

Identification of Immuno-regulatory modules and optimal treatment strategies for eliciting effector functions against different diseases

by

Piyali Ganguli

10BB16J26020

A thesis submitted to the
Academy of Scientific & Innovative Research
for the award of the degree of
DOCTOR OF PHILOSOPHY
in
SCIENCE

Under the supervision of
Dr. Ram Rup Sarkar



CSIR- National Chemical Laboratory, Pune

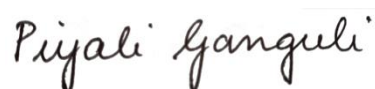


Academy of Scientific and Innovative Research
AcSIR Headquarters, CSIR-HRDC campus
Sector 19, Kamla Nehru Nagar,
Ghaziabad, U.P. – 201 002, India

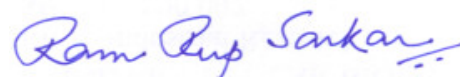
March, 2021

Certificate

This is to certify that the work incorporated in this Ph.D. thesis entitled, "Identification of Immuno-regulatory modules and optimal treatment strategies for eliciting effector functions against different diseases", submitted by Ms. Piyali Ganguli to the Academy of Scientific and Innovative Research (AcSIR) in fulfillment of the requirements for the award of the Degree of Doctor of Philosophy in Science, embodies original research work carried-out by the student. We, further certify that this work has not been submitted to any other University or Institution in part or full for the award of any degree or diploma. Research material(s) obtained from other source(s) and used in this research work has/have been duly acknowledged in the thesis. Image(s), illustration(s), figure(s), table(s) etc., used in the thesis from other source(s), have also been duly cited and acknowledged.



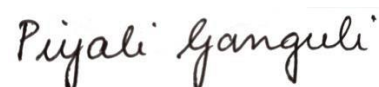
Piyali Ganguli
(Student)
31st March, 2021



Dr. Ram Rup Sarkar
(Supervisor)
31st March, 2021

STATEMENTS OF ACADEMIC INTEGRITY

I, Ms. Piyali Ganguli, a Ph.D. student of the Academy of Scientific and Innovative Research (AcSIR) with Registration No. 10BB16J26020 hereby undertake that, the thesis entitled "Identification of Immuno-regulatory modules and optimal treatment strategies for eliciting effector functions against different diseases" has been prepared by me and that the document reports original work carried out by me and is free of any plagiarism in compliance with the UGC Regulations on "*Promotion of Academic Integrity and Prevention of Plagiarism in Higher Educational Institutions (2018)*" and the CSIR Guidelines for "*Ethics in Research and in Governance (2020)*".



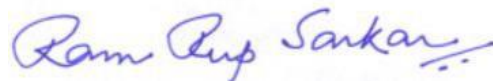
Signature of the Student

Name: Piyali Ganguli

Date : 31st March, 2021

Place : Pune

It is hereby certified that the work done by the student, under my supervision, is plagiarism-free in accordance with the UGC Regulations on "*Promotion of Academic Integrity and Prevention of Plagiarism in Higher Educational Institutions (2018)*" and the CSIR Guidelines for "*Ethics in Research and in Governance (2020)*".



Signature of the Supervisor

Name: Dr. Ram Rup Sarkar

Date : 31st March, 2021

Place : Pune

Dedicated to my parents, sister and husband

Acknowledgement

I would like to begin by expressing my sincere gratitude to each and everyone in my life, who has believed in me, inspired me, encouraged me and supported me throughout my journey in academia.

First and foremost, I would like to thank my PhD Supervisor, Dr. Ram Rup Sarkar, for being such a great mentor and teacher that has tremendously helped me pursue my research in mathematical modelling after coming from biological sciences discipline. I sincerely thank him for being patient with me through my learning procedure, putting his trust in me and believing that I could do it even when my confidence was shaken. His constant guidance, supervision and critical feedbacks throughout my PhD has helped me a lot to improvise on my mistakes, be more organised, think rationally and take up challenges with greater confidence. He has instilled in me a passion for research. From him, I have learnt how to multi-task and at the same time maintain a healthy balance between the professional and personal life. I cannot thank him enough for all his guidance and support in both academic and non-academic matters that has helped me throughout my PhD journey.

I am grateful to my Doctoral Advisory Committee (DAC) members Dr. Leelavati Narlikar, Dr. Sarika M. Bhattacharyya and Dr. Kiran Kulkarni for evaluating my progress and providing useful suggestions that have not only helped me in my doctoral research but also helped me gain new ideas and perspectives for my future work. I am sincerely thankful to Prof. Sudip Kundu, Dr. Sukla Ghosh, Dr. Nitai Pada Bhattacharyya and my professors from Department of Biophysics and Molecular Biology, University of Calcutta, who has been instrumental in shaping my research career during my Masters degree. I would also like to thank my collaborators Prof. Godefridus J. Peters, Dr. Mayur Yergeri, Dr. Manikanta Murahari, Dr. Anusree Mahanta, Dr. Pankaj Barah, Dr. Neelanjana Sarmah, Dr. Saurav Phukan, Dr. Mayuri Bora and Dr. Shashi Baruah for all their support.

I would like to thank our former Directors Dr. Saurav Pal and Prof. Ashwini K. Nangia, and the HOD of the CEPD Division, Dr. Sunil Joshi for providing the infrastructure for carrying

out my research. I would like to sincerely thank Mr. Hasso Raheja for taking initiative and solving all our problems related to the official work on several occasions. I am grateful to all the members of the Student Academic Office for entertaining our endless queries and guiding us throughout. I am also thankful to CSIR for providing me the Fellowship to continue my research and all the members of the Bills and Accounts section (especially Mrs. Shubhangi) for mediating its timely disbursal.

I do not have enough words to express gratitude towards my friend (more like a sister) and labmate-cum-roommate, Ms. Rupa Bhowmick, who has been a pillar of support during the various phases of ups and downs both in my personal and professional spheres ever since 2008. I am also tremendously thankful to Dr. Saikat Chowdhury for being such a wonderful friend and mentor and for always being there when we needed any help both in the lab and outside. I am truly indebted to both of them for making my PhD journey so memorable and smooth.

I am grateful to my lab members especially Dr. Noopur Sinha, Mr. Sutanu Nandi, Dr. Abhishek Subramanian, and Dr. Swarnendu Banerjee, for all their help, scientific discussions and guidance in the lab and all the fun memories they have created at the lab parties and during our several hangouts in and outside NCL. I would also like to thank all the new members of our lab - Gauri, Anirudh, Kshitij, Priyanka, Mudita, Malobika, Dr. Chandrakala, Bhagyashree for being such wonderful labmates. I also had the opportunity to work with some excellent and bright Summer Interns and Project Assistants of our lab that includes Shomeek, Bhavyata, Akarsh, Sashwat, Souradeep, Rituparna, Arpit, Varsha, Apoorv and many others. Thank you all so much.

My days at CSIR-NCL were brightened with the presence of some compassionate seniors that includes Dr. Manoj Kumar Nandi, Dr. Chayanika Das, Dr. Monalisa Ganguly, Dr. Atreyee Banerjee who have helped me endlessly and cared for me during my years of PhD. Special thanks to all my friends at NCL including Mr. Tushar Dubey, Dr. Sayantan Acharya, Mr. Ujjwal Nandi, Dr. Bipul Biswas, and many others. During the past seven years, I also got to

interact with some of the very talented members of the Bangiya Samitee (Bong NCL Group) who have created very beautiful memories for me to cherish all my life. I would also like to express my heartfelt gratitude to Mrs. Mousumi Sarkar for making all the countless lab parties we had, the lab trips and all the Bong celebrations so very memorable. You have always been the one person who we could trust with all our secrets, and the one we can fall back upon when we need any advice, suggestion or help in any matter. Thank you for always being by our side.

I would like to thank all my teachers Mrs. Tapati Dutta, Mrs. Subidita Kundu, Mr. Uma Shankar Sanyal, Mr. Nirmal Debnath, Mrs. Sam, Mrs. Shampa Ghosh and Mrs. Meena Chatterjee for inspiring me from my childhood and laying the foundation of my education. I will forever be indebted to them. My sincere thanks to my very close friends Dr. Deblina Basu, Dr. Samik Bose, Dr. (M.D.) Arnab Mandal, Mrs. Rima Dutta, Dr. (M.Ch.) Homagni Ghosh, Mr. Sayak Manna, Mr. Shatadru Dutta, Mr. Ameet Thakur, Mr. Ritaban Basu, Mr. Subham Bhowmick, and Dr. Saurav Mallik, for all their support throughout my journey, for always looking out for me and lending me a helping hand whenever I needed it.

Lastly, and most importantly, I want to thank my family to whom I owe everything. My entire education is an outcome of the countless sacrifices and relentless struggle of my parents (Mr. Satyananda Ganguli and Mrs. Sreerupa Ganguli) who have always believed in me and encouraged me in all my endeavours. They have been my first teachers and have taught me how to persevere in the toughest of times which helped me get through my PhD. My little sister, Miss Regina Ganguli, has been my pillar of support ever since my childhood. Not only has she constantly supported me emotionally throughout my journey and provided me with many practical solutions, but also, she has been my source of financial support when my fellowships got delayed endlessly. I am also immensely thankful to my husband Mr. Prateep Mukherjee who has always supported me emotionally as well as with several useful solutions whenever I got completely overwhelmed and frustrated with my work. He has been immensely patient and understanding with me when I lost my temper due to work pressure and freaked out. My parents, my sister and my husband are the backbone of my life.

I am also deeply indebted to my family members Mrs. Debjani Mukherjee (Mother-in-Law), Mr. Gautam Mukherjee (Father-in-law), Dr. Lopamudra Mukherjee (Sister-in-law), Dr. Vikas Singh (Brother-in-law), Mr. Jitedranath Majumdar (bhai), Mr. Sadhan Banerjee (bhaiya), Mr. Jibandhan Ganguli (great grandfather), Mrs. Laxmi Chatterjee, Mrs. Swati Chatterjee, Mrs. Gopa Goswami, Mrs. Shukla Roy, Prof. Tilak Nath Roy, Mrs. Sabita Roy, Mr. Dhruv Narayan Bhattacharyya and Mr. Suman Roy. They have always encouraged me all along in shaping my academic path and through my PhD journey.

Above all, I thank God and Sri Sri Vishuddhananda Paramahansa (Guru) for showing me the correct path and helping me in my decisions whenever I was lost.

I thank all of you from the bottom of my heart who have believed in me, have shielded me against all the patriarchy in the society and encouraged me to dream bigger at every step. My PhD would not have been possible without all your support.

Piyali Ganguli

Contents

Chapter 1 General Introduction and Scope of the Thesis	1
1.1. Background	1
1.2. Cell Signalling Pathways regulates Differentiation and Effector Function of Immune Cells.....	2
1.3. Activation and Polarization of Antigen Presenting Cells	3
1.4. Micro-environmental Cues for T-Cell Activation and Diversity	5
1.4.1. CD4 ⁺ Helper T-cell (T _H)	5
1.4.2. CD8 ⁺ Cytotoxic T-cell (T _C).....	7
1.5. Immune responses for Infectious and Non-Infectious Diseases	9
1.5.1. Immune Responses during Leishmaniasis	9
1.5.1.1. Species specific responses	11
1.5.1.2. Acute Infection	13
1.5.1.3. Chronic Infection.....	13
1.5.2. Immune Responses during Cancer.....	14
1.5.2.1. The Seed and Soil Hypothesis of Tumor Development	15
1.5.2.2. Role of Tumor Microenvironment in Immunoediting.....	17
1.6. Need for Immunotherapy in the treatment for Leishmaniasis and Cancer.....	18
1.7. Computational strategies employed for the study of immunoregulatory modules in Leishmaniasis and Cancer	20
1.8. Existing challenges in target identification for Immunostimulation and Immunopharmacology.....	24
1.9. Scope and Specific Objectives of the Thesis	26
1.10. Outline of the Thesis.....	27
Chapter 2 Materials and Methods.....	29
2.1. Collation of Signalling Pathway information	29
2.1.1. Reconstruction of T-cell Pathways and Cross talks	30
2.1.2. Reconstruction of <i>Leishmania</i> infected APC Pathways	31
2.1.2.1. Construction of gene correlation network.....	31
2.1.2.2. Integrating Intra-cellular and Inter-cellular Signalling Crosstalk of T-cell and Macrophage during Leishmaniasis	33
2.2. Logical Steady State Analysis of Signalling Pathways	37

2.2.1. Model Formulation and Transition Functions.....	39
2.2.2. Phenotypic Response Functions	40
2.2.3. Update of Logical Rules - Synchronous and Asynchronous Simulation.....	42
2.2.4. Omics Data for Model Validation.....	43
2.2.5. Binarization of Expression Data.....	45
2.2.6. Model Initialization	45
2.2.7. Attractor Analysis	46
2.2.8. <i>In-silico</i> Knock-in and Knock-out Analysis.....	47
2.3. Prediction of Protein-Protein Interactions between Host and Pathogen	47
2.3.1. Interolog Mapping from Secretome data.....	48
2.3.2. Domain-Domain Interaction Mapping	48
2.3.3. Integration and development of Host-Pathogen PPI network and Qualitative Ranking of predicted Interactors	49
2.3.4. Gene Ontology and Pathway Enrichment.....	50
2.3.5. Network Analysis	50
2.3.6. Identification of Phenotypic Response Nodes and Sub-Networks using experimental data.....	51
2.3.7. Target identification using <i>in-silico</i> perturbation based on Path distance analysis and shortest path depletion	52
2.4. Immune Cell Crosstalk in Cancer Microenvironment.....	54
2.4.1. Model Formulation	55
2.4.1.1. Tumor formation.....	55
2.4.1.2. Immune cells in the Tumor Microenvironment.....	57
2.4.1.3. Cytokines and Feedbacks.....	58
2.4.2. Model Equations	58
2.4.3. Control and Therapeutic Intervention	60
2.4.4. Designing Treatment Protocols.....	61
2.4.5. Positivity and Boundedness	63
2.4.6. Sensitivity Analysis.....	64
2.4.7. Parameter Estimation from Cancer cell line data	65
2.4.8. Experimental Data for Model Calibration	65
2.4.9. Interior Equilibria.....	67

2.4.10. Model Initialization and Numerical Simulation.....	68
Chapter 3 Study of Co-receptor and Calcium signalling crosstalks regulating T_H-cell activation and Effector functions	69
3.1. Motivation.....	69
3.2. Results.....	72
3.2.1. Reconstruction of T-cell co-receptor Signalling Pathways.....	72
3.2.2. Model Analysis - Simulation and State Transition.....	74
3.2.3. Phenotypic enrichment of output proteins	76
3.2.4. Comparison with Experimental Observations	77
3.2.5. Phenotypic Pattern Generation and Validation.....	79
3.2.6. Effect of multiple mutations on Interleukin Production	83
3.3. Discussion	87
Chapter 4 Identification of T_{H1}/T_{H2} regulatory switch to promote healing response during Leishmaniasis	91
4.1. Motivation.....	91
4.2. Results.....	95
4.2.1. Pathway Enrichment	95
4.2.2. Features of the Reconstructed Pathway.....	96
4.2.3. Model Analysis.....	98
4.2.3.1. Attractors.....	98
4.2.3.2. Model Validation with Experimental Data	99
4.2.3.3. Comparison of Uninfected and Infected Scenarios.....	103
4.2.3.4. Effect of infection on T-cell signalling cascade	104
4.2.3.5. Immune Response & Immunotherapeutic Strategies	105
4.3. Discussion	109
Chapter 5 Delineating Infection strategies and Immune Responses during Visceral Leishmaniasis	117
5.1. Motivation.....	117
5.2. Results.....	121
5.2.1. Predicted <i>L. donovani</i> -Human PPI Interactome	121
5.2.2. Structural Analysis and Sanity test of the Network.....	123
5.2.3. Functional Correlation based on Pathway Enrichment Analysis	124

5.2.4. Extraction of Phenotypic Response sub-networks targeted by <i>L. donovani</i> virulence factors based on shortest path analysis.....	125
5.2.5. Sub-networks of Phenotypic Responses reveal unique pathways regulated by the virulence factors	126
5.2.6. Study of sub-network cross-talk to identify key proteins targeted by the parasite based on nearest neighbour.....	128
5.2.7. Network Perturbation Analyses to identify important proteins that regulate each sub-network.....	129
5.2.8. Identification of protein combinations that regulate the overall phenotypic responses during <i>L. donovani</i> infection.....	133
5.3. Discussion	136
Chapter 6 Unveiling Immuno-regulatory mechanisms in the tumor microenvironment and design of protocols for triggering cancer remission.....	141
6.1. Motivation.....	141
6.2. Results.....	143
6.2.1. Model Validation with Experimental Data	143
6.2.1.1. Tumor Growth (without therapy)	143
6.2.1.2. Immune cell-ratio comparison with Cytometric data.....	145
6.2.1.3. Cytokine Production.....	147
6.2.2. Model Analysis.....	147
6.2.2.1. Development of Drug Resistance is governed by the pattern of stem cell differentiation	147
6.2.2.2. Dual Role of Tumor Associated Macrophages	149
6.2.2.3. IFN- γ and IL10 feedbacks regulate Cancer progression.....	149
6.2.3. Development of Treatment Strategies.....	152
6.2.3.1. Failure of Chemo and Radiotherapies due to the presence of resistant cells ..	152
6.2.3.2. Immune Interventions for effective Tumor Remission.....	152
6.3. Discussion	154
Chapter 7 Conclusion and Future Directions	159
7.1. Conclusion	159
7.2. Future Directions.....	163
Appendix A	166
Appendix B.....	175

Appendix C	196
Appendix D	208
References	212
Abstract	242
List of Publications	243
Publications (Thesis Related)	245

Summary

The immune system forms the sentinel of our body that protects it from infectious disease and cancer. However, the complexity of the immune regulatory network that governs the differential responses of T-cells under varied antigenic challenges, leading to immune-suppression, remains elusive through experimental approaches. In order to unveil these intricate biological regulatory mechanisms underlying immune-suppression during Cancer and Leishmaniasis (commonly known as Kala Azar, a Neglected Tropical Disease caused by the protozoan parasite *Leishmania sp.*), we have used various mathematical and computational approaches, to identify the regulatory modules of the immunological network to stimulate T cell effector functions against Leishmaniasis and Cancer, understand the role of T_H cell Plasticity/differentiation for the control disease progression and design treatment strategies to enhance immune clearance and disease prognosis.

Manual reconstruction of T-cell pathway and Boolean Modelling was used to gain a holistic understanding of the co-receptor mediated pathways. Multiple *in silico* knock-out analysis followed by synchronous and asynchronous model simulations revealed minimal combination of proteins (TCR:CD3, CRAC and OX40) that is absolutely essential to achieve sustained T-cell proliferation and activation of effector functions. Co-receptor molecules CD27 and LTBR were identified to play major role in the regulation of Interleukin expression during antigenic challenges.

To study T-cell immune-suppression during Cutaneous Leishmaniasis and identify signalling routes regulating the switching of T-cell responses from healing T_{H1} to non-healing T_{H2} response, the T-cell model was further integrated with infected APC (Antigen Presentation Cell) pathways. Here, for the first time, we report that *Leishmania* infection induced IFN- β contributes to T_{H1}/T_{H2} switching response *via* TYK2-mediated pathway. Two novel combinations have been proposed that can trigger healing immune responses for complete removal of infection. Boolean

attractor analysis was performed to compare the efficacy of each combination. Here, it was observed targeting TLR3 and SHP2 produced anti-*Leishmania* response better than conventional IFN- γ or IL12 treatment. A putative host-pathogen interactome between *Leishmania donovani* and Human has also been predicted using Interolog and Domain mapping strategies. Network analysis revealed key signalling routes mediating the host pathogen interaction. A novel combination of protein targets (UBC+1433Z+HS90A) has also been identified which governs the host immune response, parasite survival strategies and visceralization of the infection during Visceral Leishmaniasis.

To study the tumor-immune interaction, an ODE based mathematical model has been developed related to the Seed Soil hypothesis of tumor development that gives rise to tumor heterogeneity. Model analysis revealed as the differentiation of Cancer Stem Cells (CSC) shifts from symmetric to asymmetric pattern, resistant cancer cells start accumulating in the tumor that makes it refractory to therapeutic interventions. Three novel feedback regulations governing tumor progression, resistance and relapse have been proposed in the study. The model has been further used to explore the failure of conventional treatment strategies and propose improvised combinatorial protocol that shows promising results in suppressing resistant tumor for better Cancer remission.

The outcome of the research presented in the thesis cater to the experimental biologists and clinicians by providing novel target molecules and treatment strategies for infectious diseases and Cancer, while the mathematical models developed in the study acts as tools for target identification, optimization of drug dosage and time schedules for designing advanced treatment protocols in future.

List of Figures

Figure 1: Polarizing signal and transcription factors that dictate T _H cell differentiation, proliferation and effector function.....	6
Figure 2: Immune Responses generated during <i>Leishmania</i> infection.....	11
Figure 3: Simplified pathway diagram showing the <i>Leishmania</i> -APC and T-cell Interaction.....	34
Figure 4: Toy Model for LSSA: Interaction Graph, Truth Table and State Transition Graph for a Logic Based Toy Model.....	38
Figure 5: Diagrammatic representation of the Tumor-Immune interaction model...	55
Figure 6: Sensitivity Analysis and Parameter Estimation.....	66
Figure 7: Reconstructed T-cell Pathway.....	74
Figure 8: Continuous heat plot showing state transition pattern of output proteins	76
Figure 9: Cell Phenotype in different situation under LAT mutated condition.....	80
Figure 10: Effect of Co-receptor signalling on Cell fate determination.....	82
Figure 11: Changes in Cell Phenotypes and corresponding Interleukin Expression pattern due to CD27 and LTBR mutation.....	86
Figure 12: Reconstructed diagram of T-cell, APC and <i>Leishmania</i> pathogenic protein-protein interaction network.....	97
Figure 13: Boolean attractor analysis in (a) uninfected and (b) infected scenarios...	99
Figure 14: Time-course expression profile of APC output molecules.....	101
Figure 15: Expression profile of T-cell and APC during asynchronous simulation..	104
Figure 16: Expression profile of 20 T-cell proteins which shows significant de-regulation in Mann-Whitney U test.....	105
Figure 17: Response dynamics of T _{H1} , T _{H2} and NO in uninfected, infected and in different treatment scenarios.....	107
Figure 18: Attractor analysis.....	109
Figure 19: T-cell pathways de-regulated during Leishmaniasis.....	112
Figure 20: <i>L. donovani</i> and Human PPI Network prediction workflow.....	121
Figure 21: Predicted Protein Interactome.....	122
Figure 22: The three Phenotypic sub-networks representing the source and target nodes extracted from shortest path analysis.....	127

Figure 23: Network perturbation analysis.....	132
Figure 24: Pathway Depletion analysis.....	135
Figure 25: Model Validation with experimental data.....	148
Figure 26: Parameter Variation study.....	151
Figure 27: Changes in the tumor growth after therapeutic interventions.....	153
Figure 28: Regulatory Feedback Loops.....	156

List of Figures (Appendices)

Figure A. 1: Protein expression dynamics observed in Experiment, Synchronous and Asynchronous simulation.....	173
Figure B.1: Gene clusters identified in <i>Leishmania major</i> infected APC microarray data.....	175
Figure B.2: Gene clusters identified in active T-cell microarray data.....	176
Figure B. 3: Attractor analysis of the uninfected and infected scenarios under the differential activation of the splicing factors.....	182
Figure C. 1: Cellular location of direct interactors.....	201
Figure C. 2: Average shortest path length from each Virulence Factor to the response nodes of each phenotypic subnetwork.....	206
Figure C. 3: Distance deviation Analysis for the combination knockout in IR, SUR and VIS subnetworks	207
Figure D. 1: Treatment conditions under varying dose of Radiotherapy, Chemotherapy and Immunotherapy.....	211

List of Tables

Table 1: Summary of T _H cell diversity, polarizing factors and effector functions.....	8
Table 2: Validation of Results.....	79
Table 3: LAT mutation analysis.....	81
Table 4: Effect Co-receptor molecule knock-out in T cell proliferation.....	84
Table 5: Unique combinations of proteins that can be used as promising immunotherapeutic targets.....	108

List of Tables (Appendices)

Table A. 1: Logical Equations.....	166
Table A. 2: Initial Values of Nodes.....	171
Table A. 3: Functional classification of T-cell output protein.....	174
Table B.1: Pathway Enrichment of the significantly expressed genes in the microarray experiment of <i>Leishmania</i> infected APC.....	177
Table B.2: Pathway Enrichment of the significantly expressed genes in the microarray experiment of activated T-cell.....	178
Table B. 3: List of all known alternatively spliced isoforms of the output molecules of both APC and T-cell.....	179
Table B. 4: Logical Equations used to model the reaction mechanisms in T-cell and APC during <i>Leishmania</i> infection.....	184
Table B. 5: Binary initial values of the reaction nodes considered in the Logical equations from binarization of microarray expression data.....	192
Table B. 6: List of agonist and antagonist of the proposed targets.....	195
Table C. 1: <i>L.donovani</i> Virulence factors (pathogen source nodes/effector nodes) considered in the final <i>L.donovani</i> VF-Human PPI Network.....	196
Table C. 2: Statistics of the Host Pathogen Interactome.....	197
Table C. 3: Correlation of virulence factors putative function as stated by Maxwell <i>et.al</i> with their corresponding predicted partner interologs on the basis of their DAVID pathway enrichment (FDR <0.05)	197
Table C. 4: List of PRNs and their associated GO terms (biological process) for each Phenotype category.....	202
Table C. 5: Signalling Pathways enriched for each sub-network.....	204
Table C. 6: Top 10 knockout candidates identified based on Betweenness centrality measure in the three sub-networks.....	206
Table D. 1: List of Parameters.....	208
Table D. 2: List of Initial values.....	211

List of Abbreviations

Ag	Antigen
APC	Antigen Presenting Cells
CL	Cutaneous Leishmaniasis
CMI	Cell-mediated immunity
CSC	Cancer Stem Cell
DC	Dendritic Cells
DMP	Differentially Modulated Proteins
GO	Gene Ontology
HPI	Host Pathogen Interaction
IFN	Interferon
IR	Immune Response Module
LPG	Lipophosphoglycan
LSSA	Logical Steady State Analysis
M1	Macrophage (Type I- Classically Activated)
M2	Macrophage (Type II- Alternatively Activated)
MHC	Major Histocompatibility Complex
NK	Natural Killer Cell
NO	Nitric Oxide
ODE	Ordinary Differential Equations
PAMP	Pathogen-associated molecular patterns
PPI	Protein Protein Interaction
PRN	Phenotypic Response Nodes
PSP	Perturbation of shortest paths
SP	Signalling Pathway
SUR	Survival Module
TAM	Tumor Associated Macrophage
Tc	Cytotoxic T-cells
TCR	T-cell Receptor
T _{H1}	Type -I Helper T-cells
T _{H2}	Type -II Helper T-cells
TLR	Toll-like Receptor (TLR)
TNF	Tumor Necrosis Factor
VF	Virulence Factor
VIS	Visceralization Module
VL	Visceral Leishmaniasis

CHAPTER 1

GENERAL INTRODUCTION AND SCOPE OF THE THESIS

1.1. Background

The immune system forms the defence mechanism of the body that protects it from various bacterial or viral infectious diseases and cancer. The eukaryotic immune system is formed of a network of closely interacting cells that are capable of detecting foreign non-self molecules (proteins, toxins or other chemical substances) in the body called 'antigens' and undergoing differentiation into specialized activated forms, known as the Effector Cells that mediate an immune response. The Adaptive Immune system, composed mainly of the T and B lymphocytes is responsible for maintaining this defence mechanism of the body as it helps to generate immune responses specific to the type of antigenic challenge that the body encounters [1]. The Helper T-cells (T_H) forms the central orchestrators of the entire immune-regulatory network. They have been known to have essential roles in the recognition of the antigen when presented on the surface of the Antigen Presenting Cells (APC), e.g. Macrophages, Dendritic Cells (DC), etc., and secrete cytokines that aid in the proliferation of the Cytotoxic T (T_c) cells and B-cells, thereby playing an active role in stimulating both the humoral as well as the cell mediated immunity [2]. The effector functions of this immune system are mediated mainly by the cytokines and other microbicidal molecules secreted by these APCs and the T lymphocytes as a result of the activation of complex biochemical signalling pathways inside the immune cells. The T_H cells themselves produce a high amount of effector molecules (e.g. cytokines) *via* TCR and co-receptor mediated pathways that mediate apoptosis of infected and cancerous cells [3,4]. However, during Chronic Infection or Cancer, this immune-surveillance mechanism of the body is subdued by the virtue of an immune-suppressive micro-environmental condition that leads to altered immune

signalling pathways regulating the activation and differentiation of the T cells and Macrophages, which leads to immune-tolerance. This delicate balance between the immune-surveillance and immune-tolerance regulates the outcome of any disease. The changes in the signalling pathways and the gene regulatory network of these cells during infectious diseases or cancer is manifested in the form of T-cell anergy, reduced production of effector molecules, an altered pattern in the secretion of cytokines and generation of immune cell subtypes responsible for immune-suppression and further progression of the disease. Hence, in order to identify the key regulators of T cell hypo-responsiveness, it is important to delve deep into the study of the biochemical pathways to unveil the molecular mechanisms responsible for the changes in the immune response as well as design treatment strategies for controlling the disease mediated immune suppression.

1.2. Cell Signalling Pathways regulates Differentiation and Effector Function of Immune Cells

The immune responses or effector functions generated in the body on encountering a foreign antigen by the activated immune cells is regulated by a complex network of biochemical reactions that translates the cues from the diseased/infected microenvironment to the naïve T-cells and Macrophages. These intracellular and intercellular signal transduction pathways and their crosstalks activate specific transcription factors to produce effector molecules such as Cytokines (e.g. Interleukins (IL), Interferons (IFN) etc.), Chemokines and other microbicidal molecules. Depending on the cue and the polarizing signal that the immune cell receives from its microenvironment, in the form of co-stimulatory signals, polarizing cytokine milieu, and type and strength of the antigenic stimulus, various intracellular signalling pathways, such as the PI3K-AKT, JAK-STAT, Toll-like Receptor (TLR) pathways, TNF pathways, etc. as well as their cross-talking pathways, are triggered inside the cell that regulates its differentiation and effector

function specific to the antigenic challenge. The activation of these intracellular signalling pathways is intricately regulated by the various co-receptor molecules that are present on the surface of the Antigen Presenting Cells and the T-lymphocytes and the paracrine intercellular signalling cross-talks existing among them. The differential regulation of these signalling cascades culminates in the altered regulation of the sub-type specific transcription factors that lead to differentiation of the immune cells into classically activated subtypes or alternatively activated subtypes of the immune cells that have different effector functions and phenotypic responses.

1.3. Activation and Polarization of Antigen Presenting Cells

In order to elicit an effective immune response that is capable of eliminating the antigenic challenge encountered by the body, it is essential to first detect its presence as 'non-self'. The Helper T-cells (T_H) cells cannot directly recognize the presence of the antigens in the body. This antigen recognition function is carried out by phagocytic cells of Innate Immunity that act as Professional Antigen Presenting Cells (e.g. Macrophages, B-cells, Dendritic Cells). These cells can recognize the Pathogen-associated molecular patterns (PAMPs) present on the surface of the invaded microbes and other exogenous and endogenous ligands *via* complementary pattern recognition receptors (PRRs) present on their surface such as Toll-Like Receptors (TLR), Type 3 Complement Receptor (CR3), Scavenger Receptors (SR), Mannose Receptor (MR), etc [5]. The APCs then engulf the antigenic molecule, process it *via* the Antigen Processing Pathway and present it on the cell surface along with the Major Histocompatibility II (MHC II) complex that can be recognized by the T-cell Receptor (TCR).

The Dendritic Cells and Macrophages display a plethora of TLRs on its surface that triggers signal transduction pathways in its downstream. TLR1, TLR2, TLR4, TLR5,

and TLR6 are located on the cell surface and recognize bacterial components [6,7]. On the other hand TLR3, TLR7, TLR8, and TLR 9 are found mostly on membranes of the endocytic compartments [7,8]. The signalling pathways triggered by the different TLRs by recruiting the adaptor molecules MyD88, TIRAP (MAL), TRIF (TICAM1), and TRAM in various combinations, culminates in the activation of the transcription factors NF- κ B and AP-1, that leads to the production of inflammatory cytokines and chemokines. These TLRs work in a concerted way with themselves (e.g. TLR2 form heterodimers with TLR6 and TLR1) as well as with other PRRs such as CD36 and Dectin-1 to modulate the innate immune response and secretion of pro-inflammatory cytokines by the downstream activation of various signalling pathway cross-talks according to the type of antigenic challenge detected [8-10]. This classical activation pathway leads to the formation of M1 macrophages with pro-inflammatory functions and high microbicidal activities that is characterised by the secretion of IFN- γ , IL-12, TNF- α and generation of Reactive Oxygen Species (ROS) and Reactive Nitrogen Species (RNS) [11].

On the other hand, the Alternate Activation pathways triggered by the IL-4 and IL-13 pathways produce polarized M2 Macrophages that have anti-inflammatory functions with essential roles in tissue repair. While, the early source of IL-4 remains to be Basophils and mast cells, due to tissue injury, these cells can also produce IL-4 during some fungal or parasitic infections in response to chitin, a structural biopolymer [12]. These alternatively activated M2 Macrophages are often harmful to the host as they suppress the production of the pro-inflammatory cytokines and hinder the clearance of the infection. In Cancer, the Tumor Associated Macrophages (TAM) having M2 characteristics also have proven to aid in the further progression of the tumor. A comprehensive review of the Macrophage activation, polarization and effector functions have been discussed by Mosser and Edwards [12].

In addition to the functions of the innate immunity, the Macrophages and Dendritic Cells also play a crucial role in recruiting the components of adaptive immunity. For example, the M1 Macrophages produce chemokines CXCL9, CXCL10, and CXCL11 that bind to the CXCR3 receptor aiding the trafficking of CD4⁺ Helper T cells, CD8⁺ Cytotoxic T cells, and the Natural Killer (NK) cells that plays a pivotal role in the elimination of infected and cancerous cells [11,13]. Thereafter the cytokines secreted by these Macrophages and Dendritic cells create a polarizing microenvironment for the activation and differentiation of the T_H-cell into specific sub-types that is essential for generating the required immune response.

1.4. Micro-environmental Cues for T-Cell Activation and Diversity

The T lymphocytes respond to the presence of the MHC bound antigen complex (Ag-MHC) by the activation of the $\alpha\beta$ T-cell receptors (TCRs) mediated signalling pathway. The MHC molecules exist in two forms, *viz.* Class I and Class II Major Histocompatibility Complexes. In contrast to the MHC-class-II molecule, which is only expressed by professional APCs like Macrophages and Dendritic Cells, the MHC-class-I is expressed by all nucleated cells including the APCs. For optimal binding of the TCR to the Ag-MHC complex, the T cells require the additional binding of the co-receptors CD8 and CD4 to the MHC-class-I or the MHC-class-II molecules respectively. While the immature thymocytes of Lymphoid origin, called the Double Positive Cells, express both CD4 and CD8 molecules, they gradually differentiate into the CD8⁺ Cytotoxic (T_c) and the CD4⁺ Helper T_H Cells having distinct effector functions [14].

1.4.1. CD4⁺ Helper T-cell (T_H)

The CD4⁺ Helper T-cells (T_H) display high plasticity that helps them to differentiate into specialized T_H cells according to the type of the antigenic challenge and the micro-environmental conditions (**Figure 1**). The early events of the T-cell activation

play a major role in the determination of the pattern of differentiation of the naïve T_H-cell. The micro-environmental cues, in the form of cytokines, activate the signalling pathways of the T_H cells that eventually lead to the changes at the gene-regulatory levels [15]. The selective activation of specific transcription factors mediates the differentiation of the naïve cells into specialized CD4⁺ T_H effector cells, *viz.* T_{H1}, T_{H2}, T_{H17}, etc. (**Table 1**) [16]. Additionally, another type of CD4⁺ T_H cell called the Regulatory T cells (iTreg) has a role in maintaining the T_H cell homeostasis.

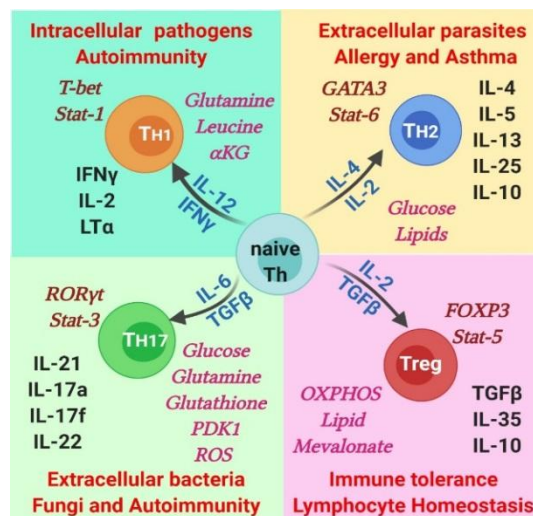


Figure 1: Polarizing signal and transcription factors that dictate T_H cell differentiation, proliferation and effector function. Signature cytokine profiles of each sub-set are also shown.

The mechanism of T-cell differentiation is governed initially by the strength of stimulus that the TCR receives from the APC. *In vitro* experiments have revealed that a stimulus of a lower strength induces the expression of the GATA-3 transcription factor, the master regulator of T_{H2} cells. Simultaneously, the expression of the IL2 cytokine activates STAT5 that synergizes with GATA-3 to transcribe IL-4 gene that eventually leads to the differentiation of the naïve cell into the T_{H2} subtype [17]. On the other hand, a stronger stimulus favours the activation of the T-bet transcription factor that helps in the differentiation into the T_{H1} subtype and triggers the production of IFN- γ and IL12 cytokines. The differentiation of naïve CD4⁺ T cells

into T_{H17} cells is induced by TGF- β /IL-6 in combination with TCR stimulation. This triggers the production of IL-23R that induces the transcription factor ROR γ t, as well as produce IL-17, and IL-21. The STAT-3 protein plays an important role in the production of the T_{H17} effector molecules and requires the activation of the ICOS co-stimulatory pathway. However, under the T_{H17} inducing conditions, the presence of IL2/STAT5 induces the expression of the Foxp3 transcription factor that leads to the differentiation of the naïve cells into iTreg cells. The strength of TCR stimulus also plays a role in the T_{H17}/iTreg determination process, where it has been observed that a weak stimulus favour the differentiation in iTreg cells that are known to have a role in immune-suppression [17].

Each of the T_H sub-type has a specific effector function to perform [15-18]. A balance between all the T_H cell subtypes is necessary for the proper functioning of the immune system. The effector molecules, in the form of Interleukins, Interferons, Tumor Necrosis Factor, etc., produced by these diverse groups of immune cells, maintain the integrity of the immune-regulatory network (**Table 1**). However, during any disease condition, this defence mechanism gets subdued.

1.4.2. CD8⁺ Cytotoxic T-cell (T_C)

The CD8⁺ Cytotoxic T-cell (T_C) recognizes the presence of intracellular pathogens and transformed cancerous by the MHC Class I molecule that combines with the antigenic peptide and is presented on the surface of the target cell. The T_C cells bind to these targets cells *via* the CD8 co-receptor that activates distinct signalling pathways and effector functions of the T_C cells. The T_C cells induce apoptosis of the target cells principally by three mechanisms [19]. The first is the secretion of cytokines (e.g. TNF- α and IFN- γ) having anti-tumour and anti-viral microbial effects. The second mechanism is the production of and release of cytotoxic granules containing the enzymes Perforin, and Granzymes [20]. While the Perforin forms a

pore in the membrane of the target cell, the granzymes, which are serine proteases, enter the infected or malignant cell. The Granzymes then cleave the proteins inside the cell and induces apoptosis of the target cell. The Tc cells, when activated can also express Fas ligand, which binds to its receptor, Fas, on the surface of the target cell and activate the caspase signalling cascade, which results in apoptosis of the target cell [20]. These CD8⁺ cytotoxic cells thus play important role in administration of immunotherapy against different diseases.

Table 1: Summary of T_H cell diversity, polarizing factors and effector functions

CD4 ⁺ Subset	Polarizing Cytokines	Transcription factors	Inhibitory transcription factors	Effector Functions
T _{H1}	IL12, IFN γ	T bet, STAT1, STAT4, Runx 3, Eomes, Hlx	GATA3	Cell mediated immunity against intracellular pathogens and phagocyte-dependent protective responses
T _{H2}	IL4, IL2	GATA3, STAT6, STAT5, STAT3, Gfi-1, c-Maf, IRF4	T-bet, Runx3	Immune response against extracellular parasites, bacteria, allergens, and toxins. They help in activation and maintenance of the humoral, or antibody-mediated, immune response and promote tissue repair
T _{H17}	IL6, IL 21, IL 23, TGF- β	ROR γ t, STAT3, ROR α , Runx1, Batf, IRF4, AHR	T-bet ⁺ Runx1, Smad3 Runx1+FOXP3	Immune response against bacterial and fungal Infection
T _{fh}	IL6, IL21	Bcl6, STAT3	Not known	Help B cells produce antibody against foreign pathogens
iTreg	TGF- β , IL2	FOXP3, Smad2, Smad3, STAT5, NFAT	Not known	Suppression of Immune Response
T _{H9}	TGF- β , IL4	IRF4	Not known	Promotes mast cell and T cell growth, stimulates mucous secretion to enhance Innate Immunity. Plays a role in allergic responses
Tr1	IL27, IL10	c-Maf, AhR	Not known	Suppression of T effector cells

1.5. Immune responses for Infectious and Non-Infectious Diseases

Changes in the micro-environmental conditions lead to alterations in the biochemical reaction network that disrupts the balance between the effector cell populations and favours the progression of the disease. This immune-suppression is observed very frequently in the cases of chronic infections (e.g., Chronic *Leishmania* infection) and Cancer. The following sections deal with the changes in the immune-regulatory network during these diseased conditions.

1.5.1. Immune Responses during Leishmaniasis

The immune responses generated during infectious diseases have baffled immunologists since ages [21]. On one hand, while in some cases, it has been observed that our immune system has been capable of protecting our body from these invading pathogens, very often these infections have led to serious diseased conditions where the immune responses generated have only favoured the continued survival of the pathogen in our body [22].

Cell-mediated immunity (CMI), responsible for confronting the infections caused due to invasion of intra-cellular pathogens, primarily involves the interactions of the phagocytic Antigen Presenting Cells (APCs) and the T-lymphocytes. This leads to the activation of a series of intra-cellular and inter-cellular biochemical signalling processes, which culminates into synthesis of certain diffusible effector molecules that includes proteins (mostly the cytokines) and microbicidal molecules (e.g. Nitric Oxide) helping in the clearance of the disease [23]. However, the activities of this defense mechanism are severely compromised during Leishmaniasis, a neglected tropical disease, caused due to infection by the protozoan parasites of the genus *Leishmania*. This is transmitted to the human through the infected bites of the Phlebotomine sand flies during their blood meal [23]. The promastigote form of the parasite once injected into the human host, is engulfed by the APC (macrophages

and dendritic cells) to form a phagolysosome, where it differentiates into its amastigote form and takes control of its entire cellular machinery in a way that reduces the immuno-competency of the immune cells thereby hindering the body's natural parasite clearance process (**Figure 2 a**) [24].

During *Leishmania* infection, the T-lymphocytes elicits either of the two types of immune responses, *viz.* healing and non-healing responses, depending on the parasite load and the host immunity [25]. The healing response is obtained in case of low parasitic load, in which a pronounced Type-I helper T-cell (or T_{H1}) response occurs due to up-regulation of the T_{H1} cytokines, such as the IFN- γ from the stimulated T-cells, and thus naturally clears the pathogen from the system [23,26]. On the other hand, higher pathogen load gives rise to a non-healing response in which an up-regulation of the T_{H2} cytokines (e.g. IL10) is observed, which favours the persistence of the *Leishmania*. Simultaneously, during this non-healing response, the production of the protective T_{H1} cytokines, such as IL12, and the microbicidal molecules, such as Nitric Oxide (NO) is also down-regulated, thus creating an immune-suppressed condition suitable for further progression of the disease [27].

This T_{H1}/T_{H2} immune response switching paradigm has perplexed both clinicians and immunologists and calls for an in-depth analysis of the biochemical pathway to unravel the mysteries of this healing versus non-healing immune responses generated during Leishmaniasis or Kala-azar that threaten the lives of millions in the tropical and sub-tropical countries ranging from the rainforests in Central and South America to deserts in western Asia and the Middle East [WHO, 2018]. Depending on the species of *Leishmania* infecting the individual and the resistance offered to the parasite by the host immune system, Leishmaniasis manifests itself as Cutaneous, Muco-cutaneous and Visceral forms. The immune responses generated during the disease vary according to the severity of the disease and the mechanism of immune modulation by the invading pathogen [21]. In this context, immune responses

during Leishmaniasis can be studied from two different perspectives, *viz.*, species specific immune responses and depending on the severity of the disease, i.e., Acute and Chronic *Leishmania* infection (Figure 2 b).

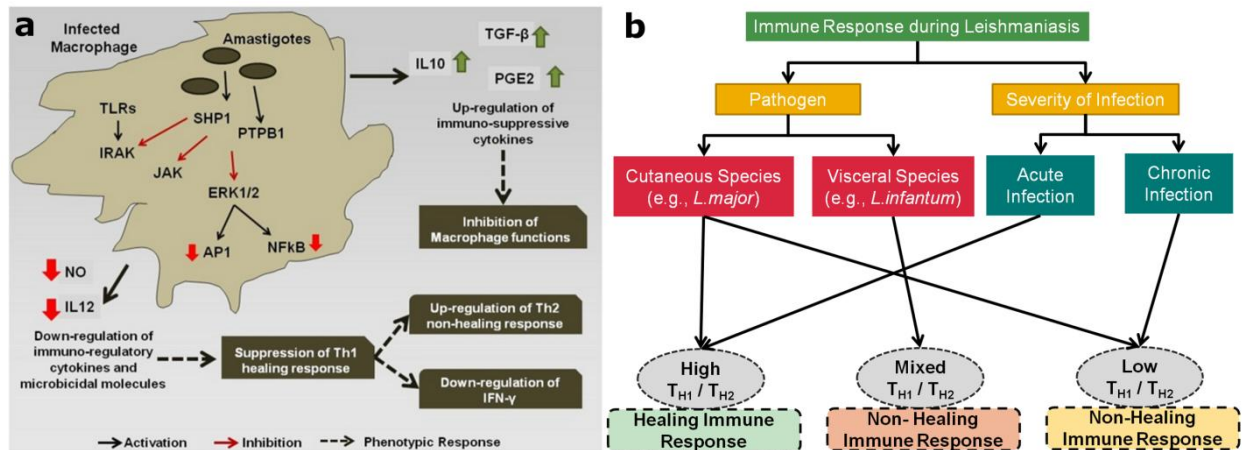


Figure 2: Immune Responses generated during *Leishmania* infection (a) Alterations in signalling pathways in the macrophages by the antigen molecules of *Leishmania*; (b) Changes in the immune responses depending on the infecting species and the severity of the infection.

1.5.1.1. Species specific responses

Cutaneous Leishmaniasis (CL), caused by the species *Leishmania major*, *Leishmania tropica*, and *Leishmania aethiopsica*, is characterized by the formation of ulcers on the skin, and disfiguring lesions on the nose, mouth and lips. However, the infection is mostly restricted to the skin. This is a less severe form of the disease and may be healed gradually by the immune mechanisms of our body [28]. The visceral form of Leishmaniasis, caused by the species such as *Leishmania infantum* and *Leishmania donovani*, is the most severe form of the disease characterized by the spread of the infection to the visceral organs like the liver and spleen, eventually leading to death. The Muco-cutaneous (MCL) and Visceral Leishmaniasis (VL) damage the mucosal lining of our body and invades the visceral organs and is highly fatal if left untreated. The antigenic challenge posed to the host by these different *Leishmania* species differs, giving rise to changes in expression of macrophage proteins, as seen in visceral versus cutaneous infections [29]. Through *in-vivo* experiments, certain

proteins have been identified in the visceral species alone, which when transfected into the cutaneous species, leads to manifestation of VL [30]. These proteins are thus characterized as Visceralizing Factor for promoting metastasis of the infected macrophages from cutaneous regions to the visceral organs [29]. In this context, *Leishmania* proteins such as A2, have been identified as the causal proteins for visceral infections [31,32], however, there are few studies that elucidate the mechanisms by which the host pathway is altered. The difference in macrophage protein expression profile, e.g. increased production of COX2 and PGE2 production in the case of *L. donovani* infection (as opposed to *L. major*) [33], indicates different *Leishmania* species selectively activates or inhibits different host pathways due to differences in the antigenic challenge. Also, *L. donovani*, which is known to cause VL, may in rare cases give rise to CL [29]. This behaviour may be attributed to host's resistance to the disease which restricts the spread of infection to visceral organs and keeps it localized to cutaneous regions [34]. From the host perspective, many groups have identified the effect of *Leishmania* antigen molecules on host signalling pathways to inhibit the functions of the Macrophage and subvert the host immune response [35]. *Leishmania* also devices regulatory mechanism to inhibit the ability of the host cell for antigen presentation to T-cells [35]. At the same time, they also modulate the activation of the co-stimulatory signalling pathways [36]. The visceral species of *Leishmania* express certain unique genes, *LinJ.15.0900*, *LinJ.28.0340*, *LinJ.36.2480* and *LinJ.22.0670*, which when inserted into the cutaneous species can cause infection to visceral organs, thereby signifying their role in visceralization of the infection [29,31,37,38]. The increased synthesis of PGE2 in *L. donovani* infected macrophages has been shown to contribute to parasite survival and visceralization [32].

Several groups of experimental biologists have studied the effect of *Leishmania* infection on macrophage expression profiles [39], the effect of altered signalling pathways on T cell responses (36), and the effect of drugs and immunostimulators

on the progression of VL [40]. However, the clinical manifestation of the disease also depends on the severity of the infection and host immune defences.

1.5.1.2. Acute Infection

During the invasion of *Leishmania* parasites into the antigen presenting cells of the host, the coat proteins of *Leishmania* interact with the Toll-like-receptor proteins present on the macrophages membrane [11]. The activation of the TLRs triggers the downstream signalling pathways such as the RAS-RAF mediated MAPK pathway, canonical and non-canonical NF κ B pathway, JAK-STAT pathway, PI3K-PLC Gamma pathway and the JNK pathway [12]. Subsequently, several transcription factors, e.g. ERK1/2, NF κ B, NFAT, AP1, STAT3, etc. gets activated in the nucleus that initiates the synthesis and secretion of several cytokines, growth factors, chemokines and anti-microbicidal molecules such as Nitric Oxide, which are responsible for a robust host immune responses [13]. During acute infection, the immune signalling pathways activated in the macrophages leads to the synthesis of an increased amount of the IL-12 cytokine. Under such micro-environmental conditions, the naïve T-cells differentiates into the T_{H1} cells that produce IFN- γ . This healing T_{H1} response helps in the elimination of the infected cells in the host.

1.5.1.3. Chronic Infection

During chronic infection, the antigenic molecules of the *Leishmania* parasite activate the phosphatases proteins in the macrophage, eg. SHP-1 and PTP1B, which leads to the dephosphorylation and deactivation of selected signalling pathways [14]. This leads to down-regulation of expression of iNOS and Nitric Oxide (NO) in the infected macrophages, thereby making the cell incompetent of performing its microbicidal functions, and creating an immune-suppressed condition, which is favourable for the continued survival of the pathogen inside APC. Simultaneously, the production of the cytokines such as IL-12 and TNF- α gets severely reduced [15].

Such changes in the cytokine expression pattern of the antigen presenting cells leads to the alteration of the phenotypic responses of the T-cells that now start showing a bias towards the non-healing T_{H2} immune response that is characterized by an increased production of IL-4, IL-10, IL-13 and TGF- β cytokines [16], and the suppression of IFN- γ that regulates the healing T_{H1} response [10]. The transcription factors T-bet and GATA3 play a pivotal role in the regulation of the T_{H1}/T_{H2} ratio during the infection [17]. Studies reveal to ensure its continued survival inside the host, *Leishmania* also inhibits the ability of the host cell for antigen presentation to other immune cells, by repressing MHC class II gene expression [18] and modulating the interaction of co-stimulatory molecules B7-1/CD28 [19] and CD40/CD40L [20].

1.5.2. Immune Responses during Cancer

In contrast to infectious diseases, the immune response generated in Cancer involves the recognition of the self-antigens as non-self-entities. These Cancer Antigens can be categorized into the following classes, viz. (a) Differentiation Antigens, e.g., melanocyte differentiation antigens, Melan-A/MART-1, tyrosinase, gp-100; (b) Mutational Antigens, e.g., abnormal forms of p53; (c) Overexpressed/Amplified Antigens, e.g., HER-2/neu; (d) Viral Antigens, e.g., EBV and HPV; and (e) Cancer-Testis (CT) Antigens [41]. Lack of expression of any of these antigen molecules on the cell-surface may help the tumor in masquerading as a normal cell, thereby escaping detection by naïve T-cells. This is one of the primary reasons that a tumor with low antigenicity is able to escape immune-surveillance, whereas an aggressive tumor with higher number of mutations can be easily detected by the immune cells [42]. Once activated, the T-cell tries to kill the cancer cells. This phase called the Elimination phase of tumor-immune interaction, where the components of both the innate and adaptive immunity attack the tumor cell with an enhanced production of IFN γ , perforin and granzymes [41]. The CD8⁺ Cytotoxic T cells and the T_{H1} helper cell are the principal mediators of this anti-tumor immune response.

However, the immune cells face many challenges in the immune-suppressive microenvironment created by the tumor that resists the elimination of the transformed cells [43]. The elimination phase is followed by a period of Equilibrium and Escape phases, where the Cancer cells take over the immune system and synthesize molecules that suppress the proliferation of the effector cells. These three phases of tumor-immune interaction, collectively termed as Tumor Immuno-editing, has been an area of active research for the past few years that have revealed the importance of the tumor microenvironment in regulation of Cancer progression [44].

1.5.2.1. The Seed and Soil Hypothesis of Tumor Development

A malignant tumor is formed of heterogeneous population of cancerous cells. According to the Cancer Stem Cell (CSC) Hypothesis, a tumor of heterogeneous cells is formed from a distinct group of cells having stem-like properties that are able to differentiate and renew for an indefinite period of time [45]. Popularly referred to as the Seed and Soil hypothesis, researchers believe that the CSCs acts like 'seed' and form the tumor initiating population of cells, which is responsible for the growth, sustenance, metastasis and relapse of Cancer [46]. These CSCs have the ability to differentiate both symmetrically and asymmetrically to form the terminally differentiated cancer cells as well as renew the pool of CSCs [47]. However, during proliferation, various extrinsic and intrinsic environmental factors give rise to random mutational events, such as, chromosomal breakage, translocation, aberrant signalling events and drug efflux, which are responsible for transformation and adaptation of the cell to resist the effect of drug and conventional therapeutic strategies [48]. This results in the formation of distinct cellular sub-populations that are drug resistant and impair the treatment of cancer.

On the other hand, the tumor microenvironment, composed mainly of the immune cells and the cytokines, plays a crucial role in determining cancer prognosis [44]. As the tumor develops, each of the tumor cell sub-populations starts manipulating the

microenvironment and induces the production of pro-tumorigenic molecules. The CSCs and the Cancer cells induce the production of immune-modulatory molecules such as IL-10, IL-13 and TGF- β that are conducive to the proliferation of the M2-Tumor Associated Macrophages (M2-TAM), the Type II T-helper (T_{H2}) cells and the T-regulatory (Treg) cells [49,50]. The IL-10 mediated positive feedback loop between the tumor and the M2-TAMs helps in the rapid proliferation of the tumor sub-populations and the progression of the disease [51]. The CSCs also express high levels of co-inhibitory molecule PD-L1 that inhibit the activation of Cytotoxic T (Tc) cells [52]. Additionally, the CSC also tries to evade recognition by the immune cell by suppressing the expression of Major Histocompatibility Complex (MHC) by the macrophage cells in the tumor microenvironment. This is achieved by the release of exosomal miRNAs, such as miR-9 and miR-21, into the microenvironment by the tumor that is taken up by the immune cells, mediating changes in the cytokine expression pattern, antigen-recognition and immune responses [53,54]. Along with these strategies of immune evasion, CSC also secretes VEGF, a growth factor that promotes angiogenesis during tumor progression and plays a pivotal role in suppressing the maturation of the T cells [55,56]. These chemokines, cytokines and growth factors secreted by the stem cells lead the system to an inflammatory state. This also mediates crosstalk between different groups of cells in the tumor microenvironment that are crucial for cancer initiation, progression and metastases formation [57,58]. These regulatory mechanisms that operate in the tumor microenvironment serve to suppress the anti-tumorigenic effect of the Cytotoxic T (Tc) cells and the Type I T-helper (T_{H1}) cells. This immune-suppressed tumor microenvironment acts as the 'soil' that nourishes and augments the growth of both the drug-sensitive as well as the drug-resistant sub-populations of the tumor, thereby posing a further challenge to the therapeutic strategies adopted to control cancer [59].

1.5.2.2. Role of Tumor Microenvironment in Immunoediting

Each of the components of the tumor microenvironment has a unique role to play in controlling the proliferation of the cancer cells at the different stages of tumor development. In the elimination phase of Tumor Immunoediting, the T_{H1} , $\gamma\delta$ -T cells and Natural Killer (NK) cells produce Interferon- γ (IFN- γ) and IL-12, the two principal cytokines that induce anti-proliferative, pro-apoptotic and angiostatic effects on the tumor. The macrophages activated by IFN- γ express tumoricidal products such as reactive oxygen and reactive nitrogen intermediates while NK cells activated either by IFN- γ kill tumor cells via TRAIL and perforin-dependent mechanisms. The cytolytic enzymes produced by the Cytotoxic T cells are also crucial mediators of anti-tumor immune response in the Elimination phase. The Tumor Associated Macrophages (TAMs) acts as the antigen-processing cells in the tumor microenvironment and manifest themselves as the M1-TAMs and the M2-TAMs [60]. While the former helps in the generation of the T_{H1} immune response, the M2-TAMs along with the T_{H2} and the Treg cells produce inflammatory cytokines such as IL-4 and IL-10 that primarily help in the sustained proliferation of the tumor by suppression of the immune effector cells [61]. This is a characteristic feature of the Escape phase where that tumor tries to program the immune cells to synthesize suppressive molecules and escape immune-surveillance. The transitions from the Elimination to Escape phase is intervened by the phase of Equilibrium where the host immune system and the tumor cell variants that have survived the elimination phase enter into a dynamic equilibrium. In this phase the tumoricidal effects of the immune cells on the tumor cells that is enough to control, but not fully extinguish these tumor clones which has reduced immunogenicity and are genetically unstable and highly mutating. This is the longest of the three phases of Cancer-Immunoediting that may last for as long as 20 years. A plausible explanation for this behavior has been attributed to the theory of Darwinian selection, where it may be said that although many of the original tumor cell variants are destroyed in the

elimination phase by the virtue of the immune cells, new variants of tumor cells arise carrying different mutations that provide them with increased resistance to immune attack. At the end of the equilibrium process, new populations of heterogeneous tumor cells arise that are resilient to any therapeutic interventions and have the potential to modulate the tumor microenvironment to ensure its own survival. The Escape phase brings in a fresh set of challenges for the immune system when the Cancer cells and the Cancer Stem Cells start proliferating rapidly and start synthesizing TGF- β and VEGF that serves to promote Angiogenesis. These molecules also induce the recruitment of Myeloid-Derived Suppressor Cells (MDSCs) that support tumor growth and metastases by the protection of tumor cells from immune-surveillance, remodelling of the tumor microenvironment, participating in the formation of a pre-metastatic niche and by facilitating the epithelial to mesenchymal transition (EMT) [62,63]. Additionally, the CSC express high levels of co-stimulatory molecule ligand (PD-L1) that inhibits the proliferation of the tumor infiltrated cytotoxic cells [64]. This helps the tumor to overpower the immunes system completely.

1.6. Need for Immunotherapy in the treatment for Leishmaniasis and Cancer

The collateral toxicity, adverse side-effects of chemotherapeutic interventions have led to the adoption of combinatorial treatment strategies for the treatment of chronic infectious diseases and cancer. This involves the use of immunotherapy along-with the chemotherapeutic drugs that can effectively overcome the immune suppression imposed by the infection or cancer and generate specific immune responses that can eliminate the disease. This is mostly achieved by immunopharmacology where small molecules and immunostimulatory drugs are administered to stimulate the production of specific cytokines by the immune cells [65]. However, in order to achieve this, the identification of important immunotherapeutic targets, signalling pathways and the study of immune-regulatory mechanisms are essential for the

design of optimal treatment strategies for diseases such as Leishmaniasis and Cancer that causes suppression of the immune effector functions.

For example, the general therapeutic strategy adopted for the treatment of Leishmaniasis is primarily aimed to expedite the process of parasite clearance for faster healing by stimulating the T_{H1} or healing response. In the case of Cutaneous Leishmaniasis therapeutics, chemotherapeutic drugs, such as pentavalent antimonials, liposomal amphotericin B has been shown to be useful to reduce the dermal lesions and the chances of further destructive mucosal inflammations and visceral infections [66,67]. However, the successive clinical studies have shown that these chemotherapeutic drugs are also associated with adverse side effects, such as nausea, intense headache, diarrhoea, musculoskeletal and abdominal pain etc. [67-71]. In several cases, relapse of the disease and developing resistant strains are also reported after the use of these drugs, which necessitates the development of better treatment protocols with higher clinical efficacy [72]. Although immunotherapeutic strategies involving the administration of exogenous IFN- γ is found to be effective in suppressing Leishmaniasis [73,74], the high production of IL10 during early stage of infection often suppresses its activity, thereby hindering NO production and disease clearance [75].

On the other hand, the low success rate of chemotherapy and radiotherapy in the treatment of tumor due to the presence of the slowly replicating Cancer Stem Cells calls for an urgent requirement of combinatorial therapies involving immune-stimulation. Literature evidences have shown the presence of few tumor associated antigens (TAA) that helps in the recognition of the tumor cells by the infiltrated T cells and the generation of effective immune responses upon Dendritic Cell (DC) vaccination which throws light on the possibility of control of the disease using immunotherapy [76]. Some studies have clearly indicated the role of Tc cells and IFN- γ in controlling Cancer progression [76]. Recent findings have suggested that

synergistic activation of Tc cells and $\gamma\delta$ -T cells are efficacious against HMLER-derived Breast Cancer stem-like cells, where $\gamma\delta$ -T cells act as an early source of IFN- γ in tumor immunity, under special *in vitro* conditions [77]. The development of Chimeric Antigen Receptor (CAR) T-cell has opened up new avenues for research in tumor immunity [78]. However, lack of truly CSC specific markers leads to on-target/off-tumor toxicity, where the CAR-T cells or any other CSC-targeted therapy kills the normal cells as well as those that display the same markers as that of CSCs [78,79].

1.7. Computational strategies employed for the study of immunoregulatory modules in Leishmaniasis and Cancer

The immune regulatory network forms a complex mesh of interacting cells and biochemical reactions that work in a coordinated fashion to eliminate the pathogen infected cells and trigger the remission of any neoplastic growth inside the body. A need to unveil these regulation mechanisms has driven experimental researchers as well as computational biologists to implement different omic studies and model the immunome under different antigenic stimulus to gain understanding from the differential gene expression as well as the pathway regulations perspectives.

Transcriptomic analysis, e.g., Microarray, RNAseq, have opened up new avenues of research that allows the analysis of gene expression profile of several patient cohorts under various disease conditions. Researchers have exploited these techniques to unearth the immunome landscape in the tumor microenvironment where the spatio-temporal dynamics of 28 different immune cell-types (immunome) have been studied using 105 human colorectal cancer patient data. Here the immunome was made up of mRNA transcripts specific for most innate and adaptive immune cell subpopulations. Using an integrative analysis, it has been elucidated that the densities of T follicular helper (Tfh) cells and innate cells increased, whereas most other T cell densities decreased along with tumor progression. However, the Tfh and

B cell numbers are inversely correlated with the disease progression and recurrence, and CXCL13 and IL21 genes are essential for the Tfh/B cell axis that is correlated with higher chances of survival of the patient [80,81].

RNAseq analyses in case of Leishmaniasis have been performed that has revealed *Leishmania* species specific differences in the expression of mammalian macrophage genes due to infection [82]. Such analyses have helped in the understanding of the changes in immune response generated during infection by unveiling the notable changes induced in the cytokine expression profiles during *Leishmania* invasion. Experiments using Microarray techniques have been used to assess the host cell genes and pathways in human dendritic cells associated with early *L. major* infection. The study revealed 728 genes were significantly differentially expressed in the infected cells and the molecular signalling pathway revealed that the type I IFN pathway was significantly enriched. Here it was elucidated that *L. major* induces expression of IRF2, IRF7, and IFIT5, which indicates that the regulation of type I IFN-associated signalling pathways is responsible for the production of IL-12. However, this is not observed in the case of *L. donovani* [83].

On the other hand, the understanding of the intra and inter cell signalling pathways involved in the generation of immune responses requires the study of a complex network of biochemical pathways under different diseases affected micro-environmental conditions. This is an extremely challenging task that can rarely be achieved using *in-vitro* or *in-vivo* experimental techniques. In order to gain insight into the immune-regulatory modules involved in T-cell functioning as well as study the immune-modulatory mechanisms employed by pathogen and the tumor cells, computational tools and mathematical modelling approaches have been extremely useful in obtaining a systems level understanding. Mathematical models have also been useful in delineating the multiplicity of the complex interactions governing the

dynamics of the tumor-immune or host-pathogen interactions that remains elusive through *in-vitro* experiments. These have also helped the researchers and medical practitioners in the identification of precise targets for immunopharmacology and immunostimulation, prediction immunotherapeutic strategies and design of combinatorial treatment protocols.

The development of the signalling pathway databases such as KEGG [84] and Reactome [85] provides the experimentalist important sources of information that contain collated pathway data from experimental studies regarding the intracellular signalling pathways in different immune cells [86,87]. Additionally, for the analysis of these biochemical pathways, the database such as BIOPYDB [88] also provide an integrated platform for performing network analysis, logical steady state analysis, knock-out analysis, etc.

For the analysis of large biochemical pathways Graph Theory and Boolean Logic based models have been extensively used for the study of cell signalling pathways and identification of drug targets for the treatment of Cancer and other diseases [89,90]. Logical models have been developed for the study of T-cell signalling pathways where the observations made from the *in-silico* analysis were experimentally validated to establish the authenticity of their logic-based model. Using this model, the authors have predicted an alternative pathway of activation from CD28 to JNK that does not involve the canonical pathway involving LAT signalosome, nor does it involve the activation of PLC γ 1 or Calcium flux, but depends on the activation of the nucleotide exchange factor Vav1 which activates MEKK1 *via* the small G-protein Rac1 [91]. Another model employing Boolean formalism has been used in the study of differentiation of naive cells into T_{H1}, T_{H2}, T_{H17} and Treg subtypes under different environmental conditions [92]. This model provides evidences that Foxp3⁺ Treg cells and T_{H17} cells are highly plastic and labile, whereas the T_{H1} and T_{H2} subtypes remain steady under different environmental

conditions. However, this model also predicts the existence of hybrid states and cyclic attractors expressing markers characteristic of two or more canonical cell types under certain environmental conditions that lay the foundation for oscillatory behaviour of T-cell differentiation. This study further elucidates that under proper polarising environments, the Treg cells may differentiate into T_{H1} or T_{H2} subtypes [92]. Later another model based on the Boolean formalism was developed to study the molecular mechanisms controlling the Cytokine-driven T_H cell differentiation and plasticity. This model explained the role of peroxisome proliferator-activated receptor gamma ($PPAR\gamma$) in the regulation of T_{H17} to iTreg cells switching that gives promising cues for the prediction of therapeutic target for deregulated immune responses and inflammation [93].

Ordinary Differential Equations (ODE) based models have also been helpful to unravel some of the intriguing problems in immunology. Several dynamic models have been developed for the study of immune responses for several diseases [94-98]. The study of Tumor Immune interaction using mathematical ODE based models has helped clinicians in the prediction of tumor evolution and the determination of dosage schedules and treatment protocols [99-101]. A seminal work by Kirschner and Panetta has led to the development of many such similar models with further improvisations [102]. The model developed by them represents an ODE based model of the Tumor-Immune interaction and the production of IL-2 that has important roles in the regulation of tumor-immune response. The model considers that the proliferation of the effector immune cells increases proportional to the antigenicity of the tumor. In this model, the antigenicity of the tumor has been considered as an essential parameter that regulates the dynamics of the effector cell population. This model explains short-term oscillations in tumor sizes as well as long-term tumor relapse. This model has been further used to explore the effects of adoptive cellular immunotherapy for tumor elimination [102]. A more recent tumor-immune

interaction model developed for understanding the dynamics of immune-mediated tumor rejection focus mainly on the role of natural killer (NK) and CD8⁺ T cells in tumor surveillance. Here the techniques of parameter estimation and sensitivity analysis have been exploited for the model calibration and validation with experimental results. This study has revealed the variable to which the model is most sensitive is patient specific and that there exists a direct positive correlation between the patient-specific efficacy of the CD8⁺ T cell response and the likelihood of a patient favourably responding to immunotherapy treatments [103].

Dynamic ODE based model has also been developed to study CD14, EGF, TNF and PI3K mediated signalling pathways and their cross-talks in *Leishmania* infected macrophage, which shows modulation of host signalling pathways that lead to immune-suppression. This model analyses revealed that EGF and TNF pathways can be considered as potent pharmacological targets to curb Leishmaniasis [104].

1.8. Existing challenges in target identification for Immunostimulation and Immunopharmacology

A comprehensive understanding of the complex regulations underlying the immune responses under different environmental conditions, antigenic challenges, the strength of stimulus has challenged the implementation of successful immunotherapy. The intricacies of the immune signalling network are far from being completely understood and the regulations governing the differential immune response of the T-cells under the varied antigenic challenges still remains elusive to immunologists. In this context, the knowledge regarding the signalling routes and their cross-talks is essential to gain a holistic understanding and identify the immunostimulatory targets precisely and understand the mechanistic regulations such as the feedback and feed-forward loops and the alternative signalling pathways that govern the production of effector molecules from the lymphocytes. Hence, an

in-depth study of the different co-receptor mediated signalling pathways and their cross-talks is essential through in-depth curation of the pathway specific data and development of detailed mathematical models that will provide valuable information regarding the pathways involved in the cytokine regulation and effector functions of the immune cells under various micro-environmental conditions.

T-cell plasticity that determines their differentiation, de-differentiation and sub-type specification under different diseased conditions is yet another area that has remained very less explored. Such studies are required to elucidate the modulations of T-cell ratios that have a substantial impact on the disease prognosis and response of a patient to an immunotherapeutic intervention. The study of T-cell plasticity under *Leishmania* infected conditions to elucidate the T_{H1}/T_{H2} switching mechanism is essential for the determination of the clinical outcome of chronic infections both in the cases of Cutaneous and Visceral Leishmaniasis. Again, the causes for the changes in the immune responses in the chronic versus the acute infection is a study of great importance that will help us gain knowledge of how to regulate the immune response generated during infection so as to trigger the healing immune responses to curb the disease. In the case of Visceral Leishmaniasis, the study of host pathogen interaction is required to predict and identify the host pathways that are triggered by the pathogenic secretome.

In the case of Cancer, the study of tumor immunity has become a field of utmost importance. Here we observe that in the tumor microenvironment, the multiple immune-regulatory effects of the effector cells on the tumor is counter balanced by an even larger number of negative regulation imposed on the immune cells by the tumor that make cancer remission difficult and highly refractory to therapeutic interventions. The role of the pleiotropic cytokines, such as IL-1, IL-6, IL-10, IL-21 and TNF, in Cancer has been poorly elucidated and many contradictory reports have

been found describing their effect in Cancer progression. The unveiling of the paradoxical roles of these pleiotropic cytokines and the Tumor Associated Macrophages promises their potential application in Oncology. Also, the studies related to cancer stem cell differentiation and their effect on the development of drug resistance is an area that remains to be further explored that will open up avenues in the design of treatment protocols for combating tumor heterogeneity and cancer relapse.

1.9. Scope and Specific Objectives of the Thesis

Identification of important immunotherapeutic targets and regulatory mechanisms is essential for the design of optimal treatment strategies for diseases such as Leishmaniasis and Cancer that causes suppression of the immune effector functions. The study of T-cell plasticity under *Leishmania* infected conditions is essential to elucidate the T_{H1}/T_{H2} switching mechanism for promoting a healing response that determines the clinical outcome of chronic Cutaneous Leishmaniasis [105,106]. The study of Visceral Leishmaniasis however requires a detailed study and prediction of the host pathogen interactome to identify the intracellular signalling routes that lead to visceralization in Leishmaniasis. On the other hand, lack of a comprehensive study of the interactions of the tumor microenvironment with the heterogeneous sub-population of tumor cells that arise from the differentiation of Cancer Stem Cells (CSC) has limited our understanding of the development of drug resistance and treatment failures in Cancer [45,107,108]. Hence a study of the deregulations of the intercellular and intracellular signalling pathways leading to the suppression of the immune system and further progression of the infectious diseases and cancer is essential for eliciting immune effector functions, which is a prerequisite to preventing relapse and a designing successful treatment strategy for these diseases. The understanding of intra and inter cell signalling pathways involved in the generation of immune responses requires the study of a complex network of

biochemical pathways under different diseases affected micro-environmental conditions. In view of the challenges in relation to infectious diseases and Cancer, the objectives of the thesis have been defined as follows:

- Identification of regulatory modules of the Immunological Network to stimulate T cell effector functions against various diseases
- Understanding the role of T_H cell Plasticity/ differentiation for the control disease progression
- Designing treatment strategies to enhance immune clearance and disease prognosis

In order to address the objectives of the thesis, detailed studies of intracellular and intercellular signalling pathways of immune cells have been performed through manual curation of the signalling pathway information available in various literature and pathway databases as well as predicting PPI for host pathogen interactions and then modelling the PPI networks using various mathematical and computational approaches to identify the key regulators of immune response in case of Leishmaniasis and Cancer.

1.10. Outline of the Thesis

In **Chapter 2**, the materials and methods used in the thesis have been discussed in details. This chapter contains the information regarding the different biochemical pathway databases and other sources that have been used to curate the information regarding the immune signalling pathways and develop the mathematical models. The software, tools, packages and computational platforms that have been used for the model simulations and parameter estimation have also been discussed here.

Chapter 3 focuses on the study of co-receptor and calcium signalling crosstalks that regulate the activation and effector functions and cytokine production of T_H-cell

using a comprehensive pathway map of T-cell activation network has been reconstructed manually and analyzed using Logical Steady State Analysis (LSSA).

In **Chapter 4**, the role of T_H cell Plasticity/differentiation for the control disease progression has been studied with respect to the infectious disease Leishmaniasis. Using a reconstructed signalling network of the intracellular and intercellular reactions between a *Leishmania* infected APC and T-cell, a LSSA based model has been proposed to predict the inhibitory effect of the *Leishmania* infected APC on the T-cell and to identify the regulators of the T_{H1}/T_{H2} -switching behaviour and immunotherapeutic targets for triggering anti-*Leishmania* immunity.

In **Chapter 5**, the host-pathogen interactome between *L. donovani* secretome derived virulence factors and the Human host proteins are predicted using Interolog and Domain mapping strategies. Pathway enrichment and graph-theory based analysis is used to model the PPI network to identify the hub proteins and signalling routes targeted by the parasite during Visceral Leishmaniasis.

In **Chapter 6**, an ODE based tumor-interaction model has been developed to study the regulations governing the stem cell differentiation and tumor development along with the influence of the tumor micro-environment. Here the model has then been used for testing known treatment protocols to explore the reasons for failure of conventional treatment strategies and propose an improvised protocol combining Chemo, Radio and Immunotherapy that shows promising results in suppressing the proliferation of all the cellular sub-populations of the tumor and restoring a healthy T_{H1}/T_{H2} ratio that assures better Cancer remission even with the presence of resistant Cancer cells.

In **Chapter 7**, the conclusions and future directions of the thesis have been discussed.

CHAPTER 2

MATERIALS AND METHODS

2.1. Collation of Signalling Pathway information

Reconstruction of the intra-cellular and inter-cellular signalling pathways is a prerequisite for gaining a holistic understanding of the regulatory networks. This has been accomplished through manual curation of protein protein interaction (PPI) data from the available literature as well as the information available in the pathway and PPI databases. To ensure the validity of the reconstructed network, only the interaction having some experimental evidences of physical interaction were considered in the development of the model.

The signalling pathway databases are important sources of information that collate pathway information from experimental studies regarding the intracellular signalling pathways in different immune cells. The KEGG database provides information regarding the core TCR-mediated pathway along with a few co-receptor signalling pathways [84]. The database also contains the pathways responsible for the T_{H1} , T_{H2} and T_{H17} differentiation. Another popular database called Reactome provides detailed the biochemical reactions involved in each step of the protein-protein interactions involved in the T-cell signalling pathway [85]. It also enlists the pathway information related to CD28 and PD-1 co-receptor mediated signalling pathways. Simultaneously, Reactome forms a very important source for Cytokine signalling pathways that include different Interleukin families, Interferons, Tumor Necrosis Factor and few Growth Hormones. However, the information regarding the intercellular cross-talks in the immune system is lacking in most of these databases that can be extracted through a thorough Literature survey.

Few databases also provide data regarding the changes in the pathway during disease condition. The KEGG database has a sufficient amount of pathway information regarding the endocytosis of the *Leishmania* pathogen as well as the signalling events that occurs inside the infected macrophage. BioLegend database contains the Cancer Immune-editing network that consists of the inter-cellular signalling cross-talks governing the immune responses generated during Cancer.

2.1.1. Reconstruction of T-cell Pathways and Cross talks

In **Chapter 3**, in order to capture all the regulations that operate to control the proliferation and activation of a T-cell, getting a comprehensive picture of the entire signalling cascade involved in the process was an essential prerequisite. Since a complete map of the pathway was lacking from any single source, the pathway had to be reconstructed by manually collating human cell specific data from about 21 popular signalling pathway databases, such as KEGG, Protein Lounge, Pathway Central, Biocarta, NetPath, etc. [84,109,110]; protein-protein interaction databases, such as, HPRD, BioGRID^{3,2}, etc. [111,112] along with more than 200 literatures published in peer reviewed journals (searched using PUBMED and Google Scholar). The protein-protein interaction data obtained were knitted together to reconstruct the entire signalling cascade (**Figure 7**). The diagram of the reconstructed pathway was drawn using CellDesigner version 4.3 [113], a freely available software package that allows to easily create gene-regulatory and biochemical network images using a graphical user interface. The overall reaction process of this pathway starts at the immunological synapse, the signal is then transduced via the T-cell membrane proteins, comprising of the receptors and co-receptors, down to the cytoplasmic proteins, which ultimately leads to the activation of certain transcription factors. These activated transcription factors then translocate into the nucleus and induce the expression of important output proteins, and cytokines (effector molecules) that are

crucial in maintaining the T-cell proliferation as well as in mediating the clearance of the antigen that has entered our body.

2.1.2. Reconstruction of *Leishmania* infected APC Pathways

In **Chapter 4**, gene correlation networks of the significantly expressed genes, observed in two independent microarray experiments for APC (E-GEOD: 42088) and T-cell (E-GEOD: 48978), were constructed. The signalling pathways from these networks were then enriched to identify the pathways significantly influenced by the invasion of *Leishmania* pathogen in APC. However, the pathways found to be enriched in this analysis do not provide a complete understanding of the molecular mechanisms through which the *Leishmania* pathogens infect the APCs. It is also unable to describe the signalling cross talks of the secreted proteins/cytokines from both APC and T-cell, and its subsequent effects on the regulation of each other's activities in both uninfected and infected scenarios, respectively. Hence, in addition to the enriched pathways, manual reconstructions of the complete inter- and intra-cellular signalling cascades, regulating the APC and T-cell functions has been performed.

2.1.2.1. Construction of gene correlation network

The time course microarray expression data of *Leishmania major* infected human dendritic cell (APC) was obtained from the EBI-ArrayExpress (ID: E-GEOD-42088) database [114]. Here the authors have predicted total of 849 genes, which are significantly expressed after the invasion of *Leishmania* pathogen in human APC. In this analysis, the time course expressions (at 0, 2, 4, 8 and 24 hours) of these 849 probes or genes were extracted and used for the construction of gene co-expression network. In order to do that, at first, the Pearson's correlation coefficients of each pair of genes across the time course microarray data samples were calculated by using the in-built function *corr* available in MATLAB R2012. This function also calculates the corresponding *P*-values of the correlation coefficient for each pair of

genes in the data set and stores them in the form of a symmetric square matrix. The P -value matrix was then used to construct an adjacency matrix (A) in which the matrix elements (A_{ij}) are either 1 (if P -value < 0.01) or 0 (otherwise). The matrix element $A_{ij} = 1$ signifies that the gene ' i ' is significantly co-expressed with the gene ' j ' and there is a connection or undirected arc present between these two genes. In this analysis, total of 139,382 arcs are present among 849 significantly expressed genes (or nodes). The possible clusters of genes, formed by at least 3 nodes in the network, are then identified from this huge network using the open source network analysis software: Cytoscape's (version 2.8) GPU enabled App AllegroMCODE (version 2.1) [115]. There are a total of 10 clusters or functional modules identified through this App. The network diagrams of the clusters generated from this analysis are shown in **Appendix B: Figure B.1**. The names of the nodes in all the cluster diagrams are assigned in the figure according to the probe IDs used in HG-U133_Plus_2 Affymetrix GeneChip for human cell. The genes from each identified functional module are then used for the further pathway enrichment analysis in bioCompendium (<http://biocompendium.embl.de/>) web servers. The names of the enriched pathways found for each of the clusters in bioCompendium pathway enrichment web servers are enlisted in **Appendix B: Table B.1**.

Similar analysis was also performed for activated, time course T-cell microarray expression datasets generated by Zhao et al., and the datasets are available in GEO (ID: GSE48978) and EBI-ArrayExpress (E-GEOD-48978) [116]. Their analysis has revealed that in the stimulated state, total of 2274 genes get significantly expressed in active T-cells. The co-expression network generated by these significant genes has 551,031 arcs. There is a total of 24 clusters identified from this huge gene co-expression network, which are depicted in **Appendix B: Figure B.2**. In the figure, the node names used in each cluster are in accordance with the probe IDs used in Affymetrix HT_HG-U133_Plus_PM array plate. The pathway enrichment analysis of

each cluster are performed in GeneCodis [117] and the enriched pathways found through this web server are enlisted in **Appendix B: Table B.2**. Only the genes/probes from first the 10 enlisted clusters gave significantly enriched pathways.

2.1.2.2. Integrating Intra-cellular and Inter-cellular Signalling Crosstalk of T-cell and Macrophage during Leishmaniasis

In order to capture the functional regulations that operate between these significantly enriched pathways within the two cells, i.e., APC and T-cell, reconstruction of a comprehensive map of signalling processes depicting the effect of *Leishmania* infection on immune response was necessary. Hence, in **Chapter 4**, a detailed T-cell and APC interaction pathway diagram was created after a thorough study of existing literatures and databases. Protein-protein interaction (PPI) and the biochemical signal transduction data were collated from various cell signalling and PPI database, and various published research articles [84,109-111]. The *Leishmania* proteins were then introduced in the network and the interactions of these proteins were established with the existing APC molecules depending on the biological evidences [118-120]. The *Leishmania* antigenic molecules used in the model, viz. LPG_L, GP63_L, LFAA_L and EF1_ALPHA_L, are known to be present in almost all the *Leishmania* species so as to create a generalized *Leishmania* infection model (LFAA_L is a hypothetical molecule which we considered in our model to show the activation of ASMASE for the production of CERAMIDE [121]; it is abbreviated for *Leishmania* factor activating ASMASE). With certain modifications (required to build the juxtacrine and paracrine interactions between the cells) the T-cell pathway (**Section 2.1.1 and Chapter 3**) was used to understand the T-cell-APC cross-talks and to monitor the immunological response generated during *Leishmania* infection [122]. A detailed description of the reconstructed pathway network has been provided.

binding Fc region of the immunoglobulin molecule) on APCs [126] which has been shown to stimulate IL10 production by directly activating ERK1/2 [119] has also been considered. During Leishmaniasis, sphingomyelinase ASMASE gets activated in the extracellular region, which produces CERAMIDE on the surface of APC [121], have also been incorporated here in our model by assuming the presence of a factor LFAA_L (abbreviated for *Leishmania* factor activating ASMASE), produced by the pathogen, that activates ASMASE for the production of CERAMIDE. CERAMIDE once produced, activates PP1 and PP2A both of which are responsible for the inhibition of PKC and de-phosphorylation of AKT in APC cytoplasm [119].

A transition line has been shown in the model indicating the entry of the flagellate motile *Leishmania* promastigote form of the pathogen inside the APC, where it differentiates into a non-motile aflagellate amastigote form. Inside the cell, the LPG molecule has been shown to interfere with the APC signalling cascade and negatively influence the PKC pathway [127]. The LPG molecule that forms a complex with MHC_CLASS_II in the APC is presented to the T cell to cause its activation. The inhibitory effects of GP63_L have also been established in our pathways by showing its inhibitory effects on AP1, NFkB, MARCKS, MRP, c_FOS and mTOR proteins in APC cytoplasm [128-131]. GP63_L also activates the phosphatases SHP1, TCPTP and PTP1B as they help in de-phosphorylation of various signalling proteins of APC during *Leishmania* invasion [132]. Another *Leishmania* protein that has been included in our model is Elongation factor 1 alpha EF1_ALPHA_L which is also known to activate SHP1 [120]. These tyrosine phosphatases (viz. SHP1, TCPTP and PTP1B) de-phosphorylates and mediates deactivation of important downstream transcription factors such as ERK1/2, P38 and JNK [118,133,134] and STAT1_ALPHA [135-137].

b) APC-T-cell interaction

In order to establish the effect of *Leishmania* infection on the outcome of the T-cell protein expression pattern and the immune responses elicited during the infection, the ligands and the output molecules expressed by the APC have been connected to the T-cells molecules. The APCs have been shown to be presenting the *Leishmania* antigen epitope in a processed form denoted as MHC_Class_II:LPG [138]. As shown in our model, the TCR: CD3 and MHC_Class_II:LPG interaction triggers the T-cell signal transduction pathways that lead to the activation of the Src family kinases LCK and FYN, and formation of the LAT signalosome [23,139,140]. After this point, the signal cascade branches out into a network of diverse signalling routes, which includes the MAPK pathway, the calcium-mediated NFAT pathway, and the NFKB pathway [141]. Upon a pathogenic invasion, the APC expresses a multitude of co-signalling molecules such as B7 and TNF-like molecules that bind with their corresponding co-receptors on the T-cell membrane to amplify the signal coming from the infected cell and thus causes a sustained T-cell proliferation [142]. Here it can be seen that while the B7 molecules (CD80 and CD86) binds to the CD28 co-receptor to activate the SOS:GRB2 mediated MAPK and the PI3K pathways, the TNF-like molecules (TNFRSF9, ICOSL, OX40L, LIGHT) propagates the signal to the interior of the cell principally through the TRAF pathway [142,143]. Apart from these juxtacrine signalling at the immunological synapse, we have also considered the CRAC channel that senses the microenvironment of the T-cell for the presence of Ca²⁺ ions and activates the Calcium Pathway. The diffusible cytokines (viz. IL1, IL2, IL10, IL12, TNF- α and IFN- β) that are produced by the APCs as a result of the pathogen load, and also by the T-cell itself has been shown to further regulate the T-cell proliferation in a paracrine and autocrine fashion respectively [144-147].

The pathway also reveals that T-cell and APC interaction has an influence on the expression of both the cells. The T-cell regulates the APC through the CD40 pathway

which activates MKP1 and MKP3 that further dephosphorylate MAPK proteins P38 and ERK1/2 respectively [148]. On the other hand, CD40 can also bind with TRAF proteins (TRAF2, TRAF3, TRAF5 and TRAF6) for the activation of MAPK proteins P38 and ERK1/2 [119,149]. Activated T-cell produces effector molecules such as IL10, IL4, IL6, IFN- γ and TNF- α , that in-turn controls the signal propagation through the JAK-STAT and TRADD-TRAF pathways of the APC cell [24,27,150].

c) Output proteins

The flow of signal from the infected extracellular environment into the cytoplasm and down to the nucleus of these immune cells leads to the activation of specific transcription factors which are responsible for the production of certain effector molecules. These effector molecules that have been included in our model comprises mostly of secreted proteins belonging to the cytokine family, which consists of different interleukins (IL10, IL12, IL1_ALPHA, IL1_BETA, etc.), interferons (IFN_GAMMA, IFN_BETA) and tumour-necrosis factors (TNF_ALPHA) having diverse functions. The other effector molecules produced by the immune cells consists of the growth factors (TGF_BETA), and microbicidal molecules (NO).

2.2. Logical Steady State Analysis of Signalling Pathways

Logical modelling is gradually being recognized as a simple yet powerful tool in Systems Biology for the study of large and complex reaction networks. Here the information flow from one node to another in a network is determined by a combination of input and their relation is specified using logic gates - AND, OR, NOT. It was first explained by Kauffman where he modeled the gene as a binary device that can be either in the 'ON' or 'OFF' stage [151]. Here he elucidated that a distinct advantage in this choice of a binary model for gene activity lies in the fact that the number of different possible rules by which a finite number (K) of inputs may affect the output behavior of a binary element is finite, i.e., 2^{2K} . This concept was

later used by Huang and Ingber [152] to model cell signalling networks for demonstrating that cellular phenotypes correspond to the dynamic steady states of the intra-cellular signalling molecules in a logic-based model. A key advantage of this strategy is that it does not require the knowledge of parameter values which is often not available for large biochemical networks.

Figure 4 shows a simple toy model of three nodes interacting with each other. The reaction network can be represented using Boolean rules or equations (**Eq 1**, **Eq. 2** and **Eq. 3**). The truth tables and the state transitions graphs of the reaction network show the temporal evolution of the states (0 or 1) of the nodes starting from different input combinations (**Figure 4**). Here, in this example we observe under the different input conditions the system tends to reach certain point steady state attractors, i.e., 0-0 and 1-1-1 or cyclic attractor, i.e. 1-0-1 \leftrightarrow 1-1-0.

- ▶ $v_1 = v_1 \text{ OR NOT } v_3$ Eq. 1
- ▶ $v_2 = v_1 \text{ AND } v_3$ Eq. 2
- ▶ $v_3 = v_2$ Eq. 3

Several software packages such as BoolNet (R-based), BooleanNet (Python based), CellNetAnalyzer (software with GUI) are available for performing Logical Steady State Analysis of large biochemical networks [153-155].

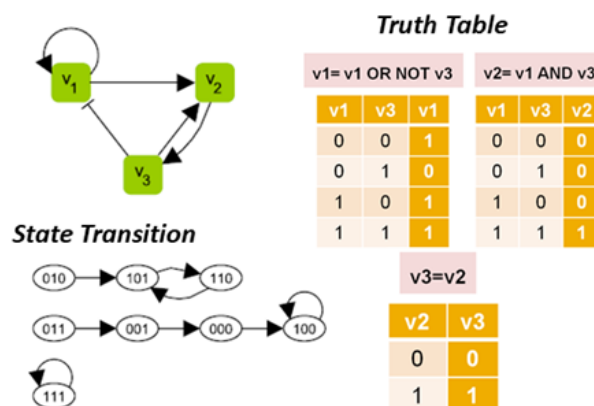


Figure 4: Toy Model for LSSA: Interaction Graph, Truth Table and State Transition Graph for a Logic Based Toy Model (Figure adapted from [156])

2.2.1. Model Formulation and Transition Functions

The dynamic analysis of such a large network requires precise kinetic data, which is rarely available and thus we had to restrict ourselves to a semi-dynamic approach of modelling this signalling pathway, i.e., “Logical Analysis”, where an up-regulation in the protein expression is considered as ‘1’ or ‘ON’, while a down-regulation of a protein expression is considered as ‘0’ or ‘OFF’ (binary states). In **Chapter 3** and **Chapter 4**, the logical equations of the target molecules have been written using different combinations of molecules (‘source’) along with ‘AND’, ‘OR’ and/or ‘NOT’ (logical gates) relations depending on how these molecules influence the expression of each other in a biologically relevant way. The molecules in the model associated with ‘AND’ operation signifies the cumulative or multiplicative effects of a combination of proteins on their downstream targets, whereas the presence of ‘OR’ operation signifies the alternative routes of signal propagation. The molecules kept in ‘NOT’ relation are principally the inhibitors of the target molecule. Different biochemical reaction mechanisms (such as phosphorylation, transcriptional activation, ubiquitylation, nuclear transport, inhibition, and different feedbacks reactions etc.) are considered in the model and transformed in terms of Boolean or logical equations.

From the reconstructed T-cell pathway that consists of 206 molecules (nodes) a complex mesh-like network formed of 435 protein-protein interactions (**Chapter 3**), the Boolean model developed consists of 167 logical equations (hyper-arcs), which control the expression pattern of the dependent variables, otherwise called the ‘target molecules’ (nodes) (**Appendix A: Table A. 1**). The remaining 39 independent ‘Input’ molecules (which did not have any transition functions governing update rules) were considered as the inputs to the system, which includes 13 ligand molecules (e.g. MHC CLASS II-Ag complex, LIGHT, B7_1, B7_2, CD70, etc.) that come into play in the extracellular environment (APC surface in case of T-cell), 2

non-protein molecules and remaining are core T-cell protein molecules. Another 39 molecules (e.g., BCL2, FKHR, P21, BCLX, IL1, IL2, etc.) were considered as the ‘Output’ of the system, many of which have a feedback that has a positive or negative impact on cell proliferation. The equations were written using Python code and simulated using the BooleanNet-1.2.4 software [157] (**Appendix A: Table A. 1**).

In **Chapter 4**, the integrated signalling network of T cell and APC, consisting of a total of 293 nodes, which includes 82 APC molecules, 206 T-cell molecules, and 5 *Leishmania* related molecules are involved in more than 400 protein-protein interactions. The interactions of the entire network, including all important regulations between T-cell and APC, were translated into Logical equations (signifying reactions or hyperacrs) using the logical gates, in a biologically meaningful way (**Appendix B: Table B. 4**). In order to capture the regulations at the post-transcriptional level, the alternatively spliced isoforms of the T-cell and APC output molecules with known functions have been also included in our model (**Appendix B: Table B. 3**). Here the selection of isoforms is based on the presence of certain cis-regulatory elements and trans-acting factors that has been collectively referred to as ‘FACTOR_i’ where [i=1, 2, ..., 23]. These 23 FACTOR_i represent specific Spliceosomes responsible for the splice site recognition in each case. The model was simulated synchronously and asynchronously until the steady state is reached [157].

2.2.2. Phenotypic Response Functions

The Logical Equations for nodes representing the Phenotypic Response functions were written using the appropriate ‘Output’ molecules (related to that particular phenotype) of the model, depending on the biological functions of the molecules and the phenotype they are associated with, respectively.

In **Chapter 3**, in order to study the effect of the co-stimulatory signals on the T-cell phenotypic response, three additional equations were formulated in the model

signifying, (a) Cell Proliferation ("Proliferating T-Cell") for the actively proliferating effector T-cells that are capable of effector functions and immune clearance; (b) Cell Survival ("Inactive T-Cell") for the inactive/naïve T-cells that do not perform any effector functions; and (c) Cell Death ("Dead T-Cell") for the T-cells that have undergone apoptosis and are eliminated from the system. The equations have been described subsequently.

a) Cell Proliferation: After encountering an Antigen Presenting Cell (APC), T cell proliferation increases. This process is regulated by different Cyclins (CYCLIN_A, CYCLIN_D1 and CYCLIN_D2) and Cyclin Dependent Kinase (CDK4) that mediate cell division [158,159], the anti-apoptotic molecule (BCLX) that prevents cell death [160], interleukins, such as, IL2, IL4 and IL6 [161-163] and TNF-like molecules (FASL) that enhances the proliferation of the immune cells [164]. The logical equation governing the fraction of cells in the proliferative state after receiving the stimulus from an APC is as follows:

$$\blacktriangleright \text{Proliferating T - Cell} = (\text{IL2 AND CYCLIN}_A \text{ AND CYCLIN}_{D1} \text{ AND CYCLIN}_{D2} \text{ AND BCLX AND CDK}_4 \text{ AND IL4 AND FASL AND IL6}) \quad \dots \text{Eq. 4}$$

b) Cell Survival: When a T cell has not encountered an APC and has not received any stimuli, it remains in its *naïve* resting state and do not proliferate, although its normal cell survival and cell division may still continue to occur. This resting state of T cell is maintained mainly by the anti-apoptotic factors (BCL2 and BCLX) that keep the T cell alive, while the normal cell homeostasis is maintained by the TNF molecules (e.g. TNF_ALPHA) [165] and cell cycle proteins-the Cyclins (CYCLIN_A, CYCLIN_D1 and CYCLIN_D2) and CDKs (CDK4) [159]. The logical equation for this phenotype of T cell is written as follows:

▶ ***Inactive T – Cell =***
(CYCLIN_A AND CYCLIN_{D1} AND CYCLIN_{D2} AND BCL2 AND BCLX AND CDK₄
AND TNF_ALPHA) Eq. 5

c) **Cell Death:** When the proteins promoting T cell proliferation and survival are absent, and an immunosuppressive condition is produced by the presence of certain molecules like IL10 [166], the chances of T cell proliferation and survival decreases and that of cell death increases. Such a situation has been termed as 'T cell death' or 'Dead T-Cell' in our model. Hence, following the logical relationship the equation for such a phenotype is written as:

▶ ***Dead T – Cell =***
(IL10 AND NOT Inactive T – Cell AND NOT Proliferating T – Cell)
.....Eq. 6

Similarly, in **Chapter 4**, three phenotypic responses equations have been formulated, viz., "TH_1_response", "TH_2_response" and "NO_response", which reflect the type of T-cell responses elicited and production of NO from the APC in response to an infection (**Eq. 7, Eq. 8 and Eq. 9**). The molecules used for defining these functions are principally the molecules involved in eliciting these responses, as reported in literatures [167].

▶ **TH_1_response =**
IL2_T AND GM-CSF_T AND TNF_ALPHA_T AND IFN_GAMMA_TEq. 7

▶ **TH_2_response = IL4_T AND IL5_T AND IL6_T AND IL10_T**Eq. 8

▶ **NO_response = NO**Eq. 9

2.2.3. Update of Logical Rules - Synchronous and Asynchronous Simulation

In **Chapter 3** and **Chapter 4**, the Boolean transition equations were updated at each step, first 'Synchronously' (for the purpose of validation), and later 'Asynchronously' (for further analysis). In Boolean models, a major assumption is

that irrespective of the nature of the reaction, all equations of the system take an equivalent amount of time for state transition. In the synchronous model, the assumption is that all molecules are updated at each step and at the same time, i.e. from t to $(t+1)$. Consequently, each state of the model at time t can transition to only one possible successor at $(t+1)$ [168]. However, in a signalling network, the protein expression levels are likely to change at different points of time and updates randomly [157]. Hence to capture such scenario, in the asynchronous model it is assumed that the update/execution of the Boolean transition functions occurs randomly at each step. In other words, as opposed to synchronous simulation where the updates of the transition functions are performed in a listed order, and the state change of the nodes are observed only at the end of the update round, in asynchronous simulation the updates of the functions are performed in random order where the states of the nodes immediately reflect the changes. This makes the asynchronous model stochastic [157]. The asynchronous model is simulated as multiple replicate simulations and the percentage of simulations that have Closure = 1 is recorded and plotted. This leads to observation of transition states of nodes as fractional values between 0 and 1. This analysis also helps us to monitor the small fluctuations in the expression pattern of the pathway species over time, which occurs due to the stochasticity in the execution of the pathway reactions inside the cell. The asynchronous simulation also ensures that the errors in the synchronous simulations, as well as attractor analysis (through selection of independent random samples) are minimized, and further presents an average behavior of the entire system over time.

2.2.4. Omics Data for Model Validation

In order to validate the model, protein expression data for the output molecules, i.e., whether the protein is up-regulated or down-regulated, were curated from various literature sources to qualitatively determine the model accuracy at steady state.

However, since the data to study the temporal variation of the protein expression were not easily available, transcriptomic data, such as Microarray expression data, that are routinely used for the study of differential gene expression and signalling pathways deregulations under various disease scenarios were used for our studies [169].

Hence in **Chapter 3**, microarray data were obtained from EBI-ARRAYEXPRESS microarray database [ArrayExpress ID: E-GEOD-48978] [170]. The differential gene expression data obtained from the database was a time-course microarray data of gene expression kinetics of human T helper cells at six time points (i.e., at 0, 2, 4, 6, 24 and 72 hours respectively) over a time period of 3 days. Array used in the experiment was an Affymetrix HT HG-U133+ PM Array Plate [116]. However, it was observed that the gene expression values of the microarray data decline after the 6 hour time-point. Since the constructed model is of T cell activation, and we are interested in the study of interleukin expression (which is highest at 6 hour time point [171]), we have not considered the expression data of 24 and 72 hour time-points, and only the values of 0, 2,4 and 6 hours values were used for further analysis.

In **Chapter 4**, in order to validate the T-cell-APC model with experimental data, time-course microarray expression data for the two cells (viz. T-cell and APC) were obtained from two separate experiments from the EBI ARRAYEXPRESS database (E-GEOD: 48978 and 42088, for T-cell and APC respectively) [170]. In these microarray experiments, expression profile of activated human T- helper cell (Affymetrix HT HG-U133+ PM Array Plate) and *Leishmania major* infected dendritic cells (Affymetrix HG-U133 Plus 2.0 Gene Chip) were studied at discrete time-points [114,116]. However, it should be noted that the experimental data for the expression of NO (Nitric Oxide) molecule is considered as proportionate to the expression values of INOS of the microarray data. In our analysis, we only considered the expression

values at 4 time-points, i.e., 0, 2, 4, and 6 hours (time-points) for T-cell and 0, 2, 4, 8 hours (time-points) for dendritic cells.

2.2.5. Binarization of Expression Data

The temporal expression data were binarized to 0 and 1 signifying down-regulation and up-regulation of expression of the nodes respectively. Here the binarization was performed using the K-means clustering method. The K-means clustering is used to partition a given set of input data in K -th partitions or cluster; in this case $K=2$, i.e. 0 and 1. In our analysis, we used this technique to binarize the time course microarray expression data [116] and then used the binarized data as input for the Boolean model. In order to perform the K-means clustering on the time series microarray expression data, we have used the binarization function in the BoolNet1.63 in R [172].

In **Chapter 3**, the expression data at time points 0, 2, 4, and 6 hours of the RNA transcripts corresponding to the proteins in our model was extracted. The expression values of the molecules considered for binarization were the mean of the expression values of the RNA transcripts of different isoforms/or subunits of the corresponding protein molecules. The mean value of the individual molecules at each of the four time points was chosen and then binarized [172]. In **Chapter 4**, the microarray expression data for the APC was also binarized using a similar technique.

2.2.6. Model Initialization

In **Chapter 3**, the binarized data at 0-hour time point was used to initialize the system (i.e., value of the simulation at time step 0). The initial value of the 7 APC molecules (viz. MHC CLASS II-Ag, B7-1, B7-2, CD70, LIGHT, PDL and TNFSF9) and 3 non-protein molecules (CRE, CALCIUM-OUT and DAG) were considered 'ON' to activate/provide a stimulus to the T-cell signalling cascade (**Appendix A : Table A. 2**).

Similarly, in **Chapter 4**, the T-cell-APC model was initialized using the binarized value at the 0th with either ON or OFF depending on whether the protein shows an up-regulation or a down-regulation at the 0th hour (**Appendix B: Table B. 5**). The initial values of the *Leishmania* proteins were considered ON in the infected scenario, and OFF in the uninfected scenario.

2.2.7. Attractor Analysis

The Boolean attractors of the T-cell-APC model in **Chapter 4** were determined by generating all possible combinations (ON or OFF) of the 51 input molecules of the system. The simulation was repeated for 20 samples, where 7 proteins have been selected from a uniform random distribution of 51 input molecules, thereby generating $2^7 \times 20$ (= 2560) combinations of input molecules. However, due to lack of Human cell specific *Leishmania major* infected RNAseq data of APC, the logical states (activation or inactivation) of the FACTORi determining alternative splicing of the output molecules could not be explicitly determined in *Leishmania* infected scenario. Hence, in our model these FACTORi were assumed to be ON in all our simulations, signifying that all the alternative isoforms have equal probability of getting expressed. The analysis was performed separately for the uninfected and the infected scenarios, which were created by initializing the *Leishmania* antigen molecules OFF and ON respectively in the two cases using synchronous Boolean update rules. The analysis was performed separately for the uninfected and the infected scenarios, which were created by initializing the *Leishmania* antigen molecules OFF and ON respectively in the two cases using synchronous Boolean update rules. Thereafter, the steady state logical values (i.e. attractor) of all the 294 nodes in 2560 different input combinations from both the scenarios were identified by using in-built functions available in BooleanNet-1.2.4 and the in-house code written in Perl script. However, to present these attractor(s) of each sample in a simplified way, only the steady state binary values of the 10 macrophage output

molecules (*viz.* IFN_BETA, IL1_ALPHA, IL1_BETA, IL10, IL12, INOS, IP10, NO, TNF_ALPHA and c_FOS) were plotted from each attractor(s) state using the network visualization software Gephi (<http://gephi.github.io/>), and were successively tested for the presence of multiple attractors in the system in uninfected and infected scenarios. On the other hand, the differential activation of the FACTORi in splicing mechanism and its role in the regulation of the network dynamics are further analyzed and discussed in **Appendix B: Table B. 3**.

2.2.8. *In-silico* Knock-in and Knock-out Analysis

The models in **Chapter 3** and **Chapter 4** were further analyzed by perturbing it with different combinations of knock-in and knock-out mutations. The *in-silico* knock-in and knock-out mutation were generated keeping the value of the target molecule as constitutively 'ON' or 'OFF' throughout the simulation by using the built-in library function 'boolean2.modify_states' in the BooleanNet-1.2.4 software [157]. In such cases, the transition or update function for the node has been eliminated from the model equation list to ensure that the node does not change its state in the following state transition step. To analyze the significant variations ($p < 0.05$) in the temporal protein expression patterns observed in mutated scenario with respect to the normal scenario, Mann Whitney U Test was performed and important proteins with significant variations are extracted [173]. Through this study, we can identify the proteins, which are being regulated upon certain perturbations and can simultaneously identify the routes along which the effect of that perturbed signal is processed.

2.3. Prediction of Protein-Protein Interactions between Host and Pathogen

In **Chapter 5**, the host pathogen interactome between the secretome proteins from *Leishmania donovani* and the human host is predicted based on sequence and structure-based data. 50 actively secreted secretory proteins identified as candidate

virulence factors by Maxwell *et al.* through the LC-MS/MS method from the secretome of *L. donovani* were used as the *Leishmania* effectors (source nodes) for prediction of the *L. donovani*-human Interactome [174]. The detailed list of these virulence factors with its information is provided in the supplementary material **Appendix C: Table C. 1.**

2.3.1. Interolog Mapping from Secretome data

To predict the interactions for the 50 secretome proteins with human proteins, Interolog Mapping approach was used. This approach identifies homolog for the query protein for which a known Host-Pathogen Interaction has been reported and the homologous HPI is transferred to the pathogen query protein and is assigned the homologous partner host protein [175]. The 50 secretory proteins were used as a query to two resources HPI-DB [176] and BIPS [177] to extract Interologs using a cut-off of $1e-20$ for E-value, minimum of 80% query coverage and 40% identity [178,179].

2.3.2. Domain-Domain Interaction Mapping

The Interologs identified were further subjected to Domain-Mapping based approach which is a form of structure-interaction based validation for the sequence-based Interolog approach. This would help to characterize the predicted interactions as more physical rather than just functional associations which are obtained from the Interolog mapping. Domain mapping for the predicted Interologs was performed using 3DID database. 3DID provided predicted domain-domain interaction pair for proteins based on structure from the Protein Data Bank [180]. 3DID contains a total of 11723 domain-domain interactions. Pfam domains for the 50 secretome proteins were extracted from UNIPROT using in-house codes. Domain-Domain Interaction (DDI) mapping was implemented such that if domain x of the query sequence (Px) is known to interact with domain y of a target sequence (Py) then the two proteins Px and Py can be established to be interacting pair of proteins. To apply this approach an in-house code was written where Pfam domain IDs of 50 secretome proteins were

mapped to 11723 3DID domain interaction pairs and the partner interacting domains were identified for 50 secretome proteins to verify the interactions predicted from the Interolog approach. To validate our predicted partners which were predicted by both HPI-DB and BIPS, but could not be verified from the 3DID database, we used the recently updated dataset from NEGATOME 2.0 to scan through our predicted protein pairs [181]. This database contains non-interacting protein pairs which are curated by manual curation of literature and by analyzing protein complexes from PDB. Domain mapping followed by NEGATOME analysis was done to eliminate false positives in our interactome predicted partners.

2.3.3. Integration and development of Host-Pathogen PPI network and Qualitative Ranking of predicted Interactors

Further to get a complete overview of the interaction between the *L. donovani* secretome proteins with the human host proteins, we integrated the predicted interactome with intra-species PPI of human as well as of *L. donovani*. The predicted interacting human partner proteins which were verified further by Domain-mapping approach were used as a query to extract human PPI from a comprehensive human PPI database PICKLE 2.0 considering only those PPI which had experimental evidence for the physical interaction reported. It is to be mentioned here that the interactions only upto the 2nd shell have been considered in our study [182]. This procedure was similarly followed for extracting *L. donovani* intra-species PPI. The secretome proteins were used as query to STRING database and the template PPI of *L. infantum* was used [183,184]. The identified PPI proteins were further mapped to *L. donovani* proteins with sequence identity cut-off of 90% and above.

Ranks were assigned to the interactions on a qualitative basis. The interactions which are predicted by Interolog by both methods (HPI-DB and BIPS) but not verified by DDI-mapping were assigned Rank 1. These PPI are however cross-

verified with the latest available data of the NEGATOME database. The interactions which are predicted by any one Interolog-source (HPI-DB/BIPS) and verified by DDI-mapping are Rank 2, interactions predicted by both the interolog-sources and also verified by DDI-mapping were assigned Rank 3. The Intra-species PPIs curated to the extended network are all assigned Rank 4 (experimentally verified). It is to be mentioned here that all the four ranks of PPI prediction have been ranked based on the source of information and bear some direct or indirect experimental proof and hence are considered equally likely in our study. The ranks have been retained for easily differentiating and filtering out the interactions if necessary, for further investigation and does not discriminate the interactions as high or low confidence.

2.3.4. Gene Ontology and Pathway Enrichment

The Gene Ontology (GO) terms for the cellular component were enriched for all the predicted host proteins using DAVID 6.8 [185]. Thereafter these proteins were enriched for the pathways that they were associated with. The predicted host proteins partners corresponding to each secretome proteins were enriched separately to identify the pathways associated with each secretome protein. This is an important step in the verification of predicted Host-Pathogen PPIs where it is expected and has been observed in various literatures that each pathogen protein targets multiple host proteins associated with related or similar biological pathways and processes.

All the GO process term enrichment, KEGG pathway enrichment, cellular component enrichment was carried out using DAVID 6.8 statistical test of Benjamini-Hochberg based validation using a p-value cut-off of 0.05 [185].

2.3.5. Network Analysis

Network analysis and topological parameters calculation were done using Cytoscape [186] and R package igraph and stats [187]. Degree distribution and

power law fit were done using Cytoscape: NetworkAnalyzer [186,188] and further plotted using R custom script. The centrality measures calculations like hubs and bottlenecks identification, betweenness centrality, eigenvector centrality were done using Cytohubba. Shortest Path distance calculations between all nodes in the network and sub-networks distance calculation was carried out using custom R script using R package igraph. All visualizations were done using Cytoscape 3.7.1 and Gephi 0.9.2 [189].

2.3.6. Identification of Phenotypic Response Nodes and Sub-Networks using experimental data

A proteomics study has identified Differentially Modulated Proteins (DMP) in THP1-cells infected with *L. donovani* at 3 time points (12 hr, 24 hr and 48 hr) by performing Liquid chromatography–mass spectrometry (LC-MS) method [190]. In this study, we hypothesize that the cause for this differential expression may be due to the presence of the secretome Virulence Factors (VFs) of the parasite that would directly or indirectly influence the host proteins upon infection. Hence, we mapped these DMPs on to our network to be further used as response proteins (target nodes). The mapping of these experimentally reported differentially modulated proteins provides a verification of the predicted network. The DMPs identified in our network were further enriched for their Biological process using DAVID 6.8 using a p-value cut-off of 0.05. From the enrichment results, we identified GO process terms relating to immunological response and pathogen’s survival and protein sets were categorized into two phenotypic response sets: (i) host response proteins involved in Immune response (IR); and (ii) host proteins involved in Intracellular survival of the pathogen (SUR). These two sets represent the early infection phase of our analysis. Since the proteomic study was limited to an infection time point of 48 hours it was not possible to check for protein sets specific for visceralization process. Through a thorough literature mining approach, a set of proteins were identified which defined

the Visceralization (VIS) phenotypic response reported by various experimental studies during the later phase of the infection [39,191-197]. The protein sets identified in these three sets were thus referred to as the “Phenotypic Response Nodes” (PRNs) in our study. Details of these individual nodes (response proteins) identified for the sub-networks are provided in **Appendix C: Table C. 4**.

To extract all possible paths from the *L. donovani* secretory Virulence Factors to the PRNs we have calculated shortest paths using Cytoscape app: PeSca’s tool: isolated nodes [198] forming three phenotype sub-networks namely, IR sub-network, SUR sub-network and VIS sub-network. This tool employs Dijkstra’s algorithm to identify the shortest paths from the given source nodes to all the target nodes. This was performed for all 24 VF nodes used as source nodes to all the response nodes as the target nodes. The three sub-networks thus consist of source nodes, i.e., *L. donovani* VFs, the path intermediates and the response nodes i.e. PRNs. Each of these sub-network was further subjected to KEGG Pathway enrichment using DAVID using statistical method of Benjamini-Hochberg FDR correction and p-value cut-off of 0.05 [185].

2.3.7. Target identification using *in-silico* perturbation based on Path distance analysis and shortest path depletion

Betweenness Centrality defines a protein as the one through which maximum shortest paths pass through and thus it will be the key information carrier in that network [188,199]. Based on this, top ten proteins were extracted based on their betweenness centrality within each sub-network and ten proteins were chosen from these 3 lists which are common in at least two of the sub-networks. These ten proteins were used for the perturbation study of the HPI network. Further, to study the effect of perturbation, each of the candidate protein was serially knocked-out *in-silico*, that is, the protein was deleted from the network along with all its associated edges which defined the connections of the target protein to the other proteins in the

network. Post knockout, the shortest path length from the secretory proteins to the response nodes were calculated again and the deviation in the average path length was calculated using Mann-Whitney test where the p-value calculated signifies the statistical significance of the deviation in path distance caused due to the perturbation created in the network upon the *in-silico* knockout.

Perturbation of shortest paths (PSP) in each sub-network upon knockout was calculated using Eq.10. The PSP scores are scaled in percentage where 0% denotes no deletion of shortest paths post knockout and thus no effect of knockout on depletion of shortest paths. The scale leads upto 100%, where 100% denotes all shortest paths to the response nodes deleted after knockout and thus indicate complete disruption of communication of that secretory protein to any of the response nodes for that sub-network. All calculations were done using the R igraph package [187]. Heatmaps were plotted using R gplots for ease of visualization to study the perturbation effects created upon knockout [200].

►
$$PSP = \frac{SP_k}{SP_T} \quad \dots \text{Eq. 10}$$

Here, SP_k indicates the number of shortest paths remaining after the knockout and SP_T is the total number of shortest paths for that sub-network.

Pathway enrichment using DAVID KEGG pathways with and FDR cutoff of 0.05 was done before and after knockout to observe deletion or addition of pathways as an effect of knockout on the perturbed sub-networks [185]. The enriched pathways were quantified in terms number of proteins from that sub-network protein set enriched for a particular pathway after the knockout. For the representation of this analysis R packages dplyr and ggplot2 were used to create bubble plots, where the bubble size reflects the count of the number of proteins enriched for a pathway in each sub-network. To normalize the observation of this depletion across all three sub-networks, we calculated the ratio of the number of enriched proteins to the total

proteins in the sub-network and have used this ratio to plot the charts. This way we could uniformly compare the depletion in the number of enriched proteins for any pathway after the knockout between the three sub-networks. Additionally, we also wanted to quantify the extent of the effect of knockout on the enriched pathways by observing the depletion in the number of proteins enriched for those pathways after knockout. Here we calculated the difference in the number of proteins enriched for the pathway before and after knockout and plotted this difference in the form of pie chart to denote the distribution of affected pathways in the perturbation study for each phenotypic sub-network.

2.4. Immune Cell Crosstalk in Cancer Microenvironment

In order to study the regulatory mechanisms involved in the immune-escape mechanism of the tumor cells, in **Chapter 6**, an ODE-based mathematical model of the tumor-immune interaction has been developed that captures the development of a malignant tumor from the 'seed', the Cancer Stem Cells (CSC), and its interaction with the 'soil', the tumor microenvironment. The tumor-immune interaction model, depicted in **Figure 5 a**, can be perceived as three regulatory modules – (i) the core tumor along with the tumor infiltrated Tc cells (red box), (ii) the immune-stimulators consisting of M1 cells, T_{H1} cells, IL2 and IFN- γ cytokines (green box) and (c) the immune-suppressors consisting of M2 cells, T_{H2} cell, Treg cells and IL10 cytokines (orange box). The interactions between these components of the model are based on known experimental evidences and immunological relevance. The tumor-immune interaction network has been modelled using 13 Ordinary Differential Equations (**Eq. 11- Eq. 23**) and 71 parameters. A detailed description of the model along with the mathematical assumptions, based on the biological phenomenon, used in its mathematical formulation has been described subsequently.

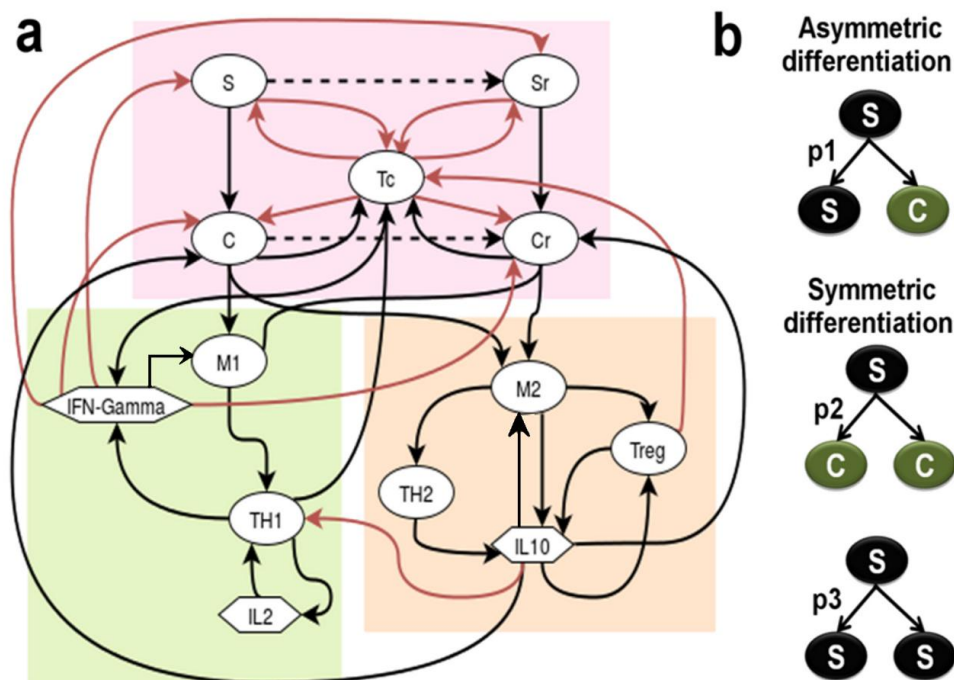


Figure 5: Diagrammatic representation of the Tumor-Immune interaction model (a) Cellular interaction network representing the key players of the tumor microenvironment, viz. Cancer Stem Cells (S), Cancer cells (C), their drug resistant counterparts (S_R and C_R), M1-TAM, M2-TAM, T_{H1} , T_{H2} , Tc, Treg immune cells, and cytokines IL10, IFN- γ and IL-2 ; The tumor microenvironment has been grouped into three parts, viz.- core tumor and infiltrated Tc cells (red box), the immune-stimulators (green box) and the immune-suppressors (orange box); the Black arrows represents Activation, while the Red arrow represent Inhibition; (b) Stem cell differentiation pattern.

The state variables and parameters used in the formulation of the model have been listed in **Appendix D: Table D. 1**. The initial values of the model variables have been listed in **Appendix D: Table D. 2**. Here the initial value of the stem cell $S_0=1$, while S_R , C, C_R have been initialized as zero such that all the tumor sub-populations develop from the symmetric and asymmetric differentiation of a single stem cell that ensures the conservation of the stem cell hypothesis.

2.4.1. Model Formulation

2.4.1.1. Tumor formation

The core tumor consists of the Cancer Stem Cells (S), the Cancer Cells (C) and their drug resistant counterparts Resistant Stem Cells (S_R) and Resistant Cancer Cells (C_R)

(**Figure 5 a**, red box). The model takes into consideration the different patterns of stem cell differentiation, *viz.* the symmetric and asymmetric stem cell differentiation (**Figure 5 b**). In the asymmetric differentiation, one stem cell (S) produces one daughter stem cell (S) and a differentiated progenitor Cancer cell (C) with probability p_1 , while in the symmetric differentiation one stem cell (S) produce either two Cancer cells (C) with probability p_2 or two stem cells (S) with probability p_3 (where, $p_1+p_2+p_3=1$). The stem cells undergoing asymmetric differentiation acquire mutation (represented with a black dotted line in **Figure 5 a**) with a probability m_S that leads to the transformation of a stem cell (S) to a resistant stem cell (S_R). Since the probability that this mutation hits the daughter stem cell and not the differentiated cancer cell is 0.5, the probability of formation of S_R from S is further multiplied by $p_1/2$. The symmetric differentiation leads to the renewal of the non-mutant stem cell (S) pool with a probability $(1-m_S)(1-p_1-p_2)$ [47]. Considering these factors (as described by Tomasetti and Levy [47]), we assume that the growth rate of S can be mathematically represented as $(\gamma_S(1 - m_S)(1 - p_1 - p_2))S$, while the rate of depletion of the stem cell pool, that includes the differentiation of S to C and the transformation S to S_R can be represented as $(\delta_S + (p_2 * \gamma_S) + \gamma_S * \frac{m_S * p_1}{2})S$. It may be mentioned here that γ_S and δ_S represent the natural birth and death rates of S cells. A similar nomenclature has been followed for all the other cell types.

The resistant stem cells are formed from the transformation of an S to S_R . The S_R follows a similar pattern of self-renewal and differentiation that leads to the replenishment of the S_R pool and the formation of differentiated C_R cells [47]. Here, it may be assumed that the S_R represents the compartment of stem cells that accumulate all the mutations in its pool, such that no separate compartment for any secondary mutations has been considered here in this model.

The Cancer cells (C) are formed from the stem cells (S) with the probability p_1+p_2 . These C cells follow a Gompertzian growth kinetics that can be mathematically represented by $\gamma_C * \log\left(\frac{C_{\max}}{C+r_1}\right)$, where C_{\max} is the carrying capacity of the tumor [201]. Here, it has been assumed that during proliferation these C cells acquire mutations with a probability m_C and get transformed into C_R cells. Hence the probability of proliferation of the non-mutant C cell is further multiplied by a factor $(1-m_C)$. The C_R cells are formed from the differentiation of the S_R cells with probability p_1+p_2 and the transformation of the C to C_R cells with probability m_C . The C_R cells also follow similar Gompertzian growth kinetics. The total carrying capacity of these non-stem tumor cells has been considered as K_{tumor} , while each of C and C_R has a carrying capacity of $K_{\text{tumor}}/2$, so that both the cell populations can use the nutrients equally and have an equal advantage in proliferation.

2.4.1.2. Immune cells in the Tumor Microenvironment

As the tumor develops the resident TAMs, both M1 and M2, encounters the C and C_R cells of the tumor and gets activated (**Figure 5 a**) [202]. It may be assumed that this cell-to-cell interaction will follow a saturating kinetics where even in the presence of a high number of tumor cells, the availability of TAMs acts as the limiting condition. Hence a Michaelis-Menten type functional form may be used to represent the TAM activation, e.g. $\gamma_{M1} * \left(\frac{M_1*(C + C_R)}{M_1 + \lambda_{M1}}\right)$. These M1 and M2 TAMs now activate the T_{H1} and T_{H2} cells respectively [203]. Here the abundance of the T_H cells acts as the limiting condition. In a similar way, the M2-TAMs also activate the Treg cells present in the tumor microenvironment [204]. The Tc cells, on the other hand, infiltrate the tumor, gets directly activated by C and C_R cells (**Figure 5 a**). However, the S and S_R cells of the tumor inhibit the Tc cell proliferation [52]. This is a bidirectional reaction, as the activated Tc also tries to kill the tumor cell sub-populations *via* its cytotoxic activity [205,206]. The Treg cells act as immune-

suppressor of the system and try to inhibit Tc proliferation, whereas the T_{H1} cells act as immune-stimulator of the system that helps in Tc proliferation and tumor infiltration [207,208]. All these cell to cell interactions tend to follow saturation growth kinetics and hence have been modelled using the Michaelis Menten form discussed earlier [102].

2.4.1.3. Cytokines and Feedbacks

Tumor formation triggers the immune system to produce cytokines. In this model, three important cytokines have been considered, *viz.* IFN- γ , IL-2 and IL-10 (**Figure 5 a**). The activation of the T_{H1} cells stimulates the production of IL-2 cytokine from them. The amount of cytokine produced is directly proportional to the abundance of effector cells activated. Hence, this has been modelled using the Law of Mass Action, e.g. $(\beta_{Th1CK3} * T_{H1})$, where β_{Th1CK3} (units: ng cell⁻¹day⁻¹) is the rate of production of IL2 from T_{H1} cells [209]. This IL2 is responsible for the auto-regulation and sustained proliferation of the T_{H1} cells. Hence, we have considered a positive feedback loop from IL2 to T_{H1} cell that has been modelled using a saturating function $\frac{\mu_{Th1CK3} * IL2 * T_{H1}}{IL2+k9}$, where the cytokine acts as the limiting factor [102,209]. Similarly, the IFN- γ is produced by T_{H1} and Tc cells which have a negative feedback effect on all the tumor cell sub-populations. The production of IL10 is regulated by M2, Treg and T_{H2} cells. An auto-regulatory positive feedback loop exists between IL10 and the Treg cells. IL10 also plays an important role in the proliferation of the C and C_R cells and inhibition of the T_{H1} cells. This IL10 mediated regulation captures the inhibitory actions of T_{H2} on T_{H1} cells that are often observed in Cancer scenario.

2.4.2. Model Equations

Based on the biological relevance and mathematical assumptions discussed above, the equations representing the tumor-immune interaction network comprising of 13

Ordinary Differential Equations (Eq. 11- Eq. 23) and 71 parameters have been enlisted below:

$$\begin{aligned} \blacktriangleright \frac{dS}{dt} &= (\gamma_S(1 - m_S)(1 - p_1 - p_2))S - \left(\delta_S + (p_2 * \gamma_S) + \gamma_S * \frac{m_S * p_1}{2} \right) S \\ &- \left(\frac{\mu_S * S * IFN\gamma}{k_1 + IFN\gamma} \right) - \left(\frac{tck * S * Tc}{k_{tc1} + Tc} \right) \end{aligned} \quad \text{.....Eq. 11}$$

$$\begin{aligned} \blacktriangleright \frac{dS_R}{dt} &= (\gamma_S(1 - p_1 - p_2) - (\delta_S + (p_2 * \gamma_S))) S_R + m_S * \gamma_S * \left(1 - \frac{p_1}{2} - p_2 \right) S - \\ &\left(\frac{\mu_{SR} * S_R * IFN\gamma}{k_2 + IFN\gamma} \right) - \left(\frac{tck * S_r * Tc}{k_{tc2} + Tc} \right) \end{aligned} \quad \text{.....Eq. 12}$$

$$\begin{aligned} \blacktriangleright \frac{dC}{dt} &= \gamma_C * (1 - m_C) * \log\left(\frac{0.5 * K_{tumor}}{C + r_1}\right) * C + \gamma_S * (p_1 + p_2) * S - \delta_C * C - m_C * \\ \gamma_C * C + \left(\frac{\mu_{C1} * C * IL10}{IL10 + k_3} \right) - \left(\frac{\mu_{C2} * C * IFN\gamma}{IFN\gamma + k_4} \right) - \left(\frac{tck * C * Tc}{k_{tc3} + Tc} \right) \end{aligned} \quad \text{.....Eq. 13}$$

$$\begin{aligned} \blacktriangleright \frac{dC_R}{dt} &= \gamma_C * C_R * \log\left(\frac{0.5 * K_{tumor}}{C_R + r_2}\right) + \gamma_S * S_R * (p_1 + p_2) + m_C * \gamma_C * C - \delta_{C_R} * \\ C_R + \left(\frac{\mu_{C1} * C_R * IL10}{IL10 + k_5} \right) - \left(\frac{\mu_{C2} * C_R * IFN\gamma}{IFN\gamma + k_6} \right) - \left(\frac{tck * C_r * Tc}{k_{tc4} + Tc} \right) \end{aligned} \quad \text{.....Eq. 14}$$

$$\blacktriangleright \frac{dM_1}{dt} = \gamma_{M1} * M_1 * \left(\frac{C + C_R}{M_1 + \lambda_{M1}} \right) - \delta_{M1} * M_1 + \left(\frac{\mu_{M1ck2} * M_1 * IFN\gamma}{IFN\gamma + k_7} \right) \quad \text{.....Eq. 15}$$

$$\blacktriangleright \frac{dM_2}{dt} = \gamma_{M2} * M_2 * \left(\frac{C + C_R}{M_2 + \lambda_{M2}} \right) - \delta_{M2} * M_2 + \left(\frac{\mu_{M2ck1} * M_2 * IL10}{IL10 + k_{10}} \right) \quad \text{.....Eq. 16}$$

$$\blacktriangleright \frac{dT_{H1}}{dt} = \gamma_{TH1} * \left(\frac{T_{H1} * M_1}{\lambda_{TH1} + T_{H1}} \right) - (\delta_{TH1} * T_{H1}) - \frac{\mu_{TH1ck1} * IL10 * T_{H1}}{IL10 + k_8} + \frac{\mu_{TH1ck3} * IL2 * T_{H1}}{IL2 + k_9} \quad \text{.....Eq. 17}$$

$$\blacktriangleright \frac{dT_{H2}}{dt} = \gamma_{TH2} * \left(\frac{T_{H2} * M_2}{\lambda_{TH2} + T_{H2}} \right) - (\delta_{TH2} * T_{H2}) \quad \text{.....Eq. 18}$$

$$\begin{aligned} \blacktriangleright \frac{dTc}{dt} &= \gamma_{Tc} * Tc * \left(\frac{C + C_R}{Tc + \lambda_{Tc1}} \right) + \gamma_{Tc} * \frac{Tc * T_{H1}}{Tc + \lambda_{Tc4}} - \mu_{TcS} * Tc * \left(\frac{S + S_R}{Tc + \lambda_{Tc2}} \right) \\ &- \delta_{Tc} * Tc - \mu_{TcTreg} * Tc * \left(\frac{T_{reg}}{\lambda_{Tc3} + T_{reg}} \right) \end{aligned} \quad \text{.....Eq. 19}$$

$$\blacktriangleright \frac{dT_{reg}}{dt} = \gamma_{Treg} * \left(\frac{T_{reg} * M_2}{T_{reg} + \lambda_{Treg2}} \right) - \delta_{Treg} * T_{reg} + \left(\mu_{Tregck1} * \frac{IL10 * T_{reg}}{T_{reg} + k_{11}} \right) \quad \text{.....Eq. 20}$$

$$\blacktriangleright \frac{dIL10}{dt} = \beta_{M2} * M_2 - \delta_{ck1} * IL10 + \beta_{Treg} * T_{reg} + \beta_{Th2} * T_{H2} \quad \text{.....Eq. 21}$$

$$\blacktriangleright \frac{dIFN\gamma}{dt} = \beta_{Th1ck2} * T_{H1} + \beta_{Tc} * Tc - \delta_{ck2} * IFN\gamma \quad \text{.....Eq. 22}$$

$$\blacktriangleright \frac{dIL2}{dt} = \beta_{Th1ck3} * T_{H1} - \delta_{ck3} * IL2 \quad \text{.....Eq. 23}$$

2.4.3. Control and Therapeutic Intervention

In order to design treatment protocols for triggering Cancer remission, in **Chapter 6**, we have introduced Radiotherapy, Chemotherapy and Immunotherapy control terms to the model.

- a. **Radiotherapy (R)** - With the aim to reduce the tumor cell proliferation, control variables were introduced in our model. Here, the control variable u_1 signifies the probability of cell death due to Radiotherapy (**Eq. 24**),

►
$$u_1 = 1 - \exp(-\alpha d_R - \beta d_R^2) \quad \dots \text{Eq. 24}$$

where α and β are the parameters governing the radio-sensitivity of the cells, and d_R is the dose of radiotherapy applied, measured in Grey (Gy) units [101]. The value of α and β depends on the oxygenation state of the cell [210]. In our model, it has been considered that Radiotherapy affects only the Cancer (C) and the Cancer Resistant (Cr) populations of the tumor. It has no effect on the stem cells owing to their slow growth rate.

- b. **Chemotherapy (C)** - The control variable u_2 , signifying chemotherapy has an effect on the drug-sensitive stem (S) and cancer (C) cells of the tumor (**Eq. 25 and Eq. 26**). u_{2_S} and u_{2_C} are defined as the probabilities of cell death, due to chemotherapy, of Stem cells and Cancer cells respectively (**Eq. 25 and Eq. 26**).

►
$$u_{2_S} = f_c * (1 - \exp(-M_c * d_c)) - k_s \quad \dots \text{Eq. 25}$$

►
$$u_{2_C} = f_c * (1 - \exp(-M_c * d_c)) \quad \dots \text{Eq. 26}$$

Here, f_c denotes the frequency of chemotherapy per day, M is defined as the efficiency of the chemotherapeutic drug in m^2mg^{-1} denoting the area of the tumor affected per mg of the drug and d_c is the concentration of the drug in $mg m^{-2}$. The efficacy of the chemotherapy of the stem cells depends on the factor k_s

that represents the inhibitory effect of IL-4 on the stem cells that reduces the efficacy of the drugs. Sequestration of IL-4 makes the stem cells sensitive to chemotherapy [211,212].

► **Immunotherapy (I)** - The parameter set was systematically screened to identify key parameters governing the negative feedback of the immune cells on the Tumor population. Then, the immunotherapy was introduced in our model as perturbations to the system in order to overcome the immunosuppressive effect of the tumor cells and to restore a healthy T_{H1}/T_{H2} balance.

► $u3_{Tc} = d_i * M_{Tc}$ Eq. 27

► $u3_{TH1} = d_i * M_{TH1}$ Eq. 28

Eq. 27 and Eq. 28 depicts the control variables for providing immune-boost to the T_c and T_{H1} cells, respectively. d_i signifies the dose of immunostimulant, measured in $mg\ day^{-1}$ that must be given to the system, while M_{Tc} and M_{TH1} are the measures of the sensitivity of the T_c and T_{H1} cells, respectively.

2.4.4. Designing Treatment Protocols

The protocols are designed using various combination of the above mentioned treatment strategies, *viz.* Radiotherapy, Chemotherapy and Immunotherapy. The dosage, time duration and number of cycles for each therapy are varied to determine the optimal combination that gives us maximum fold changes in the tumor reduction. The general form of the protocols can be described as follows:

$$DT_{200} \rightarrow (R_{tR}^{dR/n})_{nR} \rightarrow FT_{tFT} \rightarrow (Ch_{tC}^{dC})_{nC} \rightarrow (I_{tI}^{dI})_{nI}$$

Here, R denotes Radiotherapy, Ch denotes Chemotherapy, I denotes Immunotherapy and FT signifies a treatment-free period or relaxation time. The model was run till 200 days before the start of any therapeutic interventions. This has been considered as the standard detection time (DT) for a full grown tumor.

Here the subscripts (t_r , t_c and t_i) denotes the time duration for which the treatment was given, and the superscripts (d_r , d_c and d_i) represent the dosage. The subscript outside the bracket (n_r , n_c and n_i) denotes the number of cycles for which that treatment was repeated.

Protocol 1: This Protocol is an adaptation of the standard treatment protocol used for applying chemo and radiotherapy (adapted from British Columbia Cancer Agency Protocol GIGAJCPRT - <http://www.bccancer.bc.ca/>). It was applied to our model to observe the fold changes in the tumor cell population. The protocol can be summarized as follows:

$$DT_{200} \rightarrow (Ch_{14}^{800})_6 \rightarrow (R_{40}^{60/28}) \rightarrow FT_{15} \rightarrow (Ch_{14}^{800})_6$$

Protocol 2: This Protocol was designed as a combinatorial treatment protocol of Chemotherapy, Radiotherapy and Immunotherapy to enhance the treatment efficacy. Based on Protocol 1, this Protocol is an improvisation where Immunotherapy has been included that boosts both the T_{H1} and T_c simultaneously. In order to design this combinatorial treatment protocol, the dose of Radio, Chemo and Immunotherapy were varied over wide ranges in order to create 1000 treatment combinations. The treatment efficacy of each combination was plotted in a 4-dimensional scatter plot, measured in terms of fold change and T_{H1}/T_{H2} ratio (**Appendix D: Figure D. 1**). The Protocol 2 can be summarized as follows:

$$DT_{200} \rightarrow (Ch_{14}^{800})_6 \rightarrow (R_{40}^{60/28}) \rightarrow FT_{15} \rightarrow (Ch_{14}^{800})_6 \rightarrow (I_{20}^2)_{10}$$

Measuring treatment efficacy

The efficacy of a treatment protocol is measured by the reduction in the size of the tumor and the overall recovery from the immune-suppression induced by the tumor,

to ensure minimal chances of tumor relapse. Hence we have defined two parameters that can be used as an indicator of Cancer prognosis:

- a. **Fold Change** – The treatment efficacy was estimated by measuring the fold change of the tumor mass at the end of the treatment period as compared to the tumor mass measured at the time of detection.
- b. **T_{H1}/T_{H2} ratio** - In order to ensure maximum treatment efficacy and minimize chances of Cancer relapse, the T_{H1}/T_{H2} ratio was used as an indicator for disease prognosis. A minimum threshold of $T_{H1}/T_{H2} \geq 5$ was chosen to optimize treatment protocol.

2.4.5. Positivity and Boundedness

This system of equations (**Section 2.4.2, Eq. 11-23**) can be analyzed with the initial conditions (**Appendix D: Table D. 2**) defined in the thirteen-dimensional variable space

$$R_+^{13} = [(S, S_R, C, C_R, M1, M2, T_{H1}, T_{H2}, Tc, Treg, IL10, IFN\gamma, IL2) \\ \in \mathbb{R}^{13} | (S, S_R, C, C_R, M1, M2, T_{H1}, T_{H2}, Tc, Treg, IL10, IFN\gamma, IL2) \geq 0]$$

It can be proven, that all solutions of the system in R_{0+}^{13} remain in R_{0+}^{13} . Hence, R_{0+}^{13} is positively invariant, and it is sufficient to consider solutions only in R_{0+}^{13} . In this region, the usual existence, uniqueness and continuation results hold for the system. From our numerical simulations also, we have observed the existence of positive solutions. The solution set we get for the set of ODEs represents the effective cell population and protein concentrations of the species considered in the model at different time points during the tumor development. The fixed point attained by all the variables of the model is a part of this positive solution space.

Also, we observe that the right-hand side of **Eq. 11-23 (Section 2.4.2)** are smooth functions of the variables ($S, S_R, C, C_R, M1, M2, T_{H1}, T_{H2}, T_c, T_{reg}, IL10, IFN\gamma, IL2$). Also, since all the parameters are non-negative, local existence and uniqueness properties hold in R_+^{13} , and if the following necessary conditions are satisfied,

1. $S_0 > 0$
2. $p_1 + p_2 < 1$
3. $m_s < 1$
4. $m_c < 1$
5. $\gamma_s(1 - p_2) > \delta_s$

then, we can state the following proposition.

Proposition 1: All the solutions of **Eq. 11-23 (Section 2.4.2)** which initiate in R_+^{13} are uniformly bounded.

Proof: The proof of Proposition 1 is obvious as all the variables satisfy the condition of positive invariance for all the solutions of **Eq. 11-23 (Section 2.4.2)** which initiate in R_+^{13} , the assumptions and necessary conditions (stated in **Section 2.4.5**) [213].

2.4.6. Sensitivity Analysis

The sensitivity analysis of the tumor-immune interaction model (**Eq. 11 – Eq. 23**) was performed by the extended Fourier Amplitude Sensitivity Test eFAST technique using a MATLAB based toolbox [214]. The sensitivity analysis was carried out using the whole set of parameters [$k=71$]. 100 samples were chosen per search curve and resampling of the search curves was carried out 5 times [$N_s = 100, N_R = 5$]. Hence, the total number of model simulations $N = (k+1) * N_s * N_R = 36000$. The Sensitivity Indices (S_i) of the parameters ($p < 0.05$) for the variables governing the growth of the tumor sub-populations, *viz.* S, S_R, C and C_R were estimated at different stages of the tumor development (**Figure 6 a-d**). Here it may be observed that at different time points

that S_i values of the parameters change, signifying the importance of the parameters in the different stages of the tumor development. The knowledge from this sensitivity analysis was used to determine the parameters that have a maximum effect on the tumor development.

2.4.7. Parameter Estimation from Cancer cell line data

The model (in **Chapter 6**) comprises of a total of 71 parameters. The values of 21 parameters of the model were curated from the existing literature. The unknown parameters were estimated (few were ‘assumed’ within the biological feasible ranges) using the MATLAB based toolbox that employs the MCMC-DRAM algorithm for parameter estimation [215]. The time course experiment cytometric data for cancer cell proliferation obtained for 7 days in for Gastric cancer cell line (SGC7901) that was fitted for approximating the cancer cell behaviour during the growth phase (**Figure 6 f**) [216]. Parameters that were sensitive for the growth of the Cancer (C sub-population) cells were varied in biologically feasible ranges. The prior distribution was assumed to be normal and the MCMC simulation was carried out for 5,00,000 iterations to ensure the convergence of the chain (**Figure 6 e**). The estimated parameter values for the model have been listed in **Appendix D: Table D. 1**.

2.4.8. Experimental Data for Model Calibration

Apart from the parameters estimated using the MCMC method, the remaining unknown parameters governing the steady state behaviour of the system were manually adjusted within the biologically feasible ranges for the calibration of the model so as to ensure that the simulation results corroborated with the various experimental observations. These parameter values (labelled as ‘Expected’) used for the numerical simulation of the model have been enlisted in **Appendix D:Table D. 1**.

The experimental data used for this purpose were extracted from the available literature. For the validation of the growth kinetics of the resistant Cancer cells, time-course data of resistant cell lines were obtained from Breast cancer cell line MCF-7/TAX-resistant to Paclitaxel [217], Hepatocellular Carcinoma cell line SK-Hep1/CDDP3-resistant to Cisplatin [218], Colon Cancer cell lines SW-620-L-OHP and LoVo-L-OHP-resistant to Oxaliplatin [219].

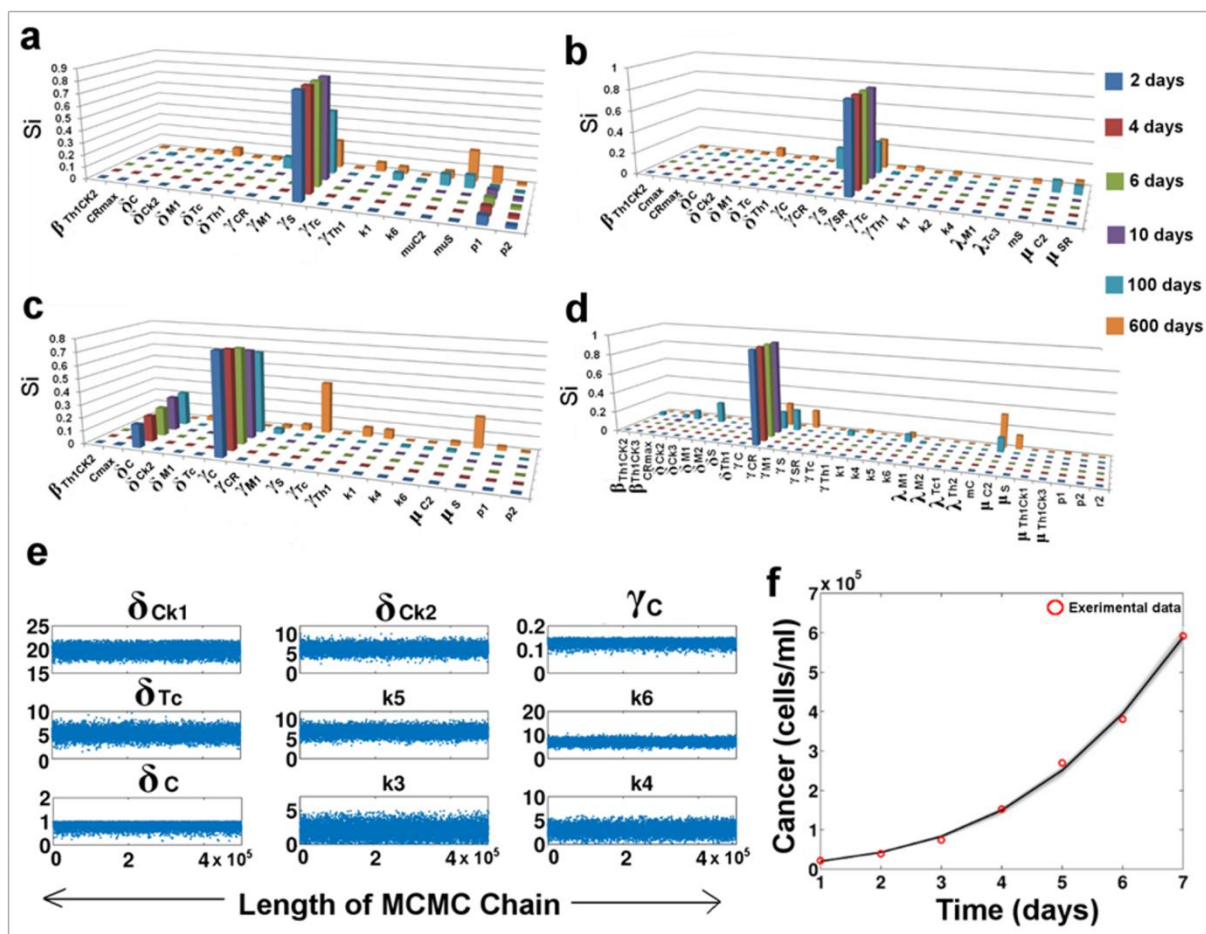


Figure 6: Sensitivity Analysis and Parameter Estimation: (a-d) Sensitivity Analysis plots for S , S_R , C and C_R respectively. The x-axis represents the parameters with $p < 0.05$; (e) Trace Plot showing the best fitting parameter values as estimated by the MCMC algorithm; (f) Predictive plot of cancer proliferation using the estimated parameter values. The red circles represent the cancer cell proliferation values as obtained from Cell Counting experiments using Gastric Cancer cell line [216].

The cytometric data obtained for the validation of the immune cell ratios were mostly obtained from Gastric Cancer, Ovarian Cancer and Osteosarcoma studies

[202,220-224]. The data for the validation of cytokine expression were obtained from cases of Gastric and Breast Cancer studies [225-227]. These data used came from heterogeneous sources as none of the previously performed experiments was found to report the values of all cytometric data in a single experiment. Moreover, the use of data from the different Cancer studies ensures that the model is generic and mimics the average behaviour observed in most Cancer studies. The use of data from both *in vitro* studies as well as data obtained from Cancer patients ensures the reliability of the model for its use in designing therapeutic control. In order to make the model specific for a single type of Cancer, one needs to simply obtain the cytometric data from a single experimental source and adjust the parameters accordingly.

2.4.9. Interior Equilibria

To ensure positivity and existence of the interior equilibrium solutions, 36000 random parameter sets were generated (as mentioned in **Section 2.4.6**) within the biologically feasible ranges. Thereafter the model is simulated up to 800 days for each set of parameter. It was observed that each model simulation led to the positive interior equilibrium solution. Hence, we can state and prove the following Proposition.

Proposition 2: Positive interior equilibria exist for the set of equations **Eq. 11-23 (Section 2.4.2)**.

Proof: The interior equilibrium points are the steady-state solutions of the **Eq. 11-23 (Section 2.4.2)** under the necessary conditions (**Section 2.4.5**) in the biologically feasible ranges of parameter values and initial conditions (**Appendix D: Table D. 1 and Table D. 2**).

2.4.10. Model Initialization and Numerical Simulation

The tumor mass is formed by the sub-populations S , S_R , C , C_R . In our model, the S cell sub-population has been initialized to 1, while all the other tumor cell sub-populations have been considered as 0. The initial values of the remaining variables have been initialized based on cytometric data and cytokine expression values of healthy individuals, curated from the literature. The details have been provided in the **Appendix D: Table D. 2**. The model was simulated numerically using the variable-step, variable order solver, `ode15s`, in MATLAB® 2017a platform.

CHAPTER 3

STUDY OF CO-RECEPTOR AND CALCIUM SIGNALLING CROSSTALKS REGULATING T_H-CELL ACTIVATION AND EFFECTOR FUNCTIONS

3.1. Motivation

The 'two signal hypothesis' of T-cell activation establishes that the complete activation of the T-cell responses and the expression of the major interleukin molecules cannot be achieved by T-cell receptor (TCR) and MHC class II protein interaction alone, but requires the successful interaction of the various co-stimulatory molecules with its co-receptors. The activation of the calcium channel has also been observed to play a crucial role in regulating the T-cell responses [142]. However, during various antigenic challenges such as Infectious diseases and Cancer, these immune signalling pathways are deregulated and the expression of effector molecules is altered. This leads to an immune-suppressed condition. To overcome such scenarios, it is necessary to have an in-depth knowledge of the intra-cellular signalling pathway crosstalks of the T_H cell that will help us to identify important immune-stimulatory modules that can elicit the desired effector functions. Experimental studies have provided us with discrete information regarding each co-receptor molecule and pathway. Several modelling and computational studies [87] on the core T-cell signalling network have revealed numerous hidden facts about this pathway, but till now none of the studies has considered the importance of all the co-receptor signalling pathways including the core network during T-cell activation. A previous study using a systems level model on the sequential phosphorylation of T-cell antigen receptor (TCR) by LCK molecule has revealed the importance of having multiple phosphorylation sites on TCR and the successive

differential binding of ZAP70 on those phosphorylated sites with ultrasensitivity or switch-like response architecture in TCR signalling network [228]. In another study, the activation mechanism of primary T-cell by TCR, CD4/CD8 co-receptor, and CD28 molecules after encountering APC has been studied using Boolean formalisms [229]. In the successive study, the same model has also been studied as a continuous model by transforming its Boolean formalisms to evaluate the temporal behavior of the entire TCR network by measuring the time course concentration level of its component protein molecules [230]. In order to encounter the stochastic effect of the protein expression pattern of T-cell signalling network in large granular lymphocyte (T-LGL) leukemia condition, a study has also been performed by using the asynchronous Boolean update rules on the T-cell network [231]. In this study, the author has mainly used core TCR network to study the network dynamics of T-LGL and successively identified 19 possible therapeutic drug targets. However, it should be noted that all of these models have mainly considered the core T-cell pathway, although the experimental studies have already revealed the importance of other co-stimulatory and co-inhibitory accessories, which also require in parallel for the proper functioning of core T-cell network [142].

For gaining a holistic understanding of the complex molecular regulations underlying the effector functions and phenotypic responses of T_H cell, it is important to employ systems level approach. Hence, in order to achieve this, the reconstruction of the complete intra-cellular T-cell signalling network that includes the core TCR pathways, co-receptor signalling pathways as well as Calcium signalling pathway is of paramount importance. This will help in identification of the regulatory modules to stimulate a sustained proliferation of the immune cell, to overcome disease induced T-cell anergy, to identify targets for stimulating of cytokine production as well as understand the mechanisms of T_H cell differentiation.

Hence, in order to address the First Objective of the Thesis, in this chapter, we aim to explore the intra-cellular signalling network of T_H cell to decipher the function of the co-receptor molecules and the Calcium channel CRAC on the regulation of the phenotypic responses and the changes in the temporal expression pattern of Interleukins and other effectors molecules from the T_H-cells.

In this work, our main hypothesis is that the temporal expression patterns of various T-cell effector molecules as well as the phenotypic responses, such as T-cell proliferation, inactivation, cell death (T cell anergy), Interleukin production, can be regulated by selective modulation of the co-receptor signalling pathways and stimulation of Ca⁺² signalling pathway. Here we aim to identify the minimum combination of pathways that are essential for the sustained proliferation of the T_H cell as well as identify the key co-receptor molecules and pathways that play the major role in regulating the Interleukin production and effector functions.

In order to accomplish this, we have manually reconstructed a comprehensive T-cell receptor mediated signalling pathway coupled with other intracellular important cell signalling pathways (e.g., MAPK, Ca⁺² signalling pathway etc.) by collating the signal propagation data from various literature and cell signalling databases (**Section 2.1.1**). Using the reconstructed pathway map of T-cell activation, and the concept of semi-dynamic Boolean or logical equations, we have constructed a mathematical model of the activation of T-cell signalling network using the 'AND', 'OR', 'NOT' logic gates (**Section 2.2, Appendix A: Table A. 1**). The initial expression levels (i.e. logical states) of all the nodes/species of this pathway are considered from the published microarray expression data (**Section 2.2.4**), which is binarized by K-means clustering method (**Section 2.2.5, Appendix A: Table A. 2**). Using this semi-dynamic computational approach, we observe various temporal protein expression

patterns and changes in phenotypic responses generated upon introducing different stimulation and co-stimulation signal on the T-cell receptor proteins.

It is to be mentioned here that, one of the main assumptions used for simulation and validation of the T-cell activation is the association of time with the Boolean model. Here, in order to gain an understanding of the temporal changes in the protein expression, each step of Boolean update was associated with a unit of time. For this, both the synchronous and asynchronous models were run for different time steps and the time step at which the simulation reached its steady state was determined (**Section 2.2.3**). The asynchronous model was simulated for 100 iterations (range =100) and the mean of the expression value for each time point of each node was taken. With the 0 hour value as the initial value and the APC molecules as 'ON', the 39 output molecules of the model were validated with 0, 2, 4 and 6 hours binarized expression data, the time when the interleukin production is highest/ at its peak and the T cell is most active [171,232]. Here each time step was assumed to be equal to 0.5 hours. This calibration of the time scale was optimized only after determining the time step at which the model reached its steady state.

3.2. Results

3.2.1. Reconstruction of T-cell co-receptor Signalling Pathways

The T cell pathway that has been reconstructed (**Figure 7**) provides a complete picture of the entire signalling cascade. The data has been collated through thorough literature survey and pathway databases (**Section 2.1**). In this pathway, we have taken into account all the co-stimulatory and co-inhibitory receptors that are expressed on the surface of the T lymphocyte and paired them with their corresponding ligand molecules expressed on the surface of the APC. These co-stimulatory pathways play a pivotal role in regulating the T cell activation, effector function and survival, without which TCR alone cannot provide the signal for the

full activation of the cell [142]. The pathway clearly shows the Antigen (Ag) in complex with the MHC Class II molecule, the 5 co-stimulatory (CD70, LIGHT, TNFSF9, OX40L and ICOSL) and 1 co-inhibitory (PD1) ligand molecules that are expressed on the APC. The B7-1 and B7-2 molecules have a dual role to play. These molecules can interact with two types of co-receptors on the T cell surface, *viz.* the CD28 co-stimulatory co-receptor and the CTLA4 co-inhibitory co-receptor [142]. In the pathway (**Figure 7**), the molecules have been coded in different colors according to their location in the membrane (dark green), cytoplasm (yellow) and nucleus (orange). The pathway shows 39 output molecules (colored light green), many of which have feedback loops (color-coded as deep pink lines) that regulate the proliferation of the T cell pathway in an auto-regulatory fashion (e.g., IL2 has a positive impact, whereas PD1 and CTLA4 have a negative effect). The functions of the co-stimulatory co-receptors have further been elucidated by different perturbation studies discussed subsequently. The pathway we report consist of 206 molecules (nodes) and complex mesh-like network formed of 435 protein-protein interactions, which is the highest as compared to other T cell signalling pathway models reported to date in Databases and Literatures [84,229].

In order to decompose this complex pathway and study how the signal propagates through this complex network of proteins and molecules, we used this pathway to construct the Logical model to understand the dynamics of protein expression during the transition of a T cell from its inactive to its activated state.

flow in the network, starting from the receptor and co-receptors down to the cytoplasmic proteins, leading to the activation of the transcription factors and finally the expression of the 39 output proteins. The model reached its steady state at 14th rounds of updates (6.5 hours) for the synchronous and at 10th time points (approx 5.5 hours) in the case of asynchronous simulation. It is worthy to note that experimental data is also taken up to 6 hours duration with 2 hours interval. In order to compare the synchronous and asynchronous temporal protein expression pattern with the experimental data, we have plotted the experimental as well as simulation data in **Figure 8**, where the state transition pattern of the 39 output molecules (**Appendix A: Table A. 3**) were plotted as a continuous heat plot (**Figure 8 A**: microarray data, **Figure 8 B**: synchronous data, **Figure 8 C**: asynchronous data). While the synchronous deterministic model simulation (**Figure 8 B**) show distinct up and down-regulation of the protein expressions of one run of simulation, the heat-plot of the asynchronous simulation (**Figure 8 C**) show a gradual change of protein expression pattern as a result of averaging the values of protein expression for each node at each of the 21 time-steps for 100 runs of the simulation. The pattern thus generated shows the dynamics and fluctuations in the protein expression over the time period of T cell activation. By using this asynchronous update, we are able to rule out certain limitations of the Boolean modelling approach (the 'all' or 'none' output), as by this method we are able to generate a protein expression pattern that clearly shows that even though some proteins in **Figure 8 B** shows a complete down-regulation at certain time points, it becomes evident from **Figure 8 C** that some amount of protein expression is still occurring in low amount (e.g. in **Figure 8 B** the proteins CTLA4, PD1, IFN- γ apparently show an absence of expression at certain time points between 1.5 – 5.0 hours, whereas **Figure 8 C** shows that the expression is not completely absent, and a low level of expression continues to occur at those time points - comparable with the microarray data). Also, **Figure 8 C** eliminates the delay

in protein expression of many interleukins and STAT proteins as shown in **Figure 8 B**, and gives us a better understanding of the change in expression dynamics of the vital T cell output proteins over time.

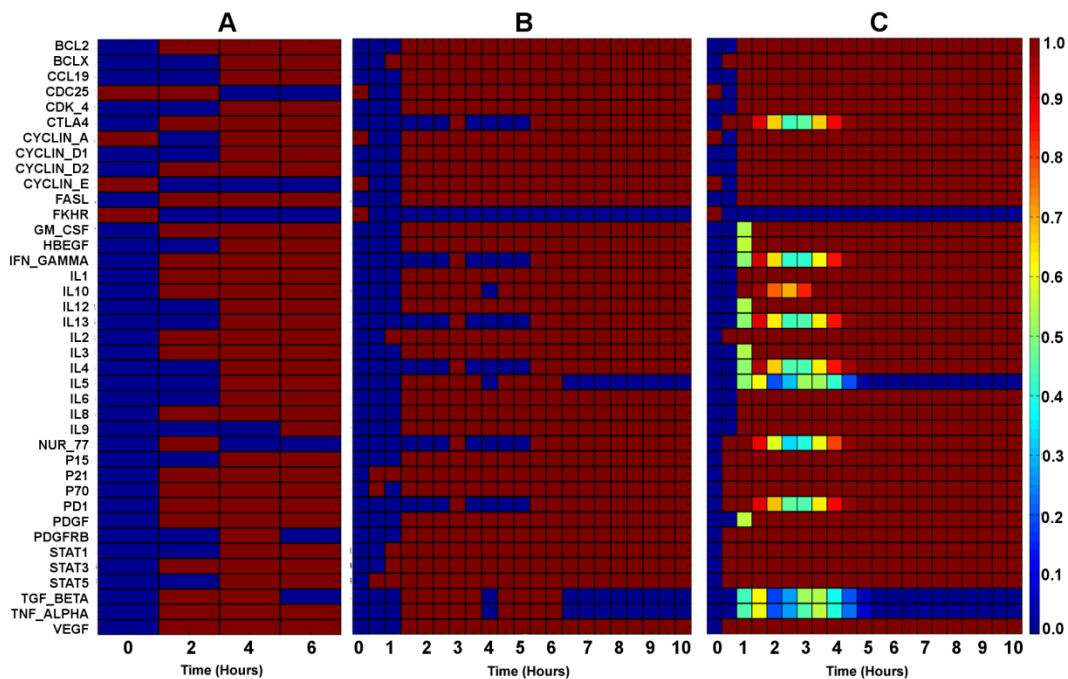


Figure 8: Continuous heat plot showing state transition pattern of output proteins. (A) Binarized microarray data of 39 T-cell output proteins at 0, 2, 4 and 6 hours, (B) Temporal protein expression pattern observed in synchronous update up to 21 time points (0 to 10 hours), (C) Temporal protein expression pattern observed in asynchronous update up to 21 time points (0 to 10 hours). Red coloured cell denotes an up-regulation in protein expression, while blue signifies down regulation.

3.2.3. Phenotypic enrichment of output proteins

The 39 output proteins were classified according to the function regulating the behaviour of a T cell (**Appendix A: Table A. 3**). The proteins were grouped into five classes - (a) T cell proliferation: consists of 12 proteins, which includes proteins/molecules responsible for the T cell survival, anti-apoptotic molecules, cell cycle proteins, TNF molecules [164], transcription factor STAT5 [233], etc.; (b) Negative regulator of T cell proliferation: consists of 7 proteins including PD1 and CTLA4 co-receptors that aid in co-inhibition of T cell pathway [234],

immunosuppressant TGF_BETA [235], NUR-77, which is a calcium-mediated T cell apoptotic factor [236], etc.; (c) Immune Response: consists of molecules responsible for initiating immune responses in the system, examples include GM-CSF [237], Interferon IFN-Gamma [238], and STAT1 and STAT3 transcription factors responsible for transcription of genes involved in eliciting an immune response [239]; (d) Interleukins: includes 11 interleukin molecules possessing different functions, e.g. IL2, IL4, and most of the other interleukins positively regulates T cell proliferation and are involved in immune responses, while IL10 is involved in T cell apoptosis [144] and (e) Growth factors: includes proteins (e.g. PDGF, PDGFRB, VEGF, HBEGF) secreted by the T cell that often acts as potent mitogenic factors for other cell and mediates immune suppression [240-243].

3.2.4. Comparison with Experimental Observations

The 14 time-steps that were required for the model to reach its steady state was scaled to 7 hours-time for the purpose of validation of the model. The time scale division was chosen keeping in mind with the experimental evidences, which indicate 6 hours to be the time required for the full activation of a *naïve* T lymphocyte, when the production of the interleukins is the highest [171,232]. In order to compare the simulation results of our model with the experimental data, the 16 time points (up to 8 hours; each time-step corresponds to 30 minutes) of both the synchronous and asynchronous simulation results were plotted along with four discrete time points (0, 2, 4 and 6 hours) from experimental observation (**Appendix A: Figure A. 1**).

The results of our simulation obtained at the time step 12 (~ 6 hours) of the 39 output proteins were then validated with the 6 hours binarized experimental data. Here, while comparing deterministic or synchronous simulation vs. experimental data, we found the logical states of 34 proteins (from synchronous updates) out of the 39

output proteins were matching with the 6 hours protein expression results observed in the experimental data. The percentage of validation of our simulation results with the experimental data have been provided in **Table 2**. Out of the remaining proteins, the expressions of which appeared to differ with the deterministic model, TGF_BETA matches with the asynchronous model with a small time-lag, while NUR_77 protein showed down-regulation in protein expression slightly earlier than the expected 6 hours time step. Both the synchronous and asynchronous simulations showed a clear match in the nature of the curves. Also, we found that the deterministic model showed a match of 14 very essential T-cell proteins (viz. BCL2, CYCLIN_D2, FASL, FKHR, GMCSF, IL1, IL2, IL3, IL8, P21, P70, PDGF, STAT3 and VEGF) with the experimental microarray data at all the four timesteps i.e., 0, 2, 4 and 6 hours respectively. It is interesting to see that the T-cell proliferating factors (such as anti-apoptosis, cell cycle progression, cell survival etc.) governed by the proteins BCL2, CYCLIN_D2, FASL were up-regulated during T-cell activation in both the synchronous and asynchronous simulation results, and successively validated against the experimental findings (**Appendix A: Figure A. 1**). On the other hand, the expression of apoptotic factor FKHR was also found to be down-regulated in our simulation result and well matched with the experimental observations (**Appendix A: Figure A. 1**). Down regulation of this protein is required during the T-cell proliferation process after T-cell activation. Simultaneously, the up-regulation of immune responsive proteins, such as, GMCSF and STAT3, and the interleukin expressions (e.g., IL1, IL2, IL3, and IL8) are also important during the T-cell activation process. In our simulation outcomes, we have found the exact outcomes, which are well corroborated with the experimental data (**Appendix A: Figure A. 1**). However, to maintain the homeostasis of T-cell proliferation, the cell cycle progression inhibitor P21 was found to be simultaneously up-regulated in our simulation results. Important growth factors, such as, PDGF and VEGF, which were

found to be up-regulated in the experimental data, were also shown to be up-regulated in the simulation outcomes. Hence, on the basis of these validation results, it can be concluded that the model outcomes generated by using synchronous and asynchronous update rules are correctly predicting the temporal protein expression patterns in T-cell signalling network during T-cell activation procedure and thus prove the robustness of our *in-silico* model.

Table 2: Validation of Results

Total number of species	206
Number of output molecules	39
No of output molecules matching at 6 hours	34 (87.18%)
No of output molecules matching at 4 hours	27 (69.23%)
No of output molecules matching at 2 hours	20 (51.28%)
No of molecules matching at every time point	14

3.2.5. Phenotypic Pattern Generation and Validation

The equations of the three nodes, *viz.* Cell Proliferation, Cell Survival and Cell Death, related to the T-cell phenotypes, contains various combinations of these output molecules according to the functions that they are associated with (**Section 2.2.2, Eq. 4, Eq. 5, Eq. 6**). The values of these three nodes were then plotted in different scenarios that were created by performing various perturbations to the system.

a) **LAT mutation scenario:** The equations for the study of the phenotype were validated by matching the change in the phenotypes observed in experimental studies after giving different perturbations to the model and simulated asynchronously. For this purpose, a study on LAT mutation was chosen, and we attempted to reproduce the experiment to observe how the phenotypic expression changes [244]. In this *in-silico* experiment, the trans-membrane protein LAT was

knocked out by keeping it constitutively in the "OFF" state so that it cannot transduce any signal downstream. The knock-out mutation of LAT, a very important protein molecule regulating the T cell signalling cascade, leads to poor proliferation of the active T-cell population (**Figure 9 A**). This poor proliferation of the T cell population could only be reverted by turning the CRAC channel constitutively ON (which reproduces the same effect as using ionomycin reported in the experiment), leading to an increased influx of calcium, which activates the calcium pathway inside the T cell.

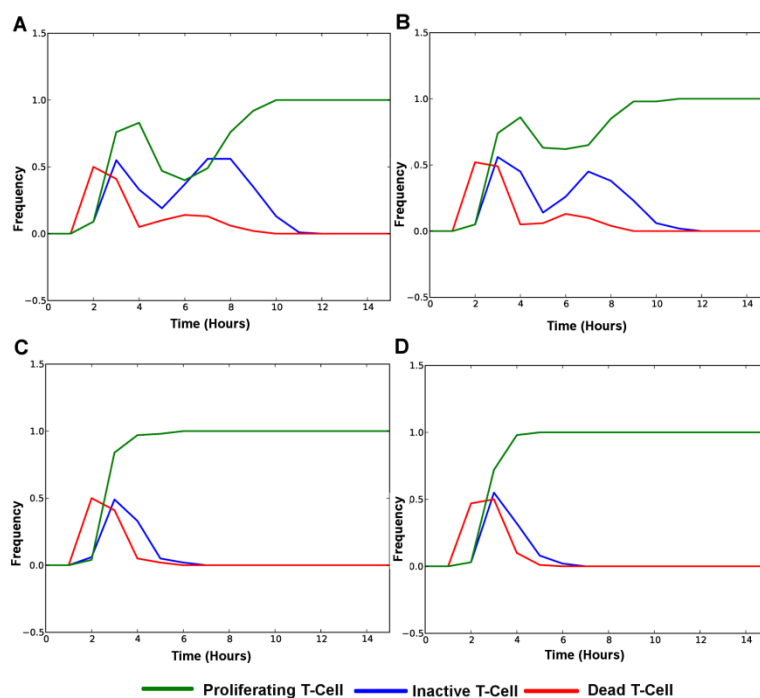


Figure 9: Cell Phenotype in different situation under LAT mutated condition. Frequencies of Proliferating T-cells, Inactive T-cells, and Dead T-cells in LAT knock-out and (A) without any stimulation; (B) TCR:CD3 and CD28 stimulation; (C) TCR:CD3, CD28 and CRAC channel stimulation; (D) only CRAC channel stimulation conditions respectively. The frequencies of Proliferating T-cell, Inactive T-Cell and Dead T-cell are shown in Green, Blue and Red lines, respectively.

Although stimulation of the TCR:CD3 complex and the CD28 co-receptor could reduce the depth of the kink in the proliferation curve, and the proliferation dynamics reached its steady state earlier compared to no stimulation scenario (proliferation reach steady state at 10th hour time-step, which signifies delayed

proliferation in **(Figure 9 A)**, and at 9th hour time-step signifying early proliferation in **(Figure 9 B)**, but it was unable to completely overcome the deficit in proliferation of the T cell population between the duration 4th to 8th hour time-steps. On the other hand, it is reported in the experiment that the CRAC channel was enough to induce a much better proliferation in the LAT mutated condition both in the presence and absence of additional stimuli, which is also observed through our simulation **(Figure 9 C- Figure 9 D)**. Similarly, in the cases of inactive T-cell frequency and T-cell death frequency curves in **Figure 9 A and Figure 9 B** show two local maxima near the 2nd and 7th hour time-points, signifying higher chances of the T cell to remain in the inactive state or die. Whereas in the CRAC active situations **(Figure 9 C- Figure 9 D)** the inactive T-cell frequency and T-cell death frequency curves show only a single peak around 2nd hour time-point signifying that in CRAC stimulated situation the probability of T cell inactivation is much reduced. The result of the simulation has also been summarized in **Table 3**.

Table 3: LAT mutation analysis

Mutation		Observation	Reference
Knock-in ('ON')	Knock-out ('OFF')		
-	LAT	Poor proliferation (Figure 4A)	[244]
TCR:CD3, CD28	LAT	Poor proliferation (Figure 4B)	
TCR:CD3, CD28, CRAC	LAT	Improved proliferation (Figure 4C)	
CRAC	LAT	Improved proliferation (Figure 4D)	

b) Effects of Co-receptor Signalling: In order to capture the effect of the co-receptor molecules and ion channel on cell phenotype dynamics, we have performed a perturbation analysis, the observations of which have been tabulated in **Table 4** and the corresponding graphs have been plotted in **Figure 10**. From here we have observed that complete sustained proliferation of the T cell population can only be achieved when TCR and co-receptors and the CRAC channel are activated together **(Figure 10 F and Figure 10 G)**. TCR when activated alone **(Figure 10 B)** show a

phenotypic behaviour similar to the no stimulation condition (all stimulations ‘OFF’ or ‘0’, **Figure 10 A**), where a high frequency of inactive cells is observed, whereas the frequency of proliferative cell is low [141].

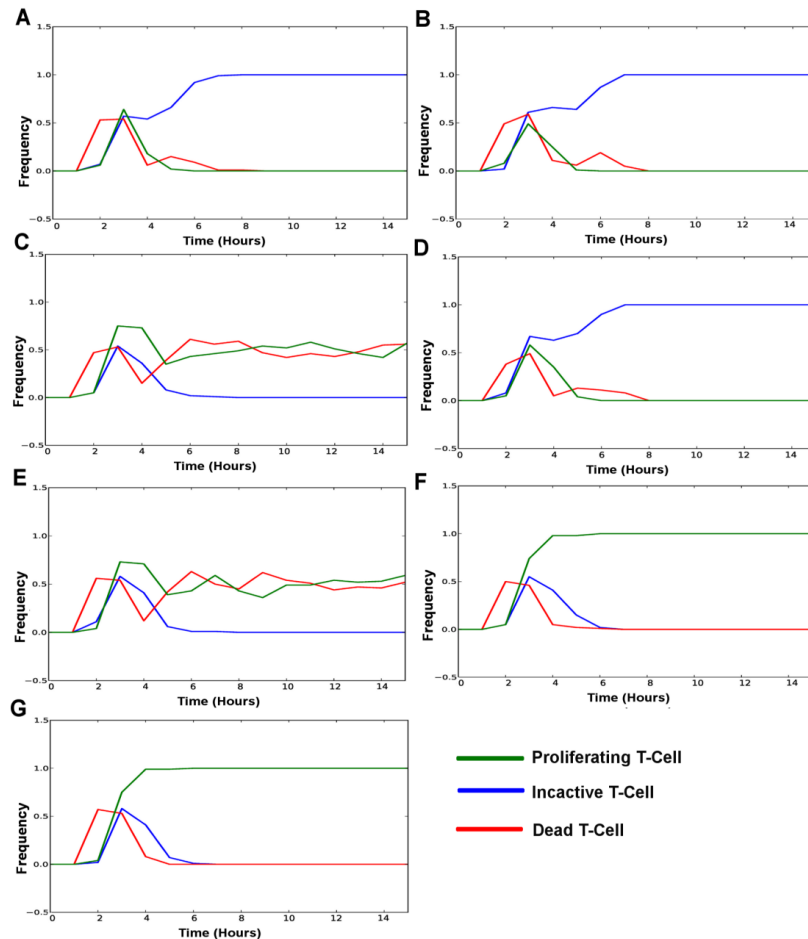


Figure 10: Effect of Co-receptor signalling on Cell fate determination. Phenotypic responses generated on different mutational analysis scenarios. (A) No stimulation. (B) TCR:CD3 stimulation. (C) Calcium channel (CRAC) as ON state. (D) Receptors and Co-receptors turned ON or activated. CRAC inhibited or OFF. (E) Only TCR:CD3 and CRAC turned ON. (F) Only TCR:CD3, CRAC and OX40 turned ON. (G) All receptors and Co-receptors turned activated or ON.

On the other hand, CRAC when activated alone (**Figure 10 C**) can lead to an increase in T cell proliferation initially [147], which after sometime starts oscillating with cell death curve due to prolonged exposure to calcium influx, which activates NFAT that controls two opposing T cell phenotypes i.e. cell proliferation and cell death

[141,147]. The situation is also similar when TCR:CD3 and CRAC are activated simultaneously (**Figure 10 E**). The importance of CRAC channel in the regulation of T cell proliferation becomes evident further in **Figure 10 D**, where we observe that in spite of all the stimulations being present, CRAC knock-down mutation blocks cell proliferation completely. The oscillation of proliferation and death curve observed in **Figure 10 C** and **Figure 10 E** could be overcome by activating the co-stimulatory receptors (**Figure 10 F** and **Figure 10 G**), where a full proliferation occurs and the cell death curve declines [160].

3.2.6. Effect of multiple mutations on Interleukin Production

Biological networks are highly robust systems, and thus a single mutation usually cannot perturb the entire signalling cascade as many alternative paths exist [245]. Diseases are mostly caused as a result of multiple mutations. The effects of such multiple mutations have also been observed in the deregulation of different cell types including T cells, where severe pathological manifestations have been observed by several research groups [89,246,247]. Simultaneously, in other experiments, significant variations in the interleukin production in different pathological conditions or diseases have also been reported [248-250]. However, the effects of multiple mutations on interleukin productions mechanism are not observed thoroughly by any other experiments and hence the mechanism, which govern these phenomenon is not clear yet. Although the effect of few co-stimulatory molecules (e.g. CD28-B7, CD40-CD40L), which regulate the interleukin production [251,252], and the deregulation in interleukin expression as a consequence of their mutation have been discretely studied, but the multiple mutation of other co-stimulatory molecules on interleukin production is yet to be analyzed extensively. Hence, in this study, we have focused on the mutations of co-stimulatory proteins CD27 and LTBR and analysed their effect on interleukin production. It is worth

mentioning that although here we have reported one multiple mutation scenario (i.e., CD27 and LTBR knockout), one can also generate different conditions using our *in-silico* model.

Table 4: Effect Co-receptor molecule knock-out in T cell proliferation

Scenario	TCR: CD3	CD4	CD28	OX40	CD40	IFNR1/R2	LTBR	TNFRSF9	TNFR	IL2R	ICOS	PD1	CTLA4	CRAC	Observation	Ref
No stimulation	0	0	0	0	0	0	0	0	0	0	0	0	0	0	No proliferation, but the cells survive in its inactive state (Figure 10 A)	[253]
TCR:CD3 stimulated	1	0	0	0	0	0	0	0	0	0	0	0	0	0	No proliferation, but the cells survive in its inactive state (Figure 10 B)	[141]
CRAC activated	0	0	0	0	0	0	0	0	0	0	0	0	0	1	T cell proliferation rises initially, but later begins to oscillate with the death curve. Number of inactive cells decline (Figure 10 C)	[147]
All activated CRAC inhibited	1	1	1	1	1	1	1	1	1	1	1	1	1	0	No proliferation (Figure 10 D)	[147]
TCR:CD3 and CRAC activated	1	0	0	0	0	0	0	0	0	0	0	0	0	1	T cell proliferation rises initially, but later begins to oscillate with the death curve. Number of inactive cells decline (Figure 10 E)	[147]
Co-stimulatory receptor activated	1	0	0	1	0	0	0	0	0	0	0	0	0	1	T cell proliferation; T cell death curve declines (Figure 10 F)	[160]
All receptors and Co-receptors activated	1	1	1	1	1	1	1	1	1	1	1	1	1	1	Full T cell proliferation observed (Figure 10 G)	[142]

a) **CD27 and LTBR knock-out scenario:** The co-stimulatory receptors CD27 and LTBR (influencing the NF κ B pathway) are involved in increased T cell proliferation [254,255], and the mutations of these molecules have been implicated in different immune-deficient conditions [256,257]. In this study, we have observed that CD27 and LTBR together are responsible for the regulation of cytokine production. Using this *in-silico* knock-down model of CD27 and LTBR proteins, we have observed that mutation of these molecules may lead to a significant decrease in cell proliferation (**Figure 11 B**) as compared to the normal scenario (**Figure 11 A**), by decreasing the interleukin production (**Figure 11 C- Figure 11 D**). As compared to the normal scenario of interleukin expression pattern (**Figure 11 B**), the mutation analysis shows these co-stimulatory receptors can regulate 6 out of 11 interleukin molecules considered in our model, out of which the expression patterns of five interleukins show an oscillatory behavior (*viz.* IL1, IL12, IL3, IL6 and IL8) while IL2 shows a delay in activation (**Figure 11 D**). The down-regulation of these six interleukins, which are mostly involved in T cell proliferation, accounts for the decrease in T cell proliferation and rise in T cell death phenotype as shown in **Figure 11 C**. As the mutation of these molecules is not involved in controlling the normal cell cycle proteins, the function defining the probability of T cell survival (denoted by the frequency of Inactive T cell) remains unchanged.

b) **Fluctuations in intermediate proteins and other output proteins:** To find out the reason/ mechanism for the deregulation of the interleukin production and the change in phenotypic dynamics, we performed the Mann Whitney U test, where we found that the mutation of these two genes leads to an altered expression of 25 genes in the entire network. Here, we observe that in addition to the NF κ B pathway (NIK-mediated non-canonical NF κ B pathway) molecules, CD27 and LTBR can also regulate the expression of the MAPK pathway molecules (MEKK, MKK4/7, COT, GCKR) and the JNK pathway molecules (T3JAM), which again is responsible for the

regulation of a collection of other important T cell molecules that regulates its proliferation, survival and effector functions. The remaining molecules that are regulated by these co-receptors include TRAF2, TRAF3, IL2R, GMCSF, CCL19, VEGF, GLK, RIP1, TAK:TAB complex and IKK-Alpha, that plays a very important role in the regulation of T cell activity. CD27 and LTBR also regulate the expression of TRAF1, which is known to have an inhibitory effect on NFKB [258]. Here, we further observed that a knock-out of TRAF1 can nullify the effect of CD27 and LTBR mutation to a great extent (data not shown).

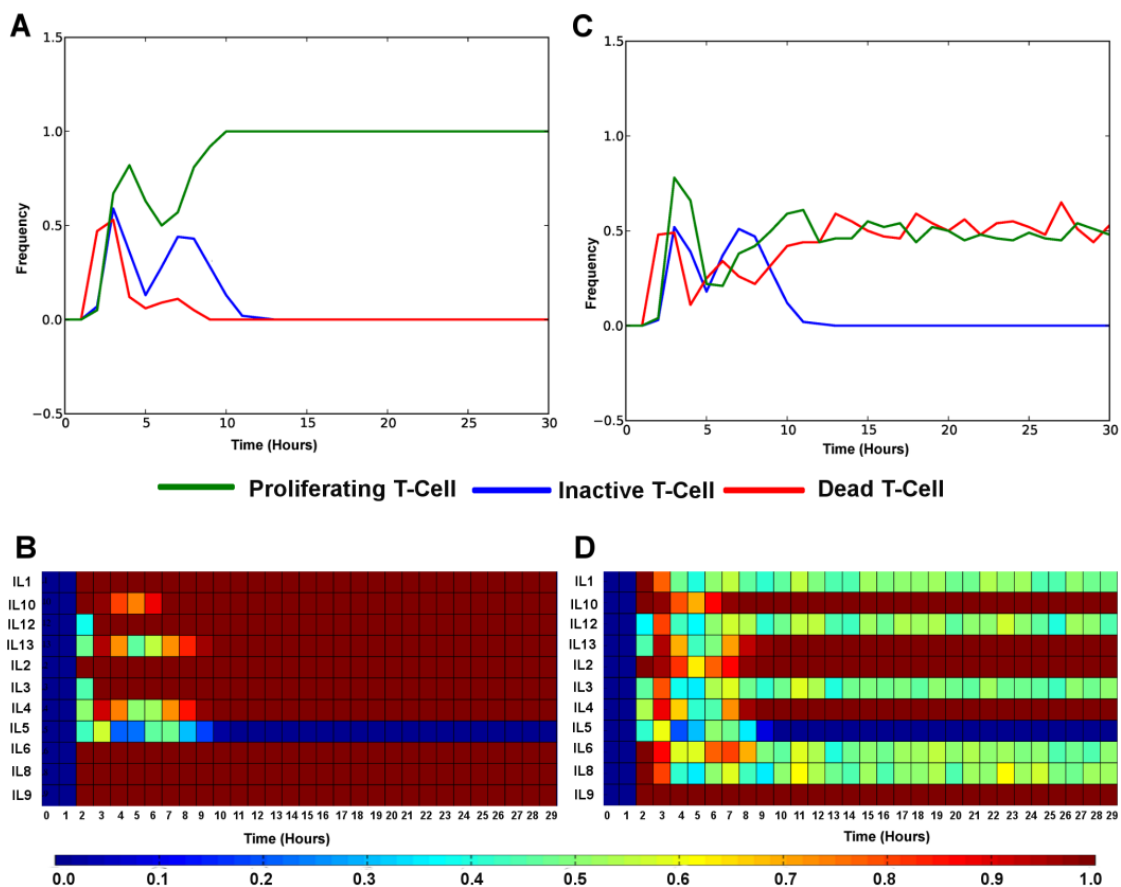


Figure 11: Changes in Cell Phenotypes and corresponding Interleukin Expression pattern due to CD27 and LTBR mutation. (A), (B) normal condition; (C), (D) CD27 and LTBR mutated condition.

3.3. Discussion

The study of T-cell signalling pathway is an essential prerequisite to the identification of the immune-stimulatory targets for the treatment of different diseases. Hence, in order to gain a holistic understanding of the signalling events regulating the T-cell activation and effector functions, the pathway data from various signalling pathway databases and literature sources (including the pathway information from the previously mentioned models) were collated. The reconstructed T-cell signalling network consists of the core TCR mediated pathway along with the pathways triggered by all the co-stimulatory, co-inhibitory receptors and the calcium channel CRAC that are crucial for the production of the various cytokines, chemokines, microbicidal molecules that mediates the T-cell immune responses and maintains its homeostasis (**Figure 7**). The pathway integrates discrete information about the regulatory mechanisms, from known experimental studies, in one frame that are missing in most of the biochemical pathway databases. Since we have used Protein-Protein Interaction (PPI) data to reconstruct the pathway and build our model, we have been able to incorporate the effect of other crosstalk molecules (e.g. components of the MAPK pathway) and feedback loops regulating the cellular phenotype to understand its role in the regulation of the T-cell immune responses and its state of activation or inactivation in response to various external stimuli and micro-environmental conditions.

Using a semi dynamic Boolean modelling approach the protein interactions of the network have then been translated into logical equations according to the regulation of a single or a combination of proteins on the expression of another downstream protein in the network, in a biologically relevant way. Binarized time series microarray data of naïve T-cell activation process was used to initialize and validate the model using synchronous and asynchronous logical update rules (**Appendix A:**

Figure A. 1 and **Table 2**). While the results from the synchronous simulation returned a deterministic value of the protein expression showing a clear up or down-regulation of the protein expression in our model, the asynchronous simulation was performed to observe the gradual variation in the protein expression pattern over time (**Figure 8**). This approach gave us the advantage of analyzing the changes in the signal propagation through the T-cell pathway in response to various *in silico* perturbations mimicking the selective activation/inactivation of the co-stimulatory pathways under various antigenic challenges. This helped us to gain a better insight into the dynamics of signalling events in the T-cell network as compared to other T-cell models that have been developed using the Boolean formalism [228-231].

The equations (**Eq.4**, **Eq.5** and **Eq.6**) formulated to study the phenotypic behaviour of the T-cell were standardized with the minimum combination of proteins that are required for the maintenance of the T-cell functional activation, which is also, validated using various perturbation experiments reported in different literatures. Using this approach, we have then tried to answer how the co-receptor molecules and the Calcium channel regulate the cellular behaviour of T-cell. Through a careful study of the signal propagation through the network using Mann-Whitney U Test we have been able to identify the precise routes of this signal propagation that regulates the Interleukin expression of the T-cells.

Our model analysis captures the effect of CRAC channel in the regulation of the T-cell proliferation, under LAT mutated conditions, where we demonstrate that the mutation of the channel leads to a suppression of proliferation under any circumstances, i.e. even if all the other stimulation and co-stimulations are present. The observation from our model corroborates well with the experimental findings [244]. Thereafter using multiple *in silico* knock-out analysis we try to identify the minimal combination of the co-receptor molecules that can stimulate and maintain a

sustained proliferation of the T-cell. Here we observed that the activation of the TCR:CD3 complex, the CRAC channel and the OX40 molecule are enough to sustain the T-cell proliferation even when the other co-receptor mediated signalling pathways are inactive. The model analysis further establishes the role of the co-receptors CD27 and LTBR in the regulation of the T-cell effector functions that are essential for the generation of T-cell immune responses. *In silico* mutation studies clearly brings out the role of these molecules in maintaining the T-cell functionalities and regulation of the levels of interleukin production *viz.* IL1, IL12, IL3, IL6, IL8 and IL2 (**Figure 11**). Our studies also reveal the precise route of signal propagation of the effects of the mutations where we have seen that deregulation of the molecules (*viz.* MEKK, MKK4/7, COT, GCKR, T3JAM etc.) involved in the MAPK and JNK pathways, as a result of the mutation, is the cause of the observed changes in the behaviour of interleukin production.

Although the main limitation of our modelling approach is its inability to capture the concentration specific data of signalling molecules for which we need better dynamic model with precise kinetic data, nevertheless the model is able to capture the dynamic regulation of the T-cell activation dynamics and agrees with the published experimental data. In this model, we have tried to integrate various aspects of T-cell activation pathway by using simple but powerful, discrete logical modelling approach. The key advantage of the model is that it only requires the logical relationship between the proteins at the time of signal transduction and does not depend on any kinetic rate parameter values; hence, it is easier to implement and simulate temporal protein expression patterns with less time and effort. Using our model, one can also perform different predictions and can monitor the temporal protein expression patterns as well as the effect of phenotypic responses *in-silico*. By generating the temporal protein expression patterns in the signal flow network for different pathological conditions, it becomes easier to monitor the proteins, which

are getting activated or inhibited throughout a specific interval of time. This proposed computational approach and analysis to study the protein expression pattern generation will not only be useful for study of various T-cell phenotypic behaviours but also be helpful for the future researchers to develop therapeutic strategies to combat against various immune diseases as has been demonstrated in **Chapter 4**.

CHAPTER 4

IDENTIFICATION OF T_{H1}/T_{H2} REGULATORY SWITCH TO PROMOTE HEALING RESPONSE DURING LEISHMANIASIS

4.1. Motivation

The general therapeutic strategy adopted for the treatment of Leishmaniasis is primarily aimed to expedite the process of parasite clearance for faster healing by stimulating the T_{H1} or healing response. In case of Cutaneous Leishmaniasis therapeutics, chemotherapeutic drugs, such as Pentavalent antimonials, liposomal amphotericin B have been shown to be useful to reduce the dermal lesions and the chances of further destructive mucosal inflammations and visceral infections [66,67]. However, the successive clinical studies have shown that these chemotherapeutic drugs are also associated with adverse side effects, such as nausea, intense headache, diarrhoea, musculoskeletal and abdominal pain etc. [67-71]. In several cases, relapse of the disease and developing resistant strains are also reported after the use of these drugs, which necessitates the development of better treatment protocols with higher clinical efficacy [72]. Although immunotherapeutic strategies involving the administration of exogenous Interferon Gamma is found to be effective in suppressing Leishmaniasis [73,74], the high production of IL10 during early stage of infection often suppresses its activity, thereby hindering the Nitric Oxide (NO) production and disease clearance [75]. Based on these experimental outcomes, a number of mathematical models have also been proposed simultaneously to untangle the complexities that appear as hurdles to devise a successful treatment strategy in Leishmaniasis [259,260]. In one of such studies, "granulomas" formation during *Leishmania donovani* infection has been modelled using Petri net analysis by considering the inter-cellular interactions of macrophage, lymphocyte, NK cells etc.

The outcomes of these cell population based models have emphasized cytokine therapy by the exogenous injection of Interferon Gamma and the suppression of IL10 to eradicate the *Leishmania* pathogens in macrophage cell [261]. However, Interferon Gamma molecule is a pro-inflammatory molecule and also has short half-life time, which in turn requires its repeated administration into the body at a regular interval of time that may have harmful consequences [262,263]. Hence, to circumvent these problems, implementation of better therapeutic strategies, by identifying novel drugs, drug target molecules and immunostimulators are required and demands higher attention from the vast majority of clinical and experimental pharmacologists.

However, in order to develop an effective immunotherapeutic strategy, it is important to have a comprehensive understanding of the T_{H1}/T_{H2} dichotomy in Leishmaniasis so as to identify the regulators through which the T_{H1}/T_{H2} switching behavior can be effectively controlled. The identification of such important molecular switch and their corresponding reaction routes through which the immunostimulation could be enhanced is highly required in this field of study. As the exact intra-cellular reaction cascades governing the T-cell response after encountering with *Leishmania* infected APCs is not clearly understood yet, the mechanisms through which this response dynamics and the Nitric Oxide (NO) production work in the immune cells is still unknown. Besides, the mechanism through which the *Leishmania* antigens override the APCs intra-cellular network by varying the expressions of the immunostimulatory proteins, and force to redirect the immune responses towards the non-healing or T_{H2} response is not comprehensively studied yet. The study of these regulatory mechanisms by analyzing such a large system using conventional experimental techniques is time consuming and also difficult to perform, and therefore *in-silico* mathematical models of inter and intra-cellular reaction cascades in APC and T-cell in presence of *Leishmania* antigens would probably be the best strategy to counteract these problems. This may also

help to address some of the unexplored questions of *Leishmania* immunotherapy, such as the limitations of the Interferon Gamma treatment, the reason for which Interferon Beta treatment is only effective at low doses and the means by which the Toll-like Receptor (TLR) molecules expressed by the APCs can regulate the immune responses of the T-cell to shift the dynamics towards a higher healing T_{H1} response [75, 264-266].

In this study, we have tried to address the above mentioned problems in *Leishmania major* infection scenario by using mathematical model and *in-silico* analysis. We have hypothesized that in order to achieve better therapeutic results without adverse side effects, the stimulation of Type-I T-helper cells (T_{H1}) and a simultaneous up-regulation of NO production by using immunostimulator would be the best therapeutic strategy to clear the *Leishmania* pathogens from the body. In order to develop a suitable *in-silico* model that may enhance our understanding of *Leishmania* immunobiology, we have manually reconstructed a comprehensive cell signalling pathway map of a *Leishmania* infected APC and a normal $CD4^+$ T-cell (helper T-cell), considering the important physical interactions and the cross-talks by the secreted diffusible molecules between the two cells (**Section 2.1.2**). The *Leishmania* infection has been introduced in the model by establishing the interaction of the *Leishmania* antigens, known from the literature and databases, with the appropriate host protein molecules in the APC. However, the dynamic analysis of such a large network is difficult to perform due to the unavailability of kinetic parameters and concentration values. Hence, to assess the gene or protein expression patterns of large scale signal transduction networks under different pathological conditions, the concept of discrete dynamic Boolean or logical modelling approach has been utilized successfully [89,267,268]. Large scale, intracellular T-cell signalling network is also analyzed by using this modelling technique and eventually various structural and functional properties of this network under normal and disease conditions are

studied successfully [269,270]. A logic based modelling technique is also applied to analyze the temporal expression patterns of the genes/proteins of T-cell, which are strongly influenced by the intra-cellular T-cell signal transduction cascade in the presence or absence of infection [122].

Here, the entire reaction mechanisms are translated into logical equations with the objective to simulate and understand the effect of the presence and absence of the *Leishmania* antigens on the signalling events of the host's APCs and T-cells (**Section 2.2, Appendix B: Table B. 4**). Followed by the Boolean attractor analysis (**Section 2.2.7**) and the successful validation of the simulation outcomes with the time-course microarray expression data as well as the phenotypic responses obtained from published experimental observations, the model is then used to compare the protein expression pattern for normal and *Leishmania* infected scenarios. With an aim to understand the mode of regulations that occur due to the infection at the molecular level inside the T-cell, the comparison of the two scenarios is then used to extract the important T-cell proteins, which are highly influenced under the pathogen burden. The result of this analysis is further used to predict the unknown changes occurring at the pathway level in the T-cell during infection. Moreover, the knowledge of these de-regulated pathways is thereafter used to predict the targets for the *in-silico* perturbation analysis. Perturbations of the logical states of proteins in the network are performed to study the effect of the known immunostimulants (*viz.* IL12 and Interferon Gamma) as well as to propose some new combinations of molecules that act as a molecular switch to regulate the T_{H1}/T_{H2} and NO response dynamics. Subsequently, these identified novel combinations of proteins were tested for stability and robustness by examining the attractors of the system under these perturbations. Thereafter it was ascertained that the proposed combinations of protein targets can be used as the potential immunomodulators, targeting of which may bypass the inhibitory activities of the pathogens and enhance the anti-

Leishmania immune responses as well as the microbicidal activities of the body's immune cells.

4.2. Results

4.2.1. Pathway Enrichment

The gene clusters identified from the co-expression networks of the two microarray expression data sets can be considered as the "functional modules" of the gene interaction networks of the *Leishmania major* infected APC and the activated T-cell respectively (**Section 2.1.2.1**). Total 10 and 24 clusters or functional modules are found from the gene co-expression networks of APC and T-cell respectively (**Appendix B: Figure B.1, Figure B.2**). Pathway enrichment analyses of the genes found in these clusters have identified various important intracellular signalling pathways (e.g. Cytokine-cytokine receptor, Toll like receptor, JAK-STAT, MAPK, mTOR, T-cell receptor, Calcium signalling, PI3 kinase, Interleukin signalling pathways etc.) of two different cells. The complete list of the pathways found to be enriched in this analysis for APC and T-cell are given in **Appendix B: Table B.1, Table B.2** respectively. These enriched pathways, corresponding to the significantly expressed genes of APC and T-cell microarray expression data sets, represent the pathways that are influenced by the *Leishmania* pathogen in the APC and in the activated T-cell. However, it should be noted that the pathways found to be enriched in this analysis do not provide a complete understanding of the molecular mechanisms through which the pathogen infect the APCs. Also, we are unable to capture the dynamic interactions of the APC and T-cells' molecules in the *Leishmania* infected scenario. Hence, the reconstructions of the complete inter- and intra cellular signalling cascades regulating the APC and T-cell functions are performed.

4.2.2. Features of the Reconstructed Pathway

The reconstructed pathway network integrates all possible inter-cellular and intra-cellular signalling events that occur between the two immune cells during *Leishmania* invasion (**Figure 12**). Here the interaction of the *Leishmania* molecules, produced from the promastigote and the amastigote forms, with the APC molecules are considered separately. The entire signalling network (i.e., intra and inter cellular) consists of a total of 293 nodes, which includes 82 APC molecules, 206 T-cell molecules, and 5 *Leishmania* related molecules, that are involved in more than 400 protein-protein interactions. The intra-cellular signalling cascades considered for modelling the APC and the T-cell consists of the major co-receptor signalling pathways, the cytokine pathways, TLR pathways, etc. that play a pivotal role in regulating the outcome of the immune cell's functional responses. In case of APC, the pathways, which are considered in our model, include the CD40 pathway, the Interleukin pathways (viz. IL4, IL6 and IL10), TLR pathways (TLR2, TLR3, TLR4), and the pathways involved in TNF_ALPHA, IFN_GAMMA signalling. Again in T-cell, in addition to the core TCR mediated signalling, seven co-receptor signalling pathways (viz. CD28, CD27, LTBR, CTLA4, ICOS, PD1 and OX40), cytokine pathways (viz. IL1, IL2, IL10, IL12, TNF and IFN mediated pathways) and the CRAC channel mediated Calcium pathway are considered.

Various crosstalk reactions are also considered in the model, which depicts the bi-directional regulation that exists between the two immune cells. These crosstalk reactions mainly comprise of the juxtacrine signalling events stimulated directly by binding of the co-receptors and the ligand molecules expressed on the T-cell and the APC membranes, and the paracrine signalling that are mediated by the diffusible output molecules (mostly cytokines) produced by each cell. Overall, 10 crosstalk interactions between the T-cell and the APC that effectively regulates the expression

pattern of each other are considered. These include IFN_GAMMA_T, IL4_T, IL6_T, IL10_T, TNF_ALPHA_T molecules secreted from the T-cell, and IFN_BETA, TNF_ALPHA, IL12 secreted from the APC that diffuses and activates their corresponding receptor/co-receptors on their neighbouring cell to trigger their downstream signalling cascades. The co-receptor ligand molecule interaction considered to be the most important in the model is the one that involves the binding of the CD40 and CD40L_T molecules [271].

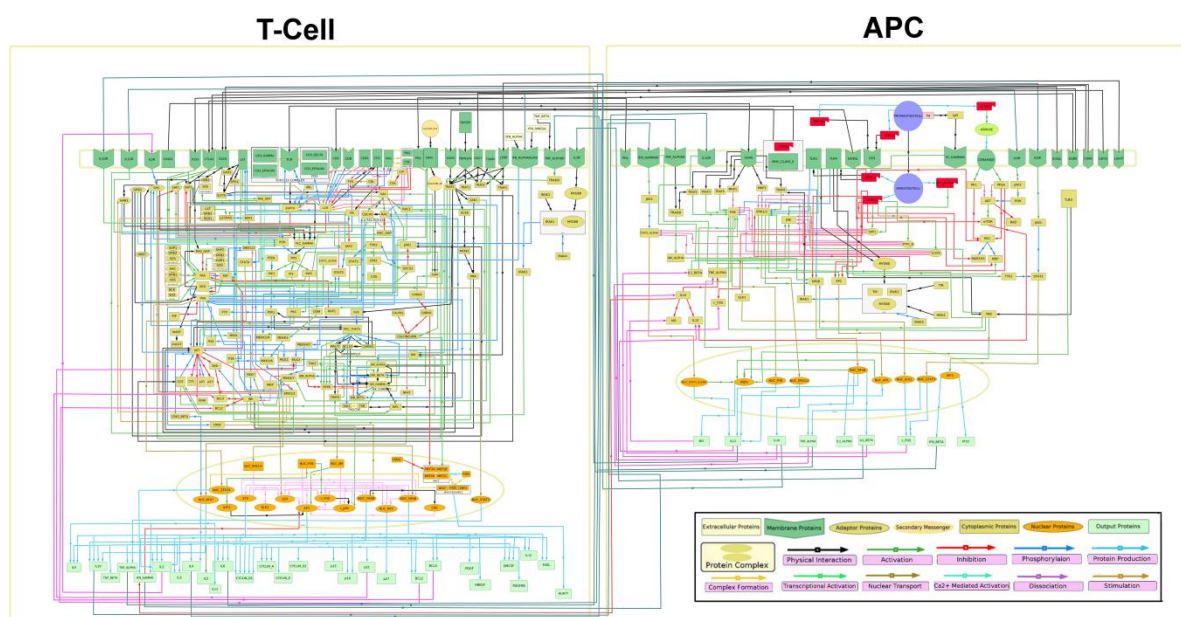


Figure 12: Reconstructed diagram of T-cell, APC and *Leishmania* pathogenic protein-protein interaction network. The diagram presents an integrated view of the T-cell and APC interaction signalling pathway during *Leishmania* infection. The different molecules involved in the signalling cascade have been color coded according to their type and cellular location. The molecules colored as red signify the *Leishmania* antigen molecules. The interaction lines have been color coded according to the type of chemical reaction such as phosphorylation (blue), inhibition (red), activation (green) etc.

The model depicts the physical binding of the T-cell and APC receptors/co-receptors with their corresponding ligands and the subsequent activation mechanism of the downstream proteins in both the cells. The model considers the activation of Toll-like-receptor proteins, present in the APC membrane, activate their downstream

proteins, which in turns diverges into important signalling routes such as the RAS-RAF mediated MAPK pathway, canonical and non-canonical NFKB pathway, JAK-STAT pathway, PI3K-PLC Gamma pathway, JNK pathway, etc., and leading to the activation of several transcription factors (e.g. ERK1_2, NFKB, NFAT, AP1, STAT3, etc.) in the nucleus, that in due course, singly or in combination with other transcriptional co-factors initiates the mRNA transcription [119]. These mRNA are then considered to undergo alternative splicing to produce different proteins isoforms with diverse biological functions that regulate the expression of the output molecules. During *Leishmania* invasion, the antigenic molecules produced by the pathogen activate certain phosphatases (e.g. SHP1, PTP1_B, TCPTP, etc.) that interfere with the signalling events of the APC. The antigen molecules considered in the network, such as LPG_L, GP63_L and EF1_Alpha, are shown to have a direct effect on the activities of the ERK1/2 and AP1 transcription factors, the former being up-regulated and the latter inhibited or degraded (a detailed description of all the signalling events have been provided in **Section 2.1.2.2**).

4.2.3. Model Analysis

4.2.3.1. Attractors

The Boolean attractor analysis performed on 20 independent random samples in the uninfected and the infected scenarios have been plotted in **Figure 13**. Here 128 combinations of input in each of the 20 samples have been grouped together with a specific color code (**Section 2.2.7**). For simplicity, for the attractor only the sequence of logical states of the molecules in the order of IFN_BETA, IL10, IL12, IL1_ALPHA, IL1_BETA, INOS, IP10, NO, TNF_ALPHA and c_FOS, is depicted in the network graph. The results of the analysis reveal that given all the FACTORs regulating alternative splicing is assumed to be in ON state, all the 2560 combinations of input (called basins of attractor; each basin is represented as a node in the network graph)

in the uninfected scenario, reaches the same Boolean attractor (...0111110111...) (**Figure 13a**), while in the infected scenario four different attractors are obtained, *viz.* (...1100001011...), (...0101100011...), (...1101101011...) and (...0100000011...) (**Figure 13 b**). However it is to be noted in the infected scenario, 2000 among the 2560 basins (i.e. 78.125%) reached the (...1100001011...) attractor (including both steady state and cyclic attractor), hereby referred to as the major attractor of the system in the infected scenario. These 2000 basins of the major attractor spans all the 20 random samples selected, among which 13 samples exclusively drive to the major attractor, while the remaining 7 samples reach multiple attractors. The (...1101101011...), (...0100000011...) and (...0101100011...) attractors have been attained from 9.375%, 9.375% and 3.125% basins respectively.

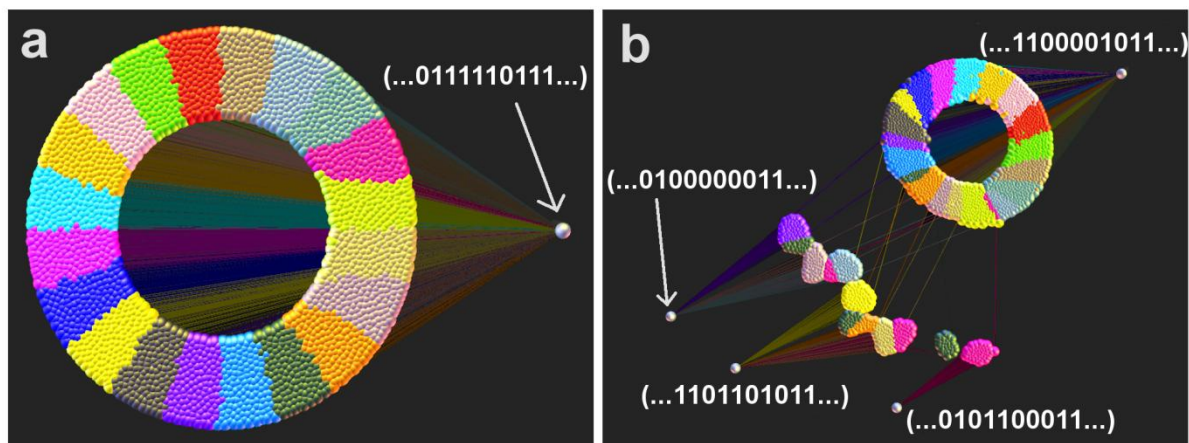


Figure 13: Boolean attractor analysis in (a) uninfected and (b) infected scenarios. The binary values shown in the attractor represents the logical steady state values of 10 macrophage output proteins in the sequence of IFN_BETA, IL1_ALPHA, IL1_BETA, IL10, IL12, INOS, IP10, NO, TNF_ALPHA, and c_FOS respectively. Different color codes are used to represent the 20 different random samples, and within each sample 128 nodes represent the input combinations of 7 proteins selected randomly from 51 inputs of the model. In total there are 2560 combination of initial states denoting the basins of attraction for the entire system.

4.2.3.2. Model Validation with Experimental Data

The temporal expression profiles of the APC output molecules *viz.* c_FOS, IL1_ALPHA, IL1_BETA, IFN_BETA, IL10, IL12, IP10, INOS, NO, TNF_ALPHA in

the infected (red) and the uninfected scenarios (green) are plotted along-with the binarized microarray data at 0, 2, 4 and 8 hours' time-points (black diamond) in **Figure 14 (Section 2.2.4)**. This figure depicts that the expression levels of all the 10 output molecules are reaching the steady state values either at 1 (i.e. up-regulation) or 0 (i.e. down-regulation). Here we observe that the expression value of the output molecules at steady state is exactly similar to the value obtained as the major attractor of the system in both the uninfected as well as the infected scenarios (**Figure 13**). Qualitative comparison of the expression values reveals that out of these 10 selected output molecules, the steady-state expression value of total 7 molecules *viz.* c_FOS, IL1_ALPHA, IL1_BETA, IL10, IL12, INOS and NO in the infected scenario shows the exact match with the experimental observations [114]. While c_FOS and IL10 show an expression value of 1 (high expression) in the infected scenario, the other output molecules such as IL1_ALPHA, IL1_BETA, IL12, INOS and NO has an expression value of 0 (low or no expression) in the infected scenario.

Also, **Figure 14** depicts that at "4 and 8 hours" time points, c_FOS and IL10 proteins get up-regulated in the simulated infected scenario, which is exactly comparable with the experimentally observed expression levels in microarray data at the same time points. However, it should be noted that although the expression level of c_FOS protein at "2 hours" time point in the simulated infected scenario is not exactly matching with the experimental findings, but the infected model is able to show the down regulation of this protein between the intervals of "0 to 1 hour" time points. Both the proteins IL1_ALPHA and IL1_BETA get up regulated at "1 hour" time point and subsequently get down regulated at "6 hours" time point of the simulated infected scenario. In the experimental data, both of them get up-regulated at "2 hours" time point and get down regulated at "4 hours" and "8 hours" time points respectively.

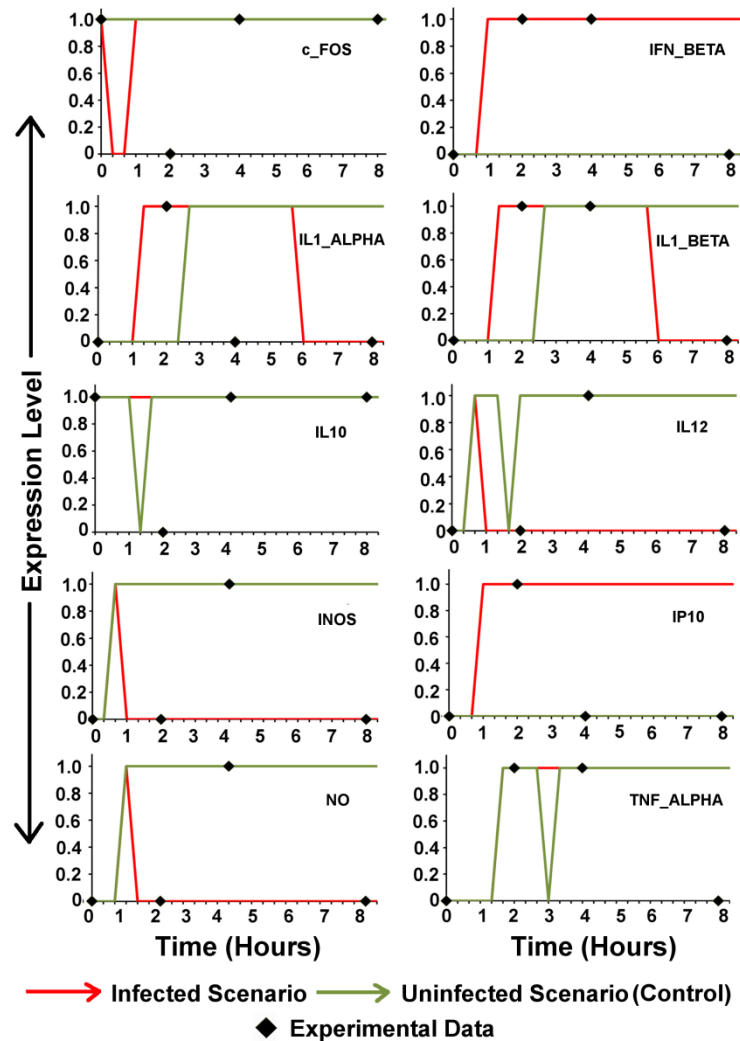


Figure 14: Time-course expression profile of APC output molecules. Expression levels of the output molecules c_FOS, IFN_BETA, IL1_ALPHA, IL1_BETA, IL10, IL12, INOS, IP10, NO and TNF_ALPHA found in infected, uninfected and experimental conditions. The validation was performed by comparing the expression levels of the infected situations (shown in red) with the microarray experimental data (black diamond).

In case of IL12, it is observed from **Figure 14** that except a small time-interval between 0 and 1 hour, this protein remains in the down regulated state throughout the rest of the time points. The time course microarray data of this protein also shows similar expression level except at “4 hours” time point, in which this protein shows up-regulation. Similarly, INOS and NO also show similar expression level at “2 and 8 hours” time points as compare to the experimental data. Altogether, the

percentage of validation of the simulated *L. major* infected scenario for all the 10 selected proteins at all the three time-points i.e., 2, 4 and 8 hours are 80%, 50% and 70% respectively.

Also, it can be observed that 9 out of 10 output molecules match exactly at least at two time-points. Even though in few cases, the simulation results of the expression values at a particular time point show an apparent mismatch with the experimental observation at that same time point, but the expression pattern essentially remains the same over time. It can be observed that although the time-course expression of c_FOS from the simulation results appear to be inconsistent with experimental data, i.e., down-regulation at 2 hours' and again up-regulation at 4 hours' time point, the overall dynamics of the expression essentially remains the same over time, with only a slight deviation of the expression levels (up or down) observed in the respective time points of experimental and simulation data. Such deviations are also observed in the expression dynamics of IL1_ALPHA, IL12, NO and INOS molecules. The successful validation of the expression levels of these molecules can be used as valuable indicators of the immune functions of the APC and can be used for fine-tuning of our model to ensure its proper functioning. On the other hand, **Figure 14** also brings out the differences in the expression of the APC output molecules due to the presence of the infection. Here it is observed that even though the steady state values of the two scenarios (viz. infected and the uninfected) is sometimes similar, as in the cases of c_FOS, IL10 and TNF_ALPHA, the overall temporal expression pattern clearly indicates the differences are emerging due to the presence of antigen molecules in the model simulation. In the uninfected scenario, the expression of the IL10 and the TNF_ALPHA remains low (in the first few hours) as compared to the infected scenario.

4.2.3.3. Comparison of Uninfected and Infected Scenarios

The interference of *Leishmania* proteins in the signalling cascade of APC cell not only modulate the expression of the output molecules and microbicidal activities of APC, but also deregulates the expression of the T-cell output molecules by manipulating the normal functioning of T-cell activation pathway [272]. Comparing the expression of the APC output proteins in infected and uninfected scenarios (**Figure 15 a, b**), the simulation results show that invasion of *Leishmania* antigen molecules severely down-regulates the expression of IL12, which is a potent T-cell stimulator [24,27]. Simultaneously, the production of INOS and Nitric Oxide (NO) is also greatly reduced in the infected APC, thereby rendering the cell incapable of performing its microbicidal functions, and creating an immune-suppressed condition, which is favourable for the continued survival of the pathogen inside APC [24,271]. Besides, in **Figure 15 b**, the production of IFN_BETA, IP10 (a chemokine) also show an up-regulation, indicating an attempt of the APC to eliminate the pathogen from the system [114,266,271]. IL1_ALPHA and IL_BETA show minor fluctuations in expression during the infection and slight down-regulation [24,273]. The effect of *Leishmania* infection on the expression pattern of T-cell output proteins (**Figure 15 c, d**) becomes evident from the fact that production of the protective cytokine from the cell, such as IFN_GAMMA_T, is down-regulated during the infection, while the productions of interleukins, such as IL10_T, IL4_T, IL5_T and IL6_T are up-regulated, which are mostly implicated as proteins favouring *Leishmania* survival [150,272,274,275]. These results supported by the previous experimental findings also strengthen the validity of our model to a greater extent and enhances its acceptability for further analysis.

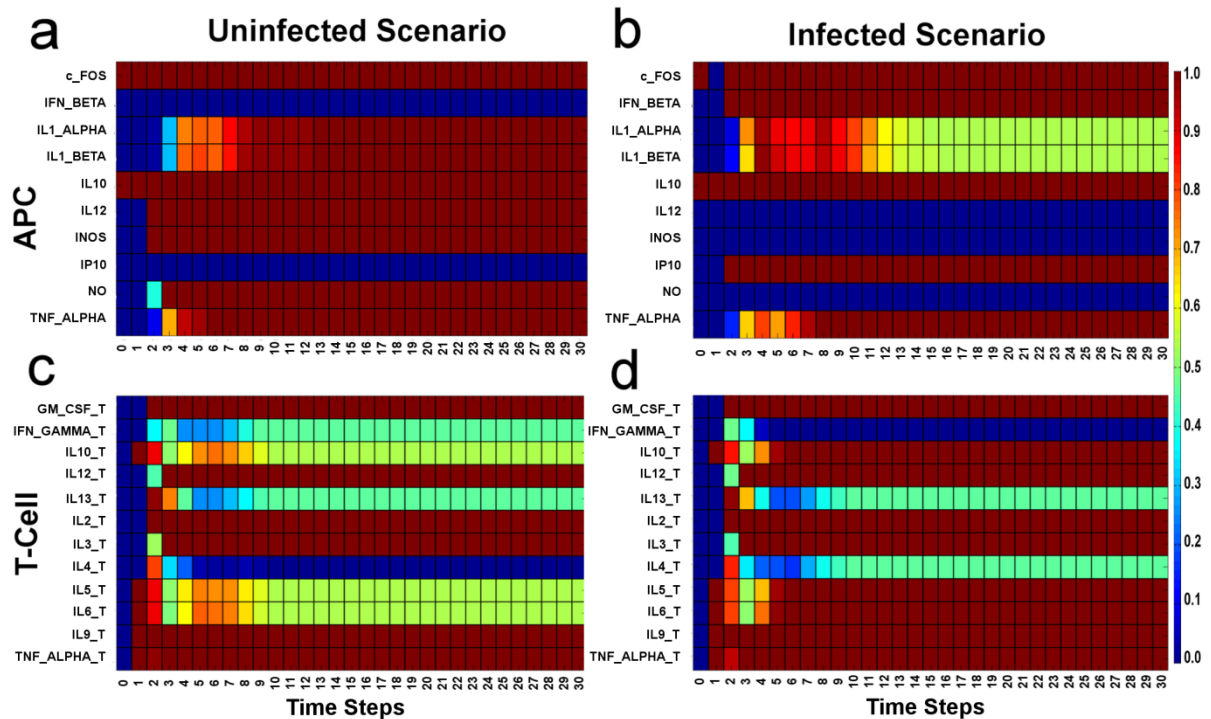


Figure 15: Expression profile of T-cell and APC during asynchronous simulation. (a) and (b) Expression of the APC output molecules in the uninfected and infected scenarios, respectively; (c) and (d) Expression of the T-cell output proteins in the uninfected and the infected scenarios, respectively.

4.2.3.4. Effect of infection on T-cell signalling cascade

The results of Mann Whitney U test reveal that out of the expression of 62 proteins in the infected scenario that exhibits a deviation from the uninfected scenario, 20 proteins get significantly de-regulated ($p < 0.05$). The temporal expression profiles of these 20 proteins (**Figure 16**) show that the *Leishmania* infection causes the significant down-regulation of the protective cytokines, such as IFN_GAMMA_T, and enhances the synthesis of TGF_BETA_T and IL10_T from the T-cell, which contributes to the decline in the immune-competency of the T-cell and formation of an immune-suppressed condition as observed during *L.major* infections in susceptible patients [26,27,276,277]. It is interesting to note that while the activation of the cytokines, such as IL4_T, IL5_T, IL6_T and the receptors, IL12R_T [275] and IL1R_T [278], show fluctuations with respect to the control (uninfected scenario), certain other

molecules, such as RAP1_T, P19_T, C3G_T, CRKL_T, TYK2_T and SOC3_T, are distinctly up-regulated as a result of the infection. Also, it is observed that the members of the JAK-STAT pathway, such as JAK2_T and STAT4_T are down-regulated in the infected scenario (**Figure 16 b**).

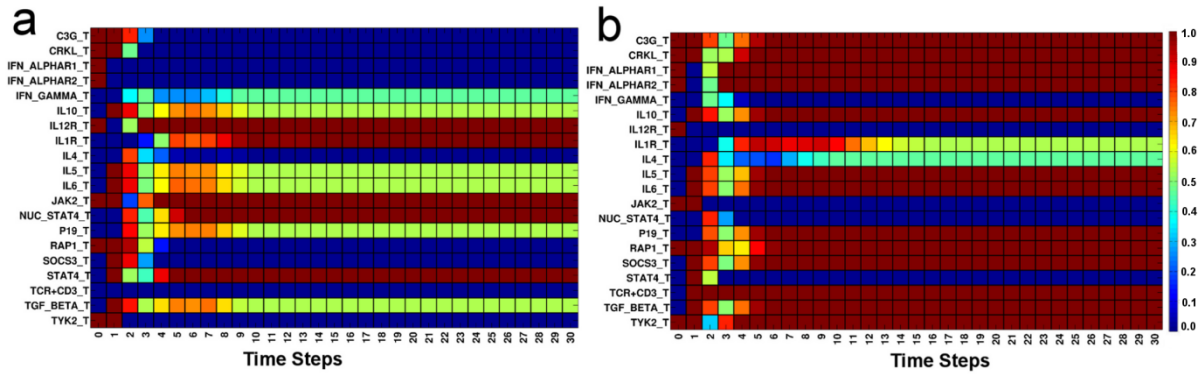


Figure 16: Expression profile of 20 T-cell proteins which shows significant de-regulation in Mann-Whitney U test. The heat maps depict the protein expression pattern of the T-cell signalling proteins under (a) Uninfected scenario (control); (b) Infected scenario. Significant changes in the expression dynamics are observed for these proteins under these two conditions, which clearly show the effect of *Leishmania* antigens in the regulation of T-cell signalling events.

4.2.3.5. Immune Response & Immunotherapeutic Strategies

The effector molecules produced at the end of the signalling processes in both T-cell and APC manifest itself in the form of a change in the phenotypic behaviours of the cell that leads to disease clearance. Through the model, these immune responses of the entire system are simulated using the functions: TH₁ response (**Eq. 7**), TH₂ response (**Eq. 8**) and NO₂ production (**Eq. 9**) - signifying healing response (green line), non-healing response (red line) and disease clearance (black triangular markers) respectively (**Figure 17**).

The pathogen load is one of the major factors, which determines the type of immune response that will be elicited during the infection [25]. When the antigens are OFF (i.e. mimicking a situation with low pathogen load, or no infection), the TH₁ and the

NO responses are higher as compared to the T_{H2} response (**Figure 17 a**) [6, 44]. On the contrary, when the antigen molecules are switched ON (i.e. infection is present), a higher T_{H2} -response is obtained (**Figure 17 b**) [25,279].

After validating these immune response functions with published literatures, these functions (**Eq. 7, 8 and 9**) confirm their acceptability and authenticity to study the effect of the conventional immunotherapeutic strategies in Leishmaniasis (i.e., IL12 and IFN_GAMMA_T), and also to predict some immunostimulatory targets to enhance anti-*Leishmania* immunity (**Table 5**). Here, at first, we have tried to study the effect of the commonly practiced IL12 (**Figure 17 c**) and IFN_GAMMA_T (**Figure 17 d**) treatments and have observed that even though these immunostimulants can enhance the T_{H1} response and down-regulate the T_{H2} response, they fail to enhance the NO response. Thereafter, through perturbation analysis we have been able to identify three T-cell molecules (viz. MKP_T, SHP2_T and SHC_T) and two APC molecules (viz. TLR3 and TLR2) that may have positive role in disease clearance. *In-silico* mutation study of these molecules reveals that in the MKP_T *in-silico* knock-in scenario (**Figure 17 e**), even though the T_{H1} response or the NO response does not increase, the T_{H2} response gets down-regulated as compared to the infected scenario (**Figure 17 b**). Knock-in mutation of the APC molecule TLR3 gives rise to an increase in NO response, although it has no significant effect on the T-cell response (**Figure 17 f**). In the case of *in-silico* knock-out mutation studies, we have observed that inhibition of SHP2_T leads to up-regulation of the T_{H1} response and down-regulation of the T_{H2} response (**Figure 17 g**). SHC_T inhibition on the other hand, does not exhibit any significant change in T-cell or NO responses as compared to the infected scenario (**Figure 17 h**). However, if we use a combinatorial therapy by activating the proteins TLR3 while simultaneously inhibiting SHP2_T, we get a better anti-*Leishmania* immune response (Combination 1, **Figure 17 j**). Alternatively, TLR3 knock-in when combined with SHC_T OFF (knock-out) and MKP_T ON (knock-in)

can also give rise to a similar effect (Combination 2, **Figure 17 k**). Besides these combinations, interestingly we have also found that if we inhibit only the expression of TLR2 protein in APC, a very high T_H1 response is obtained and simultaneously the NO production is also increased drastically (**Figure 17 i**).

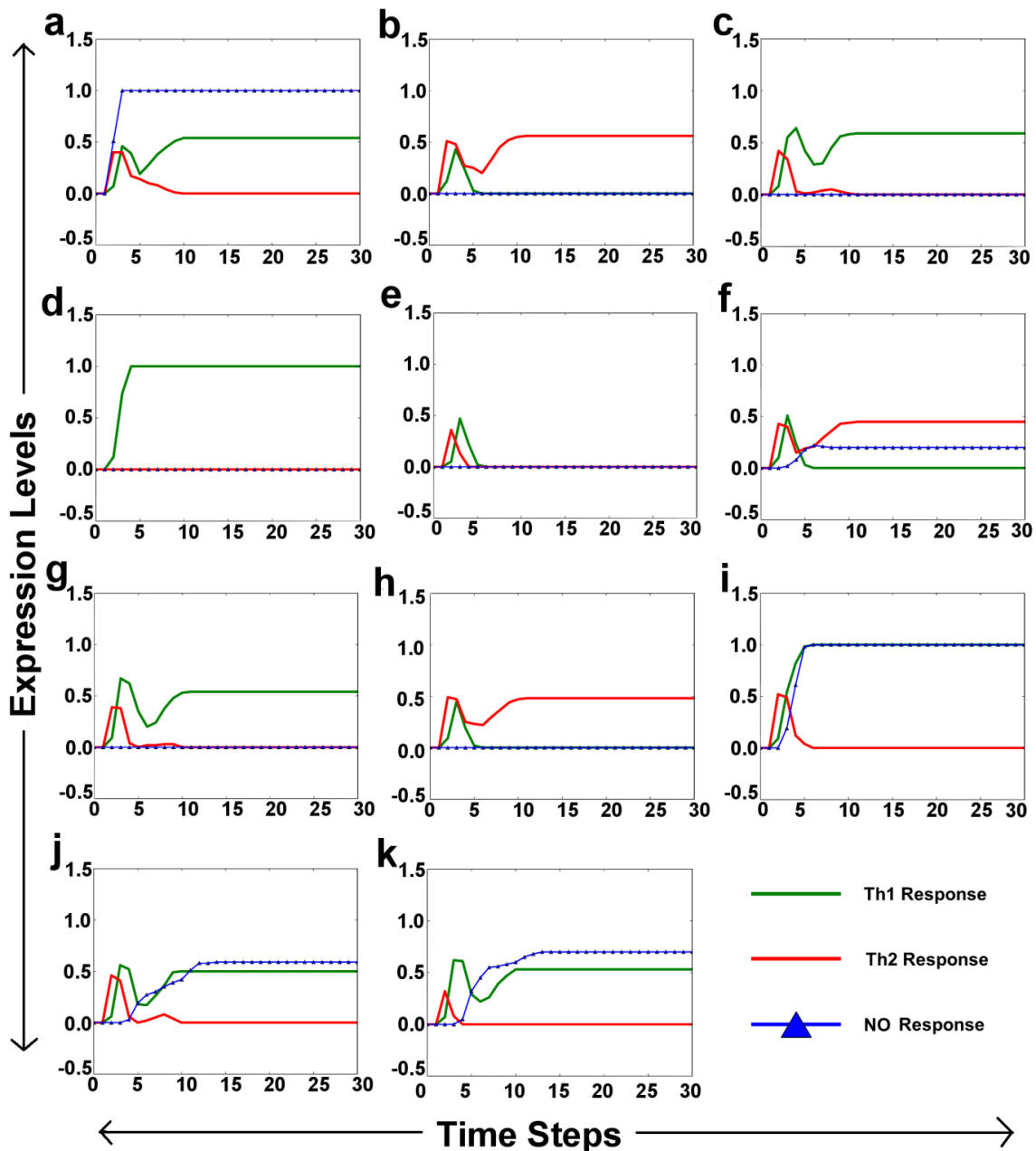


Figure 17: Response dynamics of T_H1 , T_H2 and NO in uninfected, infected and in different treatment scenarios. (a) uninfected; (b) infected; (c) IL12 [ON]; (d) IFN_GAMMA_T [ON]; (e) MKP_T [ON]; (f) TLR3 [ON]; (g) SHP2_T [OFF]; (h) SHC_T [OFF]; (i) TLR2 [OFF]; (j) TLR3 [ON] and SHP2_T [OFF]; (k) TLR3, MKP_T [ON] and SHC_T [OFF].

A summary of the combinatorial therapeutic strategies and their outcomes as observed from our analysis is provided in **Table 5**.

Table 5: Unique combinations of proteins that can be used as promising immunotherapeutic targets

Knock-in	Knock-out	T _{H1} (up)	NO (up)	T _{H2} (down)	Anti- <i>Leishmania</i> Immunity	Figure
IL12	-	Yes	No	Yes	No	17c
IFN_GAMMA_T	-	Yes	No	Yes	No	17d
MKP_T	-	No	No	Yes	No	17e
TLR3	-	No	Yes	No	No	17f
-	SHP2_T	Yes	No	Yes	No	17g
-	SHC_T	No	No	No	No	17h
-	TLR2	Yes	Yes	Yes	Yes	17i
TLR3	SHP2_T	Yes	Yes	Yes	Yes	17j
TLR3, MKP_T	SHC_T	Yes	Yes	Yes	Yes	17k

Further, the results of the Boolean attractor analysis, performed to confirm the robustness of our predictions, reveal that the uninfected and infected scenarios created in our model reaches to unique attractors, *viz.* (...110...) and (...001...) respectively (**Figure 18 a, b**). Here the attractor denotes the presence/ absence of the NO, T_{H1} and T_{H2} responses (**Figure 18**). The attractor analysis of perturbation studies reveals that the scenario with IFN_GAMMA_T treatment leads to a single attractor (...010...), which is distinct from either the infected or the uninfected attractors (**Figure 18 c**). However, our predicted targets, *viz.* TLR2 (**Figure 18 d**), Combination 1 (TLR3 ON and SHP2_T OFF; **Figure 18 e**), and Combination 2 (TLR3, MKP_T ON and SHC_T OFF; **Figure 18 f**) mostly lead to the infection-free attractor (...110...) similar to the uninfected scenario. Among these, it can be observed that all the 2560 basins in the Combination 1 scenario lead only to the infection-free attractor (...110...) (**Figure 18 e**), while in Combination 2 we observe the presence of a bi-stable attractor, oscillating between the (...100...) and (...110...) states (**Figure 18 f**). TLR2

mutation scenario also shows the presence of two attractors, i.e., (...001...) and (...110...). However, in all these three perturbations the major attractor attained by the system continues to be the desired (...110...) infection-free attractor.

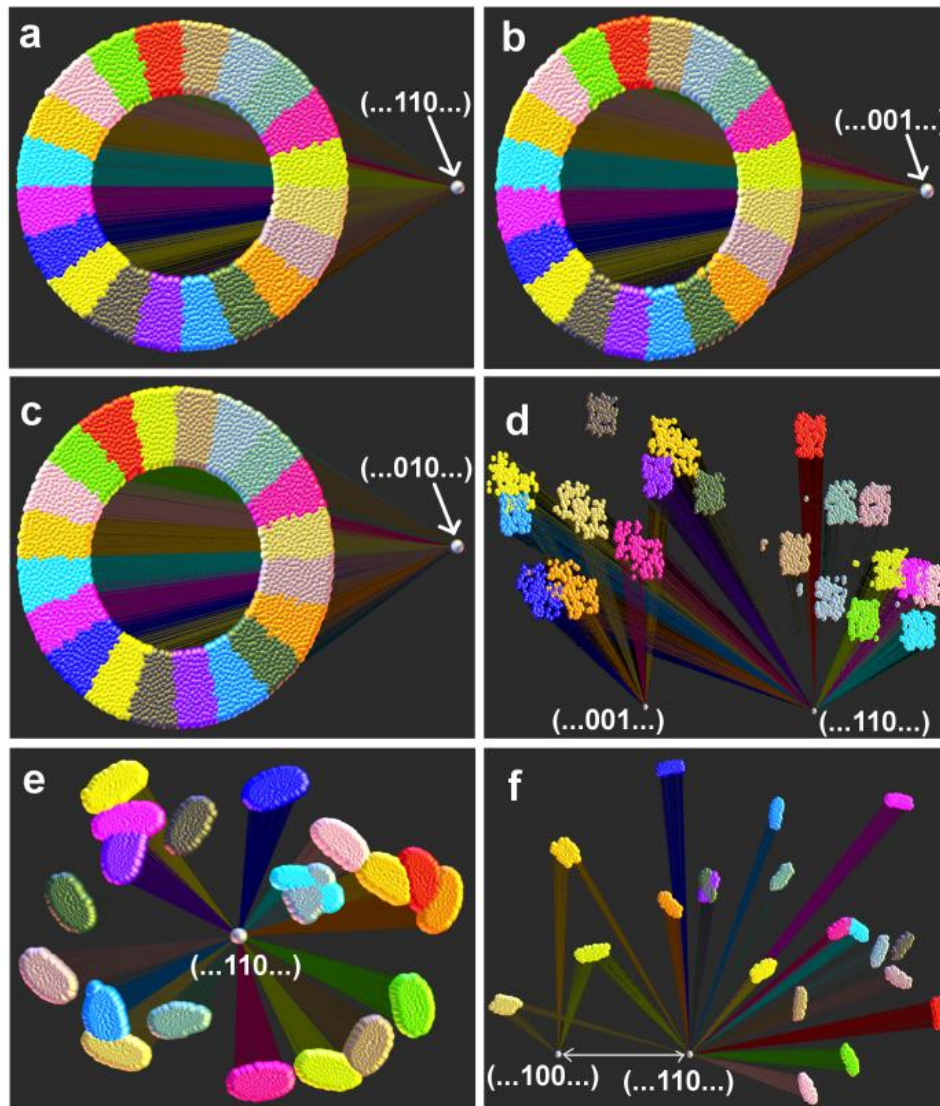


Figure 18: Attractor analysis of (a) uninfected, (b) infected, (c) IFN_GAMMA_T [ON], (d) TLR2 [OFF], (e) TLR3 [ON] and SHP2_T [OFF], (f) TLR3, MKP_T [ON] and SHC_T [OFF].

4.3. Discussion

Inadequate knowledge of the complete mechanism of *Leishmania* invasion inside the host immune system is the key reason for the low success in devising an effective

cure to Leishmaniasis. Hence, through this *in-silico* modelling study, we have tried to unravel these regulatory mechanisms by focusing on three important aspects of *Leishmania* immunobiology- (a) effect of *Leishmania* infection on the gene expression or the protein activation pattern in APC and microbicidal activities, (b) effect of the infection on the T-cell gene/protein expression pattern at the molecular level and their influence in pathway level to identify the molecular routes by which *Leishmania* inhibits T-cell functions and (c) identification of specific regulators (immunostimulators) that could act as a regulatory switch to skew the T_{H1}/T_{H2} dynamics towards the healing T_{H1} response and simultaneously enhance the NO production in order to accelerate the parasite clearance from the host cell.

In order to achieve these objectives, in this model, we have manually curated the complete signalling cascades of the immune cells depicting the detailed mechanism of regulation of the host protein-protein interaction network by the antigen molecules at various levels of signal transduction and transcriptional activities. Here, we have been able to integrate all the possible routes by which the antigen subverts the host immune responses and modulates the proper functioning of the APCs and the T-cells.

Boolean attractor analysis reveals the presence of a single attractor in the uninfected scenario and four attractors in the infected scenarios, signifying that depending on the severity of the infection and the presence or absence of certain molecules in the system, *Leishmania* infection may lead the system to multiple levels of infection with varying protein expressions and clinical manifestations (**Figure 13**). It can also be observed that the major attractor obtained in these uninfected and infected scenarios matches exactly with the expression values as obtained through our simulations using experimental data in both the scenarios. Asynchronous Boolean simulation is also performed to obtain an average behavior of the entire system under different conditions. Such comparative studies of the infected and uninfected scenarios using

asynchronous Boolean simulations brings out the effect of the *Leishmania* infection on the expression of the output molecules in both the APC and the T-cell (**Figure 14**, **Figure 15**), which nicely corroborates with previous experimental studies and strengthens the reliability and authenticity of the model outcomes. We have observed that *Leishmania* infection down-regulates the production of protective cytokines, such as IL12, IL1_ALPHA and IL1_BETA, and microbicidal molecules, such as NO, and simultaneously up-regulating the production of the chemokine, IP10 [271]. The simulation also reveals that in the infected scenario the production of the cytokine IFN_BETA is also up-regulated, which is known to have protective functions but only at low doses [266]. The T-cell expression profile shows that during *Leishmania* infection, the interleukin molecules *viz.* IL10_T, IL4_T, IL5_T and IL6_T, gets up-regulated, while the expression of IFN_GAMMA_T gets down-regulated (**Figure 15 c, d**). The higher production of the proteins, such as IL10_T and IL4_T and repression of IFN_GAMMA_T synthesis, produces conditions that favour *Leishmania* survival [274], and skews the T_{H1}/T_{H2} dynamics towards a non-healing response (**Figure 17 b**) [24,273].

A close observation on the results of our Mann-Whitney U test analysis (**Figure 16**) also predicts some novel and interesting facts about the signalling regulations imposed by the presence of the *Leishmania* infection at the pathway level. Identified from our simulation, this regulatory mechanism of the signalling cascades is presented in **Figure 19**. It can be observed that *Leishmania* infection increases the production of the protein IFN_BETA (green upward arrow) and suppresses IL12 (red downward arrow) from the APC. IFN_BETA diffuses and interacts with their corresponding receptors on the T-cell thereby enhancing the activation of its downstream TYK2 molecule (black arrow) inside the T-cell. Through this analysis, we have tried to determine the possible role of *L. major* infection in modulating the T-cell behavior at the pathway level, and infer that the pathogen up-regulates the

molecules involved in the TYK-CRKL-C3G pathway. Eventually, it enhances the production of SOCS3 and RAP1 proteins in the T-cell (**Figure 19 a**), two potential negative regulators of JAK-STAT and the RAS mediated MAPK pathways respectively (red arrow), which divulges the probable harmful effects of the high levels of IFN_BETA production from the APC that is known to occur during *Leishmania* infection [280,281]. Moreover, it can be observed that in the T-cell (**Figure 19 b**), the pathogen down-regulates the JAK2-STAT4 pathway by inhibiting the synthesis of IL12 cytokine, which results in down-regulation of IFN_GAMMA production (red downward arrow) and a consequent increase in the IL4_T, IL5_T and IL6_T expression (green upward arrow). These findings of the changes occurring at the pathway level have helped us further to identify the key regulators that can act as potential immunostimulators during the infection.

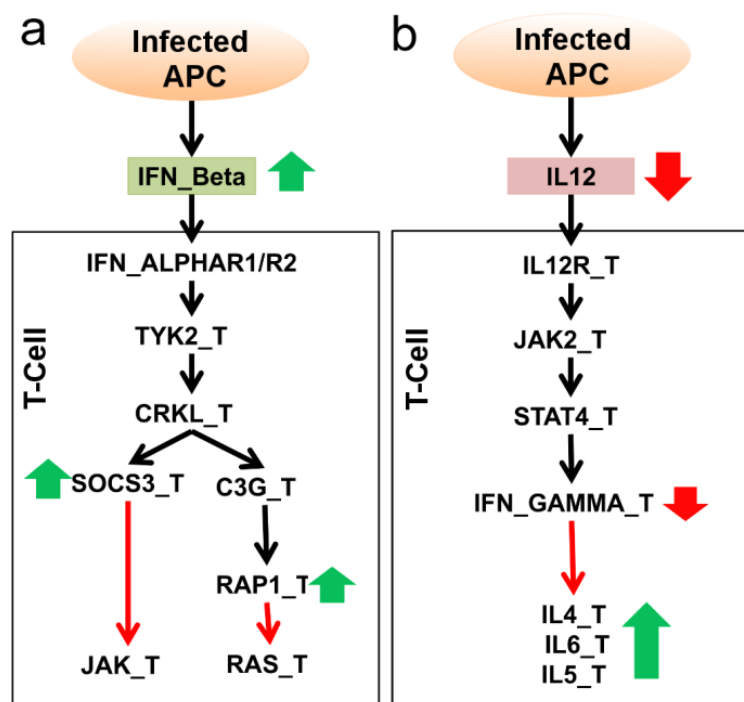


Figure 19: T-cell pathways de-regulated during Leishmaniasis. (a) Infected APC produces high amount of IFN_Beta, which up-regulates SOCS3 and RAP1 proteins that inhibits down-stream JAK-STAT and MAPK pathways; (b) Infected APC inhibits the production of the IL12 which results in up-regulation of IL4, IL5 and IL6 secretion from the T-cell by regulating the JAK/STAT and IFN_GAMMA_T protein production.

Cytokine therapy is the most widely practiced method of immunotherapy, is employed in the treatment of Leishmaniasis. Immunologists have tried to enhance the expression of IL12 and IFN_GAMMA, the two most potent T_{H1} response stimulators, which are known to play important role in the alleviation of the disease. But the most common problem faced in such immunotherapies is the inhibitory effect of the IL10 protein, which is over expressed during the infection that increases the susceptibility to the disease by inhibiting the effects of IFN Gamma treatment and often blocking the synthesis of NO [282], thereby preventing an effective anti-*Leishmania* immunity. In this work, we have tried to simulate the effect of these two immunotherapeutic strategies, viz. IL12 treatment (**Figure 17 c**) and IFN_GAMMA_T treatment (**Figure 17 d**), where we have observed that although they are able to enhance the T_{H1} response and reduce T_{H2} response, but these strategies fail to induce the NO response, which is necessary to eliminate the disease causing pathogen.

Hence, to devise a successful combinatorial immunotherapy, which can bypass the inhibitory effects of immune-suppressive molecules, various molecules that directly or indirectly influence the de-regulated T-cell pathways (i.e. JAK2-STAT4 pathway and the TYK2-mediated IFN_BETA pathways) and TLR molecules of the Antigen Presenting Cell are selectively knocked-in and knocked-out separately and then in combination (**Table 5**). Thereafter, a set of minimal combinations of protein molecules are identified that could act as regulatory switch to control the T_{H1}/T_{H2} response and also effectively enhance an anti-*Leishmania* response (**Table 5**). These molecules include three T-cell molecules (viz. SHP2_T, MKP_T and SHC_T), which are also implicated in various cancers and infectious disease treatments, and two APC molecules (viz. TLR2 and TLR3), which are popular targets in many diseases including Leishmaniasis [283-286]. A list of antagonist and agonist of these molecules is provided in **Appendix B: Table B. 6**.

Through our study, we suggest that TLR2, which is debated to have controversial roles in *Leishmania* treatment [264], helps in the parasite survival. This agrees with a recent experimental finding [265], and we propose that TLR2 inhibition can be a useful strategy to up-regulate T_{H1} and NO response (**Figure 17 i**). On the other hand, it can be understood that TLR3 alone may have a positive role to play in *Leishmania* treatment and may be a positive regulator of NO production (**Figure 17 f**). It is also interesting to note that although TLR2 inhibition alone is sufficient to drastically enhance the T_{H1} response and the NO production (**Figure 17 i**), TLR3 activation requires a synergistic inhibition of the SHP2_T molecule, a phosphatase that inhibits the activity of the JAK-STAT pathway, to gain the desired anti-*Leishmania* response (**Figure 17 j**). Surprisingly, it is also observed the MAPK phosphatase (MKP_T) when up-regulated may inhibit the non-healing T_{H2} response (**Figure 17 e**). However, MKP_P and TLR3 up-regulation when combined with the inhibition of the adapter molecule SHC_T, a positive regulator of the MAPK cascade, can act as a useful combinatorial target in Leishmaniasis treatment (**Figure 17 k**).

Nevertheless, to combat Leshmaniasis, it may be noted here that since the T_{H1} subset of helper T-cells produces inflammatory cytokines, a constant high T_{H1} response may often be undesirable in order to avoid harmful side-effects, and hence the two combinations: (i) Combination 1: up regulation of TLR3 (i.e. ON state) and down regulation of SHP2_T (i.e. OFF state) and (ii) Combination 2: up regulations of TLR3, MKP_T and down regulation of SHC_T, can be considered as better immunotherapeutic strategies than solitary TLR2 inhibition.

The robustness of our predicted combinations was further confirmed through the Boolean attractor analysis, where we observed that the major attractor attained by all the three predicted immunotherapeutic targets resembles with the infection-free attractor (...110...). This is also observed in the uninfected scenario (**Figure 18 d, e, f**),

where the NO and T_{H1} responses are high and the T_{H2} response is low. In contrast, it can be observed that none of the basins in the IFN_GAMMA_T treatment scenario is able to move the system to this desired (...110...) attractor, which clearly brings out the shortcomings of the conventional immunotherapeutic targets **(Figure 18 c)**.

The result of this analysis also highlights the controversial outcomes that may be expected from targeting TLR2 (as mentioned earlier), i.e., TLR2 knock-out may lead to two separate attractors, (...100...) and (...110...). However, it is to be noted that the major attractor obtained in the TLR2 knock-out scenario is the infection-free attractor (...110...), while only a small fraction reaches the attractor (...100...), where although the NO production is high, both the T_{H1} and the T_{H2} responses get down-regulated **(Figure 18 d)**.

A comparative analysis of the Combination 1 and Combination 2 scenarios reveals that Combination 1 may be considered a better target as compared to the others, as this is the only scenario where we can observe a complete reversal of the infected scenario to a situation (...110... attractor) similar to the uninfected scenario. However, since the Combination 2 is leading to a bi-stable attractor, which is oscillating between the major attractor (...110...) and minor attractor (...100...) states, this may also be useful in cases where a constant high NO production is required accompanied with an intermittent up-regulation of T_{H1} response for patients predisposed to inflammatory diseases.

It is important to note that in order to reduce the complexity of the model and due to lack of complete information about the functional regulations of the isoforms in *Leishmania* infected situations, we have only focused on the alternative splicing mechanism at the post-transcriptional level. However, this model may further be extended to study the effect of the alternatively spliced isoforms of the input molecules [287]. For example, TLR3 mRNA molecule is alternatively spliced to

produce a smaller 60kDa isoform, which has been observed to be over expressed in Glioblastoma cell lines. In future, RNA seq analysis of *Leishmania* infected human APC may provide further insight into the expression of such alternatively spliced isoforms in the case of the *Leishmania* infection scenario. This may also give a better understanding of the precise regulatory mechanisms underlying the differential protein expression due to the pathogenic invasion.

CHAPTER 5

DELINEATING INFECTION STRATEGIES AND IMMUNE RESPONSES DURING VISCERAL LEISHMANIASIS

5.1. Motivation

The study of host-pathogen protein interactions networks contributes to the understanding of the mechanisms of evasion of the pathogen from the host immune system, its persistence inside the host and its further replication [288-290]. One of the underlying mechanisms for host immune evasion by *Leishmania* and other intracellular pathogens involve active secretion of virulence factors (VFs) into the host cell cytosol [291,292]. These virulence factors which are secreted proteins are expected to play a major role in establishing and acquiring the host system during the infection phase of the parasite. Nevertheless, the understanding of the functionality of these virulence factors and their mode of modulation of the host responses at the time of infection is limited in case of Visceral Leishmaniasis (VL) in spite of several *in-vitro* studies which majorly focuses on proteomic analysis of the differentially modulated proteins inside the host macrophage cells [190]. A system-level understanding of the interplay between these virulence factors and host proteins is lacking, which is necessary to understand the strategies employed by the parasite to ensure its survival in the host, effective modulation of the host immune response as well as initiation of the visceralization of the infection. A deeper understanding of functional relationship between a pathogen and host can be established through identification and interrogation of protein interactions between the two species [293]. This will help in unveiling the mechanisms and the interactions of these secretory proteins that act at the interface of pathogen and the host and capture all possible signalling pathways routes that can be employed by the

parasite to regulate the host defenses. As the *in-vitro* identification of such pathogen-host interactions at a large scale is expensive and scarce, several studies have effectively implemented computational methods for predicting these interactions in various pathogens to delineate infection mechanisms [293, 294].

Pertaining to high mortality in the case of Visceral Leishmaniasis, the virulence factors secreted by the causative species *L. donovani* have been given special attention in the recent past [295]. A study carried out on *L. donovani* in its late promastigote stage has used a quantitative proteomic approach based on LC-MS/MS method to identify all possible secreted proteins in *L. donovani*. In this study, based on quantitative analysis 151 actively secreted proteins, through both classical as well as non-classical secretion pathways, have been identified [174]. Based on their general properties the putative mechanisms of secretion, as well as their functional role in the context of infection have been postulated. 50 proteins out of these are candidate virulence factors which are enriched in the medium. Although this study states the functional roles for these proteins, it is not yet identified with which host proteins these proteins interact and which pathways are elicited to establish infection. Given the high virulence and large number of identified virulence factors for this organism, one can surmise that multiple robust mechanisms exist that contribute to the infection process.

Although traditional *in vivo* methods of protein-protein interaction identification like yeast two hybrid assays, co-immunoprecipitation exist, they are expensive, time-consuming methods and also do not provide with a comprehensive overview of interactions of all these proteins together with the host proteins and the responses they elicit upon infection and post infection period. Computational methods play a key role in creating a global perspective of the interaction components under study [296]. Methods for predicting protein-protein interactions utilize high-throughput data [297] using several sequence, structure and genome based features that are

related to physical and function relationships pertaining to the interactions. Such methods include phylogenetic profile based, gene-neighbourhood and gene cluster methods and Interologs [179, 298]. Interolog-based approach assumes that homologous pair of proteins preserve their ability to interact with each other [299,300]. One such study which relies on this Interolog based approach has predicted HPI for 15 eukaryotic parasites including *Leishmania sp.* with the human proteome [288]. The pathogen proteins considered here in the study mostly includes a large number of computationally predicted secretome proteins from the pathogen proteome using the standard secretory signal peptide sequence. However, previous studies have shown that the protein secretion of *L. donovani* occurs via multiple non classical secretion pathways that are unlikely to be identified by these computational techniques that rely on the classical amino-terminal secretion signal [174]. Hence, the predicted host-pathogen interactome does not span the complete *L. donovani* secretome proteins that have been observed using quantitative mass spectrometric analysis [174].

Hence, through our study we seek to obtain a holistic understanding of the role of these secretory proteins from *L. donovani* in subverting the host defense mechanism by constructing a Host-Pathogen Interactome (HPI) between the *L. donovani* secretory Virulence Factors (VF) and the human proteins. Here, we aim to identify the major mediator proteins through which the secretory proteins approach and manipulate the immune response and cellular defense mechanisms. Using a combinatorial strategy of homology-based prediction of host-pathogen interaction from a known HPI, called Interolog-mapping and further filtering and validating these interactions based on Domain- mapping approach, we have identified putative host-pathogen interactions of high confidence (**Section 2.3**). To identify the pathways through which these secretory proteins are affecting the phenotype-associated proteins specifically playing major role in host immune responses,

parasite intracellular survival and visceralization, we extend the interactome to form a more comprehensive network of the secretome with the host system.

Further, we employ pathway enrichment and graph-theory based analysis to model the Protein-Protein Interaction (PPI) network where nodes represent proteins and edges between them represent physical interactions between those proteins [301]. As the topological and structural properties of these networks often contribute to better understanding of the functional roles of the key components in the system, we analyze the *L. donovani*-Human interaction PPI network to identify its key nodes and regulators (**Section 2.3.5**). Here we try to delineate the key signalling routes between *L. donovani* Virulence Factors (source nodes) and the deregulated host response proteins (target nodes) through analysis of shortest paths from the VFs eliciting the phenotypic host response through which the information flow occurs [301]. This led to identification of important signalling pathways involved in the host pathogen interaction. We further identify key mediator target proteins in the network by studying the global network properties using *in silico* network perturbation studies through node knockout experiments involving shortest path calculation that demonstrate the vitality of certain unique protein combinations that controls pathways to the host response proteins regulating phenotypes such as parasite survival, immune responses and visceralization during the infection (**Section 2.3.7**). Based on network perturbation analysis, our study has for the first time identified protein combination which effectively perturbs key enriched signalling pathways that are elicited by the VFs during the infection phase. This protein combination can be further tested *in vivo* in *L. donovani* infected macrophages and can serve as potential targets for drugs or immunomodulators to control phenotypic host responses during Visceralization.

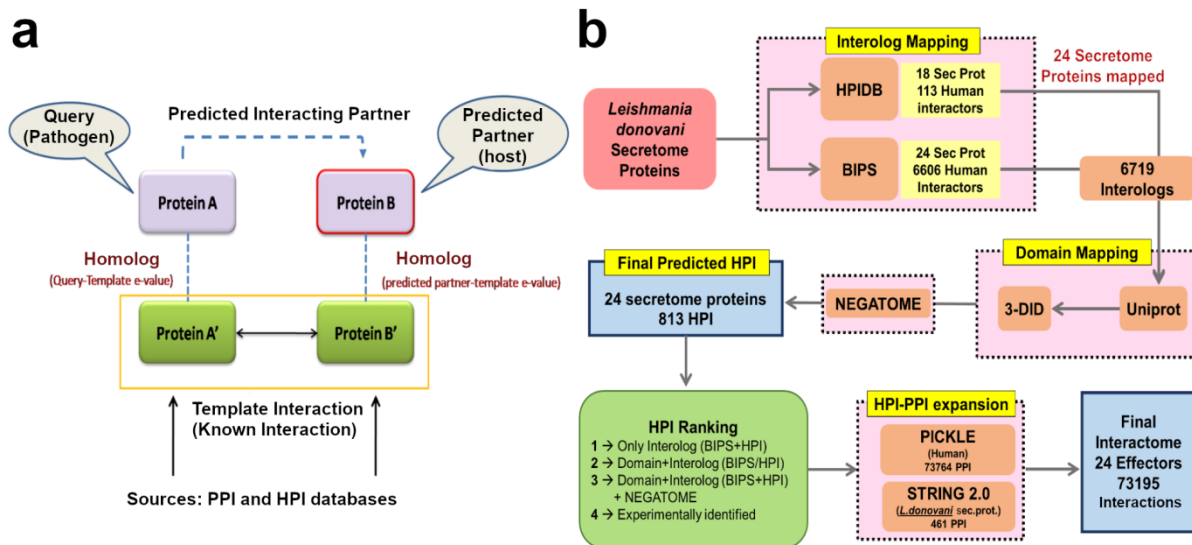


Figure 20: *L. donovani* and Human PPI Network prediction workflow: a) Interolog Mapping strategy implemented in Interactome prediction; b) Prediction Pipeline with the resultant output at each step of prediction of the Host Pathogen Interaction network prediction.

5.2. Results

5.2.1. Predicted *L. donovani*-Human PPI Interactome

The interactome map between *L. donovani* secretory proteins and the human host proteins were identified based on the Interolog-based approach using HPI-DB [176] and BIPS [177] (Figure 20) (Section 2.3). 113 human interactors from HPI-DB and 6606 from BIPS were identified. There were a total of 6719 interactions predicted for 24 out of 50 *L. donovani* secretome proteins. The remaining 26 virulence factors did not identify any significant hits from HPI-DB and BIPS and were thus not considered in the current interactome. These 6719 interactions identified were further filtered and validated by structure-knowledge based approach using experimentally verified domain-domain interaction pairs from 3DID. Domain-Interaction based filtering yielded in a total of 638 out of 6719 interactions. 175 interactions which were identified from both HPI-DB and BIPS but could not be verified by 3DID were cross-verified with the latest updated data in the NEGATOME 2.0 database and retained in the network. This step is crucial to identify any false positives in our predicted interactions as this database harbours

protein pairs which, in no capacity, can interact with each other [181]. The final inter-species Interactome PPI prediction led to a total of 813 predicted interactors for the 24 virulence factors. The detailed statistics of these interactors have been represented in the venn diagram (Figure 21 b) (Appendix C: Table C. 2).

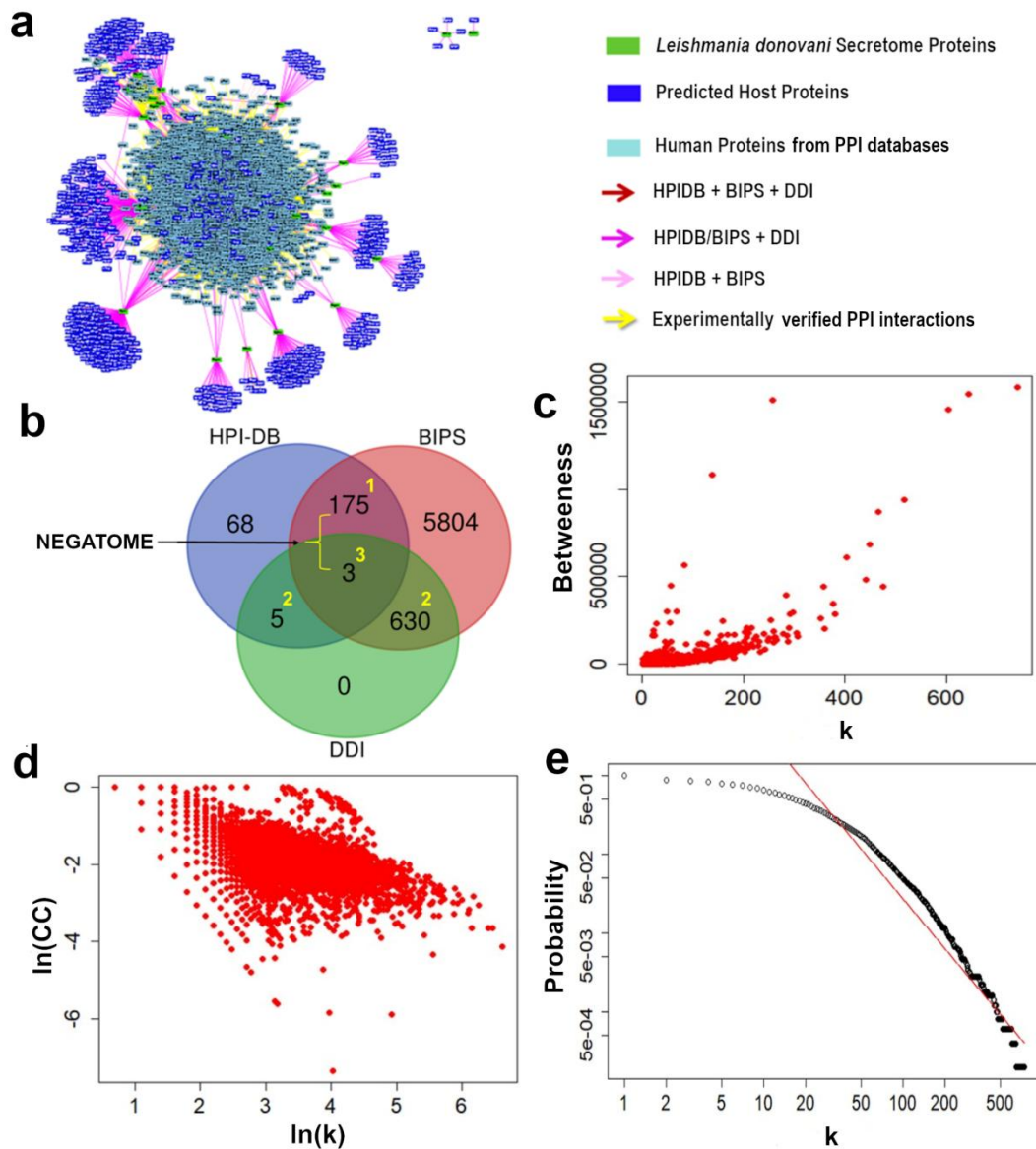


Figure 21: Predicted Protein Interactome: (a) *L. donovani*-Human PPI Network with proteins represented in the form of nodes and interactions represented in the form of edges; (b) Prediction statistics of the Network based on the resultant number of Interacting proteins obtained from Interolog and Domain Mapping resources; (c) Correlation between Degree (k) and Betweenness; (d) Correlation between Degree (k) and Clustering Coefficient (CC); (e) Degree distribution of the network follows Power Law (plot shown in log-scale).

Further integration of the predicted Interactome with the human intra-species PPI from the STRING database resulted into *L. donovani* VF- Human PPI network having a total of 73195 interactions and 24 *L. donovani* virulence factors as Effector Nodes **(Figure 21a) (Appendix C: Table C. 2)**. Since the nodes E9BSB0_LEISH and E9BQR2_LEISH were observed to be isolated from the final Integrated interactome and did not produce any results in further sub-network analysis they were eliminated from the downstream network analysis leading to final of 22 *L. donovani* VFs (Effector Nodes) in the Network **(Appendix C: Table C. 1)**. An enrichment analysis for the GO Cellular Component (CC) of these predicted interactors was performed to ensure that the location of the predicted proteins was mostly cytoplasmic or cytosolic **(Appendix C: Figure C. 1)**. It is to be mentioned here that for the initial prediction of the HPI network, tissue specificity has not been considered to gain a holistic understanding. The sub-networks created using the host response nodes was obtained from experimental studies with tissue specificity for the further analysis.

5.2.2. Structural Analysis and Sanity test of the Network

Structural analysis of the network revealed a scale free nature where the degree distribution of the network is observed to follow the power law having an α value of 2.104 [199] **(Figure 21 e)**. This structural property is observed in most biological networks and essentially indicates that the network consists of few nodes having a very high degree compared to other nodes in the network. These nodes with high number of interactions have various functional implications in the network and ensure the robustness of the network from external perturbations thus making it resistant to random errors [199].

To verify the sanity and credibility of the predicted network, the Shapiro-Wilk normality test was performed to check if any random node from the network follows a normal distribution [302]. The Shapiro-Wilk normality test conducted on the

degree distribution of the network suggested that the predicted interactions do not follow a normal distribution [303] (p-value= 2.2e-16). This test indicates that the hub proteins and their sub-networks present in the network are not by chance further indicating that the predicted interactome arises from a sturdy biological growth process and is not formed by spurious interactions.

A correlation coefficient between the Degree and Betweenness Centrality of the network using Spearman test resulted in $\rho=0.938$ thus indicating that these centralities of the network is highly positively correlated (**Figure 21 c**). On the other hand, the Spearman correlation coefficient for log of degree to the clustering coefficient was observed to have a value of $\rho= -0.385$ (**Figure 21 d**) indicating a fairly negative correlation. These patterns of correlation of topological properties have also been reported in other inter-species networks [294].

5.2.3. Functional Correlation based on Pathway Enrichment Analysis

The number of direct host interactors predicted for each virulence factor and the pathways in which they are enriched is shown in (**Appendix C: Table C. 3**). Maxwell *et al.* [174] has categorized these secretome proteins into four classes viz, 1) Intracellular survival, 2) Signal transduction, 3) Immunosuppression, 4) Vesicle Transport based on the putative biological process in which they are expected to participate. We hypothesize that the direct protein interactors predicted in the network for all these secretome derived virulence factors should be involved in a pathway whose function corroborates with these biological processes. Hence, to verify our predicted interactions based on such functional similarity, we enriched KEGG pathways for the predicted direct host Interactors corresponding to each secretome protein and compared them with their putative biological processes stated by Maxwell *et.al* (**Appendix C: Table C. 3**). It is to be mentioned here that, we opted for pathway enrichment, instead of GO Biological Process, since we wanted to investigate our predicted Interactome for pathways through which these virulence

factors regulate the host machinery. This comparison study revealed that the pathways significantly enriched (p-value<0.050) for the host interactor proteins corroborated well with the putative functions of each secretome protein. For example, the *Leishmania* virulence factor Glutathione peroxidase (E9BI90), is known to be involved in mediating intracellular survival of the parasite by its antioxidant properties [174]. From our analysis, we observe that the predicted protein targets are enriched for the pathways such as Glutathione metabolism, Purine and Pyrimidine metabolism and p53 signalling pathway. Similarly, the predicted protein targets of Mitogen-activated protein kinase (E9BA99) of the parasite are enriched for MAPK, Neurotrophin, ErBB, GnRH and related pathways. On the other hand, Peptidyl-prolyl cis-trans isomerase (E9BHJ8) having immunosuppressive properties targets host pathways related to VEGF, B cell receptor pathway and T cell receptor signalling pathway. Similar observation is consistent with other secretory proteins and their predicted protein partners (**Appendix C: Table C. 3**).

5.2.4. Extraction of Phenotypic Response sub-networks targeted by *L. donovani* virulence factors based on shortest path analysis

The infection process by the parasite elicits various types of phenotypic responses inside the host. One of the key goals of this study is to identify how the secretome derived virulence factors play a role in modulating these phenotypic responses of the host during the infection. In order to identify the host proteins from our network that are deregulated by the parasite and are responsible for causing the changes in the phenotypic response, we identified a total of 136 (111 for early phase infection and 25 for late phase infection) differentially modulated proteins (DMPs) of the host from the literature from various experimental studies performed using *L. infantum* and *L. donovani* which mapped in our network (**Section 2.3.6**). In order to associate these DMPs to the phenotypic responses, they were enriched for their GO biological process terms and segregated to specific phenotypic responses. The three major

phenotypic responses selected for the study were Immune Response (IR), Intracellular survival (SUV) of the parasite, and Visceralization (VIS). The DMPs selected for each of these three sub-networks resulted in identification of 20 phenotypic response nodes (PRNs) for IR Phenotype, 14 PRNs for SUR phenotype and 25 PRNs for VIS phenotype (**Appendix C: Table C. 4**).

Subsequently, in order to study the effect of the virulence factors on these PRNs we extracted all the shortest paths through which these virulence factors (source/Effector Nodes) interact with the PRNs (sink/Target Nodes). This shortest path extraction led to formation of three sub-networks-IR, SUR and VIS exhibiting three phenotypes under study, each containing paths from all 24 virulence factors to their respective PRNs in that phenotype class (**Figure 22 a-c**). The resulting sub-networks consist of 372 shortest paths for IR, 127 shortest paths for SUR and 614 shortest paths for VIS comprising of direct source-sink interaction or alternate cross-talking pathway routes connecting the parasite (source) and host PRNs (sink).

5.2.5. Sub-networks of Phenotypic Responses reveal unique pathways regulated by the virulence factors

Pathway enrichment of the three sub-networks revealed that the virulence factors primarily target some common pathways such as MAPK Pathway, T-cell receptor signalling pathway, Toll-like receptor signalling pathway, PI3K-Akt signalling pathway, TNF signalling pathway, Ras signalling pathway (**Appendix C: Table C. 5**). The Neurotrophin Signalling pathway is also one of the major pathways targeted by the parasite that is involved in the Nitric Oxide production. This pathway has also been implicated in Macrophage chemotaxis that may be responsible for visceralization of infection. The parasite also targets the ErbB signalling pathway that is responsible for immune responses as well as visceralization.

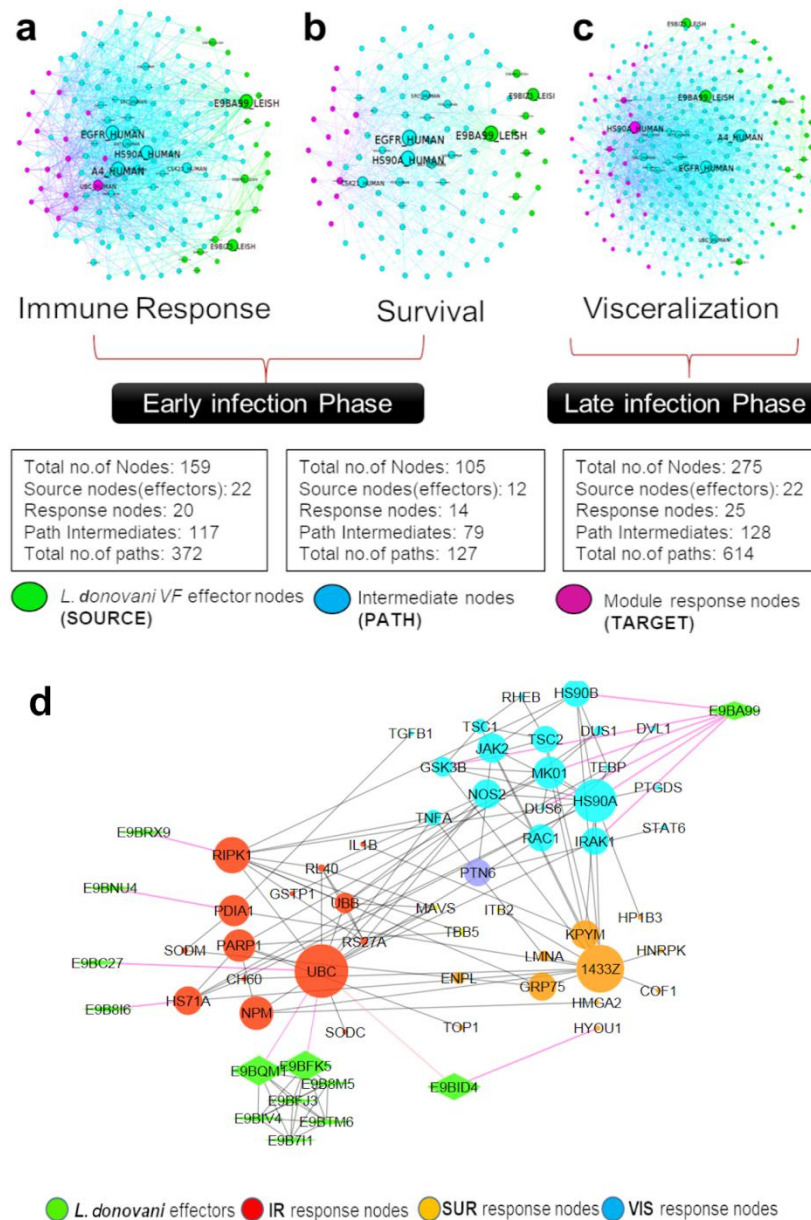


Figure 22: The three Phenotypic sub-networks representing the source and target nodes extracted from shortest path analysis: (a) Immune Response, (b) Survival, (c) Visceralization; (d) Protein interactions sub-graph from the Network showing inter-linking of the direct interactors of the Virulence factors from all three phenotypic responses. Node size arranged based on increasing order of betweenness centrality values.

In VIS sub-network the virulence factors of *Leishmania* is observed to enact through mTOR pathway. mTOR plays a crucial role in regulation of M2 macrophage polarization and direct the innate immune homeostasis towards parasite survival inside host [304].

Through this study we identified certain unique pathways enriched from the VIS sub-network which included Hippo signalling pathway, Glucagon signalling pathway, Antigen processing and presentation, protein processing in endoplasmic reticulum which have not been previously reported. It is known that some released proteases can directly modulate the activity of macrophage by interacting directly with the host cell surface or following entry into the macrophage Endoplasmic reticulum (ER) from the phagosome [305]. The enrichment of pathway for protein processing in ER for the VIS sub-network in our network suggests that this modulation activity specifically contributes majorly for visceralization and infection prolongation inside the host. Hippo signalling pathway that has been reported to play a pivotal role in Cancer metastasis and cell migration has also been identified from our VIS sub-network. The involvement of these pathways in visceralization of the Leishmaniasis have not been reported earlier.

5.2.6. Study of sub-network cross-talk to identify key proteins targeted by the parasite based on nearest neighbour

In order to study the PRNs of the sub-networks that are in direct contact with the virulence factors and the cross-talks amongst each other, we extracted the sub-network of all direct interactions (having the least shortest path length) from virulence factors to the PRNs of all three sub-networks in unison to observe the cross-talks (**Figure 22 d**). This reveals that the virulence factors E9BQM1, E9BKF5 and E9BC27 have direct interaction (shortest path length=1) with the host UBC protein, which has highest Betweenness centrality for the IR subnetwork. The virulence factors are observed to target 1433Z as the most central protein in SUR sub-network through direct interaction (shortest path length=2). For the VIS sub-network we observed that the virulence factor E9BA99 alone has a direct interaction (shortest path length=1) with 6 PRNs with the HS90A protein with highest betweenness centrality of that sub-network. These results highlight the importance

of the protein UBC for the IR phenotype being distance wise close to the virulence factors and similarly that of the proteins 1433Z for SUR and HS90A for VIS phenotypes.

Further, the comparison of the average shortest path distances from all virulence factors to each sub-network and to the whole network revealed that all three sub-networks were observed to be closer to the virulence factors with average shortest path distance of 2.77 for IR, 2.90 for SUR and 2.91 for VIS as compared to the distance to the whole network which was 3.17 (p-value <0.05). The immune response (IR) phenotype is observed to be the closest phenotype to the virulence factors set indicating that one of the key strategies employed by the parasite is targeting the host immune signalling pathways. The virulence factor E9BA99, MAP Kinase is observed to be the closest to all the sub-networks with lowest average shortest path distance of 2.02 to the three sub-networks compared to other virulence factors (**Appendix C: Figure C. 2**). This protein is also observed to have maximum number of direct interactions with PRNs belonging to the VIS phenotype as stated earlier. Our analysis highlights the importance of influence of the MAP kinase E9BA99 virulence factor in pathogenesis and specifically in the visceralization process.

5.2.7. Network Perturbation Analyses to identify important proteins that regulate each sub-network

Key regulators of any biological network system are characterized by the nodes in that network whose absence perturbs the structure of the network. In this study our network represents a static state of interaction between the *L. donovani* virulence factors with the human host proteins. The key components in any biological network are positioned to be important for diffusion of information and signal throughout the network and thus tend to be easy targets in the infection process by any virus or parasite. The hubs which are characterized by high Degree are important for local

network organization whereas the bottlenecks which are characterized by high Betweenness centrality are important for global diffusion of information throughout the network. If such candidate proteins having a considerably high degree and betweenness centrality are removed from the network, it is expected to perturb the information flow and the natural signalling process in the network. Thus, such proteins can be identified as key modulatory proteins important for regulating the phenotypic responses in the host. In our case, we associated the break in information flow or perturbation of network structure to be measured in the form of two analyses: 1) significant increase in average shortest path distance 2) Percent depletion of shortest paths (**Section 2.3.7**).

In order to identify the candidate proteins from the host for the knockout analysis, top 10 proteins were identified based on the betweenness centrality from the three sub-networks, *viz.* EGFR, A4, 1433Z, UBC, HS90A, AKT1, SRC, MK01, TRAF6 and GSK3B (**Appendix C: Table C. 6**). Individual knockouts of these 10 proteins and the associated deviation in average shortest path distance, as well as the percent depletion in shortest paths, have been depicted in **Figure 23**. To identify the knockout analysis which is statistically significant the non-parametric Mann Whitney's test was performed.

First, the distance analysis shows that for the IR sub-network, UBC and A4 knockouts significantly increase average path distance for majority of the virulence factors with a p-value of 0.00098 and 0.02386 respectively, for the SUR sub-network, 1433Z and A4 have significant impact with p-value of 0.0003 and 0.0486 respectively whereas for VIS sub-network it is observed that HS90A, UBC, A4 and EGFR have significant impact with p-value of 0.0001, 0.02953, 0.04734 and 0.04876 respectively (p-value<0.05) (**Figure 23 a**). It was also observed that the UBC knockout completely

disrupted the interaction of the virulence factor E9BC27, myo-inositol-1-phosphate with all the PRNs of all three phenotypic sub-networks.

The second analysis of percent path depletion also showed similar results. The heatmaps representing detailed individual knockout effect on the shortest path percent depletion is shown in **Figure 23 d-f**. For the IR phenotype, impact of UBC knockout alone was observed with 100% path depletion from virulence factors E9BC27, E9BFJ3, E9BFK5, E9BID4, E9B8M5 and E9BQM1, about 70-80% depletion from virulence factors E9BN59 and E9B7I1 and about 40-50% depletion from virulence factors E9BQ78, E9BIZ5, E9BTM6 and E9BIV4. Affecting overall 12 virulence factors post knockout it showed a p-value of 0.0003404 proving to be statistically significant impact. The maximum impact was for the virulence factors belonging to the proteasome assembly as well as inositol and heat shock protein. For SUR phenotype, impact of 1433Z knockout alone was observed with 100% path depletion from virulence factors E9B7I1, E9BQ78, E9BU45 and E9B8M5, about 70-80% path depletion from virulence factors E9BIZ5 and about 40-50% depletion from virulence factors E9BK16, E9BI90 and E9BA99. Affecting overall 8 virulence factors post knockout it showed a p-value of 0.005988 thus proving a statistically significant impact. The maximum impact was on the virulence factor category of MAP kinases, proteasome assembly and 1433Z host proteins. Finally, for the VIS phenotype knockout of UBC and HS90A was observed to be statistically significant with a p-value of 0.01552 and 0.000126 respectively.

The UBC knockout resulted in 100% path depletion for virulence factors E9BQM1 and E9BC27, about 70-80% path depletion for E9BFK5 and about 40-50% depletion for E9BID4 whereas HS90A knockout resulted in 100% path depletion for virulence factors E9BI90, about 70-80% depletion for E9BIV4 and about 40-50% depletion for E9B8I6 and E9B7I1. The overall effect was on 5 virulence factors by UBC and 4

virulence factors by HS90A with maximum impact on the VF category of Proteasome assembly and inositol by UBC and Glutathione peroxidase by HS90A.

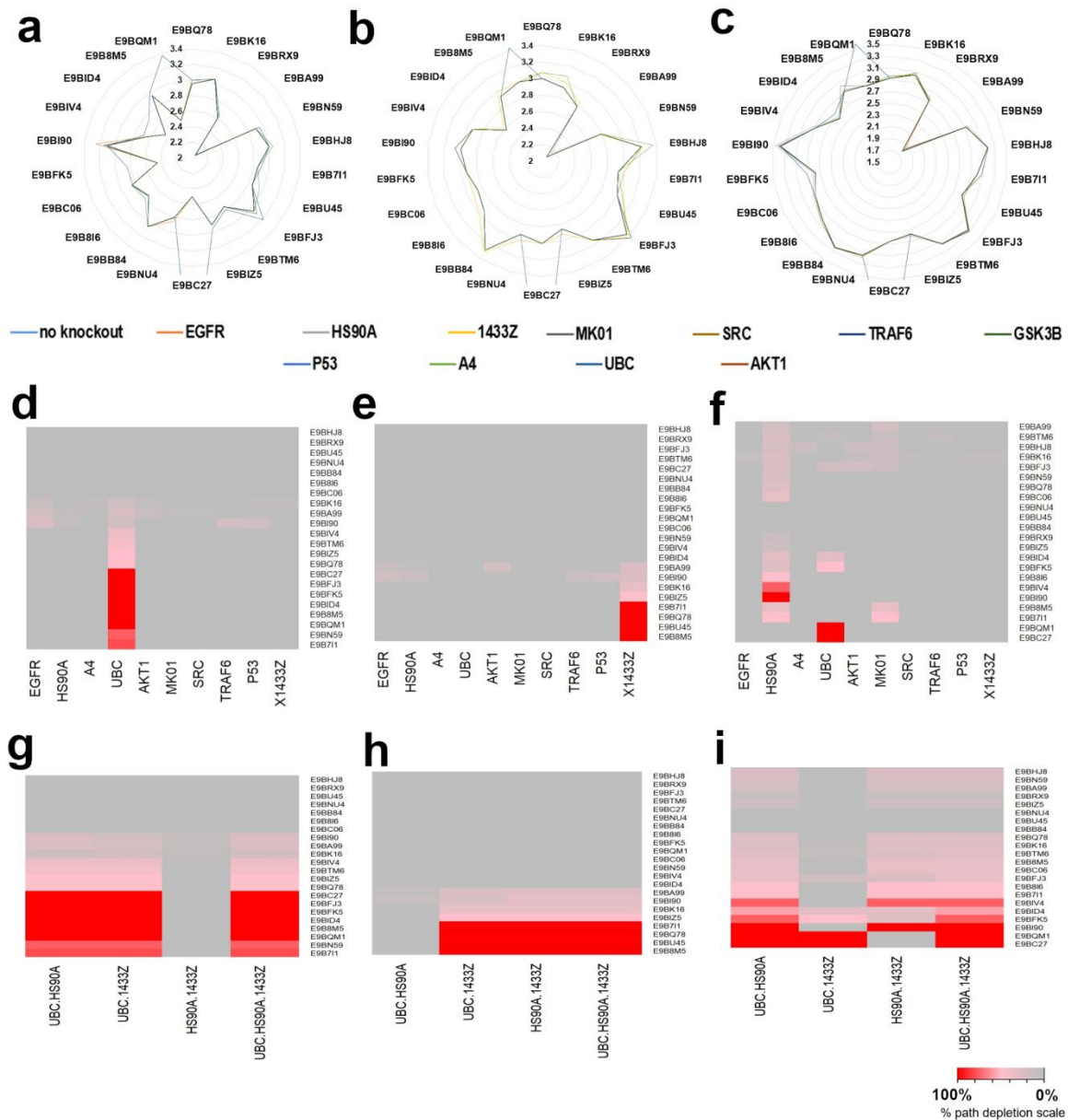


Figure 23: Network perturbation analysis: (a, b, c) Distance Analysis Web-graph representing deviation in the average shortest path distance upon individual knockout by each candidate protein from each Virulence factor to the phenotypic response node of all three sub-networks IR, SUR, VIS respectively; (d,e,f) Heatplots showing depletion in number of shortest paths upon individual knockout by each candidate protein. The scale 0%-100% represents 0% indicating no shortest path deleted to 100% indicating all shortest path deleted; (g, h, i) Heat plots representing percent shortest path depletion analysis of final four combinations of shortlisted knockout candidates.

5.2.8. Identification of protein combinations that regulate the overall phenotypic responses during *L. donovani* infection

Combining the results from individual knock-out studies, we identified three common host proteins UBC, HS90A and 1433Z creating statistically significant impact individually on the three phenotypic sub-networks (**Figure 23**). In order to identify a combination of proteins which can potentially act as key modulators in the early as well as late infection phase, knockout analyses were performed for all possible combinations of the three identified candidate proteins UBC, HS90A and 1433Z. The possible combinations were UBC+HS90A, UBC+1433Z, HS90A+1433Z and UBC+HS90A+1433Z. The distance analysis for these combinations reveals that all combinations showed a statistically significant ($p < 0.05$) impact of knockout on all three phenotypes except the combination of HS90A+1433Z which did not show any significant impact on IR phenotype (**Figure 23 g-i**). The distance analyses are also depicted in the form of Probability Density distribution of each VF to the target nodes in each sub-network as a function of their average distances before and after knock-out (**Appendix C: Figure C. 3**). This additional analysis was done to observe the shift in Gaussian Curve peak for the shift in the average shortest path distance post knockout for each combination.

The path depletion analysis shows that for IR phenotype the combination HS90A+1433Z showed a poor impact with p-value of 0.09072 whereas all other three combinations showed a statistically significant impact with p-values < 0.05 . For SUR phenotype the combination 1433Z+HS90A showed a poor impact with a p-value of 0.17290 whereas all other three combinations showed statistically significant impact with p-values < 0.05 . For VIS phenotype we observed that all combinations were impacting in a significant way (p-value < 0.05) (**Figure 23 g-i**).

Pertaining to above results from both analyses it was clear that the combinations HS90A+1433Z and UBC+HS90A were to be eliminated due to poor impact. This

resulted in only two possible significant combinations UBC+1433Z and UBC+HS90A+1433Z. We carried out Pathway enrichment analysis of the three sub-networks before and after knockout in case of both knockout combinations, i.e., (a) UBC+1433Z and (b) UBC+1433Z+HS90A. Here we aimed to observe depletion of one or many pathways amongst the significantly enriched signalling pathways or at least depletion in the number of proteins enriched for a particular pathway after the knockout. This analysis would reflect the effect of the perturbation of the protein combination to disturb the identified signalling pathways that are targeted by the VFs for the three phenotypic outcomes during infection. In case of UBC+1433Z combination, it did not yield any significant difference in depletion of enriched pathways post knockout thus reflecting a lower perturbation effect. Significant perturbation effect on depletion of pathways was observed for the knockout of combination UBC+1433Z+HS90A.

Figure 24 (a, b and c) represent the pathways statistically significantly ($FDR < 0.05$) enriched in the three sub-networks where the bubble size corresponds to the number of proteins from the sub-network enriched for the corresponding pathway depicted on y-axis and the fraction of proteins involved in that enriched pathway out of the total proteins in the sub network depicts the ratio value spanning across the x-axis. The signalling pathways like PI3K-Akt, MAPK, Neurotrophin and chemokine are observed to be amongst the highest enriched pathways in all three sub-networks. Certain unique pathways are also observed to be enriched in specific phenotypes such as NF-kappa B signalling pathway in IR (**Figure 24 a**), cAMP signalling pathway in SUR (**Figure 24 b**) and Adipocytokine, Oxytocin and Wnt signalling pathway in VIS phenotype (**Figure 24 c**). The pie chart representation of the analysis depicts the difference in the proteins enriched for the pathways after knockout. Insulin Signalling Pathway (SP) enriched in the IR and SUR sub-network was

observed to have maximum impact with respect to highest loss of proteins enriched for that pathway after knockout (**Figure 24 d**).

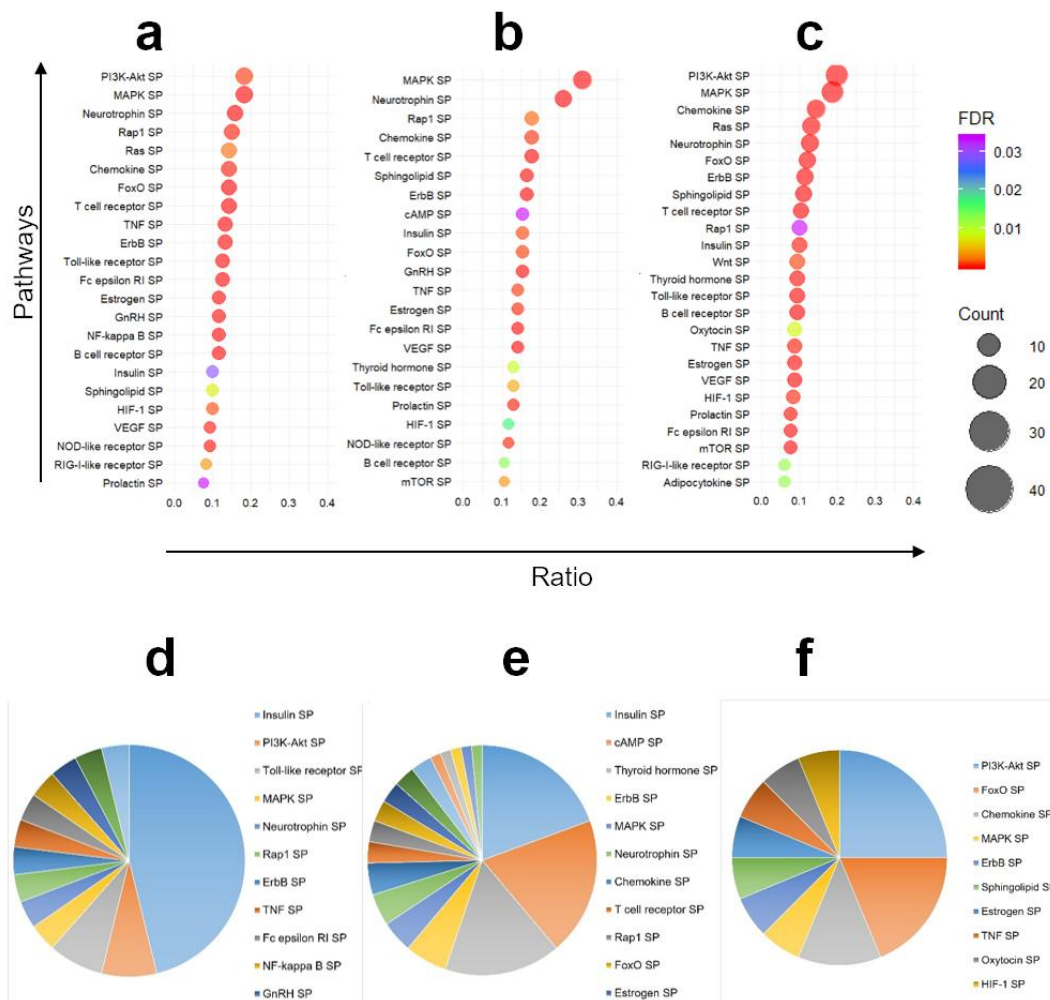


Figure 24: Pathway Depletion analysis: Upper Panel: Pathways statistically significantly enriched for the shortest paths for each sub-network **a) IR**, **b) SUR** and **c) VIS**. The circle size represents count of genes/proteins enriched from the sub-network for that particular pathway and the color scale represents enrichment confidence in the form of FDR value. Lower Panel: Charts representing fraction of enriched genes/proteins from corresponding pathways depleted after the knockout UBC+HS90A+1433Z for the enriched pathways previously identified in each sub-network **d) IR**, **e) SUR** and **f) VIS** respectively.

Additionally, this effect was observed in SUR sub-network for cAMP and thyroid hormone signalling pathway. In VIS sub-network highest protein loss was observed for pathway PI3K-Akt, FoxO and Chemokine signalling pathway. Here it is to be noted that cAMP signalling pathway was also observed to be uniquely enriched for the SUR sub-network thus implying the ability of the VFs to attack phenotype-

specific pathways through these modulatory proteins UBC, 1433Z and HS90A. This highlights the importance of the role of these modulator proteins used as key mediators by the parasite to attack the host defences activated during the parasite survival process.

The components of Adipocytokine signalling pathway, essentially secretions from fat cells include proteins such as IL-6, IL1 β , TNF α . TNF α is up-regulated PRN whereas IL1 β is down-regulated. Previous studies suggest macrophage apoptosis inhibition during intracellular *L. donovani* infection by induced gene expression of TNF α , TGF β and IL-6 [306,307]. These cytokines in our VIS sub-network are PRNs. Above observations suggest that these PRNs are triggered by *L. donovani* VFs (E9BK16_LEISH) LACK (Activated protein kinase C) protein, (E9BRX9_LEISH) Casein kinase, (E9BHJ8_LEISH) peptidyl-prolyl cis-trans isomerase, (E9BFJ3_HUMAN) proteasome, (E9BTM6_HUMAN) proteasome-subunit and (E9BIZ5_HUMAN) Small GTP-binding protein Rab1 based on our shortest path analysis. Also, it is recently observed that inhibition of Wnt5a signalling pathway during *L. donovani* infection antagonizes Visceralization since this pathway is specifically targeted in Visceral Leishmaniasis [191].

5.3. Discussion

The study of host-pathogen interaction (HPI) networks has been invaluable for understanding infection strategies and identification of drug targets for various infectious diseases. In case of Leishmaniasis, although much work has already been done for Cutaneous Leishmaniasis, a holistic understanding of Visceral Leishmaniasis (VL) is still scarce due to scanty knowledge of the mechanism of visceralization and parasitic survival strategies. The inadequate knowledge of Visceral Leishmaniasis at the pathway level also makes the device of an effective treatment strategy difficult. Hence, in this study, using the Interolog and Domain mapping approach we predict a total of 813 Host Pathogen interactions for 24

secretome derived VFs of *L. donovani*. Further extension of the HPI with the intra-species Human and *L. donovani* network resulted in a total Interactome of 73195 interactions (**Figure 20 and Figure 21**). Thereafter, the network has been validated qualitatively based on its topological and functional properties and mapped with experimentally obtained expression data for the extraction and study of important sub-networks responsible for the immune response (IR), parasite survival (SUR) and visceralization (VIS) of the disease.

Based on these sub-networks IR, SUR and VIS (**Figure 22**), we have identified the shortest paths through which the VFs modulate the host response proteins (PRNs) during the early and late phases of infection. Pathway enrichment analysis divulge some pathways common in all three sub-networks which includes MAPK, Neurotrophin, Toll-like receptor, Wnt, TNF, p53, VEGF [308]. Some of these have been previously reported to play important role in infection process of *L. donovani* leading to fatalities of VL. On the other hand, amongst the uniquely enriched pathways for Visceralization, we found two pathways which have not been studied in *L. donovani* infection or Visceral Leishmaniasis in Humans. These include Hippo and Glucagon signalling pathway. It is known that Hippo signalling pathway, identified as one of the central pathways has previously been associated with cancer [309] and viral infectious diseases [310-312]. Along with its key role in determination of cell polarity, tissue regeneration, apoptosis and cell proliferation, it has also been identified as a key regulator in the mammalian adaptive immune responses and cell migrations which may play a vital role in the visceralization of the infected cells [313]. However, the role of Glucagon signalling pathway in VL remains to be elucidated although it may have some implications towards M2 polarization of the Macrophages.

On the other hand, from the parasite perspective, our analysis of shortest path distance from the VFs to the phenotypic sub-networks and the whole network

revealed that the VF E9BA99, which is a MAP Kinase, is the closest to all three phenotypic responses. This observation produces a possibility of this secretory protein in the involvement in modulating the MAPK pathway for subverting the proinflammatory responses that is crucial for eliciting immune responses aiding parasite clearance which is compromised during Visceral Leishmaniasis. Further investigation is warranted for this observation through *in vitro* and *in vivo* experiments.

The phenotypic sub-networks constructed from the predicted Interactome prompted to further answer questions such as which key proteins in the host act as the central regulators to modulate the phenotypic responses? In this study we have implemented an *in-silico* knockout strategy to identify these key modulators driving all the paths for the VFs towards the phenotypic response proteins. One of the most striking observations seen from the individual knockouts of the candidate proteins was that UBC knockout completely disrupted the path of E9BC27 to the response nodes in all three phenotypic sub-networks through both distance as well as path depletion analysis (**Figure 23**). The shortest paths extracted for this protein for IR sub-network is only one direct interaction i.e., path length 1 of E9BC27 with UBC, no shortest path to any SUR response nodes and 4 shortest paths of path length 2 to four response nodes of VIS sub-network namely, RAC1, NOS2, IRAK1 and TNFA. All these paths pass through the UBC protein. Maxwell *et al.* [174] has stated this protein E9BC27 to have massive export with the highest relative abundance ratio and thus the most enriched secretory protein in the conditioned medium. Myo-inositol-1-phosphate synthase is required for *de novo* biosynthesis of myo-inositol, a precursor of vital inositol phospholipids such as those found in the GPI membrane anchors of nearly all *Leishmania* surface proteins and other glycoconjugates such as GP63 and lipophosphoglycan. This study states its putative role in intracellular survival since it is known to be essential for cell growth and survival in inositol-

limited environments [174]. A *Leishmania* myo-inositol-1-phosphate synthase knockout study has shown complete avirulence in mice [314]. Our knockout study for the first time identifies the host protein UBC in human through which this virulence protein modulates the infection responses inside the host. We thus postulate that the modulation of Ubiquitin-C expression can be effectively implemented to impart avirulence and can be further tested in Human infected subjects to develop effective immunomodulators [315].

Similarly, we also observed the effects of these knockouts on other VFs. Our analysis shows that the complete disruption of paths to VFs (E9BC27, E9BFJ3, E9BFK5, E9BID4, E9B8M5 and E9BQM1) belonging to the proteasome signalling family (**Figure 23**) in the IR sub-network indicates these VFs mainly targets the induced host protective immune responses through modulation of UBC protein to subvert the immune response pathways such as TLR2 signalling pathway. A previous study shows that *L. donovani* promastigote interferes with the ubiquitination of TRAF6 by activation of host de-ubiquitinating enzyme A20 through the mechanism of TLR2-mediated suppression [316]. This is done through inhibition of IKK-NF- κ B cascade. However how this modulation of host A20 deubiquitination occurs is not yet clear. Inhibition of ubiquitination of TRAF6 leads to persistence of TRAF3 in signalosome complex during infection thereby leading to deactivation of MAPK pathway which thereby facilitates parasite survival in host macrophages [317]. TRAF6 and TRAF3 have been observed as intermediate nodes in the phenotypic sub-networks. Our results suggest the involvement of UBC modulation by the parasite through proteasome assembly in its secretome which in turn assists in de-ubiquitination. This Ubiquitin-proteasome pathway plays crucial role in canonical and non-canonical pathways of NF- κ B activation. The pathway enrichment results support this observation as it shows the enrichment of NF- κ B signalling pathway for all three phenotypes. This also shows the interlinking of the modulation of immune

responses as a phenotype supporting the parasite survival inside the host environment. This observation also validates the inclusion of VFs in the category of putatively involved in intracellular survival of the parasite by Maxwell *et.al.* [174]. UBC knockout has also shown significant impact on disruption of all paths in the Visceralization phenotype sub-network for the VFs E9BQM1 and E9BC27. We observed that all the shortest paths for these VFs to the VIS response nodes were through UBC and affected nodes were NOS2, IRAK1, RAC1 and TNFA.

Thereafter we have identified a combination of protein molecules i.e., UBC+HS90A+1433Z, which has a significant impact in the regulation of all three phenotypes under study in the *L. donovani*-Human HPI. Our analysis revealed knock-out of the combination lead to deletion of a significant number of shortest paths from each sub-network which involved loss of genes regulating important pathways e.g. Insulin and PI3k-Akt signalling pathway. Although this combination could not significantly perturb the unique pathways for VIS phenotype response, the identified pathways play a crucial role in the overall infection process from immune response generation to infecting visceral organs. These pathways and genes altered due to the knock-out may be targeted for therapeutic interventions as they play crucial role in progression of the disease. However, it may be mentioned here that one major drawback of this study is that it involves a static analysis of the HPI and the inferences are drawn completely on the basis of graph theoretical analysis alone. A further analysis of the network using LSSA may further give useful insights into the dynamics of the system. Nevertheless, the proposed HPI will be invaluable for gaining a holistic understanding of the *L. donovani* Human interactions and will be extremely useful for the generation of new testable hypothesis and identification of new targets to fight Visceral Leishmaniasis.

CHAPTER 6

UNVEILING IMMUNO-REGULATORY MECHANISMS IN THE TUMOR MICROENVIRONMENT AND DESIGN OF PROTOCOLS FOR TRIGGERING CANCER REMISSION

6.1. Motivation

The tumor microenvironment comprising of the immune cells and cytokines acts as the ‘soil’ that nourishes a developing tumor. Lack of a comprehensive study of the interactions of this tumor microenvironment with the heterogeneous sub-population of tumor cells that arise from the differentiation of Cancer Stem Cells (CSC), i.e. the ‘seed’, has limited our understanding of the development of drug resistance and treatment failures in Cancer.

Mathematical models have been useful in delineating the multiplicity of the complex interactions governing the dynamics of the tumor-immune interaction that remains elusive through *in-vitro* experiments. In this context, *in-silico* studies have shown light on the CSC differentiation pattern and its effect on the tumor growth dynamics [47]. Here it has been observed that symmetric stem cell division shows a correlation with cancer progression [47]. This is in contrast to another report that mentions symmetric stem cell division lowers cancer risk as it reduces the accumulation of cellular damage [318]. However, the effect of CSC differentiation on drug-resistivity and the outcome of the interaction of these differentiated cells with the tumor microenvironment have not been explored sufficiently. On the other hand, models on tumor-immune interaction considering the involvement of tumor, immune effector cell and IL2 have enhanced our understanding about oscillations in tumor sizes, long-term tumor relapse and the conditions under which tumor elimination may be achieved using Adoptive Cellular Immunotherapy [102]. Mathematical

models are now being exploited for the study of the efficacy of adaptive immunity for the elimination of aggressive tumors [103,319], the existence of an angiogenic switch that regulates Cancer progression [320] and as a powerful tool in the design of optimal control strategies for Cancer [321,322].

However, the study of the CSC differentiation pattern and the outcome of the interaction of these heterogeneous tumor cell sub-populations with the immune cells and cytokines present in the microenvironment is a challenge yet to be achieved in both experiments as well as modelling studies. With the aim to gain a clearer and unambiguous picture of the regulatory mechanisms involved in the immune-escape mechanism of the tumor cells, we propose a 13 variable ODE-based mathematical model of the tumor-immune interaction (**Figure 5, Eq. 11- Eq. 23**) that captures the development of a malignant tumor from the 'seed', the CSCs, and its interaction with the 'soil', the tumor microenvironment (**Section 2.4**). In this model, we consider the three different modes of CSC differentiation, as well as the effect of random mutations and ask the question, how the stem cell differentiation patterns regulate the different cellular sub-populations in the tumor and how it affects the development of drug resistance? Using this model we have tried to address the unresolved question of the correlation of M2 macrophages with more resistant tumors by exploring the regulatory feedback loops that govern the dynamics of the tumor-sub-population and the roles of the cytokine feedbacks in shaping the tumor microenvironment. Prior to these studies, the model has been calibrated and the unknown parameters of the model have been estimated by fitting the initial growth kinetics of the model with data obtained from Gastric Cancer cell line using the MCMC-DRAM algorithm [216] (**Section 2.4.7 and 2.4.8**). Moreover, the steady state behaviours of the entire model variables have been quantifiably validated with previously reported experimental data obtained from cytometric and protein expression studies from both *in-vitro* studies as well as data obtained from different

Cancer patients to establish the generic behaviour of our model and ensure its acceptability in the design of treatment strategies.

In order to design treatment protocols for triggering the Cancer remission, we have introduced radio and chemotherapeutic strategies and observed the fold changes in the tumor mass in the presence and in the absence of resistant cells, where we demonstrate the failure of the conventional treatment strategies for curing Cancer. Thereafter, we have ventured the use of immunotherapy that has also been a popular choice for the elimination of the CSCs that are resistant to chemo and radio-therapeutic interventions [76,323]. Hence, using the leads from our model analysis, we have attempted to propose combinatorial treatment strategies and design protocols that help in better suppression of the tumor, even in the presence of resistant cells. However, it may be mentioned here that a vital assumption in our model is that the drug-sensitive and drug-resistant population of tumor cells elicit similar immune responses. The resistant population of cells represents a fraction of the tumor cells that are unresponsive to the conventional treatment strategies. Thus, the difference in their behaviour arises when the treatment/control is applied. Our novel modelling approach and strategy for the design of treatment protocol throws light on the ways to optimize drug schedules, dosage and treatment cycles required for the elimination of the tumor cells. This model may be used as a potential tool for the prediction of Cancer prognosis and calculation of fold changes in the tumor sub-populations in response to a new treatment regimen.

6.2. Results

6.2.1. Model Validation with Experimental Data

6.2.1.1. Tumor Growth (without therapy)

The growth kinetics of the tumor is estimated by four variables of our model, S , S_R , C and C_R , signifying the four sub-populations of cells that are found in the tumor. In

order to validate the growth kinetics of these tumor cell sub-populations of our model, we have used data from different experimental and theoretical studies of tumor growth estimation. The early temporal growth kinetics of the Stem (S) and Resistant Stem cells (S_R) were validated over a period of 5 days, with the reports of Tomasetti and Levy [47], by choosing the parameter values $\gamma_S = 2 \text{ day}^{-1}$ and $\delta_S = 0.2 \text{ day}^{-1}$ (**Figure 25 a**). Here, it was observed that the Stem cells (S) start proliferating exponentially during this initial growth phase of tumor formation. During this time frame, the stem cells also start acquiring mutations and start producing the Resistant Stem Cells (S_R) that gradually starts proliferating slowly and is maintained in very low numbers inside the tumor [47]. It is to be noted that for all our subsequent simulations we have used $\gamma_S = 0.15 \text{ day}^{-1}$ and $\delta_S = 2 \times 10^{-7} \text{ day}^{-1}$, as reported in **Appendix D: Table D. 1**.

Temporal behaviours of the Cancer (C) and Resistant Cancer (C_R) sub-populations have been simulated to validate our model with experimental data (**Figure 6 f and Figure 25 b**). **Figure 25 b** depicts the temporal growth kinetics of the Breast cancer cell line MCF-7/TAX-resistant to Paclitaxel [217], Hepatocellular Carcinoma cell line SK-Hep1/CDDP3-resistant to Cisplatin [218], and Colon Cancer cell lines SW-620-L-OHP and LoVo-L-OHP-resistant to Oxaliplatin [219]. Our simulation result mimics the average behaviour of the resistant cancer cell lines over the time period of 5 days (**Figure 25 b**), using the parameter set estimated through the MCMC method (**Section 2.4.7**).

The model was simulated for a sufficiently long time to study the temporal evolution of the drug-sensitive and drug-resistant cancer cells without any therapeutic interventions (**Figure 25 c**). Here, it was observed that during the early stages of tumor development, the stem cells (S) show a very slow rate of proliferation. According to our simulation results, it is observed that although a

single stem cell initiates the formation of the entire tumor, the stem cells maintain a very low number during the first few months of tumor development. The rapid proliferation of the Cancer cells (C) during the early growth phase leads to their transformation to the resistant C_R species that soon start proliferating rapidly, thereby giving rise to a tumor. At the end of the exponential growth phase, the cancer progression is impeded by the activated M1, T_{HI} and T_c immune cells. This phase mimics the Elimination Phase of Tumor Immunoediting. The systems stay relatively stable for some time (Equilibrium phase) until the stem cells start proliferating exponentially and form the main bulk of the tumor (Escape Phase). Our simulation results indicate that the first resistant stem cell of the tumor is detected at 400 days. Around 800 days the model reaches its steady state. The total tumor density at steady state can be estimated to be around 2.5×10^{10} cells/ml, i.e., 25 times higher than the reported minimum threshold of a clinically detectable tumor [47]. From here we calculate the relative abundance of the sub-populations of the tumor cells and derive that at steady state, the tumor is composed of 94.59% Stem cells (S), 4.49% Cancer cells (C), 1% Cancer Resistant cells (C_R) and small fraction of Stem Resistant cells (S_R) that comprises 0.001% of the tumor mass.

6.2.1.2. Immune cell-ratio comparison with Cytometric data

Our simulations results revealed the dynamics of the adaptive immune responses generated during the tumor development (**Figure 25 c**). Here we observe that as the tumor sub-populations begins to proliferate, the T_c cells show enhanced activation that is required for the natural regression of the tumor (**Figure 25 c**). However, as the tumor continues to proliferate and the resistant cancer cells (C_R) peaks to 1.5×10^9 cells/ml, there is a sharp rise in the M1 and T_{HI} cells proliferation. The combined effect of the T_c , M1 and T_{HI} cells helps to impede the tumor development and decrease it by 3 folds which then falls below the limit of tumor detection (i.e. 10^9

cells/ml, [47]) and apparently stays dormant till 400 days. Thereafter, as the stem (S) and resistant stem (S_R) cells start proliferating, the adaptive immunity becomes active again. However, this is also accompanied with the increase in abundance of M2 and Treg cells (**Figure 25 c**), which helps in the sustenance and continued survival of the tumor cells.

In order to analyse the changes in the immune activation state before and after tumor formation, the immune cell ratio values obtained at the steady state are estimated and compared to the cell ratios in the normal disease-free condition (**Figure 25 f**). It may be mentioned here, in **Figure 25 e** and **Figure 25 f**, CD4 depicts the summation of both the T_{H1} and T_{H2} cells of our model, while CD8 implies Tc cells. From our model analysis, we observe that, during Cancer, the ratio of CD4 and CD8 cells reaches a mean value of 2.75, that is in sharp contrast to the normal healthy individuals which show a value of 1.48 (**Figure 25 f**) [220]. On the other hand, the value of CD4:Treg ratio in Cancer shows a value of 15.2 that is higher than the ratio observed in the normal scenario. This happens due to the enhanced T_{H2} proliferation during tumor development. This also explains the reason for the elevated CD4/Treg ratio. However, the CD8:Treg ratio shows a decrease in Cancer patients and reaches to about 5.5, which is a characteristic of resistant tumors in mammals [221]. In **Figure 25 e**, we have compared these results of our numerical simulation with experimental data obtained from various literatures. Here, we clearly observe that our simulation corroborates very well with the experimental observations made from blood samples of Cancer patients (**Figure 25 e**) [222, 223]. Additionally, we have observed the changes in the $T_{H1}:T_{H2}$ and M1:M2 ratios that have important implications in Cancer prognosis. We find that both $T_{H1}:T_{H2}$ ratio and M1:M2 ratio get decreased during Cancer as compared to the normal disease-free conditions (**Figure 25 f**) [202,224]. These results are in excellent agreement to the literature that suggests Cancer patients showing $T_{H1}:T_{H2}$ ratio below 8 show poor disease prognosis [224].

6.2.1.3. Cytokine Production

IL10 production is a characteristic feature for Cancer detection. During Cancer, the marked increase in IL10 production has been noted in blood samples of various cancer patients, where an average concentration of 0.01 ng/ml has been recorded in various protein expression studies [225-227]. The temporal protein expression profile, from our simulations, suggests the IL10 expression starts increasing around the 15th day until it reaches to a concentration of 0.005 ng/ml (**Figure 25 d**). The IFN- γ production begins along with the proliferation of the Tc cells and increases sharply with the activation of the T_{H1} cells (**Figure 25 d**). This is accompanied by IL2 production that helps in the continued proliferation of the T_{H1} cells. After the proliferation of the stem cells, the cytokine production increases further. The IL10 concentration starts increasing rapidly and attains a concentration of 0.009 ng/ml at steady state. The steady state concentrations of IFN- γ and IL2 reach 9.6 ng/ml and 0.6 ng/ml respectively. The cytokine expression levels from our simulation lie close to the experimentally observed ranges of protein expression in tumor microenvironment prior to their treatment [225].

6.2.2. Model Analysis

6.2.2.1. Development of Drug Resistance is governed by the pattern of stem cell differentiation

With the assumption that the stem cells predominantly tend to renew their pool of stem cells, i.e., with a probability p_3 , we have varied p_1 and p_2 to observe the effect of the asymmetric and symmetric differentiation of the stem cell on the development of drug resistance (**Figure 26 a-d**). Here it may be observed that as we increase the values of p_1 and p_2 , the rate of the stem cell renewal decreases gradually, thereby leading to decrease in the steady state values of S and S_R (**Figure 26 a-b**).

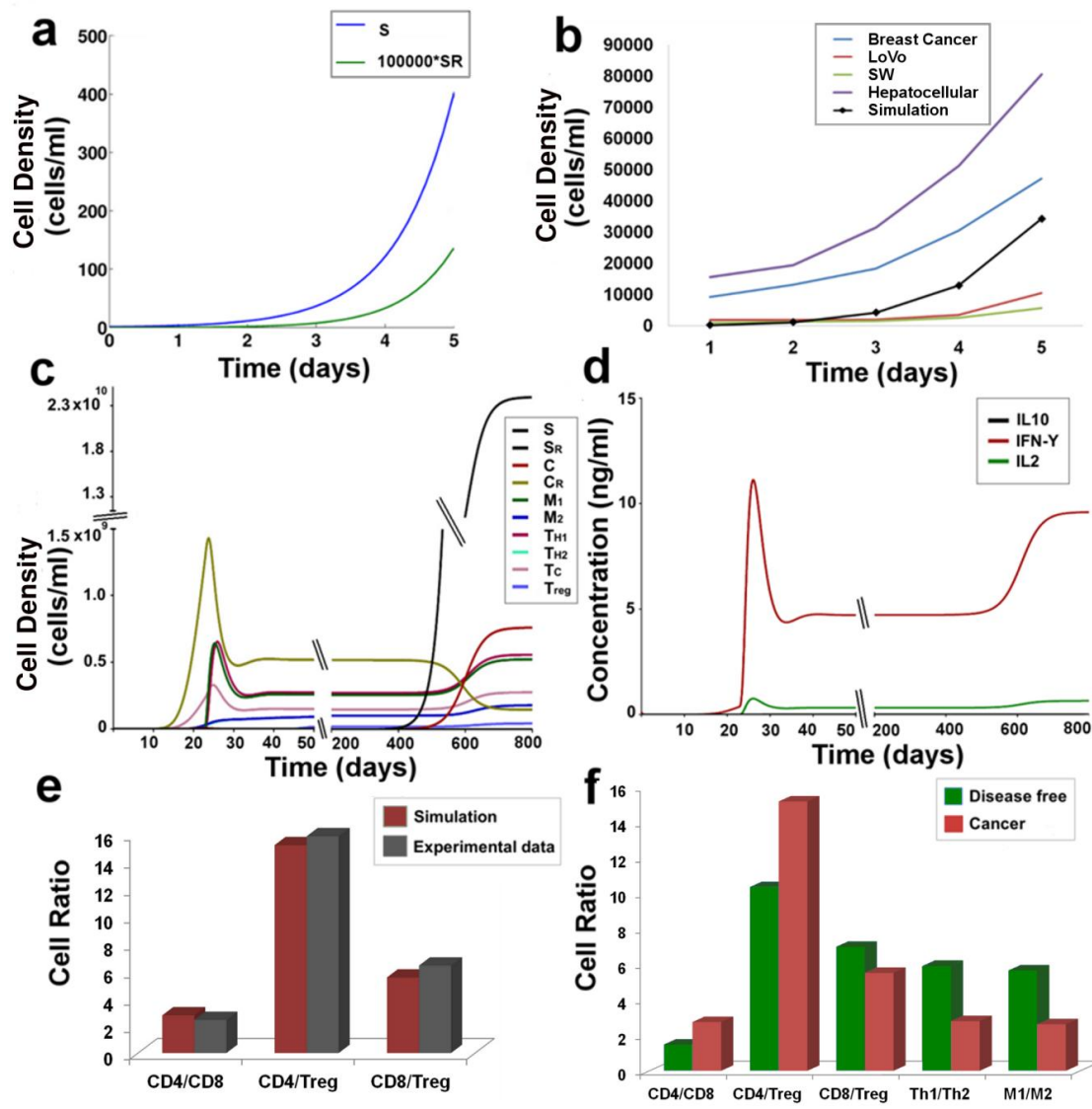


Figure 25: Model Validation with experimental data: (a) Stem and Stem resistant cell proliferation at $\gamma_s=2 \text{ day}^{-1}$ and $\delta_s=0.2 \text{ day}^{-1}$; (b) Proliferation of the Cancer Resistant cells as observed in experiments along with the observations from our simulation; figure depicts growth kinetics of the Breast cancer cell line MCF-7/TAX-resistant to Paclitaxel, Hepatocellular Carcinoma cell line SK-Hep1/CDDP3-resistant to Cisplatin, and Colon Cancer cell lines SW-620-L-OHP and LoVo-L-OHP-resistant to Oxaliplatin; (c) Temporal cellular behavior of the components of the model during tumor formation showing the Elimination, Equilibrium and Escape phases of Tumor Immunoediting; (d) Temporal cytokine expression pattern during tumor formation; (e) Immune Cell Ratio at steady state-experiment versus simulation results (f) Immune cell ratio in the disease free condition versus cancer scenario. Note: $CD4= T_{H1} + T_{H2}$; $CD8=T_c$

However, in the case of C cells (Figure 26 c), we observe that as we increase the value of p_1 , the steady state values of C decreases, whereas the variation of p_2 has little effect on the steady states of C (Figure 26 c). The steady state level of C_R on the

other hand is greatly influenced by p_1 and p_2 (**Figure 26 d**). With the increase in the value of p_1 and p_2 , the steady states value of C_R increases, signifying as the mode of stem cell differentiation changes, the tumor cell sub-populations tend to transform into the resistant Cancer cells. Hence, from our results, we may infer that higher asymmetric stem cell division may be associated with a high rate of drug resistance.

6.2.2.2. Dual Role of Tumor Associated Macrophages

The differential regulatory behaviour of the type I and type II TAMs on the tumor cells was studied by varying the γ_{M1} and γ_{M2} parameters, governing the growth rate of the M1 and M2 macrophages (**Figure 26 e-h**). Here it was observed, as we increase the birth rate of M1, the steady state values of all the sub-populations of the tumor decreases. However, on varying γ_{M2} , we observe that although the S , S_R and C sub-populations show a decrease in the steady state values, the C_R population increases (**Figure 26 e-h**). This result corroborates with the experimental observations that indicate that while M1 macrophages may have an important role in suppression of the tumor growth, a higher abundance of M2 macrophages may lead to poor disease prognosis [324]. From our model analysis, we infer that a higher proliferation of M2 TAMs leads to an increased accumulation of resistant cancer cells in the tumor. This is primarily because of the feedback regulations that govern the dynamics of the tumor-immune interaction network.

6.2.2.3. IFN- γ and IL10 feedbacks regulate Cancer progression

The cytokines are the key regulators of the Tumor-Immune interaction network. The IFN- γ produced by the T_{H1} cells helps in maintaining the steady state dynamics of the entire system. Parameter variation studies reveal that as we increase IFN- γ production from the T_{H1} cells by changing the value of β_{Th1ck2} between 10^{-7} and 10^{-2} ng/cell/day, the S and S_R cells show a dampening oscillation in their temporal

behaviour and these stem cell populations gradually decrease to a very low value. On the other hand, with the increasing β_{Th1ck2} values, the temporal behaviour of C and C_R cell population changes from dampening to stable oscillations at $\beta_{\text{Th1ck2}} = 0.1$ (**Figure 26 i**). The increased production of IFN- γ leads to the rapid killing of the S and S_R populations, whose oscillations dampen with time resulting in complete elimination of the stem cells from the system (**Figure 26 j**). However, the high rate of C proliferation balances out the negative feedback effect of the high IFN- γ production, which keeps oscillating the system (**Figure 26 k**). The phase-plot depicts the feedback regulation that operates between the Cancer (C) cells and IFN- γ that regulates the Cancer relapse. As the Cancer proliferation reaches 4×10^6 cells, the IFN- γ production starts increasing which reduces the Cancer proliferation. When the Cancer cells fall below 1×10^6 cells, the IFN- γ production also starts decreasing. However, at low levels IFN- γ , the Cancer cells start proliferating again (**Figure 26 k**). This leads the system into stable steady state oscillations.

Another important feedback regulation that is crucial for the determination of tumor progression is the negative feedback effect of the IL10 cytokine on the T_{H1} proliferation. This is governed by the parameter μ_{Th1ck1} . As the value of μ_{Th1ck1} is increased, the $T_{\text{H1}}/T_{\text{H2}}$ ratio decreased rapidly (**Figure 26 l**). This results in the further proliferation of all the tumor sub-populations, i.e., S, S_R , C and C_R , and the fold changes in the steady state values of all four increases with increasing μ_{Th1ck1} values (**Figure 26 m**). Here it may be observed that inhibition of T_{H1} cells by IL10, results in higher fold changes of the steady state of S_R cells.

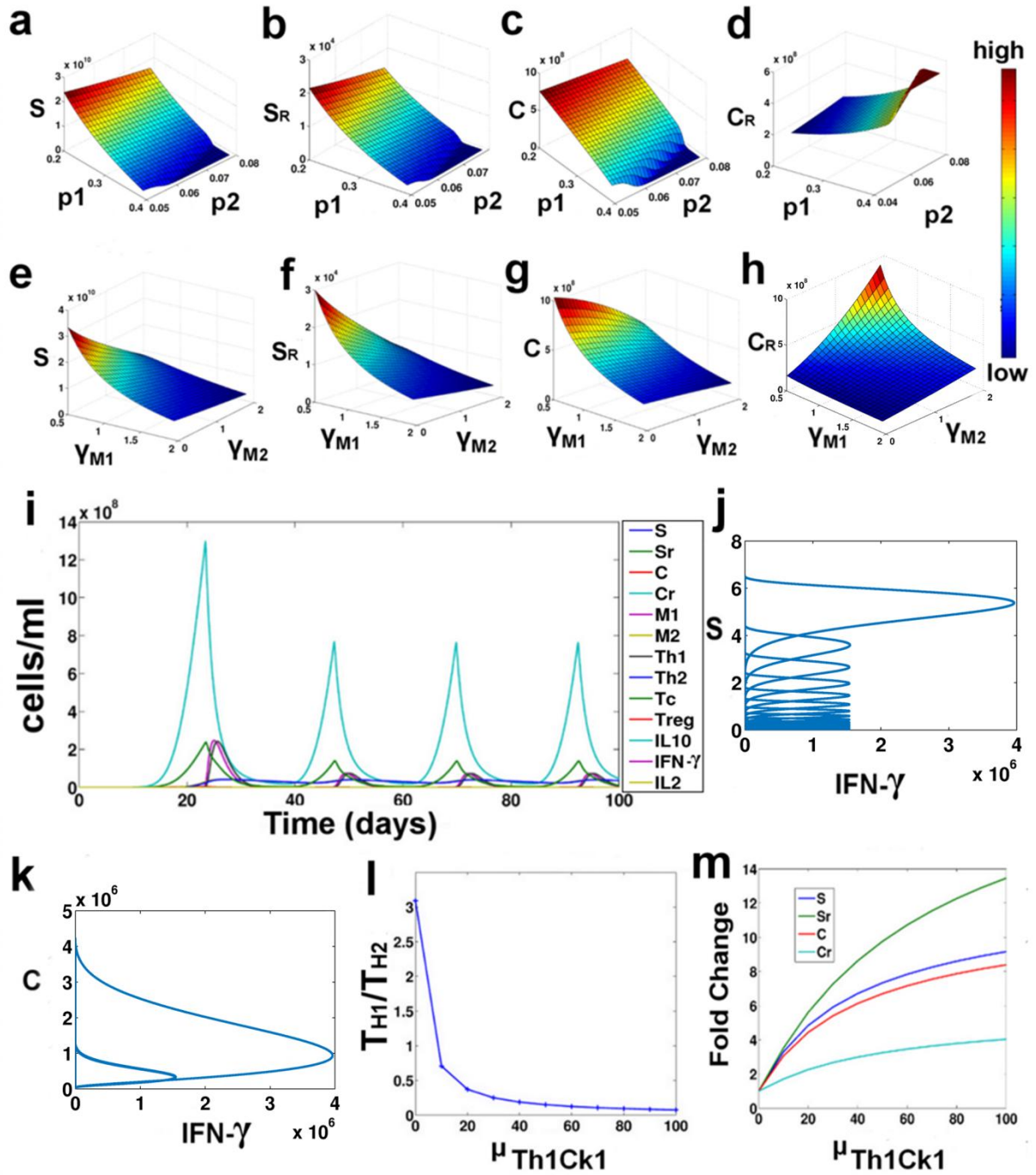


Figure 26: Parameter Variation study. (a-d) Surface plot of the steady state values of S, S_R , C and C_R under varying p_1 and p_2 ; (e-h) Surface plot of the steady state values of S, S_R , C and C_R under varying γ_{M1} and γ_{M2} ; (i) Temporal Plot at $\beta_{Th1Ck2}=0.1$; (j-k) Phase plane of S vs. IFN- γ and C vs. IFN- γ at $\beta_{Th1Ck2}=0.1$; (l) T_{H1}/T_{H2} ratio at varying μ_{Th1Ck1} ; (m) Fold change in steady states at varying μ_{Th1Ck1}

6.2.3. Development of Treatment Strategies

6.2.3.1. Failure of Chemo and Radiotherapies due to the presence of resistant cells

Chemotherapy and Radiotherapy are effective for controlling tumor proliferation in the absence of the resistant cells, i.e., when the rate of transformation of the stem and cancer cells to their resistant counterparts reduces. Here we have tried to simulate the cancer scenario without any mutational pressure, i.e., $m_c = 0$ and $m_s = 0$. Under such conditions, when we apply the Treatment Protocol 1, we observe the Stem and the Cancer cells population decreases rapidly and an overall reduction in the tumor population is observed (**Figure 27**). However, during the formation of a tumor, a certain fraction of the tumor cells acquire resistance to drugs. Under such conditions, i.e. $m_c > 0$ and $m_s > 0$, when the Treatment Protocol 1 is applied at the end of the detection time (DT=200 days), we observe that even though the drug-sensitive populations *viz.* S and C decreases, the resistant populations S_R and C_R remain unaffected during the chemotherapeutic cycles. Thereafter, during the Radiotherapy cycles, the S_R cell population being completely unaffected by radiation proliferates rapidly, while the C and C_R population sharply decreases for some time and then becomes stable. In the next treatment-free stage, S_R , C and C_R start proliferating again. This activates the IFN- γ from the T_{H1} and Tc cells that help to bring down the S_R and C_R populations a little, that are then sustained by the M2 and the Treg cells of the tumor microenvironment. The last phase of Chemotherapy does not have any effect on S_R and C_R populations. Hence the reduction in the overall tumor mass is not substantial. Also, it may be noticed here that at the end of this treatment regimen the T_{H1}/T_{H2} ratio is reduced to 2.5 that is indicative of a poor disease prognosis.

6.2.3.2. Immune Interventions for effective Tumor Remission

Combinatorial treatment protocol was designed to reduce the tumor burden and restore healthy T_{H1}/T_{H2} ratio. Parameter variation studies revealed the importance of

the T_C and the T_{H1} cells in the regulation of the steady state levels of the tumor cells. Here, Immunotherapy was introduced as two control variables, i.e., $u3_{Tc}$ and $u3_{T_{H1}}$, which boost the production of the T_C and T_{H1} respectively.

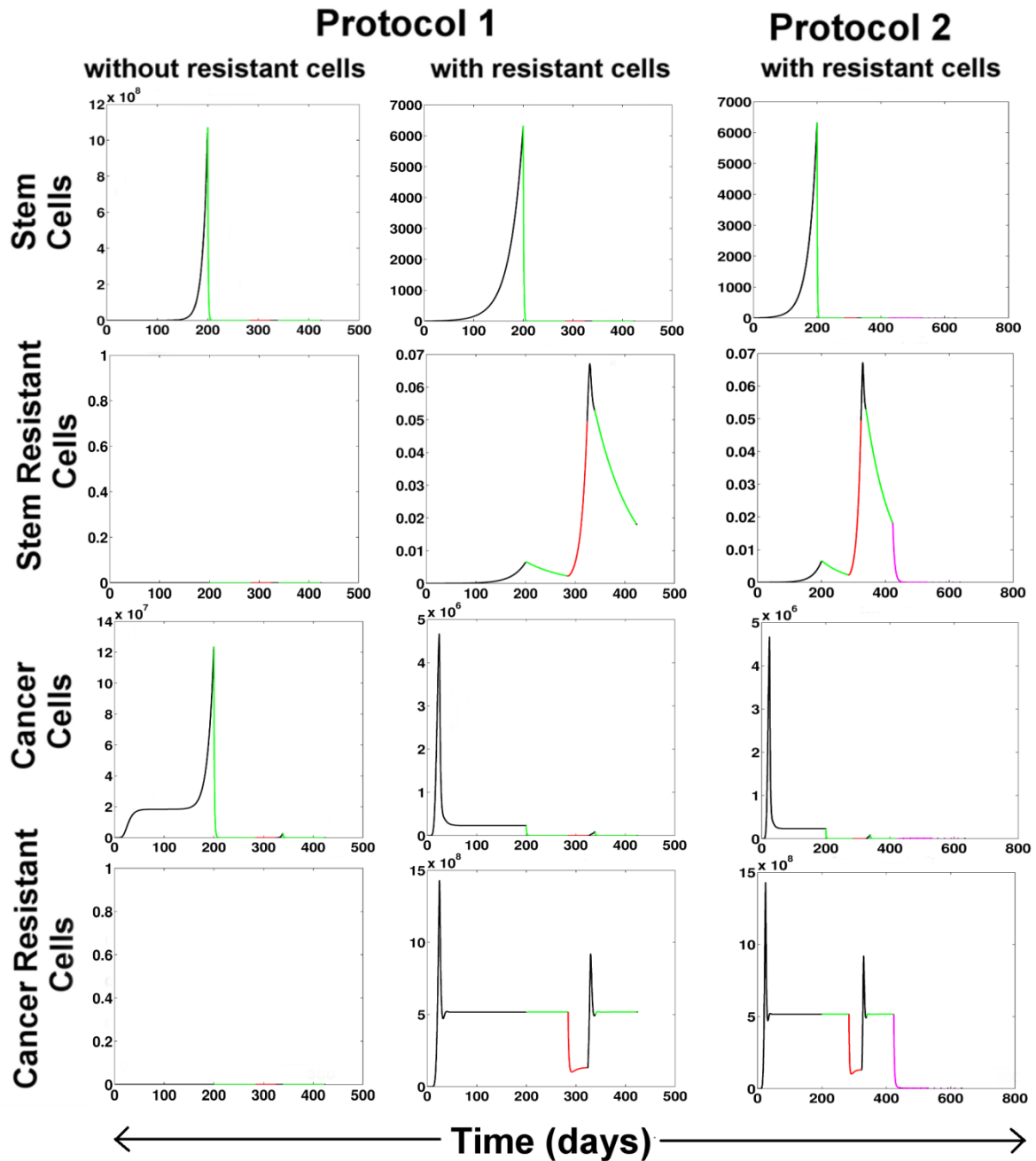


Figure 27: Changes in the tumor growth after therapeutic interventions. Protocol 1 has been applied without and with the presence of resistant cells. Protocol 2 efficiently suppresses tumor in spite of the presence of resistant cells. Color code: Black-without treatment, Green-Chemotherapy, Red-Radiotherapy, Pink-Immunotherapy

The stimulus to the T_{H1} and T_C cells was started at the end of the last chemotherapeutic cycle and was administered for 20 days followed by 1 day rest. This was repeated for 10 cycles. The dosage of each therapy was varied in wide ranges, and it was observed that when Immunotherapy is low, the change in Radio and Chemotherapies does not affect the tumor population significantly which is reflected in the very small tumor fold change and low T_{H1}/T_{H2} ratio (**Appendix D: Figure D. 1**). As the Immunotherapy is increased, the fold change of tumor population increases along with the T_{H1}/T_{H2} . However at very high doses of immunostimulation, the fold changes decreases and the T_{H1}/T_{H2} ratio increases abruptly that leads to extreme suppression of the T_{H2} cells in the system. Hence the region $1.5 < d_I < 2.5$ can be considered as the ideal dosage of immunostimulation required for triggering the remission of Tumor. Using the leads from this analysis, the Protocol 2 was designed. At the end of this treatment regimen, it was observed that all the four tumor sub-populations showed a huge reduction in their proliferation, i.e., 136 fold reduction in tumor mass (Protocol 2). The T_{H1}/T_{H2} ratio was boosted to 8.8.

6.3. Discussion

The model developed here throws light into the development of a full-grown tumor from a single cancer stem cell (S), and the influence of the tumor microenvironment during its maturation. The study of the temporal evolution of tumor development from our model captures the three phases of Immuno-editing – Elimination, Equilibrium and Escape phases (**Figure 25 c**). The model shows that although the CSC forms the ‘seed’ from which the tumor emanates, the stem cell population remains low in the beginning. These cancer stem cells, owing to their slow replication, are intrinsically resistant to radiotherapy and are only partially sensitive to chemotherapy [211,325]. Additionally, the stem cell sub-populations have a strong immune-suppressive effect on the tumor microenvironment [326]. This phenomenon

has been captured in our model in the study of the temporal evolution of the tumor-immune interaction dynamics, where we observe that coincident with the proliferation of the stem and resistant stem cell there is also an increased proliferation of the M2 and Treg cells (**Figure 25 c**). This consequently leads to the lowering of the M1/M2 and T_{H1}/T_{H2} ratio that is associated with the formation of resistant tumors (**Figure 25 f**). Moreover, it has been observed in our study that the proliferation of stem cell sub-populations leads to suppression of the Tc cells and the activation of the Treg cells, that results in the lowering the CD8/Treg ratio during Cancer (**Figure 25 f**). This happens primarily because of the direct negative regulatory effects of the stem and resistant stem cells on the growth of the Tc cells. Hence, an early detection of the tumor is crucial for an effective treatment, when the stem cell population in the tumor remains low and the resistant stem cell population is not yet formed.

The model also captures the different patterns of CSC differentiation and its role in determining the fate of the tumor. Here, it has been observed that as the differentiation pattern of CSC shifts towards the asymmetric pattern, the CSC pool begins to deplete and the CSC starts producing the terminally differentiated cancer cells that have a finite lifespan. The reduction in the stem cell population helps in the reduction of its immune-suppressive effects on the Tc cells. At the same time, the differentiation of the stem into the cancer cells stimulates the Tc cells to get activated that now inhibit the tumor *via* the negative feedback regulation. However, the steady state value of the resistant cancer cells increases and overrides the negative feedback effect of the immune cells, reinforcing the observations that a higher asymmetric stem cell differentiation may be associated with the formation of more resistant tumors. Our model analysis also indicates that at low p_1 value, as the probability of symmetric differentiation (p_2) of stem cells is increased, the steady state levels of stem cells rapidly decrease, however it has little effect on the steady state value of

Cancer cells. On the contrary, at high p_1 value, the increase in p_2 leads to the transformation of the cancer to resistant cancer cells. These results signify that reduction in stem cell symmetric renewal (p_3) of the cell leads to its differentiation into more resistant tumors.

The model further elucidates a dual role of the M2-TAMs in regulating the tumor formation (**Figure 26 e-h**). Here we observe that on one hand, the M2-TAMs aid in the suppression of the S , S_R and C cells of the tumor. This is because M2 is a prime source for the production of IL10 cytokine that has an important role in positively regulating the proliferation of the Cancer (C) cells. Hence, as the M2-TAMs increase in abundance, the cancer cells begin to proliferate *via* a positive feedback loop. This leads to the activation of both the T_c and T_{H1} cells that inhibits the tumor cells *via* their negative feedback by producing a higher amount of IFN- γ and higher cytotoxic activity of the T_c cells (**Figure 28 a**). However, on the other hand, it may be observed that M2-TAMs help in the growth of the C_R cells *via* the positive feedback loop, while the negative feedback has little effect on the C_R sub-population. This observation explains the reason for the refractory behavior of the tumor to treatment strategies under the presence of the M2-TAMs [327].

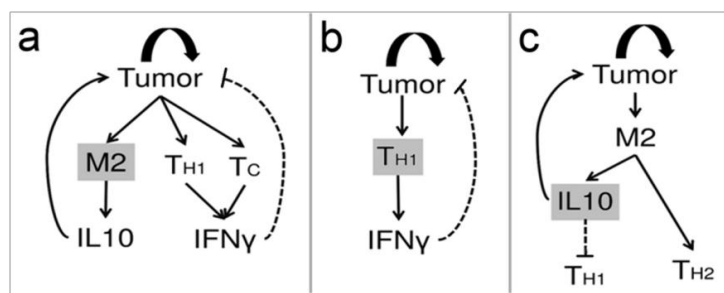


Figure 28: Regulatory Feedback Loops. (a) The M2 macrophage triggers two feedback loops. The first loop through IL10 is a positive feedback that triggers tumor proliferation. This, in turn, activates the second loop through IFN- γ that inhibits the tumor; (b) T_{H1} derived IFN- γ inhibits the tumor via a negative feedback that leads to an oscillation in the population of tumor cells; (c) Positive feedback loop through IL10 is responsible for the maintenance of tumor and suppression of T_{H1}/ T_{H2} ratio.

Our study reveals the functional behavior of the feedback mechanisms that regulate the behaviour of the entire tumor-immune interaction network. From our parameter

variation studies, the importance of the IFN- γ production in regulating the temporal behavior of the tumor development is observed. Here, we found that as the rate of IFN- γ production from the T_{H1} cells increases, the negative feedback effect of IFN- γ on the tumor helps in the suppression of the tumor cells (**Figure 26 i** and **Figure 28 b**). However, the replicative potential of the Cancer and resistant Cancer balances out the negative effect of the IFN- γ leading to an oscillatory tumor-relapsing behaviour, whereas the slowly replicating stem and resistant cells sub-populations gradually get eliminated from the tumor due to the high production of the IFN- γ cytokine (**Figure 26 j-k**). This finding explains the IFN- γ paradox and has important implications in the design of Immunotherapeutic protocols, where we observe the differential behaviour of the tumor cells in response to high IFN- γ production [328,329]. Using our model, we further explore the effects of the negative feedback of the IL10 cytokine on the T_{H1} cells (**Figure 26 l-m** and **Figure 28 c**). We also make an important observation, where we find that as the sensitivity of T_{H1} cells to IL10 increases, the T_{H1}/T_{H2} ratio decreases sharply. This leads to the increased proliferation of the tumor cells. The fold change in the steady values of the resistant stem cells is the greatest signifying the prognostic role of the T_{H1}/T_{H2} ratio in predicting tumor progression and the formation of a resistant tumor with higher proportion of resistant stem cells.

With the knowledge of the regulatory mechanisms governing the differential response of the tumor sub-populations to the microenvironment, we have tried to explore the effect of treatment strategies conventionally adopted for the treatment of Cancer (**Figure 27**). Using our model, we have been able to show that the reason for the failure of conventional Chemotherapy and Radiotherapy is primarily due to the formation of the resistant cancer stem cells S_R and resistant cancer cells C_R within the tumor. Under the conditions where there are no mutations conferring drug resistivity to the tumor, a significant reduction in tumor mass may be achieved using

Chemo and Radio therapy alone. However, in reality, a small population of resistant tumor cells exists in the tumor that remains refractory to these treatment protocols. In order to successfully remove the tumor, a combination of the conventional treatment protocol along with Immuno-therapy can help alleviate the disease scenario. There can be several ways of boosting the immune system. However, in this work, we propose that a synergistic stimulus to both T_{H1} and Tc cells is required for the generation of an adaptive immune response that is capable of reducing both the drug-sensitive as well as the drug-resistant sub-populations of the tumor. In order to achieve this, dosage of Radio, Chemo and Immunotherapies were varied to create 1000 different treatment combinations and thereafter a treatment protocol (Protocol 2) has been designed to ensure maximal reduction in the tumor mass, as well as the restoration of a healthy T_{H1}/T_{H2} balance.

In this model, we try to capture the high complexity of the tumor microenvironment with a simple ODE model that represents the interaction of the tumor cell sub-populations and the immune cells at the phenotypic level. Here we assume that the parameters governing these cellular interactions are a cumulative outcome of the various molecular and intracellular signalling events occurring in the microenvironment that influence the immune evasion but have not been explicitly considered in this model for its simplification. However, it is worth mentioning that depending on the availability of data and hybrid modelling techniques involving a combination of different mathematical tools and strategies, this model may further be improvised by considering the effect of the various molecular events such as angiogenesis, the role of the miRNA, exosomes and chemokines in mediating the cellular interactions, the metabolic pathways as well as the hypoxic conditions [330], that may further help us unravel unknown regulations underlying the tumor immune interaction and the development of drug-resistance.

CHAPTER 7

CONCLUSION AND FUTURE DIRECTIONS

7.1. Conclusion

Identification of important immunotherapeutic targets and regulatory mechanisms is essential for the design of optimal treatment strategies for infectious diseases (e.g. Leishmaniasis) and Cancer that causes suppression of the immune effector functions. However, the complexity of the immune regulatory network that governs the differential immune response of the T-cells under varied antigenic challenges still remains elusive. In this context, the knowledge regarding the signalling pathway cross talks is essential to understand the mechanistic regulations that govern the effector functions of the lymphocytes. Hence, in this thesis, we aim to delve deep into the intricate network of intracellular and intercellular signalling pathway crosstalks that regulate the immune responses and effector functions during Leishmaniasis and Cancer using mathematical modelling and computational approaches.

In order to gain insight into the immune-regulatory modules involved in T-cell functioning as well as study the immune-modulatory mechanisms employed by pathogen and the tumor cells, the study of T-cell signalling pathway is an essential prerequisite to the identification of the immune-stimulatory targets for the treatment of different diseases. Hence in **Chapter 3**, first we have aimed to study the role of various T-cell co-receptor molecules and calcium channel CRAC in the maintenance of cell's functional responses and regulation of the production of effector molecules, principally the cytokines mediating T cell immune response. Here, through manual reconstruction of the pathway map of T-cell activation and model development using LSSA, the role of co-receptor molecules has been studied that govern the

expression patterns of Interleukins under a variety of micro environmental conditions and stimuli, the changes in the phenotypic behaviours of the T-cell population and the signalling routes through which the response is propagated in the cytoplasm. This integrative computational approach serves as a valuable technique to study the changes in protein expression patterns and helps to predict variations in the cellular behaviour through which we identify that a sustained T-cell proliferation can only be achieved when the TCR:CD3 complex, the Ca^{+2} channel CRAC and the T-cell co-receptor molecule OX40 are stimulated simultaneously. The model also throws light on the role of the co-receptors CD27 and LTBR in the regulation of Interleukins IL1, IL12, IL3, IL6, IL8 and IL2 expression which are essential for the T-helper cell immune functions during an antigenic challenge [122].

Thereafter, the role of T_H cell Plasticity/ differentiation for the control of disease progression has been studied with respect to the infectious disease Leishmaniasis, caused by *Leishmania sp.*, which devices its survival strategy by suppressing the host's immune functions leading to switching of the T-cell responses from a healing T_{H1} response to a non-healing T_{H2} response. Using a reconstructed signalling network of the intracellular and intercellular reactions between a *Leishmania* infected APC and T-cell, we propose a LSSA based model to predict the inhibitory effect of the *Leishmania* infected APC on the T-cell and to identify the regulators of this T_{H1}/T_{H2} -switching behavior as observed during *Leishmania* infection. This has important implications in developing strategies for effective regulation of the switching mechanism for devising a proper cure for the disease. In **Chapter 4**, we have been able to capture some of the vital aspects of *Leishmania* infection and the mechanism through which the interaction of the *Leishmania* antigen molecules with the APC signalling proteins modulate the microbicidal activity of both the APC and T-cell. Although our model does not deal with the dynamics of the entire system due to the large number of unknown parameter sets, but through the logical analysis of the

integrated *Leishmania*-APC-T-cell model, we have been able to precisely highlight the inhibitory effects of *Leishmania* infection on the T-cell's signalling routes and T_{H1}/T_{H2} immune responses. Here we observe that *Leishmania* infection enhances the secretion of the IFN_BETA from the APC, which in turn can up-regulate the production of the RAP1 and SOCS3 proteins inside the T-cell, the potential inhibitors of MAPK and JAK-STAT signalling pathways respectively, *via* the TYK2-mediated pathway; the other T-cell pathway affected in *Leishmania* infection being the JAK2-STAT4 pathway. Enhancing the activity of this pathway in the T-cell by inhibition of the phosphatase SHP2, and simultaneously regulating the activity of the TLR3 molecule in the APC, we have also been able to identify certain unique combinations of proteins, which can act as regulatory switch to shift the T_{H2} response towards the T_{H1} response, and at the same time can increase the production of NO. The study highlights a negative role of the T-cell SHC molecule and a positive role of the MKP molecule in Leishmaniasis treatment. Attractor analysis study firmly establishes the reasons for the failure of the conventional immunotherapeutic targets, such as IFN_GAMMA_T treatment, and ensures that our proposed combinations of protein molecules when targeted reverts the system to an infection-free attractor. This study not only enhances our knowledge in understanding the T_{H1}/T_{H2} regulatory switch to promote healing response during leishmaniasis but also helps to identify combinations of target molecules can be efficiently used as potent immunostimulators to yield an effective anti-*Leishmania* immune response and expedite the process of parasite clearance from the system [331,332].

In **Chapter 5**, we address the problem of Visceral Leishmaniasis, where we aim to identify the important regulatory modules to study the parasite strategies to subvert the host immune responses, secure its survival inside the host and further the spread of infection to the visceral organs. Here the host pathogen interaction network between secretome derived virulence factors of *Leishmania donovani*, one of the

causative agents of Visceral Leishmaniasis, and the Human Protein Protein Interaction (PPI) network has been proposed using Interlog and Domain mapping strategies. Shortest path analysis and extraction of important sub-networks governing distinct phenotypes lead to the identification of important signalling pathways targeted by the parasite. Thereafter we propose a novel combination of protein targets (UBC, HS90A and 1433Z), using graph theoretical analysis to determine the pathways which are significantly de-regulated in shortest path depletion analysis and can be implicated to play a crucial role in regulating the phenotypic responses such as Immune Response, Parasite Survival and Visceralization in the predicted *L. donovani* and Human host pathogen interactome.

On the other hand, lack of a comprehensive study of the interactions of the tumor microenvironment with the heterogeneous sub-population of tumor cells that arise from the differentiation of Cancer Stem Cells (CSC) has limited our understanding of the development of drug resistance and treatment failures in Cancer [45,107,108]. Hence, in **Chapter 6**, with respect to the long standing ‘seed and soil’ hypothesis, we propose a model that throws light into the previously unexplored regulations governing tumor-immune interaction. This novel approach of developing of a tumor-immune interaction model considering both the stem cell differentiation pattern as well as the effect of the microenvironment has helped us in unveiling the effect of stem cell differentiation on the development of drug resistance and the different mechanistic regulations governing the tumor-immune interaction dynamics. However, this model does not capture the diffusion kinetics of the cytokines or the time delay associated with the cytokine regulations. Nonetheless, the observations derived from the model have been corroborated extensively with the experimental observations in cytometric and protein expression studies that strengthen the reliability of our model for the prediction of mechanistic regulations of tumor-immune interaction and design of the treatment protocols.

Using this model we report that as the CSC differentiation shifts from symmetric to asymmetric pattern, resistant cancer cells start accumulating in the tumor that makes it refractory to therapeutic interventions. Model analyses unveiled the presence of feedback loops that establish the dual role of M2 macrophages in regulating tumor proliferation and a shift towards the formation of more resistant tumors. The study further revealed oscillations in the tumor sub-populations in the presence of T_{H1} derived IFN- γ that eliminates CSC but retains a fraction of the differentiated cells that explains the IFN- γ paradigm in the treatment of Cancer; and the role of IL10 feedback in the regulation of T_{H1}/T_{H2} ratio. These analyses expose important observations that are indicative of Cancer prognosis. Further, the model has been used for testing known treatment protocols to explore the reasons of failure of conventional treatment strategies and propose an improvised protocol that shows promising results in suppressing the proliferation of all the cellular sub-populations of the tumor and restoring a healthy T_{H1}/T_{H2} ratio that assures better Cancer remission [333].

7.2. Future Directions

The study on the T cell pathway provides a comprehensive understanding of the crosstalks of the co-receptor mediated pathways that are essential for gaining a holistic understanding of the Helper T cell responses. The outcome of the thesis provides several testable hypotheses for the design of immunotherapy for Leishmaniasis and Cancer. The insights gained into the pathway regulations of the T cells during *Leishmania* infection provides a fundamental understanding of the parasite strategies in suppressing the host immune responses that paves the path for further experimental studies conforming the effect of *Leishmania* infection on immune suppression and T cell differentiation and polarization. On the other hand, the proposed combinations of target molecules predicted through the study can be efficiently used as potent immunostimulators to yield an effective anti-

Leishmania immune response and expedite the process of parasite clearance from the system. Immuno-pharmacological studies involving virtual screening and molecular docking studies can be further performed to identify the drug-like small molecules that may help to regulate these identified targets to elicit a robust anti-*Leishmania* immune response. The pathways reconstructed and the models developed for the study of Cutaneous and Visceral Leishmaniasis provides useful insights into the study and prediction of host pathogen interactions for other infectious diseases that devices its survival strategy by mediating immune suppression of the host.

Additionally, the study on tumor immune interaction provides insights into the mechanisms regulating the development of tumor heterogeneity and resistance as well as throw light into feedback regulations that answers few of the major questions of tumor biology. Simultaneously, the model developed in the study caters to the oncologists to optimize treatment strategies, drug dosage and time schedules for designing advanced treatment protocols for Cancer.

As a continuation of the work on the tumor development presented in the thesis, we have also been able to develop a mathematical to study the effect of drug combinations, comprising of novel Acridone derivatives (AC26, AC2 and AC7) and Temozolomide (TMZ), on heterogeneous tumor subpopulations [334]. Here using our modelling strategy the dosage combinations of the novel drugs that show high tumor cytotoxicity and high synergy and efficacy towards the reduction of TMZ resistant Glioma have been determined. Our model outcomes nicely corroborate with our *in vitro* studies on two Glioma cell lines (T-98 and U-87). Molecular Docking studies have been further performed to unveil the interaction of the Acridone derivatives with the drug resistance causing proteins P-GP, MGMT, MRP that explains the plausibility of the drug synergy. The drugs show high cytotoxicity and lipophilicity. *In silico* analysis has also been performed to predict the Blood Brain Barrier permeability. Through this study we propose three novel drug combinations

with the optimal dosages that provide new hopes for the treatment of drug resistant Glioma as well as develop a mathematical model that will be an invaluable tool to estimate dosage and effectiveness of other drugs for Glioma therapy in future. To establish the clinical usefulness of the proposed combinations, further *in vitro* and *in vivo* assays using orthotropic xenografts can be performed for determining the clinical efficacy and estimation of the other important pharmacokinetic parameters of the drugs.

Thus, the outcomes of the thesis not only contribute to the understanding of the fundamental questions of T-cell biology, but also through the development of the mathematical models we have been able to provide several tools for identification of important immune-stimulatory targets for better treatment and alleviation of infectious diseases and Cancer.

APPENDIX A

Table A. 1: Logical Equations

1.	$AKT^* = (CARMA1) \text{ or } (CDC42+RAC) \text{ or } (COT) \text{ or } (GRB7) \text{ or } (IKK_ALPHA \text{ and } IKK_BETA) \text{ or } (PAK) \text{ or } (PDK1) \text{ or } (PKC)$
2.	$AP1^* = (\text{not } GSK3_BETA) \text{ or } (ATF2 \text{ and } JUN \text{ and } \text{not } GSK3_BETA) \text{ or } (CRE \text{ and } ATF2 \text{ and } JUN \text{ and } \text{not } GSK3_BETA) \text{ or } (CRE \text{ and } JUN \text{ and } \text{not } GSK3_BETA) \text{ or } (FOS \text{ and } JUN \text{ and } \text{not } GSK3_BETA) \text{ or } (JUN \text{ and } \text{not } GSK3_BETA) \text{ or } (NUC_ERK1_2 \text{ and } FOS \text{ and } JUN \text{ and } \text{not } GSK3_BETA) \text{ or } (NUC_JNK \text{ and } FOS \text{ and } JUN) \text{ or } (NUC_P38 \text{ and } FOS \text{ and } JUN \text{ and } \text{not } GSK3_BETA)$
3.	$ASK1^* = (TRAF2)$
4.	$ATF2^* = (NUC_P38)$
5.	$BAD^* = (\text{not } AKT) \text{ or } (JNK \text{ and } \text{not } AKT)$
6.	$BCL10^* = (CARMA1 \text{ and } PKC_THETA \text{ and } \text{not } IKK_ALPHA \text{ and } \text{not } IKK_BETA \text{ and } \text{not } IKK_GAMMA)$
7.	$BCL2^* = (\text{not } JNK) \text{ or } (ETS) \text{ or } (NUC_CREB)$
8.	$BCLX^* = (\text{not } BAD) \text{ or } (\text{not } JNK) \text{ or } (ETS) \text{ or } (NUC_NFKB)$
9.	$C3G^* = (CRK_L)$
10.	$CABIN1^* = (\text{not } CAMK4)$
11.	$CALCINEURIN^* = (\text{not } CABIN1 \text{ and } CAM) \text{ or } (CAM \text{ and } \text{not } CALCIPRESSIN \text{ and } \text{not } CABIN1)$
12.	$CALCIUM_IN^* = (CRAC \text{ and } CALCIUM_OUT)$
13.	$CAM^* = (CALCIUM_IN) \text{ or } (VAV \text{ and } CALCIUM_IN)$
14.	$CAMK4^* = (CAM)$
15.	$CARMA1^* = (PKC_THETA)$
16.	$CCL19^* = (NUC_NFKB)$
17.	$CD2^* = (FYN) \text{ or } (LCK)$
18.	$CD3^* = (LCK)$
19.	$CD4^* = (LCK)$
20.	$CD8^* = (LCK)$
21.	$CDC25^* = (NUC_MYC)$
22.	$CDC42^* = (PAK) \text{ or } (RAS) \text{ or } (VAV)$
23.	$CDC42+RAC^* = (VAV \text{ and } \text{not } RAC_GAP)$
24.	$CDK_4^* = (NUC_MYC)$
25.	$COT^* = (RIP1) \text{ or } (TRAF2)$
26.	$CRAC^* = (IP3)$
27.	$CREB^* = (RSK) \text{ or } (\text{not } GSK3_BETA)$

28.	CRK_L*=(TYK2)
29.	CYCLIN_A*=(AP1 and not GSK3_BETA) or (NUC_CREB) or (NUC_MYC)
30.	CYCLIN_D1*=(AP1 and not GSK3_BETA) or (ETS) or (NUC_CREB) or (NUC_MYC) or (NUC_NFKB)
31.	CYCLIN_D2*=(NUC_MYC)
32.	CYCLIN_E*=(NUC_MYC)
33.	DAG*=(PIP2)
34.	ELK1*=(NUC_ERK1_2)
35.	ERK1_2*=(MEK1_2 and not MKP)
36.	ETS*=(NUC_ERK1_2)
37.	FASL*=(ETS) or (NUC_NFKB)
38.	FKHR*=(not AKT)
39.	FOS*=(ELK1) or (ETS) or (JUN) or (NUC_P38)
40.	FYN*=(not PAG+CSK) or (CD45 and not PAG+CSK and not CBL)
41.	GAB1*=(ERK1_2) or (SHC)
42.	GCKR*=(TRAF2)
43.	GLK*=(TRAF2)
44.	GM-CSF*=(ETS and NUC_NFKB) or (ETS and NUC_NFKB and AP1)
45.	GRB2+SOS*=(B7_1 and CD28) or (B7_2 and CD28) or (RAS_GRP)
46.	GSK3_BETA*=(not AKT) or (IFN_GAMMA)
47.	HBEGF*=(ETS)
48.	HPK1*=(LAT)
49.	IFN_GAMMA*=(NUC_NFAT and AP1)
50.	IKB_ALPHA*=(not IKK_BETA)
51.	IKB_BETA*=(not IKK_ALPHA and not IKK_BETA) or (not IKK_ALPHA and not IKK_BETA and not IKK_GAMMA)
52.	IKK_ALPHA*=(NIK) or (TRAF2)
53.	IKK_BETA*=(BCL10) or (IKK_ALPHA) or (PKC_THETA) or (TRAF2)
54.	IKK_GAMMA*=(BCL10 and MALT1 and CARMA1) or (CARMA1 and MALT1 and BCL10 and IKK_ALPHA and IKK_BETA) or (IKK_ALPHA and IKK_BETA) or (RIP1) or (TAK1+TAB and RIP1) or (TRAF6 and MALT1)
55.	IL1*=(NUC_NFKB)
56.	IL10*=(AP1 and CREB and not GSK3_BETA) or (NUC_NFAT)
57.	IL12*=(ETS and NUC_NFKB)
58.	IL13*=(NUC_NFAT and AP1)
59.	IL2*=(AP1 and NUC_NFAT and not GSK3_BETA) or (ETS and NUC_NFKB) or (NUC_NFAT and AP1) or (NUC_NFKB)
60.	IL2R*=(NUC_NFKB)

61.	IL3*=(ETS and NUC_NFKB)
62.	IL4*=(AP1 and NUC_NFAT) or (AP1 and NUC_NFAT and not GSK3_BETA)
63.	IL5*=(AP1 and not GSK3_BETA)
64.	IL6*=(AP1 and CREB and not GSK3_BETA) or (NUC_NFKB)
65.	IL8*=(NUC_NFKB)
66.	IL9*=(AP1) or (NUC_NFAT) or (NUC_NFKB)
67.	IP3*=(PIP2)
68.	ITK*=(CD2) or (LCK)
69.	JAK*=(not SOCS3) or (GRB2) or (IFN_ALPHA and IFNAR1_R2) or (IFNAR1_R2 and IFN_BETA) or (IFNAR1_R2 and IFN_OMEGA) or (SHC)
70.	JAK2*=(not SHP2)
71.	JNK*=(MKK) or (MKK4_7 and not MKP) or (MKK7) or (T3JAM)
72.	JUN*=(FOS) or (NUC_JNK)
73.	LAT*=(ITK) or (ZAP70)
74.	LAT+GRB2+SOS1*=(LAT and GRB2 and SOS1)
75.	LCK*=(not PAG+CSK and not LYP) or (not PAG+CSK and CD4 and MHC_CLASS_II+AG) or (CD4 and MHC_CLASS_II+AG and not PAG+CSK and not LYP) or (CD45 and CD4 and MHC_CLASS_II+AG and CD28 and not CBL and not LYP and not PAG+CSK)
76.	LYP*=(not CSK)
77.	MALT1*=(CARMA1) or (PKC_THETA)
78.	MEF2*=(CALCINEURIN and P300) or (CALCINEURIN and P300 and not CABIN1 and not HDAC) or (MEF2A and MEF2B and MEF2C and MEF2D)
79.	MEK1_2*=(PAK and not MKP) or (RAF and not MKP) or (RAF1 and not MKP)
80.	MEKK*=(CDC42+RAC) or (GCKR) or (HPK1) or (PAK)
81.	MEKK1_4*=(CDC42+RAC) or (RAC1)
82.	MEKK3*=(OSM)
83.	MEKK4_7*=(CDC42+RAC)
84.	MKK*=(ASK1) or (MEKK)
85.	MKK3_6*=(MEKK1_4) or (MEKK3) or (MLK3)
86.	MKK4_7*=(ASK1) or (COT and not MKP) or (MEKK4_7 and not MKP)
87.	MKK7*=(MEKK) or (TAK1)
88.	MLK2*=(PAK)
89.	MLK3*=(CDC42 and not AKT) or (RAC)
90.	NCK*=(not RAS) or (PKC and not RAS)
91.	NCK+SOS*=(NCK and SOS)
92.	NFAT*=(CALCINEURIN)
93.	NFAT+P300+MEF2*=(NFAT and P300 and MEF2)

94.	NFKB*=(OX40 and OX40L and PKC_THETA and TRAF2 and RIP1 and CARMA1 and MALT1 and BCL10 and IKK_ALPHA and IKK_BETA and IKK_GAMMA and not IKB_ALPHA and not IKB_BETA) or (not TRAF1) or (not IKB_BETA and not IKB_ALPHA and NIK)
95.	NIK*=(COT) or (TRAF2) or (TRAF5)
96.	NUC_CREB*=(CREB) or (NUC_ERK1_2)
97.	NUC_ERK1_2*=(ERK1_2)
98.	NUC_JNK*=(JNK)
99.	NUC_MYC*=(NUC_ERK1_2) or (NUC_NFKB)
100.	NUC_NFAT*=(NFAT) or (NFAT and not GSK3_BETA)
101.	NUC_NFKB*=(NFKB) or (NFKB and IL1)
102.	NUC_P38*=(P38)
103.	NUR_77*=(NFAT+P300+MEF2)
104.	OSM*=(RAC1)
105.	P15*=(NUC_MYC)
106.	P21*=(AKT) or (NUC_MYC)
107.	P21RAS*=(JAK2) or (LAT+GRB2+SOS1)
108.	P38*=(MKK3_6)
109.	P70*=(PDK1)
110.	PAG+CSK*=(PAG and CSK and FYN and not CD45) or (PAG and CSK and LCK and not CD45)
111.	PAK*=(ERK1_2 and not PIP) or (GRB2) or (NCK and not PIP)
112.	PDGF*=(ETS)
113.	PDGFRB*=(NUC_MYC)
114.	PDK1*=(CARMA1) or (PIP3)
115.	PI3K*=(B7_1 and CD28) or (B7_2 and CD28) or (GAB1) or (GRB2) or (ICOSL and ICOS) or (RAS) or (SHP2)
116.	PIP2*=(PI3K) or (PLC_GAMMA)
117.	PIP3*=(PIP2) or (PTEN)
118.	PKC*=(JAK)
119.	PKC_THETA*=(AKT) or (DAG) or (GLK) or (PDK1)
120.	PLC_GAMMA*=(GAB1) or (GRB2) or (ITK) or (LAT) or (SHC) or (SHP2)
121.	RAC*=(PAK and not RAC_GAP) or (RAS and not RAC_GAP) or (VAV and not RAC_GAP)
122.	RAC_GAP*=(DAG)
123.	RAC1*=(NCK) or (VAV)
124.	RAF*=(PAK) or (PKC and not AKT) or (RAS)
125.	RAF1*=(P21RAS)

126.	RAP1*=(C3G)
127.	RAS*=(not RAP1) or (not RAS_GAP) or (GRB2+SOS) or (GRB7 and not RAS_GAP and not RAP1) or (NCK+SOS and not RAS_GAP and not RAP1) or (RAS_GRP) or (SHC+GRB2+SOS and not RAS_GAP and not RAP1) or (SHP1+GRB2+SOS and not RAS_GAP and not RAP1) or (SHP2+GRB2+GAB1+SOS and not RAS_GAP and not RAP1)
128.	RAS_GAP*=(GRB2) or (NCK)
129.	RAS_GRP*=(DAG and IP3) or (LAT)
130.	RIP1*=(TRAF2)
131.	RSK*=(ERK1_2)
132.	SHC*=(IL2 and IL2R) or (PI3K) or (PKC)
133.	SHC+GRB2+SOS*=(SHC and GRB2 and SOS)
134.	SHP1*=(not ERK1_2) or (B7_1 and CTLA4) or (B7_2 and CTLA4) or (PDL and PD1)
135.	SHP1+GRB2+SOS*=(SHP1 and GRB2 and SOS)
136.	SHP2*=(not LCK) or (B7_1 and CTLA4) or (B7_2 and CTLA4) or (ERK1_2) or (SHC)
137.	SHP2+GRB2+GAB1+SOS*=(SHP2 and GRB2 and GAB1 and SOS)
138.	SLP76*=(ITK)
139.	SOCS3*=(CRK_L) or (NCK)
140.	SOS1*=(ERK1_2)
141.	STAT1*=(PKC)
142.	STAT3*=(PKC)
143.	STAT5*=(not SHP2) or (JAK2) or (P38) or (PAK)
144.	T3JAM*=(TRAF3)
145.	TAK1*=(BCL10)
146.	TAK1+TAB*=(RIP1)
147.	TCR+CD3*=(TCR and CD3)
148.	TGF_BETA*=(AP1 and not GSK3_BETA)
149.	TNF_ALPHA*=(AP1 and not GSK3_BETA)
150.	TRADD*=(TNF_ALPHA and TNFR) or (TNF_BETA and TNFR)
151.	TRAF1*=(TNFSF9 and TNFRSF9) or (NUC_NFKB)
152.	TRAF2*=(CD70 and CD27) or (LIGHT and LTBR) or (OX40L and OX40) or (TNFSF9 and TNFRSF9) or (TRADD)
153.	TRAF3*=(CD70 and CD27) or (LIGHT and LTBR) or (TNFSF9 and TNFRSF9)
154.	TRAF5*=(CD70 and CD27) or (LIGHT and LTBR)
155.	TRAF6*=(MALT1)
156.	TYK2*=(IFNAR1_R2 and IFN_ALPHA) or (IFNAR1_R2 and IFN_BETA) or (IFNAR1_R2 and IFN_OMEGA)
157.	VAV*=(JAK) or (LAT and GADS and SLP76)

158.	VEGF*=(NUC_NFKB)
159.	WASP*=(NCK)
160.	ZAP70*=(ABL and TCR+CD3 and MHC_CLASS_II+AG and not SHP1) or (LCK and not SHP1) or (LCK and TCR+CD3 and not LYP and FYN and ABL and VAV and not SHP1 and MHC_CLASS_II+AG) or (TCR+CD3 and MHC_CLASS_II+AG and FYN and not SHP1)
161.	CTLA4*=(NUC_NFAT)
162.	CD28*=(not TNF_ALPHA)
163.	P53*=(ETS and NUC_P38)
164.	PD1*=(NUC_NFAT)
165.	GRB2*=(PAK or SHC)
166.	GRB7*=(SHC)
167.	PAG*=(not CD45 and LCK) or (not CD45 and FYN)

*Target nodes

Table A. 2: Initial Values of Nodes

MHC_CLASS_II+AG =True	FYN=False	MEKK1_4=True	STAT1=False
B7_1=True	GAB1=True	MEKK3=True	STAT3=False
B7_2=True	GADS=False	MEKK4_7=True	STAT5=False
CALCIUM_OUT=True	GCKR=False	MKK3_6=False	T3JAM=True
CRE=True	GLK=True	MKK4_7=False	TAK1=True
PDL=True	GM_CSF=False	MKK7=True	TCR=True
LIGHT=True	GRB2=False	MKP=False	TCR+CD3=False
CD70=True	GRB7=False	MLK3=False	TGF_BETA=False
TNFSF9=True	GSK3_BETA=True	NCK=True	TNF_ALPHA=False
ABL=False	HBEGF=False	NFAT=False	TNF_BETA=False
AKT=True	HDAC=True	NFKB=False	TNFR=False
ATF2=False	HPK1=True	NIK=False	TNFRSF9=False
BAD=True	ICOS=False	NUR_77=False	TRADD=True
BCL10=False	ICOSL=False	OX40=False	TRAF1=False
BCL2=False	IFN_ALPHA=False	OX40L=True	TRAF2=False
BCLX=False	IFN_BETA=False	P15=False	TRAF3=False
C3G=True	IFN_GAMMA =False	P21=False	TRAF5=True
CABIN1=True	IFN_OMEGA=True	P21RAS=False	TRAF6=False
CALCINEURIN=False	IFNAR1_R2=True	P300=True	TYK2=True
CALCIPRESSIN=True	IKB_ALPHA=False	P38=False	VAV=False
CAM=True	IKB_BETA=False	P53=False	VEGF=False
CAMK4=True	IKK_BETA=True	P70=False	ZAP70=False
CARMA1=False	IKK_GAMMA =False	PAG=True	AP1=False

CBL=True	IL1=False	PAK=False	ASK1=False
CCL19=False	IL10=False	PD1=False	CALCIUM_IN=False
CD2=False	IL12=False	PDGF=False	CDC42+RAC=False
CD27=True	IL13=False	PDGFRB=False	GRB2+SOS=False
CD28=False	IL2=False	PDK1=True	IKK_ALPHA=False
CD3=True	IL2R=False	PI3K=True	IP3=False
CD4=True	IL3=False	PIP=False	LAT+GRB2+SOS1=False
CD45=True	IL4=False	PKC=False	MKK=False
CD8=False	IL5=False	PKC_THETA=True	MLK2=False
CDC25=True	IL6=False	PLC_GAMMA=True	NCK+SOS=False
CDC42=False	IL8=False	PTEN=True	NFAT+P300+MEF2=False
CDK_4=False	IL9=False	RAC=False	NUC_CREB=False
COT=False	ITK=False	RAC_GAP=True	NUC_ERK1_2=False
CRAC=True	JAK=True	RAC1=False	NUC_JNK=False
CREB=False	JAK2=True	RAF=True	NUC_MYC=False
CRK_L=True	JNK=True	RAF1=True	NUC_NFAT=False
CSK=True	JUN=False	RAP1=True	NUC_NFKB=False
CTLA4=False	LAT=False	RAS=False	NUC_P38=False
CYCLIN_A=True	LCK=True	RAS_GAP=False	OSM=False
CYCLIN_D1=False	LTBR=True	RAS_GRP=True	PAG+CSK=False
CYCLIN_D2=False	LYP=False	RIP1=True	PIP2=False
CYCLIN_E=True	MALT1=False	RSK=True	PIP3=False
DAG=True	MEF2=True	SHC=False	SHC+GRB2+SOS=False
ELK1=False	MEF2A=False	SHP1=False	SHP1+GRB2+SOS=False
ERK1_2=True	MEF2B=True	SHP2=False	SHP2+GRB2+GAB1+SOS=False
ETS=False	MEF2C=True	SLP76=False	TAK1+TAB=False
FASL=False	MEF2D=False	SOCS3=False	WASP=False
FKHR=True	MEK1_2=True	SOS=True	
FOS=False	MEKK=True	SOS1=True	

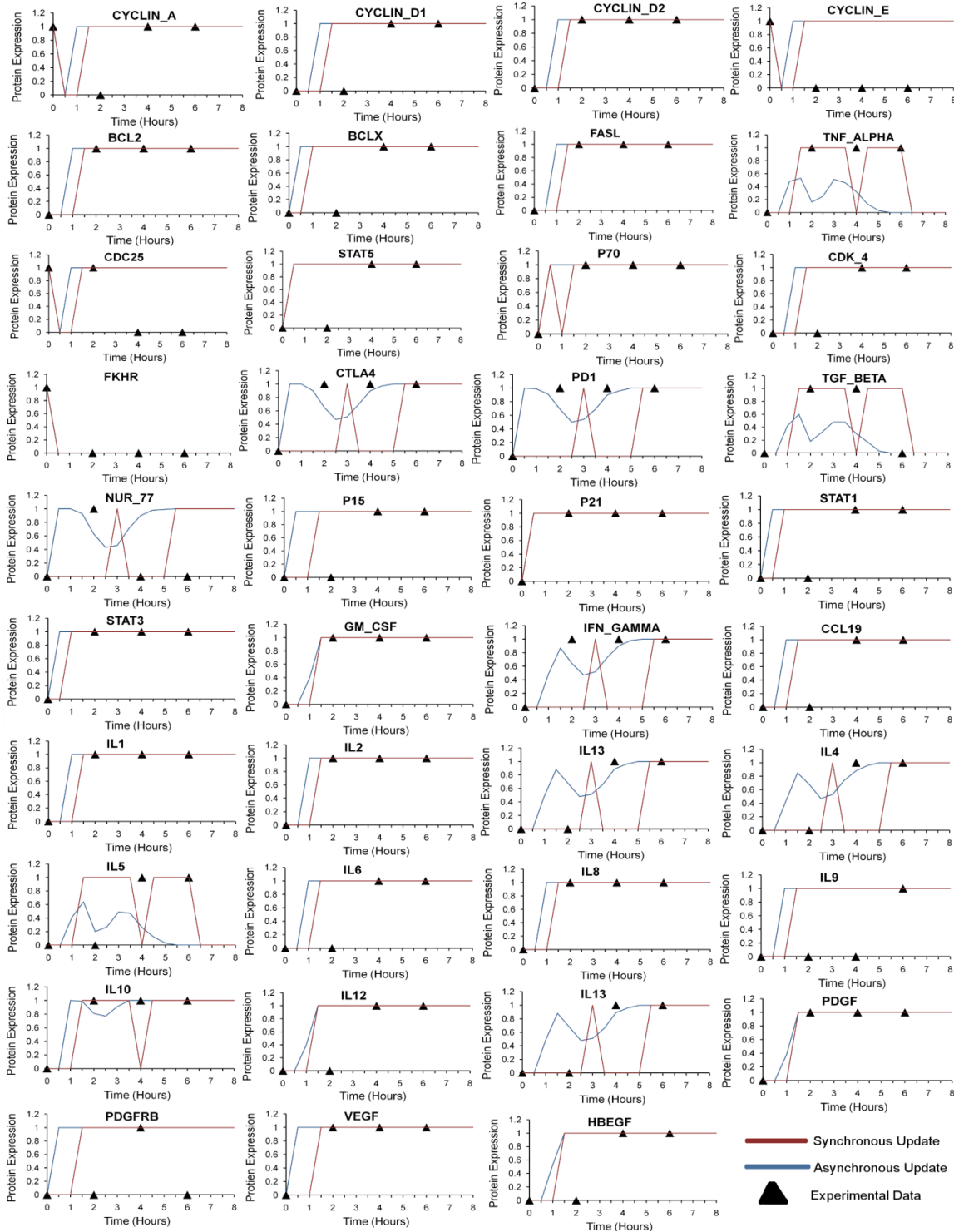


Figure A. 1: Protein expression dynamics observed in Experiment, Synchronous and Asynchronous simulation. 'Experimental' data is the binarized time course microarray expression data of total 39 output proteins of the model, which is compared against the 'synchronous' and 'asynchronous' simulation results. Out of the 39 output proteins, the expressions of total 34 proteins match at 6th hour, while the temporal expression patterns of 14 proteins (viz. BCL2, CYCLIN_D2, FASL, FKHR, GMCSF, IL1, IL2, IL3, IL8, P21, P70, PDGF, STAT3 and VEGF) from the simulations match exactly with the experimental data at all the four time points (0, 2, 4, and 6 hours).

Table A. 3: Functional classification of T-cell output protein

No. of molecules	List of molecules	Function	Ref
T cell Proliferation (12)	CYCLIN A,CYCLIN- D1, CYCLIN D2, CYCLIN E, CDK4	Cell cycle progression	[158,159]
	BCL2, BCLX	Anti-apoptosis	[160,335]
	FASL, TNF_ALPHA, CDC25, STAT5, P70	T cell proliferation, survival	[164,165,233 ,336,337]
Negative Regulator of T cell Proliferation (7)	P21, FKHR, CTLA4, PD1,TGF_BETA, NUR77, P15	Co-inhibitory signal transduction, Immunosuppression, inhibition of cell cycle progression	[234- 236,338-340]
Immune Response (5)	STAT1, STAT3, GM-CSF, IFN- GAMMA, CCL19	Immunity against parasitic infection, T cell homing, T cell homeostasis, as immune adjuvant, dendritic cell maturation, control of allergic diseases	[237- 239,341,342]
Interleukins (11)	IL1	T helper cell proliferation and differentiation	[343]
	IL2	Proliferation	[161]
	IL3	Immune Response; critical for the development, survival and function of mast cells and basophils, role in allergic diseases	[344]
	IL4	T cell proliferation, differentiation, inflammatory response	[144,162]
	IL5	Differentiation and function of myeloid cells; leads to growth, activation, mobilization, differentiation, and survival of eosinophils	[144]
	IL6	T cell proliferation	[163]
	IL8	Proinflammatory cytokine, chemotactic factor	[345]
	IL9	Growth factor for T cells and mast cells	[346]
	IL10	T cell suppression	[166]
	IL12	T cell proliferation	[347]
	IL13	Antibody class switching, activation of eosinophils and mast cells, defense against parasite infections	[144]
Growth Factors (4)	PDGF, PDGFRB, VEGF, HBEGF	Growth factors secreted by T cells acting as potent mitogens for other cells	[240-243]

APPENDIX B

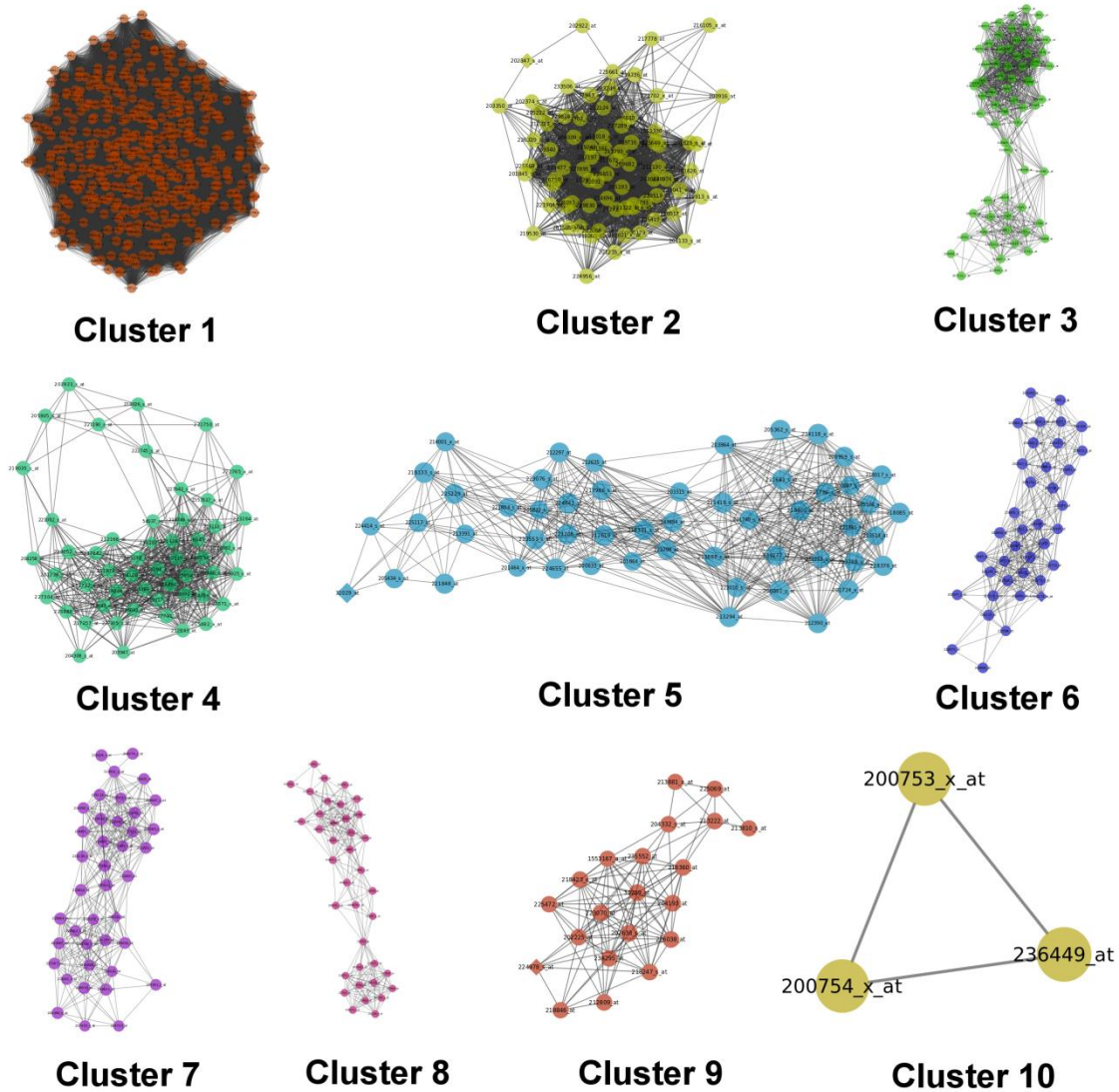


Figure B.1: Gene clusters identified in *Leishmania major* infected APC microarray data. This figure contains total 10 clusters or functions modules, which have been identified from the gene co-expression network generated from the time course microarray expression data of *Leishmania major* infected APC [EBI-ArrayExpress (ID: E-GEOD-42088)]. The names of the nodes in all the cluster diagrams are assigned according to the probe IDs used in HG-U133_Plus_2 Affymetrix GeneChip for human cell.

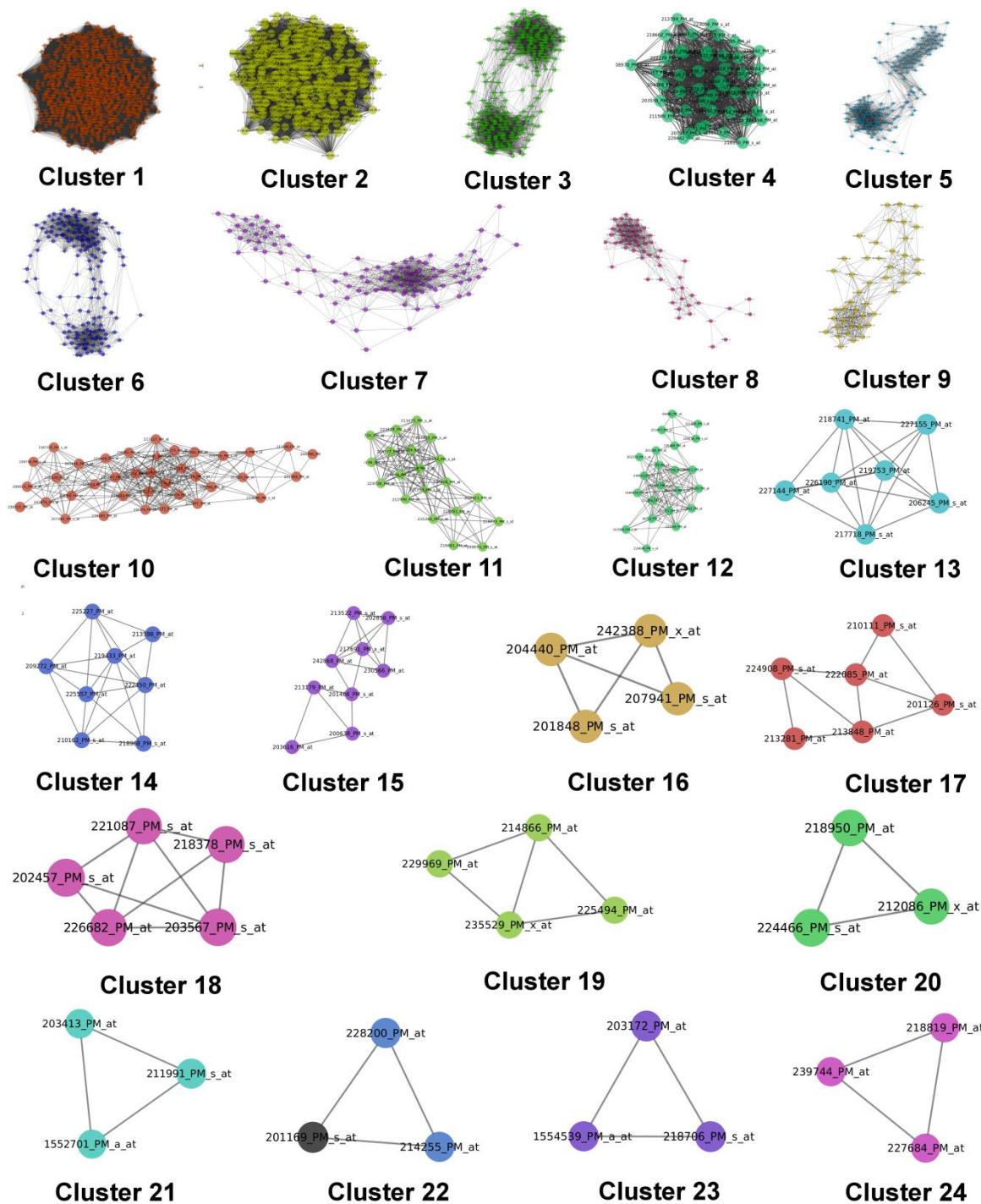


Figure B.2: Gene clusters identified in active T-cell microarray data. This figure contains total 24 clusters or functions modules, which have been identified from the gene co-expression network generated from the time course microarray expression data of activate T-cell [EBI-ArrayExpress (E-GEOD-48978)]. The node names used in each cluster are in accordance with the probe IDs used in Affymetrix HT_HG-U133_Plus_PM array plate.

Table B.1: Pathway Enrichment of the significantly expressed genes in the microarray experiment of *Leishmania* infected APC

Clusters	Pathway Enrichment
Cluster 1	Cytokine-cytokine receptor interaction, Fc gamma R-mediated phagocytosis, Toll-like receptor signalling pathway, MAPK signalling pathway, Jak-STAT signalling pathway, mTOR signalling pathway, Antigen processing and presentation, Chemokine signalling pathway, Apoptosis, Nitrogen metabolism, etc.
Cluster 2	Endocytosis, Toll-like receptor signalling pathway, Fc gamma R-mediated phagocytosis, Cytokine-cytokine receptor interaction, Jak-STAT signalling pathway, MAPK signalling pathway, Chemokine signalling pathway, Spliceosome, etc.
Cluster 3	Fc gamma R-mediated phagocytosis, Phosphatidylinositol signalling system, TGF-beta signalling pathway, Cell cycle, Cell adhesion molecules (CAMs), etc.
Cluster 4	Cytokine-cytokine receptor interaction, Fc gamma R-mediated phagocytosis, MAPK signalling pathway, Phosphatidylinositol signalling system, Spliceosome, Cell cycle, etc.
Cluster 5	Toll-like receptor signalling pathway, Cytosolic DNA-sensing pathway, Jak-STAT signalling pathway, MAPK signalling pathway, mTOR signalling pathway, T cell receptor signalling pathway, Chemokine signalling pathway, etc.
Cluster 6	MAPK signalling pathway, p53 signalling pathway, TGF-beta signalling pathway, Leukocyte trans-endothelial migration, etc.
Cluster 7	Jak-STAT signalling pathway, Phosphatidylinositol signalling system, Fc gamma R-mediated phagocytosis, Chemokine signalling pathway, Antigen processing and presentation, Nitrogen metabolism, Spliceosome, etc.
Cluster 8	Antigen processing and presentation, Cytokine-cytokine receptor interaction, Apoptosis, Ubiquitin mediated proteolysis, etc.
Cluster 9	Phosphatidylinositol signalling system, Chemokine signalling pathway, Leukocyte transendothelial migration, Calcium signalling pathway, Cell adhesion molecules (CAMs), etc.
Cluster 10	Spliceosome

Table B.2: Pathway Enrichment of the significantly expressed genes in the microarray experiment of activated T-cell

Cluster	Pathway Enrichment
Cluster 1	T cell receptor signalling pathway, Calcium signalling pathway, Cytokine-cytokine receptor interaction, Chemokine signalling pathway, Interleukin signalling pathway, Toll-like receptor signalling pathway, MAPK signalling pathway, Ras Pathway, Jak-STAT signalling pathway, PI3 kinase pathway, Antigen processing and presentation, p53 signalling pathway, Cell cycle, Apoptosis, Ubiquitin mediated proteolysis, Spliceosome, etc.
Cluster 2	T cell receptor signalling pathway, Cytokine-cytokine receptor interaction, Chemokine signalling pathway, Jak-STAT signalling pathway, Apoptosis, Spliceosome, etc.
Cluster 3	T cell receptor signalling pathway, T cell activation, MAPK signalling pathway, Chemokine signalling pathway, PI3 kinase pathway, Inflammation mediated by chemokine and cytokine signalling pathway, Apoptosis, etc.
Cluster 4	DNA replication, Tryptophan metabolism, etc.
Cluster 5	Interleukin signalling pathway, Cell cycle, TGF-beta signalling pathway, etc.
Cluster 6	T cell receptor signalling pathway, Interleukin signalling pathway, MAPK signalling pathway, Calcium signalling pathway, Jak-STAT signalling pathway, Ras Pathway, PI3 kinase pathway, Chemokine signalling pathway, Inflammation mediated by chemokine and cytokine signalling pathway, Apoptosis signalling pathway, Spliceosome, etc.
Cluster 7	MAPK signalling pathway, Apoptosis signalling pathway, Leukocyte trans-endothelial migration, Regulation of actin cytoskeleton, etc.
Cluster 8	T cell receptor signalling pathway, Interleukin signalling pathway, Cytokine-cytokine receptor interaction, MAPK signalling pathway, Jak-STAT signalling pathway, Inflammation mediated by chemokine and cytokine signalling pathway, etc.
Cluster 9	Cytokine-cytokine receptor interaction
Cluster 10	Cytokine-cytokine receptor interaction, MAPK signalling pathway, Inflammation mediated by chemokine and cytokine signalling pathway, Leukocyte trans-endothelial migration, Cell adhesion molecules (CAMs), etc.

Table B. 3: List of all known alternatively spliced isoforms of the output molecules of both APC and T-cell

A. Isoforms considered included in our model

I. Isoforms with similar function

Protein (as used in the model)	Principal Isoform (canonical isoform)	Alternatively spliced Isoforms (non-canonical isoforms)	Functional significance of spliced variants
PDGF_T	PDGF_AL_T (211)	PDGF_AS_T (196)	PDGF_AL_T and PDGF_AS_T differ in their ability to associate with the extracellular matrix and to bind heparin in vitro. PDGFA_S_T has a lower binding affinity. The overall function remains similar [348].
TGF_BETA_T	TGFB1_T(390), TGFB2_T(414), TGFB3_T(414)	Several minor isoforms	All TGF Beta isoforms have similar effect on immune cells. Functions of minor isoforms not known [349].
CYCLIN_D1_T	CYCLIN_D1a_T	CYCLIN_D1b_T	Functions of both the isoforms are similar. Unlike CYCLIN_D1a_T, the non-canonical oncogenic CYCLIN_D1b_T isoform is found only in the nucleus. However CYCLIN_D1b_T is expressed only in cancer derived cell lines [350].
CYCLIN_D2_T	CYCLIN_D2_iso1_T(289)	CYCLIN_D2_iso2_T(209)	Functions similar. CYCLIN_D2_iso2_T is overexpressed in certain types of cancer [351].
C_FOS	C_FOS_canonical	C_FOS_2 (169)	C_FOS_2 is degraded at a faster rate than the C_FOS_canonical isoform [352].
P15_T	P15_138aa_T (138)	P10_T (78)	P15 inhibits cell cycle progression by binding to CDK4 and CDK6 and also via p53 pathway. P10 also inhibits the cell cycle progression, but its function is mediated only via the p53 pathway. P10 does not interact with CDK4 and CDK6 [353].
PDGFRB_T	PDGFRB_iso1_T (1106)	PDGFRB_iso2_T (336)	Functions similarly [354].

II. Isoforms with antagonistic functions

Protein (as used in the model)	Principal Isoform (canonical isoform)	Alternatively spliced Isoforms (non-canonical isoforms)	Functional significance of spliced variants
IL4_T	IL4_long_T (153)	IL4_short_T (137)	The shorter IL4 isoform (IL4delta2) antagonizes the function of the longer canonical IL4 isoform [355].
IL6_T	IL6_native_T	IL6_Delta4_T	IL6_Delta4_T antagonizes the function of the native IL6 protein [356].
FASL_T	FASLm_T (281)	FASLs_T (127)	FAS ligand membrane and soluble isoforms has functional differences. The membrane bound form induces apoptosis while the soluble form does not [357,358].
BCLX_T	BCLX_L_T (233)	BCLX_S_T (170), BCLX_BETA_T (227)	BCLX_L_T is anti-apoptotic. BCLX_S_T inhibits the function of BCL-2, hence indirectly helps in apoptosis. The function of BCLX_BETA_T is unknown [359].

B. Isoforms not included in our model

I. Proteins with Single Functional Isoform

	Protein (as used in the model)	Principal Isoform (canonical isoform)
1.	P19_T	P19_T(166)
2.	P21_T	P21_T(164)
3.	HBEGF_T	HBEGF_T(208)
4.	GM_CSF_T	GM_CSF_T(144)
5.	IL2_T	IL2_T(153)
6.	IL3_T	IL3_T(152)
7.	IFN_GAMMA_T	IFN_GAMMA_T(166)
8.	IL9_T	IL9_T(144)
9.	IL10_T	IL10_T(178)
10.	TNF_ALPHA_T	TNF_ALPHA_T(233)
11.	IFN_BETA	IFN_BETA(187)
12.	IL10	IL10 (178)
13.	TNF_ALPHA	TNF_ALPHA (233)
14.	IP10	IP10(98)
15.	IL1_ALPHA	IL1_ALPHA (271)
16.	IL1_BETA	IL1_BETA (269)
17.	IL5_T	IL5_T(134)
18.	INOS	iNOS
19.	CYCLIN_A_T	CYCLIN_A2_T (432)

II. Functional Significance of Alternatively Spliced (non-canonical) Isoforms not known

	Protein (as used in the model)	Principal Isoform (canonical isoform)	Alternatively spliced Isoforms (non-canonical isoforms)
1.	BCL2_T	BCL2_ALPHA_T(239)	BCL2_BETA_T(205)
2.	NUR77_T	NUR77_T(598)	Two other isoforms of length 611aa and 325aa have been identified.
3.	IL12_T	IL12p40a_T(375); IL12p35_T (328)	IL12p40b_T(330), IL12p40c_T(330);
4.	P27_T	P27_T(198)	Two other isoforms of length 205aa and 104aa have been identified.
5.	IL13_T	IL13_T(146)	Another isoform of length 144aa has been isolated
6.	IL12	IL12p40a(375); IL12p35(328)	IL12p40b(330), IL12p40c (330);
7.	CYCLIN_E_T	CYCLIN_E1L_T(410)	CYCLIN_E1S_T(367), CYCLIN_E1_iso3_T(395)

Here, the expressions of different isoforms from single gene transcript are dependent on the presence of certain cis-regulatory elements and trans-acting factors that has been collectively referred as 'FACTOR' in our model. These FACTORS represents specific Spliceosomes responsible for the splice site recognition in each case. However, due to lack of Human cell specific *Leishmania major* infected RNA seq data of APC, the logical states (activation or inactivation) of the FACTORS determining alternative splicing of the output molecules could not be explicitly determined in *Leishmania* infected scenario. Hence, in our model these FACTORS were assumed to be ON in all our simulations, signifying that all the alternative isoforms have equal probability of getting expressed.

However, the concept of attractor analysis was further exploited to understand the differential regulations of the identified 23 FACTORS [$FACTOR_i$ where $(i=1, 2, \dots, 23)$] associated with the splicing events of 11 output genes. Hence, to observe the effects of the differential activations of all these 23 FACTORS in the production of the corresponding isoforms and the regulation of the dynamics of the entire network, in

total 2^{23} combinations of initial states of all the FACTORS have to be considered. Since, finding the attractors of this huge number of input combinations is computationally difficult; hence, to achieve this goal, we have randomly changed the logical states (i.e., 0 or 1) of the 23 FACTORS, and generated 1000 input random samples for both the uninfected and infected scenarios. The inputs files of each of these samples are then used for the simulations and followed by the attractor identifications of uninfected and infected scenarios.

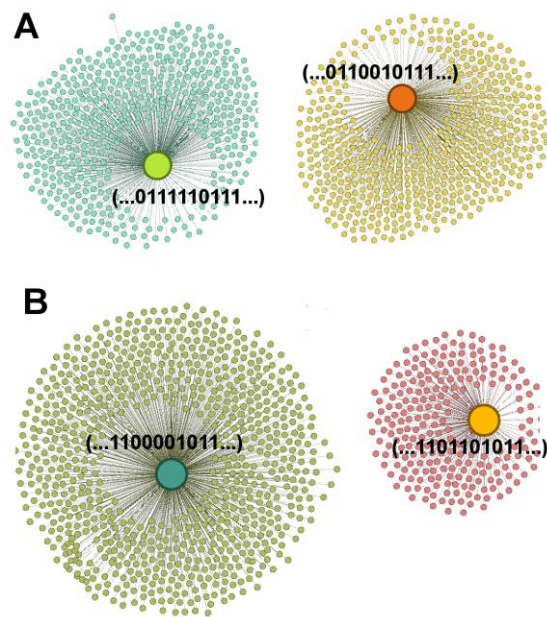


Figure B. 3: Attractor analysis of the uninfected and infected scenarios under the differential activation of the splicing factors. (A) In the uninfected scenario the system reaches two stable steady state attractors, in which the expressions of IFN_BETA, IL10, IL12, IL1_ALPHA, IL1_BETA, INOS, IP10, NO, TNF_ALPHA and C_FOS proteins are (0111110111) or (0110010111). (B) In the infected scenario, the system reaches two stable steady state attractors namely (1100001011) and (1101101011), respectively.

From the simulations of the uninfected and infected scenarios it is observed that both the scenarios are reaching at two stable attractors separately (**Figure B. 3**). It is also observed in the uninfected scenario that the system has reached at two stable steady state attractors, in which the expressions of IFN_BETA, IL10, IL12, IL1_ALPHA, IL1_BETA, INOS, IP10, NO, TNF_ALPHA and C_FOS proteins are either (0111110111) or (0110010111). The first attractor (0111110111) was also found in the simulation in which the probabilities of all the splicing isoforms were taken equally i.e., the initial

logical states of all the FACTORs were kept at ON state (**Figure 13 a**). Hence, it can be assumed that the emergence of the second attractor (0110010111) in the simulation is occurring due to the differential expressions and the dynamic interactions of the isoforms in the model. In **Figure B. 3A**, these two attractor nodes (placed at the middle of the circular layouts) are represented by light green and orange colors respectively. The other small nodes, which are connected to these two nodes, are the different samples. Moreover, the subsequent analysis of the logical steady states of NO production, T_{H1} Response, and T_{H2} Response are reaching at only one steady state (i.e., 110), which is also accordance with the experimental observations found in the previous studies.

On the other hand, in case of infected scenario, the system is also reaching at two different steady state attractors (1100001011) and (1101101011). Similar to the uninfected scenario, the first attractor (1100001011) is same as the attractor found while keeping all FACTORs at ON state (**Figure 13 b**), and the other attractor (1101101011) is found due to the differential expressions of the different splicing factors in the model. In (**Figure B. 3 B**), these two attractor nodes are shown by deep green and deep yellow colors at the middle of the circular layout or network. The logical steady states of NO production, T_{H1} Response, and T_{H2} Responses observed in the 1000 samples are reaching at two different steady states i.e., either at (001) or (000) and are corresponding to the observed logical steady state attractors (1100001011) and (1101101011), respectively. The logical states of the immune responses (001) are also in accordance with the clinical observations of the *Leishmania* infected APCs. However, the states (000) do not comply with the real biological situation of *Leishmania* infected immune response patterns. Hence, we have excluded the samples which are driving the systems of the infected scenario towards the second attractor (1101101011) and only take the samples, which are going to the first attractor (1100001011) for further perturbation or drug target identification studies.

Table B. 4: Logical Equations used to model the reaction mechanisms in T-cell and APC during *Leishmania* infection

AKT_T* = (CARMA1_T) OR (CDC42+RAC_T) OR (COT_T) OR (GRB7_T) OR (IKK_ALPHA_T AND IKK_BETA_T) OR (PAK_T) OR (PDK1_T) OR (PKC_T)
AKT* = (IL4R AND JAK3 AND PI3K AND IL4_T)
AP1_T* = (NOT IFN_GAMMA_T) OR (ATF2_T AND C_JUN_T AND NOT IFN_GAMMA_T) OR (C_FOS_T AND C_JUN_T AND NOT IFN_GAMMA_T) OR (C_JUN_T AND NOT IFN_GAMMA_T) OR (CRE_T AND ATF2_T AND C_JUN_T AND NOT IFN_GAMMA_T) OR (CRE_T AND C_JUN_T AND NOT IFN_GAMMA_T) OR (NUC_ERK1_2_T AND C_FOS_T AND C_JUN_T AND NOT IFN_GAMMA_T) OR (NUC_JNK_T AND C_FOS_T AND C_JUN_T) OR (NUC_P38_T AND C_FOS_T AND C_JUN_T AND NOT IFN_GAMMA_T)
AP1* = (NOT GP63_L AND ERK1_2) OR (NOT LPG_L AND ERK1_2)
ARP2_3_T* = (WASP_T)
ASK1_T* = (TRAF2_T)
ATF2_T* = (NUC_P38_T)
BAD_T* = (NOT AKT_T) OR (JNK_T AND NOT AKT_T)
BAD* = (NOT AKT)
BCL10_T* = (CARMA1_T) OR (PKC_THETA_T)
BCL2_T* = (NOT JNK_T) OR (ETS_T) OR (NUC_CREB_T)
BCLX_L_T* = (NOT BAD_T AND FACTOR20 OR NOT FACTOR21) OR (NOT JNK_T AND FACTOR20 OR NOT FACTOR21) OR (ETS_T AND FACTOR20 OR NOT FACTOR21) OR (NUC_NFKB_T AND FACTOR20 OR NOT FACTOR21)
BCLX_S_T* = (NOT BAD_T AND FACTOR21 OR NOT FACTOR20) OR (NOT JNK_T AND FACTOR21 OR NOT FACTOR20) OR (ETS_T AND FACTOR21 OR NOT FACTOR20) OR (NUC_NFKB_T AND FACTOR21 OR NOT FACTOR20)
BCLX_T* = (BCLX_L_T AND NOT BCLX_S_T) OR (BCLX_L_T)
C_FOS_2* = (ERK1_2 AND NOT GP63_L AND FACTOR11 OR NOT FACTOR10) OR (NUC_STAT3 AND FACTOR11 OR NOT FACTOR10) OR (NUC_ELK1 AND FACTOR11 OR NOT FACTOR10)
C_FOS_CANONICAL* = (ERK1_2 AND NOT GP63_L AND FACTOR10 OR NOT FACTOR11) OR (NUC_STAT3 AND FACTOR10 OR NOT FACTOR11) OR (NUC_ELK1 AND FACTOR10 OR NOT FACTOR11)
C_FOS_T* = (C_JUN_T) OR (ELK1_T) OR (ETS_T) OR (NUC_P38_T)
C_FOS* = (C_FOS_CANONICAL OR C_FOS_2)
C_JUN_T* = (C_FOS_T) OR (NUC_JNK_T)
C3G_T* = (CRKL_T)
CABIN1_T* = (NOT CAMK4_T)
CALCINEURIN_T* = (NOT CABIN1_T AND CAM_T) OR (CAM_T AND NOT CALCIPRESSIN_T AND NOT CABIN1_T)
CALCIUM_IN_T* = (CRAC_T AND CALCIUM_OUT_T)
CAM_T* = (CALCIUM_IN_T) OR (VAV_T AND CALCIUM_IN_T)

CAMK4_T*=(CAM_T)
CARMA1_T*=(PKC_THETA_T)
CD2_T*=(FYN_T) OR (LCK_T)
CD3_T*=(LCK_T)
CD4_T*=(LCK_T) OR (MHC_CLASS_II+LPG_L)
CD40*=(CD40L_T)
CD8_T*=(LCK_T)
CDC42_T*=(PAK_T) OR (RAS_T) OR (VAV_T)
CDC42+RAC_T*=(VAV_T AND NOT RAC_GAP_T)
CERAMIDE*=(LFAA_L AND ASMASE)
COT_T*=(RIP1_T) OR (TRAF2_T)
CR3*=(GP63_L) OR (LPG_L)
CRAC_T*=(IP3_T)
CREB_T*=(RSK_T)
CRKL_T*=(TYK2_T)
CTLA4_T*=(NUC_NFAT_T)
CYC_T*=(NOT AKT_T)
CYCLIN_A_T*=(AP1_T AND NOT IFN_GAMMA_T) OR (NUC_CREB_T) OR (NUC_MYC_T)
CYCLIN_D1_T*=(CYCLIN_D1A_T OR CYCLIN_D1B_T)
CYCLIN_D1A_T*=(AP1_T AND NOT IFN_GAMMA_T AND FACTOR6 OR NOT FACTOR7) OR (ETS_T AND FACTOR6 OR NOT FACTOR7) OR (NUC_CREB_T AND FACTOR6 OR NOT FACTOR7) OR (NUC_MYC_T AND FACTOR6 OR NOT FACTOR7) OR (NUC_NFKB_T AND FACTOR6 OR NOT FACTOR7)
CYCLIN_D1B_T*=(AP1_T AND NOT IFN_GAMMA_T AND FACTOR7 OR NOT FACTOR6) OR (ETS_T AND FACTOR7 OR NOT FACTOR6) OR (NUC_CREB_T AND FACTOR7 OR NOT FACTOR6) OR (NUC_MYC_T AND FACTOR7 OR NOT FACTOR6) OR (NUC_NFKB_T AND FACTOR7 OR NOT FACTOR6)
CYCLIN_D2_ISO1_T*=(NUC_MYC_T AND FACTOR8 OR NOT FACTOR9)
CYCLIN_D2_ISO2_T*=(NUC_MYC_T AND FACTOR9 OR NOT FACTOR8)
CYCLIN_D2_T*=(CYCLIN_D2_ISO1_T OR CYCLIN_D2_ISO2_T)
CYCLIN_E_T*=(NUC_MYC_T)
DAG_T*=(PIP2_T)
ELK1_T*=(NUC_ERK1_2_T)
ELK1*=(ERK1_2)
ERK1_2_T*=(MEK1_2_T AND NOT MKP_T)
ERK1_2*=(CD40 AND MKP3) OR (NOT PP2A) OR (NOT SHP1 AND NOT TCPTP AND NOT PTP1B AND TLR4 AND TRIF) OR (NOT SHP1 AND NOT TCPTP AND TRIF AND NOT PTP1B AND TLR3) OR (LPG_L AND TLR2)
ETS_T*=(NUC_ERK1_2_T)
FASL_T*=(FASLM_T AND NOT FASLS_T) OR (FASLM_T)
FASLM_T*=(ETS_T AND FACTOR16 OR NOT FACTOR17) OR (NUC_NFKB_T AND FACTOR16 OR NOT FACTOR17)

FASLS_T*= (ETS_T AND FACTOR17 OR NOT FACTOR16) OR (NUC_NFKB_T AND FACTOR17 OR NOT FACTOR16)
FKHR_T*= (NOT AKT_T)
FYN_T*= (NOT PAG+CSK_T) OR (CD45_T AND NOT PAG+CSK_T AND NOT CBL_T)
GAB1_T*= (ERK1_2_T) OR (SHC_T)
GCKR_T*= (TRAF2_T)
GLK_T*= (TRAF2_T)
GM_CSF_T*= (NUC_NFKB_T) OR (ETS_T AND AP1_T)
GRB2_T*=PAK_T OR SHC_T
GRB2+SOS_T*= (CD80 AND CD28_T) OR (CD86 AND CD28_T) OR (RAS_GRP_T)
GRB7_T*=SHC_T
GSK3_BETA_T*= (NOT AKT_T)
HBEGF_T*= (ETS_T)
HPK1_T*= (LAT_T)
IFN_ALPHAR1_T*= IFN_BETA
IFN_ALPHAR2_T*= IFN_BETA
IFN_BETA*= (TLR3 AND TRIF AND IRF3) OR (TLR4 AND TRIF AND IRF3)
IFN_GAMMA_T*= (NUC_NFAT_T AND AP1_T AND NUC_STAT4_T) OR (NOT IL10)
IFN_GAMMAR*= IFN_GAMMA_T
IKB_ALPHA_T*= (NOT IKK_ALPHA_T AND NOT IKK_BETA_T) OR (NOT IKK_BETA_T)
IKB_BETA_T*= (NOT IKK_ALPHA_T AND NOT IKK_BETA_T AND NOT IKK_GAMMA_T)
IKK_ALPHA_T*= (NIK_T) OR (TRAF2_T)
IKK_ALPHA*= (TRADD)
IKK_BETA_T*= (BCL10_T) OR (IKK_ALPHA_T) OR (PKC_THETA_T) OR (TRAF2_T)
IKK_GAMMA_T*= (BCL10_T AND MALT1_T AND CARMA1_T) OR (CARMA1_T AND MALT1_T AND BCL10_T AND IKK_ALPHA_T AND IKK_BETA_T) OR (IKK_ALPHA_T AND IKK_BETA_T) OR (RIP1_T) OR (TRAF6_T AND MALT1_T)
IL1_ALPHA*= (NUC_NFKB)
IL1_BETA*= (NUC_NFKB)
IL10_T*= (AP1_T AND CREB_T AND NOT IFN_GAMMA_T) OR (NUC_NFAT_T AND NOT IFN_GAMMA_T)
IL10*= (NUC_ERK1_2)
IL10R*= (IL10_T) OR (IL10)
IL12_T*= (ETS_T AND NUC_NFKB_T)
IL12*= (NOT MTOR AND NOT IL10 AND NUC_P38 AND NUC_NFKB AND NUC_STAT1_ALPHA_P) OR (NUC_AP1)
IL12R_T*= (IL12)
IL12R*= IL12
IL13_T*= (NUC_NFAT_T AND AP1_T)
IL1R_T*= (IL1_BETA)
IL2_T*= (AP1_T AND NUC_NFAT_T AND NOT IFN_GAMMA_T) OR (ETS_T AND NUC_NFKB_T) OR (NUC_NFAT_T AND AP1_T) OR (NUC_NFKB_T)

IL2R_T*=(NUC_NFKB_T)
IL3_T*=(ETS_T AND NUC_NFKB_T)
IL4_LONG_T*=(AP1_T AND NUC_NFAT_T AND NOT IFN_GAMMA_T AND FACTOR12 OR NOT FACTOR13)
IL4_SHORT_T*=(AP1_T AND NUC_NFAT_T AND NOT IFN_GAMMA_T AND FACTOR13 OR NOT FACTOR12)
IL4_T*=(IL4_LONG_T AND NOT IL4_SHORT_T) OR (IL4_LONG_T)
IL4R*=(IL4_T)
IL5_T*=(AP1_T AND NOT IFN_GAMMA_T)
IL6_DELTA4_T*=(AP1_T AND CREB_T AND NOT IFN_GAMMA_T AND FACTOR15 OR NOT FACTOR14) OR (NUC_NFKB_T AND AP1_T AND CREB_T AND NOT IFN_GAMMA_T AND FACTOR15 OR NOT FACTOR14)
IL6_NATIVE_T*=(AP1_T AND CREB_T AND NOT IFN_GAMMA_T AND FACTOR14 OR NOT FACTOR15) OR (NUC_NFKB_T AND AP1_T AND CREB_T AND NOT IFN_GAMMA_T AND FACTOR14 OR NOT FACTOR15)
IL6_T*=(IL6_NATIVE_T AND NOT IL6_DELTA4_T) OR (IL6_NATIVE_T)
IL6R*=(IL6_T)
IL9_T*=(AP1_T) OR (NUC_NFAT_T) OR (NUC_NFKB_T)
INOS*=(TLR3 AND NUC_NFKB AND NUC_STAT1_ALPHA_P AND P38 AND TLR2) OR (NUC_AP1) OR (NOT IL10)
IP10*=(TLR3 AND TRIF AND IRF3) OR (TLR4 AND TRIF AND IRF3)
IP3_T*=(PIP2_T)
IRAK1_P*=(IRAK4 AND MYD88+TIR+IRAK1)
IRF3*=(LPG_L AND TLR4 AND TRIF) OR (TLR3 AND TRIF)
ITK_T*=(CD2_T) OR (LCK_T)
JAK1_T*=(NOT SOCS3_T) OR (GRB2_T) OR (IFN_ALPHAR1_T AND IFN_ALPHA_T) OR (IFN_ALPHAR1_T AND IFN_OMEGA_T) OR (IFN_ALPHAR2_T AND IFN_ALPHA_T) OR (IFN_ALPHAR2_T AND IFN_OMEGA_T) OR (SHC_T) OR (IFN_ALPHAR1_T AND IFN_BETA) OR (IFN_ALPHAR2_T AND IFN_BETA)
JAK1*=(IL6_T AND IL6R)
JAK2_T*=(NOT SHP2_T) OR (IL12R_T AND IL12)
JAK2*=(IFN_GAMMA_T AND IFN_GAMMAR) OR (IL12 AND IL12R)
JAK3*=(IL4_T AND IL4R)
JNK_T*=(MKK_T) OR (MKK4_7_T AND NOT MKP_T) OR (MKK7_T) OR (T3JAM_T)
JNK*=(NOT SHP1 AND NOT TCPTP AND NOT PTP1B AND IL1_BETA) OR (NOT SHP1 AND NOT TCPTP AND NOT PTP1B AND TNF_ALPHA) OR (TLR3 AND TRIF) OR (TLR4 AND TRIF)
LAT_T*=(ITK_T) OR (ZAP70_T)
LAT+GRB2+SOS1_T*=(LAT_T AND GRB2_T AND SOS1_T)
LCK_T*=(NOT PAG+CSK_T AND NOT LYP_T) OR (NOT PAG+CSK_T AND CD4_T AND MHC_CLASS_II+LPG_L) OR (CD4_T AND MHC_CLASS_II+LPG_L AND NOT PAG+CSK_T AND NOT LYP_T) OR (CD45_T AND CD4_T AND MHC_CLASS_II+LPG_L AND CD28_T AND

NOT CBL_T AND NOT LYP_T AND NOT PAG+CSK_T)
LYP_T*=(NOT CSK_T)
MALT1_T*=(CARMA1_T) OR (PKC_THETA_T)
MARCKS*=(NOT GP63_L AND PKC)
MEF2_T*=(CALCINEURIN_T AND P300_T) OR (CALCINEURIN_T AND P300_T AND NOT CABIN1_T AND NOT HDAC_T) OR (MEF2A_T AND MEF2B_T AND MEF2C_T AND MEF2D_T)
MEK1_2_T*=(PAK_T AND NOT MKP_T) OR (RAF_T AND NOT MKP_T) OR (RAF1_T AND NOT MKP_T)
MEKK_T*=(CDC42+RAC_T) OR (GCKR_T) OR (HPK1_T) OR (PAK_T)
MEKK1_4_T*=(CDC42+RAC_T) OR (RAC1_T)
MEKK3_T*=(OSM_T)
MEKK4_7_T*=(CDC42+RAC_T)
MHC_CLASS_II+LPG_L*=(MHC_CLASS_II AND LPG_L)
MKK_T*=(ASK1_T) OR (MEKK_T)
MKK3_6_T*=(MEKK1_4_T) OR (MEKK3_T)
MKK4_7_T*=(ASK1_T) OR (COT_T AND NOT MKP_T) OR (MEKK4_7_T AND NOT MKP_T)
MKK7_T*=(MEKK_T) OR (TAK1_T)
MLK2_T*=(PAK_T)
MLK3_T*=(CDC42_T AND NOT AKT_T) OR (RAC_T)
MRP*=(NOT GP63_L AND PKC) OR (IFN_GAMMAR AND IFN_GAMMA_T)
MTOR*=(NOT PP1 AND NOT PP2A AND NOT GP63_L AND AKT) OR (AKT AND IL4R AND IL4_T)
MYD88*=(LPG_L AND TLR4) OR (LPG_L AND TLR2)
MYD88+TIR*=(MYD88 AND TIR)
MYD88+TIR+IRAK1*=(MYD88+TIR AND IRAK1)
NCK_T*=(NOT RAS_T) OR (PKC_T AND NOT RAS_T)
NCK+SOS_T*=(NCK_T AND SOS_T)
NFAT_T*=(CALCINEURIN_T)
NFAT+P300+MEF2_T*=(NFAT_T AND P300_T AND MEF2_T)
NFKB_T*=(NOT IKB_BETA_T AND NOT IKB_ALPHA_T) OR (NIK_T) OR (OX40_T AND OX40L AND PKC_THETA_T AND TRAF2_T AND RIP1_T AND CARMA1_T AND MALT1_T AND BCL10_T AND IKK_ALPHA_T AND IKK_BETA_T AND IKK_GAMMA_T AND NOT IKB_ALPHA_T AND NOT IKB_BETA_T) OR (TRAF6_T AND TAK1_T AND IKK_BETA_T AND NOT IKB_BETA_T)
NFKB*=(ERK1_2 AND TLR3 AND TRIF) OR (ERK1_2 AND TLR4 AND TRIF AND NOT MTOR) OR (NOT GP63_L AND ERK1_2 AND TLR3 AND TRIF) OR (NOT GP63_L AND ERK1_2 AND TLR4 AND TRIF) OR (IRAK1_P AND TRAF6) OR (TRAF2 AND IKK_ALPHA AND NOT MTOR)
NIK_T*=(COT_T) OR (TRAF2_T) OR (TRAF5_T)
NO*=(INOS)
NUC_AP1*=(AP1)
NUC_CREB_T*=(CREB_T) OR (NUC_ERK1_2_T)

NUC_ELK1*=(ELK1)
NUC_ERK1_2_T*=(ERK1_2_T)
NUC_ERK1_2*=(CD40 AND TRAF6 AND ERK1_2) OR (ERK1_2) OR (IGG AND FC_GAMMAR AND ERK1_2)
NUC_JNK_T*=(JNK_T)
NUC_MYC_T*=(NUC_ERK1_2_T) OR (NUC_NFKB_T)
NUC_NFAT_T*=(NFAT_T)
NUC_NFKB_T*=(NFKB_T)
NUC_NFKB*=(NFKB)
NUC_P38_T*=(P38_T)
NUC_P38*=(CD40 AND TRAF2 AND P38) OR (CD40 AND TRAF3 AND P38) OR (CD40 AND TRAF5 AND P38) OR (P38)
NUC_STAT1_ALPHA_P*=(STAT1_ALPHA_P)
NUC_STAT3_T*=(STAT3_T)
NUC_STAT3*=(STAT3)
NUC_STAT4_T*=(STAT4_T)
NUR77_T*=(NFAT+P300+MEF2_T)
OSM_T*=(RAC1_T)
P10_T*=(NUC_MYC_T AND FACTOR19 OR NOT FACTOR18)
P15_138AA_T*=(NUC_MYC_T AND FACTOR18 OR NOT FACTOR19)
P15_T*=(P15_138AA_T OR P10_T)
P19_T*=(AP1_T AND NUC_NFKB_T AND NOT IFN_GAMMA_T)
P21_T*=(AKT_T) OR (NUC_MYC_T)
P21RAS_T*=(JAK2_T) OR (LAT+GRB2+SOS1_T)
P27_T*=(NOT AKT) OR (NUC_MYC_T)
P38_T*=(MKK3_6_T)
P38*=(CD40 AND MKP1) OR (NOT SHP1 AND NOT TCPTP AND NOT PTP1B AND IL1_BETA) OR (NOT SHP1 AND NOT TCPTP AND NOT PTP1B AND TNF_ALPHA) OR (LPG_L AND TLR4) OR (TLR3 AND TRIF) OR (TLR4 AND TRIF)
P53_T*=(ETS_T AND NUC_P38_T)
P70_T*=(PDK1_T)
PAG_T*=(NOT CD45_T AND LCK_T) OR (NOT CD45_T AND FYN_T)
PAG+CSK_T*=(PAG_T AND CSK_T AND FYN_T AND NOT CD45_T) OR (PAG_T AND CSK_T AND LCK_T AND NOT CD45_T)
PAK_T*=(ERK1_2_T AND NOT PIP_T) OR (GRB2_T) OR (NCK_T AND NOT PIP_T)
PD1_T*=NUC_NFAT_T
PDGF_AL_T*=(ETS_T AND FACTOR1 OR NOT FACTOR2)
PDGF_AS_T*=(ETS_T AND FACTOR2 OR NOT FACTOR1)
PDGF_T*=(PDGF_AL_T OR PDGF_AS_T)
PDGFRB_ISO1_T*=(NUC_MYC_T AND FACTOR22 OR NOT FACTOR23)
PDGFRB_ISO2_T*=(NUC_MYC_T AND FACTOR23 OR NOT FACTOR22)
PDGFRB_T*=(PDGFRB_ISO1_T OR PDGFRB_ISO2_T)

PKD1_T*=(CARMA1_T) OR (PIP3_T)
PI3K_T*=(CD80 AND CD28_T) OR (CD86 AND CD28_T) OR (GAB1_T) OR (GRB2_T) OR (ICOSL AND ICOS_T) OR (RAS_T) OR (SHP2_T)
PIP2_T*=(PI3K_T) OR (PLC_GAMMA_T)
PIP3_T*=(PIP2_T) OR (PTEN_T)
PKC_T*=(JAK1_T)
PKC_THETA_T*=(AKT_T) OR (DAG_T) OR (GLK_T) OR (PDK1_T)
PKC*=(NOT PP1 AND NOT LPG_L) OR (NOT PP2A AND NOT LPG_L)
PLC_GAMMA_T*=(GAB1_T) OR (GRB2_T) OR (ITK_T) OR (LAT_T) OR (SHC_T) OR (SHP2_T)
PP1*=(CERAMIDE)
PP2A*=(CERAMIDE)
PTP1B*=(GP63_L)
RAC_GAP_T*=(DAG_T)
RAC_T*=(PAK_T AND NOT RAC_GAP_T) OR (RAS_T AND NOT RAC_GAP_T) OR (VAV_T AND NOT RAC_GAP_T)
RAC1_T*=(NCK_T) OR (VAV_T)
RAF_T*=(PAK_T) OR (PKC_T AND NOT AKT_T) OR (RAS_T)
RAF1_T*=(P21RAS_T)
RAP1_T*=(C3G_T)
RAS_GAP_T*=(GRB2_T) OR (NCK_T)
RAS_GRP_T*=(DAG_T AND IP3_T) OR (LAT_T)
RAS_T*=(NOT RAP1_T) OR (NOT RAS_GAP_T) OR (GRB2+SOS_T) OR (GRB7_T AND NOT RAS_GAP_T AND NOT RAP1_T) OR (NCK+SOS_T AND NOT RAS_GAP_T AND NOT RAP1_T) OR (RAS_GRP_T) OR (SHC+GRB2+SOS_T AND NOT RAS_GAP_T AND NOT RAP1_T) OR (SHP1+GRB2+SOS_T AND NOT RAS_GAP_T AND NOT RAP1_T) OR (SHP2+GRB2+GAB1+SOS_T AND NOT RAS_GAP_T AND NOT RAP1_T)
RIP1_T*=(TRAF2_T)
RSK_T*=(ERK1_2_T)
SHC_T*=(GRB7_T) OR (IL2_T AND IL2R_T) OR (PI3K_T) OR (PKC_T)
SHC+GRB2+SOS_T*=(SHC_T AND GRB2_T AND SOS_T)
SHP1_T*=(NOT ERK1_2_T) OR (CD80 AND CTLA4_T) OR (CD86 AND CTLA4_T) OR (PDL AND PD1_T)
SHP1*=(EF1_ALPHA_L) OR (GP63_L)
SHP1+GRB2+SOS_T*=(SHP1_T AND GRB2_T AND SOS_T)
SHP2_T*=(NOT LCK_T) OR (CD80 AND CTLA4_T) OR (CD86 AND CTLA4_T) OR (ERK1_2_T) OR (SHC_T)
SHP2+GRB2+GAB1+SOS_T*=(SHP2_T AND GRB2_T AND GAB1_T AND SOS_T)
SLP76_T*=(ITK_T)
SOCS3_T*=(CRKL_T) OR (NCK_T)
SOS1_T*=(ERK1_2_T)
STAT1_ALPHA_P*=(IFN_GAMMAR AND JAK2 AND IFN_GAMMA_T) OR (STAT1_ALPHA)
STAT1_ALPHA*=(PTP1B AND STAT1_ALPHA_P) OR (SHP1 AND STAT1_ALPHA_P) OR

(TCPTP AND STAT1_ALPHA_P)
STAT1_T*=(PKC_T)
STAT3_T*=(PKC_T) OR (IL10R_T AND TYK2_T AND IL10)
STAT3*=(IL6R AND JAK1 AND IL6_T) OR (IL10R AND TYK2 AND IL10_T) OR (IL12 AND IL12R AND JAK2)
STAT4_T*=(JAK2_T AND IL12R_T AND IL12) OR (JAK2_T)
STAT5_T*=(NOT SHP2_T) OR (JAK2_T) OR (P38_T) OR (PAK_T)
T3JAM_T*=(TRAF3_T)
TAK1_T*=(BCL10_T)
TAK1+TAB_T*=(RIP1_T)
TCPTP*=(GP63_L)
TCR+CD3_T*=(MHC_CLASS_II+LPG_L) OR (TCR_T AND CD3_T)
TGF_BETA_T*=(TGFB1_T OR TGFB2_T OR TGFB3_T)
TGFB1_T*=(AP1_T AND NOT IFN_GAMMA_T AND FACTOR3 OR NOT FACTOR4 OR NOT FACTOR5)
TGFB2_T*=(AP1_T AND NOT IFN_GAMMA_T AND FACTOR4 OR NOT FACTOR3 OR NOT FACTOR5)
TGFB3_T*=(AP1_T AND NOT IFN_GAMMA_T AND FACTOR5 OR NOT FACTOR3 OR NOT FACTOR4)
TLR2*= LPG_L
TNF_ALPHA_T*=(AP1_T AND NOT IFN_GAMMA_T) OR (NUC_STAT3_T)
TNF_ALPHA*=(NOT IL10 AND NUC_NFKB) OR (NUC_STAT3)
TNF_ALPHAR_T*=(TNF_ALPHA)
TNF_ALPHAR*=(TNF_ALPHA_T)
TRADD_T*=(TNF_ALPHA_T AND TNF_ALPHAR_T) OR (TNF_BETA_T AND TNF_ALPHAR_T) OR (TNF_ALPHA AND TNF_ALPHAR_T)
TRADD*=(TNF_ALPHA AND TNF_ALPHAR) OR (TNF_ALPHA_T AND TNF_ALPHAR)
TRAF1_T*=(TNFSF9_T AND TNFSF9R_T)
TRAF2_T*=(TNFSF9_T AND TNFSF9R_T)
TRAF2*=(TNF_ALPHAR AND TRADD AND TNF_ALPHA_T) OR (OX40L AND OX40_T)
TRAF3_T*=(CD70 AND CD27_T) OR (LIGHT AND LTBR_T)
TRAF3*=(CD40L_T AND CD40)
TRAF5_T*=(CD70 AND CD27_T) OR (LIGHT AND LTBR_T)
TRAF5*=(CD40L_T AND CD40)
TRAF6_T*=(MALT1_T) OR (IL1R_T AND IRAK1_T AND IRAK4_T AND IL1_BETA AND MYD88_T)
TRAF6*=(CD40L_T AND CD40)
TRIF*=(LPG_L AND TLR4) OR (TLR3)
TYK2_T*=(IFN_ALPHAR1_T AND IFN_ALPHA_T) OR (IFN_ALPHAR1_T AND IFN_OMEGA_T) OR (IFN_ALPHAR2_T AND IFN_ALPHA_T) OR (IFN_ALPHAR2_T AND IFN_OMEGA_T) OR (IFN_ALPHAR1_T AND IFN_BETA) OR (IFN_ALPHAR2_T AND IFN_BETA)

VAV_T*=(JAK1_T) OR (LAT_T AND GADS_T AND SLP76_T)
WASP_T*=(NCK_T)
ZAP70_T*=(ABL_T AND TCR+CD3_T AND MHC_CLASS_II+LPG_L AND NOT SHP1_T) OR (LCK_T AND NOT SHP1_T) OR (LCK_T AND TCR+CD3_T AND NOT LYP_T AND FYN_T AND ABL_T AND VAV_T AND NOT SHP1_T AND MHC_CLASS_II+LPG_L) OR (TCR+CD3_T AND MHC_CLASS_II+LPG_L AND FYN_T AND NOT SHP1)
TH_1_RESPONSE*=IL2_T AND GM_CSF_T AND TNF_ALPHA_T AND IFN_GAMMA_T
TH_2_RESPONSE*=IL4_T AND IL5_T AND IL6_T AND IL10_T
NO_PRODUCTION*=NO

*Target Nodes

Here, the nodes *FACTOR_i* (where $i=1, 2, \dots, 23$) are the combinations of the cis and trans-regulatory factors associated with the alternative splicing of the isoforms.

Table B. 5: Binary initial values of the reaction nodes considered in the Logical equations from binarization of microarray expression data

ABL_T=False	IL4_T=False	PIP3_T=False
AKT_T=True	IL4R=False	PKC_T=True
AKT=True	IL5_T=False	PKC_THETA_T=True
AP1_T=False	IL6_T=False	PKC=True
AP1=True	IL6R=False	PLC_GAMMA_T=True
ARP2_3_T=False	IL9_T=False	PP1=False
ASK1_T=False	INOS=False	PP2A=False
ASMASE=True	IP10=False	PTEN_T=True
ATF2_T=False	IP3_T=False	PTP1B=False
BAD_T=True	IRAK1_P=True	RAC_GAP_T=True
BAD=True	IRAK1_T=False	RAC_T=False
BCL10_T=False	IRAK1=True	RAC1_T=False
BCL2_T=False	IRAK4_T=True	RAF_T=True
BCLX_T=False	IRAK4=True	RAF1_T=True
C_FOS_T=False	IRF3=True	RAP1_T=True
C_FOS=True	ITK_T=False	RAS_GAP_T=False
C_JUN_T=False	JAK1_T=True	RAS_GRP_T=True
C3G_T=True	JAK1=False	RAS_T=False
CABIN1_T=True	JAK2_T=True	RIP1_T=True
CALCINEURIN_T=False	JAK2=False	RSK_T=True
CALCIPRESSIN_T=True	JAK3=False	SHC_T=False
CALCIUM_IN_T=False	JNK_T=True	SHC+GRB2+SOS_T=False
CALCIUM_OUT_T=Random	JNK=True	SHP1_T=False
CAM_T=True	LAT_T=False	SHP1+GRB2+SOS_T=False
CAMK4_T=True	LAT+GRB2+SOS1_T=False	SHP1=True

CARMA1_T=False	LCK_T=True	SHP2_T=False
CBL_T=True	LFAA_L=True	SHP2+GRB2+GAB1+SOS_T=False
CD2_T=False	LIGHT=False	SLP76_T=False
CD27_T=True	LPG_L=True	SOCS3_T=False
CD28_T=False	LTBR_T=True	SOS_T=True
CD3_T=True	LYP_T=False	SOS1_T=True
CD4_T=False	MALT1_T=False	STAT1_ALPHA_P=False
CD40=False	MARCKS=False	STAT1_ALPHA=False
CD40L_T=False	MEF2_T=True	STAT1_T=False
CD45_T=True	MEF2A_T=False	STAT3_T=False
CD70=False	MEF2B_T=True	STAT3=False
CD8_T=False	MEF2C_T=True	STAT4_T=False
CD80=False	MEF2D_T=False	STAT5_T=False
CD86=False	MEK1_2_T=True	T3JAM_T=True
CDC42_T=False	MEKK_T=True	TAK1_T=True
CDC42+RAC_T=False	MEKK1_4_T=True	TAK1+TAB_T=False
CERAMIDE=True	MEKK3_T=True	TCPTP=True
COT_T=False	MEKK4_7_T=True	TCR_T=False
CR3=False	MHC_CLASS_II+LPG_L=True	TCR+CD3_T=False
CRAC_T=True	MHC_CLASS_II=True	TGF_BETA_T=False
CRE_T=False	MKK_T=False	TIR=True
CREB_T=False	MKK3_6_T=False	TLR2=True
CRKL_T=True	MKK4_7_T=False	TLR3=False
CSK_T=True	MKK7_T=True	TLR4=True
CTLA4_T=False	MKP_T=False	TNF_ALPHA_T=False
CYC_T=False	MKP1=True	TNF_ALPHA=False
CYCLIN_A_T=True	MKP3=True	TNF_ALPHAR_T=False
CYCLIN_D1_T=False	MLK2_T=False	TNF_ALPHAR=True
CYCLIN_D2_T=False	MLK3_T=False	TNF_BETA_T=False
CYCLIN_E_T=True	MRP=False	TNFSF9_T=False
DAG_T=True	MTOR=False	TNFSF9R_T=False
EF1_ALPHA_L=True	MYD88_T=True	TRADD_T=True
ELK1_T=False	MYD88+TIR+IRAK1=False	TRADD=False
ELK1=False	MYD88+TIR=False	TRAF1_T=False
ERK1_2_T=True	MYD88=False	TRAF2_T=False
ERK1_2=True	NCK_T=True	TRAF2=False
ETS_T=False	NCK+SOS_T=False	TRAF3_T=False
FASL_T=False	NFAT_T=False	TRAF3=False
FC_GAMMAR=False	NFAT+P300+MEF2_T=False	TRAF5_T=False
FKHR_T=True	NFKB_T=False	TRAF5=True
FYN_T=False	NFKB=False	TRAF6_T=True
GAB1_T=True	NIK_T=False	TRAF6=False
GADS_T=False	NO=False	TRIF=False

GCKR_T=False	NUC_AP1=False	TYK2_T=True
GLK_T=True	NUC_CREB_T=False	TYK2=True
GM_CSF_T=False	NUC_ELK1=False	VAV_T=False
GP63_L=True	NUC_ERK1_2_T=False	WASP_T=False
GRB2_T=False	NUC_ERK1_2=True	ZAP70_T=False
GRB2+SOS_T=False	NUC_JNK_T=False	NO_PRODUCTION=False
GRB7_T=False	NUC_MYC_T=False	TH_1_RESPONSE=False
GSK3_BETA_T=True	NUC_NFAT_T=False	TH_2_RESPONSE=False
HBEGF_T=False	NUC_NFKB_T=False	FACTOR1= TRUE
HDAC_T=True	NUC_NFKB=False	FACTOR2= TRUE
HPK1_T=True	NUC_P38_T=False	FACTOR3= TRUE
ICOS_T=False	NUC_P38=False	FACTOR4= TRUE
ICOSL=False	NUC_STAT1_ALPHA_P=False	FACTOR5= TRUE
IFN_ALPHA_T=False	NUC_STAT3_T=False	FACTOR6= TRUE
IFN_ALPHAR1_T=True	NUC_STAT3=False	FACTOR7= TRUE
IFN_ALPHAR2_T=True	NUC_STAT4_T=False	FACTOR8= TRUE
IFN_BETA=False	NUR77_T=False	FACTOR9= TRUE
IFN_GAMMA_T=False	OSM_T=False	FACTOR10= TRUE
IFN_GAMMAR=True	OX40_T=False	FACTOR11= TRUE
IFN_OMEGA_T=True	OX40L=False	FACTOR12= TRUE
IGG=True	P15_T=False	FACTOR13= TRUE
IKB_ALPHA_T=False	P19_T=False	FACTOR14= TRUE
IKB_BETA_T=False	P21_T=False	FACTOR15= TRUE
IKK_ALPHA_T=False	P21RAS_T=False	FACTOR16= TRUE
IKK_ALPHA=False	P27_T=True	FACTOR17= TRUE
IKK_BETA_T=True	P300_T=True	FACTOR18= TRUE
IKK_GAMMA_T=False	P38_T=False	FACTOR19= TRUE
IL1_ALPHA=False	P38=False	FACTOR20= TRUE
IL1_BETA=False	P53_T=False	FACTOR21= TRUE
IL10_T=False	P70_T=False	FACTOR22= TRUE
IL10=True	PAG_T=True	FACTOR23= TRUE
IL10R_T=True	PAG+CSK_T=False	
IL10R=False	PAK_T=False	
IL12_T=False	PD1_T=False	
IL12=False	PDGF_T=False	
IL12R_T=True	PDGFRB_T=False	
IL12R=True	PDK1_T=True	
IL13_T=False	PDL=False	
IL1R_T=False	PI3K_T=True	
IL2_T=False	PI3K=True	
IL2R_T=False	PIP_T=False	
IL3_T=False	PIP2_T=False	

Table B. 6: List of agonist and antagonist of the proposed targets

Targets	Antagonist/ Agonist	Reference
TLR2	Antagonist- C16H15NO4	[360]
TLR3	Agonist- polyIC ₁₂ U	[361]
MKP	Agonist- JWH015	[362]
SHC	Antagonist- PP2 Inhibitor of Shc/Grb2 interaction- actinomycin D	[363,364]
SHP2	Antagonist- 8-hydroxy-7-(6-sulfonaphthalen-2-yl) diazanyl-quinoline-5-sulfonic acid (NSC-87877)	[365]

APPENDIX C

Table C. 1: *L. donovani* Virulence factors (pathogen source nodes/effector nodes) considered in the final *L. donovani* VF-Human PPI Network

No.	Secretome protein Functional Category [366]	<i>L.donovani</i> Virulence factors (Source node)	Protein Name (Description)
1	Signalling	E9BQ78_LEISH	Mitogen activated protein kinase, putative
2		E9BK16_LEISH	Activated protein kinase c receptor (LACK)
3		E9BRX9_LEISH	Casein kinase, putative
4		E9BA99_LEISH	Mitogen-activated protein kinase (EC 2.7.11.24)
5		E9BN59_LEISH	ADP-ribosylation factor, putative
6	Intracellular Survival	E9B7I1_LEISH	Proteasome regulatory non-ATPase subunit 6, putative
7		E9BU45_LEISH	14-3-3 protein-like protein
8		E9BFJ3_LEISH	Proteasome subunit alpha type (EC 3.4.25.1)
9		E9BTM6_LEISH	Proteasome subunit alpha type (EC 3.4.25.1)
10		E9BC27_LEISH	Myo-inositol-1-phosphate synthase
11		E9BNU4_LEISH	Superoxide dismutase (EC 1.15.1.1)
12		E9BB84_LEISH	Carboxypeptidase, putative
13		E9B8I6_LEISH	Dipeptidyl peptidase 3 (EC 3.4.14.4) (Dipeptidyl aminopeptidase III) (Dipeptidyl peptidase III)
14		E9BC06_LEISH	Enolase
15		E9BFK5_LEISH	Proteasome subunit alpha type (EC 3.4.25.1)
16		E9BI90_LEISH	Glutathione peroxidase
17		E9BIV4_LEISH	Proteasome endopeptidase complex (EC 3.4.25.1)
18		E9BID4_LEISH	Heat shock protein 70-related protein
19		E9B8M5_LEISH	Proteasome subunit beta (EC 3.4.25.1)
20		E9BQM1_LEISH	Proteasome regulatory non-ATP-ase subunit 11, putative
21	Immunosuppression	E9BHJ8_LEISH	Peptidyl-prolyl cis-trans isomerase (PPIase) (EC 5.2.1.8)
22	Vesicle transport	E9BIZ5_LEISH	Small GTP-binding protein Rab1, putative

Table C. 2: Statistics of the Host Pathogen Interactome

Statistics	Interaction type (Rank)	No. of Interactions	Source
HPI+BIPS	1	175	Prediction
HPI/BIPS+DDI	2	635	
HPI+BIPS+DDI	3	3	
Experimental	4	74225	STRING
Total No. of Interactions		75038	

- ▶ Total Interactions (Edges) of Interactome predicted: 75038
- ▶ No. of Self loops: 1843
- ▶ **No. of Interactors in the final network: 73195**

Table C. 3: Correlation of virulence factors putative function as stated by Maxwell *et.al* with their corresponding predicted partner interologs on the basis of their DAVID pathway enrichment (FDR <0.05)

<i>L.donovani</i> Virulence factor	Protein Name	No. of Predicted Interactors	DAVID enriched pathways for the interactors (KEGG/Reactome)	Putative function of VFs from Proteomic analysis [366]
Intracellular Survival				
E9B7I1	Proteasome regulatory non-ATPase subunit 6, putative	36	Proteasome	Proteolysis (Intracellular survival)
E9BTM6	Proteasome subunit alpha type (EC 3.4.25.1)	09	Endocytosis	Proteolysis (Intracellular survival)
E9BU45	14-3-3 protein-like protein	11	1)AMPK signalling pathway 2)cGMP-PKG signalling pathway	Anti-apoptotic (Intracellular survival)
E9BNU4	Superoxide dismutase (EC 1.15.1.1)	28	1)Chromatin Organization 2) RMT Methylate histone arginines (arginine methylation)	Antioxidant (Intracellular survival)
E9BQM1	Proteasome regulatory non-	3	1)DNA Repair-DNA	Proteolysis

	ATP-ase subunit 11, putative		damage recognition in GG-NER DNA repair 2)Formation of TC-NER Pre-incision complex	(Intracellular survival)
E9B8I6	Dipeptidyl peptidase 3 (EC 3.4.14.4) (Dipeptidyl aminopeptidase III) (Dipeptidyl peptidase III)	23	1)Antigen processing and presentation 2)Estrogen signalling pathway 3)Spliceosome 4)Protein processing in endoplasmic reticulum 5)Endocytosis 6)MAPK signalling pathway	Proteolysis (Intracellular survival)
E9B8M5	Proteasome subunit beta (EC 3.4.25.1)	16	Proteasome	Proteolysis (Intracellular survival)
E9BC06	Enolase	15	1)Glycolysis / Gluconeogenesis 2)RNA degradation 3)HIF-1 signalling pathway	Plasminogen binding, Invasion (Intracellular survival)
E9BFJ3	Proteasome subunit alpha type (EC 3.4.25.1)	8	Proteasome	Proteolysis (Intracellular Survival)
E9BFK5	Proteasome subunit alpha type (EC 3.4.25.1)	54	1)Chemokine signalling pathway 2)Cytokine-cytokine receptor interaction 3)Cysteine and methionine metabolism	Proteolysis (Intracellular survival)
E9BI90	Glutathione peroxidase	8	1)Purine metabolism 2)Glutathione metabolism 3)p53 signalling pathway 4)Pyrimidine metabolism	Antioxidant (Intracellular survival)
E9BID4	Heat shock protein 70-related protein	47	5)Protein processing in endoplasmic reticulum	Protein stability (Intracellular survival)

E9BSB0	Aminopeptidase P, Putative	1	No significant Pathway Enrichment Molecular Function: plays important role in collagen metabolism Go process: Cellular aminoacid metabolic process	Proteolysis (Intracellular Survival)
E9BB84	Carboxypeptidase, putative	2	No significant Pathway Enrichment Function: Go process: proteasomal protein catabolic process, negative regulation of proteolysis, protein localization to cytosolic proteasome complex involved in ERAD pathway, apoptotic process, immune response-activating cell surface receptor signalling pathway Go function: proteasome binding	Proteolysis (intracellular survival)
E9BC27	Myo-inositol-phosphate synthase	1	No significant Pathway Enrichment KEGG pathway annotation: PPAR Singalling Pathway	Inositol biosynthesis (Intracellular survival)
E9BIV4	Proteasome alpha 7 subunit, putative	25	1)SLBP independent Processing of Histone Pre-mRNAs (Homo sapiens) 2)SLBP Dependent Processing of Replication-Dependent Histone Pre-mRNAs (Homo sapiens) 3)snRNP Assembly (Homo sapiens) 4)mRNA Splicing – Minor Pathway	Proteolysis (intracellular survival)

			(Homo sapiens)	
E9BQR2	Putative uracil phosphoribosyltransferase	5	No significant Pathway Enrichment GO process: Actin cytoskeleton organization, barbed-end actin filament capping	Pyrimidine Salvage (Intracellular survival)
Signal Transduction				
E9BRX9	Casein kinase, putative	24	1)Apoptosis 2)RIG-I-like receptor signalling pathway 3)Toll-like receptor signalling pathway 4)TNF signalling pathway	Kinase (Signal transduction)
E9BA99	Mitogen-activated protein kinase (EC 2.7.11.24)	257	1)MAPK signalling pathway 2)Neurotrophin signalling pathway 3)Fc epsilon RI signalling pathway 4)ErbB signalling pathway 5)GnRH signalling pathway 6)T cell receptor signalling pathway 7)TNF signalling pathway 8)Toll-like receptor signalling pathway 9)Insulin signalling pathway	Kinase (Signal transduction)
E9BK16	Activated protein kinase c receptor (LACK)	23	1)Ras signalling pathway 2)Chemokine signalling pathway	Kinase receptor (Signal transduction)
E9BN59	ADP-ribosylation factor, putative	56	1)Endocytosis 2)Fc gamma R-mediated phagocytosis 3)Lysosome	GTPase mediated signal transduction (Signal transduction)
E9BQ78	Mitogen activated protein kinase, putative	3	1)GnRH signalling pathway 2)MAPK signalling	Kinase (Signal transduction)

			pathway	
Immunosuppression				
E9BHJ8	Peptidyl-prolyl cis-trans isomerase (PPIase) (EC 5.2.1.8)	20	1)VEGF signalling pathway 2)B cell receptor signalling pathway 3)T cell receptor signalling pathway	Immunosuppressive (Immunosuppressive protein)
Vessical Transport				
E9BIZ5	Small GTP-binding protein Rab1, putative	137	1)Endocytosis 2)Phagosome	Endosome/Golgi trafficking (Vessical transport processes)

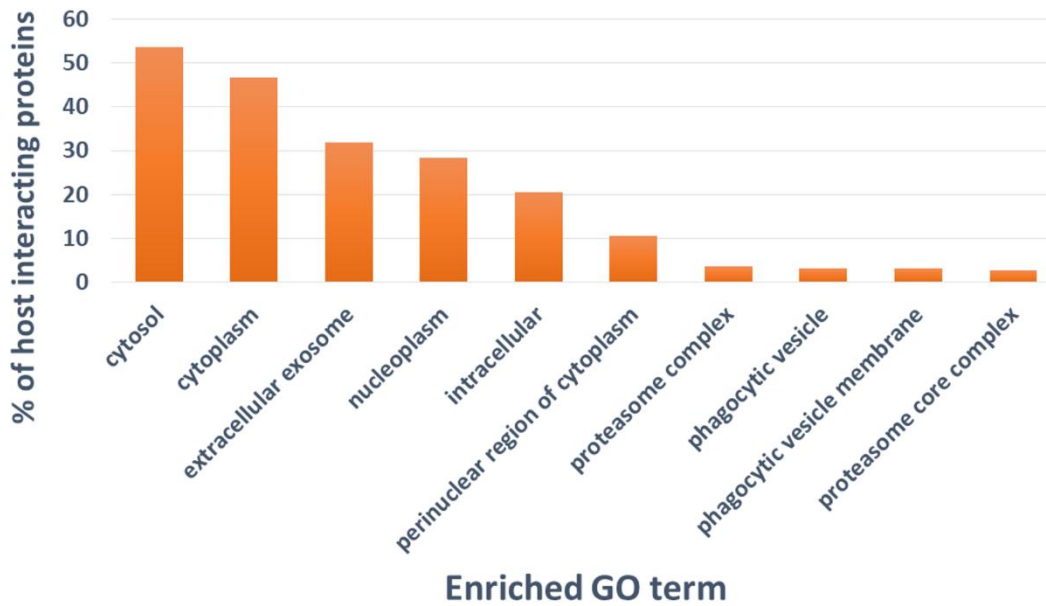


Figure C. 1: Cellular location of direct interactors: predicted interolog partner proteins) of virulence factors based on GO Term (CC) enrichment (Benjamini-Hochberg correction FDR <0.05)

Table C. 4: List of PRNs* and their associated GO terms (biological process) for each Phenotype category (Early infection)- 1) IR 2) SUR and Literature-curated for (late infection) 3) VIS#

Early Infection Phase		Late Infection Phase
IR PRNs	SUR PRNs	VIS PRNs
1. CH60_HUMAN	1. 1433Z_HUMAN	1. TNFA_HUMAN
2. GSTP1_HUMAN	2. ANXA5_HUMAN	2. COX2_HUMAN
3. HS71A_HUMAN	3. COF1_HUMAN	3. DVL1_HUMAN
4. IL1B_HUMAN	4. EF1A2_HUMAN	4. GSK3B_HUMAN
5. ITB2_HUMAN	5. ENPL_HUMAN	5. TSC1_HUMAN
6. MAVS_HUMAN	6. GRP75_HUMAN	6. TSC2_HUMAN
7. NPM_HUMAN	7. HMGA2_HUMAN	7. SFRP4_HUMAN
8. PARP1_HUMAN	8. HNRPK_HUMAN	8. SFRP2_HUMAN
9. PDIA1_HUMAN	9. HP1B3_HUMAN	9. RHEB_HUMAN
10. PRDX3_HUMAN	10. HYOU1_HUMAN	10. RAC1_HUMAN
11. PTN6_HUMAN	11. KPVM_HUMAN	11. NOS2_HUMAN
12. RIPK1_HUMAN	12. LMNA_HUMAN	12. TGFB1_HUMAN
13. RL40_HUMAN	13. SCRIB_HUMAN	13. STAT6_HUMAN
14. RS27A_HUMAN	14. TOP1_HUMAN	14. CXCR2_HUMAN
15. SODC_HUMAN		15. TEBP_HUMAN
16. SODM_HUMAN		16. PTGDS_HUMAN
17. TBB4B_HUMAN		17. LTBP2_HUMAN
18. TBB5_HUMAN		18. HS90A_HUMAN
19. UBB_HUMAN		19. HS90B_HUMAN
20. UBC_HUMAN		20. JAK2_HUMAN
		21. DUS6_HUMAN
		22. MK01_HUMAN
		23. PTPA_HUMAN
		24. DUS1_HUMAN
		25. IRAK1_HUMAN
GO TERMS for IR	GO TERMS for SUR	The PRNs for the VIS module have been identified from the experimental studies reported in the Literature.
<ul style="list-style-type: none"> GO:0051092~positive regulation of NF-kappaB transcription factor activity GO:0035666~TRIF-dependent toll-like receptor signalling pathway GO:0032480~negative regulation of type I interferon production GO:0010803~regulation of tumor necrosis factor-mediated signalling pathway GO:0002755~MyD88-dependent toll-like receptor signalling pathway GO:0032479~regulation of type I interferon production 	<ul style="list-style-type: none"> GO:0043066~negative regulation of apoptotic process GO:0010939~regulation of necrotic cell death GO:0043065~positive regulation of apoptotic process GO:0006977~DNA damage response, signal transduction by p53 class mediator resulting in cell cycle arrest GO:0071456~cellular response to hypoxia GO:2001240~negative regulation of extrinsic 	

<ul style="list-style-type: none"> • GO:0002756~MyD88-independent toll-like receptor signalling pathway • GO:0000302~response to reactive oxygen species • GO:0007249~I-kappaB kinase/NF-kappaB signalling • GO:0032757~positive regulation of interleukin-8 production • GO:0030512~negative regulation of transforming growth factor beta receptor signalling pathway • GO:0007179~transforming growth factor beta receptor signalling pathway • GO:0043123~positive regulation of I-kappaB kinase/NF-kappaB signalling • GO:0042542~response to hydrogen peroxide • GO:0042267~natural killer cell mediated cytotoxicity • GO:0033209~tumor necrosis factor-mediated signalling pathway • GO:0038061~NIK/NF-kappaB signalling • GO:0016236~macroautophagy • GO:0045429~positive regulation of nitric oxide biosynthetic process • GO:0000303~response to superoxide 	<p>apoptotic signalling pathway in absence of ligand</p> <ul style="list-style-type: none"> • GO:2001237~negative regulation of extrinsic apoptotic signalling pathway • GO:0012501~programmed cell death • GO:0050665~hydrogen peroxide biosynthetic process • GO:0034599~cellular response to oxidative stress 	
--	--	--

*These PRNs are categorized for each Early infection Phenotype (IR/SUR) based on the GO Biological process terms which were curated based on the association of the biological process of the 111 DMPs [367] with the infection phenotype to be studied. For example, the GO terms “TRIF-dependent toll-like receptor signalling pathway” and “negative regulation of type I interferon production” were assumed to be associated with the phenotype IR and thus corresponding DMPs enriched for these terms were categorized into IR PRNs and similar was followed for the SUR PRNs.

#The PRNs for Late infection phenotype (VIS) were curated from Literature (Literature sources referred in the main manuscript) as the DMPs identified in Singh *et.al* [367] study was not identified for sufficiently longer period of incubation (>72 hrs) which is previously observed to be required for the visceralization process to be established during the infection.

Table C. 5: Signalling Pathways enriched for each sub-network

IR	SUR	VIS
hsa04722: Neurotrophin signalling pathway	hsa04722: Neurotrophin signalling pathway	hsa04010: MAPK signalling pathway
hsa04664: Fc epsilon RI signalling pathway	hsa04010: MAPK signalling pathway	hsa04012: ErbB signalling pathway
hsa04660: T cell receptor signalling pathway	hsa04660: T cell receptor signalling pathway	hsa04014: Ras signalling pathway
hsa04012: ErbB signalling pathway	hsa04012: ErbB signalling pathway	hsa04015: Rap1 signalling pathway
hsa04662: B cell receptor signalling pathway	hsa04370: VEGF signalling pathway	hsa04022: cGMP-PKG signalling pathway
hsa04668: TNF signalling pathway	hsa04664: Fc epsilon RI signalling pathway	hsa04024: cAMP signalling pathway
hsa04068: FoxO signalling pathway	hsa04912: GnRH signalling pathway	hsa04062: Chemokine signalling pathway
hsa04010: MAPK signalling pathway	hsa04071: Sphingolipid signalling pathway	hsa04064: NF-kappa B signalling pathway
hsa04064: NF-kappa B signalling pathway	hsa04917: Prolactin signalling pathway	hsa04066: HIF-1 signalling pathway
hsa04620: Toll-like receptor signalling pathway	hsa04621: NOD-like receptor signalling pathway	hsa04068: FoxO signalling pathway
hsa04912: GnRH signalling pathway	hsa04915: Estrogen signalling pathway	hsa04071: Sphingolipid signalling pathway
hsa04915: Estrogen signalling pathway	hsa04062: Chemokine signalling pathway	hsa04115: p53 signalling pathway
hsa04621: NOD-like receptor signalling pathway	hsa04668: TNF signalling pathway	hsa04150: mTOR signalling pathway
hsa04370: VEGF signalling pathway	hsa04068: FoxO signalling pathway	hsa04151: PI3K-Akt signalling pathway
hsa04015: Rap1 signalling pathway	hsa04910: Insulin signalling pathway	hsa04152: AMPK signalling pathway
hsa04062: Chemokine signalling pathway	hsa04015: Rap1 signalling pathway	hsa04310: Wnt signalling pathway
hsa04151: PI3K-Akt signalling pathway	hsa04150: mTOR signalling pathway	hsa04370: VEGF signalling pathway
hsa04066: HIF-1 signalling	hsa04620: Toll-like receptor	hsa04390: Hippo signalling

pathway	signalling pathway	pathway
hsa04014: Ras signalling pathway	hsa04919: Thyroid hormone signalling pathway	hsa04550: Signalling pathways regulating pluripotency of stem cells
hsa04622: RIG-I-like receptor signalling pathway	hsa04662: B cell receptor signalling pathway	hsa04620: Toll-like receptor signalling pathway
hsa04071: Sphingolipid signalling pathway	hsa04066: HIF-1 signalling pathway	hsa04621: NOD-like receptor signalling pathway
hsa04910: Insulin signalling pathway	hsa04024: cAMP signalling pathway	hsa04622: RIG-I-like receptor signalling pathway
hsa04917: Prolactin signalling pathway	hsa04151: PI3K-Akt signalling pathway	hsa04660: T cell receptor signalling pathway
hsa04024: cAMP signalling pathway	hsa04014: Ras signalling pathway	hsa04662: B cell receptor signalling pathway
hsa04919: Thyroid hormone signalling pathway	hsa04022: cGMP-PKG signalling pathway	hsa04664: Fc epsilon RI signalling pathway
hsa04022: cGMP-PKG signalling pathway	hsa04622: RIG-I-like receptor signalling pathway	hsa04668: TNF signalling pathway
hsa04921: Oxytocin signalling pathway	hsa04550: Signalling pathways regulating pluripotency of stem cells	hsa04722: Neurotrophin signalling pathway
hsa04115: p53 signalling pathway	hsa04064: NF-kappa B signalling pathway	hsa04910: Insulin signalling pathway
hsa04152: AMPK signalling pathway	hsa04115: p53 signalling pathway	hsa04912: GnRH signalling pathway
hsa04310: Wnt signalling pathway	hsa04921: Oxytocin signalling pathway	hsa04915: Estrogen signalling pathway
hsa04920: Adipocytokine signalling pathway	hsa04920: Adipocytokine signalling pathway	hsa04917: Prolactin signalling pathway
hsa04550: Signalling pathways regulating pluripotency of stem cells	hsa04310: Wnt signalling pathway	hsa04919: Thyroid hormone signalling pathway
		hsa04920: Adipocytokine signalling pathway
		hsa04921: Oxytocin signalling pathway
		hsa04922: Glucagon signalling pathway

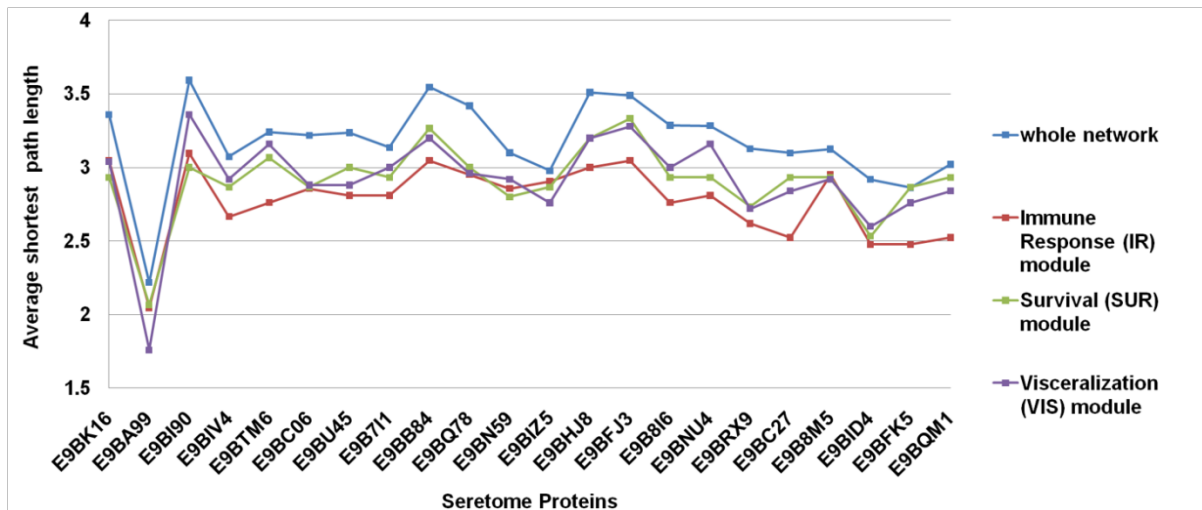


Figure C. 2: Average shortest path length from each Virulence Factor to the response nodes of each phenotypic subnetwork. E9BA99 is observed to be closest to all the phenotypes.

Table C. 6: Top 10 knockout candidates identified based on Betweenness centrality measure in the three sub-networks

No .	Knockout Candidate Protein (Node)	Protein	Betweenness Centrality	Degree
1	A4_HUMAN	Amyloid-beta precursor protein	0.06405442	740
2	EGFR_HUMAN	Epidermal growth factor receptor	0.06245475	644
3	HS90A_HUMAN	Heat shock protein HSP 90-alpha	0.05881114	604
4	UBC_HUMAN	Polyubiquitin-C	0.03804491	518
5	P53_HUMAN	Cellular tumor antigen p53	0.01793926	476
6	SRC_HUMAN	Proto-oncogene tyrosine-protein kinase Src	0.02759134	449
7	AKT1_HUMAN	RAC-alpha serine/threonine-protein kinase	0.02456149	403
8	TRAF6_HUMAN	TNF receptor-associated factor 6	0.01380817	377
9	1433Z_HUMAN	14-3-3 protein zeta/delta	0.01051357	352
10	GSK3B_HUMAN	Glycogen synthase kinase-3 beta	0.01578974	283

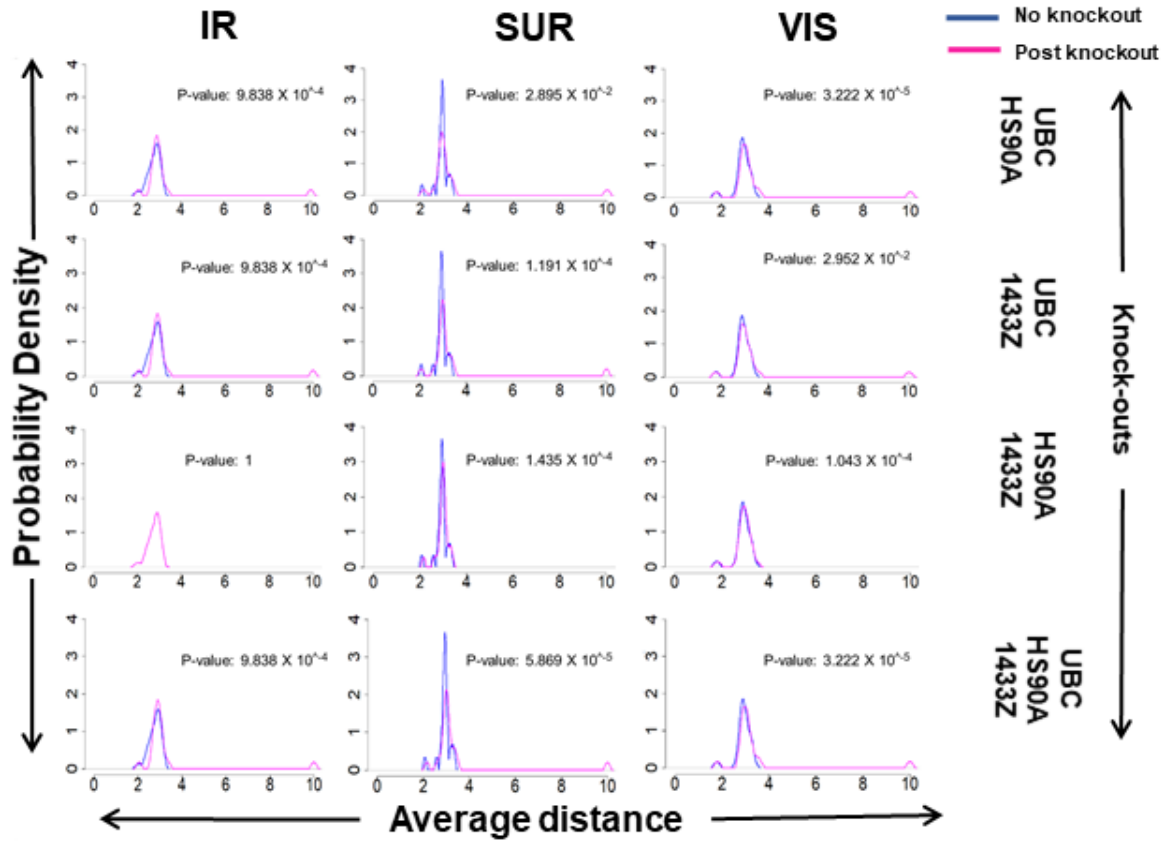


Figure C. 3: Distance deviation Analysis for the combination knockout in IR, SUR and VIS subnetworks. Probability density graphs using Gaussian curve based Epanechnikov method representing the deviation in the average shortest path distance before and after knockout.

APPENDIX D

Table D. 1: List of Parameters

	Parameter	Description	Units	Value	Reference [#]
1.	β_{M2}	Rate of IL-10 production from M2 cells	ng cell ⁻¹ day ⁻¹	1x10 ⁻¹⁵	Expected
2.	β_{Tc}	Rate of IFN- γ production from Tc cells	ng cell ⁻¹ day ⁻¹	1x10 ⁻⁸	Expected
3.	β_{Th1CK2}	Rate of IFN- γ production from TH1 cells	ng cell ⁻¹ day ⁻¹	1x10 ⁻⁷	Expected
4.	β_{Th1CK3}	Rate of IL-2 production from TH1 cells	ng cell ⁻¹ day ⁻¹	1 x10 ⁻⁸	Expected
5.	β_{Th2}	Rate of IL-10 production from TH2 cells	ng cell ⁻¹ day ⁻¹	1 x10 ⁻⁹	Expected
6.	β_{Treg}	Rate of IL-10 production from Treg cells	ng cell ⁻¹ day ⁻¹	1 x10 ⁻¹⁰	Expected
7.	γ_C	Birth rate of Cancer cells	day ⁻¹	0.1282	Estimated
8.	γ_{CR}	Birth rate of Cancer resistant cells	day ⁻¹	0.1282	Expected
9.	γ_{M1}	Birth rate of M1 cells	day ⁻¹	0.7	Expected
10.	γ_{M2}	Birth rate of M2 cells	day ⁻¹	0.01	Expected
11.	γ_S	Birth rate of Stem cells	day ⁻¹	0.15	Expected
12.	γ_{Tc}	Birth rate of Tc cells	day ⁻¹	1.0	[368]
13.	γ_{Th1}	Birth rate of TH1 cells	day ⁻¹	2.0	[369]
14.	γ_{Th2}	Birth rate of TH2 cells	day ⁻¹	2.0	[369]
15.	γ_{Treg}	Birth rate of Treg cells	day ⁻¹	0.3	[370]
16.	δ_C	Death rate of Cancer cells	day ⁻¹	0.8055	Estimated
17.	δ_{Ck1}	Degradation rate of IL-10	day ⁻¹	19.757	Estimated
18.	δ_{Ck2}	Degradation rate of IFN- γ	day ⁻¹	6.1212	Estimated
19.	δ_{Ck3}	Degradation rate of IL-2	day ⁻¹	8.664339	Calculated [100]
20.	δ_{CR}	Death rate of Resistant Cancer cells	day ⁻¹	5.37 x10 ⁻⁵	Estimated
21.	δ_{M1}	Death rate of M1 cells	day ⁻¹	1.02	[371]
22.	δ_{M2}	Death rate of M2 cells	day ⁻¹	0.05	[371]
23.	δ_S	Death rate of Stem cells	day ⁻¹	2 x10 ⁻⁷	Expected
24.	δ_{Tc}	Death rate of Tc cells	day ⁻¹	5.2939	Estimated
25.	δ_{Th1}	Death rate of TH1 cells	day ⁻¹	2.0	[372]
26.	δ_{Th2}	Death rate of TH2 cells	day ⁻¹	2.0	Expected
27.	δ_{Treg}	Death rate of Treg cells	day ⁻¹	1.0	[373]
28.	λ_{M1}	Saturation constant for M1 activation	cells ml ⁻¹	1x10 ⁸	Expected
29.	λ_{M2}	Saturation constant for M2 activation	cells ml ⁻¹	1 x10 ⁶	Expected
30.	λ_{Tc1}	Saturation constant for Tc	cells ml ⁻¹	1 x10 ⁵	Expected

		activation by cancer cells			
31.	λ_{Tc2}	Saturation constant for Tc inhibition by stem cells	cells ml ⁻¹	5 x10 ⁵	Expected
32.	λ_{Tc3}	Saturation constant for Tc inhibition by Treg cells	cells ml ⁻¹	5 x10 ¹⁰	Expected
33.	λ_{Tc4}	Saturation constant for Tc activation by T _{H1} cells	cells ml ⁻¹	1 x10 ⁵	Expected
34.	λ_{Th1}	Saturation constant for T _{H1}	cells ml ⁻¹	1 x10 ⁵	Expected
35.	λ_{Th2}	Saturation constant for T _{H2}	cells ml ⁻¹	1 x10 ⁵	Expected
36.	λ_{Treg2}	Saturation constant for Treg	cells ml ⁻¹	1 x10 ⁷	Expected
37.	μ_{C1}	Rate of activation of C and C _R by IL-10	day ⁻¹	0.75	[374]
38.	μ_{C2}	Rate of killing of C and C _R by IFN- γ	day ⁻¹	0.9	[375]
39.	μ_S	Rate of killing of S by IFN-gamma	day ⁻¹	0.17	[375]
40.	μ_{SR}	Rate of killing of S _R by IFN-gamma	day ⁻¹	0.18	Expected
41.	μ_{TcS}	Rate of Tc killing by S and S _R cells	day ⁻¹	1 x10 ⁻¹⁰	[376]
42.	μ_{TcTreg}	Rate of Tc killing by Treg cells	day ⁻¹	1.5x10 ⁻⁵	[377]
43.	μ_{Th1ck1}	Rate of T _{H1} killing by IL-10	day ⁻¹	1 x10 ⁻⁹	[378]
44.	μ_{Th1ck3}	Rate of T _{H1} activation by IL-2	day ⁻¹	0.1245	[102]
45.	$\mu_{TregCk1}$	Rate of Treg activation by IL-10	day ⁻¹	1 x10 ⁻⁷	Expected
46.	$C_{max}=K_{tumor}/2$	Carrying capacity for Cancer cells , where $K_{tumor}=2 \times 10^{10}$ is the total Carrying capacity of non-stem tumor cells	cells ml ⁻¹	1 x10 ¹⁰	[47]
47.	$CR_{max}=K_{tumor}/2$	Carrying capacity for Resistant Cancer cells, where $K_{tumor}=2 \times 10^{10}$ is the total Carrying capacity of non-stem tumor cells	cells ml ⁻¹	1 x10 ¹⁰	Expected
48.	$k1$	Saturation constant for inhibition of S by IFN- γ	ng ml ⁻¹	10.0	Expected
49.	$k11$	Saturation constant for activation of Treg by IL-10	ng ml ⁻¹	0.001	Expected
50.	$k2$	Saturation constant for inhibition of S _R by IFN- γ	ng ml ⁻¹	10.0	Expected
51.	$k3$	Saturation constant for activation of C by IL-10	ng ml ⁻¹	2.0531	Estimated
52.	$k4$	Saturation constant for inhibition of C by IFN- γ	ng ml ⁻¹	3.02	Estimated
53.	$k5$	Saturation constant for activation of C _R by IL-10	ng ml ⁻¹	6.7979	Estimated
54.	$k6$	Saturation constant for inhibition of C _R by IFN- γ	ng ml ⁻¹	6.9937	Estimated

55.	k8	Saturation constant for inhibition of T_{H1} by IL-10	ng ml ⁻¹	0.01	Expected
56.	k9	Saturation constant for activation of T_{H1} by IL-2	ng ml ⁻¹	0.001	Expected
57.	ktc1	Saturation constant for inhibition of S by Tc	cell ml ⁻¹	1 x10 ⁹	Expected
58.	ktc2	Saturation constant for inhibition of S_R by Tc	cell ml ⁻¹	1 x10 ⁸	Expected
59.	ktc3	Saturation constant for inhibition of C by Tc	cell ml ⁻¹	1 x10 ⁹	Expected
60.	ktc4	Saturation constant for inhibition of C_R by Tc	cell ml ⁻¹	1 x10 ⁹	Expected
61.	mc	Probability of Stem cell transformation into Stem resistant cells	-	0.01	Expected
62.	ms	Probability of Cancer cell transformation into Cancer resistant cells	-	4 x10 ⁻⁷	[47]
63.	p1	Probability of Asymmetric differentiation of stem cells	-	0.2	[47]
64.	p2	Probability of Symmetric differentiation into two differentiated cancer cells	-	0.05	[47]
65.	r1	constant		0.0001	Expected
66.	r2	constant		1x x10 ⁻⁵	Expected
67.	Tck	Rate of killing of tumor by Tc cells	day ⁻¹	0.1	Expected
68.	μ_{M1CK2}	Rate of M1 activation by IFN-γ	day ⁻¹	0.01	Expected
69.	μ_{M2CK1}	Rate of M2 activation by IL10	day ⁻¹	0.01	Expected
70.	k7	Saturation constant for proliferation of M1 by IFN-γ	ng ml ⁻¹	0.2	Expected
71.	k10	Saturation constant for proliferation of M2 by IL10	ng ml ⁻¹	0.01	Expected

Estimated parameter values have been determined by the MCMC techniques using the time course experiment cytometric data for cancer cell proliferation for Gastric cancer cell line (SGC7901) (Section 2.4.7).

Expected parameter values are estimated by varying the parameters within the biologically feasible ranges found in various Literatures so as to determine its expected value to calibrate the model with experimental observations.

Table D. 2: List of Initial values

Variable	Symbol	Initial Values	Reference
Stem Cell	S	1	-
Stem Resistant Cell	S_R	0	-
Cancer Cell	C	0	-
Cancer Resistant Cell	C_R	0	-
Type-I Tumor Associated Macrophage	M1	85000	Calculated [371]
Type-II Tumor Associated Macrophage	M2	15000	Calculated [371]
Type-I Helper T Cell	T_{H1}	71000	[16]
Type-II Helper T Cell	T_{H2}	12000	[16]
Cytotoxic T Cell	T_c	56000	[16]
Regulatory T Cell	Treg	8000	[16]
Interleukin-10	IL10	0.0085	[17]
Interferon- γ	IFN- γ	0.12	[17]
Interleukin-2	IL2	0.0094	[17]

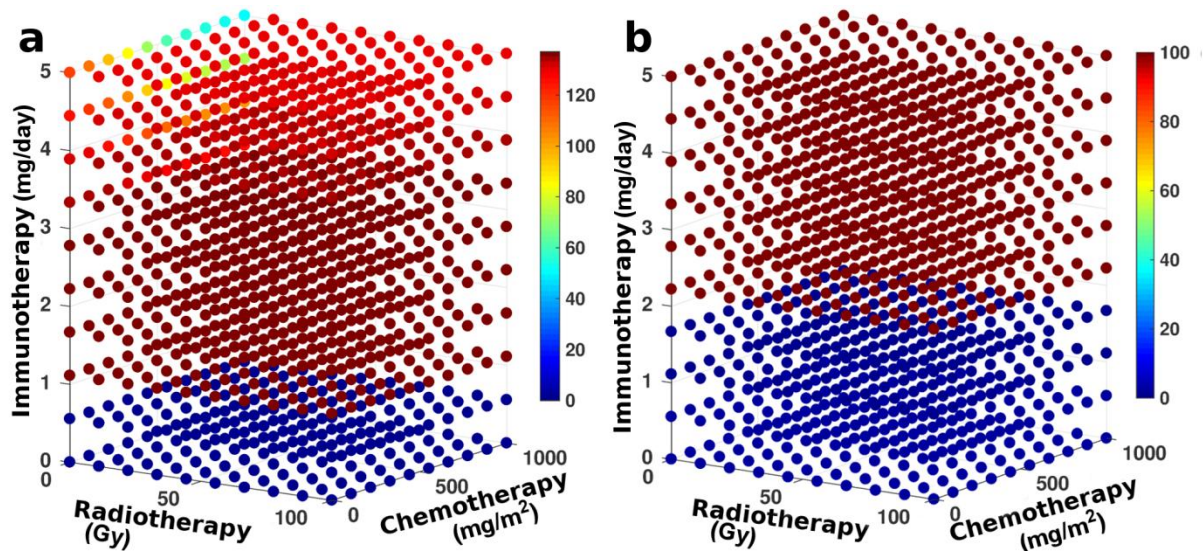


Figure D. 1: Treatment conditions under varying dose of Radiotherapy, Chemotherapy and Immunotherapy. The scatter plot depicts (a) the fold change of tumor population and (b) T_{H1}/T_{H2} ratio under 1000 treatment combinations.

REFERENCES

1. Cruse JM, Lewis RE and Wang H (2004) Chapter 1 - Molecules, Cells, and Tissues of Immunity. In *Immunology Guidebook*. San Diego: Elsevier Academic Press. pp. 1-15, doi: 10.1016/B978-012198382-6/50025-X
2. Rabb H (2002) The T cell as a bridge between innate and adaptive immune systems: Implications for the kidney. *Kidney International* 61: 1935-1946, doi: 10.1046/j.1523-1755.2002.00378.x
3. Moticka EJ (2016) Chapter 20 - Activation of T Lymphocytes and MHC Restriction. A Historical Perspective on Evidence-Based Immunology. Amsterdam: Elsevier. pp. 169-179, doi: 10.1016/B978-0-12-398381-7.00020-4
4. Moticka EJ (2016) Chapter 37 - Tumor Immunology. A Historical Perspective on Evidence-Based Immunology. Amsterdam: Elsevier. pp. 329-339, doi: 10.1016/B978-0-12-398381-7.00037-X
5. Gordon S (2002) Pattern recognition receptors: doubling up for the innate immune response. *Cell* 111: 927-930, doi: 10.1016/s0092-8674(02)01201-1
6. Hemmi H, Akira S (2005) TLR signalling and the function of dendritic cells. *Mechanisms of Epithelial Defense: Chemical Immunology and Allergy*. Basel, Karger, 86:120-135, doi:10.1159/000086657
7. Akira S, Uematsu S, Takeuchi O (2006) Pathogen recognition and innate immunity. *Cell* 124(4): 783-801, doi: 10.1016/j.cell.2006.02.015
8. Lee MS, Kim Y-J (2007) Signaling pathways downstream of pattern-recognition receptors and their cross talk. *Annual Review in Biochemistry* 76: 447-480, doi: 10.1146/annurev.biochem.76.060605.122847
9. Kawasaki T, Kawai T (2014) Toll-like receptor signaling pathways. *Frontiers in Immunology* 5: 461, doi: 10.3389/fimmu.2014.00461
10. Kaisho T, Akira S (2003) Regulation of dendritic cell function through Toll-like receptors. *Current Molecular Medicine* 3(8): 759-771, doi: 10.2174/1566524033479366
11. Wager CL, Wormley F (2014) Classical versus alternative macrophage activation: the Ying and the Yang in host defense against pulmonary fungal infections. *Mucosal Immunology* 7: 1023-1035, doi: 10.1038/mi.2014.65
12. Mosser DM, Edwards JP (2008) Exploring the full spectrum of macrophage activation. *Nature Reviews Immunology* 8: 958-969, doi: 10.1038/nri2448
13. Najafi M, Hashemi Goradel N, Farhood B, Salehi E, Nashtaei MS, et al. (2019) Macrophage polarity in cancer: A review. *Journal of Cellular Biochemistry* 120: 2756-2765, doi: 10.1002/jcb.27646
14. Germain RN (2002) T-cell development and the CD4-CD8 lineage decision. *Nature Reviews Immunology* 2: 309-322, doi: 10.1038/nri798

-
15. Zhu J, Yamane H, Paul WE (2010) Differentiation of effector CD4 T cell populations. *Annual Reviews in Immunology* 28: 445-489, doi: 10.1146/annurev-immunol-030409-101212
 16. Luckheeram RV, Zhou R, Verma AD, Xia B (2012) CD4+T Cells: Differentiation and Functions. *Clinical and Developmental Immunology* 2012: 12, doi: 10.1155/2012/925135
 17. Yamane H, Paul WE (2013) Early signaling events that underlie fate decisions of naive CD4(+) T cells towards distinct T-helper cell subsets. *Immunological Reviews* 252: 12-23, doi: 10.1111/imr.12032
 18. Geginat J, Paroni M, Maglie S, Alfen JS, Kastirr I, et al. (2014) Plasticity of human CD4 T cell subsets. *Frontiers in Immunology* 5: 630, doi: 10.3389/fimmu.2014.00630
 19. Janeway CA Jr, Travers P, Walport M, et al. (2001) *Immunobiology: The Immune System in Health and Disease*. 5th edition. New York: Garland Science; <https://www.ncbi.nlm.nih.gov/books/NBK10775/>
 20. Kagi D, Vignaux F, Ledermann B, Burki K, Depraetere V, et al. (1994) Fas and perforin pathways as major mechanisms of T cell-mediated cytotoxicity. *Science* 265: 528-530, doi: 10.1126/science.7518614
 21. Gregory DJ, Olivier M (2005) Subversion of host cell signalling by the protozoan parasite *Leishmania*. *Parasitology* 130: S27-S35, doi: 10.1017/S0031182005008139
 22. Gupta G, Oghumu S, Satoskar AR (2013) Mechanisms of Immune Evasion in Leishmaniasis. *Advances in Applied Microbiology* 82: 155-184, doi: 10.1016/B978-0-12-407679-2.00005-3
 23. Kaye P, Scott P (2011) Leishmaniasis: complexity at the host-pathogen interface. *Nature Reviews Microbiology* 9: 604-615, doi: 10.1038/nrmicro2608
 24. Olivier M, Gregory DJ, Forget G (2005) Subversion mechanisms by which *Leishmania* parasites can escape the host immune response: a signaling point of view. *Clinical Microbiology Reviews* 18: 293-305, doi: 10.1128/CMR.18.2.293-305.2005
 25. Menon JN, Bretscher PA (1998) Parasite dose determines the Th1/Th2 nature of the response to *Leishmania major* independently of infection route and strain of host or parasite. *European Journal of Immunology* 28: 4020-4028, doi: 10.1002/(SICI)1521-4141(199812)28:12<4020::AID-IMMU4020>3.0.CO;2-3
 26. Sharma U, Singh S (2009) Immunobiology of leishmaniasis. *Indian Journal of Experimental Biology* 47: 412.
 27. Liu D, Uzonna JE (2012) The early interaction of *Leishmania* with macrophages and dendritic cells and its influence on the host immune response. *Frontiers in Cell Infection and Microbiology* 2: 83, doi: 10.3389/fcimb.2012.00083
 28. Reithinger R, Dujardin J-C, Louzir H, Pirmez C, Alexander B, et al. (2007) Cutaneous Leishmaniasis. *The Lancet Infectious Diseases* 7: 581-596, doi: 10.1016/S1473-3099(07)70209-8

-
29. Zhang WW, Matlashewski G (2010) Screening *Leishmania donovani*-specific genes required for visceral infection. *Molecular microbiology* 77: 505-517, doi: 10.1007/978-1-4939-1438-8_20
 30. Chauhan N, Vidyarthi AS, Poddar R (2011) Comparative multivariate analysis of codon and amino acid usage in three *Leishmania* genomes. *Genomics, Proteomics & Bioinformatics* 9: 218-228, doi: 10.1016/S1672-0229(11)60025-9
 31. Zhang W-W, Mendez S, Ghosh A, Myler P, Ivens A, et al. (2003) Comparison of the A2 gene locus in *Leishmania donovani* and *Leishmania major* and its control over cutaneous infection. *Journal of Biological Chemistry* 278: 35508-35515, doi: 10.1074/jbc.M305030200
 32. Gregory DJ, Sladek R, Olivier M, Matlashewski G (2008) Comparison of the effects of *Leishmania major* or *Leishmania donovani* infection on macrophage gene expression. *Infection and immunity* 76: 1186-1192, doi: 10.1128/IAI.01320-07
 33. Rezende AM, Folador EL, Resende DdM, Ruiz JC (2012) Computational prediction of protein-protein interactions in *Leishmania* predicted proteomes. *PloS ONE* 7: e51304, doi: 10.1371/journal.pone.0051304
 34. Gradoni L, Gramiccia M (1994) *Leishmania infantum* Tropism: Strain genotype or host immune status? *Parasitology Today* 10: 264-267, doi: 10.1016/0169-4758(94)90142-2
 35. Olivier M, Gregory DJ, Forget G (2005) Subversion mechanisms by which *Leishmania* parasites can escape the host immune response: a signaling point of view. *Clinical Microbiology Reviews* 18: 293-305, doi: 10.1128/CMR.18.2.293-305.2005
 36. Soong L, Xu J-C, Grewal IS, Kima P, Sun J, et al. (1996) Disruption of CD40-CD40 ligand interactions results in an enhanced susceptibility to *Leishmania amazonensis* infection. *Immunity* 4: 263-273, doi: 10.1016/s1074-7613(00)80434-3
 37. McCall L-I, Zhang W-W, Matlashewski G (2013) Determinants for the development of visceral leishmaniasis disease. *PLoS Pathogens* 9: e1003053, doi: 10.1371/journal.ppat.1003053
 38. Zhang W-W, Chan KF, Song Z, Matlashewski G (2011) Expression of a *Leishmania donovani* nucleotide sugar transporter in *Leishmania major* enhances survival in visceral organs. *Experimental Parasitology* 129: 337-345, doi: 10.1016/j.exppara.2011.09.010
 39. Shadab M, Ali N (2011) Evasion of host defence by *Leishmania donovani*: subversion of signaling pathways. *Molecular Biology International* 2011, doi: 10.4061/2011/343961
 40. Sharma G, Kar S, Ball WB, Ghosh K, Das PK (2014) The curative effect of fucoidan on visceral leishmaniasis is mediated by activation of MAP kinases through specific protein kinase C isoforms. *Cellular & Molecular Immunology* 11: 263, doi: 10.1038/cmi.2013.68
 41. Dunn GP, Old LJ, Schreiber RD (2004) The Three Es of Cancer Immunoediting. *Annual Review of Immunology* 22: 329-360, doi: 10.1146/annurev.immunol.22.012703.104803
 42. Beatty GL, Gladney WL (2015) Immune escape mechanisms as a guide for cancer immunotherapy. *Clinical Cancer Research* 21: 687-692, doi: 10.1158/1078-0432.CCR-14-1860

-
43. Rabinovich GA, Gabrilovich D, Sotomayor EM (2007) Immunosuppressive strategies that are mediated by tumor cells. *Annual Reviews in Immunology* 25: 267-296, doi: 10.1146/annurev.immunol.25.022106.141609
 44. Chew V, Toh HC, Abastado JP (2012) Immune microenvironment in tumor progression: characteristics and challenges for therapy. *Journal of Oncology* 2012: 608406, doi: 10.1155/2012/608406
 45. Tan BT, Park CY, Ailles LE, Weissman IL (2006) The cancer stem cell hypothesis: a work in progress. *Laboratory Investigation* 86: 1203-1207, doi: 10.1038/labinvest.3700488
 46. Fidler IJ (2003) The pathogenesis of cancer metastasis: the 'seed and soil' hypothesis revisited. *Nature Reviews Cancer* 3: 453-458, doi: 10.1038/nrc1098
 47. Tomasetti C, Levy D (2010) Role of symmetric and asymmetric division of stem cells in developing drug resistance. *Proceedings of the National Academy of Sciences USA* 107: 16766-16771, doi: 10.1073/pnas.1007726107
 48. Zahreddine H, Borden KLB (2013) Mechanisms and insights into drug resistance in cancer. *Frontiers in Pharmacology* 4: 28, doi: 10.3389/fphar.2013.00028
 49. Papaccio F, Paino F, Regad T, Papaccio G, Desiderio V, et al. (2017) Concise review: cancer cells, cancer stem cells, and mesenchymal stem cells: influence in cancer development. *Stem cells Translational Medicine* 6: 2115-2125, doi: 10.1002/sctm.17-0138
 50. Bellone G, Turletti A, Artusio E, Mareschi K, Carbone A, et al. (1999) Tumor-associated transforming growth factor- β and interleukin-10 contribute to a systemic Th2 immune phenotype in pancreatic carcinoma patients. *The American Journal of Pathology* 155: 537-547, doi: 10.1016/s0002-9440(10)65149-8
 51. Ostuni R, Kratochvill F, Murray PJ, Natoli G (2015) Macrophages and cancer: from mechanisms to therapeutic implications. *Trends in Immunology* 36: 229-239, doi: 10.1016/j.it.2015.02.004
 52. Hirohashi Y, Torigoe T, Tsukahara T, Kanaseki T, Kochin V, et al. (2016) Immune responses to human cancer stem-like cells/cancer-initiating cells. *Cancer Science* 107: 12-17, doi: 10.1111/cas.12830
 53. Bell E, Taylor MA (2017) Functional roles for exosomal microRNAs in the tumour microenvironment. *Computational and Structural Biotechnology Journal* 15: 8-13, doi: 10.1186/s13046-020-01570-6
 54. Neviani P, Fabbri M (2015) Exosomic microRNAs in the tumor microenvironment. *Frontiers in Medicine* 2: 47, doi: 10.1186/s13046-020-01570-6
 55. Ohm JE, Gabrilovich DI, Sempowski GD, Kisseleva E, Parman KS, et al. (2003) VEGF inhibits T-cell development and may contribute to tumor-induced immune suppression. *Blood* 101: 4878-4886, doi: 10.1182/blood-2002-07-1956
 56. Ziogas AC, Gavalas NG, Tsiatas M, Tsitsilonis O, Politi E, et al. (2012) VEGF directly suppresses activation of T cells from ovarian cancer patients and healthy individuals via

-
- VEGF receptor Type 2. *International Journal of Cancer* 130: 857-864, doi: 10.1038/bjc.2012.468
57. Paino F, La Noce M, Di Nucci D, Nicoletti GF, Salzillo R, et al. (2017) Human adipose stem cell differentiation is highly affected by cancer cells both in vitro and in vivo: implication for autologous fat grafting. *Cell Death & Disease* 8: e2568, doi: 10.1038/cddis.2016.308
 58. Stellavato A, La Noce M, Corsuto L, Pirozzi AVA, De Rosa M, et al. (2017) Hybrid complexes of high and low molecular weight hyaluronans highly enhance HASCs differentiation: implication for facial bioremodelling. *Cellular Physiology and Biochemistry* 44: 1078-1092, doi: 10.1159/000485414
 59. Whiteside TL (2008) The tumor microenvironment and its role in promoting tumor growth. *Oncogene* 27: 5904-5912, doi: 10.1038/onc.2008.271
 60. Hao NB, Lu MH, Fan YH, Cao YL, Zhang ZR, et al. (2012) Macrophages in tumor microenvironments and the progression of tumors. *Clinical and Development Immunology* 2012: 948098, doi: 10.1155/2012/948098
 61. Corthay A (2009) How do regulatory T cells work? *Scandinavian Journal of Immunology* 70: 326-336, doi: 10.1111/j.1365-3083.2009.02308.x
 62. Gabrilovich DI, Nagaraj S (2009) Myeloid-derived suppressor cells as regulators of the immune system. *Nature Reviews Immunology* 9: 162, doi: 10.1038/nri2506
 63. Toh B, Wang X, Keeble J, Sim WJ, Khoo K, et al. (2011) Mesenchymal Transition and Dissemination of Cancer Cells Is Driven by Myeloid-Derived Suppressor Cells Infiltrating the Primary Tumor. *PLoS Biology* 9: e1001162, doi: 10.1371/journal.pbio.1001162
 64. Hirohashi Y, Torigoe T, Tsukahara T, Kanaseki T, Kochin V, et al. (2016) Immune responses to human cancer stem-like cells/cancer-initiating cells. *Cancer Science* 107: 12-17, doi: 10.1111/cas.12830
 65. Tiligada E, Ishii M, Riccardi C, Spedding M, Simon H-U, et al. (2015) The expanding role of immunopharmacology: IUPHAR Review 16. *British Journal of Pharmacology* 172: 4217-4227, doi: 10.1111/bph.13219
 66. Saha P, Mukhopadhyay D, Chatterjee M (2011) Immunomodulation by chemotherapeutic agents against Leishmaniasis. *International Immunopharmacology* 11: 1668-1679, doi: 10.1016/j.intimp.2011.08.002
 67. Oliveira LF, Schubach AO, Martins MM, Passos SL, Oliveira RV, et al. (2011) Systematic review of the adverse effects of cutaneous leishmaniasis treatment in the New World. *Acta Tropica* 118: 87-96, doi: 10.1016/j.actatropica.2011.02.007
 68. Markle WH, Makhoul K (2004) Cutaneous leishmaniasis: recognition and treatment. *American Family Physician* 69: 1455-1460, PMID: 15053410
 69. Frézard F, Demicheli C, Ribeiro RR (2009) Pentavalent Antimonials: New Perspectives for Old Drugs. *Molecules* 14: 2317-2336, doi: 10.3390/molecules14072317

-
70. Mishra M, Biswas UK, Jha DN, Khan AB (1992) Amphotericin versus pentamidine in antimony-unresponsive kala-azar. *The Lancet* 340: 1256-1257, doi: 10.1016/0140-6736(92)92952-C
 71. Haldar AK, Sen P, Roy S (2011) Use of Antimony in the Treatment of Leishmaniasis: Current Status and Future Directions. *Molecular Biology International* 2011: 23, doi: 10.4061/2011/571242
 72. Croft SL, Sundar S, Fairlamb AH (2006) Drug resistance in leishmaniasis. *Clinical Microbiology Reviews* 19: 111-126, doi: 10.1128/CMR.19.1.111-126.2006
 73. Kolde G, Luger T, Sorg C, Sunderkötter C (1996) Successful treatment of cutaneous leishmaniasis using systemic interferon-gamma. *Dermatology* 192: 56-60, doi: 10.1159/000246316
 74. Li J, Sutterwala S, Farrell JP (1997) Successful therapy of chronic, nonhealing murine cutaneous leishmaniasis with sodium stibogluconate and gamma interferon depends on continued interleukin-12 production. *Infection and immunity* 65: 3225-3230, doi: 10.1128/IAI.65.8.3225-3230.1997
 75. Chatelain R, Mauze S, Coffman RL (1999) Experimental *Leishmania major* infection in mice: role of IL-10. *Parasite immunology* 21: 211-218, doi: 10.1046/j.1365-3024.1999.00224.x.
 76. Gammaitoni L, Leuci V, Mesiano G, Giraudo L, Todorovic M, et al. (2014) Immunotherapy of cancer stem cells in solid tumors: initial findings and future prospective. *Expert Opinion on Biological Therapy* 14: 1259-1270, doi: 10.1517/14712598.2014.918099
 77. Chen HC, Joalland N, Bridgeman JS, Alchami FS, Jarry U, et al. (2017) Synergistic targeting of breast cancer stem-like cells by human $\gamma\delta$ T cells and CD8⁺ T cells. *Immunology and Cell Biology* 95: 620-629, doi: 10.1038/icb.2017.21
 78. Guo Y, Feng K, Wang Y, Han W (2018) Targeting cancer stem cells by using chimeric antigen receptor-modified T cells: a potential and curable approach for cancer treatment. *Protein & Cell* 9: 516-526, doi: 10.1007/s13238-017-0394-6
 79. Agliano A, Calvo A, Box C. (2017) The challenge of targeting cancer stem cells to halt metastasis. *Seminars in Cancer Biology* pp. 25-42, doi: 10.1016/j.semcancer.2017.03.003
 80. Bindea G, Mlecnik B, Tosolini M, Kirilovsky A, Waldner M, et al. (2013) Spatiotemporal Dynamics of Intratumoral Immune Cells Reveal the Immune Landscape in Human Cancer. *Immunity* 39: 782-795, doi: 10.1016/j.immuni.2013.10.003
 81. Fridman WH, Pagès F, Sautès-Fridman C, Galon J (2012) The immune contexture in human tumours: impact on clinical outcome. *Nature Reviews Cancer* 12: 298, doi: 10.1038/nrc3245
 82. Dillon LAL, Suresh R, Okrah K, Corrada Bravo H, Mosser DM, et al. (2015) Simultaneous transcriptional profiling of *Leishmania major* and its murine macrophage

-
- host cell reveals insights into host-pathogen interactions. *BMC Genomics* 16: 1108, doi: 10.1186/s12864-015-2237-2
83. Favila MA, Geraci NS, Zeng E, Harker B, Condon D, et al. (2014) Human Dendritic Cells exhibit a pronounced type I IFN signature following *Leishmania major* infection that is required for IL-12 induction. *Journal of Immunology (Baltimore, Md : 1950)* 192: 5863-5872, doi: 10.4049/jimmunol.1203230
 84. Kanehisa M, Goto S (2000) KEGG: kyoto encyclopedia of genes and genomes. *Nucleic Acids Research* 28: 27-30, doi: 10.1093/nar/28.1.27
 85. Croft D, O'Kelly G, Wu G, Haw R, Gillespie M, et al. (2011) Reactome: a database of reactions, pathways and biological processes. *Nucleic Acids Research* 39: D691-D697, doi: 10.1093/nar/gkq1018
 86. Chowdhury S, Sarkar RR (2015) Comparison of human cell signaling pathway databases—evolution, drawbacks and challenges. *Database*, doi: 10.1093/database/bau126
 87. Sherriff M, Sarkar RR (2008) Computational approaches and modelling of signaling processes in immune system. *Proceedings of Indian National Science Academy* 74(4):187-200
 88. Chowdhury S, Sinha N, Ganguli P, Bhowmick R, Singh V, Nandi S, Sarkar RR (2018) BIOPYDB: a dynamic human cell specific biochemical pathway database with advanced computational analyses platform. *Journal of Integrative Bioinformatics* 15, doi: 10.1515/jib-2017-0072
 89. Chowdhury S, Pradhan RN, Sarkar RR (2013) Structural and logical analysis of a comprehensive hedgehog signaling pathway to identify alternative drug targets for glioma, colon and pancreatic cancer. *PLoS ONE* 8: e69132, doi: 10.1371/journal.pone.0069132
 90. Chowdhury S, Sarkar R (2013) Drug targets and biomarker identification from computational study of human notch signaling pathway. *Journal of Clinical and Experimental Pharmacology* 3: 2161-1459.1000137, doi: 10.4172/2161-1459.1000137
 91. Saez-Rodriguez J, Simeoni L, Lindquist JA, Hemenway R, Bommhardt U, et al. (2007) A Logical Model Provides Insights into T Cell Receptor Signaling. *PLoS Computational Biology* 3: e163, doi: 10.1371/journal.pcbi.0030163
 92. Naldi A, Carneiro J, Chaouiya C, Thieffry D (2010) Diversity and Plasticity of Th Cell Types Predicted from Regulatory Network Modelling. *PLoS Computational Biology* 6: e1000912, doi: 10.1371/journal.pcbi.1000912
 93. Carbo A, Hontecillas R, Kronsteiner B, Viladomiu M, Pedragosa M, et al. (2013) Systems Modeling of Molecular Mechanisms Controlling Cytokine-driven CD4+ T Cell Differentiation and Phenotype Plasticity. *PLoS Computational Biology* 9: e1003027, doi: 10.1371/journal.pcbi.1003027

-
94. Beerenwinkel N, Schwarz RF, Gerstung M, Markowitz F (2015) Cancer evolution: mathematical models and computational inference. *Systematic Biology* 64: e1-25, doi: 10.1093/sysbio/syu081
 95. Banerjee S, Sarkar RR (2008) Delay-induced model for tumor-immune interaction and control of malignant tumor growth. *Biosystems* 91: 268-288, doi: 10.1016/j.biosystems.2007.10.002
 96. d'Onofrio A, Gatti F, Cerrai P, Freschi L (2010) Delay-induced oscillatory dynamics of tumour-immune system interaction. *Mathematical and Computer Modelling* 51: 572-591, doi: 10.1016/j.mcm.2009.11.005
 97. dePillis L, Caldwell T, Sarapata E, Williams H (2013) Mathematical modeling of regulatory T cell effects on renal cell carcinoma treatment. *Discrete and Continuous Dynamical Systems - Series B* 18: 915-943, doi: 10.3934/dcdsb.2013.18.915
 98. d'Onofrio A (2008) Metamodeling tumor-immune system interaction, tumor evasion and immunotherapy. *Mathematical and Computer Modelling* 47: 614-637, doi: 10.1016/j.mcm.2007.02.032
 99. Leder K, Pitter K, Laplant Q, Hambarzumyan D, Ross BD, et al. (2014) Mathematical modeling of PDGF-driven glioblastoma reveals optimized radiation dosing schedules. *Cell* 156: 603-616, doi: 10.1016/j.cell.2013.12.029
 100. Robertson-Tessi M, El-Kareh A, Goriely A (2012) A mathematical model of tumor-immune interactions. *Journal of Theoretical Biology* 294: 56-73, doi: 10.1016/j.jtbi.2011.10.027
 101. Powathil GG, Adamson DJ, Chaplain MA (2013) Towards predicting the response of a solid tumour to chemotherapy and radiotherapy treatments: clinical insights from a computational model. *PLoS Computational Biology* 9: e1003120, doi: 10.1371/journal.pcbi.1003120
 102. Kirschner D, Panetta JC (1998) Modeling immunotherapy of the tumor-immune interaction. *Journal of Mathematical Biology* 37: 235-252, doi: 10.1007/s002850050127
 103. de Pillis LG, Radunskaya AE, Wiseman CL (2005) A Validated Mathematical Model of Cell-Mediated Immune Response to Tumor Growth. *Cancer Research* 65: 7950, doi: 10.1158/0008-5472.CAN-05-0564
 104. Mol M, Patole MS, Singh S (2013) Signaling networks in *Leishmania* macrophages deciphered through integrated systems biology: a mathematical modeling approach. *Systems and synthetic biology* 7: 185-195, doi: 10.1007/s12015-013-0008-3
 105. Kaye P, Scott P (2011) Leishmaniasis: complexity at the host-pathogen interface. *Nature Reviews Microbiology* 9: 604-615, doi: 10.1038/nrmicro2608
 106. Liu D, Uzonna JE (2012) The early interaction of *Leishmania* with macrophages and dendritic cells and its influence on the host immune response. *Frontiers in Cellular and Infection Microbiology* 2: 83, doi: 10.3389/fcimb.2012.00083

-
107. Tomasetti C, Levy D (2010) Role of symmetric and asymmetric division of stem cells in developing drug resistance. *Proceedings of the National Academy of Sciences USA* 107: 16766-16771, doi: 10.1073/pnas.1007726107
 108. Fidler IJ (2003) The pathogenesis of cancer metastasis: the 'seed and soil' hypothesis revisited. *Nature Reviews Cancer* 3: 453-458, doi: 10.1038/nrc1098
 109. Nishimura D (2001) BioCarta. *Biotech Software & Internet Report* 2(3): 117-120, doi: 10.1089/152791601750294344
 110. Kandasamy K, Mohan SS, Raju R, Keerthikumar S, Kumar GS, et al. (2010) NetPath: a public resource of curated signal transduction pathways. *Genome biology* 11: R3, doi: 10.1186/gb-2010-11-1-r3
 111. Chatr-aryamontri A, Breitkreutz B-J, Heinicke S, Boucher L, Winter A, et al. (2013) The BioGRID interaction database: 2013 update. *Nucleic Acids Research* 41: D816-D823, doi: 10.1093/nar/gks1158
 112. Prasad TK, Goel R, Kandasamy K, Keerthikumar S, Kumar S, et al. (2009) Human protein reference database—2009 update. *Nucleic Acids Research* 37: D767-D772, doi: 10.1093/nar/gkn892
 113. Funahashi A, Morohashi M, Kitano H, Tanimura N (2003) CellDesigner: a process diagram editor for gene-regulatory and biochemical networks. *Biosilico* 1: 159-162, doi: 10.1016/S1478-5382(03)02370-9
 114. Favila MA, Geraci NS, Zeng E, Harker B, Condon D, et al. (2014) Human dendritic cells exhibit a pronounced type I IFN signature following *Leishmania major* infection that is required for IL-12 induction. *The Journal of Immunology* 192(12): 5863-5872, doi: 10.4049/jimmunol.1203230
 115. Smoot ME, Ono K, Ruscheinski J, Wang P-L, Ideker T (2011) Cytoscape 2.8: new features for data integration and network visualization. *Bioinformatics* 27: 431-432, doi: 10.1093/bioinformatics/btq675
 116. Zhao S, Fung-Leung WP, Bittner A, Ngo K, Liu X (2014) Comparison of RNA-Seq and microarray in transcriptome profiling of activated T cells. *PLoS ONE* 9: e78644, doi: 10.1371/journal.pone.0078644
 117. Tabas-Madrid D, Nogales-Cadenas R, Pascual-Montano A (2012) GeneCodis3: a non-redundant and modular enrichment analysis tool for functional genomics. *Nucleic Acids Research* 40: W478-W483, doi: 10.1093/nar/gks402
 118. Halle M, Gomez MA, Stuible M, Shimizu H, McMaster WR, et al. (2009) The *Leishmania* surface protease GP63 cleaves multiple intracellular proteins and actively participates in p38 mitogen-activated protein kinase inactivation. *Journal of Biological Chemistry* 284: 6893-6908, doi: 10.1074/jbc.M805861200
 119. Bhardwaj S, Srivastava N, Sudan R, Saha B (2010) *Leishmania* interferes with host cell signaling to devise a survival strategy. *Journal of Biomedicine and Biotechnology* 2010: 109189, doi: 10.1155/2010/109189

-
120. Nandan D, Yi T, Lopez M, Lai C, Reiner NE (2002) *Leishmania* EF-1alpha activates the Src homology 2 domain containing tyrosine phosphatase SHP-1 leading to macrophage deactivation. *Journal of Biological Chemistry* 277(51): 50190-50197, doi: 10.1074/jbc.M209210200
 121. Majumder S, Dey R, Bhattacharjee S, Rub A, Gupta G, et al. (2012) *Leishmania*-induced biphasic ceramide generation in macrophages is crucial for uptake and survival of the parasite. *Journal of Infectious Diseases* 205: 1607-1616, doi: 10.1093/infdis/jis229
 122. Ganguli P, Chowdhury S, Bhowmick R, Sarkar RR (2015) Temporal Protein Expression Pattern in Intracellular Signaling Cascade during T cell Activation: A Computational Study. *Journal of Biosciences* 40: 769-789, doi: 10.1007/s12038-015-9561-1
 123. Russell DG, Wright S (1988) Complement receptor type 3 (CR3) binds to an Arg-Gly-Asp-containing region of the major surface glycoprotein, gp63, of *Leishmania* promastigotes. *The Journal of Experimental Medicine* 168: 279-292, doi: 10.1084/jem.168.1.279
 124. Talamás-Rohana P, Wright SD, Lennartz MR, Russell DG (1990) Lipophosphoglycan from *Leishmania mexicana* promastigotes binds to members of the CR3, p150, 95 and LFA-1 family of leukocyte integrins. *The Journal of Immunology* 144: 4817-4824, PMID: 1972169
 125. Saraiva M, O'Garra A (2010) The regulation of IL-10 production by immune cells. *Nature Review Immunology* 10: 170-181, doi: 10.1038/nri2711
 126. Cunningham AC (2002) Parasitic Adaptive Mechanisms in Infection by *Leishmania*. *Experimental and Molecular Pathology* 72: 132-141, doi: 10.1006/exmp.2002.2418
 127. Turco SJ (1999) Adversarial relationship between the *Leishmania* lipophosphoglycan and protein kinase C of host macrophages. *Parasite Immunology* 21: 597-600, doi: 10.1046/j.1365-3024.1999.00266.x
 128. Contreras I, Gomez MA, Nguyen O, Shio MT, McMaster RW, et al. (2010) *Leishmania*-induced inactivation of the macrophage transcription factor AP-1 is mediated by the parasite metalloprotease GP63. *PLoS Pathogens* 6: e1001148, doi: 10.1371/journal.ppat.1001148
 129. Corradin S (1999) MARCKS-related Protein (MRP) Is a Substrate for the *Leishmania* major Surface Protease Leishmanolysin (gp63). *Journal of Biological Chemistry* 274: 25411-25418, doi: 10.1074/jbc.274.36.25411
 130. Chawla M, Vishwakarma RA (2003) Alkylacylglycerolipid domain of GPI molecules of *Leishmania* is responsible for inhibition of PKC-mediated c-fos expression. *Journal of Lipid Research* 44: 594-600, doi: 10.1194/jlr.M200296-JLR200
 131. Jaramillo M, Gomez MA, Larsson O, Shio MT, Topisirovic I, et al. (2011) *Leishmania* repression of host translation through mTOR cleavage is required for parasite survival and infection. *Cell Host Microbe* 9: 331-341, doi: 10.1016/j.chom.2011.03.008

-
132. Gomez MA, Contreras I, Halle M, Tremblay ML, McMaster RW, et al. (2009) *Leishmania* GP63 alters host signaling through cleavage-activated protein tyrosine phosphatases. *Science Signaling* 2: ra58, doi: 10.1126/scisignal.2000213
 133. Mookerjee Basu J, Mookerjee A, Sen P, Bhaumik S, Sen P, et al. (2006) Sodium antimony gluconate induces generation of reactive oxygen species and nitric oxide via phosphoinositide 3-kinase and mitogen-activated protein kinase activation in *Leishmania donovani*-infected macrophages. *Antimicrobial Agents and Chemotherapy* 50: 1788-1797, doi: 10.1128/AAC.50.5.1788-1797.2006
 134. Blanchette J, Abu-Dayyeh I, Hassani K, Whitcombe L, Olivier M (2009) Regulation of macrophage nitric oxide production by the protein tyrosine phosphatase Src homology 2 domain phosphotyrosine phosphatase 1 (SHP-1). *Immunology* 127: 123-133, doi: 10.1111/j.1365-2567.2008.02929.x
 135. Forget G, Gregory DJ, Whitcombe LA, Olivier M (2006) Role of host protein tyrosine phosphatase SHP-1 in *Leishmania donovani*-induced inhibition of nitric oxide production. *Infection and Immunity* 74: 6272-6279, doi: 10.1128/IAI.00853-05
 136. Zhu W, Mustelin T, David M (2002) Arginine methylation of STAT1 regulates its dephosphorylation by T cell protein tyrosine phosphatase. *Journal of Biological Chemistry* 277: 35787-35790, doi: 10.1074/jbc.C200346200
 137. Xu H, An H, Hou J, Han C, Wang P, et al. (2008) Phosphatase PTP1B negatively regulates MyD88- and TRIF-dependent proinflammatory cytokine and type I interferon production in TLR-triggered macrophages. *Molecular Immunology* 45: 3545-3552, doi: 10.1016/j.molimm.2008.05.006
 138. Awasthi A, Mathur RK, Saha B (2004) Immune response to *Leishmania* infection. *Indian Journal of Medical Research* 119: 238-258, PMID: 15243162
 139. Moll H, Röllinghoff M (1991) T-cell reactivity to purified lipophosphoglycan from *Leishmania major*: A model for analysis of the cellular immune response to microbial carbohydrates. *Behring Inst Mitt* 88: 161-169, PMID: 2049034
 140. Brownlie RJ, Zamoyska R (2013) T cell receptor signalling networks: branched, diversified and bounded. *Nature Reviews Immunology* 13: 257-269, doi: 10.1038/nri3403
 141. Yamagishi M, Watanabe T (2012) New Paradigm of T cell Signaling: Learning from Malignancies. *Journal of Clinical and Cellular Immunology* S12: 2, doi: 10.4172/2155-9899.S12-007
 142. Chen L, Flies DB (2013) Molecular mechanisms of T cell co-stimulation and co-inhibition. *Nature Reviews Immunology* 13: 227-242, doi: 10.1038/nri3405
 143. Fathman CG, Lineberry NB (2007) Molecular mechanisms of CD4+ T-cell anergy. *Nature Review Immunology* 7: 599-609, doi: 10.1038/nri2131

-
144. Akdis M, Burgler S, Cramer R, Eiwegger T, Fujita H, et al. (2011) Interleukins, from 1 to 37, and interferon-gamma: receptors, functions, and roles in diseases. *The Journal of Allergy and Clinical Immunology* 127: 701-721 e701-770, doi: 10.1016/j.jaci.2010.11.050
 145. Bak RO, Mikkelsen JG (2010) Review Regulation of cytokines by small RNAs during skin inflammation. *Journal of Biomedical Science* 17(1):53 doi: 10.1186/1423-0127-17-53
 146. Feske S (2013) Ca(2+) influx in T cells: how many ca(2+) channels? *Frontiers in Immunology* 4: 99, doi: 10.3389/fimmu.2013.00099
 147. Qu B, Al-Ansary D, Kummerow C, Hoth M, Schwarz EC (2011) ORAI-mediated calcium influx in T cell proliferation, apoptosis and tolerance. *Cell Calcium* 50: 261-269, doi: 10.1016/j.ceca.2011.05.015
 148. Srivastava N, Sudan R, Saha B (2011) CD40-modulated dual-specificity phosphatases MAPK phosphatase (MKP)-1 and MKP-3 reciprocally regulate *Leishmania major* infection. *Journal of Immunology* 186: 5863-5872, doi: 10.4049/jimmunol.1003957
 149. Rub A, Dey R, Jadhav M, Kamat R, Chakkaramakkil S, et al. (2009) Cholesterol depletion associated with *Leishmania major* infection alters macrophage CD40 signalosome composition and effector function. *Nature Immunology* 10: 273-280, doi: 10.1038/ni.1705
 150. Kemp K (2000) Cytokine-producing T cell subsets in human leishmaniasis. *Archivum Immunologiae et Therapiae Experimentalis-English Edition-* 48(3): 173-176, PMID: 10912621
 151. Kauffman SA (1969) Metabolic stability and epigenesis in randomly constructed genetic nets. *Journal of Theoretical Biology* 22: 437-467, doi: 10.1016/0022-5193(69)90015-0
 152. Huang S, Ingber DE (2000) Shape-dependent control of cell growth, differentiation, and apoptosis: switching between attractors in cell regulatory networks. *Experimental Cell Research* 261: 91-103, doi: 10.1006/excr.2000.5044
 153. Müssel C, Hopfensitz M, Kestler HA (2010) BoolNet—an R package for generation, reconstruction and analysis of Boolean networks. *Bioinformatics* 26: 1378-1380, doi: 10.1093/bioinformatics/btq124
 154. Albert I, Thakar J, Li S, Zhang R, Albert R (2008) Boolean network simulations for life scientists. *Source code for biology and medicine* 3: 16, doi: 10.1186/1751-0473-3-16
 155. Klamt S, Saez-Rodriguez J, Gilles ED (2007) Structural and functional analysis of cellular networks with CellNetAnalyzer. *BMC systems biology* 1: 2, doi: 10.1186/1752-0509-1-2
 156. Bhowmick R, Ganguli P, Sarkar RR (2020) Chapter 6- T-Cell Activation and Differentiation: Role of Signaling and Metabolic Cross-Talk. In *Systems and Synthetic Immunology*, Ed. Shailza Singh: Springer, Singapore. pp. 153-182, doi: 10.1007/978-981-15-3350-1_6
 157. Albert I, Thakar J, Li S, Zhang R, Albert R (2008) Boolean network simulations for life scientists. *Source code for biology and medicine* 3: 16, doi: 10.1186/1751-0473-3-16

-
158. Wells AD, Morawski PA (2014) New roles for cyclin-dependent kinases in T cell biology: linking cell division and differentiation. *Nature Review Immunology* 14: 261-270, doi: 10.1038/nri3625
 159. Berridge Michael J (2012) *Cell Signalling Biology: Module 9 - Cell Cycle and Proliferation*. *Biochemical Journal* 9, 1-39.
 160. Rogers PR, Song J, Gramaglia I, Killeen N, Croft M (2001) OX40 promotes Bcl-xL and Bcl-2 expression and is essential for long-term survival of CD4 T cells. *Immunity* 15: 445-455, doi: 10.1016/s1074-7613(01)00191-1
 161. Cantrell D, Collins M, Crumpton M (1988) Autocrine regulation of T-lymphocyte proliferation: differential induction of IL-2 and IL-2 receptor. *Immunology* 65(3):343-9, PMID: 3264805
 162. Kupper T, Horowitz M, Lee F, Robb R, Flood PM (1987) Autocrine growth of T cells independent of interleukin 2: identification of interleukin 4 (IL 4, BSF-1) as an autocrine growth factor for a cloned antigen-specific helper T cell. *The Journal of Immunology* 138: 4280-4287, PMID: 2953803
 163. Van Epps HL (2006) IL-6 drives T cell proliferation. *The Journal of Experimental Medicine* 203: 1387b-1387b, doi: 10.1084/jem.2036iti3
 164. Suzuki I, Martin S, Boursalian TE, Beers C, Fink PJ (2000) Fas ligand costimulates the in vivo proliferation of CD8+ T cells. *The Journal of Immunology* 165: 5537-5543, doi: 10.4049/jimmunol.165.10.5537
 165. Shi M, Ye Z, Umeshappa KS, Moyana T, Xiang J (2007) Alpha tumor necrosis factor contributes to CD8(+) T cell survival in the transition phase. *Biochemical and Biophysical Research Communications* 360: 702-707, doi: 10.1016/j.bbrc.2007.06.126
 166. Akdis CA, Joss A, Akdis M, Faith A, Blaser K (2000) A molecular basis for T cell suppression by IL-10: CD28-associated IL-10 receptor inhibits CD28 tyrosine phosphorylation and phosphatidylinositol 3-kinase binding. *The FASEB Journal* 14: 1666-1668, doi: 10.1096/fj.99-0874fje
 167. Romagnani S (1992) Type 1 T helper and type 2 T helper cells: functions, regulation and role in protection and disease. *International Journal of Clinical and Laboratory Research* 21: 152-158, doi: 10.1007/BF02591635
 168. Schwab JD, Kühlwein SD, Ikonomi N, Kühl M, Kestler HA (2020) Concepts in Boolean network modeling: What do they all mean? *Computational and Structural Biotechnology Journal* 18: 571-582, doi: 10.1016/j.csbj.2020.03.001
 169. Ramachandran A, Black MA, Shelling AN, Love DR (2008) Microarrays--analysis of signaling pathways. *Methods in Molecular Medicine* 141: 115-130, PMID: 18453087
 170. Parkinson H, Sarkans U, Shojatalab M, Abeygunawardena N, Contrino S, et al. (2005) ArrayExpress--a public repository for microarray gene expression data at the EBI. *Nucleic Acids Research* 33: D553-555, doi: 10.1093/nar/gki056

-
171. Yeh JH, Sidhu SS, Chan AC (2008) Regulation of a late phase of T cell polarity and effector functions by Crtam. *Cell* 132: 846-859, doi: 10.1016/j.cell.2008.01.013
 172. Müssel C, Hopfensitz M, Zhou D, Kestler H, Kestler MH (2010) BoolNet--an R package for generation, reconstruction and analysis of Boolean networks. *Bioinformatics* 26(10):1378-80. doi: 10.1093/bioinformatics/btq124
 173. McKnight PE, Najab J (2010) Mann-Whitney U Test. *Corsini Encyclopedia of Psychology*, 1-1.
 174. Maxwell MJ, Chan SK, Robinson DP, Dwyer DM, Nandan D, et al. (2008) Proteomic analysis of the secretome of *Leishmania donovani*. *Genome Biology* 9(2), 1-21, doi: 10.1186/gb-2008-9-2-r35
 175. von Mering C, Jensen LJ, Kuhn M, Chaffron S, Doerks T, et al. (2007) STRING 7 - Recent developments in the integration and prediction of protein interactions. *Nucleic Acids Research* 35, no. suppl_1 (2007): D358-D362, doi: 10.1093/nar/gkl825
 176. Ammari MG, Gresham CR, McCarthy FM, Nanduri B (2016) HPIDB 2.0: a curated database for host-pathogen interactions. *Database* (2016), doi: 10.1093/database/baw103
 177. Garcia-Garcia J, Schleker S, Klein-Seetharaman J, Oliva B (2012) BIPS: BIANA Interolog Prediction Server. A tool for protein-protein interaction inference. *Nucleic Acids Research* 40(W1), W147-W151, doi: 10.1093/nar/gks553
 178. Kshirsagar M, Carbonell J, Klein-Seetharaman J. (2013) Multitask learning for host-pathogen protein interactions. *Bioinformatics* 29(13), i217-i226, doi: 10.1093/bioinformatics/btt245
 179. Huo T, Liu W, Guo Y, Yang C, Lin J, et al. (2015) Prediction of host - pathogen protein interactions between *Mycobacterium tuberculosis* and *Homo sapiens* using sequence motifs. *BMC Bioinformatics* 16(1), 1-9, doi: 10.1186/s12859-015-0535-y
 180. Stein A, Céol A, Aloy P (2011) 3did: Identification and classification of domain-based interactions of known three-dimensional structure. *Nucleic Acids Research* 39, no. suppl_1 (2011): D718-D723, doi: 10.1093/nar/gkq962
 181. Blohm P, Frishman G, Smialowski P, Goebels F, Wachinger B, et al. (2014) Negatome 2.0: A database of non-interacting proteins derived by literature mining, manual annotation and protein structure analysis. *Nucleic Acids Research* 42(D1), D396-D400, doi: 10.1093/nar/gkt1079
 182. Gioutlakis A, Klapa MI, Moschonas NK (2017) PICKLE 2.0: A human protein-protein interaction meta-database employing data integration via genetic information ontology. *PLoS ONE* 12(10), e0186039, doi: 10.1371/journal.pone.0186039
 183. Szklarczyk D, Gable AL, Lyon D, Junge A, Wyder S, et al. (2019) STRING v11: Protein-protein association networks with increased coverage, supporting functional discovery in genome-wide experimental datasets. *Nucleic Acids Research* 47(D1), D607-D613, doi: 10.1093/nar/gky1131

-
184. von Mering C, Jensen LJ, Snel B, Hooper SD, Krupp M, et al. (2005) STRING: Known and predicted protein-protein associations, integrated and transferred across organisms. *Nucleic Acids Research* 33, no. suppl_1 (2005): D433-D437, doi: 10.1093/nar/gki005
 185. Huang DW, Sherman BT, Lempicki RA, Huang Dw SBTLRA (2009) DAVID Functional Annotation Bioinformatics Microarray Analysis. *Nature Protocols* 4(1):44-57 doi: 10.1038/nprot.2008.211
 186. Shannon P, Markiel A, Ozier O, Baliga NS, Wang JT, et al. (2003) Cytoscape: A software Environment for integrated models of biomolecular interaction networks. *Genome Research* 13(11), 2498-2504, doi: 10.1101/gr.1239303
 187. Csardi G, Nepusz T (2006) The igraph software package for complex network research. *International Journal of Complex Systems* 1695(5), 1-9
 188. Doncheva NT, Assenov Y, Domingues FS, Albrecht M (2012) Topological analysis and interactive visualization of biological networks and protein structures. *Nature Protocols* 7(4), 670, doi: 10.1038/nprot.2012.004
 189. Bastian M, Heymann S, Jacomy M (2009) Gephi: An Open Source Software for Exploring and Manipulating Networks. *Third International AAAI Conference on Weblogs and Social Media Vol. 3. No. 1. 2009*, doi: 10.1136/qshc.2004.010033
 190. Singh AK, Pandey RK, Siqueira-Neto JL, Kwon YJ, Freitas-Junior LH, et al. (2015) Proteomic-based approach to gain insight into reprogramming of THP-1 cells exposed to *Leishmania donovani* over an early temporal window. *Infection and Immunity* 83(5), 1853-1868, doi: 10.1128/IAI.02833-14
 191. Chakraborty A, Kurati SP, Mahata SK, Sundar S, Roy S, et al. (2017) Wnt5a Signaling Promotes Host Defense against *Leishmania donovani* Infection. *The Journal of Immunology* 199(3), 992-1002, doi: 10.4049/jimmunol.1601927
 192. Osorio EY, Zhao W, Espitia C, Saldarriaga O, Hawel L, et al. (2012) Progressive visceral leishmaniasis is driven by dominant parasite-induced STAT6 activation and STAT6-dependent host arginase 1 expression. *PLoS Pathogens* 8(1): e1002417, doi: 10.1371/journal.ppat.1002417
 193. Das P, De T, Chakraborti T (2014) *Leishmania donovani* secretory serine protease alters macrophage inflammatory response via COX-2 mediated PGE-2 production. *Indian Journal of Biochemistry & Biophysics* 51(6):542-51, PMID: 25823228
 194. Kar S, Ukil A, Sharma G, Das PK (2010) MAPK-directed phosphatases preferentially regulate pro- and anti-inflammatory cytokines in experimental visceral leishmaniasis: involvement of distinct protein kinase C isoforms. *Journal of Leukocyte Biology* 88(1): 9-20, doi: 10.1189/jlb.0909644
 195. Paul J, Naskar K, Chowdhury S, Chakraborti T, De T (2014) TLR mediated GSK3 β activation suppresses CREB mediated IL-10 production to induce a protective immune response against murine visceral leishmaniasis. *Biochimie* 107 (2014): 235-246, doi: 10.1016/j.biochi.2014.09.004

-
196. Rostan O, Gangneux JP, Piquet-Pellorce C, Manuel C, McKenzie ANJ, et al. (2013) The IL-33/ST2 axis is associated with human visceral leishmaniasis and suppresses Th1 responses in the livers of BALB/c mice infected with *Leishmania donovani*. *MBio* 4(5), doi: 10.1128/mBio.00383-13
 197. Kumar P, Sundar S, Singh N (2007) Degradation of pteridine reductase 1 (PTR1) enzyme during growth phase in the protozoan parasite *Leishmania donovani*. *Experimental Parasitology*, 116.2 (2007): 182-189. doi: 10.1016/j.exppara.2006.12.008
 198. Scardoni G, Tosadori G, Pratap S, Spoto F, Laudanna C (2015) Finding the shortest path with PesCa: a tool for network reconstruction. *F1000Research* 4(2015), doi: 10.12688/f1000research.6769.1
 199. Pavlopoulos GA, Secrier M, Moschopoulos CN, Soldatos TG, Kossida S, et al. (2011) Using graph theory to analyze biological networks. *BioData mining* 4(1): 1-27 doi: 10.1186/1756-0381-4-10
 200. Warnes GR, Bolker B, Bonebakker L, Gentleman R, Liaw WHA, et al. (2016) Package "gplots": Various R programming tools for plotting data. R package (2016).
 201. Demicheli R, Pratesi G, Foroni R (1991) The exponential-Gompertzian tumor growth model: data from six tumor cell lines in vitro and in vivo. Estimate of the transition point from exponential to Gompertzian growth and potential clinical implications. *Tumori* 77: 189-195, PMID: 1862544
 202. Zhang M, He Y, Sun X, Li Q, Wang W, et al. (2014) A high M1/M2 ratio of tumor-associated macrophages is associated with extended survival in ovarian cancer patients. *Journal of Ovarian Research* 7: 19-19, doi: 10.1186/1757-2215-7-19
 203. Mills CD, Ley K (2014) M1 and M2 Macrophages: The Chicken and the Egg of Immunity. *Journal of Innate Immunity* 6: 716-726, doi: 10.1159/000364945
 204. Sun W, Wei F-Q, Li W-J, Wei J-W, Zhong H, et al. (2017) A positive-feedback loop between tumour infiltrating activated Treg cells and type 2-skewed macrophages is essential for progression of laryngeal squamous cell carcinoma. *British Journal of Cancer* 117: 1631, doi: 10.1038/bjc.2017.329
 205. Kwiatkowska-Borowczyk EP, Gąbka-Buszek A, Jankowski J, Mackiewicz A (2015) Immunotargeting of cancer stem cells. *Contemporary Oncology* 19: A52-A59, doi: 10.5114/wo.2014.47129
 206. Beavis PA, Petley EV, Darcy PK (2017) A novel combination strategy for effectively targeting cancer stem-like cells. *Immunology and Cell Biology* 95: 573, doi: 10.1038/icb.2017.39
 207. Chen M-L, Pittet MJ, Gorelik L, Flavell RA, Weissleder R, et al. (2005) Regulatory T cells suppress tumor-specific CD8 T cell cytotoxicity through TGF- β signals in vivo. *Proceedings of the National Academy of Sciences USA* 102: 419, doi: 10.1073/pnas.0408197102

-
208. Huang H, Hao S, Li F, Ye Z, Yang J, et al. (2007) CD4(+) Th1 cells promote CD8(+) Tc1 cell survival, memory response, tumor localization and therapy by targeted delivery of interleukin 2 via acquired pMHC I complexes. *Immunology* 120: 148-159, doi: 10.1111/j.1365-2567.2006.02452.x
 209. dePillis, L., Caldwell, T., Sarapata, E., & Williams, H. (2013). Mathematical modeling of regulatory T cell effects on renal cell carcinoma treatment. *Discrete & Continuous Dynamical Systems-B*, 18(4): 915, doi: 10.3934/dcdsb.2013.18.915
 210. Powathil G, Kohandel M, Milosevic M, Sivaloganathan S (2012) Modeling the spatial distribution of chronic tumor hypoxia: implications for experimental and clinical studies. *Computational and Mathematical Methods in Medicine* 2012: 410602, doi: 10.1155/2012/410602
 211. Rich JN, Bao S (2007) Chemotherapy and cancer stem cells. *Cell Stem Cell* 1: 353-355, doi: 10.1016/j.stem.2007.09.011
 212. Abdullah LN, Chow EK (2013) Mechanisms of chemoresistance in cancer stem cells. *Clinical and Translational Medicine* 2: 3, doi: 10.1186/2001-1326-2-3
 213. Birkhoff G, Rota G (1978) *Ordinary differential equations*, John Wiley & Sons. ISBN: 978-0-471-86003-7
 214. Marino S, Hogue IB, Ray CJ, Kirschner DE (2008) A methodology for performing global uncertainty and sensitivity analysis in systems biology. *Journal of Theoretical Biology* 254: 178-196, doi: 10.1016/j.jtbi.2008.04.011
 215. Haario H, Laine M, Mira A, Saksman E (2006) DRAM: efficient adaptive MCMC. *Statistics and Computing* 16: 339-354, doi: 10.1007/s11222-006-9438-0
 216. Ning X, Sun S, Hong L, Liang J, Liu L, et al. (2007) Calcyclin-binding protein inhibits proliferation, tumorigenicity, and invasion of gastric cancer. *Molecular Cancer Research* 5: 1254-1262, doi: 10.1158/1541-7786.MCR-06-0426
 217. Chen S-Y, Hu S-S, Dong Q, Cai J-X, Zhang W-P, et al. (2013) Establishment of Paclitaxel-resistant Breast Cancer Cell Line and Nude Mice Models, and Underlying Multidrug Resistance Mechanisms in Vitro and in Vivo. *Asian Pacific Journal of Cancer Prevention* 14: 6135-6140, doi: 10.7314/apjcp.2013.14.10.6135
 218. Ling X, Wen L, Zhou Y (2012) Role of mitochondrial translocation of telomerase in hepatocellular carcinoma cells with multidrug resistance. *International Journal of Medical Sciences* 9: 545-554, doi: 10.7150/ijms.4648
 219. Liu Z, Qiu M, Tang QL, Liu M, Lang N, et al. (2010) Establishment and biological characteristics of oxaliplatin-resistant human colon cancer cell lines. *Chinese Journal of Cancer* 29: 661-667, doi: 10.5732/cjc.009.10666
 220. Markowska J, Lacki J, Jaroszewski J, Wiktorowicz K (1995) The usefulness of CD4/CD8 ratio evaluation in monitoring of ovarian cancer patients. *European Journal of Gynaecological Oncology* 16: 54-58, PMID: 7744118

-
221. Biller BJ, Guth A, Burton JH, Dow SW (2010) Decreased Ratio of CD8+ T Cells to Regulatory T Cells Associated with Decreased Survival in Dogs with Osteosarcoma. *Journal of veterinary internal medicine* 24: 1118-1123, doi: 10.1111/j.1939-1676.2010.0557.x
 222. Liu K, Yang K, Wu B, Chen H, Chen X, et al. (2015) Tumor-Infiltrating Immune Cells Are Associated With Prognosis of Gastric Cancer. *Medicine* 94: e1631, doi: 10.1097/MD.0000000000001631
 223. Balachandran VP, Cavnar MJ, Zeng S, Bamboat ZM, Ocuin LM, et al. (2011) Imatinib potentiates antitumor T cell responses in gastrointestinal stromal tumor through the inhibition of Ido. *Nature Medicine* 17: 1094-1100, doi: 10.1038/nm.2438
 224. Ubukata H, Motohashi G, Tabuchi T, Nagata H, Konishi S, et al. (2010) Evaluations of interferon-gamma/interleukin-4 ratio and neutrophil/lymphocyte ratio as prognostic indicators in gastric cancer patients. *Journal of Surgical Oncology* 102: 742-747, doi: 10.1002/jso.21725
 225. Hong CC, Yao S, McCann SE, Dolnick RY, Wallace PK, et al. (2013) Pretreatment levels of circulating Th1 and Th2 cytokines, and their ratios, are associated with ER-negative and triple negative breast cancers. *Breast Cancer Research and Treatment* 139: 477-488, doi: 10.1007/s10549-013-2549-3
 226. Szaflarska A, Szczepanik A, Siedlar M, Czupryna A, Sierzega M, et al. (2009) Preoperative plasma level of IL-10 but not of proinflammatory cytokines is an independent prognostic factor in patients with gastric cancer. *Anticancer Research* 29: 5005-5012, PMID: 20044609
 227. Gupta M, Han JJ, Stenson M, Maurer M, Wellik L, et al. (2012) Elevated serum IL-10 levels in diffuse large B-cell lymphoma: a mechanism of aberrant JAK2 activation. *Blood* 119: 2844-2853, doi: 10.1182/blood-2011-10-388538
 228. Mukhopadhyay H, Cordoba S-P, Maini PK, van der Merwe PA, Dushek O (2013) Systems model of T cell receptor proximal signaling reveals emergent ultrasensitivity. *PLoS Computational Biology* 9: e1003004, doi: 10.1371/journal.pcbi.1003004
 229. Saez-Rodriguez J, Simeoni L, Lindquist JA, Hemenway R, Bommhardt U, et al. (2007) A logical model provides insights into T cell receptor signaling. *PLoS Comput Biol* 3: e163, doi: 10.1371/journal.pcbi.0030163
 230. Wittmann DM, Krumsiek J, Saez-Rodriguez J, Lauffenburger DA, Klamt S, et al. (2009) Transforming Boolean models to continuous models: methodology and application to T-cell receptor signaling. *BMC systems biology* 3: 1-21, doi: 10.1186/1752-0509-3-98
 231. Saadatpour A, Wang R-S, Liao A, Liu X, Loughran TP, et al. (2011) Dynamical and structural analysis of a T cell survival network identifies novel candidate therapeutic targets for large granular lymphocyte leukemia. *PLoS Computational Biology* 7: e1002267, doi: 10.1371/journal.pcbi.1002267

-
232. Fukushima A (2003) Ag-Specific Recognition, Activation, and Effector Function of T Cells in the Conjunctiva with Experimental Immune-Mediated Blepharconjunctivitis. *Investigative Ophthalmology & Visual Science* 44: 4366-4374, doi: 10.1167/iovs.02-1323
 233. Welte T (1999) STAT5 Interaction with the T Cell Receptor Complex and Stimulation of T Cell Proliferation. *Science* 283: 222-225, doi: 10.1126/science.283.5399.222
 234. Parry RV, Chemnitz JM, Frauwirth KA, Lanfranco AR, Braunstein I, et al. (2005) CTLA-4 and PD-1 receptors inhibit T-cell activation by distinct mechanisms. *Molecular & Cellular Biology* 25: 9543-9553, doi: 10.1128/MCB.25.21.9543-9553.2005
 235. Delisle JS, Giroux M, Boucher G, Landry JR, Hardy MP, et al. (2013) The TGF-beta-Smad3 pathway inhibits CD28-dependent cell growth and proliferation of CD4 T cells. *Genes & Immunity* 14: 115-126, doi: 10.1038/gene.2012.63
 236. Youn H-D, Liu JO (2000) Cabin1 represses MEF2-dependent Nur77 expression and T cell apoptosis by controlling association of histone deacetylases and acetylases with MEF2. *Immunity* 13: 85-94, doi: 10.1016/s1074-7613(00)00010-8
 237. Shi Y, Liu CH, Roberts AI, Das J, Xu G, et al. (2006) Granulocyte-macrophage colony-stimulating factor (GM-CSF) and T-cell responses: what we do and don't know. *Cell Res* 16: 126-133, doi: 10.1038/sj.cr.7310017
 238. Green AM, Difazio R, Flynn JL (2013) IFN-gamma from CD4 T cells is essential for host survival and enhances CD8 T cell function during Mycobacterium tuberculosis infection. *Journal of Immunology* 190: 270-277, doi: 10.4049/jimmunol.1200061
 239. Barbi J, Snider HM, Bhardwaj N, Lezama-Davila CM, Durbin JE, et al. (2009) Signal transducer and activator of transcription 1 in T cells plays an indispensable role in immunity to *Leishmania major* by mediating Th1 cell homing to the site of infection. *FASEB Journal* 23: 3990-3999, doi: 10.1096/fj.09-138057
 240. Mor F, Quintana FJ, Cohen IR (2004) Angiogenesis-Inflammation Cross-Talk: Vascular Endothelial Growth Factor Is Secreted by Activated T Cells and Induces Th1 Polarization. *The Journal of Immunology* 172: 4618-4623, doi: 10.4049/jimmunol.172.7.4618
 241. Ohm JE, Gabrilovich DI, Sempowski GD, Kisseleva E, Parman KS, et al. (2003) VEGF inhibits T-cell development and may contribute to tumor-induced immune suppression. *Blood* 101: 4878-4886, doi: 10.1182/blood-2002-07-1956
 242. Blotnick S, Peoples GE, Freeman MR, Eberlein TJ, Klagsbrun M (1994) T lymphocytes synthesize and export heparin-binding epidermal growth factor-like growth factor and basic fibroblast growth factor, mitogens for vascular cells and fibroblasts: differential production and release by CD4+ and CD8+ T cells. *Proceedings of the National Academy of Sciences* 91: 2890-2894, doi: 10.1073/pnas.91.8.2890
 243. Daynes RA, Dowell T, Araneo BA (1991) Platelet-derived growth factor is a potent biologic response modifier of T cells. *The Journal of Experimental Medicine* 174: 1323-1333, doi: 10.1084/jem.174.6.1323

-
244. Sommers CL, Park CS, Lee J, Feng C, Fuller CL, et al. (2002) A LAT mutation that inhibits T cell development yet induces lymphoproliferation. *Science* 296: 2040-2043, doi: 10.1126/science.1069066
 245. Barabasi AL, Oltvai ZN (2004) Network biology: understanding the cell's functional organization. *Nature Review Genetics* 5: 101-113, doi: 10.1038/nrg1272
 246. Loeb LA, Loeb KR, Anderson JP (2003) Multiple mutations and cancer. *Proceedings of the National Academy of Sciences USA* 100: 776-781, doi: 10.1073/pnas.0334858100
 247. Buckley RH (2004) Molecular defects in human severe combined immunodeficiency and approaches to immune reconstitution. *Annual Review of Immunology* 22: 625-655, doi: 10.1146/annurev.immunol.22.012703.104614
 248. Street MGA (1995) Investigation of the deregulation of interleukin-6 in two non-Hodgkin's lymphoma cell lines. ProQuest Dissertations Publishing, 1995. 9617063
 249. Hirooka Y, Kayama M, Ohga S, Kimura M, Hasegawa M, et al. (1993) Deregulated production of interleukin-4 (IL4) in autoimmune thyroid disease assayed with a new radioimmunoassay. *Clinica Chimica Acta* 216(1-2):1-10, doi: 10.1016/0009-8981(93)90134-p
 250. Hirano T, Kishimoto T (1989) Interleukin-6: possible implications in human diseases. *Research in Clinic and Laboratory* 19: 1-10, doi: 10.1007/BF02871787
 251. Cella M, Scheidegger D, Palmer-Lehmann K, Lane P, Lanzavecchia A, et al. (1996) Ligation of CD40 on dendritic cells triggers production of high levels of interleukin-12 and enhances T cell stimulatory capacity: T-T help via APC activation. *The Journal of experimental medicine* 184: 747-752, doi: 10.1084/jem.184.2.747
 252. Harris NL, Ronchese F (1999) The role of B7 costimulation in T-cell immunity. *Immunology and cell biology* 77: 304-311, doi: 10.1046/j.1440-1711.1999.00835.x
 253. Bell J (2002) Wake-up call. *Nature Reviews Immunology* 2: 143-143, doi: 10.1038/nri766
 254. DeBarros A, Chaves-Ferreira M, d'Orey F, Ribot JC, Silva-Santos B (2011) CD70-CD27 interactions provide survival and proliferative signals that regulate T cell receptor-driven activation of human gammadelta peripheral blood lymphocytes. *European Journal of Immunology* 41: 195-201, doi: 10.1002/eji.201040905
 255. Wang J, Fu Y-X (2004) The role of LIGHT in T cell-mediated immunity. *Immunologic Research* 30(2): 201-214, doi: 10.1385/IR:30:2:201
 256. van Montfrans JM, Hoepelman AI, Otto S, van Gijn M, van de Corput L, et al. (2012) CD27 deficiency is associated with combined immunodeficiency and persistent symptomatic EBV viremia. *Journal of Allergy and Clinical Immunology* 129: 787-793 e786, doi: 10.1016/j.jaci.2011.11.013
 257. Seymour R, Sundberg JP, Hogenesch H (2006) Abnormal lymphoid organ development in immunodeficient mutant mice. *Veterinary Pathology* 43(4): 401-423, doi: 10.1354/vp.43-4-401

-
258. Zapata JM, Reed JC (2002) TRAF1: lord without a RING. *Science Signaling* 133(2002): pe27, doi: 10.1126/stke.2002.133.pe27
 259. Mol M, Patole MS, Singh S (2014) Immune signal transduction in leishmaniasis from natural to artificial systems: Role of feedback loop insertion. *Biochimica et Biophysica Acta (BBA) - General Subjects* 1840: 71-79, doi: 10.1016/j.bbagen.2013.08.018
 260. Mol M, Patole MS, Singh S (2013) Signaling networks in *Leishmania* macrophages deciphered through integrated systems biology: a mathematical modeling approach. *Systems and Synthetic Biology* 7: 185-195, doi: 10.1007/s11693-013-9111-9
 261. Albergante L, Timmis J, Beattie L, Kaye PM (2013) A Petri Net Model of Granulomatous Inflammation: Implications for IL-10 Mediated Control of *Leishmania donovani* Infection. *PLoS Computational Biology* 9: e1003334, doi: 10.1371/journal.pcbi.1003334
 262. Hattori K, Nishikawa M, Watcharanurak K, Ikoma A, Kabashima K, et al. (2010) Sustained exogenous expression of therapeutic levels of IFN-gamma ameliorates atopic dermatitis in NC/Nga mice via Th1 polarization. *Journal of Immunology* 184: 2729-2735, doi: 10.4049/jimmunol.0900215
 263. Williams J, Jurkovich G, Hahnel G, Maier R (1992) Macrophage priming by interferon gamma: a selective process with potentially harmful effects. *Journal of Leukocyte Biology* 52: 579-584, doi: 10.1002/jlb.52.6.579
 264. Faria MS, Reis FC, Lima AP (2012) Toll-like receptors in *Leishmania* infections: guardians or promoters? *Journal of Parasitology Research* 2012: 930257, doi: 10.1155/2012/930257
 265. Srivastava S, Pandey SP, Jha MK, Chandel HS, Saha B (2013) *Leishmania* expressed lipophosphoglycan interacts with Toll-like receptor (TLR)-2 to decrease TLR-9 expression and reduce anti-leishmanial responses. *Clinical and Experimental Immunology* 172: 403-409, doi: 10.1111/cei.12074
 266. Mattner J, Wandersee-Steinhäuser A, Pahl A, Röllinghoff M, Majeau GR, et al. (2004) Protection against Progressive Leishmaniasis by IFN- β . *The Journal of Immunology* 172: 7574-7582, doi: 10.4049/jimmunol.172.12.7574
 267. Chowdhury S, Sarkar R (2013) Drug Targets and Biomarker Identification from Computational Study of Human Notch Signaling Pathway. *Clinical and Experimental Pharmacology* 3: 2161-1459.1000137, doi: 10.4172/2161-1459.1000137
 268. Fumiã HF, Martins ML (2013) Boolean Network Model for Cancer Pathways: Predicting Carcinogenesis and Targeted Therapy Outcomes. *PLoS ONE* 8: e69008, doi: 10.1371/journal.pone.0069008
 269. Saez-Rodriguez J, Simeoni L, Lindquist JA, Hemenway R, Bommhardt U, et al. (2007) A Logical Model Provides Insights into T Cell Receptor Signaling. *PLoS Computational Biology* 3: e163, doi: 10.1371/journal.pcbi.0030163
 270. Zhang R, Shah MV, Yang J, Nyland SB, Liu X, et al. (2008) Network model of survival signaling in large granular lymphocyte leukemia. *Proceedings of the National Academy of Sciences USA* 105: 16308-16313, doi: 10.1073/pnas.0806447105

-
271. Shio MT, Hassani K, Isnard A, Ralph B, Contreras I, et al. (2012) Host cell signalling and *Leishmania* mechanisms of evasion. *Journal of Tropical Medicine* 2012: 819512, doi: 10.1155/2012/819512
 272. Muller I, Pedrazzini T, Farrell JP, Louis J (1989) T-cell responses and immunity to experimental infection with *Leishmania major*. *Annual Review of Immunology* 7: 561-578, doi: 10.1146/annurev.iy.07.040189.003021
 273. Von Stebut E, Ehrchen JM, Belkaid Y, Kostka SL, Molle K, et al. (2003) Interleukin 1alpha promotes Th1 differentiation and inhibits disease progression in *Leishmania major*-susceptible BALB/c mice. *The Journal of Experimental Medicine* 198: 191-199, doi: 10.1084/jem.20030159
 274. McMahon-Pratt D, Alexander J (2004) Does the *Leishmania major* paradigm of pathogenesis and protection hold for New World cutaneous leishmaniases or the visceral disease? *Immunological Reviews* 201: 206-224, doi: 10.1111/j.0105-2896.2004.00190.x
 275. Himmelrich H, Parra-Lopez C, Tacchini-Cottier F, Louis JA, Launois P (1998) The IL-4 rapidly produced in BALB/c Mice after infection with *Leishmania major* down-regulates IL-12 Receptor β 2-Chain expression on CD4+ T Cells resulting in a state of unresponsiveness to IL-12. *The Journal of Immunology* 161: 6156-6163, PMID: 9834101
 276. El-On J (2009) Current status and perspectives of the immunotherapy of Leishmaniasis. *The Israel Medical Association journal: IMAJ* 11: 623-628, PMID: 20077951
 277. Reiner SL, Zheng S, Wang ZE, Stowring L, Locksley RM (1994) *Leishmania* promastigotes evade interleukin 12 (IL-12) induction by macrophages and stimulate a broad range of cytokines from CD4+ T cells during initiation of infection. *The Journal of Experimental Medicine* 179: 447-456, doi: 10.1084/jem.179.2.447
 278. Kostka SL, Knop J, Konur A, Udey MC, von Stebut E (2006) Distinct roles for IL-1 receptor type I signaling in early versus established *Leishmania major* infections. *Journal of Investigative Dermatology* 126: 1582-1589, doi: 10.1038/sj.jid.5700309
 279. O'Garra A (1998) Cytokines Induce the Development of Functionally Heterogeneous T Helper Cell Subsets. *Immunity* 8: 275-283, doi: 10.1016/S1074-7613(00)80533-6
 280. Rawlings JS, Rosler KM, Harrison DA (2004) The JAK/STAT signaling pathway. *Journal of Cell Science* 117: 1281-1283, doi: 10.1242/jcs.00963
 281. Stork PJS (2003) Does Rap1 deserve a bad Rap? *Trends in Biochemical Sciences* 28: 267-275, doi: 10.1016/s0968-0004(03)00087-2
 282. Okwor I, Uzonna JE (2009) Immunotherapy as a strategy for treatment of leishmaniasis: a review of the literature. *Immunotherapy* 1: 765-776, doi: 10.2217/imt.09.40
 283. Zuany-Amorim C, Hastewell J, Walker C (2002) Toll-like receptors as potential therapeutic targets for multiple diseases. *Nature Review Drug Discovery* 1: 797-807, doi: 10.1038/nrd914

-
284. Bakken T, He M, Cannon ML (2010) The phosphatase Shp2 is required for signaling by the Kaposi's sarcoma-associated herpesvirus viral GPCR in primary endothelial cells. *Virology* 397: 379-388, doi: 10.1016/j.virol.2009.11.030
285. Flandin JF, Chano F, Descoteaux A (2006) RNA interference reveals a role for TLR2 and TLR3 in the recognition of *Leishmania donovani* promastigotes by interferon-gamma-primed macrophages. *European Journal of Immunology* 36: 411-420, doi: 10.1002/eji.200535079
286. Tuon FF, Amato VS, Bacha HA, Almusawi T, Duarte MI, et al. (2008) Toll-like receptors and leishmaniasis. *Infection and Immunity* 76: 866-872, doi: 10.1128/IAI.01090-07
287. Yang EJ, Shin JS, Kim H, Park HW, Kim MH, et al. (2004) Cloning of TLR3 Isoform. *Yonsei Med J* 45: 359-361, doi: 10.3349/ymj.2004.45.2.359
288. Cuesta-Astroz Y, Santos A, Oliveira G, Jensen LJ (2019) Analysis of predicted host-parasite interactomes reveals commonalities and specificities related to parasitic lifestyle and tissues tropism. *Frontiers in Immunology*, doi: 10.3389/fimmu.2019.00212
289. Bahia D, Satoskar AR, Dussurget O (2018) Editorial: Cell signaling in host-pathogen interactions: The host point of view. *Frontiers in Immunology* 9:221. doi: 10.3389/fimmu.2018.00221
290. Zuck M, Austin LS, Danziger SA, Aitchison JD, Kaushansky A (2017) The promise of systems biology approaches for revealing host pathogen interactions in malaria. *Frontiers in Microbiology* 8:2183. doi: 10.3389/fmicb.2017.02183
291. Lambertz U, Silverman JM, Nandan D, McMaster WR, Clos J, et al. (2012) Secreted virulence factors and immune evasion in visceral leishmaniasis. *Journal of Leukocyte Biology*, doi: 10.1189/jlb.0611326
292. Silva-Almeida M, Pereira BAS, Ribeiro-Guimarães ML, Alves CR (2012) Proteinases as virulence factors in *Leishmania* spp. infection in mammals. *Parasites & Vectors* 5(1):1-10 doi: 10.1186/1756-3305-5-160
293. Li H, Zhou Y, Zhang Z (2017) Network analysis reveals a common host-pathogen interaction pattern in Arabidopsis immune responses. *Frontiers in Plant Science*, doi: 10.3389/fpls.2017.00893
294. Kumar S, Lata KS, Sharma P, Bhairappanavar SB, Soni S, et al. (2019) Inferring pathogen-host interactions between *Leptospira interrogans* and *Homo sapiens* using network theory. *Scientific Reports*, doi: 10.1038/s41598-018-38329-1
295. Avilán L, Gualdrón-López M, Quiñones W, González-González L, Hannaert V, et al. (2011) Enolase: A key player in the metabolism and a probable virulence factor of trypanosomatid parasites - Perspectives for its use as a therapeutic target. *Enzyme Research* 2011(932549), doi: 10.4061/2011/932549
296. Rao VS, Srinivas K, Sujini GN, Kumar GNS (2014) Protein-Protein Interaction Detection: Methods and Analysis. *International Journal of Proteomics*, doi: 10.1155/2014/147648

-
297. Liu ZP, Chen L (2012) Proteome-wide prediction of protein-protein interactions from high-throughput data. *Protein & Cell* 3(7): 508-520, doi: 10.1007/s13238-012-2945-1
 298. Chang JW, Zhou YQ, Ul Qamar MT, Chen LL, Ding YD (2016) Prediction of protein-protein interactions by evidence combining methods. *International Journal of Molecular Sciences* 17(11): 1946 doi: 10.3390/ijms17111946
 299. Liu ZP, Wang J, Qiu YQ, Leung RKK, Zhang XS, et al. (2011) Inferring protein-protein interactions based on sequences and interologs in *Mycobacterium tuberculosis*. *International Conference on Intelligent Computing*. Springer, Berlin, Heidelberg pp. 91-96, doi: 10.1007/978-3-642-24553-4_14
 300. Liu ZP, Wang J, Qiu YQ, Leung RKK, Zhang XS, et al. (2012) Inferring a protein interaction map of *Mycobacterium tuberculosis* based on sequences and interologs. *BMC Bioinformatics*, doi: 10.1186/1471-2105-13-S7-S6
 301. Rubanova N, Morozova N (2019) Centrality and the shortest path approach in the human interactome. *Journal of Bioinformatics and Computational Biology*, doi: 10.1142/S0219720019500276
 302. Ghasemi A, Zahediasl S (2012) Normality tests for statistical analysis: A guide for non-statisticians. *International Journal of Endocrinology and Metabolism*, doi: 10.5812/ijem.3505
 303. Öztuna D, Elhan AH, Tüccar E (2006) Investigation of four different normality tests in terms of type 1 error rate and power under different distributions. *Turkish Journal of Medical Sciences* 36 (3): 171-176
 304. Kumar A, Das S, Mandal A, Verma S, Abhishek K, et al. (2018) *Leishmania* infection activates host mTOR for its survival by M2 macrophage polarization. *Parasite Immunology* 40(11), e12586, doi: 10.1111/pim.12586
 305. Olivier M, Gregory DJ, Forget G (2005) Subversion mechanisms by which *Leishmania* parasites can escape the host immune response: A signaling point of view. *Clinical Microbiology Reviews* 18(2), 293-305, doi: 10.1128/CMR.18.2.293-305.2005
 306. Dayakar A, Chandrasekaran S, Kuchipudi SV, Kalangi SK (2019) Cytokines: Key determinants of resistance or disease progression in visceral leishmaniasis: Opportunities for novel diagnostics and immunotherapy. *Frontiers in immunology* 10, 670, doi: 10.3389/fimmu.2019.00670
 307. Moore KJ, Matlashewski G (1994) Intracellular infection by *Leishmania donovani* inhibits macrophage apoptosis. *Journal of Immunology (Baltimore, Md : 1950)*, 152(6):2930-7, PMID: 8144893
 308. Bose D, Banerjee S, Das S, Chatterjee N, Saha KD (2016) Heat killed attenuated *Leishmania* induces apoptosis of HepG2 cells through ROS mediated p53 dependent mitochondrial pathway. *Cellular Physiology and Biochemistry* 38(4), 1303-1318, doi: 10.1159/000443125

-
309. Harvey KF, Zhang X, Thomas DM (2013) The Hippo pathway and human cancer. *Nature Reviews Cancer* 13.4 (2013): 246-257, doi: 10.1038/nrc3458
 310. Boro M, Singh V, Balaji KN (2016) Mycobacterium tuberculosis-triggered Hippo pathway orchestrates CXCL1/2 expression to modulate host immune responses. *Scientific Reports* 6(1), 1-14, doi: 10.1038/srep37695
 311. Lee PC, Machner MP (2018) The Legionella Effector Kinase LegK7 Hijacks the Host Hippo Pathway to Promote Infection. *Cell Host and Microbe* 24(3), 429-438, doi: 10.1016/j.chom.2018.08.004
 312. Garcia G, Paul S, Beshara S, Ramanujan VK, Ramaiah A, et al. (2020) Hippo Signaling Pathway Has a Critical Role in Zika Virus Replication and in the Pathogenesis of Neuroinflammation. *American Journal of Pathology* 190(4), 844-861, doi: 10.1016/j.ajpath.2019.12.005
 313. Zhao B, Wei X, Li W, Udan RS, Yang Q, et al. (2007) Inactivation of YAP oncoprotein by the Hippo pathway is involved in cell contact inhibition and tissue growth control. *Genes and Development* 21(21), 2747-2761, doi: 10.1101/gad.1602907
 314. Al-Salabi MI, De Koning HP (2005) Purine nucleobase transport in amastigotes of *Leishmania mexicana*: Involvement in allopurinol uptake. *Antimicrobial Agents and Chemotherapy* 49(9), 3682-3689, doi: 10.1128/AAC.49.9.3682-3689.2005
 315. Boer DR, Bijlmakers MJ (2019) Differential Inhibition of Human and Trypanosome Ubiquitin E1S by TAK-243 Offers Possibilities for Parasite Selective Inhibitors. *Scientific Reports* 9(1), 1-14, doi: 10.1038/s41598-019-52618-3
 316. Srivastav S, Kar S, Chande AG, Mukhopadhyaya R, Das PK (2012) *Leishmania donovani* Exploits Host Deubiquitinating Enzyme A20, a Negative Regulator of TLR Signaling, To Subvert Host Immune Response. *The Journal of Immunology* 189(2), 924-934, doi: 10.4049/jimmunol.1102845
 317. Gupta P, Giri J, Srivastav S, Chande AG, Mukhopadhyaya R, et al. (2014) *Leishmania donovani* targets tumor necrosis factor receptor-associated factor (TRAF) 3 for impairing TLR4-mediated host response. *FASEB Journal* 28(4), 1756-1768, doi: 10.1096/fj.13-238428
 318. McHale PT, Lander AD (2014) The Protective Role of Symmetric Stem Cell Division on the Accumulation of Heritable Damage. *PLoS Computational Biology* 10: e1003802, doi: 10.1371/journal.pcbi.1003802
 319. De Boer RJ, Hogeweg P, Dullens HF, De Weger RA, Den Otter W (1985) Macrophage T lymphocyte interactions in the anti-tumor immune response: a mathematical model. *The Journal of Immunology* 134: 2748, PMID: 3156189
 320. Robertson-Tessi M, El-Kareh A, Goriely A (2012) A mathematical model of tumor-immune interactions. *Journal of Theoretical Biology* 294: 56-73, doi: 10.1016/j.jtbi.2011.10.027

-
321. De Pillis LG, Radunskaya A (2001) A mathematical tumor model with immune resistance and drug therapy: an optimal control approach. *Journal of Theoretical Medicine* 3: 79-100, doi: 10.1080/10273660108833067
 322. Krishnapriya P, Pitchaimani M (2015) Optimal control of mixed immunotherapy and chemotherapy of tumours with discrete delay. *International Journal of Dynamics and Control* 5(3), 872-892, doi: 10.1007/s40435-015-0221-y
 323. Pan Q, Li Q, Liu S, Ning N, Zhang X, et al. (2015) Concise Review: Targeting Cancer Stem Cells Using Immunologic Approaches. *Stem Cells* 33: 2085-2092, doi: 10.1002/stem.2039
 324. Yuan A, Hsiao Y-J, Chen H-Y, Chen H-W, Ho C-C, et al. (2015) Opposite Effects of M1 and M2 Macrophage Subtypes on Lung Cancer Progression. *Scientific Reports* 5: 14273, doi: 10.1038/srep14273
 325. Kim Y, Joo KM, Jin J, Nam D-H (2009) Cancer Stem Cells and Their Mechanism of Chemo-Radiation Resistance. *International Journal of Stem Cells* 2: 109-114, doi: 10.15283/ijsc.2009.2.2.109
 326. Hazem G, Monther A-A (2013) Do Cancer Stem Cells have an Immunomodulatory Role Different from the Bulk of Tumor Cells? *Journal of Carcinogenesis & Mutagenesis* 14 (2013): 003, doi: 10.4172/2157-2518.S14-003
 327. Jiang X (2015) Macrophage-produced IL-10 limits the chemotherapy efficacy in breast cancer. *Journal of Zhejiang University Science B* 16: 44-45, doi: 10.1631/jzus.B1400352
 328. Zaidi MR (2018) The Interferon-Gamma Paradox in Cancer. *Journal of Interferon & Cytokine Research* 39: 30-38, doi: 10.1089/jir.2018.0087
 329. Mojic M, Takeda K (2017) The Dark Side of IFN- γ : Its Role in Promoting Cancer Immuno-evasion. *International journal of molecular sciences*, 19(1), 89, doi: 10.3390/ijms19010089
 330. Mele L, Paino F, Papaccio F, Regad T, Boocock D, et al. (2018) A new inhibitor of glucose-6-phosphate dehydrogenase blocks pentose phosphate pathway and suppresses malignant proliferation and metastasis in vivo. *Cell death & disease* 9: 572, doi: 10.1038/s41419-018-0635-5
 331. Mahanta A, Ganguli P, Barah P, Sarkar RR, Sarmah N, et al. (2018) Integrative Approaches to Understand the Mastery in Manipulation of Host Cytokine Networks by Protozoan Parasites with Emphasis on *Plasmodium* and *Leishmania* Species. *Frontiers in Immunology* 9:296, doi: 10.3389/fimmu.2018.00296
 332. Ganguli P, Chowdhury S, Chowdhury S, Sarkar RR (2015) Identification of Th1/Th2 regulatory switch to promote healing response during leishmaniasis: a computational approach. *EURASIP Journal on Bioinformatics and Systems Biology* 2015: 13, doi: 10.1186/s13637-015-0032-7

-
333. Ganguli P, Sarkar RR (2018) Exploring immuno-regulatory mechanisms in the tumor microenvironment: Model and design of protocols for cancer remission. *PLoS ONE* 13: e0203030, doi: 10.1371/journal.pone.0203030
 334. Chakravarty M, Ganguli P, Murahari M, Sarkar RR, Peters GJ, et al. (2021) Study of Combinatorial Drug Synergy of Novel Acridone Derivatives With Temozolomide Using in-silico and in-vitro Methods in the Treatment of Drug-Resistant Glioma. *Frontiers in Oncology* 11(640), doi: 10.3389/fonc.2021.625899
 335. Watts TH (2010) Staying alive: T cell costimulation, CD28, and Bcl-xL. *Journal of Immunology* 185: 3785-3787, doi: 10.4049/jimmunol.1090085
 336. Nargi JL, Woodford-Thomas TA (1994) Cloning and characterization of a cdc25 phosphatase from mouse lymphocytes. *Immunogenetics* 39: 99-108, doi: 10.1007/BF00188612
 337. Brennan P, Babbage J, Thomas G, Cantrell D (1999) p70s6k integrates phosphatidylinositol 3-kinase and rapamycin-regulated signals for E2F regulation in T lymphocytes. *Molecular and cellular biology* 19: 4729-4738, doi: 10.1128/mcb.19.7.4729
 338. Arias CF, Ballesteros-Tato A, Garcia MI, Martin-Caballero J, Flores JM, et al. (2007) p21CIP1/WAF1 Controls Proliferation of Activated/Memory T Cells and Affects Homeostasis and Memory T Cell Responses. *The Journal of Immunology* 178: 2296-2306, doi: 10.4049/jimmunol.178.4.2296
 339. Dijkers PF, Birkenkamp KU, Lam EW, Thomas NS, Lammers JW, et al. (2002) FKHR-L1 can act as a critical effector of cell death induced by cytokine withdrawal: protein kinase B-enhanced cell survival through maintenance of mitochondrial integrity. *The Journal of Cell Biology* 156: 531-542, doi: 10.1083/jcb.200108084
 340. Patsoukis N, Sari D, Boussiotis VA (2012) PD-1 inhibits T cell proliferation by upregulating p27 and p15 and suppressing Cdc25A. *Cell Cycle* 11: 4305-4309, doi: 10.4161/cc.22135
 341. Lee JK, Won C, Yi EH, Seok SH, Kim MH, et al. (2013) Signal transducer and activator of transcription 3 (Stat3) contributes to T-cell homeostasis by regulating pro-survival Bcl-2 family genes. *Immunology* 140: 288-300, doi: 10.1111/imm.12133
 342. Takamura K, Fukuyama S, Nagatake T, Kim DY, Kawamura A, et al. (2007) Regulatory Role of Lymphoid Chemokine CCL19 and CCL21 in the Control of Allergic Rhinitis. *The Journal of Immunology* 179: 5897-5906, doi: 10.4049/jimmunol.179.9.5897
 343. Ben-Sasson SZ, Hu-Li J, Quiel J, Cauchetaux S, Ratner M, et al. (2009) IL-1 acts directly on CD4 T cells to enhance their antigen-driven expansion and differentiation. *Proceedings of the National Academy of Sciences USA* 106: 7119-7124, doi: 10.1073/pnas.0902745106
 344. Lantz CS, Boesiger J, Song CH, Mach N, Kobayashi T, et al. (1998) Role for interleukin-3 in mast-cell and basophil development and in immunity to parasites. *Nature* 392: 90-93, doi: 10.1038/32190

-
345. Wechsler AS, Gordon MC, Dendorfer U, LeClair KP (1994) Induction of IL-8 expression in T cells uses the CD28 costimulatory pathway. *The Journal of Immunology* 153: 2515-2523, PMID: 8077662
 346. Goswami R, Kaplan MH (2011) A brief history of IL-9. *The Journal of Immunology* 186: 3283-3288, doi: 10.4049/jimmunol.1003049
 347. Yoo JK, Cho JH, Lee SW, Sung YC (2002) IL-12 Provides Proliferation and Survival Signals to Murine CD4⁺ T Cells Through Phosphatidylinositol 3-Kinase/Akt Signaling Pathway. *The Journal of Immunology* 169: 3637-3643, doi: 10.4049/jimmunol.169.7.3637
 348. Pollock RA, Richardson WD (1992) The alternative-splice isoforms of the PDGF A-chain differ in their ability to associate with the extracellular matrix and to bind heparin in vitro. *Growth Factors* 7: 267-277, doi: 10.3109/08977199209046409
 349. Gorelik L, Flavell RA (2002) Transforming growth factor-beta in T-cell biology. *Nature Review Immunology* 2: 46-53, doi: 10.1038/nri704
 350. Lu F, Gladden AB, Diehl JA (2003) An alternatively spliced cyclin D1 isoform, cyclin D1b, is a nuclear oncogene. *Cancer Research* 63: 7056-7061, PMID: 14612495
 351. Denicourt C, Legault P, McNabb FA, Rassart E (2008) Human and mouse cyclin D2 splice variants: transforming activity and subcellular localization. *Oncogene* 27: 1253-1262, doi: 10.1038/sj.onc.1210750
 352. Jurado J, Fuentes-Almagro CA, Prieto-Alamo MJ, Pueyo C (2007) Alternative splicing of c-fos pre-mRNA: contribution of the rates of synthesis and degradation to the copy number of each transcript isoform and detection of a truncated c-Fos immunoreactive species. *BMC Molecular Biology* 8: 83, doi: 10.1186/1471-2199-8-83
 353. de Castro IP, Benet M, Jiménez M, Alzabin S, Malumbres M, et al. (2005) Mouse p10, an alternative spliced form of p15INK4b, inhibits cell cycle progression and malignant transformation. *Cancer Research* 65: 3249-3256, doi: 10.1158/0008-5472.CAN-03-3445
 354. Jin P, Zhang J, Sumariwalla PF, Ni I, Jorgensen B, et al. (2008) Novel splice variants derived from the receptor tyrosine kinase superfamily are potential therapeutics for rheumatoid arthritis. *Arthritis Research and Therapy* 10: R73, doi: 10.1186/ar2447
 355. Arinobu Y, Atamas SP, Otsuka T, Niuro H, Yamaoka K, et al. (1999) Antagonistic effects of an alternative splice variant of human IL-4, IL-4 δ 2, on IL-4 activities in human monocytes and B cells. *Cellular Immunology* 191: 161-167, doi: 10.1006/cimm.1998.1431
 356. Bihl MP, Heinemann K, Rudiger JJ, Eickelberg O, Perruchoud AP, et al. (2002) Identification of a novel IL-6 isoform binding to the endogenous IL-6 receptor. *American Journal of Respiratory Cell and Molecular Biology* 27: 48-56, doi: 10.1165/ajrcmb.27.1.4637
 357. Hohlbaum AM, Moe S, Marshak-Rothstein A (2000) Opposing effects of transmembrane and soluble Fas ligand expression on inflammation and tumor cell survival. *The Journal of Experimental Medicine* 191: 1209-1220, doi: 10.1084/jem.191.7.1209

-
358. Ayroldi E, D'Adamio F, Zollo O, Agostini M, Moraca R, et al. (1999) Cloning and expression of a short Fas ligand: a new alternatively spliced product of the mouse Fas ligand gene. *Blood* 94: 3456-3467, PMID: 10552956
 359. Boise LH, González-García M, Postema CE, Ding L, Lindsten T, et al. (1993) *bcl-x*, a *bcl-2*-related gene that functions as a dominant regulator of apoptotic cell death. *Cell* 74: 597-608, doi: 10.1016/0092-8674(93)90508-n
 360. Mistry P, Laird MH, Schwarz RS, Greene S, Dyson T, et al. (2015) Inhibition of TLR2 signaling by small molecule inhibitors targeting a pocket within the TLR2 TIR domain. *Proceedings of the National Academy of Sciences USA* 112: 5455-5460, doi: 10.1073/pnas.1422576112
 361. Nicodemus CF, Berek JS (2010) TLR3 agonists as immunotherapeutic agents. *Immunotherapy* 2: 137, doi: 10.2217/imt.10.8
 362. Romero-Sandoval EA, Horvath R, Landry RP, DeLeo JA (2009) Cannabinoid receptor type 2 activation induces a microglial anti-inflammatory phenotype and reduces migration via MKP induction and ERK dephosphorylation. *Molecular Pain* 5: 25, doi: 10.1186/1744-8069-5-25
 363. Brown JE, Zeiger SL, Hettinger JC, Brooks JD, Holt B, et al. (2010) Essential role of the redox-sensitive kinase p66shc in determining energetic and oxidative status and cell fate in neuronal preconditioning. *Journal of Neuroscience* 30: 5242-5252, doi: 10.1523/JNEUROSCI.6366-09.2010
 364. Kim HK, Jeong MJ, Kong MY, Han MY, Son KH, et al. (2005) Inhibition of Shc/Grb2 protein-protein interaction suppresses growth of B104-1-1 tumors xenografted in nude mice. *Life Sciences* 78: 321-328, doi: 10.1016/j.lfs.2005.04.067
 365. Chen L, Sung SS, Yip ML, Lawrence HR, Ren Y, et al. (2006) Discovery of a novel shp2 protein tyrosine phosphatase inhibitor. *Molecular Pharmacology* 70: 562-570, doi: 10.1124/mol.106.025536
 366. Silverman JM, Chan SK, Robinson DP, Dwyer DM, Nandan D, et al. (2008) Proteomic analysis of the secretome of *Leishmania donovani*. *Genome Biology* 9: R35, doi: 10.1186/gb-2008-9-2-r35
 367. Singh AK, Pandey RK, Siqueira-Neto JL, Kwon YJ, Freitas-Junior LH, et al. (2015) Proteomic-based approach to gain insight into reprogramming of THP-1 cells exposed to *Leishmania donovani* over an early temporal window. *Infection and Immunity* 83: 1853-1868, doi: 10.1128/iai.02833-14
 368. Macallan DC, Asquith B, Irvine AJ, Wallace DL, Worth A, et al. (2003) Measurement and modeling of human T cell kinetics. *European Journal of Immunology* 33: 2316-2326, doi: 10.1002/eji.200323763
 369. Jansson A, Fagerlind M, Karlsson D, Nilsson P, Cooley M (2006) In silico simulations suggest that Th-cell development is regulated by both selective and instructive

-
- mechanisms. *Immunology and Cell Biology* 84: 218-226, doi: 10.1111/j.1440-1711.2006.01425.x
370. Vukmanovic-Stejic M, Zhang Y, Cook JE, Fletcher JM, McQuaid A, et al. (2006) Human CD4(+) CD25(hi) Foxp3(+) regulatory T cells are derived by rapid turnover of memory populations in vivo. *Journal of Clinical Investigation* 116: 2423-2433, doi: 10.1172/JCI28941
371. Italiani P, Boraschi D (2014) From Monocytes to M1/M2 Macrophages: Phenotypical vs. Functional Differentiation. *Frontiers in Immunology* 5: 514, doi: 10.3389/fimmu.2014.00514
372. Zhang X, Brunner T, Carter L, Dutton RW, Rogers P, et al. (1997) Unequal death in T helper cell (Th) 1 and Th2 effectors: Th1, but not Th2, effectors undergo rapid Fas/FasL-mediated apoptosis. *Journal of Experimental Medicine* 185: 1837-1849, doi: 10.1084/jem.185.10.1837
373. Xing S, Fu J, Zhang Z, Gao Y, Jiao Y, et al. (2010) Increased turnover of FoxP3^{high} regulatory T cells is associated with hyperactivation and disease progression of chronic HIV-1 infection. *JAIDS Journal of Acquired Immune Deficiency Syndromes* 54: 455-462, doi: 10.1097/QAI.0b013e3181e453b9
374. Enewold L, Mechanic LE, Bowman ED, Zheng Y-L, Yu Z, et al. (2009) Serum concentrations of cytokines and lung cancer survival in African Americans and Caucasians. *Cancer Epidemiology and Prevention Biomarkers* 18: 215-222, doi: 10.1158/1055-9965.EPI-08-0705
375. Briesemeister D, Sommermeyer D, Loddenkemper C, Loew R, Uckert W, et al. (2011) Tumor rejection by local interferon gamma induction in established tumors is associated with blood vessel destruction and necrosis. *International Journal of Cancer* 128: 371-378, doi: 10.1002/ijc.25350.
376. Hof-Nahor I, Leshansky L, Shivtiel S, Eldor L, Aberdam D, et al. (2012) Human mesenchymal stem cells shift CD8⁺ T cells towards a suppressive phenotype by inducing tolerogenic monocytes. *Journal of Cell Science* 125: 4640, doi: 10.1242/jcs.108860
377. McNally A, Hill GR, Sparwasser T, Thomas R, Steptoe RJ (2011) CD4⁺ CD25⁺ regulatory T cells control CD8⁺ T-cell effector differentiation by modulating IL-2 homeostasis. *Proceedings of the National Academy of Sciences USA* 108: 7529, doi: 10.1073/pnas.1103782108
378. Sakamoto T, Saito H, Tatebe S, Tsujitani S, Ozaki M, et al. (2006) Interleukin-10 expression significantly correlates with minor CD8⁺ T-cell infiltration and high microvessel density in patients with gastric cancer. *International Journal of Cancer* 118: 1909-1914, doi: 10.1002/ijc.21598

ABSTRACT

Name of the Student: Piyali Ganguli

Registration No.: 10BB16J26020

Faculty of Study: Biological Sciences (BS)

Year of Submission: 2021

CSIR Lab: CSIR-NCL, Pune

Name of the Supervisor: Dr. Ram Rup Sarkar

Title of the thesis: Identification of Immuno-regulatory modules and optimal treatment strategies for eliciting effector functions against different diseases

The immune system protects it from various infectious disease and cancer. However, regulations governing suppression of T-cells under varied antigenic challenges remains elusive through experimental approaches. In order to unveil the regulatory mechanisms underlying immune-suppression during Cancer and Leishmaniasis, we have used various mathematical and computational approaches, to identify the regulatory modules of the immunological network and design novel treatment strategies.

Manual reconstruction of T-cell pathway and Boolean Modelling was used to gain a holistic understanding of the co-receptor mediated pathways. *In silico* knock-out analysis revealed minimal combination of proteins (TCR:CD3, CRAC and OX40) that are absolutely essential to achieve sustained T-cell proliferation and activation of effector functions. Co-receptor molecules CD27 and LTBR were identified to play major role in the regulation of Interleukin expression during antigenic challenges.

For Cutaneous Leishmaniasis, signalling routes regulating the switching of T-cell responses from healing T_{H1} to non-healing T_{H2} response, were identified using Logical Steady State Analysis. Novel targets for eliciting robust anti-*Leishmania* immune response are also proposed through this study. For the study of Visceral Leishmaniasis, a putative host-pathogen interactome between *Leishmania donovani* and Human has been predicted using Interlog and Domain mapping strategies. Network analysis revealed key signalling routes mediating the host pathogen interaction. A novel combination of protein targets (UBC+1433Z+HS90A) has also been identified which governs the host immune response, parasite survival strategies and visceralization of the infection during Visceral Leishmaniasis.

To study the tumor-immune interaction, an ODE based model has been developed related to the Seed Soil hypothesis of tumor development. Model analysis revealed the role of Cancer Stem Cell differentiation pattern on the development o drug resistance. Three novel feedback regulations governing tumor progression, resistance and relapse have been proposed in the study. The model has been further used to propose improvised combinatorial treatment protocol that shows promising results in suppressing resistant tumor for better Cancer remission.

LIST OF PUBLICATIONS

Related to Thesis

1. **Ganguli P**, Chowdhury S, Bhowmick R, and Sarkar RR (2015) Temporal protein expression pattern in intracellular signalling cascade during T-cell activation: A computational study. *Journal of Biosciences*, 40(4), pp 769-789, DOI: 10.1007/s12038-015-9561-1
2. **Ganguli P**, Chowdhury S, Chowdhury S, and Sarkar RR (2015) Identification of Th1/Th2 regulatory switch to promote healing response during leishmaniasis: a computational approach. *Eurasip Journal on Bioinformatics and Systems Biology*, 2015(1), pp 1-19, DOI: 10.1186/s13637-015-0032-7
3. Mahanta A#, **Ganguli P#**, Barah P, Sarkar RR, Sarmah N, Phukan S, Bora M and Baruah S (2018) Integrative approaches to understand the mastery in manipulation of host cytokine networks by protozoan parasites with emphasis on *Plasmodium* and *Leishmania* species. *Frontiers in Immunology*, 9: 296, DOI: 10.3389/fimmu.2018.00296 (**#Equal First Authors**)

[This article also appears as Book Chapter In: Morrot A. (eds) *Immune evasion strategies in protozoan-host interactions*, *Frontiers*, pp 478-485, ISSN 1664-8714; ISBN 978-2-88966-294-4; DOI: 10.3389/978-2-88966-294-4 (Published October 2020)]
4. **Ganguli P** and Sarkar RR (2018) Exploring immuno-regulatory mechanisms in the tumor microenvironment: Model and design of protocols for cancer remission. *PloS ONE*, 13(9), e0203030, DOI: 10.1371/journal.pone.0203030
5. Bhowmick R, **Ganguli P** and Sarkar RR (2020) T-Cell Activation and Differentiation: Role of Signalling and Metabolic Cross-Talk. (Chapter 6) In: Singh S. (eds) *Systems and Synthetic Immunology*. *Springer*, Singapore, pp 153-182, Online ISBN: 978-981-15-3350-1, DOI: 10.1007/978-981-15-3350-1_6
6. Chakravarty M#, **Ganguli P#**, Murahari M, Sarkar RR, Peters GJ, Yergeri MC (2021) Study of combinatorial drug synergy of novel acridone derivatives with Temozolomide using in-silico and in-vitro methods in the treatment of drug - resistant Glioma. *Frontiers in Oncology* 11(640), DOI: 10.3389/fonc.2021.625899 (**#Equal First Authors**)

-
- Panditrao G, **Ganguli P** and Sarkar RR (2021) Delineating infection strategies of *Leishmania donovani* secretory proteins in Human through Host-Pathogen protein Interactome prediction (Submitted, Under review)

Other Publications

- Chowdhury S, Sinha N, **Ganguli P**, Bhowmick R, Singh V, Nandi S and Sarkar RR (2018) BIOPYDB: A Dynamic Human Cell Specific Biochemical Pathway Database with Advanced Computational Analyses Platform, *Journal of Integrative Bioinformatics*, 15(3), 20170072, DOI: 10.1515/jib-2017-0072
- Nandi S, **Ganguli P** and Sarkar RR (2020) Essential gene prediction using limited gene essentiality information – An Integrative Semi-supervised Machine Learning Strategy, *PLoS ONE*, 15 (11), e0242943, DOI: 10.1371/journal.pone.0242943

Patent

- Sarkar RR, **Ganguli P**, Chowdhury S (2015) Identification of minimal combinations of molecules that act as probable immunostimulators against Leishmaniasis. Patent Application No. 3691/DEL/2015 filed on December 11, 2015. (WO2017081703A1)

**PUBLICATIONS
(THESIS RELATED)**

Temporal protein expression pattern in intracellular signalling cascade during T-cell activation: A computational study

PIYALI GANGULI¹, SAIKAT CHOWDHURY^{1,2}, RUPA BHOWMICK¹ and RAM RUP SARKAR^{1,2,*}

¹Chemical Engineering and Process Development Division, CSIR-National Chemical Laboratory, Pune 411 008, India

²Academy of Scientific & Innovative Research (AcSIR), New Delhi 110 001, India

*Corresponding author (Fax, +91-20-2590 2621; Email, rr.sarkar@ncl.res.in)

Various T-cell co-receptor molecules and calcium channel CRAC play a pivotal role in the maintenance of cell's functional responses by regulating the production of effector molecules (mostly cytokines) that aids in immune clearance and also maintaining the cell in a functionally active state. Any defect in these co-receptor signalling pathways may lead to an altered expression pattern of the effector molecules. To study the propagation of such defects with time and their effect on the intracellular protein expression patterns, a comprehensive and largest pathway map of T-cell activation network is reconstructed manually. The entire pathway reactions are then translated using logical equations and simulated using the published time series microarray expression data as inputs. After validating the model, the effect of *in silico* knock down of co-receptor molecules on the expression patterns of their downstream proteins is studied and simultaneously the changes in the phenotypic behaviours of the T-cell population are predicted, which shows significant variations among the proteins expression and the signalling routes through which the response is propagated in the cytoplasm. This integrative computational approach serves as a valuable technique to study the changes in protein expression patterns and helps to predict variations in the cellular behaviour.

[Ganguli P, Chowdhury S, Bhowmick R and Sarkar RR 2015 Temporal protein expression pattern in intracellular signalling cascade during T-cell activation: A computational study. *J. Biosci.* **40** 769–789] DOI 10.1007/s12038-015-9561-1

1. Introduction

Exhibition of diverse patterns in the biological world has been observed in various systems, starting from ecosystems to embryogenesis and organogenesis (Othmer *et al.* 1993). Precise understanding of such patterns, evolved in nature, requires knowledge of the underlying mechanisms through which various components of that system interact with each other and subsequently emerge towards different configurations. Reaction-Diffusion model of morphogens (Turing effect) in the development of embryo is one of the most studied areas in the field of pattern formation in biological system. In this model it is assumed that a well-structured pre-pattern of morphogen is

formed before the embryogenesis and accordingly the cells within the embryo respond, proliferate and develop into a well-structured morphology (Turing 1952). Chemical rate parameters and diffusion co-efficient of morphogen determine the chemical stability of the entire systems, which in certain cases leads to the oscillation or unstable dynamics that may further develop different spatial structures (Turing 1952; Maini *et al.* 1997). Many such models have been developed to study the biological systems, most of which discuss either the pattern generation in ecological systems (e.g. host–parasite interaction, consumer–resource interactions, habitat and species richness, etc.) or the development of body pigmentation, embryogenesis and physiological activities (e.g. heart beats, information

Keywords. Boolean model; co-receptors and CRAC channel; synchronous and asynchronous simulation; T-cell signalling pathway; temporal gene expression patterns

Supplementary materials pertaining to this article are available on the *Journal of Biosciences* Website at <http://www.ias.ac.in/jbiosci/oct2015/supp/Ganguli.pdf>

processing in neural network, synaptic pattern recognition of immune cells, etc.) of living organisms (Cohen and Grossberg 1983; Sinha *et al.* 1984; Qi *et al.* 2001; Gilad *et al.* 2004; Potse *et al.* 2006; Rietkerk and Van de Koppel 2008).

The counter proposal of Turing model of morphogen has also been proposed where it is assumed that the distribution of cellular density forms the mechano-chemical gradient in the developing tissue and helps the cell differentiations and proliferation (Murray 2003). Although later it is proven that the phenotypic responses (e.g. cellular growth, cell death, proliferation, pigmentation, etc.) shown by a cell is not only dependent on morphogen or mechano-chemical gradient, but also dependent on its intracellular biochemical signalling cascades, which eventually turn on or off specific sets of genes responsible for such phenotypic responses (Rasopovic *et al.* 2014; Srinivasan *et al.* 2014). However, it is still not clear that how these genes are regulated by these extracellular fluctuations and how their concerted effort develops different robust biological patterns (Eldar *et al.* 2002). During the last few decades, the advancement of molecular biology, genomics and proteomics experiments have come up with several significant discoveries indicating the role of various signalling networks in different cellular physiologies and pattern formation (Álvarez-Buylla and Ihrie 2014; Gaarenstroom and Hill 2014; Rentzsch and Adamska 2014). Although most of the mathematical models have focused on the pattern formation of the phenotypic signatures of tumour growth and embryological development, very few models have discussed on the context of molecular basis (e.g. gene, protein expression, signalling and metabolic network, etc.) of such pattern development processes. One of the major reasons behind this is the unavailability of detailed molecular mechanisms through which the information or signal upon interacting with different extracellular fluctuations is passed from one molecule to another molecule inside the cell. On the other hand, analysis of temporal protein expression patterns have proven to be important by various experimental groups (Velardo *et al.* 2004; Li *et al.* 2014), and is of utmost importance to study different physiological and development processes. Hence, integrating the cellular responses with the gene/protein expression patterns inside the cell, a comprehensive study using suitable mathematical and computational approaches is required.

Several attempts have been made to study the progression of various cancers, birth defects, organogenesis, etc., in human cells and tissues by studying different signalling pathways, such as Hedgehog, Notch, MAPK, WNT, etc. (Rosner *et al.* 2002; Corson *et al.* 2003; Chowdhury *et al.* 2013; Chowdhury and Sarkar 2013; Hall *et al.* 2014). Moreover, during the last few decades, researchers have also focused on the evolution of temporal gene/protein expression patterns observed in our immune system under different immunological disorders (Rangel *et al.* 2004; Rosenwald *et al.* 2001). The immune system, the central defence system of our body against the foreign invaders (i.e. antigens), is constituted by different cell types, such as

lymphocytes, macrophages, etc. Out of the other cell types of our immune system, study of gene or protein expression patterns in intracellular activation network of T-cell (one of the most important components of immune system) has been performed by several research groups, by using different experimental and computational tools and techniques (Rangel *et al.* 2004; Coombs *et al.* 2011; Teku *et al.* 2014). However, one of the main drawbacks of these techniques is that most of these methods deal with the gene expression data obtained from microarray experiment, which is inherently unable to correlate various functional responses with temporal protein expression patterns involved in T-cell signalling pathway. Hence, in order to understand the activity of our immune systems properly, it is very important to study this particular cell type from various aspects.

Activation of T-cell is also a delicate system and pattern recognition process which functions in response to different external stimuli. At the time of activation of naive T-cell into cytotoxic or T-helper cells, the population of naive T-cells has to pass through the pattern recognition process of the identification of antigenic peptide sequences (self or non-self antigen), which in turn decides whether the naive T-cells will be converted into the active T-cells (which will further proliferate) or inactive T-cells (no further proliferation but the cells will survive) or dead T-cells (which will further trigger apoptotic pathway and cell death) (Carter 2000; Coombs and Goldstein 2005). Hence, certain deregulation of this sensitive mechanism can destabilize our body's immune system and can trigger various diseases, like auto-immune diseases, severe combined immune deficiency syndrome (SCID), etc. (Shlomchik *et al.* 1987; Fischer *et al.* 2005; Baecklund *et al.* 2014). However, the complete activation of the T-cell responses and the expression of the major interleukin molecules cannot be achieved by T-cell receptor (TCR) and MHC class II protein interaction alone, but requires the successful interaction of the various co-stimulator molecules with its co-receptors and the activation of the calcium channel as well (Chen and Flies 2013). The exact molecular pathways involved in the regulation of the T-cell effector molecules by the co-signalling and the calcium pathways are still not clear and thus require a better understanding of the intracellular T-cell activation network. After receiving the signal (by interacting with the antigen presenting cell) and the successive activation of the TCR-mediated pathway, the co-signalling pathways, and the calcium pathways, the expression of different cytosolic and nuclear proteins inside the T-cell is changed, and hence such temporal protein expression pattern can then decide the phenotypic responses to be expressed. In this work, our main hypothesis is that the temporal protein expression patterns of various T-cell signalling component proteins as well as the phenotypic responses (such as proliferation, inactivation, cell death, interleukin production, etc.) can be regulated by tuning various co-stimulatory and co-inhibitory molecules including Ca^{+2} signalling pathway. Several other previously published models on T-

cell network have not considered the effect of these parallel pathways along with the core T-cell signalling cascades and thus are unable to discuss the effect of these membrane bound co-receptor molecules in the downstream of T-cell intracellular network as well as the cross-talks with other pathways inside the cell.

In order to accomplish this work successfully, we have manually reconstructed a new, comprehensive T-cell signalling pathway coupled with other intracellular important signalling pathways (e.g. MAPK, Ca⁺² signalling pathway etc.) by collating the signal propagation data from various literatures and cell signalling databases. The reconstructed pathway map of T-cell activation, which has been used in our model, is the largest T-cell activation pathway to the best of our knowledge till date. Using this collated signal transduction data and the concept of semi-dynamic Boolean or logical equations, we have constructed a mathematical model of the activation of T-cell signalling network. The initial expression levels (i.e. logical states) of all the nodes/species of this pathway were considered from the published microarray expression data, which is binarized by K-means clustering method. Using this semi-dynamic computational approach, we have been able to observe various temporal protein expression patterns, generated upon introducing different stimulation and co-stimulation signal on the T-cell receptor proteins. We also tried to correlate the temporal expression of proteins with three T-cell populations, i.e. Activated or Proliferated T-cells, Inactive T-cells and Dead T-cells. Using our model, we have been able to reproduce such phenotypic responses of T-cells reported in different published experimental results. We have also been able to predict *in silico* temporal protein expression patterns and its effect on cellular phenotypic responses by perturbing the expression of two important co-stimulatory proteins, viz. CD27 and LTBR. Through this work, we are proposing a novel computational approach, which is easy to implement for understanding the correlation of temporal protein expression pattern with different phenotypic expressions generated upon the activation of T-cell signalling network. Moreover, by successfully simulating different experimental scenarios with the protein knock-out and/or knock-in conditions, our model depicts its potential to predict future drug targets for the treatment of various T-cells, immune-related diseases. We hope this approach will be helpful for the theoretical and experimental biologists to dissect its intricate complexities while studying various pathological disorders directed by T-cell activation process.

2. Materials and methods

2.1 Pathway reconstruction

In order to capture all the regulations that operate to control the proliferation and activation of a T-cell, getting a

comprehensive picture of the entire signalling cascade involved in the process was an essential prerequisite. Since a complete map of the pathway was lacking from any single source, the pathway had to be reconstructed by manually collating human cell specific data from about 21 popular signalling pathway databases, such as, KEGG, Protein Lounge, Pathway Central, Biocarta, NetPath, etc. (Kanehisa and Goto 2000; Nishimura 2001, Kandasamy *et al.* 2010); protein-protein interaction databases, such as, HPRD, BioGRID^{3,2}, etc. (Prasad *et al.* 2009; Chatr-aryamontri *et al.* 2013) along with more than 200 literatures published in peer reviewed journals (searched using PUBMED and Google Scholar). The protein-protein interaction data obtained were knitted together to reconstruct the entire signalling cascade. The diagram of the reconstructed pathway was drawn using CellDesigner version 4.3 (Funahashi *et al.* 2003), a freely available software package that allows to easily create gene-regulatory and biochemical network images using a graphical user interface. The overall reaction process of this pathway starts at the immunological synapse, the signal is then transduced via the T-cell membrane proteins, comprising of the receptors and co-receptors, down to the cytoplasmic proteins, which ultimately leads to the activation of certain transcription factors. These activated transcription factors then translocate into the nucleus and induce the expression of important output proteins, and cytokines (effector molecules) that are crucial in maintaining the T-cell proliferation as well as in mediating the clearance of the antigen that has entered our body.

2.2 Logical analysis

The dynamic analysis of such large network requires precise kinetic data, which is rarely available and thus we had to restrict ourselves to a semi-dynamic approach of modeling this signalling pathway, i.e. 'Logical Analysis', where an up-regulation in the protein expression is considered as '1' or 'ON', while a down-regulation of a protein expression is considered as '0' or 'OFF' (binary states). The logical equations of the target molecules have been written using different combinations of molecules ('source') along with 'AND', 'OR' and/or 'NOT' (logical gates) relations depending on how these molecules influence the expression of each other in a biologically relevant way. The molecules in the model associated with 'AND' operation signifies the cumulative or multiplicative effects of a combination of proteins on their downstream targets, whereas the presence of 'OR' operation signifies the alternative routes of signal propagation. The molecules kept in 'NOT' relation are principally the inhibitors of the target molecule. Different biochemical reaction mechanisms (such as phosphorylation, transcriptional acti-

vation, ubiquitylation, nuclear transport, inhibition, and different feedbacks reactions, etc.) are considered in the model and transformed in terms of Boolean or logical equations.

For example, the Src family kinase (SFK), FYN is regulated by the complex formed by the association of the transmembrane adaptor protein PAG and protein tyrosine kinase CSK (PAG:CSK). These two proteins remain associated with each other which inhibit the activation of the FYN protein. The other two proteins regulating the expression of FYN are tyrosine phosphatase CD45, which positively regulates the activation of Fyn, and the proto-oncogene CBL, which has an inhibitory effect. The PAG:CSK complex being a strong negative regulator of FYN, its absence is absolutely necessary even in the presence of its positive regulator CD45. Using this biologically relevant information from the literature sources, one can thus write the following equation of the above reaction mechanisms (Andoniou *et al.* 2000; Brdička *et al.* 2000; Trowbridge and Thomas 1994).

$$FYN^* = (\text{NOT } PAG:CSK) \text{ OR} \quad (1)$$

$$[CD45 \text{ AND } (\text{NOT } PAG:CSK) \text{ AND } (\text{NOT } CBL)]$$

From the reconstructed pathway consisting of 206 molecules (nodes) and complex mesh-like network formed of 435 protein–protein interactions, our model consists of such 167 logical equations (hyper-arcs), which control the expression pattern of the dependent variables, otherwise called the ‘target molecules’ (nodes). The remaining 39 independent ‘Input’ molecules (which did not have any transition functions governing update rules) were considered as the inputs to the system, which includes 13 ligand molecules (e.g. MHC CLASS II-Ag complex, LIGHT, B7_1, B7_2, CD70, etc.) that come into play in the extracellular environment (APC surface in case of T-cell), 2 non-protein molecules and

remaining are core T-cell protein molecules. Another 39 molecules (e.g. BCL2, FKHR, P21, BCLX, IL1, IL2, etc.) were considered as the ‘Output’ of the system, many of which have a feedback that has a positive or negative impact on cell proliferation. The equations were written using Python code and simulated using the BooleanNet-1.2.4 software (Albert *et al.* 2008).

2.3 Functional response

Three additional nodes were added to the model signifying, Cell Proliferation (‘Proliferating T-Cell’), Cell Survival (‘Inactive T-Cell’) and Cell Death (‘Dead T-Cell’). The Logical Equations for these nodes were written using the appropriate ‘Output’ molecules (related to that particular phenotype) of the model, depending on the biological functions of the molecules and the phenotype they are associated with, respectively. The details of the logical constructions of these nodes and corresponding equations according to their biological functions are discussed subsequently.

2.3.1 Cell proliferation: After encountering an Antigen Presenting Cell (APC), T-cell proliferation increases. This process is regulated by different Cyclins (CYCLIN_A, CYCLIN_D1 and CYCLIN_D2) and Cyclin Dependent Kinase (CDK_4) that mediate cell division (Berridge 2014; Wells and Morawski 2014), the anti-apoptotic molecule (BCLX) that prevents cell death (Rogers *et al.* 2001), interleukins, such as, IL2, IL4 and IL6 (Kupper *et al.* 1987; Cantrell *et al.* 1988; Van Epps 2006) and TNF-like molecules (FASL) that enhances the proliferation of the immune cells (Suzuki *et al.* 2000). The logical equation governing the fraction of cells in the proliferative state after receiving the stimulus from an APC is as follows:

$$Proliferating\ T\text{-}Cell = [IL2 \text{ AND } CYCLIN_A \text{ AND } CYCLIN_D1 \text{ AND } CYCLIN_D2 \text{ AND } BCLX \text{ AND } CDK_4 \text{ AND } IL4 \text{ AND } FASL \text{ AND } IL6] \quad (2)$$

2.3.2 Cell survival: When a T-cell has not encountered an APC and has not received any stimuli, it remains in its naïve resting state and do not proliferate, although its normal cell survival and cell division may still continue to occur. This resting state of T-cell is maintained mainly by the anti-apoptotic factors (BCL2 and BCLX) that

keep the T-cell alive, while the normal cell homeostasis is maintained by the TNF molecules (e.g. TNF_ALPHA) (Shi *et al.* 2007), and cell cycle proteins: Cyclins (CYCLIN_A, CYCLIN_D1 and CYCLIN_D2) and CDKs (CDK_4) (Berridge 2014). The logical equation for this phenotype of T-cell is written as follows:

$$Inactive\ T\text{-}Cell = [CYCLIN_A \text{ AND } CYCLIN_D1 \text{ AND } CYCLIN_D2 \text{ AND } BCL2 \text{ AND } BCLX \text{ AND } CDK_4 \text{ AND } TNF_ALPHA] \quad (3)$$

2.3.3 Cell death: The probability of T-cell proliferation and survival decreases and that of cell death increases whenever the proteins promoting T-cell proliferation as well as survival are absent, and an immunosuppressive condition is produced by the presence of certain molecules, like IL10 (Akdis *et al.* 2000). Such a situation has been termed as ‘T-cell death’ or ‘Dead T-Cell’ in our model. Hence, following the logical relationship the equation for such a phenotype is written as:

$$\begin{aligned} & \text{Dead T-Cell} \\ & = [\text{IL10 AND (NOT Inactive T-Cell) AND (NOT Proliferating T-Cell)}] \end{aligned} \quad (4)$$

2.4 Update rule of transition functions

The Boolean transition equations were updated at each step, first ‘Synchronously’ (for the purpose of validation), and later ‘Asynchronously’ (for further analysis). In the synchronous model, the assumption is that all molecules are updated at the same time. However in a signalling network the protein expression levels are likely to change at different points of time and updates randomly (Albert *et al.* 2008), hence to capture such scenario, in the asynchronous model we have assumed asynchronous/random update/execution of the Boolean transition equations.

2.5 Microarray data extraction

After constructing the model, the next most important step was to assign initial values to the individual nodes. The value of all the nodes at step 0 (time point 0 h) was initialized using the binarized values of the extracted microarray data obtained from EBI-ARRAYEXPRESS microarray database [ArrayExpress ID: E-GEOD-48978] (Parkinson *et al.* 2005). The differential gene expression data obtained from the database was a time-course microarray data of gene expression kinetics of human T helper cells at six time points (i.e. at 0, 2, 4, 6, 24 and 72 h respectively) over a time period of 3 days. Array used in the experiment was an Affymetrix HT HG-U133+ PM Array Plate (Zhao *et al.* 2014). However, it was observed that the protein expression values of the microarray data decline after the 6 h time-point. Since the constructed model is of T-cell activation, and we are interested in the study of interleukin expression (which is highest at 6 h time point (Yeh *et al.* 2008)), we have not considered the expression data of 24 and 72 h time-points, and only the

values of 0, 2, 4 and 6 h values were used for further analysis.

2.5.1 Binarization of expression data: The expression data at time points 0, 2, 4, and 6 h of the RNA transcripts corresponding to the proteins in our model was extracted. Out of the 206 molecules in our model, data of 168 molecules was obtained. The remaining molecules were not found in the array which consisted of 7 APC molecules, 7 inorganic molecules, 11 protein complexes, 7 nuclear components of transcription factors of NFkB, NFAT, etc. (their cytoplasmic counterparts were already considered among the 168 molecules extracted), and 6 other protein molecules. The expression values of the 168 molecules considered for binarization were the mean of the expression values of the RNA transcripts of different isoforms/or subunits of the corresponding protein molecules. The mean value of the individual molecules at each of the four time points was chosen and then binarized in ‘R’ using the BoolNet 1.63 package’s binarization function (Müssel *et al.* 2010). The binarization was done using K-means clustering method (discussed in the next sub-section).

The binarized data at 0 h time point was used to initialize the system (i.e. value of the simulation at time step 0). The initial value of the 7 APC molecules (viz. MHC CLASS II-Ag, B7-1, B7-2, CD70, LIGHT, PDL and TNFSF9) and 3 non-protein molecules (CRE, CALCIUM-OUT and DAG) were considered ‘ON’ to activate/provide a stimulus to the T-cell signalling cascade. All the remaining molecules, the expression data of which could not be obtained from the microarray expression data could safely be initialized as ‘OFF’, since all of them will get updated in the next step of iteration using the transition functions considered in the model.

2.5.2 K-means clustering: K-means clustering is used to partition a given set of input data in K -th partitions or cluster. However, in our analysis we used this powerful statistical technique to binarize the time course micro array expression data (Zhao *et al.* 2014) and then used the binarized data as input for Boolean model. In order to perform the K-means clustering on the time series microarray expression data, we have used Boolnet (a software package of ‘R’) (Müssel *et al.* 2010).

2.6 Simulation of the model

2.6.1 Validation: In order to validate the model, both the synchronous and asynchronous models were run for

different time steps and the time step at which the simulation reached its steady state was determined. The asynchronous model was simulated for 100 times (range = 100) and the mean of the expression value for each time point of each node was taken. With the 0 h value as initial value and the APC molecules as 'ON', the 39 output molecules of the model were validated with 0, 2, 4 and 6 h binarized expression data, the time when the interleukin production is highest/ at its peak and the T-cell is most active (Fukushima 2003; Yeh *et al.* 2008). Here each time step was assumed to be equal to 0.5 h. This calibration of the time scale was optimized only after determining the time step at which the model reached its steady state.

2.6.2 Perturbation analysis: The model was further analysed by perturbing it with different combinations of knock-in and knock-out mutations. The *in silico* knock-in and knock-out mutation were generated keeping the value of the target molecule as constitutively 'ON' or 'OFF' throughout the simulation by using the built-in library function 'boolean2.modify_states' in the BooleanNet-1.2.4 software (Albert *et al.* 2008). To analyse the significant variations ($p < 0.05$) in the temporal protein expression patterns observed in mutated scenario with respect to the normal scenario, Mann Whitney U Test was performed and important proteins with significant variations are extracted (McKnight and Najab 2010). Through this study, we can identify the proteins, which are being regulated upon certain perturbations, and can simultaneously identify the routes along which the effect of that perturbed signal is processed.

3. Results

3.1 Reconstructed T-cell signalling pathway

The T-cell pathway that has been reconstructed (shown in figure 1) provides a complete picture of the entire signalling cascade. In this pathway, we have taken into account all the co-stimulatory and co-inhibitory receptors that are expressed on the surface of the T lymphocyte and paired them with their corresponding ligand molecules expressed on the surface of the APC. These co-stimulatory pathways play a pivotal role in regulating the T-cell activation, effector function and survival, without which TCR alone cannot provide the signal for the full activation of the cell (Chen and Flies 2013). The pathway clearly shows the Antigen (Ag) in complex with the MHC Class II molecule, the 5 co-stimulatory (CD70, LIGHT, TNFSF9, OX40L and ICOSL) and 1 co-inhibitory (PD1) ligand molecules that are expressed on the APC. The B7_1 and B7_2 molecules have a dual role to play. These molecules can interact with two types of co-receptors on the T-cell surface, viz. the CD28 co-stimulatory co-receptor and the CTLA4 co-inhibitory co-

receptor (Chen and Flies 2013). In the pathway (figure 1), the molecules have been coded in different colours according to their location in the membrane (dark green), cytoplasm (yellow) and nucleus (orange). The pathway shows 39 output molecules (coloured light green), many of which have feedback loops (colour-coded as deep pink lines) that regulate the proliferation of the T-cell pathway in an auto-regulatory fashion (e.g. IL2 has a positive impact, whereas PD1 and CTLA4 have a negative effect). The functions of the co-stimulatory co-receptors have further been elucidated by different perturbation studies discussed subsequently. The pathway we report consist of 206 molecules (nodes) and complex mesh-like network formed of 435 protein-protein interactions, which is the highest as compared to other T-cell signalling pathway models reported till date in different databases and literatures (Kanehisa and Goto 2000; Saez-Rodriguez *et al.* 2007).

In order to decompose this complex pathway and study the propagation of signal through this complex network of proteins and molecules, it was essential to further analyse this pathway using Network Analysis and the semi-dynamic Boolean approach (Chowdhury *et al.* 2013). But since our aim was to study the dynamics of the signal propagation over time we did not perform network analysis, which is a static approach. Rather, we used this pathway to construct the logical model to understand the dynamics of protein expression during the transition of a T-cell from its inactive to its activated state.

3.2 Model analysis

3.2.1 Simulation and state transition: The Boolean model constructed was simulated first synchronously and then asynchronously. The input for both the cases was the 0 h binarized data extracted from mRNA expression profile of normal human T-cell (Zhao *et al.* 2014). The models were iterated for 21 rounds of update (time-steps) to see the pattern of signal flow in the network, starting from the receptor and co-receptors down to the cytoplasmic proteins, leading to the activation of the transcription factors and finally the expression of the 39 output proteins. The model reached its steady state at 14th rounds of updates (i.e. 7 h) for the synchronous and at 10th time points (i.e. 5 h) in the case of asynchronous simulation. It is worthy to note that experimental data is also taken up to 6 h durations with 2 h interval. In order to compare the synchronous and asynchronous temporal protein expression pattern with the experimental data, we have plotted the experimental as well as simulation data in figure 2, where the state transition pattern of the 39 output molecules (see supplementary table 1) were plotted as a continuous heat plot (figure 2A: microarray data, figure 2B: synchronous data, figure 2C: asynchronous data). While the synchronous deterministic model simulation

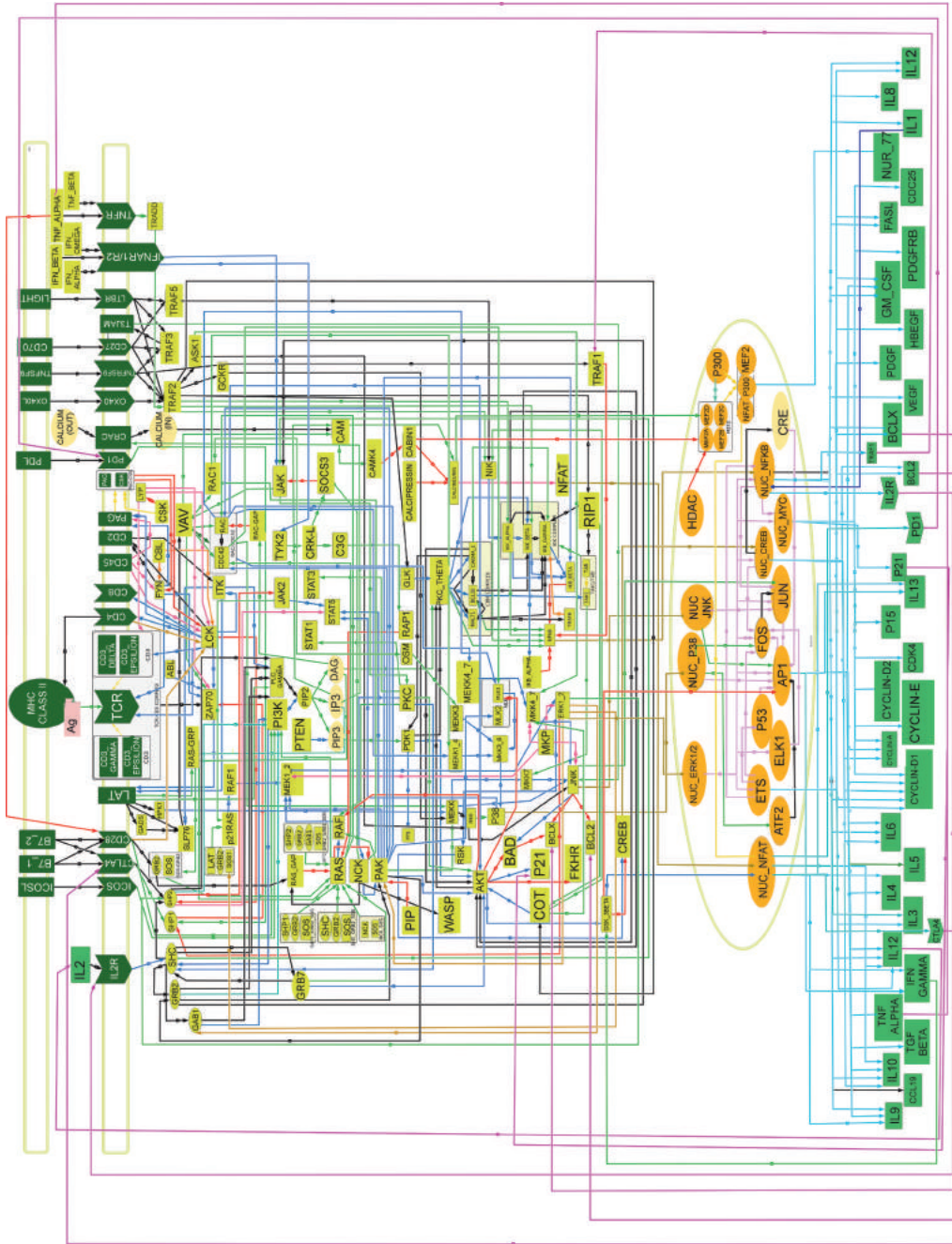


Figure 1. Reconstructed T-cell pathway. The pathway consists of 206 molecules and 435 protein-protein interactions. The interaction lines have been colour-coded according to their types: activation (green), inhibition (red), phosphorylation (blue), transcriptional activation (light pink), feedback (deep pink), nuclear transport (yellow-brown), complex formation (yellow), ubiquitylation (orange), physical interaction (black). The protein molecules in the network have been differently colour-coded according to its location: membrane (dark green), cytoplasm (yellow), nucleus (orange), and output molecules (light green). For denoting the non-protein molecules a light yellow-coloured oval shape has been used.

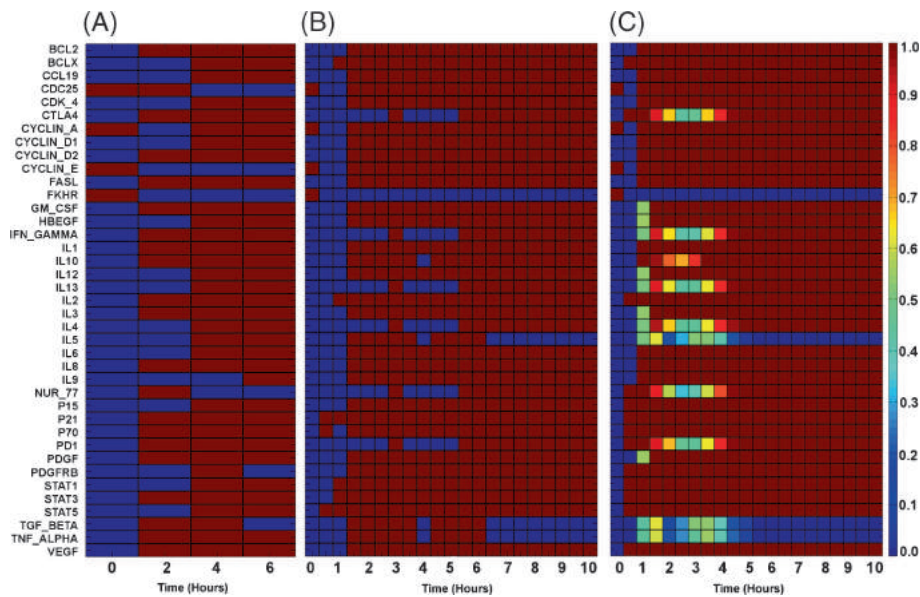


Figure 2. Continuous heat plot showing state transition pattern of output proteins. (A) Binarized microarray data of 39 T-cell output proteins at 0, 2, 4 and 6 h, (B) temporal protein expression pattern observed in synchronous update up to 21 time points (0 to 10 h), (C) temporal protein expression pattern observed in asynchronous update up to 21 time points (0 to 10 h). Red-coloured cell denotes an up-regulation in protein expression, while blue signifies down-regulation.

(figure 2B) show distinct up and down-regulation of the protein expressions of one run of simulation, the heat-plot of the asynchronous simulation (figure 2C) show a gradual change of protein expression pattern as a result of averaging the values of protein expression for each node at each of the 21 time-steps for 100 runs of the simulation. The pattern thus generated shows the dynamics and fluctuations in the protein expression over the time period of T-cell activation. By using this asynchronous update, we are able to rule out certain limitations of the deterministic or synchronous Boolean modeling approach (the ‘all’ or ‘none’ output), as by this method we are able to generate a protein expression pattern that clearly shows that even though some proteins in figure 2B shows a complete down-regulation at certain time points, it becomes evident from figure 2C that some amount of protein expression is still occurring in low amount (e.g. in figure 2B the proteins CTLA4, PD1, IFN-Gamma apparently show an absence of expression at certain time points between 1.5 and 5.0 h, whereas figure 2C shows that the expression is not completely absent, and a low level of expression continues to occur at those time points – comparable with the microarray data). Also, figure 2C eliminates the delay in protein expression of many interleukins and STAT proteins as shown in figure 2B, and gives us a better understanding of the change in expression dynamics of the vital T-cell output proteins over time.

3.2.2 Phenotypic enrichment of output proteins: The 39 output proteins were classified according to the function regulating the behaviour of a T-cell (supplementary table 1). The proteins

were grouped into five classes: (a) *T-cell proliferation*: consists of 12 proteins, which includes proteins/molecules responsible for the T-cell survival, anti-apoptotic molecules, cell cycle proteins, TNF molecules (Suzuki *et al.* 2000), transcription factor STAT5 (Welte 1999), etc.; (b) *Negative regulator of T-cell proliferation*: consists of 7 proteins including PD1 and CTLA4 co-receptors that aid in co-inhibition of T-cell pathway (Parry *et al.* 2005), immunosuppressant TGF_BETA (Delisle *et al.* 2013), NUR_77, which is a calcium-mediated T-cell apoptotic factor (Youn and Liu 2000), etc.; (c) *Immune Response*: consists of molecules responsible for initiating immune responses in the system, examples include GMCSF (Shi *et al.* 2006), Interferon IFN-Gamma (Green *et al.* 2013), and STAT1 and STAT3 transcription factors responsible for transcription of genes involved in eliciting the immune response (Barbi *et al.* 2009); (d) *Interleukins*: includes 11 interleukin molecules possessing different functions, e.g. IL2, IL4, and most of the other interleukins positively regulates T-cell proliferation and are involved in immune responses, while IL10 is involved in T-cell apoptosis (Akdis *et al.* 2011) and (e) *Growth factors*: includes proteins (e.g. PDGF, PDGFRB, VEGF, HBEGF) secreted by the T-cell that often acts as potent mitogenic factors for other cell and mediates immunosuppression (Blotnick *et al.* 1994; Daynes *et al.* 1991; Mor *et al.* 2004; Ohm *et al.* 2003).

3.2.3 Comparison with experimental observations: The 14 time-steps that were required for the model to reach its steady

state was scaled to 7 h time for the purpose of validation of the model. The time scale division was chosen keeping in mind the experimental evidences, which indicate 6 h to be the time required for the full activation of a *naïve* T lymphocyte, when the production of the interleukins is at the highest peak (Fukushima 2003; Yeh *et al.* 2008). In order to compare the simulation results of our model with the experimental data, the 16 time points (up to 8 h; each time-step corresponds to 30 minutes) of both the synchronous and asynchronous simulation results have been plotted along with four discrete time points (0, 2, 4 and 6 h) from the experimental observation (figure 3 and supplementary figure 1).

The results of our simulation obtained at the time step 12 (~6 h) of the 39 output proteins were then validated with the 6 h binarized experimental data. Here, while comparing deterministic or synchronous simulation vs. experimental data, we found the logical states of 34 proteins (from synchronous updates) out of the 39 output proteins were matching with the 6 h protein expression results observed in the experimental data. The percentage of validation of our simulation results with the experimental data have been provided in table 1. Out of the remaining proteins, the expressions of which appeared to differ with the deterministic model, TGF_BETA matches with the asynchronous model with a small time lag, while NUR_77 protein showed down-regulation in protein expression slightly earlier than the expected 6 h time step. Both the synchronous and asynchronous simulations showed a clear match in the nature of the curves. Also, we found that the deterministic model showed a beautiful match of 14 very essential T-cell proteins (viz. BCL2, CYCLIN_D2, FASL, FKHR, GMCSF, IL1, IL2, IL3, IL8, P21, P70, PDGF, STAT3 and VEGF) with the experimental microarray data at all the four time steps i.e. 0, 2, 4 and 6 h respectively. In supplementary table 1, the corresponding phenotypic responses of these 14 protein molecules are mentioned. It is interesting to see that the T-cell proliferating factors (such as anti-apoptosis, cell cycle progression, cell survival etc.) governed by the proteins BCL2, CYCLIN_D2, FASL were up-regulated during T-cell activation in both the synchronous and asynchronous simulation results, and successfully validated against the experimental findings (figure 3). On the other hand, the expression of apoptotic factor FKHR was also found to be down-regulated in our simulation result and well matched with the experimental observations (figure 3). Down-regulation of this protein is required during the T-cell proliferation process after T-cell activation. Simultaneously, the up-regulation of immunoresponsive proteins, such as, GMCSF and STAT3, and the interleukin expressions (e.g. IL1, IL2, IL3, and IL8) are also important during the T-cell activation process. In our simulation outcomes, we have found the exact outcomes, which are well corroborated with the experimental data (figure 3). However, to maintain the homeostasis of T-cell proliferation, the cell cycle progression

inhibitor P21 was found to be simultaneously up-regulated in our simulation results. Important growth factors, such as, PDGF and VEGF, which were found to be up-regulated in the experimental data, were also shown to be up-regulated in the simulation outcomes. Hence, on the basis of these validation results, it can be concluded that the model outcomes generated by using synchronous and asynchronous update rules are correctly predicting the temporal protein expression patterns in T-cell signalling network during T-cell activation procedure and thus prove the robustness of our *in silico* model.

3.3 Phenotypic pattern generation

3.3.1 Scenario Creation: The equations of the three nodes, viz. Cell Proliferation, Cell Survival and Cell Death, related to the T-cell phenotypes, which have been defined in section 2 contains various combinations of these output molecules according to the functions that they are associated with. The values of these three nodes were then plotted in different scenarios that were created by performing various perturbations to the system.

(i) Validation of equations depicting different phenotypes

- a) **LAT mutation:** The equations for the study of the phenotypes were validated by comparing the change in the phenotypes observed in experimental studies after performing different perturbations to the model and asynchronous simulation. For this purpose, a study on LAT mutation was chosen, and we attempted to reproduce the experiment to observe the changes in the phenotypic expression patterns (Sommers *et al.* 2002). In this *in silico* experiment, the trans-membrane protein LAT was knocked out by keeping it constitutively in the 'OFF' state, so that it cannot transduce any signal downstream. The knock-out mutation of LAT, a very important protein molecule regulating the T-cell signalling cascade, leads to poor proliferation of the active T-cell population (figure 4A). This poor proliferation of the T-cell population could only be reverted by turning the CRAC channel constitutively ON (which reproduces the same effect as using Inonomycin reported in the experiment), leading to an increased influx of calcium, which activates the calcium pathway inside the T-cell (Sommers *et al.* 2002).

Although the stimulation of the TCR:CD3 complex and the CD28 co-receptor molecules in LAT knocked-out T-cells (figure 4B) reached its proliferation dynamics (shown as green lines) at steady state (i.e. proliferation reached steady state at 10th h time-step, which signifies delayed proliferation in figure 4A, and at 9th h time-step signifying early proliferation in figure 4B)

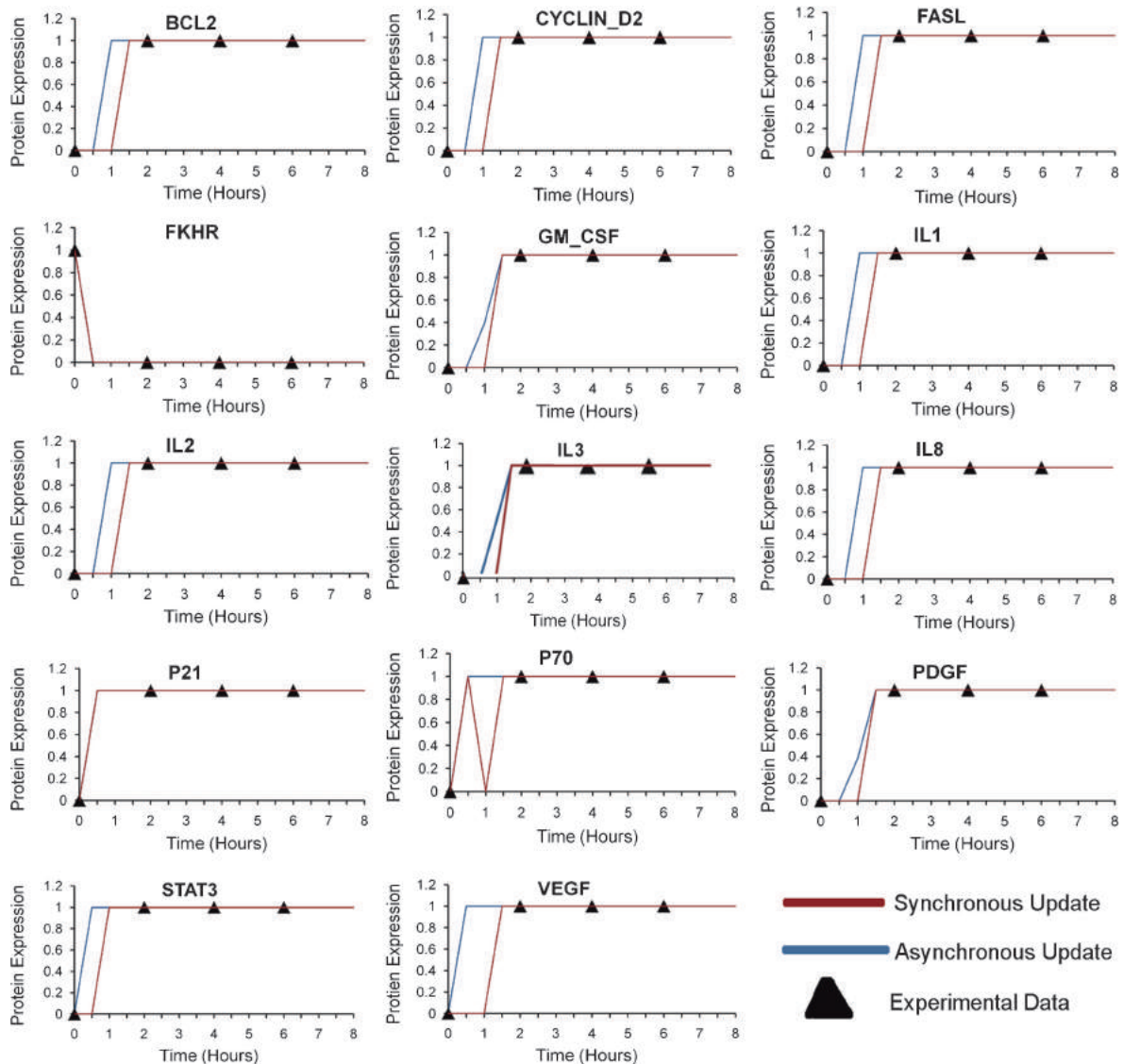


Figure 3. Protein expression dynamics observed in Experiment, Synchronous and Asynchronous simulation. ‘Experimental’ data is the binarized time course microarray expression data of total 39 output proteins of the model, which is compared against the ‘synchronous’ and ‘asynchronous’ simulation results. Out of the 39 output proteins, the expressions of total 34 proteins match at 6th h, while the temporal expression patterns of 14 proteins (viz. BCL2, CYCLIN_D2, FASL, FKHR, GMCSF, IL1, IL2, IL3, IL8, P21, P70, PDGF, STAT3 and VEGF) from the simulations match exactly with the experimental data at all the four time points (0, 2, 4, and 6 h). The expression dynamics of the remaining 25 proteins are presented in supplementary figure 1.

earlier than the no stimulation scenario (figure 4A), but it was unable to completely overcome the deficit in proliferation of the T-cell population between the duration 4th to 8th h time-steps. On the other hand it is reported in the experiment that the CRAC channel was enough to induce a much better proliferation in the LAT mutated condition both in presence and absence of additional stimuli, which was also observed through our simulation (figure 4C-4D) (Sommers *et al.* 2002).

Similarly in the cases of inactive T-cell frequency and T-cell death frequency curves in figure 4A and 4B show two local maxima near the 2nd and 7th h time-points, signifying higher chances of the T-cell to remain in the inactive state or die. Whereas in the CRAC active situations (figure 4C and D) the inactive T-cell frequency and T-cell death frequency curves show only a single peak around 2nd h time-point signifying that in CRAC stimulated situation the probability of

Table 1. Validation of results

Total number of species	206
Number of output* molecules	39
No of output molecules matching at 6 h	34 (87.18%)
No of output molecules matching at 4 h	27 (69.23%)
No of output molecules matching at 2 h	20 (51.28%)
No of molecules matching at every time point	14

* Protein molecules (e.g. Interleukins, cytokines, growth factors) which are expressed at the end of the signalling pathway.

T-cell inactivation is much reduced. The result of the simulation has also been summarized in table 2.

- b) **Effects of co-receptor signalling:** The ‘two-signal model’ states that, for the activation of naïve T-cell, two signals are required: (i) signal elicited from the interaction of the TCR: CD3 complex with the MHC:Antigen complex presented on the APC membrane; and (ii) the co-stimulatory signals emanating from APC that leads to the activation of the co-receptors present on the T-cell surface (Chen and Flies 2013). Without this second co-stimulatory signal, the T-cell cannot sustain its proliferation for long, and this will ultimately lead to a state of unresponsiveness, called ‘T-cell anergy’ or cell death (Yamagishi and Watanabe 2012).

In order to capture the effect of these co-receptor molecules and ion channel on cell phenotype dynamics, we have performed a perturbation analysis, the observations of which have been tabulated in table 3 and the corresponding graphs have been plotted in figure 5A–G. Here we observed that complete sustained proliferation of the T-cell population can only be achieved when TCR along with the co-receptor molecules and the CRAC channel are activated together (figure 5F and 5G). TCR when activated alone (figure 5B) showed a phenotypic behaviour similar to the no stimulation condition (all stimulations ‘OFF’, figure 5A), where a high frequency of inactive cells was observed, and the frequency of proliferative cells was low (Yamagishi and Watanabe 2012). On the other hand, CRAC when activated alone (figure 5C) can lead to an increase in T-cell proliferation initially (Qu *et al.* 2011), which after sometime started oscillating with cell death curve due to prolonged exposure to calcium influx, which activates NFAT that controls two opposing T-cell phenotypes, i.e. cell proliferation and cell death (Qu *et al.* 2011; Yamagishi and

Watanabe 2012). The situation was also similar when TCR:CD3 and CRAC were activated simultaneously (figure 5E). The importance of CRAC channel in the regulation of T-cell proliferation becomes evident further in figure 5D, where we observed that in spite of all the stimulations being present, CRAC knocked-down mutation blocked cell proliferation completely. The oscillation of proliferation and death curve observed in figure 5C and 5E could be overcome by activating the co-stimulatory receptors (figure 5F and 5G), where a full proliferation occurred and the cell death curve declined (Rogers *et al.* 2001).

(ii) **Effect of multiple mutations on Interleukin Production**

Biological networks are highly robust systems, and thus a single mutation usually cannot perturb the entire signalling cascade as many alternative paths exist (Barabasi and Oltvai 2004). Diseases are mostly caused as a result of multiple mutations. The effects of such multiple mutations have also been observed in the deregulation of different cell types including T-cells, where severe pathological manifestations have been observed by several research groups (Loeb *et al.* 2003; Buckley 2004; Chowdhury *et al.* 2013). Simultaneously, in other experiments, significant variations in interleukin production in different pathological conditions or diseases have also been reported (Hirano and Kishimoto 1989; Hirooka *et al.* 1993; Street 1995). However, the effects of multiple mutations on interleukin productions mechanism are not observed thoroughly by any other experiments and hence the mechanism, which govern these phenomenon is not clear yet. Although the effect of few co-stimulatory molecules (e.g. CD28-B7, CD40-CD40L), which regulate the interleukin production (Cella *et al.* 1996; Harris and Ronchese 1999), and the deregulation in interleukin expression as a consequence of their mutation have been discretely studied, but the multiple mutation of other co-stimulatory molecules on interleukin production is yet to be analysed extensively. Hence, in this study we have focused on the mutations of co-stimulatory proteins CD27 and LTBR and analysed their effect on interleukin production. It is worth to mention that although here we have created one multiple mutation scenario, but one can also generate different conditions using our *in-silico* model by altering the logical states of different pathway components.

- a) **CD27 and LTBR knock-out scenario:** The co-stimulatory receptors CD27 and LTBR (influencing the NF κ B pathway) are involved in increased T-cell proliferation (DeBarros *et al.* 2011; Wang and Fu 2004), and the mutations of these molecules have

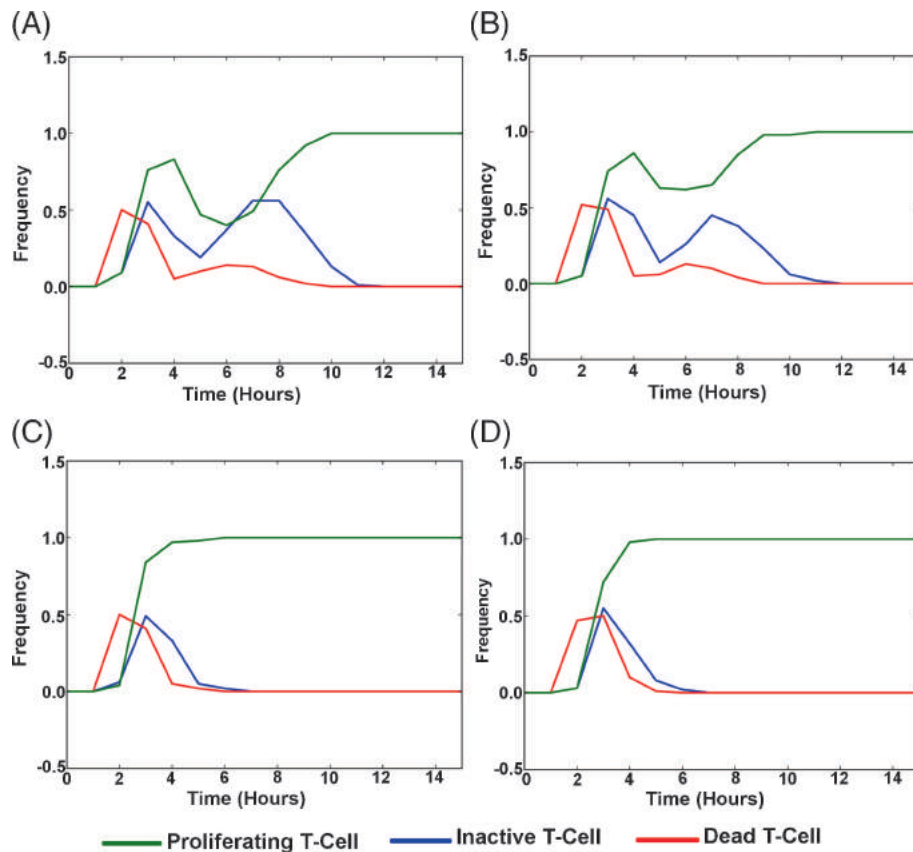


Figure 4. Cell Phenotype in different situation under LAT mutated condition. Frequencies of Proliferating T-cells, Inactive T-cells, and Dead T-cells in LAT knock-out and (A) without any stimulation; (B) TCR:CD3 and CD28 stimulation; (C) TCR:CD3, CD28 and CRAC channel stimulation; (D) only CRAC channel stimulation conditions respectively. The frequencies of Proliferating T-cell, Inactive T-Cell and Dead T-cell are shown in Green, Blue and Red lines, respectively.

been implicated in different immune-deficient conditions (Seymour *et al.* 2006; van Montfrans *et al.* 2012). In this study, we have observed that CD27 and LTBR together are responsible for the regulation of cytokine production. Using this *in-silico* knock-down model of CD27 and LTBR proteins, we observed that the mutation of these molecules may lead to significant decrease in cell proliferation (figure 6B) as compared to the normal scenario (figure 6A), by decreasing the interleukin production (figure 6C–D). As compared to the normal scenario of interleukin expression pattern (figure 6B), the mutational analysis showed these co-stimulatory receptors can regulate 6 out of 11 interleukin molecules considered in our model, out of which the expression patterns of five interleukins showed an oscillatory behaviour (viz. IL1, IL12, IL3, IL6 and IL8) while IL2 showed a delay in activation (figure 6D). The down-regulation of these six interleukins, which are mostly involved in T-cell

proliferation (see supplementary table 1 for individual function), accounted for the decrease in T-cell proliferation and rise in T-cell death phenotype as shown in figure 6C. As the mutation of these molecules are not involved in controlling the normal cell cycle proteins, the function defining the probability of T-cell survival (denoted by the frequency of Inactive T-cell) remains unchanged.

- b) **Fluctuations in intermediate proteins and other output proteins:** To find out the reason/ mechanism for the deregulation of the interleukin production and the change in phenotypic dynamics (mentioned above), we performed the Mann Whitney U test, where we found that the mutation of these two genes leads to an altered expression of 25 genes in the entire network. Here, we observed that in addition to the NFKB pathway (NIK-mediated non-canonical NFKB pathway) molecules, CD27 and LTBR can also regulate the expression of the MAPK pathway molecules (MEKK, MKK4/7, COT, GCKR) and the JNK

Table 2. LAT mutation analysis

Mutation		Observation	Reference
Knock-in ('ON')	Knock-out ('OFF')		
-	LAT	Poor proliferation (figure 4A)	Sommers <i>et al.</i> 2002
TCR:CD3, CD28	LAT	Poor proliferation (figure 4B)	
TCR:CD3, CD28, CRAC	LAT	Improved proliferation (figure 4C)	
CRAC	LAT	Improved proliferation (figure 4D)	

pathway molecules (T3JAM), which again is responsible for the regulation of a collection of other important T-cell molecules that regulates its proliferation, survival and effector functions. The remaining molecules that are regulated by these two co-receptor molecules include TRAF2, TRAF3, IL2R, GMCSF, CCL19, VEGF, GLK, RIP1, TAK:TAB complex and IKK-Alpha, all of which plays a very important role in the regulation of T-cell activity. CD27 and LTBR also regulate the expression of TRAF1 protein, which is known to have an inhibitory effect on NFkB (Zapata and Reed 2002). From our model, we further observed that a knock-out mutation of TRAF1 can nullify this effect (i.e. the effect of CD27 and LTBR mutation) of down-regulation of cell proliferation to a great extent (data not shown).

4. Discussion

Integration of apparently diverse two biological phenomena – gene/protein expression and phenotypic responses can only be done by analysing different signalling pathways (e.g. Hedgehog, Notch, T-cell receptor pathway, etc.), which play a vital role in receiving the signal from extracellular regions, processing the signal in the cytoplasm followed by the regulation of gene transcription network inside the nucleus (Chowdhury *et al.* 2013). Hence, successful execution of these reaction mechanisms requires proper regulation of the activity of some biomolecules (e.g. genes, proteins, ions, metabolites, etc.) at precise time points. As a matter of fact, it is obvious that certain deregulation of these concerted efforts may trigger various abnormalities in our body and can cause various diseases such as cancer, tumour, auto-immune diseases, etc. (Parekh 2010; Chowdhury *et al.* 2013). In order to know these diseases properly, it is indeed necessary to understand the temporal protein expression patterns which are associated with these severe diseases through different signalling pathways.

However, monitoring the temporal protein expression patterns at the time of signal propagation in intracellular

signalling pathway is a time-consuming and complicated process. Hence, in this context, a well-established computational approach can perform better and can generate expected results for studying different intracellular pathways within a short interval of time (Orton *et al.* 2005; Chowdhury *et al.* 2013; Chowdhury and Sarkar 2013). The importance of T-cell signalling pathway study needs no special mention. Several modelling and computational studies (Sherriff and Sarkar 2008) on the core T-cell signalling network have revealed numerous hidden facts about this pathway, but so far no study has considered the importance of all the co-receptor signalling pathways including the core network during T-cell activation. A previous study using systems level model on the sequential phosphorylation of T-cell antigen receptor (TCR) by LCK molecule has revealed the importance of having multiple phosphorylation sites on TCR and the successive differential binding of ZAP70 on those phosphorylated sites with ultrasensitivity or switch-like response architecture in TCR signalling network (Mukhopadhyay *et al.* 2013). In another study, the activation mechanism of primary T-cell by TCR, CD4/CD8 co-receptor, and CD28 molecules after encountering with APC has been studied using Boolean formalisms (Saez-Rodriguez *et al.* 2007). In the successive study, the same model has also been studied as a continuous model by transforming its Boolean formalisms to evaluate the temporal behaviour of the entire TCR network by measuring the time course concentration level of its component protein molecules (Wittmann *et al.* 2009). In order to encounter the stochastic effect of the protein expression pattern of T-cell signalling network in large granular lymphocyte (T-LGL) leukemia condition, a study has also been performed by using the asynchronous Boolean update rules on the T-cell network (Saadatpour *et al.* 2011). In this study, the author has mainly used core TCR network to study the network dynamics of T-LGL and successively identified 19 possible therapeutic drug targets. However, it should be noted that all of these models have mainly considered the core T-cell pathway, although the experimental studies have already revealed the importance of other co-stimulatory and co-inhibitory accessories, which also require in parallel for the proper functioning of core T-cell network (Chen and Flies 2013). The effect of temporal protein expression patterns of the T-cell output molecules by

Table 3. Importance of co-receptor signalling in cell proliferation regulation from *in silico* mutation studies

Scenario	TCR: CD3	CD4	CD28	OX40	CD40	IFN γ /R2	LTBR	TNFR SF9	TNFR	IL2R	ICOS	PDI	CTLA4	CRAC	Observation	Reference
No stimulation	OFF	OFF	OFF	OFF	OFF	OFF	OFF	OFF	OFF	OFF	OFF	OFF	OFF	OFF	No proliferation, but the cells survives in its inactive state (figure 5A)	Bell 2002
TCR:CD3 stimulated	ON	OFF	OFF	OFF	OFF	OFF	OFF	OFF	OFF	OFF	OFF	OFF	OFF	OFF	No proliferation, but the cells survives in its inactive state (figure 5B)	Yamagishi and Watanabe 2012
Calcium channel activated	OFF	OFF	OFF	OFF	OFF	OFF	OFF	OFF	OFF	OFF	OFF	OFF	OFF	ON	T-cell proliferation rises initially, but later begins to oscillate with the death curve. Number of inactive cells decline (figure 5C)	Qu et al. 2011
Receptors turned activated. CRAC inhibited	ON	ON	ON	ON	ON	ON	ON	ON	ON	ON	ON	ON	ON	OFF	No proliferation (figure 5D)	Qu et al. 2011
TCR:CD3 and CRAC activated	ON	OFF	OFF	OFF	OFF	OFF	OFF	OFF	OFF	OFF	OFF	OFF	OFF	ON	T-cell proliferation rises initially, but later begins to oscillate with the death curve. Number of inactive cells decline (figure 5E)	Qu et al. 2011
Co-stimulatory receptor activated	ON	OFF	OFF	ON	OFF	OFF	OFF	OFF	OFF	OFF	OFF	OFF	OFF	ON	T-cell proliferation; T-cell death curve declines (figure 5F)	Rogers et al. 2001
All receptors and Co-receptors activated	ON	ON	ON	ON	ON	ON	ON	ON	ON	ON	ON	ON	ON	ON	Full T-cell proliferation observed (figure 5G)	Chen and Flies 2013

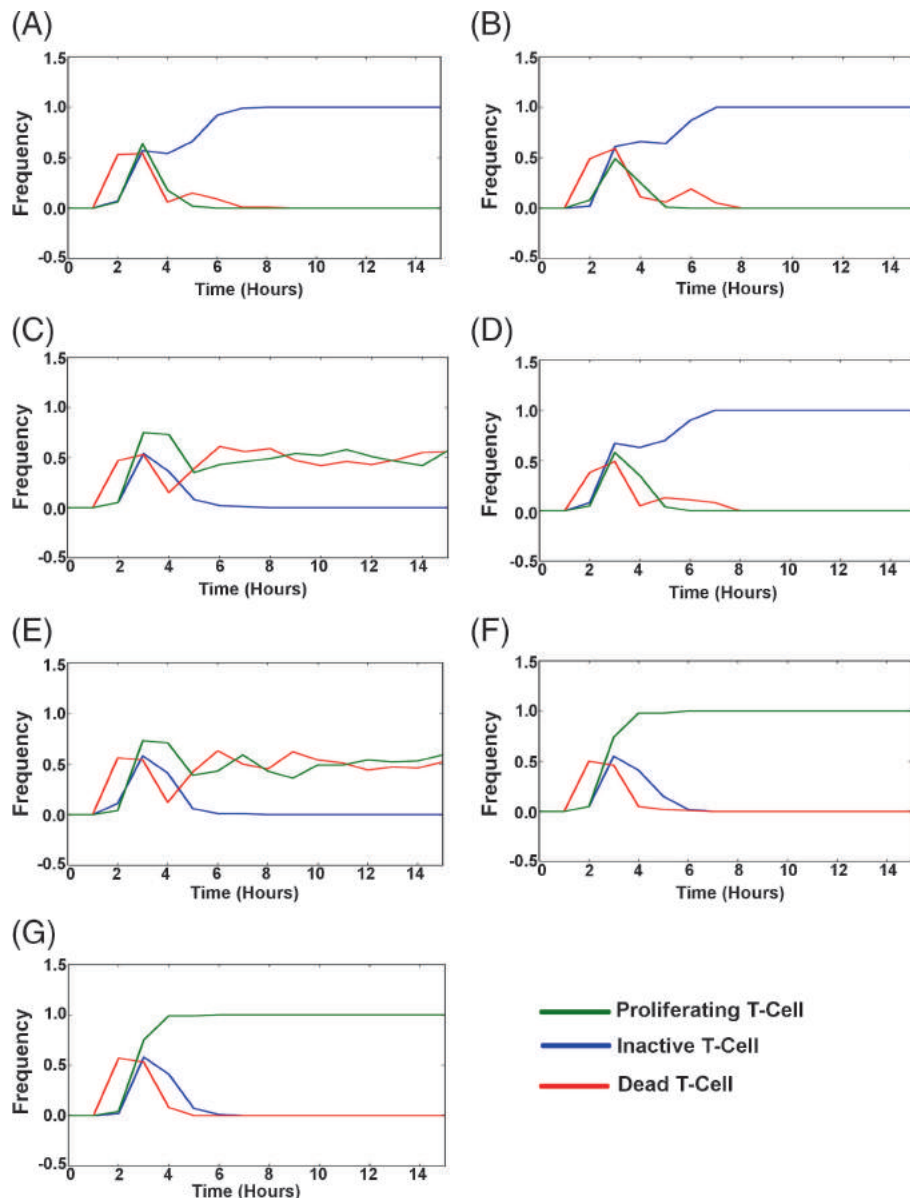


Figure 5. Effect of co-receptor signalling on cell fate determination. Phenotypic responses generated on different mutational analysis scenarios. (A) No stimulation. (B) TCR:CD3 stimulation. (C) Calcium channel (CRAC) as ON state. (D) Receptors and Co-receptors turned ON or activated. CRAC inhibited or OFF. (E) Only TCR:CD3 and CRAC turned ON. (F) Only TCR:CD3, CRAC and OX40 turned ON. (G) All receptors and Co-receptors turned activated or ON.

regulating the T-cell co-receptor pathway is not extensively studied in these models and hence was included in our newly developed model. Moreover, to identify the important regulators in T-cell network, the study of the effects of various components of this pathway with different phenotypic responses of T-cells (i.e. T-cells in proliferative, inactive and dead stages) was also performed in this work. Through this analysis we have also been able to show the necessity of various co-receptor molecules in regulating the normal functioning of T-cell network during T-cell activation.

Hence, to perform the above-mentioned analysis and to overcome the limitations of the previous models, in this work, we first collated the pathway data from various signalling databases and literature sources (including the pathway information from the previously mentioned models) to reconstruct the entire T-cell signalling network consisting of the core TCR mediated pathway along with the pathways triggered by all the co-stimulatory and co-inhibitory receptors (e.g. CD27, LTBR, PD1, CTLA4, etc.) that are crucial for the proper functioning of the T-cell pathway and

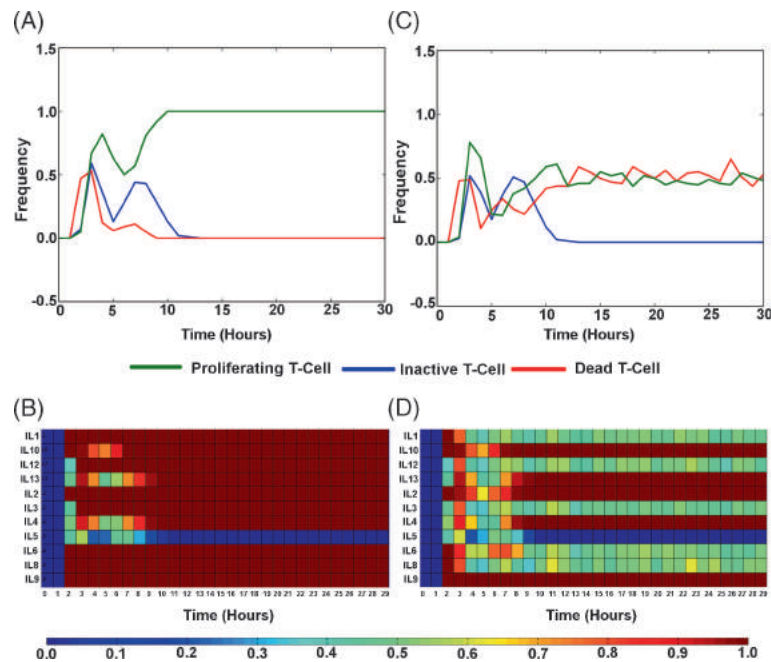


Figure 6. Changes in Cell Phenotypes and corresponding Interleukin Expression pattern due to CD27 and LTBR mutation. (A) and (B) Normal condition; (C) and (D) Cd27 and LTBR mutated condition.

regulation of its effector functions, which includes interleukin production. This reconstructed pathway map is the largest as compared to other T-cell signalling pathway models reported till date. The pathway itself provides a lot of scattered information about the T-cell regulation, compiled into one frame, which are missing in most of the publicly available databases and previously published literatures. Since we have used Protein–Protein Interaction (PPI) data to reconstruct the pathway and build our model, we have been able to provide a comprehensive picture of the T-cell signalling pathway regulation by other cross-talk molecules. We have also considered the calcium signalling pathway, which plays a very important role in the regulation of the T-cell proliferation. By incorporating all the probable co-receptor signalling pathways and the calcium pathway, we were able to capture a more realistic scenario of T-cell regulation, which the other previously published works were not able to show in their respective models. Previous models on T-cell network which considered the core T-cell network including co-receptors CD4/CD8 and CD28 have shown the effects of these molecules in wild type and knock-out T-cell pathway during its activation process, and the identification of the probable activation pathways between the proteins of interest (Saez-Rodriguez *et al.* 2007). That study is limited to only these two co-receptor molecules, but our study has focused more number of co-receptor pathways including CD4/CD8 and CD28, and their downstream effects to regulate other pathways (e.g. MAPK, JNK, NFKB pathways,

etc.). On the other hand, the logical model on T-cell signalling network in T-LGL leukemia cell has tried to search the potential therapeutic targets in T-cell signalling network to perturb the T-cell activation process in T-LGL (Saadatpour *et al.* 2011). However, our model does not address such question in this work, but has the ability to perform such analysis by creating diseased conditions, and *in silico* perturbation study to identify potential therapeutic targets etc. In this work, we have also shown the effects of perturbation analyses by tuning various co-receptors and other pathway molecules to reproduce the experimental observations, which provides an additional advantage of our model for future therapeutic studies. Moreover, the phenotypes such as cell proliferation, survival and death considered in our model as 3 additional nodes allow us to easily monitor the changes in cell fate dynamics due to any mutation related to any diseased condition. Also, the interleukin expression pattern generated using our model provides an immediate idea about the reasons for the change in cell phenotype in any pathological condition.

The reconstructed comprehensive pathway diagram (figure 1) is further used as a master model for the *in silico* simulation studies. In this work, by using the semidynamic logical modelling approach we have performed a computational study of the reconstructed T-cell activation network (i.e. on the master model) to understand the dynamics of protein expression pattern over a time period. For this, the reconstructed T-cell pathway was used to build a model where all the

protein–protein interactions are translated into logical equations using the ‘AND’, ‘OR’ or ‘NOT’ logical gates according to the regulation of a single or a combination of proteins on the expression of another protein, in a biologically relevant way. Extensive literature searches have helped us to extract different types of signal cascade reactions, which govern the regulation of each protein in this pathway. Using this collated information, a total of 167 logical equations were written to transform the whole biochemical reaction cascades of the newly reconstructed T-cell network in terms of logical equations. The model consists total 206 molecules, out of which 39 molecules are inputs (having no incoming signal), 128 molecules are intermediate (having both incoming and outgoing signal) and 39 molecules are output or target nodes (having only incoming signal). The detailed description of the model formulation is provided in section 2 (subsection 3.2). Time series microarray data of naïve T-cell activation process were extracted and binarized using K-means clustering method, which were then used as the initial values for running the simulation both synchronously and asynchronously. The use of binarized microarray data helped us to assign the initial values of the nodes in a more biologically relevant manner and also to validate our model for temporal protein expression pattern during T-cell activation in the normal scenario. The results from the synchronous simulation returned a deterministic value of the protein expression showing a clear up or down-regulation of the protein expression in our model, whereas the asynchronous simulation results showed the gradual variation in the protein expression pattern over time.

Hence, to capture the small fluctuations in protein expression over time, and also to observe the probability of lower levels of protein expressions, which is overlooked in the synchronous update (i.e. deterministic Boolean analysis), we used the asynchronous update rule that eliminates such errors that might creep in due to the use of synchronous or deterministic Boolean approach. This approach gives us the liberty to get a more dynamic way of analysing the large T-cell network as compared to other logical models published earlier (Saez-Rodriguez *et al.* 2007; Wittmann *et al.* 2009; Saadatpour *et al.* 2011; Mukhopadhyay *et al.* 2013). In this study, the asynchronous update of the Boolean transition equations reveals the fluctuations and oscillation patterns of protein expression in many diseased/mutated conditions performed *in silico* (e.g. as shown in the case of CD27 and LTBR mutations in figure 6).

While formulating equations of the cell phenotype behaviour, we are also able to standardize the minimum combination of proteins that are required for the maintenance of the T-cell proliferation, which is also validated using various perturbation experiments reported in different literatures. These equations (2–4) depicting the phenotypic behaviour of the T-cell can further be used in various mutation studies for predicting the behaviour of the T-cell. The reason for the

change in the phenotypic behaviour under such mutated scenarios can then be concluded by a careful analysis of the change in the protein expression pattern over time using our model. Moreover, through our modelling approach, for the first time we have been able to reproduce the effect of CRAC channel in the regulation of the T-cell proliferation, such that its mutation may lead to a complete suppression of proliferation under any circumstances, i.e. even if all the stimulation and co-stimulations are present. The necessity of the different co-receptor molecules in T-cell biology, such as OX40, CD27 and LTBR, becomes clear in the different mutations studies performed by our model simulation, where we have also observed that not only the presence of the TCR:CD3 and the activation of CRAC channel are required for the proliferation of the T-cell, but the activation of the co-receptor signalling pathways is necessary for its continued proliferation (figure 5E–F). Finally through our study, the impact of the co-receptors CD27 and LTBR mutation clearly brings out the role of these molecules maintaining the T-cell functionalities and regulation of the levels of interleukin production, and their prime target molecules are IL1, IL12, IL3, IL6, IL8 and IL2 (figure 6D). Our studies also reveals the precise route of signal propagation of the effects of the mutations where we have seen that a deregulation of the molecules (e.g. MEKK, MKK4/7, COT, GCKR, T3JAM, etc.) involved in the MAPK and JNK pathways, as a result of the mutation, is the cause of the observed changes in the behaviour of interleukin production.

The main drawback of our model is its inability to capture the concentration specific data of signalling molecules for which we need better dynamic model with precise kinetic data. However, despite this drawback, our model is close enough to capture the dynamic regulation of the T-cell activation dynamics and agrees with the published experimental data. In this model, we have tried to integrate various aspects of T-cell activation pathway by using simple but powerful, discrete logical modelling approach. As our model only requires the logical relationship between the proteins at the time of signal transduction and does not depend on any kinetic rate parameter values, it is easier to implement and simulate temporal protein expression patterns with less time and effort. Using our model, one can also perform different predictions and can monitor the temporal protein expression patterns as well as the effect of phenotypic responses *in silico*. By generating the temporal protein expression patterns in the signal flow network for different pathological conditions, it becomes easier to monitor the proteins, which are getting activated or inhibited throughout a specific interval of time. We hope the proposed computational approach and analysis to study the protein expression pattern generation will not only be useful for study of various T-cell phenotypic behaviours but also be helpful for the future researchers to develop therapeutic strategies to combat against various immune diseases.

Acknowledgments

We thank Department of Biotechnology, India (Project Code: BT/PR13689/BID/07/363/2010), and Council of Scientific and Industrial Research, XII Five Year Plan Project 'GENESIS' (BSC0121) for providing financial support to perform this work. SC acknowledges the research fellowship from DST-INSPIRE fellowship program. The authors also acknowledge Mr Shomeek Chowdhury for his effort to collate few pathway specific data used in this work.

References

- Akdis CA, Joss A, Akdis M, Faith A and Blaser K 2000 A molecular basis for T cell suppression by IL-10: CD28-associated IL-10 receptor inhibits CD28 tyrosine phosphorylation and phosphatidylinositol 3-kinase binding. *FASEB J.* **14** 1666–1668
- Akdis M, Burgler S, Cramer R, Eiwegger T, Fujita H, Gomez E, Klunker S, Meyer N, et al. 2011 Interleukins, from 1 to 37, and interferon-gamma: receptors, functions, and roles in diseases. *J. Allergy Clin. Immunol.* **127** e701–e770
- Albert I, Thakar J, Li S, Zhang R and Albert R 2008 Boolean network simulations for life scientists. *Source Code Biol. Med.* **3** 1–8
- Álvarez-Buylla A and Ihrie RA 2014 Sonic hedgehog signalling in the postnatal brain. *Semin. Cell Dev. Biol.* **33** 105–111
- Andoniou CE, Lill NL, Thien CB, Luper ML, Ota S, Bowtell DDL, Scaife RM, Langdon WY, et al. 2000 The Cbl proto-oncogene product negatively regulates the Src-family tyrosine kinase Fyn by enhancing its degradation. *Mol. Cell. Biol.* **20** 851–867
- Arias CF, Ballesteros-Tato A, Garcia MI, Martin-Caballero J, Flores JM, Martinez-A C and Balomenos D 2007 p21CIP1/WAF1 controls proliferation of activated/memory T cells and affects homeostasis and memory T cell responses. *J. Immunol.* **178** 2296–2306
- Baecklund E, Smedby KE, Sutton L-A, Askling J and Rosenquist R 2014 Lymphoma development in patients with autoimmune and inflammatory disorders—what are the driving forces? *Semin. Cancer Biol.* **24** 61–70
- Barabasi AL and Oltvai ZN 2004 Network biology: understanding the cell's functional organization. *Nat. Rev. Genet.* **5** 101–113
- Barbi J, Snider HM, Bhardwaj N, Lezama-Davila CM, Durbin JE and Satoskar AR 2009 Signal transducer and activator of transcription 1 in T cells plays an indispensable role in immunity to *Leishmania major* by mediating Th1 cell homing to the site of infection. *FASEB J.* **23** 3990–3999
- Bell J 2002 Wake-up call. *Nat. Rev. Immunol.* **2** 143
- Ben-Sasson SZ, Hu-Li J, Quiel J, Cauchetaux S, Ratner M, Shapira I, Dinarello CA and Paul WE 2009 IL-1 acts directly on CD4 T cells to enhance their antigen-driven expansion and differentiation. *Proc. Natl. Acad. Sci. USA* **106** 7119–7124
- Berridge MJ 2014 Cell signalling biology: module 9 - cell cycle and proliferation. *Biochem. J.* doi:10.1042/csb0001009
- Blotnick S, Peoples GE, Freeman MR, Eberlein TJ and Klagsbrun M 1994 T lymphocytes synthesize and export heparin-binding epidermal growth factor-like growth factor and basic fibroblast growth factor, mitogens for vascular cells and fibroblasts: differential production and release by CD4+ and CD8+ T cells. *Proc. Natl. Acad. Sci. USA* **91** 2890–2894
- Brdička T, Pavlišťová D, Leo A, Bruyns E, Korinek V, Angelisová P, Scherer J, Shevchenko A, et al. 2000 Phosphoprotein associated with glycosphingolipid-enriched microdomains (Pag), a novel ubiquitously expressed transmembrane adaptor protein, binds the protein tyrosine kinase Csk and is involved in regulation of T cell activation. *J. Exp. Med.* **191** 1591–1604
- Brennan P, Babbage J, Thomas G and Cantrell D 1999 p70s6k integrates phosphatidylinositol 3-kinase and rapamycin-regulated signals for E2F regulation in T lymphocytes. *Mol. Cell. Biol.* **19** 4729–4738
- Buckley RH 2004 Molecular defects in human severe combined immunodeficiency and approaches to immune reconstitution. *Annu. Rev. Immunol.* **22** 625–655
- Cantrell D, Collins M and Crumpton M 1988 Autocrine regulation of T-lymphocyte proliferation: differential induction of IL-2 and IL-2 receptor. *Immunology.* **65** 343
- Carter JH 2000 The immune system as a model for pattern recognition and classification. *J. Am. Med. Assoc. Inform. Assoc.* **7** 28–41
- Cella M, Scheidegger D, Palmer-Lehmann K, Lane P, Lanzavecchia A and Alber G 1996 Ligation of CD40 on dendritic cells triggers production of high levels of interleukin-12 and enhances T cell stimulatory capacity: T help via APC activation. *J. Exp. Med.* **184** 747–752
- Chatr-aryamontri A, Breitkreutz B-J, Heinicke S, Boucher L, Winter A, Stark C, Nixon J, Ramage L, et al. 2013 The BioGRID interaction database: 2013 update. *Nucleic Acids Res.* **41** D816–D823
- Chen L and Flies DB 2013 Molecular mechanisms of T cell costimulation and co-inhibition. *Nat. Rev. Immunol.* **13** 227–242
- Chowdhury S, Pradhan RN and Sarkar RR 2013 Structural and logical analysis of a comprehensive hedgehog signalling pathway to identify alternative drug targets for glioma, colon and pancreatic cancer. *PLoS One* **8** e69132
- Chowdhury S and Sarkar RR 2013 Drug targets and biomarker identification from computational study of human notch signalling pathway. *Clin. Exp. Pharmacol.* **3** 137
- Cohen MA and Grossberg S 1983 Absolute stability of global pattern formation and parallel memory storage by competitive neural networks. *IEEE Trans. Syst. Man. Cybern.* **SMC-13** 815–826
- Coombs D, Dushek O and van der Merwe PA 2011 A review of mathematical models for T cell receptor triggering and antigen discrimination; in *Mathematical models and immune cell biology* (eds MP Carmen and L Grant (New York: Springer) pp 25–45
- Coombs D and Goldstein B 2005 T cell activation: kinetic proof-reading, serial engagement and cell adhesion. *J. Comput. Appl. Math.* **184** 121–139
- Corson LB, Yamanaka Y, Lai K-MV and Rossant J 2003 Spatial and temporal patterns of ERK signalling during mouse embryogenesis. *Development* **130** 4527–4537
- Daynes RA, Dowell T and Araneo BA 1991 Platelet-derived growth factor is a potent biologic response modifier of T cells. *J. Exp. Med.* **174** 1323–1333

- DeBarros A, Chaves-Ferreira M, d'Orey F, Ribot JC and Silva-Santos B 2011 CD70-CD27 interactions provide survival and proliferative signals that regulate T cell receptor-driven activation of human gamma delta peripheral blood lymphocytes. *Eur. J. Immunol.* **41** 195–201
- Delisle JS, Giroux M, Boucher G, Landry JR, Hardy MP, Lemieux S, Jones RG, Wilhelm BT, *et al.* 2013 The TGF-beta-Smad3 pathway inhibits CD28-dependent cell growth and proliferation of CD4 T cells. *Genes Immun.* **14** 115–126
- Dijkers PF, Birkenkamp KU, Lam EW, Thomas NS, Lammers JW, Koenderman L and Coffey PJ 2002 FKHR-L1 can act as a critical effector of cell death induced by cytokine withdrawal: protein kinase B-enhanced cell survival through maintenance of mitochondrial integrity. *J. Cell Biol.* **156** 531–542
- Eldar A, Dorfman R, Weiss D, Ashe H, Shilo B-Z and Barkai N 2002 Robustness of the BMP morphogen gradient in *Drosophila* embryonic patterning. *Nature* **419** 304–308
- Fischer A, Le Deist F, Haccin-Bey-Abina S, André-Schmutz I, De Saint Basile G, De Villartay JP and Cavazzana-Calvo M 2005 Severe combined immunodeficiency. A model disease for molecular immunology and therapy. *Immunol. Rev.* **203** 98–109
- Fukushima A 2003 Ag-specific recognition, activation, and effector function of T cells in the conjunctiva with experimental immune-mediated blepharconjunctivitis. *Invest. Ophthalmol. Vis. Sci.* **44** 4366–4374
- Funahashi A, Morohashi M, Kitano H and Tanimura N 2003 Cell designer: a process diagram editor for gene-regulatory and biochemical networks. *Biosilico.* **1** 159–162
- Gaarenstroom T and Hill CS 2014 TGF- β signalling to chromatin: how Smads regulate transcription during self-renewal and differentiation. *Semin. Cell Dev. Biol.* **32** 107–118
- Gilad E, Von Hardenberg J, Provenzale A, Shachak M and Meron E 2004 Ecosystem engineers: from pattern formation to habitat creation. *Phys. Rev. Lett.* **93** 098105
- Goswami R and Kaplan MH 2011 A brief history of IL-9. *J. Immunol.* **186** 3283–3288
- Green AM, Difazio R and Flynn JL 2013 IFN-gamma from CD4 T cells is essential for host survival and enhances CD8 T cell function during *Mycobacterium tuberculosis* infection. *J. Immunol.* **190** 270–277
- Hall BA, Jackson E, Hajnal A and Fisher J 2014 Logic programming to predict cell fate patterns and retrodict genotypes in organogenesis. *J. R. Soc. Interface.* **11** 20140245
- Harris NL and Ronchese F 1999 The role of B7 costimulation in T-cell immunity. *Immunol. Cell Biol.* **77** 304–311
- Hirano T and Kishimoto T 1989 Interleukin-6: possible implications in human diseases. *Ric. Clin. Lab.* **19** 1–10
- Hirooka Y, Kayama M, Ohga S, Kimura M, Hasegawa M, Shin K, Nogimori T, Ishizuki Y, *et al.* 1993 Deregulated production of interleukin-4 (IL4) in autoimmune thyroid disease assayed with a new radioimmunoassay. *Clin. Chim. Acta.* **216** 1–10
- Kandasamy K, Mohan SS, Raju R, Keerthikumar S, Kumar GS, Venugopal AK, Telikicherla D, Navarro JD, *et al.* 2010 NetPath: a public resource of curated signal transduction pathways. *Genome Biol.* **11** R3
- Kanehisa M and Goto S 2000 KEGG: kyoto encyclopedia of genes and genomes. *Nucleic Acids Res.* **28** 27–30
- Kupper T, Horowitz M, Lee F, Robb R and Flood PM 1987 Autocrine growth of T cells independent of interleukin 2: identification of interleukin 4 (IL 4, BSF-1) as an autocrine growth factor for a cloned antigen-specific helper T cell. *J. Immunol.* **138** 4280–4287
- Lantz CS, Boesiger J, Song CH, Mach N, Kobayashi T, Mulligan RC, Nawa Y, Dranoff G, *et al.* 1998 Role for interleukin-3 in mast-cell and basophil development and in immunity to parasites. *Nature* **392** 90–93
- Lee JK, Won C, Yi EH, Seok SH, Kim MH, Kim SJ, Chung MH, Lee HG, *et al.* 2013 Signal transducer and activator of transcription 3 (Stat3) contributes to T-cell homeostasis by regulating pro-survival Bcl-2 family genes. *Immunology* **140** 288–300
- Li G, Wang D, Yang R, Logan K, Chen H, Zhang S, Skaggs MI, Lloyd A, *et al.* 2014 Temporal patterns of gene expression in developing maize endosperm identified through transcriptome sequencing. *Proc. Natl. Acad. Sci. USA* **111** 7582–7587
- Loeb LA, Loeb KR and Anderson JP 2003 Multiple mutations and cancer. *Proc. Natl. Acad. Sci. USA* **100** 776–781
- Maini P, Painter K and Chau HP 1997 Spatial pattern formation in chemical and biological systems. *J. Chem. Soc Faraday Trans.* **93** 3601–3610
- McKnight PE and Najab J 2010 Mann-Whitney U Test; in *Corsini Encyclopedia of Psychology* doi:10.1002/9780470479216.corpsy0524
- Mor F, Quintana FJ and Cohen IR 2004 Angiogenesis-inflammation cross-talk: vascular endothelial growth factor is secreted by activated T cells and induces Th1 polarization. *J. Immunol.* **172** 4618–4623
- Mukhopadhyay H, Cordoba SP, Maini PK, van der Merwe PA and Dushek O 2013 Systems model of T cell receptor proximal signalling reveals emergent ultrasensitivity. *PLoS Comput. Biol.* **9** e1003004
- Murray JD 2003 On the mechanochemical theory of biological pattern formation with application to vasculogenesis. *C. R. Biol.* **326** 239–252
- Müssel C, Hopfensitz M, Zhou D, Kestler H and Kestler MH 2010 BoolNet—an R package for generation, reconstruction and analysis of Boolean networks. *Bioinformatics* **26** 1378–1380
- Nargi JL and Woodford-Thomas TA 1994 Cloning and characterization of a cdc25 phosphatase from mouse lymphocytes. *Immunogenetics* **39** 99–108
- Nishimura D 2001 BioCarta. *Biotech. Soft. Int. Rep. Comput. Softw. J. Scient.* **2** 117–120
- Ohm JE, Gabrilovich DI, Sempowski GD, Kisseleva E, Parman KS, Nadaf S and Carbone DP 2003 VEGF inhibits T-cell development and may contribute to tumor-induced immune suppression. *Blood* **101** 4878–4886
- Orton R, Oxae S, Vysheirsky V, Calder M, Dzar G and Kolch W 2005 Computational modelling of the receptor-tyrosine-kinase-activated MAPK pathway. *Biochem. J.* **392** 249–261
- Othmer HG, Maini PK and Murray JD 1993 *Experimental and theoretical advances in biological pattern formation* (New York: Plenum Press)
- Parekh AB 2010 Store-operated CRAC channels: function in health and disease. *Nat. Rev. Drug Discov.* **9** 399–410
- Parkinson H, Sarkans U, Shojatalab M, Abeygunawardena N, Contrino S, Coulson R, Farne A, Lara GG, *et al.* 2005

- ArrayExpress—a public repository for microarray gene expression data at the EBI. *Nucleic Acids Res.* **33** D553–D555
- Parry RV, Chemnitz JM, Frauwirth KA, Lanfranco AR, Braunstein I, Kobayashi SV, Linsley PS, Thompson CB, et al. 2005 CTLA-4 and PD-1 receptors inhibit T-cell activation by distinct mechanisms. *Mol. Cell. Biol.* **25** 9543–9553
- Patsoukis N, Sari D and Boussiotis VA 2012 PD-1 inhibits T cell proliferation by upregulating p27 and p15 and suppressing Cdc25A. *Cell Cycle* **11** 4305–4309
- Potse M, Dubé B, Richer J, Vinet A and Gulrajani RM 2006 A comparison of monodomain and bidomain reaction-diffusion models for action potential propagation in the human heart. *IEEE Trans. Biomed. Eng.* **53** 2425–2435
- Prasad TK, Goel R, Kandasamy K, Keerthikumar S, Kumar S, Mathivanan S, Telikicherla D, Raju R, et al. 2009 Human protein reference database—2009 update. *Nucleic Acids Res.* **37** D767–D772
- Qi S, Groves JT and Chakraborty AK 2001 Synaptic pattern formation during cellular recognition. *Proc. Natl. Acad. Sci. USA* **98** 6548–6553
- Qu B, Al-Ansary D, Kummerow C, Hoth M and Schwarz EC 2011 ORAI-mediated calcium influx in T cell proliferation, apoptosis and tolerance. *Cell Calcium* **50** 261–269
- Rangel C, Angus J, Ghahramani Z, Lioumi M, Sotheran E, Gaiba A, Wild DL and Falciani F 2004 Modeling T-cell activation using gene expression profiling and state-space models. *Bioinformatics* **20** 1361–1372
- Raspopovic J, Marcon L, Russo L and Sharpe J 2014 Digit patterning is controlled by a Bmp-Sox9-Wnt Turing network modulated by morphogen gradients. *Science* **345** 566–570
- Rentzsch F and Adamska M 2014 Unravelling the developmental regulatory networks in early animals. *BioEssays*. **36** 427–430
- Rietkerk M and Van de Koppel J 2008 Regular pattern formation in real ecosystems. *Trends Ecol. Evol.* **23** 169–175
- Rogers PR, Song J, Gramaglia I, Killeen N and Croft M 2001 OX40 promotes Bcl-xL and Bcl-2 expression and is essential for long-term survival of CD4 T cells. *Immunity* **15** 445–455
- Rosenwald A, Alizadeh AA, Widhopf G, Simon R, Davis RE, Yu X, Yang L, Pickeral OK, et al. 2001 Relation of gene expression phenotype to immunoglobulin mutation genotype in B cell chronic lymphocytic leukemia. *J. Exp. Med.* **194** 1639–1648
- Rosner A, Miyoshi K, Landesman-Bollag E, Xu X, Seldin DC, Moser AR, MacLeod CL, Shyamala G, et al. 2002 Pathway pathology: histological differences between ErbB/Ras and Wnt pathway transgenic mammary tumors. *Am. J. Pathol.* **161** 1087–1097
- Saadatpour A, Wang R-S, Liao A, Liu X, Loughran TP, Albert I and Albert R 2011 Dynamical and structural analysis of a T cell survival network identifies novel candidate therapeutic targets for large granular lymphocyte leukemia. *PLoS Comput. Biol.* **7** e1002267
- Saez-Rodriguez J, Simeoni L, Lindquist JA, Hemenway R, Bommhardt U, Arndt B, Haus UU, Weismantel R, et al. 2007 A logical model provides insights into T cell receptor signalling. *PLoS Comput. Biol.* **3**, e163
- Seymour R, Sundberg JP and Hogenesch H 2006 Abnormal lymphoid organ development in immunodeficient mutant mice. *Vet. Pathol.* **43** 401–423
- Sherriff MR and Sarkar RR 2008 Computational approaches and modeling of signalling processes in the Immune System. *Proc. Indian Natl. Sci. Acad.* **74** 187–200
- Shi M, Ye Z, Umeshappa KS, Moyana T and Xiang J 2007 Alpha tumor necrosis factor contributes to CD8(+) T cell survival in the transition phase. *Biochem. Biophys. Res. Commun.* **360** 702–707
- Shi Y, Liu CH, Roberts AI, Das J, Xu G, Ren G, Zhang Y, Zhang L, et al. 2006 Granulocyte-macrophage colony-stimulating factor (GM-CSF) and T-cell responses: what we do and don't know. *Cell Res.* **16** 126–133
- Shlomchik MJ, Marshak-Rothstein A, Wolfowicz CB, Rothstein TL and Weigert MG 1987 The role of clonal selection and somatic mutation in autoimmunity. *Nature* **328** 805–811
- Sinha S, Joshi N, Rao JS and Mookerjee S 1984 A four-variable model for the pattern-forming mechanism in Hydra. *Biosystems* **17** 15–22
- Sommers CL, Park CS, Lee J, Feng C, Fuller CL, Grinberg A, Hildebrand JA, Lacana E, et al. 2002 A LAT mutation that inhibits T cell development yet induces lymphoproliferation. *Science* **296** 2040–2043
- Srinivasan S, Hu JS, Curre DS, Fung ES, Hayes WB, Lander AD and Monuki ES 2014 A BMP-FGF morphogen toggle switch drives the ultrasensitive expression of multiple genes in the developing forebrain. *PLoS Comput. Biol.* **10**, e1003463
- Street MGA 1995 Investigation of the deregulation of interleukin-6 in two non-Hodgkin's lymphoma cell lines (Texas: Texas Medical Center Dissertations)
- Suzuki I, Martin S, Boursalian TE, Beers C and Fink PJ 2000 Fas ligand costimulates the in vivo proliferation of CD8+ T cells. *J. Immunol.* **165** 5537–5543
- Takamura K, Fukuyama S, Nagatake T, Kim DY, Kawamura A, Kawauchi H and Kiyono H 2007 Regulatory role of lymphoid chemokine CCL19 and CCL21 in the control of allergic rhinitis. *J. Immunol.* **179** 5897–5906
- Teku GN, Ortutay C and Vihinen M 2014 Identification of core T cell network based on immunome interactome. *BMC Syst. Biol.* **8** 17
- Trowbridge IS and Thomas ML 1994 CD45: an emerging role as a protein tyrosine phosphatase required for lymphocyte activation and development. *Annu. Rev. Immunol.* **12** 85–116
- Turing AM 1952 The chemical basis of morphogenesis. *Phil. Trans. R. Soc. B.* **237** 37–72
- Van Epps HL 2006 IL-6 drives T cell proliferation. *J. Exp. Med.* **203** 1387
- van Montfrans JM, Hoepelman AI, Otto S, van Gijn M, van de Corput L, de Weger RA, Monaco-Shawver L, Banerjee PP, et al. 2012 CD27 deficiency is associated with combined immunodeficiency and persistent symptomatic EBV viremia. *J. Allergy Clin. Immunol.* **129** 787–793 e786
- Velardo MJ, Burger C, Williams PR, Baker HV, López MC, Mareci TH, White TE, Muzyczka N, et al. 2004 Patterns of gene expression reveal a temporally orchestrated wound healing response in the injured spinal cord. *J. Neurosci.* **24** 8562–8576
- Wang J and Fu Y-X 2004 The role of LIGHT in T cell-mediated immunity. *Immunol. Res.* **30** 201–214
- Watts TH 2010 Staying alive: T cell costimulation, CD28, and Bcl-xL. *J. Immunol.* **185** 3785–3787

- Wechsler AS, Gordon MC, Dendorfer U and LeClair KP 1994 Induction of IL-8 expression in T cells uses the CD28 costimulatory pathway. *J. Immunol.* **153** 2515–2523
- Wells AD and Morawski PA 2014 New roles for cyclin-dependent kinases in T cell biology: linking cell division and differentiation. *Nat. Rev. Immunol.* **14** 261–270
- Welte T 1999 STAT5 interaction with the T cell receptor complex and stimulation of T cell proliferation. *Science* **283** 222–225
- Wittmann DM, Krumsiek J, Saez-Rodriguez J, Lauffenburger DA, Klamt S and Theis FJ 2009 Transforming Boolean models to continuous models: methodology and application to T-cell receptor signalling. *BMC Syst. Biol.* **3** 98
- Yamagishi M and Watanabe T 2012 New paradigm of T cell signalling: learning from malignancies. *J. Clin. Cell Immunol.* **S 12** 2
- Yeh JH, Sidhu SS and Chan AC 2008 Regulation of a late phase of T cell polarity and effector functions by Crtam. *Cell* **132** 846–859
- Yoo JK, Cho JH, Lee SW and Sung YC 2002 IL-12 provides proliferation and survival signals to murine CD4+ T cells through phosphatidylinositol 3-Kinase/Akt signalling pathway. *J. Immunol.* **169** 3637–3643
- Youn H-D and Liu JO 2000 Cabin1 represses MEF2-dependent Nur77 expression and T cell apoptosis by controlling association of histone deacetylases and acetylases with MEF2. *Immunity* **13** 85–94
- Zapata JM and Reed JC 2002 TRAF1: lord without a RING. *Sci. STKE* **2002** pe27
- Zhao S, Fung-Leung WP, Bittner A, Ngo K and Liu X 2014 Comparison of RNA-Seq and microarray in transcriptome profiling of activated T cells. *PLoS One* **9** e78644

RESEARCH

Open Access



Identification of Th1/Th2 regulatory switch to promote healing response during leishmaniasis: a computational approach

Piyali Ganguli¹, Saikat Chowdhury^{1,2}, Shomeek Chowdhury¹ and Ram Rup Sarkar^{1,2*}

Abstract

Leishmania devises its survival strategy by suppressing the host's immune functions. The antigen molecules produced by *Leishmania* interferes with the host's cell signaling cascades and consequently changes the protein expression pattern of the antigen-presenting cell (APC). This creates an environment suitable for the switching of the T-cell responses from a healing Th1 response to a non-healing Th2 response that is favorable for the continued survival of the parasite inside the host APC. Using a reconstructed signaling network of the intracellular and intercellular reactions between a *Leishmania* infected APC and T-cell, we propose a computational model to predict the inhibitory effect of the *Leishmania* infected APC on the T-cell and to identify the regulators of this Th1-/Th2-switching behavior as observed during *Leishmania* infection. In this work, we hypothesize that a complete removal of the parasite could only be achieved with a simultaneous up-regulation of the healing Th1 response and stimulation of nitric oxide (NO) production from the APCs, and downregulation of the non-healing Th2 response and thereby propose several unique combinations of protein molecules that could elicit this anti-*Leishmania* immune response. Our results indicate that TLR3 may play a positive role in eliciting NO synthesis, while TLR2 may be responsible for inhibiting an anti-*Leishmania* immune response. Also, TLR3 overexpression (in the APC), when combined with SHP2 inhibition (in the T cell), produces an anti-*Leishmania* response that is better than the conventional IFN-gamma or IL12 treatment. A similar anti-*Leishmania* response is also obtained in another combination where TLR3 (in APC) is overexpressed, and SHC and MKP (of T cell) are inhibited and activated, respectively. Through our study, we also observe that *Leishmania* infection may induce an upregulation of IFN-beta production from the APC that may lead to an upregulation of the RAP1 and SOCS3 proteins inside the T cell, the potential inhibitors of MAPK and JAK-STAT signaling pathways, respectively, via the TYK2-mediated pathway. This study not only enhances our knowledge in understanding the Th1/Th2 regulatory switch to promote healing response during leishmaniasis but also helps to identify novel combinations of proteins as potential immunomodulators.

Keywords: T cell and APC signaling pathways, *Leishmania*, Th1/Th2 response, NO synthesis, Logical model, Immunotherapy, Combinatorial drug targets

* Correspondence: rr.sarkar@ncl.res.in

¹Chemical Engineering and Process Development Division, CSIR-National Chemical Laboratory, Pune, Maharashtra 411008, India

²Academy of Scientific & Innovative Research (AcSIR), CSIR-National Chemical Laboratory, Pune, India

1 Introduction

Cell-mediated immunity (CMI), responsible for confronting the infections caused due to invasion of intracellular pathogens, primarily involves the interactions of the phagocytic antigen-presenting cells (APCs) and the T-lymphocytes. This leads to the activation of a series of intra-cellular and inter-cellular biochemical signaling processes, which culminates into synthesis of certain diffusible effector molecules that includes proteins (mostly the cytokines) and microbicidal molecules (e.g., nitric oxide) helping in the clearance of the disease [1]. However, the activities of this defense mechanism are severely compromised during leishmaniasis, a neglected tropical disease, caused due to infection by the protozoan parasites of the genus *Leishmania*. This is transmitted to the human through the infected bites of the phlebotomine sand flies during their blood meal [1]. The promastigote form of the parasite, once injected into the human host, is engulfed by the APC (macrophages and dendritic cells) to form a phagolysosome, where it differentiates into its amastigote form and takes control of its entire cellular machineries in a way that reduces the immuno-competency of the immune cells thereby hindering the body's natural parasite clearance process [2].

The surface molecules produced by *Leishmania*, such as, lipophosphoglycan (LPG), glycoprotein 63 (GP63), and the elongation factor EF1-alpha directly or indirectly activate a series of phosphatases inside the human APCs (e.g., SHP1, PTP1B, and TCP1P), that leads to dephosphorylation and de-activation of important signaling molecules inside the host cell [3]. Inside the APC, the LPG molecules act as antigens and are presented to the surrounding T-lymphocytes to elicit either of the two types of immune responses, viz. healing and non-healing responses, depending on the parasite load and the host immunity [4]. The healing response is obtained in case of low parasitic load, in which a pronounced Type-I helper T-cell (or Th1) response occurs due to up-regulation of the Th1 cytokines, such as the interferon-gamma from the stimulated T cells, and thus naturally clears the pathogen from the system [1, 5]. On the other hand, higher pathogen load gives rise to a non-healing response in which an upregulation of the Th2 cytokines (e.g., IL10) is observed, that favors the persistence of the *Leishmania*. Simultaneously, during this non-healing response, the production of the protective Th1 cytokines, such as IL12, and the microbicidal molecules, such as nitric oxide is also downregulated, thus creating an immune-suppressed condition suitable for the further progression of the disease [6].

It is experimentally shown that all types of leishmaniasis viz. cutaneous, muco-cutaneous, and visceral leishmaniasis elicit these types of immune responses in

human body [7]. Hence, the general therapeutic strategy adopted for the treatment of Leishmaniasis is primarily aimed to expedite the process of parasite clearance for faster healing by stimulating the Th1 or healing response. In case of cutaneous leishmaniasis therapeutics, chemotherapeutic drugs, such as pentavalent antimonials, liposomal amphotericin B has been shown to be useful to reduce the dermal lesions and the chances of further destructive mucosal inflammations and visceral infections [8, 9]. However, the successive clinical studies have shown that these chemotherapeutic drugs are also associated with adverse side effects, such as nausea, intense headache, diarrhea, musculoskeletal and abdominal pain etc. [9–13]. In several cases, relapse of the disease and developing resistant strains are also reported after the use of these drugs, which necessitates the development of better treatment protocols with higher clinical efficacy [14]. Although immunotherapeutic strategies involving the administration of exogenous interferon-gamma is found to be effective in suppressing leishmaniasis [15, 16], the high production of IL10 during early stage of infection often suppresses its activity, thereby hindering NO production and disease clearance [17]. Based on these experimental outcomes, a number of mathematical models have also been proposed simultaneously to untangle the complexities that appear as hurdles to devise a successful treatment strategy in leishmaniasis [18, 19]. In one of such studies, “granulomas” formation during *Leishmania donovani* infection has been modeled using Petri net analysis by considering the inter-cellular interactions of macrophage, lymphocyte, NK cells etc. The outcomes of these cell population based models have emphasized cytokine therapy by the exogenous injection of interferon-gamma and the suppression of IL10 to eradicate the *Leishmania* pathogens in macrophage cell [20]. However, interferon-gamma molecule is a pro-inflammatory molecule and also has short half-life time, which in turn requires its repeated administration into the body at a regular interval of time that may have harmful consequences [21, 22]. Hence, to circumvent these problems, implementation of better therapeutic strategies, by identifying novel drugs, drug target molecules and immunostimulators are required and demands higher attention from the vast majority of clinical and experimental pharmacologists.

However, in order to develop an effective immunotherapeutic strategy, it is important to have a comprehensive understanding of the Th1/Th2 dichotomy in leishmaniasis so as to identify the regulators through which the Th1/Th2 switching behavior can be effectively controlled. This mechanism still remains very less explored. The identification of such important molecular switch and their corresponding reaction routes through which the immunostimulation could be enhanced is highly required in this field of study.

As the exact intra-cellular reaction cascades governing the T cell response after encountering with *Leishmania* infected APCs is not clearly understood yet, the mechanisms through which this response dynamics and the nitric oxide (NO) production work in the immune cells is still unknown. Besides, the mechanism through which the *Leishmania* antigens override the APCs intra-cellular network by varying the expressions of the immunostimulatory proteins, and force to redirect the immune responses towards the non-healing or Th2 response is not comprehensively studied yet. The study of these regulatory mechanisms by analyzing such a large system using conventional experimental techniques is time consuming and also difficult to perform, and therefore *in silico* mathematical models of inter and intra-cellular reaction cascades in APC and T cell in presence of *Leishmania* antigens would probably be the best strategy to counteract these problems. This may also help to address some of the unexplored questions of *Leishmania* immunotherapy, such as the limitations of the interferon-gamma treatment, the reason for which interferon-beta treatment is only effective at low doses, and the means by which the toll-like receptor (TLR) molecules expressed by the APCs can regulate the immune responses of the T cell to shift the dynamics towards a higher healing Th1 response [17, 23–25].

In this study, we have tried to address the above mentioned problems in *Leishmania major* infection scenario by using mathematical model and *in silico* analysis. We have hypothesized that in order to achieve better therapeutic results without adverse side effects, the stimulation of type-I T-helper cells and a simultaneous upregulation of NO production by using immunostimulator would be the best therapeutic strategy to clear the *Leishmania* pathogens from the body. In order to develop a suitable *in silico* model that may enhance our understanding of *Leishmania* immunobiology, we have manually reconstructed a comprehensive cell signaling pathway map of a *Leishmania* infected APC and a normal CD4⁺ T cell (helper T cell), considering the important physical interactions and the cross-talks by the secreted diffusible molecules between the two cells. The *Leishmania* infection has been introduced in the model by establishing the interaction of the *Leishmania* antigens, known from the literature and databases, with the appropriate host protein molecules in the APC. However, the dynamic analysis of such a large network is difficult to perform due to the unavailability of kinetic parameters and concentration values. Hence, to assess the gene or protein expression patterns of large scale signal transduction networks under different pathological conditions, the concept of discrete dynamic Boolean or logical modeling approach has been utilized successfully [26–28]. Large scale, intracellular T cell signaling network is also analyzed by using this

modeling technique and eventually various structural and functional properties of this network under normal and disease conditions are studied successfully [29, 30]. A logic-based modeling technique is also applied to analyze the temporal expression patterns of the genes/proteins of T cell, which are strongly influenced by the intra-cellular T cell signal transduction cascade in presence or absence of infection [31].

Here, the entire reaction mechanisms are translated into logical equations with the objective to simulate and understand the effect of the presence and absence of the *Leishmania* antigens on the signaling events of the host's APCs and T cells. Followed by the Boolean attractor analysis and the successful validation of the simulation outcomes with the time-course microarray expression data as well as the phenotypic responses obtained from published experimental observations, the model is then used to compare the protein expression pattern for normal and *Leishmania*-infected scenarios. With an aim to understand the mode of regulations that occur due to the infection at the molecular level inside the T cell, the comparison of the two scenarios is then used to extract the important T cell proteins, which are highly influenced under the pathogen burden. The result of this analysis is further used to predict the unknown changes occurring at the pathway level in the T cell during infection. Moreover, the knowledge of these deregulated pathways is thereafter used to predict the targets for the *in silico* perturbation analysis. Perturbations of the logical states of proteins in the network are performed to study the effect of the known immunostimulants (*viz.* IL12 and interferon-gamma) as well as to propose some new combinations of molecules that act as a molecular switch to regulate the Th1/Th2 and NO response dynamics. Subsequently, these identified novel combinations of proteins were tested for stability and robustness by examining the attractors of the system under these perturbations. Thereafter, it was ascertained that the proposed combinations of protein targets can be used as the potential immunomodulators, targeting of which may bypass the inhibitory activities of the pathogens and enhance the anti-*Leishmania* immune responses as well as the microbicidal activities of the body's immune cells.

2 Materials and methods

2.1 Construction of gene correlation network

Gene correlation networks of the significantly expressed genes, observed in two independent microarray experiments for APC (E-GEOD: 42088) and T cell (E-GEOD: 48978), were constructed in this work by calculating the Pearson correlation coefficient of each pair of genes from the temporal gene expression data followed by the calculation of *P* values. The *P* values of all pair of genes from the two microarray data sets were stored in symmetric square

matrices from which the corresponding adjacency matrices were generated. In the adjacency matrices, the elements are either 1 (P value < 0.01) or 0 (otherwise). These adjacency matrices are then used for the construction of co-expression or correlation networks of the two microarray gene expression datasets. The networks are then analyzed for the identification of probable clusters (or functional modules) in Cytoscape (version 2.8) GPU based App AllegroMCODE (version 2.1) [32]. The genes from each functional module identified in this analysis are further used for the pathway enrichment analysis in bioCompendium (<http://biocompendium.embl.de/>) and GeneCodis [33] web servers [Additional file 1: Text S1/ Table S1 and Text S2/ Table S2]. The pictorial representations of each cluster are provided in Additional file 2: Figure S1 and Additional file 3: Figure S2.

2.2 Pathway reconstruction/integration

In order to capture the functional regulations that operate between these significantly enriched pathways within the two cells, i.e., APC and T cell, reconstruction of a comprehensive map of signaling processes depicting the effect of *Leishmania* infection on immune response was necessary. Hence, a detailed T cell and APC interaction pathway diagram was created after a thorough study of existing literatures and databases. Protein-protein interaction (PPI) and the biochemical signal transduction data were collated from various cell signaling and PPI databases, such as KEGG, Protein Lounge, Pathway Central, Biocarta, NetPath, BIOGRID, etc. and various published research articles [34–37]. The *Leishmania* proteins were then introduced in the network and the interactions of these proteins were established with the existing APC molecules depending on the biological evidences [38–40]. The *Leishmania* antigenic molecules used in the model, viz. LPG_L, GP63_L, LFAA_L, and EF1_ALPHA_L, are known to be present in almost all the *Leishmania* species so as to create a generalized *Leishmania* infection model (LFAA_L is a hypothetical molecule which we considered in our model to show the activation of ASMASE for the production of CERAMIDE [41]; it is abbreviated for *Leishmania* factor activating ASMASE). With certain modifications (required to build the juxtacrine and paracrine interactions between the cells), the T cell pathway reported in our previous work was used to understand the T cell-APC cross-talks and to monitor the immunological response generated during *Leishmania* infection [31]. The pathway figure was drawn using Cell Designer software (version 4.3) [42]. The signaling molecules (nodes) and interactions were color coded in accordance with cellular locations and their chemical nature, respectively. Also, in order to differentiate the redundant *Leishmania* and T cell molecules from the APC molecules, the

names of the protein/non-protein molecules were denoted with suffix “L” and “T” for *Leishmania* and T cell, respectively (Additional file 4: Figure S3 and Additional file 1: Text S3).

2.3 Model formulation

The interactions of the entire network, including all important regulations between T cell and APC, were translated into logical equations (signifying reactions or hyperacrs) using the AND, OR, and NOT logical gates, in a biologically meaningful way (Additional file 1: Text S5). In order to capture the regulations at the post-transcriptional level, the alternatively spliced isoforms of the T cell and APC output molecules with known functions have been also included in our model (Additional file 1: Text S4/ Table S3). Here, the selection of isoforms is based on the presence of certain cis-regulatory elements and trans-acting factors that have been collectively referred to as “FACTOR_i” where $\{i = 1, 2, \dots, 23\}$. These 23 FACTOR_i represent specific spliceosomes responsible for the splice site recognition in each case.

The model was simulated synchronously (i.e., all equations updated simultaneously) and asynchronously (i.e., random execution of the equations) using BooleanNet-1.2.4 software until the steady state is reached [43]. In this model, we also defined three functions, viz. “TH_1_response*”, “TH_2_response*”, and “NO_response*”, which reflect the type of T cell responses elicited and production of NO from the APC in response to an infection (Eqs. 1, 2, and 3; * denotes the $(t+1)^{\text{th}}$ logical state of the responses). The molecules used for defining these functions are principally the molecules involved in eliciting these responses, as reported in literatures [44].

$$\text{TH_1_response}^* = \text{IL2_T AND GM_CSF_T AND TNF_ALPHA_T AND IFN_GAMMA_T} \quad (1)$$

$$\text{TH_2_response}^* = \text{IL4_T AND IL5_T AND IL6_T AND IL10_T} \quad (2)$$

$$\text{NO_response}^* = \text{NO} \quad (3)$$

2.4 Boolean attractor, experimental data and validation

The Boolean attractors of the model were determined by generating all possible combinations (ON or OFF) of the 51 input molecules of the system. The simulation was repeated for 20 samples, where 7 proteins have been selected from a uniform random distribution of 51 input molecules, thereby generating $2^7 \times 20$ (=2560) combinations of input molecules. However, due to lack of human cell-specific *Leishmania major*-infected RNA seq data of APC, the logical states (activation or inactivation) of the FACTOR_i determining that alternative splicing of the

output molecules could not be explicitly determined in *Leishmania*-infected scenario. Hence, in our model, these FACTORi were assumed to be ON in all our simulations, signifying that all the alternative isoforms have equal probability of getting expressed. The analysis was performed separately for the uninfected and the infected scenarios, which were created by initializing the *Leishmania* antigen molecules OFF and ON, respectively, in the two cases using synchronous Boolean update rules. Thereafter, the steady state logical values (i.e., attractor) of all the 294 nodes in 2560 different input combinations from both the scenarios were identified by using in-built functions available in BooleanNet-1.2.4 and the in house code written in Perl script. However, to present these attractor(s) of each sample in a simplified way, only the steady state binary values of the ten macrophage output molecules (viz. IFN_BETA, IL1_ALPHA, IL1_BETA, IL10, IL12, INOS, IP10, NO, TNF_ALPHA, and c_FOS) were plotted from each attractor(s) state using the network visualization software Gephi (<http://gephi.github.io/>) and were successively tested for the presence of multiple attractors in the system in uninfected and infected scenarios. On the other hand, the differential activation of the FACTORi in splicing mechanism and its role in the regulation of the network dynamics is further analyzed and discussed in Additional file 1: Text S4 and Additional file 5: Figure S4.

Furthermore, in order to validate our model with experimental data, time-course microarray expression data for the two cells (viz. T cell and APC) were obtained from two separate experiments from the EBI ARRAYEXPRESS database (E-GEOD: 48978 and 42088, for T cell and APC, respectively) [45]. In these microarray experiments, expression profile of activated human T-helper cell (Affymetrix HT HG-U133+ PM Array Plate) and *Leishmania major* infected dendritic cells (Affymetrix HG-U133 Plus 2.0 Gene Chip) were studied at discrete time-points [46, 47]. In our analysis, we only considered the expression values at four time-points, i.e. 0, 2, 4, and 6-h time-points for T-cell and 0, 2, 4, 8-h time-points for dendritic cells. These expression data were then extracted and binarized using the BOOLNET software that employs K-means clustering algorithm [48]. The zeroth hour-binarized data was used to initialize all the nodes of the respective cells, with either ON or OFF depending on whether the protein shows an up-regulation or a down-regulation at the zeroth hour (BooleanNet Software uses TRUE and FALSE for ON and OFF, respectively; Additional file 1: Text S6). The initial values of the *Leishmania* proteins were considered ON in the infected scenario and OFF in the uninfected scenario. The model was then simulated using the synchronous update rule and validated by comparing the expression of the ten APC output

molecules in the infected scenario with the binarized time-course microarray data of the APC [46]. However, it should be noted that the experimental data for the expression of NO molecule is considered as proportionate to the expression values of INOS of the microarray data. The model reached its steady state at the 19th time-step in the infected scenario. As a control of the experiment an uninfected scenario was also created. However, to calibrate the four experimental time-points used in microarray data (i.e. 0, 2, 4, and 6 h) with the discrete time points of our simulation results, logical states of the proteins up to 24 discrete time-steps were considered in this analysis (after comparing the steady state values for both the experimental and simulation results). Thus, a 1-h duration of experimental data was associated by three time-steps of the simulations. The temporal expression profile of the ten output molecules were plotted till the 24th step (i.e., 8 h of experimental data). It is to be mentioned here that since the expression of the output proteins is the best reflection of functioning of the entire signaling cascade, the validation of these previously mentioned ten output molecules is assumed to be sufficient to demonstrate the authenticity of the entire model. The T cell model was also validated in a similar way, i.e., by comparing the time-course expression profile of the output protein molecules as obtained in the synchronous simulation with the experimental data [31].

2.5 Model analysis and perturbation studies

The model was simulated asynchronously (until steady state was reached) to make a qualitative analysis of differences in the expression profiles and functional responses of the APC and T cell output molecules in the infected and the uninfected scenarios. The model was iterated 100 times, and the average values of all the simulations at each time-point were plotted for further analysis. This analysis also helped us to monitor the small fluctuations in the expression pattern of the pathway species over time, which occurs due to the stochasticity in the execution of the pathway reactions inside the cell. The asynchronous simulation also ensures that the errors in the synchronous simulations as well as attractor analysis (through selection of independent random samples) are minimized and further presents an average behavior of the entire system over time. In order to unravel the effect of *Leishmania* infection on the entire T cell signaling cascade at the individual protein level, and then to understand the changes at the pathway level, two-tailed Mann-Whitney U test was carried out on the expression of the 163 T cell intermediate and output molecules. This helped us to identify the proteins that get significantly de-regulated during the infection (at 5 % level of significance). Thereafter, the model was used to predict

the phenotypic responses (using Eqs. 1, 2, and 3) in various treatment scenarios using several gene knock-in and knock-out experiments created *in silico* by trying different combinations of ON and OFF of the protein molecules using the in-built “boolean2.modify_states” function of the BooleanNet-1.2.4 software [43]. In order to further confirm the robustness of our predicted combinations of immunotherapeutic targets, Boolean attractor analysis was performed for the perturbation scenarios by varying the input molecules of the model (as mentioned earlier). Logical steady states of all the 296 nodes of the model from different scenarios (i.e., uninfected, infected and perturbed) were identified and out of these steady state sequences, only the steady state values of NO, Th1, and Th2 responses were extracted for the comparisons of the effect of different perturbations in the infected scenario. Hence, following this methodology, this study aims to find the effectiveness of our proposed treatment strategies to revert the infected scenario to an infection-free attractor similar to the uninfected scenario.

3 Result

3.1 Pathway enrichment analysis

The gene clusters identified from the co-expression networks of the two microarray expression data sets can be considered as the “functional modules” of the gene interaction networks of the *Leishmania major* infected APC and the activated T cell, respectively. A total of 10 and 24 clusters or functional modules are found from the gene co-expression networks of APC and T cell, respectively (Additional file 2: Figure S1 and Additional file 3: Figure S2). Pathway enrichment analyses of the genes found in these clusters have identified various important intracellular signaling pathways (e.g., cytokine-cytokine receptor, toll-like receptor, JAK-STAT, MAPK, mTOR, T cell receptor, calcium signaling, PI3 kinase, interleukin signaling pathways etc.) of two different cells. The complete list of the pathways found to be enriched in this analysis for APC and T-cell are given in Additional file 1: Text S1/Table S1 and Text S2/Table S2, respectively. These enriched pathways, corresponding to the significantly expressed genes of APC and T cell microarray expression data sets, represent the pathways that are influenced by the *Leishmania* pathogen in the APC and in the activated T cell. However, it should be noted that the pathways found to be enriched in this analysis do not provide the complete understandings of the molecular mechanisms through which the pathogen infect the APCs. Also, we are unable to capture the dynamic interactions of the APC and T cells’ molecules in the *Leishmania* infected scenario. Hence, the reconstructions of the complete inter- and intra-cellular

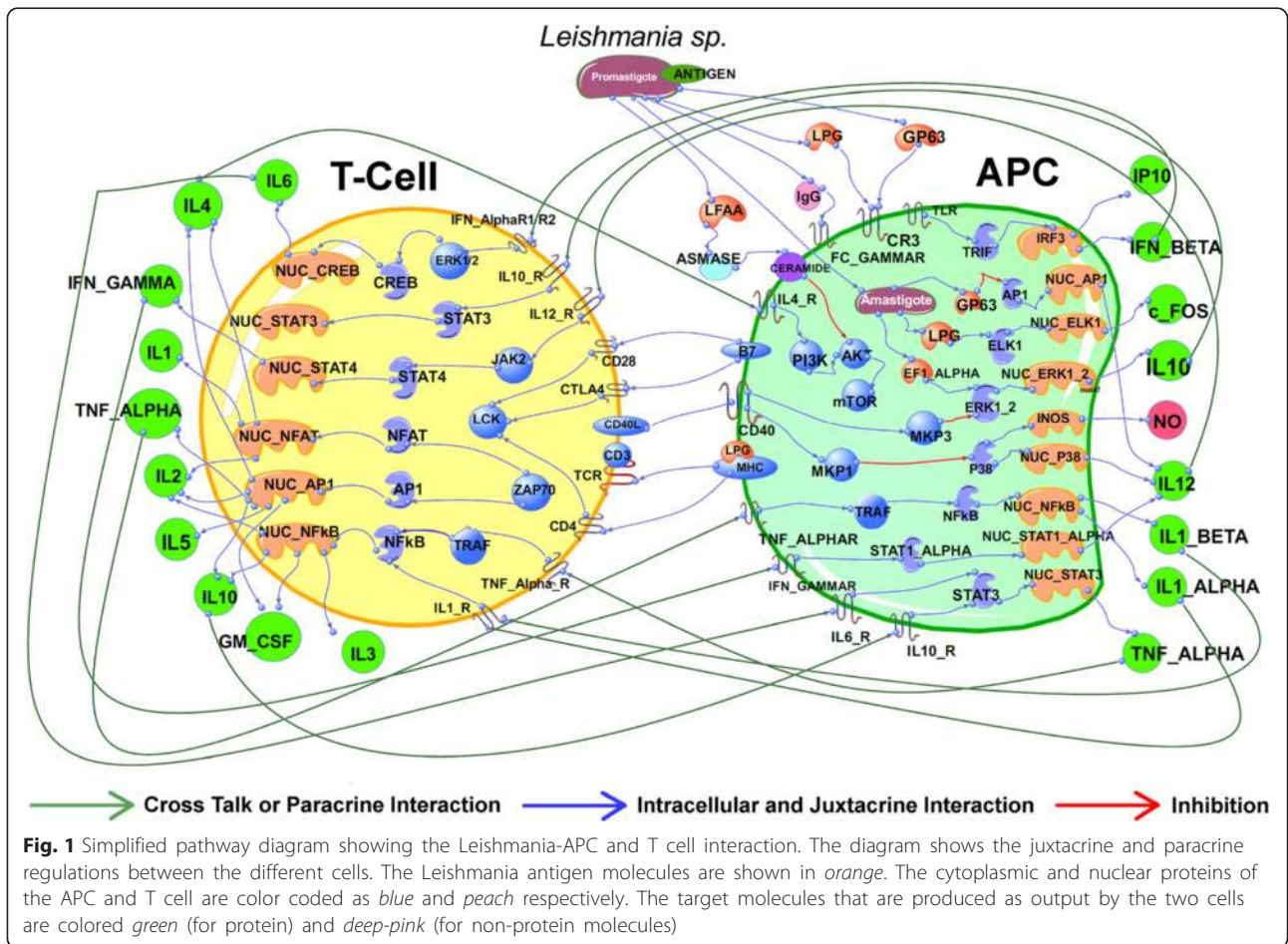
signaling cascades regulating the APC and T cell functions are performed.

3.2 Features of the reconstructed pathway

In Fig. 1, a simplified version of the newly reconstructed pathway diagram is presented to provide the brief description of the entire reaction cascade. In this simplified figure, the major inter- and intra-cellular signaling events triggered by important molecules (e.g., MHC, CD40, IL10 etc.) of both the cells and pathogen are provided for the sake of simplicity.

The complete diagram of the newly reconstructed *Leishmania*-APC-T-cell pathway model is provided in Additional file 4: Figure S3. It integrates all possible inter-cellular and intra-cellular signaling events that occur between the two immune cells during *Leishmania* invasion. Here, the interaction of the *Leishmania* molecules, produced from the promastigote and the amastigote forms, with the APC molecules are considered separately. The entire signaling network (i.e. intra- and inter-cellular) consists of a total of 293 nodes, which includes 82 APC molecules, 206 T cell molecules, and 5 *Leishmania*-related molecules, that are involved in more than 400 protein-protein interactions. The intra-cellular signaling cascades considered for modeling the APC and the T cell consists of the major co-receptor signaling pathways, the cytokine pathways, TLR pathways, etc. that play a pivotal role in regulating the outcome of the immune cell’s functional responses. In case of APC, the pathways, which are considered in our model, include the CD40 pathway, the interleukin pathways (viz. IL4, IL6, and IL10), TLR pathways (TLR2, TLR3, TLR4), and the pathways involved in TNF_ALPHA, IFN_GAMMA signaling. Again in T cell, in addition to the core TCR-mediated signaling, seven co-receptor signaling pathways (viz. CD28, CD27, LTBR, CTLA4, ICOS, PD1, and OX40), cytokine pathways (viz. IL1, IL2, IL10, IL12, TNF, and IFN-mediated pathways) and the CRAC channel-mediated calcium pathway are considered.

Various crosstalk reactions are also considered in the model, which depict the bi-directional regulation that exists between the two immune cells. These crosstalk reactions mainly comprise of the juxtacrine signaling events stimulated directly by binding of the co-receptors and the ligand molecules expressed on the T cell and the APC membranes, and the paracrine signaling that are mediated by the diffusible output molecules (mostly cytokines) produced by each cell. Overall 10 crosstalk interactions between the T cell and the APC that effectively regulates the expression pattern of each other are considered. These includes IFN_GAMMA_T, IL4_T, IL6_T, IL10_T, TNF_ALPHA_T molecules secreted from the T cell, and IFN_BETA, TNF_ALPHA, IL12 secreted from the APC that diffuses and activates their



corresponding receptor/co-receptors on their neighboring cell to trigger their downstream signaling cascades. The co-receptor ligand molecule interaction considered to be the most important in the model is the one that involves the binding of the CD40 and CD40L_T molecules [3].

The signaling events that begin at the membrane region is then considered to transduce the signal downstream to activate the major signaling pathways, such as, the MAPK, JNK, NFkB, JAK-STAT cascades, which activate a series of transcription factors, that eventually transcribes the output molecules. During *Leishmania* invasion, the antigenic molecules produced by the pathogen activate certain phosphatases (e.g. SHP1, PTP1_B, TCPTP etc.) that interfere with the signaling events of the APC. The antigen molecules considered in the network, such as LPG_L, GP63_L and EF1_Alpha, are shown to have a direct effect on the activities of the ERK1/2 and AP1 transcription factors, the former being upregulated and the latter inhibited or degraded (a detailed description of all the signaling events have been provided in Additional file 1: Text S3).

3.3 Model analysis

3.3.1 Attractors

The Boolean attractor analysis performed on 20 independent random samples in the uninfected and the infected scenarios have been plotted in Fig. 2. Here, 128 combinations of input in each of the 20 samples have been grouped together with a specific color code. For simplicity, for the attractor only the sequence of logical states of the molecules in the order of IFN_BETA, IL10, IL12, IL1_ALPHA, IL1_BETA, INOS, IP10, NO, TNF_ALPHA, and c_FOS, is depicted in the network graph. The results of the analysis reveal that given all the FACTORS regulating alternative splicing is assumed to be in ON state, all the 2560 combinations of input (called basins of attractor; each basin is represented as a node in the network graph) in the uninfected scenario, reaches the same Boolean attractor (...0111110111...) (Fig. 2a), while in the infected scenario four different attractors are obtained, viz (...1100001011...), (...0101100011...), (...1101101011...) and (...0100000011...) (Fig. 2b). However, it is to be noted in the infected scenario, 2000 among the 2560 basins (i.e., 78.125 %) reached

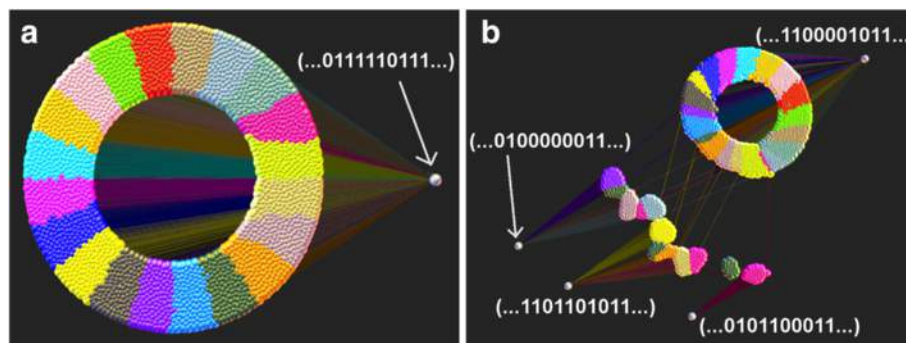


Fig. 2 Boolean attractor analysis in uninfected (a) and infected scenarios (b). The binary values shown in the attractor represents the logical steady state values of 10 macrophage output proteins in the sequence of IFN_BETA, IL1_ALPHA, IL1_BETA, IL10, IL12, INOS, IP10, NO, TNF_ALPHA, and c_FOS, respectively. Different color codes are used to represent the 20 different random samples, and within each sample, 128 nodes represent the input combinations of 7 proteins selected randomly from 51 inputs of the model. In total, there are 2560 combination of initial states denoting the basins of attraction for the entire system

the (...1100001011...) attractor (including both steady state and cyclic attractor), hereby referred as the major attractor of the system in the infected scenario. These 2000 basins of the major attractor spans all the 20 random samples selected, among which 13 samples exclusively drive to the major attractor, while the remaining 7 samples reach multiple attractors. The (...1101101011...), (...0100000011...), and (...0101100011...) attractors have been attained from 9.375, 9.375, and 3.125 % basins, respectively.

3.3.2 Model validation with experimental data

The temporal expression profiles of the APC output molecules viz. c_FOS, IL1_ALPHA, IL1_BETA, IFN_BETA, IL10, IL12, IP10, INOS, NO, TNF_ALPHA in the infected (red) and the uninfected scenarios (green) are plotted along-with the binarized microarray data at 0, 2, 4 and 8 h time-points (black diamond) in Fig. 3. This figure depicts that the expression levels of all the 10 output molecules are reaching the steady state values either at 1 (i.e., up-regulation) or 0 (i.e., down-regulation). Here, we observe that expression value of the output molecules at steady state is exactly similar to the value obtained as the major attractor of the system in both the uninfected as well as the infected scenarios (Fig. 2). Qualitative comparison of the expression values reveals that out of these 10 selected output molecules, the steady-state expression value of total 7 molecules viz. c_FOS, IL1_ALPHA, IL1_BETA, IL10, IL12, INOS, and NO in the infected scenario show the exact match with the experimental observations [46]. While c_FOS and IL10 show an expression value of 1 (high expression) in the infected scenario, the other output molecules such as IL1_ALPHA, IL1_BETA, IL12, INOS, and NO have an expression value of 0 (low or no expression) in the infected scenario.

Also, Fig. 3 depicts that at “4 and 8 h” time points, c_FOS and IL10 proteins get upregulated in the simulated infected scenario, which is exactly comparable with the experimentally observed expression levels in microarray data at the same time-points. However, it should be noted that although the expression level of c_FOS protein at “2 h” time point in the simulated infected scenario is not exactly matching with the experimental findings, but the infected model is able to show the downregulation of this protein between the intervals of “0 to 1 h” time points. Both the proteins IL1_ALPHA and IL1_BETA get up regulated at “1 h” time point and subsequently get downregulated at “6 h” time point of the simulated infected scenario. In the experimental data, both of them get upregulated at “2 h” time-point and get downregulated at “4 h” and “8 h” time-points, respectively. In case of IL12, it is observed from Fig. 3 that except a small time interval between 0 and 1 h, this protein remains in the downregulated state throughout the rest of the time-points. The time course microarray data of this protein also shows similar expression level except at “4 h” time-point, in which this protein shows upregulation. Similarly, INOS and NO also show similar expression level at “2 and 8 h” time points as compare to the experimental data. Altogether, the percentage of validation of the simulated *L.major* infected scenario for all the 10 selected proteins at all the three time-points, i.e., 2, 4 and 8 h are 80, 50, and 70 %, respectively.

Also it can be observed that 9 out of 10 output molecules match exactly at least at two time-points. Even though in few cases, the simulation results of the expression values at a particular time point show an apparent mismatch with the experimental observation at that same time-point, but the expression pattern essentially remains the same over time. It can be observed that although the time-course expression of c_FOS from the

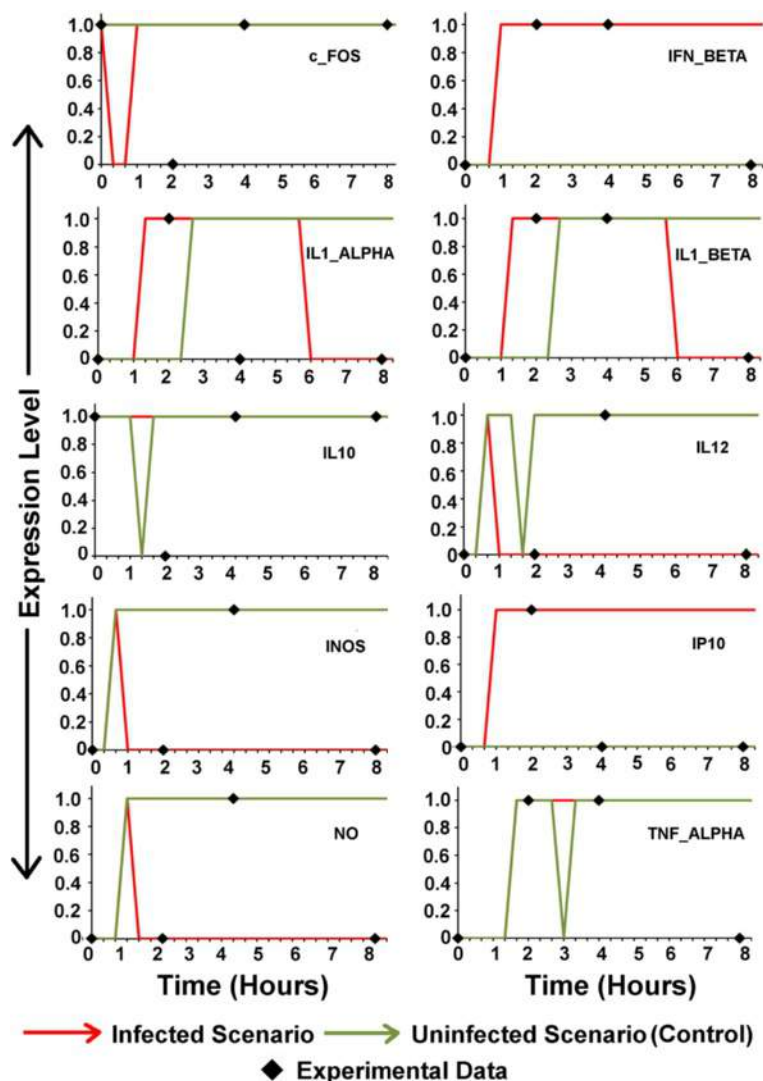


Fig. 3 Time-course expression profile of APC output molecules. Expression levels of the output molecules c_FOS, IFN_BETA, IL1_ALPHA, IL1_BETA, IL10, IL12, INOS, IP10, NO, and TNF_ALPHA found in infected, uninfected and experimental conditions. The validation was performed by comparing the expression levels of the infected situations (shown in red) with the microarray experimental data (black diamond)

simulation results appear to be inconsistent with experimental data, i.e., downregulation at 2 h and again upregulation at 4 h time-point, the overall dynamics of the expression essentially remains the same over time, with only a slight deviation of the expression levels (up or down) observed in the respective time-points of experimental and simulation data. Such deviations are also observed in the expression dynamics of IL1_ALPHA, IL12, NO, and INOS molecules. The successful validation of the expression levels of these molecules can be used as valuable indicators of the immune functions of the APC and can be used for fine-tuning of our model to ensure its proper functioning. On the other hand, Fig. 3 also brings out the differences in the expression of the APC output molecules due to the presence of the infection.

Here, it is observed that even though the steady state values of the two scenarios (viz. infected and the uninfected) is sometimes similar, as in the cases of c_FOS, IL10, and TNF_ALPHA, the overall temporal expression pattern clearly indicates that the differences are emerging due to the presence of antigen molecules in the model simulation. In the uninfected scenario, the expression of the IL10 and the TNF_ALPHA remains low (in the first few hours) as compared to the infected scenario.

3.3.3 Comparison of uninfected and infected scenarios

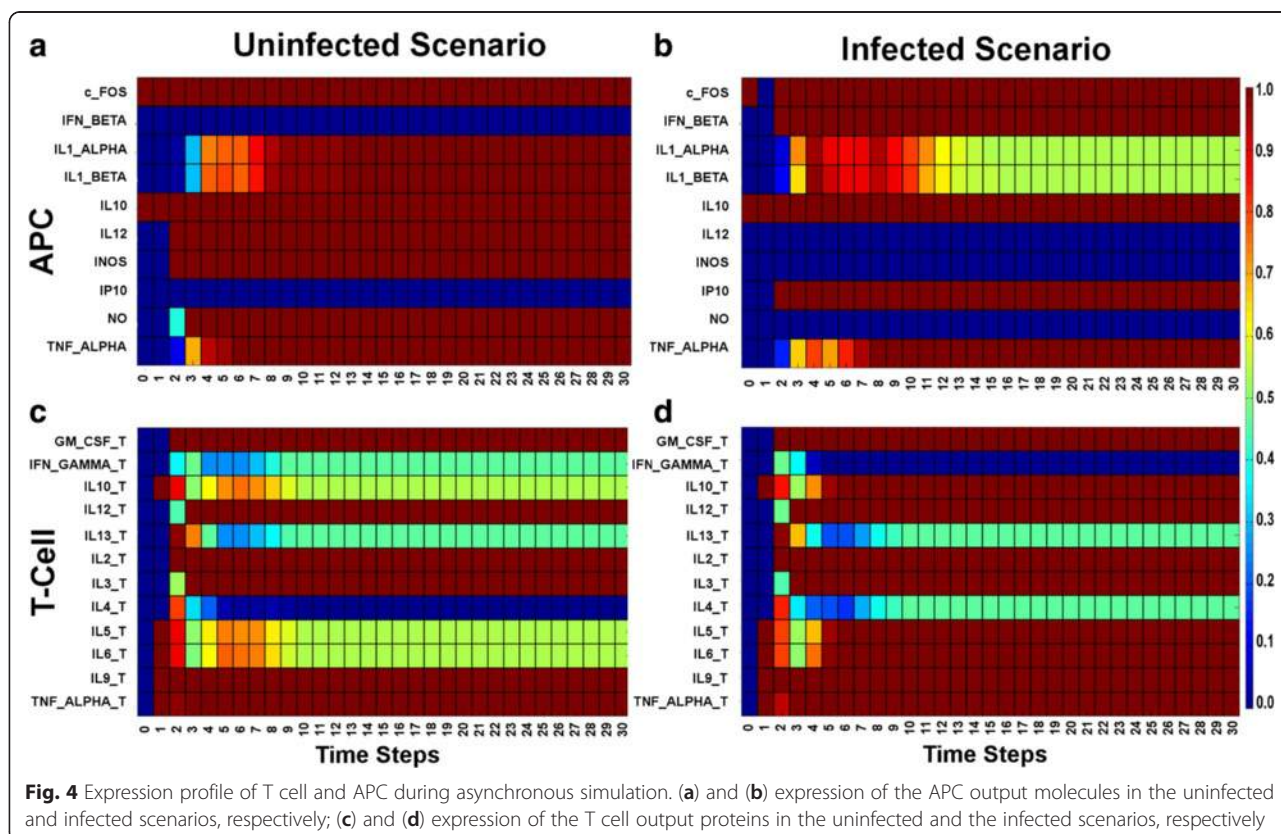
The interference of *Leishmania* proteins in the signaling cascade of APC cell not only modulates the expression of the output molecules and microbicidal

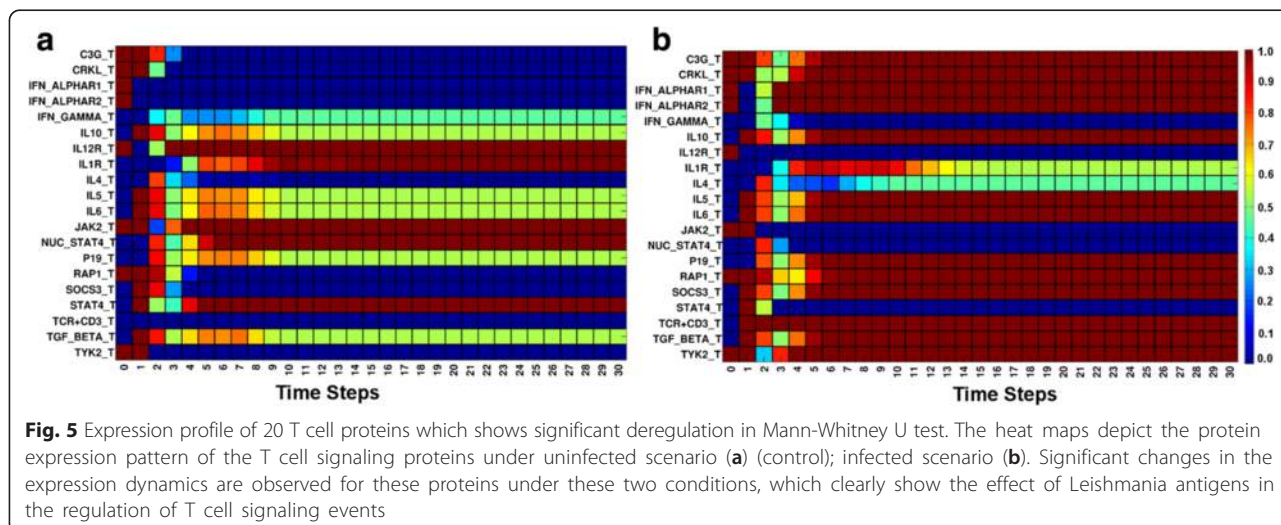
activities of APC, but also deregulates the expression of the T cell output molecules by manipulating the normal functioning of T cell activation pathway [49]. Comparing the expression of the APC output proteins in infected and uninfected scenarios (Fig. 4a, b), the simulation results show that invasion of *Leishmania* antigen molecules severely downregulates the expression of IL12, which is a potent T cell stimulator [2, 6]. Simultaneously, the production of INOS and nitric oxide (NO) is also greatly reduced in the infected APC, thereby rendering the cell incapable of performing its microbicidal functions, and creating an immune-suppressed condition, which is favorable for the continued survival of the pathogen inside APC [2, 3]. Besides, in Fig. 4b, the production of IFN- β , IP10 (a chemokine) also show an upregulation, indicating an attempt of the APC to eliminate the pathogen from the system [3, 25, 46]. IL1- α and IL- β show minor fluctuations in expression during the infection and slight downregulation [2, 50]. The effect of *Leishmania* infection on the expression pattern of T cell output proteins (Fig. 4c, d) becomes evident from the fact that production of the protective cytokine from the cell, such as IFN- γ , is downregulated during the infection, while the productions of interleukins, such as IL10, IL4, IL5, and IL6 are upregulated, which are mostly implicated as proteins favoring *Leishmania* survival [7, 49, 51, 52]. These results supported by the

previous experimental findings also strengthen the validity of our model to a greater extent and enhances its acceptability for further analysis.

3.3.4 Effect of infection on T cell signaling cascade

The results of Mann-Whitney U test reveals that out of the expression of 62 proteins in the infected scenario that exhibit a deviation from the uninfected scenario, 20 proteins get significantly deregulated ($P < 0.05$). The temporal expression profiles of these 20 proteins (Fig. 5) show that the *Leishmania* infection causes the significant downregulation of the protective cytokines, such as IFN- γ , and enhances the synthesis of TGF- β , and IL10 from the T cell, which contributes to the decline in the immune-competency of the T cell and formation of an immune-suppressed condition as observed during *L. major* infections in susceptible patients [5, 6, 53, 54]. It is interesting to note that while the activation of the cytokines, such as IL4, IL5, IL6, and the receptors, IL12R and IL1R [55], show fluctuations with respect to the control (uninfected scenario), certain other molecules, such as RAP1, P19, C3G, CRKL, TYK2, and SOCS3, are distinctly upregulated as a result of the infection. Also, it is observed that the members of the JAK-STAT pathway, such as JAK2 and STAT4 are downregulated in the infected scenario (Fig. 5b).





3.3.5 Immune response and immunotherapeutic strategies

The effector molecules produced at the end of the signaling processes in both T cell and APC manifest itself in the form of a change in the phenotypic behaviors of the cell that leads to disease clearance. Through the model, these immune responses of the entire system are simulated using the functions: TH₁ response (Eq. 1), TH₂ response (Eq. 2), and NO production (Eq. 3)—signifying healing response (green line), non-healing response (red line) and disease clearance (black triangular markers), respectively (Fig. 6). The pathogen load is one of the major factors, which determines the type of immune response that will be elicited during the infection [4]. When the antigens are OFF (i.e., mimicking a situation with low pathogen load, or no infection), the Th₁ and the NO responses are higher as compared to the Th₂ response (Fig. 6a) [6, 44]. On the contrary, when the antigen molecules are switched ON (i.e., infection is present), a higher Th₂-response is obtained (Fig. 6b) [4, 56].

After validating these immune response functions with published literatures, these functions (Eqs. 1, 2, and 3) confirm their acceptability and authenticity to study the effect of the conventional immunotherapeutic strategies in Leishmaniasis (i.e., IL12 and IFN_GAMMA_T), and also to predict some immunostimulatory targets to enhance anti-*Leishmania* immunity (Table 1). Here, at first, we have tried to study the effect of the commonly practiced IL12 (Fig. 6c) and IFN_GAMMA_T (Fig. 6d) treatments and have observed that even though these immunostimulants can enhance the Th₁ response and downregulate the Th₂ response, they fail to enhance the NO response. Thereafter, through perturbation analysis we have been able to identify three T cell molecules (viz. MKP_T, SHP2_T, and SHC_T) and two APC molecules (viz. TLR3 and TLR2) that may have a positive role in disease clearance. Single in silico mutation study of these

molecules reveals that in the MKP_T in silico knock-in scenario (Fig. 6e), even though the Th₁ response of the NO response does not increase, the Th₂ response gets downregulated as compared to the infected scenario (Fig. 6b). Knock-in mutation of the APC molecule TLR3 gives rise to an increase in NO response, although it has no significant effect on the T cell response (Fig. 6f). In the case of in silico knock-out mutation studies, we have observed that inhibition of SHP2_T leads to upregulation of the Th₁ response and downregulation of the Th₂ response (Fig. 6g). SHC_T inhibition on the other hand, does not exhibit any significant change in T cell or NO responses as compared to the infected scenario (Fig. 6h). However, if we use a combinatorial therapy by activating the proteins TLR3 while simultaneously inhibiting SHP2_T, we get a better anti-*Leishmania* immune response (combination 1, Fig. 6j). Alternatively, TLR3 knock-in when combined with SHC_T OFF (knock-out) and MKP_T ON (knock-in) can also give rise to a similar effect (combination 2, Fig. 6k). Besides these combinations, interestingly we have also found that if we inhibit only the expression of TLR2 protein in APC, a very high Th₁ response is obtained and simultaneously the NO production is also increased drastically (Fig. 6i). A summary of the combinatorial therapeutic strategies and their outcomes as observed from our analysis is provided in Table 1.

Further, the results of the Boolean attractor analysis, performed to confirm the robustness of our predictions, reveal that the uninfected and infected scenarios created in our model reaches to unique attractors, viz. (...110...) and (...001...), respectively (Fig. 7 a, b). Here, the attractor denotes the presence/absence of the NO, Th₁, and Th₂ responses (Fig. 7). The attractor analysis of perturbation studies reveals that the scenario with IFN_GAMMA_T treatment leads to

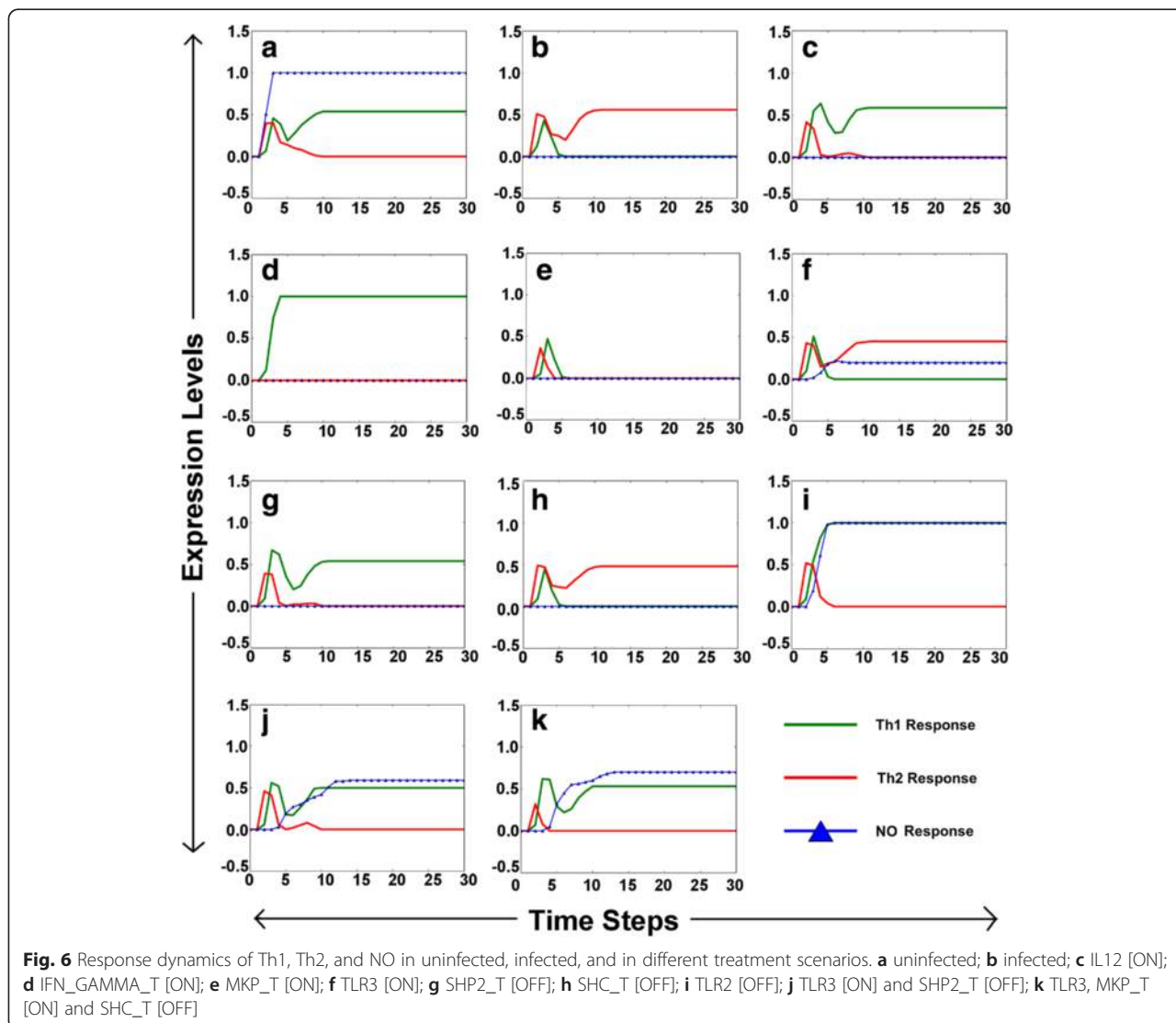


Table 1 Unique combinations of proteins that can be used as promising immunotherapeutic targets

Knock-in	Knock-out	Th1 response up-regulation	NO increase	Th2 response down-regulation	Anti-Leishmania Immunity ^b	Figure
IL12 ^a	–	Yes	No	Yes	No	6c
IFN_GAMMA_T ^a	–	Yes	No	Yes	No	6d
MKP_T	–	No	No	Yes	No	6e
TLR3	–	No	Yes	No	No	6f
–	SHP2_T	Yes	No	Yes	No	6g
–	SHC_T	No	No	No	No	6h
–	TLR2	Yes	Yes	Yes	Yes	6i
TLR3 ^c	SHP2_T ^c	Yes	Yes	Yes	Yes	6j
TLR3, MKP_T ^d	SHC_T ^d	Yes	Yes	Yes	Yes	6k

^arepresents previously known and commonly used immunotherapeutic targets; ^brepresents anti-Leishmania immunity that implies to a state when Th1 and NO response is up-regulated and the Th2 response is down-regulated; ^crepresents the proposed Combination 1; ^drepresents the proposed combination 2 treatment strategy

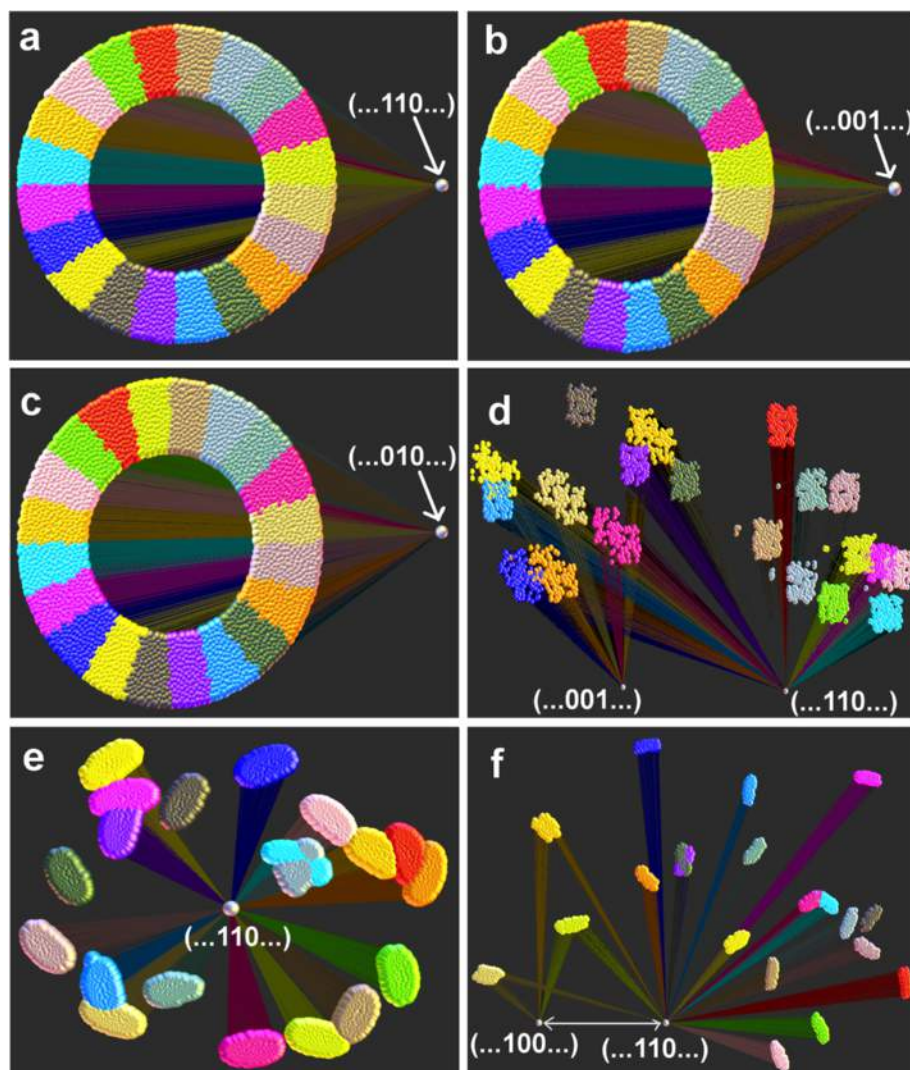


Fig. 7 Attractor analysis of the uninfected (**a**), infected (**b**), and in silico treatment scenarios (**c–f**). Here, the binary values at the attractor states represent only the logical steady states of NO, Th1, and Th2 responses under uninfected (**a**), infected (**b**), IFN_GAMMA_T [ON] (**c**), TLR2 [OFF] (**d**), TLR3 [ON] and SHP2_T [OFF] (**e**), TLR3, MKP_T [ON] and SHC_T [OFF] (**f**). The logical states of the other nodes/protein molecules are not shown here for the sake of better visualization. The *color codes* are kept same as used in Fig. 2

a single attractor (...010...), which is distinct from either the infected or the uninfected attractors (Fig. 7c). However, our predicted targets, viz. TLR2 (Fig. 7d), combination 1 (TLR3 ON and SHP2_T OFF; Fig. 7e), and combination 2 (TLR3, MKP_T ON and SHC_T OFF; Fig. 7f) mostly lead to the infection-free attractor (...110...) similar to the uninfected scenario. Among these, it can be observed that all the 2560 basins in the combination 1 scenario lead only to the infection-free attractor (...110...) (Fig. 7e), while in combination 2, we observe the presence of a bi-stable attractor, oscillating between the (...100...) and (...110...) states (Fig. 7f). TLR2 mutation scenario also shows the presence of two attractors, i.e., (...001...) and (...110...). However, in all these three perturbations the major attractor attained by the

system continues to be the desired (...110...) infection-free attractor.

4 Discussion

Inadequate knowledge of the complete mechanism of *Leishmania* invasion inside the host immune system is the key reason for the low success in devising an effective cure to leishmaniasis. In order to overcome this short-coming, it is necessary to gain insight into the precise mechanism of the regulation by which the *Leishmania* antigen molecules takes control of the host cell's signaling processes. Through this in silico modeling study, we have tried to unravel these regulatory mechanisms by focusing on three important aspects of *Leishmania* immunobiology—(a) effect of *Leishmania* infection on the gene expression or

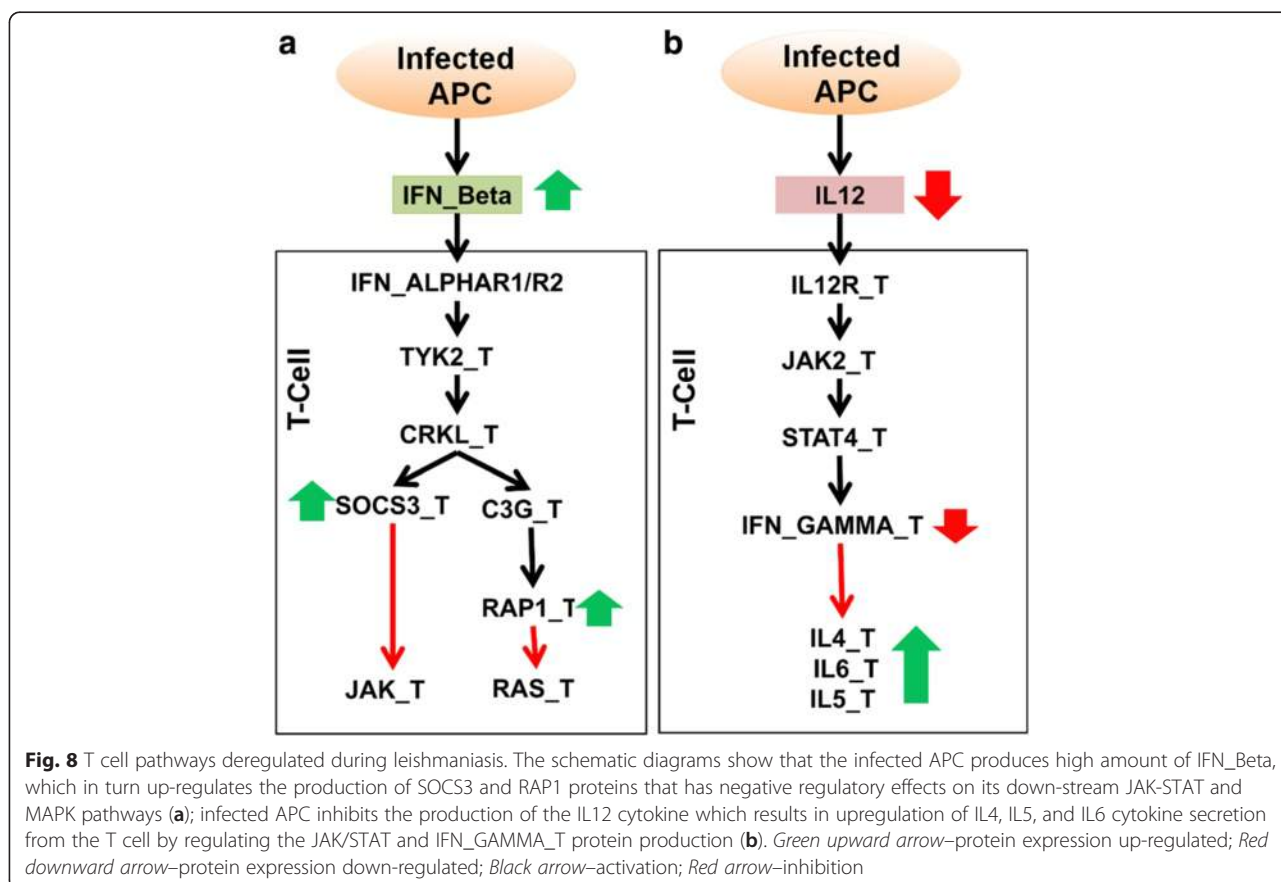
the protein activation pattern in APC and microbicidal activities, (b) effect of the infection on the T cell gene/protein expression pattern at the molecular level and their influence in pathway level to identify the molecular routes by which *Leishmania* inhibits T cell functions, and (c) identification of specific regulators (immunostimulators) that could act as a regulatory switch to skew the Th1/Th2 dynamics towards the healing Th1 response and simultaneously enhance the NO production in order to accelerate the parasite clearance from the host cell.

In this model, we have manually curated the complete signaling cascades of the immune cells depicting the detailed mechanism of regulation of the host protein-protein interaction network by the antigen molecules at various levels of signal transduction and transcriptional activities. Here, we have been able to integrate all the possible routes by which the antigen subverts the host immune responses and modulates the proper functioning of the sentinels of our immune systems, viz. the APCs and the T cells. The model (Additional file 4: Figure S3) depicts the physical binding of the T cell and APC receptors/co-receptors with their corresponding ligands and the subsequent activation mechanism of the downstream proteins in both the cells. The model considers the activation of toll-like-receptor proteins, present in the APC membrane, activate their downstream proteins, which in turns diverges into important signaling routes such as the RAS-RAF mediated MAPK pathway, canonical, and non-canonical NFKB pathway, JAK-STAT pathway, PI3K-PLC Gamma pathway, JNK pathway, etc., and leading to the activation of several transcription factors (e.g., ERK1_2, NFKB, NFAT, AP1, STAT3, etc.) in the nucleus, that in due course, singly or in combination with other transcriptional co-factors initiates the mRNA transcription [39]. These mRNA are then considered to undergo alternative splicing to produce different proteins isoforms with diverse biological functions that regulates the expression of the output molecules. These proteins (principally the cytokines, growth factors, and the cell cycle proteins) synthesized at the end of the cascade, in response to the pathogenic invasion, manifest externally in the form of a change in the cellular behavior, here referred to as a “phenotypic response” viz. the Th1-response, Th2-response, and NO-response (Eqs. 1, 2, and 3) [5].

Boolean attractor analysis reveals the presence of a single attractor in the uninfected scenario and four attractors in the infected scenarios, signifying that depending on the severity of the infection and the presence or absence of certain molecules in the system, *Leishmania* infection may lead the system to multiple levels of infection with varying protein expressions and clinical manifestations (Fig. 2). It can also be observed that the major attractor obtained in these uninfected and infected scenarios matches exactly with the expression values as obtained through our simulations using experimental data in both

the scenarios. Asynchronous Boolean simulation is also performed to obtain an average behavior of the entire system under different conditions. Such comparative studies of the infected and uninfected scenarios using asynchronous Boolean simulations brings out the effect of the *Leishmania* infection on the expression of the output molecules in both the APC and the T cell (Figs. 3 and 4), which nicely corroborates with previous experimental studies and strengthens the reliability and authenticity of the model outcomes. We have observed that *Leishmania* infection down-regulates the production of protective cytokines, such as IL12, IL1_ALPHA and IL1_BETA, and microbicidal molecules, such as NO, and simultaneously up-regulating the production of the chemokine, IP10 [3]. The simulation also reveals that in the infected scenario the production of the cytokine IFN_BETA is also upregulated, which is known to have protective functions but only at low doses [25]. The T cell expression profile shows that during *Leishmania* infection, the interleukin molecules viz. IL10_T, IL4_T, IL5_T, and IL6_T, gets upregulated, while the expression of IFN_GAMMA_T gets downregulated (Fig. 4c, d). The higher production of the proteins, such as IL10_T and IL4_T and repression of IFN_GAMMA_T synthesis, produces conditions that favor *Leishmania* survival [7], and skews the Th1/Th2 dynamics towards a non-healing response (Fig. 6b) [2, 50].

A close observation on the results of our Mann-Whitney *U* test analysis (Fig. 5) also predicts some novel and interesting facts about the signaling regulations imposed by the presence of the *Leishmania* infection at the pathway level. Identified from our simulation, this regulatory mechanism of the signaling cascades is presented in Fig. 8. It can be observed that *Leishmania* infection increases the production of the protein IFN_BETA (green upward arrow) and suppresses IL12 (red downward arrow) from the APC. IFN_BETA diffuses and interacts with their corresponding receptors on the T cell thereby enhancing the activation of its downstream TYK2 molecule (black arrow) inside the T cell. Through this analysis, we have tried to determine the possible role of *L. major* infection in modulating the T-cell behavior at the pathway level, and infer that the pathogen upregulates the molecules involved in the TYK-CRKL-C3G pathway. Eventually, it enhances the production of SOCS3 and RAP1 proteins in the T cell (Fig. 8a), two potential negative regulators of JAK-STAT and the RAS-mediated MAPK pathways, respectively (red arrow), which divulges the probable harmful effects of the high levels of IFN_BETA production from the APC that is known to occur during *Leishmania* infection [57, 58]. Moreover, it can be observed that in the T cell (Fig. 8b), the pathogen downregulates the JAK2-STAT4 pathway by inhibiting the synthesis of IL12 cytokine, which results in downregulation of IFN_GAMMA production (red downward arrow) and a



consequent increase in the IL4_T, IL5_T, and IL6_T expression (green upward arrow). These findings of the changes occurring at the pathway level have helped us further to identify the key regulators that can act as potential immunostimulators during the infection.

Cytokine therapy is the most widely practiced method of immunotherapy, is employed in the treatment of Leishmaniasis. Immunologists have tried to enhance the expression of IL12 and IFN_GAMMA, the two most potent Th1 response stimulators, which are known to play important role in alleviation of the disease. But, the most common problem faced in such immunotherapies is the inhibitory effect of the IL10 protein, which is overexpressed during the infection that increases the susceptibility to the disease by inhibiting the effects of interferon-gamma treatment and often blocking the synthesis of NO [59], thereby preventing an effective anti-*Leishmania* immunity. In this work, we have tried to simulate the effect of these two immunotherapeutic strategies, viz. IL12 treatment (Fig. 6c) and IFN_GAMMA_T treatment (Fig. 6d), where we have observed that although they are able to enhance the Th1 response and reduce Th2 response, but these strategies fail to induce the NO response, which is necessary to eliminate the disease causing

pathogen. Hence, to devise a successful combinatorial immunotherapy, which can bypass the inhibitory effects of immune-suppressive molecules, various molecules that directly or indirectly influence the de-regulated T cell pathways (i.e., JAK2-STAT4 pathway and the TYK2-mediated IFN_BETA pathways) and TLR molecules of the antigen-presenting cell are selectively knocked-in and knocked-out separately and then in combination (Table 1). Thereafter, a set of minimal combinations of protein molecules are identified that could act as regulatory switch to control the Th1/Th2 response and also effectively enhance an anti-*Leishmania* response (Table 1). These molecules include three T cell molecules (viz. SHP2_T, MKP_T and SHC_T), which are also implicated in various cancers and infectious disease treatments, and two APC molecules (viz. TLR2 and TLR3), which are popular targets in many diseases including leishmaniasis [60–63]. A list of antagonists and agonists of these molecules is provided in Additional file 1: Table S4.

Through our study, we suggest that TLR2, which is debated to have the controversial roles in *Leishmania* treatment [23], helps in the parasite survival. This agrees with a recent experimental finding [24], and we propose that TLR2 inhibition can be a useful strategy to up-

regulate Th1 and NO response (Fig. 6i). On the other hand it can be understood that TLR3 alone may have a positive role to play in *Leishmania* treatment and may be a positive regulator of NO production (Fig. 6f). It is also interesting to note that although TLR2 inhibition alone is sufficient to drastically enhance the Th1 response and the NO production (Fig. 6i), TLR3 activation requires a synergistic inhibition of the SHP2_T molecule, a phosphatase that inhibits the activity of the JAK-STAT pathway, to gain the desired anti-*Leishmania* response (Fig. 6j). Surprisingly, it is also observed the MAPK phosphatase (MKP_T) when upregulated may inhibit the non-healing Th2 response (Fig. 6e). However, MKP_P and TLR3 upregulation when combined with the inhibition of the adapter molecule SHC_T, a positive regulator of the MAPK cascade, can act as a useful combinatorial target in leishmaniasis treatment (Fig. 6k). Nevertheless to combat leishmaniasis, it may be noted here that since the Th1 subset of helper T cells produces inflammatory cytokines, a constant high Th1 response may often be undesirable in order to avoid harmful side-effects, and hence the two combinations: (1) combination 1: upregulation of TLR3 (i.e. ON state) and downregulation of SHP2_T (i.e., OFF state) and (2) combination 2: upregulations of TLR3, MKP_T, and downregulation of SHC_T, can be considered as better immunotherapeutic strategies than solitary TLR2 inhibition.

The robustness of our predicted combinations was further confirmed through the Boolean attractor analysis, where we observed that the major attractor attained by all the three predicted immunotherapeutic targets resembles with the infection-free attractor (...110...). This is also observed in the uninfected scenario (Fig. 7 d–f), where the NO and Th1 responses are high and the Th2 response is low. In contrast, it can be observed that none of the basins in the IFN_GAMMA_T treatment scenario is able to move the system to this desired (...110...) attractor, which clearly brings out the shortcomings of the conventional immunotherapeutic targets (Fig. 7c). The result of this analysis also highlights the controversial outcomes that may be expected from targeting TLR2 (as mentioned earlier), i.e., TLR2 knock-out may lead to two separate attractors, (...100...) and (...110...). However, it is to be noted that the major attractor obtained in the TLR2 knock-out scenario is the infection-free attractor (...110...), while only a small fraction reaches the attractor (...100...), where although the NO production is high, both the Th1 and the Th2 responses gets downregulated (Fig. 7d). Also, a comparative analysis of the combination 1 and combination 2 scenarios reveals that combination 1 may be considered a better target as compared to the others, as this is the only scenario where we can observe a complete reversal of the infected

scenario to a situation (...110... attractor) similar to the uninfected scenario. However, since the combination 2 is leading to a bi-stable attractor, which is oscillating between the major attractor (...110...) and minor attractor (...100...) states, this may also be useful in cases where a constant high NO production is required accompanied with an intermittent up-regulation of Th1 response for patients pre-disposed to inflammatory diseases.

It is important to note that in order to reduce the complexity of the model and due to lack of complete information about the functional regulations of the isoforms in *Leishmania* infected situation, we have only focused on the alternative splicing mechanism at the post-transcriptional level. However, this model may further be extended to study the effect of the alternatively spliced isoforms of the input molecules [64]. For example, TLR3 mRNA molecule is alternatively spliced to produce a smaller 60 kDa isoform, which has been observed to be overexpressed in Glioblastoma cell lines. In future, RNA seq analysis of *Leishmania* infected human APC may provide further insight into the expression of such alternatively spliced isoforms in case of *Leishmania* infection scenario. This may also give a better understanding of the precise regulatory mechanisms underlying the differential protein expression due to the pathogenic invasion.

5 Conclusions

The switching between the Th1/Th2 responses during *Leishmania* invasion has important implications in Leishmaniasis treatment, and hence effective regulation of this switching mechanism is important for devising a proper cure for the disease. In this work, we have been able to capture some of the vital aspects of *Leishmania* infection and the mechanism through which the interaction of the *Leishmania* antigen molecules with the APC signaling proteins modulate the microbicidal activity of both the APC and T cell. Although our model does not deal with the dynamics of the entire system due to the large number of unknown parameter sets, but through the logical analysis of the integrated *Leishmania*-APC-T-cell model, we have been able to precisely highlight the inhibitory effects of *Leishmania* infection on the T cell's signaling routes and Th1/Th2 immune responses. Here, we suggest that *Leishmania* infections enhances the secretion of the IFN_BETA from the APC, which in turn can up-regulate the production of the RAP1 and SOCS3 proteins inside the T cell, the potential inhibitors of MAPK and JAK-STAT signaling pathways, respectively, via the TYK2-mediated pathway. The other T cell pathway affected in *Leishmania* infection is the JAK2-STAT4 pathway. Enhancing the activity of this

pathway in the T cell by inhibition of the phosphatase SHP2, and simultaneously regulating the activity of the TLR3 molecule in the APC, we have also been able to identify certain unique combinations of proteins, which can act as regulatory switch to shift the Th2 response towards the Th1 response, and at the same time can increase the production of NO. The study highlights a negative role of the T cell SHC molecule and a positive role of the MKP molecule in leishmaniasis treatment. Attractor analysis study firmly establishes the reasons for the failure of the conventional immunotherapeutic targets, such as IFN_GAMMA_T treatment, and ensures that our proposed combinations of protein molecules when targeted reverts the system to an infection-free attractor. Hence, it may be inferred that the proposed combinations of target molecules can be efficiently used as potent immunostimulators to yield an effective anti-*Leishmania* immune response and expedite the process of parasite clearance from the system. We also hope that in future this computational study will be a useful tool for identification of important immunostimulatory targets for better treatment and alleviation of leishmaniasis.

6 Additional files

Additional file 1: This file contains the following Supplementary Materials. Text S1. Construction of gene co-expression network from *Leishmania* infected APC time course microarray data. **Table S1.** Pathway Enrichment of the significantly expressed genes in the microarray experiment of *Leishmania* infected APC. **Text S2.** Construction of gene co-expression network from time course activated T-cell microarray data. **Table S2.** Pathway Enrichment of the significantly expressed genes in the microarray experiment of activated T-cell. **Text S3.** Brief description of the *Leishmania*-APC-T-cell Signaling Pathways. **Text S4.** Differential regulation of different splicing FACTORS and isoforms. **Table S3.** List of all known alternatively spliced isoforms of the output molecules of both APC and T-cell. **Text S5.** Logical Equations used to model the reaction mechanisms in T-cell and APC during *Leishmania* infection. **Text S6.** Binary initial values of the reaction nodes considered in the Logical equations from binarization of microarray expression data. **Table S4.** List of agonist and antagonist of the proposed targets (DOCX 128 kb)

Additional file 2: Figure S1. Gene clusters identified in *Leishmania major* infected APC microarray data. This figure contains total 10 clusters or functional modules, which have been identified from the gene co-expression network generated from the time course microarray expression data of *Leishmania major* infected APC [EBI-ArrayExpress (ID: E-GEOD-42088)]. The names of the nodes in all the cluster diagrams are assigned according to the probe IDs used in HG-U133_Plus_2 Affymetrix GeneChip for human cell. (TIF 2077 kb)

Additional file 3: Figure S2. Gene clusters identified in active T-cell microarray data. This figure contains total 24 clusters or functional modules, which have been identified from the gene co-expression network generated from the time course microarray expression data of activate T-cell [EBI-ArrayExpress (E-GEOD-48978)]. The node names used in each cluster are in accordance with the probe IDs used in Affymetrix HT_HG-U133_Plus_PM array plate. (TIF 4656 kb)

Additional file 4: Figure S3. Comprehensive diagram of T-cell, APC and *Leishmania* pathogenic protein-protein interaction network. The diagram presents an integrated view of the T-cell and APC interaction

signaling pathway during *Leishmania* infection. The different molecules involved in the signaling cascade have been color coded according to its type and cellular location. The molecules colored as red signify the *Leishmania* antigen molecules. The interaction lines have been color coded according to the type of chemical reaction such as phosphorylation (blue), inhibition (red), activation (green) etc. (TIF 5212 kb)

Additional file 5: Figure S4. Attractor analysis of the uninfected and infected scenarios under the differential activation of the splicing factors. (A) In the uninfected scenario the system reach two stable steady state attractors, in which the expressions of IFN_BETA, IL10, IL12, IL1_ALPHA, IL1_BETA, INOS, IP10, NO, TNF_ALPHA and C_FOS proteins are (0111110111) or (0110010111). (B) In the infected scenario, the system reach two stable steady state attractors namely (1100010111) and (1101101011), respectively. (TIF 339 kb)

Abbreviations

APC: antigen-presenting cell; Th1 response: type I T-helper cell cytokine response; Th2 response: type II T-helper cell cytokine response; NO: nitric oxide molecule; LPG: lipophosphoglycan; PPI: protein-protein interaction; CMI: cell-mediated immunity.

Competing interests

The authors declare no conflict of interests.

Authors' contribution

Conceived the study: RRS Designed and performed the experiment: PG and SC¹ Data curation and pathway reconstruction: PG and SC² Model development and data analysis: RRS, PG, SC¹ and SC² Result interpretation and manuscript writing: RRS, PG and SC¹

Acknowledgements

We thank Council of Scientific and Industrial Research, XII Five Year Plan Project "HOPE" (BSC0114) for providing financial support to perform this work. Saikat Chowdhury acknowledges the research fellowship from DST-INSPIRE fellowship program.

Received: 4 August 2015 Accepted: 18 November 2015

Published online: 01 December 2015

References

1. P Kaye, P Scott, Leishmaniasis: complexity at the host-pathogen interface. *Nat Rev Micro* **9**, 604–615 (2011)
2. M Olivier, DJ Gregory, G Forget, Subversion mechanisms by which *Leishmania* parasites can escape the host immune response: a signaling point of view. *Clin. Microbiol. Rev.* **18**, 293–305 (2005)
3. MT Shio, K Hassani, A Isnard, B Ralph, I Contreras, MA Gomez et al., Host cell signalling and leishmania mechanisms of evasion. *J Trop Med* **2012**, 819512 (2012)
4. JN Menon, PA Bretscher, Parasite dose determines the Th1/Th2 nature of the response to *Leishmania major* independently of infection route and strain of host or parasite. *Eur. J. Immunol.* **28**, 4020–4028 (1998)
5. U Sharma, S Singh, Immunobiology of leishmaniasis. *Indian J. Exp. Biol.* **47**, 412 (2009)
6. D Liu, JE Uzonna, The early interaction of *Leishmania* with macrophages and dendritic cells and its influence on the host immune response. *Front Cell Infect Microbiol* **2**, 83 (2012)
7. D McMahon-Pratt, J Alexander, Does the *Leishmania major* paradigm of pathogenesis and protection hold for New World cutaneous leishmaniases or the visceral disease? *Immunol. Rev.* **201**, 206–224 (2004)
8. P Saha, D Mukhopadhyay, M Chatterjee, Immunomodulation by chemotherapeutic agents against Leishmaniasis. *Int. Immunopharmacol.* **11**, 1668–1679 (2011)
9. LF Oliveira, AO Schubach, MM Martins, SL Passos, RV Oliveira, MC Marzochi et al., Systematic review of the adverse effects of cutaneous leishmaniasis treatment in the New World. *Acta Trop.* **118**, 87–96 (2011)
10. WH Markle, K Makhoul, Cutaneous leishmaniasis: recognition and treatment. *Am. Fam. Physician* **69**, 1455–1460 (2004)
11. F Frézard, C Demicheli, RR Ribeiro, Pentavalent antimonials: New perspectives for Old drugs. *Molecules* **14**, 2317–2336 (2009)

12. M Mishra, UK Biswas, DN Jha, AB Khan, Amphotericin versus pentamidine in antimony-unresponsive kala-azar. *Lancet* **340**, 1256–1257 (1992)
13. AK Haldar, P Sen, S Roy, Use of antimony in the treatment of leishmaniasis: current status and future directions. *Mol Biol Int* **2011**, 23 (2011)
14. SL Croft, S Sundar, AH Fairlamb, Drug resistance in leishmaniasis. *Clin. Microbiol. Rev.* **19**, 111–126 (2006)
15. G Kolde, T Luger, C Sorg, C Sunderkötter, Successful treatment of cutaneous leishmaniasis using systemic interferon-gamma. *Dermatology* **192**, 56–60 (1996)
16. J Li, S Sutterwala, JP Farrell, Successful therapy of chronic, nonhealing murine cutaneous leishmaniasis with sodium stibogluconate and gamma interferon depends on continued interleukin-12 production. *Infect. Immun.* **65**, 3225–3230 (1997)
17. R Chatelain, S Mauze, RL Coffman, Experimental Leishmania major infection in mice: role of IL-10. *Parasite Immunol.* **21**, 211–218 (1999)
18. M Mol, MS Patole, S Singh, Immune signal transduction in leishmaniasis from natural to artificial systems: role of feedback loop insertion. *Biochim. Biophys. Acta Gen. Subj.* **1840**, 71–79 (2014)
19. M Mol, MS Patole, S Singh, Signaling networks in Leishmania macrophages deciphered through integrated systems biology: a mathematical modeling approach. *Syst. Synth. Biol.* **7**, 185–195 (2013)
20. L Albergante, J Timmis, L Beattie, PM Kaye, A petri Net model of granulomatous inflammation: implications for IL-10 mediated control of Leishmania donovani infection. *PLoS Comput. Biol.* **9**, e1003334 (2013)
21. K Hattori, M Nishikawa, K Watcharanurak, A Ikoma, K Kabashima, H Toyota et al., Sustained exogenous expression of therapeutic levels of IFN-gamma ameliorates atopic dermatitis in NC/Nga mice via Th1 polarization. *J. Immunol.* **184**, 2729–2735 (2010)
22. J Williams, G Jurkovich, G Hahnel, R Maier, Macrophage priming by interferon gamma: a selective process with potentially harmful effects. *J. Leukoc. Biol.* **52**, 579–584 (1992)
23. MS Faria, FC Reis, AP Lima, Toll-like receptors in leishmania infections: guardians or promoters? *J Parasitol Res* **2012**, 930257 (2012)
24. S Srivastava, SP Pandey, MK Jha, HS Chandel, B Saha, Leishmania expressed lipophosphoglycan interacts with Toll-like receptor (TLR)-2 to decrease TLR-9 expression and reduce anti-leishmanial responses. *Clin. Exp. Immunol.* **172**, 403–409 (2013)
25. J Mattner, A Wandersee-Steinhäuser, A Pahl, M Röllinghoff, GR Majeau, PS Hochman et al., Protection against progressive Leishmaniasis by IFN- β . *J. Immunol.* **172**, 7574–7582 (2004)
26. S Chowdhury, RN Pradhan, RR Sarkar, Structural and logical analysis of a comprehensive hedgehog signaling pathway to identify alternative drug targets for glioma, colon and pancreatic cancer. *PLoS One* **8**, e69132 (2013)
27. S Chowdhury, R Sarkar, Drug targets and biomarker identification from computational study of human notch signaling pathway. *Clin. Exp. Pharmacol.* **3**, 2161–1459.1000137 (2013)
28. HF Fumiã, ML Martins, Boolean network model for cancer pathways: predicting carcinogenesis and targeted therapy outcomes. *PLoS ONE* **8**, e69008 (2013)
29. J Saez-Rodriguez, L Simeoni, JA Lindquist, R Hemenway, U Bommhardt, B Arndt et al., A logical model provides insights into T cell receptor signaling. *PLoS Comput. Biol.* **3**, e163 (2007)
30. R Zhang, MV Shah, J Yang, SB Nyland, X Liu, JK Yun et al., Network model of survival signaling in large granular lymphocyte leukemia. *Proc. Natl. Acad. Sci. U. S. A.* **105**, 16308–16313 (2008)
31. P Ganguli, S Chowdhury, R Bhowmick, RR Sarkar, Temporal protein expression pattern in intracellular signaling cascade during T cell activation: a computational study. *J. Biosci.* **40**, 769–789 (2015)
32. ME Smoot, K Ono, J Ruscchinski, P-L Wang, T Ideker, Cytoscape 2.8: new features for data integration and network visualization. *Bioinformatics* **27**, 431–432 (2011)
33. D Tabas-Madrid, R Nogales-Cadenas, A Pascual-Montano, GeneCodis3: a non-redundant and modular enrichment analysis tool for functional genomics. *Nucleic Acids Res.* **40**, W478–W483 (2012)
34. M Kanehisa, S Goto, KEGG: kyoto encyclopedia of genes and genomes. *Nucleic Acids Res.* **28**, 27–30 (2000)
35. D Nishimura, BioCarta. *Biotech Soft & Internet Rep: Comput Softw J for Scient* **2**, 117–120 (2001)
36. K Kandasamy, SS Mohan, R Raju, S Keerthikumar, GS Kumar, AK Venugopal et al., NetPath: a public resource of curated signal transduction pathways. *Genome Biol.* **11**, R3 (2010)
37. A Chatr-aryamontri, B-J Breitkreutz, S Heinicke, L Boucher, A Winter, C Stark et al., The BioGRID interaction database: 2013 update. *Nucleic Acids Res.* **41**, D816–D823 (2013)
38. M Halle, MA Gomez, M Stuble, H Shimizu, WR McMaster, M Olivier et al., The Leishmania surface protease GP63 cleaves multiple intracellular proteins and actively participates in p38 mitogen-activated protein kinase inactivation. *J. Biol. Chem.* **284**, 6893–6908 (2009)
39. S Bhardwaj, N Srivastava, R Sudan, B Saha, Leishmania interferes with host cell signaling to devise a survival strategy. *J. Biomed. Biotechnol.* **2010**, 109189 (2010)
40. D Nandan, T Yi, M Lopez, C Lai, NE Reiner, Leishmania EF-1 α activates the Src homology 2 domain containing tyrosine phosphatase SHP-1 leading to macrophage deactivation. *J. Biol. Chem.* **277**, 50190–50197 (2002)
41. S Majumder, R Dey, S Bhattacharjee, A Rub, G Gupta, SB Majumdar et al., Leishmania-induced biphasic ceramide generation in macrophages is crucial for uptake and survival of the parasite. *J. Infect. Dis.* **205**, 1607–1616 (2012)
42. A Funahashi, M Morohashi, H Kitano, N Tanimura, Cell Designer: a process diagram editor for gene-regulatory and biochemical networks. *Biosilico* **1**, 159–162 (2003)
43. I Albert, J Thakar, S Li, R Zhang, R Albert, Boolean network simulations for life scientists. *Source Code Biol Med* **3**, 1–8 (2008)
44. S Romagnani, Type 1 T helper and type 2 T helper cells: functions, regulation and role in protection and disease. *Int. J. Clin. Lab. Res.* **21**, 152–158 (1992)
45. H Parkinson, U Sarkans, M Shojatalab, N Abeygunawardena, S Contrino, R Coulson et al., ArrayExpress—a public repository for microarray gene expression data at the EBI. *Nucleic Acids Res.* **33**, D553–555 (2005)
46. MA Favila, NS Geraci, E Zeng, B Harker, D Condon, RN Cotton et al., Human dendritic cells exhibit a pronounced type I IFN signature following Leishmania major infection that is required for IL-12 induction. *J. Immunol.* **192**, 5863–5872 (2014)
47. S Zhao, WP Fung-Leung, A Bittner, K Ngo, X Liu, Comparison of RNA-Seq and microarray in transcriptome profiling of activated T cells. *PLoS One* **9**, e78644 (2014)
48. C Müssel, M Hopfensitz, HA Kestler, BoolNet—an R package for generation, reconstruction and analysis of Boolean networks. *Bioinformatics* **26**, 1378–1380 (2010)
49. I Müller, T Pedrazzini, JP Farrell, J Louis, T-cell responses and immunity to experimental infection with Leishmania major. *Annu. Rev. Immunol.* **7**, 561–578 (1989)
50. E Von Stebut, JM Ehrchen, Y Belkaid, SL Kostka, K Molle, J Knop et al., Interleukin 1 α promotes Th1 differentiation and inhibits disease progression in Leishmania major-susceptible BALB/c mice. *J. Exp. Med.* **198**, 191–199 (2003)
51. K Kemp, Cytokine-producing T cell subsets in human leishmaniasis. *Arch Immunol Ther Exp* **48**, 173–176 (2000)
52. H Himmelrich, C Parra-Lopez, F Tacchini-Cottier, JA Louis, P Launois, The IL-4 rapidly produced in BALB/c mice after infection with Leishmania major downregulates IL-12 receptor β -chain expression on CD4+ T cells resulting in a state of unresponsiveness to IL-12. *J. Immunol.* **161**, 6156–6163 (1998)
53. J El-On, Current status and perspectives of the immunotherapy of leishmaniasis. *Isr Med Assoc J* **11**, 623–628 (2009)
54. SL Reiner, S Zheng, ZE Wang, L Stowring, RM Locksley, Leishmania promastigotes evade interleukin 12 (IL-12) induction by macrophages and stimulate a broad range of cytokines from CD4+ T cells during initiation of infection. *J Exp Med* **179**, 447–456 (1994)
55. SL Kostka, J Knop, A Konur, MC Udey, E von Stebut, Distinct roles for IL-1 receptor type I signaling in early versus established Leishmania major infections. *J Invest Dermatol* **126**, 1582–1589 (2006)
56. A O'Garra, Cytokines induce the development of functionally heterogeneous T helper cell subsets. *Immunity* **8**, 275–283 (1998)
57. JS Rawlings, KM Rosler, DA Harrison, The JAK/STAT signaling pathway. *J. Cell Sci.* **117**, 1281–1283 (2004)
58. PJS Stork, Does Rap1 deserve a bad Rap? *Trends Biochem. Sci.* **28**, 267–275 (2003)
59. I Okwor, JE Uzonna, Immunotherapy as a strategy for treatment of leishmaniasis: a review of the literature. *Immunotherapy* **1**, 765–776 (2009)

60. C Zuany-Amorim, J Hastewell, C Walker, Toll-like receptors as potential therapeutic targets for multiple diseases. *Nat. Rev. Drug Discov.* **1**, 797–807 (2002)
61. T Bakken, M He, ML Cannon, The phosphatase Shp2 is required for signaling by the Kaposi's sarcoma-associated herpesvirus viral GPCR in primary endothelial cells. *Virology* **397**, 379–388 (2010)
62. JF Flandin, F Chano, A Descoteaux, RNA interference reveals a role for TLR2 and TLR3 in the recognition of *Leishmania donovani* promastigotes by interferon-gamma-primed macrophages. *Eur. J. Immunol.* **36**, 411–420 (2006)
63. FF Tuon, VS Amato, HA Bacha, T Almusawi, MI Duarte, NV Amato, Toll-like receptors and leishmaniasis. *Infect. Immun.* **76**, 866–872 (2008)
64. EJ Yang, JS Shin, H Kim, HW Park, MH Kim et al., Cloning of TLR3 Isoform. *Yonsei Med. J.* **45**, 359–361 (2004)

Submit your manuscript to a SpringerOpen[®] journal and benefit from:

- ▶ Convenient online submission
- ▶ Rigorous peer review
- ▶ Immediate publication on acceptance
- ▶ Open access: articles freely available online
- ▶ High visibility within the field
- ▶ Retaining the copyright to your article

Submit your next manuscript at ▶ springeropen.com



Integrative Approaches to Understand the Mastery in Manipulation of Host Cytokine Networks by Protozoan Parasites with Emphasis on *Plasmodium* and *Leishmania* Species

OPEN ACCESS

Edited by:

Alexandre Morrot,
Universidade Federal do Rio de Janeiro, Brazil

Reviewed by:

Danielle Oliveira Nascimento,
Universidade Federal do Rio de Janeiro, Brazil
Elisangela Costa Da Silva,
State University of Norte Fluminense, Brazil

*Correspondence:

Shashi Baruah
sbaruah@tezu.ernet.in,
sashibaruah@gmail.com

[†]Joint first author

Specialty section:

This article was submitted to
Microbial Immunology,
a section of the journal
Frontiers in Immunology

Received: 14 November 2017

Accepted: 01 February 2018

Published: 23 February 2018

Citation:

Mahanta A, Ganguli P, Barah P, Sarkar RR, Sarmah N, Phukan S, Bora M and Baruah S (2018) Integrative Approaches to Understand the Mastery in Manipulation of Host Cytokine Networks by Protozoan Parasites with Emphasis on *Plasmodium* and *Leishmania* Species. *Front. Immunol.* 9:296. doi: 10.3389/fimmu.2018.00296

Anusree Mahanta^{1,2†}, Piyali Ganguli^{3,4†}, Pankaj Barah¹, Ram Rup Sarkar^{3,4}, Neelanjana Sarmah¹, Saurav Phukan¹, Mayuri Bora¹ and Shashi Baruah^{1*}

¹Department of Molecular Biology and Biotechnology, Tezpur University, Tezpur, India, ²Institute of Stem Cell Biology and Regenerative Medicine, Bengaluru, India, ³Chemical Engineering and Process Development, CSIR- National Chemical Laboratory, Pune, India, ⁴Academy of Scientific and Innovative Research (AcSIR), CSIR-NCL Campus, Pune, India

Diseases by protozoan pathogens pose a significant public health concern, particularly in tropical and subtropical countries, where these are responsible for significant morbidity and mortality. Protozoan pathogens tend to establish chronic infections underscoring their competence at subversion of host immune processes, an important component of disease pathogenesis and of their virulence. Modulation of cytokine and chemokine levels, their crosstalks and downstream signaling pathways, and thereby influencing recruitment and activation of immune cells is crucial to immune evasion and subversion. Many protozoans are now known to secrete effector molecules that actively modulate host immune transcriptome and bring about alterations in host epigenome to alter cytokine levels and signaling. The complexity of multi-dimensional events during interaction of hosts and protozoan parasites ranges from microscopic molecular levels to macroscopic ecological and epidemiological levels that includes disrupting metabolic pathways, cell cycle (*Toxoplasma* and *Theileria* sp.), respiratory burst, and antigen presentation (*Leishmania* spp.) to manipulation of signaling hubs. This requires an integrative systems biology approach to combine the knowledge from all these levels to identify the complex mechanisms of protozoan evolution *via* immune escape during host–parasite coevolution. Considering the diversity of protozoan parasites, in this review, we have focused on *Leishmania* and *Plasmodium* infections. Along with the biological understanding, we further elucidate the current efforts in generating, integrating, and modeling of multi-dimensional data to explain the modulation of cytokine networks by these two protozoan parasites to achieve their persistence in host *via* immune escape during host–parasite coevolution.

Keywords: cytokine networks, manipulation, *Plasmodium*, *Leishmania*, inflammation, signalling hubs, cross regulation, system biology

INTRODUCTION

Parasitic protozoa are responsible for some of the major diseases of humans affecting several million people each year resulting in significant morbidity and mortality and loss of economic activity. There have been some gains in reducing the incidence of these diseases owing to better intervention strategies, but in absence of effective vaccines, diseases like malaria, leishmaniasis, trypanosomiasis still pose a major public health problem. These protozoans typically establish chronic infections validating their success in evasion and manipulation of host defense and of metabolic processes for their survival, proliferation, and transmission. Many of these pathogenic protozoa have adapted to intracellular habitat as seen in infections by *Plasmodium* spp., *Leishmania* spp., and others. The intracellular niche makes them vulnerable to lysosomal enzymes, reactive oxygen intermediates, and detection by cytosolic sensors of infection, but also offers some protection from adaptive immunity (1). This dynamic host–pathogen interaction, leads to the activation of a series of intracellular and intercellular biochemical signaling processes leading to synthesis of diffusible effector molecules that includes cytokines and reactive oxygen species. “The earliest stages of infection are a parasite’s first opportunity to establish itself within its host and conversely, it is also the host’s chance to mount a rapid and effective response to clear, or at least control the infection” (2). Recent studies demonstrate that pathogens including protozoa modulate the host cell environment by manipulating the host transcriptome by epigenetic modifications besides targeting the major signaling hubs of metabolic, immune, and cell cycle processes to promote their growth, multiplication and survival (3–9). Many protozoans secrete effector molecules that actively modulate host immune transcriptome to alter cytokine levels and signaling either to escape immune processes as in liver stages of *P. falciparum* or to drive their growth as seen in the blood stages of this pathogen.

Considering the diversity of protozoan pathogenesis, this review will focus on manipulation and hijacking of cytokine networks by *Leishmania* and *Plasmodium* spp. for their survival in human host. We will highlight few recently published representative omics and systems biology based studies on *Leishmania* and *Plasmodium* parasites, toward understanding modulation of cytokine and chemokine networks in the host by the parasite to achieve their persistence in host *via* immune escape.

CYTOKINES AND CYTOKINE REGULATION

Cytokines are small molecules of the immune system, synthesized by various cell types that by virtue of binding to their receptors present on a multitude of cells mediate immune cell activation, differentiation, and cross talk to maintain immune homeostasis (10, 11). Synthesis and regulation of cytokine expression depends on the type of stimulus, cell type, and its state of activation (12–14). Expression of cytokine genes is also regulated by epigenetic modifications that include DNA methylation, histone modifications, and higher order chromatin interactions (15, 16) and posttranscriptional regulation by micro RNA-mediated

mechanisms (16–19). Differentiation of immune cells as in T cell subpopulations and macrophage phenotypes is determined and regulated by cytokine environment (4, 16, 20, 21) and epigenetic modifications at cytokine gene loci (22, 23). Cytokine crosstalk between IFN α/β and TNF- α was noted to be at level of chromatin wherein IFNs in addition to regulating interferon signaling genes, also potentiated the TNF genes (4). Similarly, emerging data suggest extensive crosstalk between NLR family proteins of inflammation complex for IL-1 β and IL-18 secretion and other cytokines integrated signalosome facilitating integration of diverse pathways for optimal immune response (24). H3K27, methyltransferase enhancer of zeste homolog 1 is reported to promote TLR-triggered inflammatory cytokine production by suppressing the TLR negative regulator toll-interacting protein, thereby contributing to the full activation of the innate immune response against invading pathogens (25).

CYTOKINE SIGNALING MANIPULATION BY PROTOZOAN PATHOGENS

Intracellular protozoa modulate cytokine gene expression and signaling by some common themes that include targeting of transcription factors (15, 23) phosphorylation status of signaling molecules like STATs, immune check point molecules like CTLA-4 and PD-1 to drive regulatory pathways (26) as well as kinases (5, 6, 27). The pathways usually targeted by pathogens include NF- κ B, cell cycle, interferons, MAP Kinase JAK–STAT and pathways mediated by TLR and NLR receptors because of their wide range of functionality and core association with the host genome (28–30).

Toxoplasma spp. secrete dense granular protein (GRA) and Rhoptry proteins that activate host kinases and possess kinase activity, respectively, into host cell, which by phosphorylating STAT3 and STAT6, nuclear translocation of NF- κ B or activation status of MAPK pathways modulate the levels of IL-4, IL-6, IL-12, and IFN-g (31–35). “*T. gondii* inhibitor of STAT1 transcriptional is another secretory protein that recruits the host nucleosome remodeling and deacetylase complex to block STAT1-mediated gene transcription” (36). *Trypanosoma cruzi* modulates NF- κ B pathway by TLR and NLR mediated signaling for favorable cytokine environment (37–39) However, the protozoa is also reported to manipulate TGF β pathway (40) and also induces the production of IL-10 (40, 41) and arginase for its survival and replication.

PLASMODIUM AND HOST INFLAMMATORY RESPONSE

Malaria, caused by *Plasmodium* spp. of Apicomplexa phylum, has been the strongest evolutionary selective force in recent human history and has shaped human genome (42) and is one of the major causes of mortality of children below 5 years of age particularly in WHO African region, taking the life of a child every 2 min (43). The life cycle of the parasite is complex and completed in multiple stages in the human and in the mosquito (female *Anopheles* spp.) hosts with stage specific gene and protein signatures (44). Briefly, sporozoites inoculated into human

host by bite of infected mosquito travel to liver to mature into merozoites that infect RBCs to continue asexual cycle and also develop into gametocytes which, after fertilization in mosquito gut, develop and mature into sporozoites.

During the liver stages of the parasite, the host immune response tends to be tolerogenic and circumsporozoite protein was seen to inhibit NADPH oxidase and IL-12 and suppressed IL-6 and TNF- α secretion with simultaneous increase of IL-10 levels, allowing parasite to escape detection by immune system (45, 46).

Inflammation is recognized as pivotal feature of immune response to blood stages of *Plasmodium* infection (47). Notably, clinical manifestations of the disease are related to erythrocytic stage of infection. An early and finely balanced inflammatory response with increase in levels of pro-inflammatory IL-12, IFN- γ , TNF- α , IL-1 β , and IL-6 and of anti-inflammatory IL-10 and TGF- β is essential for resolution of parasitemia and of disease (48–52). However, pathological activation of exaggerated levels of the very same pro-inflammatory cytokines (cytokine storm) concomitant with lower levels of regulatory mechanisms has been attributed to severe and cerebral malaria syndromes (14, 53–57). A recent study examined the levels of different biomarkers of immune response and found high concentrations of sCDI63 and Fractalkine, which are involved in immune response downregulation and modulation of anti-inflammatory responses in asymptomatic malaria (58). These authors also reported high levels of Neopterin, which is related to increased cell-mediated immune responses and macrophage activation in severe and cerebral malaria patients, indicating an overall sustained state of inflammation supporting the hypothesis of intense and prolonged inflammatory response in severe and in cerebral malaria patients.

The question then arises is that why and how would the parasite drive intense inflammatory response that has the potential to be fatal which could limit parasite transmission and hence not be in interest of the pathogen? The answer appears to lie in (a) enhanced expression of adhesion molecules on endothelial cells by pro-inflammatory cytokines (IFN γ and TNF α) (59) and (b) by requirement for endothelial adhesion mediated by *P. falciparum* membrane protein 1 (PfEMP1) with CD36 and endothelial protein C receptor (EPCR) (60, 61). From the parasite view, endothelial sequestration is essential to escape clearance in spleen and to facilitate *falciparum* merozoite maturation. The highly diverse PfEMP1 proteins encoded by parasite *var* genes contain a Duffy-binding like and cysteine-rich interdomain region (CIDR) domains. Most CIDR α 1 domains bind to EPCR and CIDR α 2–6 bind CD36 (60, 61). Notably, interaction of EPCR with its ligand the activated protein C (APC) has a role in anti-inflammatory, coagulation homeostasis, and endothelial barrier protection functions (62) and its blockade of these functions by PfEMP1–EPCR interaction that is postulated to contribute to cerebral malaria pathology (59, 61). Interestingly, Smith et al. (61) found increased association of severe malaria with EPCR binding CIDR α 1 domain containing isolates supporting the contention. Interactions with CD36 are also reported to inhibit IL-12 synthesis and suppressing dendritic cell (DC) maturation and T cell activation.

It is, therefore, not unimaginable that parasite manipulates NF- κ B and Type 1 interferon pathway to drive inflammation.

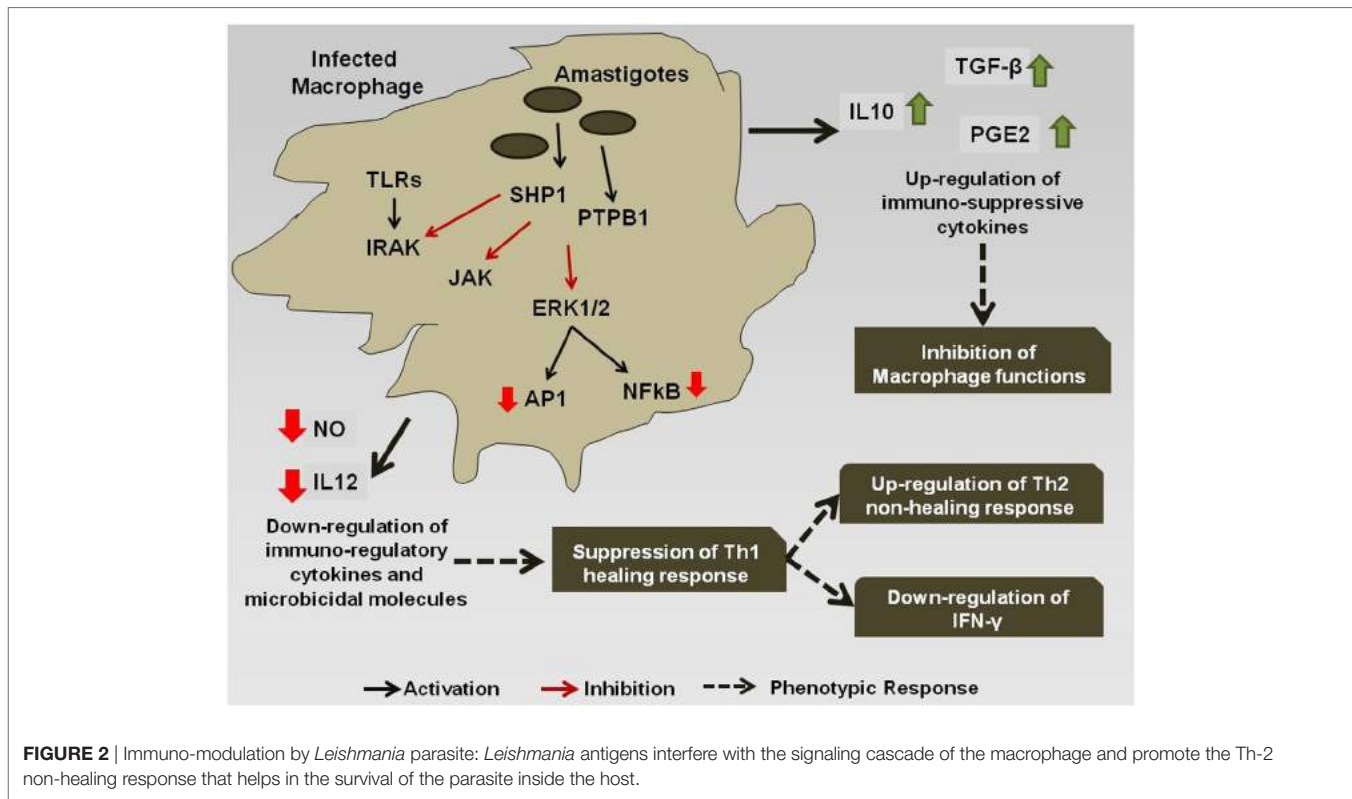
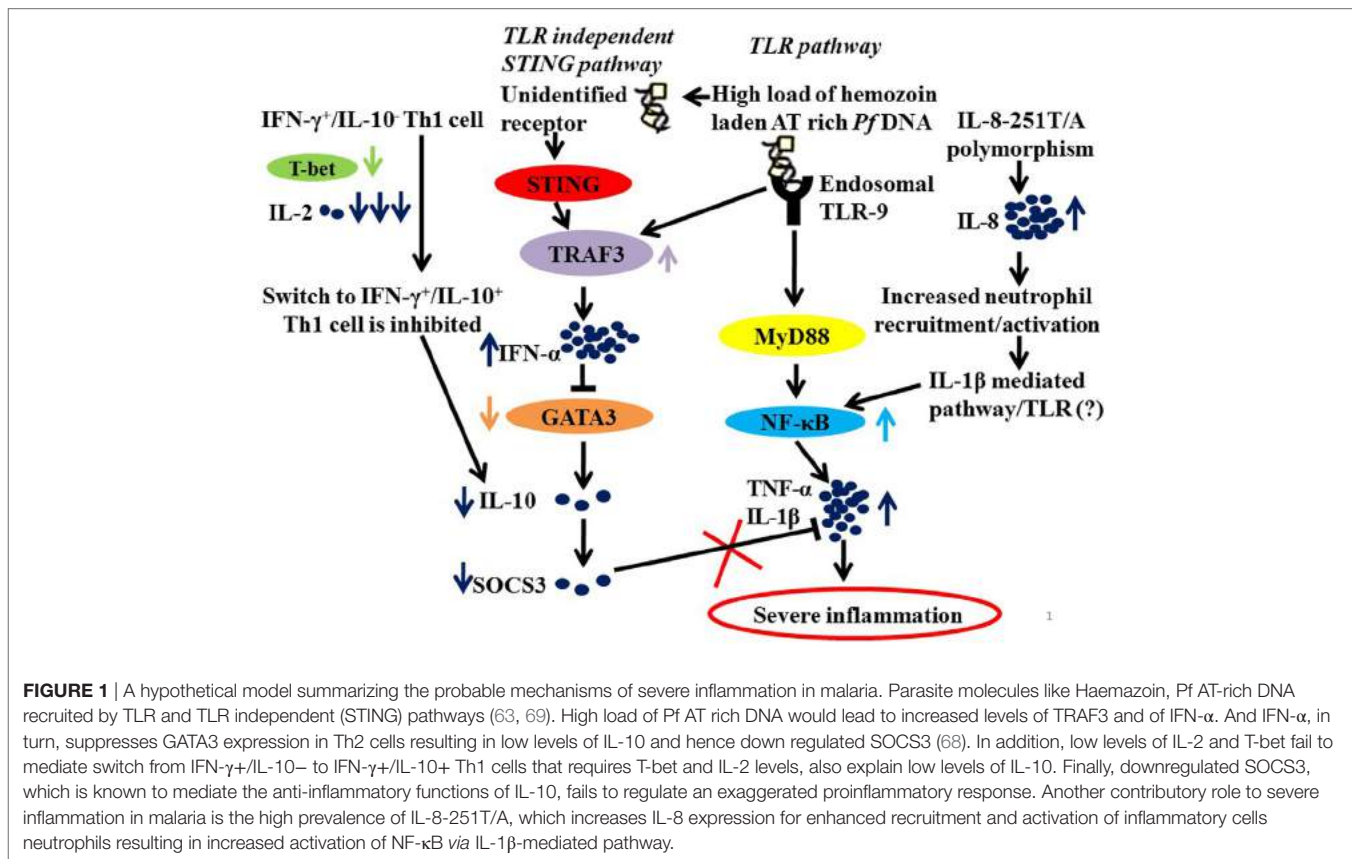
Plasmodium-derived PAMPs that include GPI anchors, CpG motifs, AT-rich motifs, and haemazoin are sensed by PRRs of host that include TLRs, NLRs, and AIM2 on cells of monocyte/macrophage lineage and on DCs (61, 63–65). These ligand–receptor interactions initiate MyD88 and STING-IRF3 mediated downstream signaling leading to activation of NF- κ B and IRF3 pathways and synthesis of pro-inflammatory cytokines and interferon α/β (55, 65–68). It is the exaggerated activation of these pathways “mediated by IFN- γ pro-inflammatory priming with extreme levels of pro-inflammatory mediators” with concomitant loss of regulatory cytokines that drives malaria pathogenesis (46, 57, 68). It has also been proposed that in addition to driving inflammation, *P. falciparum* by downregulating GATA3 expression suppresses IL-10 and SOCS3 that are necessary to control inflammation, possibly by exploiting the IFN α/β pathway as summarized in **Figure 1**.

LEISHMANIA: T CELL DIFFERENTIATION AND CROSS REGULATION OF CYTOKINE SIGNALING

Leishmaniasis caused by *Leishmania* spp. is a public health problem with 1.3 million reported Leishmaniasis cases worldwide which is intensified by availability of few effective drugs (70) and vaccine (71, 72). Being an intracellular parasite, it needs to overcome host-resistance mechanisms and exploit host environment for survival. From the parasite context, metabolism of *Leishmania* possesses a unique metabolic organization that can re-route metabolites, the uptake of which is constrained in different host environments toward synthesis of specific biomass metabolites; thereby providing novel mechanisms for metabolic adaptations (73, 74). From the host context, the contribution of specific virulence factors in immune suppression or the inability of the host to generate a sufficient immune response against the parasite, which promotes infection. Survival strategy of *Leishmania* is to modulate the signaling pathways of the macrophages after entering the phagolysosome. Depending on the type of infection and the parasite burden, either Th-1 healing or the Th-2 non-healing immune responses are generated, but detailed mechanism is poorly explored. This can be largely understood with respect to the interaction of parasite molecules with the host signaling pathways to suppress host immunity against infection (71).

During invasion, the surface molecules of *Leishmania* interact with the toll-like-receptor proteins present on the macrophages membrane (75). The activation of the TLRs triggers the downstream signaling pathways such as the RAS–RAF-mediated MAPK pathway, canonical and non-canonical NF- κ B pathway, JAK–STAT pathway, PI3K–PLC Gamma pathway, and the JNK pathway (76). Subsequently several transcription factors, such as ERK1/2, NF- κ B, NFAT, AP1, STAT3, are activated that initiate the synthesis and secretion of several cytokines, growth factors, chemokines and antimicrobial molecules which are responsible for the host immune responses during the infection (77).

However, during chronic infection (**Figure 2**), the antigenic molecules of the *Leishmania* parasite activate the phosphatase proteins in the macrophage, e.g., SHP-1 and PTP1B, which leads



to the dephosphorylation and deactivation of selected signaling pathways (78). This leads to downregulation of expression of iNOS and nitric oxide in the infected macrophages, thereby compromising microbicidal functions of the cell and creating an immune-suppressed condition, which is favorable for the continued survival of the pathogen inside APC. Simultaneously, the production of the cytokines, such as IL-12 and TNF- α , gets severely reduced. Such changes in the cytokine expression pattern of the antigen-presenting cells leads to the alteration of the phenotypic responses of the T-cells that now start showing a bias toward the non-healing Th-2 immune response that is characterized by an increased production of IL-4, IL-10, IL-13, and TGF- β cytokines (79), and the suppression of IFN- γ that regulates the healing Th-1 response (71). The transcription factors T-bet and GATA3 play a pivotal role in the regulation of the Th-1/Th-2 ratio during the infection (80). *Leishmania* also inhibits the ability of the host cell for antigen presentation to other immune cells, by repressing the MHC class II gene expression (81) and by modulating the interaction of the co-stimulatory molecules B7-1/CD28 (82) and CD40/CD40L (83).

The difference in the antigenic challenge posed to the host gives rise to differences in expression of the macrophage proteins, as seen in visceral versus the cutaneous infections (84). The difference in macrophage protein expression profile, as exemplified by increased production of COX2 and PGE2 production in case of *L. donovani* infection (as opposed to *L. major*) (85) indicates different *Leishmania* species selectively activate or inhibits different host pathways due to differences in the antigenic challenge. Also, it has been observed in a study that *L. donovani*, which is known to cause visceral leishmaniasis, may in rare cases give rise to cutaneous leishmaniasis (86). This behavior of *L. donovani* infection may be attributed to host's resistance to the disease which restricts the spread of the infection to the visceral organs and keeps it localized to cutaneous regions (86).

The CD4+ CD25+ regulatory T cells also play a major role in regulating the persistence of the parasite *L. major* inside the host. Inhibition of the T-reg promoting cytokines such as IL-10 leads to the clearance of the pathogen from the host (87). However, during Leishmaniasis the low production of the IFN- γ and IL-12 cytokines leads to the increased proliferation of the T-reg cells that leads to the re-activation of the *Leishmania* parasites inside the host (87).

SYSTEMS BIOLOGY BASED INTEGRATIVE APPROACHES FOR UNDERSTANDING THE HOST-PARASITE INTERACTION AND CO-EVOLUTIONARY PATTERNS IN PROTOZOAN DISEASES

During the interaction of hosts and protozoan parasites, both employ mutual selective pressures on each other, which may facilitate rapid reciprocal adaptation. Different stages of the parasite life cycle introduce another layer of complexity (88). Significant amount of molecular, omics, clinical, epidemiological as well as ecological data has been generated at *in vitro* and

in vivo levels using various pathogens and respective diseases. Integrative analysis of such discretely generated and located data from the host and protozoan parasite variants, in laboratory as well as natural populations is the most essential necessity to identify the complex mechanisms of protozoan evolution *via* immune escape during host-parasite coevolution. Public resources such as EuPathDB (89), Pathogen-Host Interactions (90), ProtozoaDB (91), together with protozoan species-specific databases are tremendously useful to collect useful information for initiating systems based integrative analysis. The key steps in such integrative approach involves data generation/data collection, data organization, data integration, integrative network construction, network analyses, and finally computer-based mathematical simulation and predictive modeling (92). As an example, using a reconstructed genome scale metabolic model of *Leishmania infantum* adaptations, (73) have identified the robustness of the parasite metabolic network against accidental errors and demonstrated the wide array of choices for the parasite to achieve optimal survival (73).

Recent advancement in RNA-Seq based techniques has facilitated the simultaneous sequencing of both host and parasite (including non-model parasites) transcriptomes (93). In a first of its kind RNA-seq experiment in control human neutrophils during priming with pro-inflammatory cytokines (TNF- α and GM-CSF), Wright et al. have shown the rapid expression of a common set of transcripts for cytokines, chemokines, and cell surface receptors (CXCL1, CXCL2, IL1A, IL1B, IL1RA, ICAM1) (94). They have demonstrated the utility of this approach to define functional changes in neutrophils following cytokine exposure. During a mega scale analysis of 116 malaria patients and infecting *P. falciparum* parasite, Yamagishi et al. have identified variable behaviors of the field malaria parasites, which were far more complex than those observed under laboratory conditions (95). Pittman et al. have generated a large scale *T. gondii*-host interactome, using dual transcriptional profiling of mice and parasite during acute and chronic infection (96) to demonstrate the influence of parasite development on host gene transcription as well as the epigenetic influence of the host environment on parasite gene transcription. Various systems-wide studies on malaria parasites have reported posttranscriptional (97) and translational (98) control at various points of the parasite lifecycle. One of such controlling mechanism is translational delay, by which protein expression in parasite is actively suspended for expressed mRNA transcripts. It was shown in *P. falciparum* that by suppressing more than 30% of its genes, the parasite rapidly adapts to new environments within the host by remaining undetected to the host immune system and undergo developmental switching in order to survive (99).

CONCLUSION AND FUTURE PERSPECTIVES

There is large apparent heterogeneity in offense strategies employed by the protozoan pathogen in human infections. In contrast to this, there appears to be a broad consensus on the major signaling hubs manipulated by the pathogens. It would

be worthwhile to dissect the host–pathogen interactions at cellular, molecular, and systems level to discriminate between infections that are virulent with potential for fatal outcomes from asymptomatic or uncomplicated infections with limited morbidity. It may be hypothesized that immuno regulatory mechanisms that confer disease tolerance are distinct from immune and metabolic responses to severe diseases and demand to be determined by large global studies employing different protozoan pathogen systems. However, despite the availability of huge amount of multi-dimensional data in host–protozoan interaction, functional characterization, and annotation of parasite genomes is severely limited by lack of both genetic tools and resources in protozoa. Given the size, heterogeneity and complexity of the host–parasite interaction data, development of new computational tools and user-friendly methods for integrating heterogeneous “Big Data” will facilitate to fill up the missing links. This will be beneficial for better understanding of the evolutionary arm race between the host and the parasite, and finally for the efficient management and control of the protozoan diseases in humans.

AUTHOR CONTRIBUTIONS

SB: manuscript design and contributed the introduction and sections on cytokines, malaria and *Toxoplasma* and future perspectives, PB: contributed the section on systems biology-based integrative approaches to understand host–parasite interaction and future perspectives, RRS: contributed in the sections on

Leishmaniasis and *Trypanosoma*, AM: contributed to the section on malaria, NS: contributed to the section on cytokines and cytokine regulation, SP: contributed to the section on *Toxoplasma*, MB: contributed to the section on *Toxoplasma*, and PG: contributed in the sections on Leishmaniasis and *Trypanosoma*. SP and MB: contributed to section on Cytokine Signalling Manipulation by Protozoan parasites.

ACKNOWLEDGMENTS

We would like to thank all the participants in the study and the Clinical Collaborators in the grant and infrastructure support of University Grants Commission. This study was funded by Department of Biotechnology (Grant Nos: BT/22/NE/2011, BT/CP/11/NE/TBP/2010 and BT/PR14958/BID/7/537/2015).

FUNDING

This work was supported by the Department of Biotechnology Institutional Biotech Hub (Grant no: BT/22/NE/2011) and the Department of Biotechnology (Grant no: BT/CP/11/NE/TBP/2010). This work supported with a grant provided to RRS by the Department of Biotechnology, Government of India project [BT/PR14958/BID/7/537/2015]. The authors also acknowledge the infrastructure support from University Grants Commission. PG acknowledges the Junior Research Fellowship from CSIR, India.” and SB acknowledges clinical support from Prof. Kakati, AMC&H, Dibrugarh.

REFERENCES

- Sacks D, Sher A. Evasion of innate immunity by parasitic protozoa. *Nat Immunol* (2002) 3:1041–7. doi:10.1038/ni1102-1041
- McGovern KE, Wilson EH. Dark side illuminated: imaging of *Toxoplasma gondii* through the decades. *Parasit Vectors* (2013) 6:334. doi:10.1186/1756-3305-6-334
- de Monerri NCS, Kim K. Pathogens hijack the epigenome A new twist on host–pathogen interactions. *Am J Pathol* (2014) 184:897–911. doi:10.1016/j.ajpath.2013.12.022
- Park SH, Kang K, Giannopoulos E, Qiao Y, Kang K, Kim G, et al. Type I interferons and the cytokine TNF cooperatively reprogram the macrophage epigenome to promote inflammatory activation. *Nat Immunol* (2017) 18:1104. doi:10.1038/ni.3818
- Bougdour A, Tardieux I, Hakimi MA. *Toxoplasma* exports dense granule proteins beyond the vacuole to the host cell nucleus and rewires the host genome expression. *Cell Microbiol* (2014) 16:334–43. doi:10.1111/cmi.12255
- Schneider AG, Abdallah DSA, Butcher BA, Denkers EY. *Toxoplasma gondii* triggers phosphorylation and nuclear translocation of dendritic cell STAT1 while simultaneously blocking IFN gamma-induced STAT1 transcriptional activity. *PLoS One* (2013) 8. doi:10.1371/journal.pone.0060215
- Escoll P, Mondino S, Rolando M, Buchrieser C. Targeting of host organelles by pathogenic bacteria: a sophisticated subversion strategy. *Nat Rev Microbiol* (2016) 14:5–19. doi:10.1038/nrmicro.2015.1
- Hanein D. *Toxoplasma gondii* targets the host actin cytoskeleton during invasion, GO figure. *Biophys J* (2013) 104:140a. doi:10.1016/j.bpj.2012.11.796
- Lee SH, Lee BY, Min DY, Kim JM, Ahn MH. Role of cytoskeleton in host cell invasion by intracellular protozoa *Toxoplasma gondii*. *J Microbiol Biotechnol* (2002) 12:628–34.
- Jones MJ, Fejes AP, Kobor MS. DNA methylation, genotype and gene expression: who is driving and who is along for the ride? *Genome Biol* (2013) 14:126. doi:10.1186/gb-2013-14-7-126
- Iwasaki A, Medzhitov R. Regulation of adaptive immunity by the innate immune system. *Science* (2010) 327:291–5. doi:10.1126/science.1183021
- Mayer-Barber KD, Yan B. Clash of the cytokine titans: counter-regulation of interleukin-1 and type I interferon-mediated inflammatory responses. *Cell Mol Immunol* (2017) 14:22–35. doi:10.1038/cmi.2016.25
- Kubo M, Motomura Y. Transcriptional regulation of the anti-inflammatory cytokine IL-10 in acquired immune cells. *Front Immunol* (2012) 3:275. doi:10.3389/fimmu.2012.00275
- Freitas do Rosario AP, Lamb T, Spence P, Stephens R, Lang A, Roers A, et al. IL-27 promotes IL-10 production by effector Th1 CD4+ T cells: a critical mechanism for protection from severe immunopathology during malaria infection. *J Immunol* (2012) 188:1178–90. doi:10.4049/jimmunol.1102755
- Falvo JV, Jasenosky LD, Kruidenier L, Goldfeld AE. Epigenetic control of cytokine gene expression: regulation of the TNF/LT locus and T helper cell differentiation. *Adv Immunol* (2013) 118:37–128. doi:10.1016/B978-0-12-407708-9.00002-9
- Mia S, Warnecke A, Zhang XM, Malmstrom V, Harris RA. An optimized protocol for human M2 macrophages using M-CSF and IL-4/IL-10/TGF-beta yields a dominant immunosuppressive phenotype. *Scand J Immunol* (2014) 79:305–14. doi:10.1111/sji.12162
- Xiao C, Rajewsky K. MicroRNA control in the immune system: basic principles. *Cell* (2009) 136:26–36. doi:10.1016/j.cell.2008.12.027
- Baltimore D, Boldin MP, O’Connell RM, Rao DS, Taganov KD. MicroRNAs: new regulators of immune cell development and function. *Nat Immunol* (2008) 9:839–45. doi:10.1038/ni.f.209
- Asirvatham AJ, Magner WJ, Tomasi TB. miRNA regulation of cytokine genes. *Cytokine* (2009) 45:58–69. doi:10.1016/j.cyto.2008.11.010
- McGovern KE, Wilson EH. Role of chemokines and trafficking of immune cells in parasitic infections. *Curr Immunol Rev* (2013) 9:157–68. doi:10.2174/1573395509666131217000000
- Diaz-Gandarilla JA, Osorio-Trujillo C, Hernandez-Ramirez VI, Talamas-Rohana P. PPAR activation induces M1 macrophage polarization via cPLA(2)-COX-2 inhibition, activating ROS production against *Leishmania mexicana*. *Biomed Res Int* (2013) 2013:215283. doi:10.1155/2013/215283

22. Lee CG, Sahoo A, Im SH. Epigenetic regulation of cytokine gene expression in T lymphocytes. *Yonsei Med J* (2009) 50:322–30. doi:10.3349/ymj.2009.50.3.322
23. Zhu JF, Jankovic D, Oler AJ, Wei G, Sharma S, Hu GQ, et al. The transcription factor T-bet is induced by multiple pathways and prevents an endogenous Th2 cell program during Th1 cell responses. *Immunity* (2012) 37:660–73. doi:10.1016/j.immuni.2012.09.007
24. Barker BR, Taxman DJ, Ting JP. Cross-regulation between the IL-1beta/IL-18 processing inflammasome and other inflammatory cytokines. *Curr Opin Immunol* (2011) 23:591–7. doi:10.1016/j.coi.2011.07.005
25. Liu Y, Zhang Q, Ding Y, Li X, Zhao D, Zhao K, et al. Histone lysine methyltransferase Ezh1 promotes TLR-triggered inflammatory cytokine production by suppressing Tollip. *J Immunol* (2015) 194:2838–46. doi:10.4049/jimmunol.1402087
26. Wykes MN, Lewin SR. Immune checkpoint blockade in infectious diseases. *Nat Rev Immunol* (2018) 18:91–104. doi:10.1038/nri.2017.112
27. Cheeseman K, Weitzman JB. Host-parasite interactions: an intimate epigenetic relationship. *Cell Microbiol* (2015) 17:1121–32. doi:10.1111/cmi.12471
28. Ghosh D, Stumhofer JS. Do you see what I see: recognition of protozoan parasites by toll-like receptors. *Curr Immunol Rev* (2013) 9:129–40. doi:10.2174/1573395509666131203225929
29. Sibley LD. Invasion and intracellular survival by protozoan parasites. *Immunol Rev* (2011) 240:72–91. doi:10.1111/j.1600-065X.2010.00990.x
30. Kim BH, Shenoy AR, Kumar P, Bradfield CJ, MacMicking JD. IFN-inducible GTPases in host cell defense. *Cell Host Microbe* (2012) 12:432–44. doi:10.1016/j.chom.2012.09.007
31. Du J, An R, Chen L, Shen Y, Chen Y, Cheng L, et al. *Toxoplasma gondii* virulence factor ROP18 inhibits the host NF-kappaB pathway by promoting p65 degradation. *J Biol Chem* (2014) 289:12578–92. doi:10.1074/jbc.M113.544718
32. Saeij JPJ, Collier S, Boyle JP, Jerome ME, White MW, Boothroyd JC. *Toxoplasma* co-opts host gene expression by injection of a polymorphic kinase homologue. *Nature* (2007) 445:324–7. doi:10.1038/nature05395
33. Rosowski EE, Lu D, Julien L, Rodda L, Gaiser RA, Jensen KD, et al. Strain-specific activation of the NF-kappaB pathway by GRA15, a novel *Toxoplasma gondii* dense granule protein. *J Exp Med* (2011) 208:195–212. doi:10.1084/jem.20100717
34. Franco M, Shastri AJ, Boothroyd JC. Infection by *Toxoplasma gondii* specifically induces host c-Myc and the genes this pivotal transcription factor regulates. *Eukaryot Cell* (2014) 13:483–93. doi:10.1128/EC.00316-13
35. Peixoto L, Chen F, Harb OS, Davis PH, Beiting DP, Brownback CS, et al. Integrative genomic approaches highlight a family of parasite-specific kinases that regulate host responses. *Cell Host Microbe* (2010) 8:208–18. doi:10.1016/j.chom.2010.07.004
36. Bougdour A, Durandau E, Brenier-Pinchart MP, Ortet P, Barakat M, Kieffer S, et al. Host cell subversion by *Toxoplasma* GRA16, an exported dense granule protein that targets the host cell nucleus and alters gene expression. *Cell Host Microbe* (2013) 13:489–500. doi:10.1016/j.chom.2013.03.002
37. Cardoso MS, Reis-Cunha JL, Bartholomeu DC. Evasion of the immune response by *Trypanosoma cruzi* during acute infection. *Front Immunol* (2015) 6:659. doi:10.3389/fimmu.2015.00659
38. Rodrigues MM, Oliveira AC, Bellio M. The immune response to *Trypanosoma cruzi*: role of toll-like receptors and perspectives for vaccine development. *J Parasitol Res* (2012) 2012:507874. doi:10.1155/2012/507874
39. Silva GK, Gutierrez FR, Guedes PM, Horta CV, Cunha LD, Mineo TW, et al. Cutting edge: nucleotide-binding oligomerization domain 1-dependent responses account for murine resistance against *Trypanosoma cruzi* infection. *J Immunol* (2010) 184:1148–52. doi:10.4049/jimmunol.0902254
40. DosReis GA. Evasion of immune responses by *Trypanosoma cruzi*, the etiological agent of Chagas disease. *Braz J Med Biol Res* (2011) 44:84–90. doi:10.1590/S0100-879X2011007500005
41. Cribb P, Perdomo V, Alonso VL, Manarin R, Barrios-Payan J, Marquina-Castillo B, et al. *Trypanosoma cruzi* high mobility group B (TcHMG) can act as an inflammatory mediator on mammalian cells. *Plos Negl Trop Dis* (2017) 11:e0005350. doi:10.1371/journal.pntd.0005350
42. Hedrick PW. Population genetics of malaria resistance in humans. *Heredity* (2011) 107:283–304. doi:10.1038/hdy.2011.16
43. World Health Organization. *Malaria Fact Sheet No 94*. Available from www.who.int/mediacentre/factsheets/fs375/en/
44. Joice R, Narasimhan V, Montgomery J, Sidhu AB, Oh K, Meyer E, et al. Inferring developmental stage composition from gene expression in human malaria. *PLoS Comput Biol* (2013) 9:e1003392. doi:10.1371/journal.pcbi.1003392
45. Zheng H, Tan Z, Xu W. Immune evasion strategies of pre-erythrocytic malaria parasites. *Mediators Inflamm* (2014) 2014:362605. doi:10.1155/2014/362605
46. Bertolino P, Bowen DG. Malaria and the liver: immunological hide-and-seek or subversion of immunity from within? *Front Microbiol* (2015) 6:41. doi:10.3389/fmicb.2015.00041
47. Clark IA, Budd AC, Alleva LM, Cowden WB. Human malarial disease: a consequence of inflammatory cytokine release. *Malar J* (2006) 5:85. doi:10.1186/1475-2875-5-85
48. Rovira-Vallbona E, Moncunill G, Bassat Q, Aguilar R, Machevo S, Puyol L, et al. Low antibodies against *Plasmodium falciparum* and imbalanced pro-inflammatory cytokines are associated with severe malaria in Mozambican children: a case-control study. *Malar J* (2012) 11:181. doi:10.1186/1475-2875-11-181
49. Anyona SB, Kempaiah P, Raballah E, Ouma C, Were T, Davenport GC, et al. Functional promoter haplotypes of interleukin-18 condition susceptibility to severe malarial anemia and childhood mortality. *Infect Immun* (2011) 79:4923–32. doi:10.1128/IAI.05601-11
50. Ayimba E, Hegewald J, Segbena AY, Gantini RG, Lechner CJ, Agossou A, et al. Proinflammatory and regulatory cytokines and chemokines in infants with uncomplicated and severe *Plasmodium falciparum* malaria. *Clin Exp Immunol* (2011) 166:218–26. doi:10.1111/j.1365-2249.2011.04474.x
51. Boeuf PS, Loizon S, Awandare GA, Tetteh JKA, Addae MM, Adjei GO, et al. Insights into deregulated TNF and IL-10 production in malaria: implications for understanding severe malarial anaemia. *Malar J* (2012) 11:253. doi:10.1186/1475-2875-11-253
52. Mendonca VRR, Queiroz ATL, Lopes FM, Andrade BB, Barral-Netto M. Networking the host immune response in *Plasmodium vivax* malaria. *Malar J* (2013) 12:69. doi:10.1186/1475-2875-12-69
53. Ockenhouse CF, Hu WC, Kester KE, Cummings JF, Stewart A, Heppner DG, et al. Common and divergent immune response signaling pathways discovered in peripheral blood mononuclear cell gene expression patterns in presymptomatic and clinically apparent malaria. *Infect Immun* (2006) 74:5561–73. doi:10.1128/IAI.00408-06
54. Sharma S, DeOliveira RB, Kalantari P, Parroche P, Goutagny N, Jiang Z, et al. Innate immune recognition of an AT-rich stem-loop DNA motif in the *Plasmodium falciparum* genome. *Immunity* (2011) 35:194–207. doi:10.1016/j.immuni.2011.05.016
55. Mahanta A, Kar SK, Kakati S, Baruah S. Heightened inflammation in severe malaria is associated with decreased IL-10 expression levels and neutrophils. *Innate Immun* (2015) 21:546–52. doi:10.1177/1753425914561277
56. Storm J, Craig AG. Pathogenesis of cerebral malaria-inflammation and cytoadherence. *Front Cell Infect Microbiol* (2014) 4:100. doi:10.3389/fcimb.2014.00100
57. Lourebam SD, Sawian CE, Baruah S. Dysregulation of cytokines expression in complicated *falciparum* malaria with increased TGF-beta and IFN-gamma and decreased IL-2 and IL-12. *Cytokine* (2013) 64:503–8. doi:10.1016/j.cyto.2013.08.007
58. Tahar R, Albergaria C, Zeghidour N, Ngane VF, Basco LK, Roussillon C. Plasma levels of eight different mediators and their potential as biomarkers of various clinical malaria conditions in African children. *Malar J* (2016) 15:337. doi:10.1186/s12936-016-1378-3
59. Engwerda CR, Mynott TL, Sawhney S, De Souza JB, Bickle QD, Kaye PM. Locally up-regulated lymphotoxin alpha, not systemic tumor necrosis factor alpha, is the principle mediator of murine cerebral malaria. *J Exp Med* (2002) 195:1371–7. doi:10.1084/jem.20020128
60. Hsieh FL, Turner L, Bolla JR, Robinson CV, Lavtsen T, Higgins MK. The structural basis for CD36 binding by the malaria parasite. *Nat Commun* (2016) 7:12837. doi:10.1038/ncomms12837
61. Bernabeu M, Danziger SA, Avril M, Vaz M, Babar PH, Brazier AJ, et al. Severe adult malaria is associated with specific PfEMP1 adhesion types and high parasite biomass. *Proc Natl Acad Sci U S A* (2016) 113:E3270–9. doi:10.1073/pnas.1524294113
62. Sarangi PP, Lee HW, Kim M. Activated protein C action in inflammation. *Br J Haematol* (2010) 148:817–33. doi:10.1111/j.1365-2141.2009.08020.x

63. Gazzinelli RT, Kalantari P, Fitzgerald KA, Golenbock DT. Innate sensing of malaria parasites. *Nat Rev Immunol* (2014) 14:744–57. doi:10.1038/nri3742
64. Franchi L, Munoz-Planillo R, Nunez G. Sensing and reacting to microbes through the inflammasomes. *Nat Immunol* (2012) 13:325–32. doi:10.1038/ni.2231
65. Kalantari P, DeOliveira RB, Chan J, Corbett Y, Rathinam V, Stutz A, et al. Dual engagement of the NLRP3 and AIM2 inflammasomes by *Plasmodium*-derived hemozoin and DNA during malaria. *Cell Rep* (2014) 6:196–210. doi:10.1016/j.celrep.2013.12.014
66. Durai P, Govindaraj RG, Choi S. Structure and dynamic behavior of toll-like receptor 2 subfamily triggered by malarial glycosylphosphatidylinositols of *Plasmodium falciparum*. *FEBS J* (2013) 280:6196–212. doi:10.1111/febs.12541
67. Pichyangkul S, Yongvanitchit K, Kum-Arb U, Hemmi H, Akira S, Krieg AM, et al. Malaria blood stage parasites activate human plasmacytoid dendritic cells and murine dendritic cells through a toll-like receptor 9-dependent pathway. *J Immunol* (2004) 172:4926–33. doi:10.4049/jimmunol.172.8.4926
68. Mahanta A, Baruah S. Lower expression of GATA3 and T-bet correlates with downregulated IL-10 in severe *falciparum* malaria. *Clin Transl Immunology* (2015) 4:e49. doi:10.1038/cti.2015.30
69. Shaham SH. *IL-10 Regulation in Complicated Malaria*. [dissertation/master's thesis], Tezpur University.
70. Croft SL, Seifert K, Yardley V. Current scenario of drug development for leishmaniasis. *Indian J Med Res* (2006) 123:399–410.
71. Ganguli P, Chowdhury S, Sarkar RR. Identification of Th1/Th2 regulatory switch to promote healing response during leishmaniasis: a computational approach. *EURASIP J Bioinform Syst Biol* (2015) 2015(1):13. doi:10.1186/s13637-015-0032-7
72. Kumar R, Engwerda C. Vaccines to prevent leishmaniasis. *Clin Transl Immunology* (2014) 3:e13. doi:10.1038/cti.2014.4
73. Subramanian A, Sarkar RR. Revealing the mystery of metabolic adaptations using a genome scale model of *Leishmania infantum*. *Sci Rep* (2017) 7:10262. doi:10.1038/s41598-017-10743-x
74. Saunders EC, Ng WW, Kloehn J, Chambers JM, Ng M, McConville MJ. Induction of a stringent metabolic response in intracellular stages of *Leishmania mexicana* leads to increased dependence on mitochondrial metabolism. *PLoS Pathog* (2014) 10:e1003888. doi:10.1371/journal.ppat.1003888
75. Tuon FF, Amato VS, Bacha HA, Almusawi T, Duarte MI, Amato Neto V. Toll-like receptors and leishmaniasis. *Infect Immun* (2008) 76:866–72. doi:10.1128/IAI.01090-07
76. Faria MS, Reis FC, Lima AP. Toll-like receptors in *Leishmania* infections: guardians or promoters? *J Parasitol Res* (2012) 2012:930257. doi:10.1155/2012/930257
77. Bhardwaj S, Srivastava N, Sudan R, Saha B. *Leishmania* interferes with host cell signaling to devise a survival strategy. *J Biomed Biotechnol* (2010) 2010:109189. doi:10.1155/2010/109189
78. Shio MT, Hassani K, Isnard A, Ralph B, Contreras I, Gomez MA, et al. Host cell signalling and leishmania mechanisms of evasion. *J Trop Med* (2012) 2012:819512. doi:10.1155/2012/819512
79. Cummings HE, Tuladhar R, Satoskar AR. Cytokines and their STATs in cutaneous and visceral leishmaniasis. *J Biomed Biotechnol* (2010) 2010:294389. doi:10.1155/2010/294389
80. Diaz YR, Rojas R, Valderrama L, Saravia NG. T-bet, GATA-3, and Foxp3 expression and Th1/Th2 cytokine production in the clinical outcome of human infection with *Leishmania* (Viannia) species. *J Infect Dis* (2010) 202:406–15. doi:10.1086/653829
81. Olivier M, Gregory DJ, Forget G. Subversion mechanisms by which *Leishmania* parasites can escape the host immune response: a signaling point of view. *Clin Microbiol Rev* (2005) 18:293. doi:10.1128/CMR.18.2.293-305.2005
82. Kaye PM, Rogers NJ, Curry AJ, Scott JC. Deficient expression of co-stimulatory molecules on *Leishmania*-infected macrophages. *Eur J Immunol* (1994) 24:2850–4. doi:10.1002/eji.1830241140
83. Soong L, Xu JC, Grewal IS, Kima P, Sun J, Longley BJ Jr., et al. Disruption of CD40-CD40 ligand interactions results in an enhanced susceptibility to *Leishmania amazonensis* infection. *Immunity* (1996) 4:263–73. doi:10.1016/S1074-7613(00)80434-3
84. McMahon-Pratt D, Alexander J. Does the *Leishmania major* paradigm of pathogenesis and protection hold for New World cutaneous leishmaniasis or the visceral disease? *Immunol Rev* (2004) 201:206–24. doi:10.1111/j.0105-2896.2004.00190.x
85. Gregory DJ, Sladek R, Olivier M, Matlashewski G. Comparison of the effects of *Leishmania major* or *Leishmania donovani* infection on macrophage gene expression. *Infect Immun* (2008) 76:1186–92. doi:10.1128/IAI.01320-07
86. McCall LI, Zhang WW, Matlashewski G. Determinants for the development of visceral leishmaniasis disease. *PLoS Pathog* (2013) 9:e1003053. doi:10.1371/journal.ppat.1003053
87. Mendez S, Reckling SK, Piccirillo CA, Sacks D, Belkaid Y. Role for CD4(+) CD25(+) regulatory T cells in reactivation of persistent leishmaniasis and control of concomitant immunity. *J Exp Med* (2004) 200:201–10. doi:10.1084/jem.20040298
88. Hill AV, Jepson A, Plebanski M, Gilbert SC. Genetic analysis of host-parasite coevolution in human malaria. *Philos Trans R Soc Lond B Biol Sci* (1997) 352:1317–25. doi:10.1098/rstb.1997.0116
89. Aurrecochea C, Barreto A, Basenko EY, Brestelli J, Brunk BP, Cade S, et al. EuPathDB: the eukaryotic pathogen genomics database resource. *Nucleic Acids Res* (2017) 45:D581–91. doi:10.1093/nar/gkw1105
90. Urban M, Pant R, Raghunath A, Irvine AG, Pedro H, Hammond-Kosack KE. The pathogen-host interactions database (PHI-base): additions and future developments. *Nucleic Acids Res* (2015) 43:D645–55. doi:10.1093/nar/gku1165
91. Davila AM, Mendes PN, Wagner G, Tschoeke DA, Cuadrat RR, Liberman F, et al. ProtozoaDB: dynamic visualization and exploration of protozoan genomes. *Nucleic Acids Res* (2008) 36:D547–52. doi:10.1093/nar/gkm820
92. Swann J, Jamshidi N, Lewis NE, Winzeler EA. Systems analysis of host-parasite interactions. *Wiley Interdiscip Rev Syst Biol Med* (2015) 7:381–400. doi:10.1002/wsbm.1311
93. Westermann AJ, Gorski SA, Vogel J. Dual RNA-seq of pathogen and host. *Nat Rev Microbiol* (2012) 10:618–30. doi:10.1038/nrmicro2852
94. Wright HL, Thomas HB, Moots RJ, Edwards SW. RNA-Seq reveals activation of both common and cytokine-specific pathways following neutrophil priming. *PLoS One* (2013) 8:e58598. doi:10.1371/journal.pone.0058598
95. Yamagishi J, Natori A, Tolba MEM, Mongan AE, Sugimoto C, Katayama T, et al. Interactive transcriptome analysis of malaria patients and infecting *Plasmodium falciparum*. *Genome Res* (2014) 24:1433–44. doi:10.1101/gr.158980.113
96. Pittman KJ, Aliota MT, Knoll LJ. Dual transcriptional profiling of mice and *Toxoplasma gondii* during acute and chronic infection. *BMC Genomics* (2014) 15:806. doi:10.1186/1471-2164-15-806
97. Doerig C, Rayner JC, Scherf A, Tobin AB. Post-translational protein modifications in malaria parasites. *Nat Rev Microbiol* (2015) 13:160–72. doi:10.1038/nrmicro3402
98. Cui LW, Lindner S, Miao J. Translational regulation during stage transitions in malaria parasites. *Ann N Y Acad Sci* (2015) 1342:1–9. doi:10.1111/nyas.12573
99. Bunnik EM, Chung DWD, Hamilton M, Potts N, Saraf A, Prudhomme J, et al. Polysome profiling reveals translational control of gene expression in the human malaria parasite *Plasmodium falciparum*. *Genome Biol* (2013) 14:R128. doi:10.1186/gb-2013-14-11-r128

Conflict of Interest Statement: The authors declare that the research was conducted in the absence of any commercial or financial relationships that could be construed as a potential conflict of interest.

The reviewer DN and handling editor declared their shared affiliation.

Copyright © 2018 Mahanta, Ganguli, Barah, Sarkar, Sarmah, Phukan, Bora and Baruah. This is an open-access article distributed under the terms of the Creative Commons Attribution License (CC BY). The use, distribution or reproduction in other forums is permitted, provided the original author(s) and the copyright owner are credited and that the original publication in this journal is cited, in accordance with accepted academic practice. No use, distribution or reproduction is permitted which does not comply with these terms.

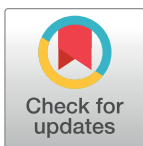
RESEARCH ARTICLE

Exploring immuno-regulatory mechanisms in the tumor microenvironment: Model and design of protocols for cancer remission

Piyali Ganguli^{1,2}, Ram Rup Sarkar^{1,2*}

1 Chemical Engineering and Process Development Division, CSIR-National Chemical Laboratory, Pune, Maharashtra, India, **2** Academy of Scientific & Innovative Research (AcSIR), CSIR-NCL Campus, Pune, India

* rr.sarkar@ncl.res.in



Abstract

The tumor microenvironment comprising of the immune cells and cytokines acts as the ‘soil’ that nourishes a developing tumor. Lack of a comprehensive study of the interactions of this tumor microenvironment with the heterogeneous sub-population of tumor cells that arise from the differentiation of Cancer Stem Cells (CSC), i.e. the ‘seed’, has limited our understanding of the development of drug resistance and treatment failures in Cancer. Based on this seed and soil hypothesis, for the very first time, we have captured the concept of CSC differentiation and tumor-immune interaction into a generic model that has been validated with known experimental data. Using this model we report that as the CSC differentiation shifts from symmetric to asymmetric pattern, resistant cancer cells start accumulating in the tumor that makes it refractory to therapeutic interventions. Model analyses unveiled the presence of feedback loops that establish the dual role of M2 macrophages in regulating tumor proliferation. The study further revealed oscillations in the tumor sub-populations in the presence of T_{H1} derived IFN- γ that eliminates CSC; and the role of IL10 feedback in the regulation of T_{H1}/T_{H2} ratio. These analyses expose important observations that are indicative of Cancer prognosis. Further, the model has been used for testing known treatment protocols to explore the reasons of failure of conventional treatment strategies and propose an improvised protocol that shows promising results in suppressing the proliferation of all the cellular sub-populations of the tumor and restoring a healthy T_{H1}/T_{H2} ratio that assures better Cancer remission.

OPEN ACCESS

Citation: Ganguli P, Sarkar RR (2018) Exploring immuno-regulatory mechanisms in the tumor microenvironment: Model and design of protocols for cancer remission. PLoS ONE 13(9): e0203030. <https://doi.org/10.1371/journal.pone.0203030>

Editor: Gianpaolo Papaccio, Università degli Studi della Campania, ITALY

Received: July 19, 2018

Accepted: August 14, 2018

Published: September 5, 2018

Copyright: © 2018 Ganguli, Sarkar. This is an open access article distributed under the terms of the [Creative Commons Attribution License](https://creativecommons.org/licenses/by/4.0/), which permits unrestricted use, distribution, and reproduction in any medium, provided the original author and source are credited.

Data Availability Statement: All relevant data are within the manuscript and its Supporting Information files.

Funding: We thank SERB, Department of Science and technology, Govt. of India (file no. EMR/2016/000516), for providing financial support to Ram Rup Sarkar. Piyali Ganguli acknowledges Council of Scientific & Industrial Research (CSIR) for the Junior Research Fellowship. The funders had no role in study design, data collection and analysis, decision to publish, or preparation of the manuscript.

1. Introduction

A malignant tumor is formed of heterogeneous population of cells. According to Cancer Stem Cell (CSC) Hypothesis, this tumor of heterogeneous cells is formed from a distinct group of cells having stem-like properties that are able to differentiate and renew for an indefinite period of time [1]. Popularly referred to as the Seed and Soil hypothesis, researchers believe that the CSCs acts like ‘seed’ and form the tumor initiating population of cells, that is responsible for the growth, sustenance, metastasis and relapse of Cancer [2]. These CSCs have the

Competing interests: The authors have declared that no competing interests exist.

ability to differentiate both symmetrically and asymmetrically to form the terminally differentiated cancer cells as well as renew the pool of CSCs [3]. However, during proliferation, various extrinsic and intrinsic environmental factors give rise to random mutational events, such as, chromosomal breakage, translocation, aberrant signalling events and drug efflux, which are responsible for transformation and adaptation of the cell to resist the effect of drug and conventional therapeutic strategies [4]. This results in the formation of distinct cellular sub-populations that are drug resistant and impair the treatment of cancer.

On the other hand, the tumor microenvironment, composed mainly of the immune cells and the cytokines, plays a crucial role in determining cancer prognosis [5]. As the tumor develops, each of the tumor cell sub-populations starts manipulating the microenvironment and induces the production of pro-tumorigenic molecules. The CSCs and the Cancer cells induce the production of immune-modulatory molecules such as IL-10, IL-13 and TGF- β that are conducive to the proliferation of the M2-Tumor Associated Macrophages (M2-TAM), the Type II T-helper (T_{H2}) cells and the T-regulatory (Treg) cells [6, 7]. The IL-10 mediated positive feedback loop between the tumor and the M2-TAMs helps in the rapid proliferation of the tumor sub-populations and the progression of the disease [8]. The CSCs also express high levels of co-inhibitory molecule PD-L1 that inhibit the activation of Cytotoxic T (Tc) cells [9]. Additionally, the CSC also tries to evade recognition by the immune cell by suppressing the expression of Major Histocompatibility Complex (MHC) by the macrophage cells in the tumor microenvironment. This is achieved by the release of exosomal miRNAs, such as miR-9 and miR-21, into the microenvironment by the tumor that are taken up by the immune cells, mediating changes in the cytokine expression pattern, antigen-recognition and immune responses [10, 11]. Along with these strategies of immune evasion, CSC also secretes VEGF, a growth factor that promotes angiogenesis during tumor progression and plays a pivotal role in suppressing the maturation of the T cells [12, 13]. These chemokines, cytokines and growth factors secreted by the stem cells lead the system to an inflammatory state. This also mediates a crosstalk between different groups of cells in the tumor microenvironment that are crucial for cancer initiation, progression and metastases formation [14, 15]. These regulatory mechanisms that operate in the tumor microenvironment serve to suppress the anti-tumorigenic effect of the Cytotoxic T (Tc) cells and the Type I T-helper (T_{H1}) cells. This immune-suppressed tumor microenvironment acts as the 'soil' that nourishes and augments the growth of both the drug-sensitive as well as the drug-resistant sub-populations of the tumor, thereby posing a further challenge to the therapeutic strategies adopted to control cancer [16]. However, literature evidences showing the presence of a few tumor associated antigens (TAA) that helps in the recognition of these tumor cell sub-populations by the infiltrated T cells and the generation of effective immune responses upon Dendritic Cell (DC) vaccination throws light on the possibility of control of the disease using immunotherapy [17]. Hence a thorough understanding of the tumor-immune interaction, considering tumor sub-populations, is crucial to overcome the immune-suppression induced by the tumor.

In order to gain insight into the regulatory mechanisms governing these tumor-immune interactions, several studies have been performed using both theoretical as well as experimental techniques. Such studies have clearly indicated the role of Tc cells and IFN- γ in controlling Cancer progression [18]. Recent findings have suggested that synergistic activation of Tc cells and $\gamma\delta$ -T cells are efficacious against HMLER-derived Breast Cancer stem-like cells, where $\gamma\delta$ -T cells act as an early source of IFN- γ in tumor immunity, under special *in vitro* conditions [19]. The development of Chimeric Antigen Receptor (CAR) T-cell has opened up new avenues for research in tumor immunity [20]. However, lack of truly CSC specific markers leads to on-target/off-tumor toxicity, where the CAR-T cells or any other CSC-targeted therapy kills the normal cells as well that display the same markers as that of CSCs [20, 21].

Mathematical models have been useful in delineating the multiplicity of the complex interactions governing the dynamics of the tumor-immune interaction that remains elusive through *in-vitro* experiments. In this context, *in-silico* studies have shown light on the CSC differentiation pattern and its effect on the tumor growth dynamics [3]. Here it has been observed that symmetric stem cell division shows a correlation with cancer progression [3]. This is in contrast to another report that mentions symmetric stem cell division lowers cancer risk as it reduces the accumulation of cellular damage [22]. However, the effect of CSC differentiation on drug-resistivity and the outcome of the interaction of these differentiated cells with the tumor microenvironment have not been explored sufficiently. On the other hand, models on tumor-immune interaction considering the involvement of tumor, immune effector cell and IL2 have enhanced our understanding about oscillations in tumor sizes, long-term tumor relapse and the conditions under which tumor elimination may be achieved using Adoptive Cellular Immunotherapy [23]. Mathematical models are now being exploited for the study of the efficacy of adaptive immunity for the elimination of aggressive tumors [24, 25], the existence of an angiogenic switch that regulates Cancer progression [26] and as a powerful tool in the design of optimal control strategies for Cancer [27, 28].

However, the study of the CSC differentiation pattern and the outcome of the interaction of these heterogeneous tumor cell sub-populations with the immune cells and cytokines present in the microenvironment is a challenge yet to be achieved in both experiments as well as modelling studies. With the aim to gain a clearer and unambiguous picture of the regulatory mechanisms involved in the immune-escape mechanism of the tumor cells, we propose an ODE-based mathematical model of the tumor-immune interaction that captures the development of a malignant tumor from the 'seed', the CSCs, and its interaction with the 'soil', the tumor microenvironment. In this model, we consider the three different modes of CSC differentiation, as well as the effect of random mutations and ask the question, how the stem cell differentiation patterns regulate the different cellular sub-populations in the tumor and how it affects the development of drug resistance? Using this model we have tried to address the unresolved question of the correlation of M2 macrophages with more resistant tumors by exploring the regulatory feedback loops that govern the dynamics of the tumor-sub-population and the roles of the cytokine feedbacks in shaping the tumor microenvironment. Prior to these studies, the model has been calibrated and the unknown parameters of the model have been estimated by fitting the initial growth kinetics of the model with data obtained from Gastric Cancer cell line using the MCMC-DRAM algorithm [29]. Moreover, the steady state behaviors of all the model variables have been quantifiably validated with previously reported experimental data obtained from cytometric and protein expression studies from both *in-vitro* studies as well as data obtained from different Cancer patients to establish the generic behavior of our model and ensure its acceptability in the design of treatment strategies.

In order to design treatment protocols for triggering the Cancer remission, we have introduced radio and chemotherapeutic strategies and observed the fold changes in the tumor mass in the presence and in the absence of resistant cells, where we demonstrate the failure of the conventional treatment strategies for curing Cancer. Thereafter, we have ventured the use of immunotherapy that has also been a popular choice for the elimination of the CSCs that are resistant to chemo and radio-therapeutic interventions [17, 30]. Hence, using the leads from our model analysis, we have attempted to propose combinatorial treatment strategies and design protocols that help in better suppression of the tumor, even in the presence of resistant cells. However, it may be mentioned here that a vital assumption in our model is that the drug-sensitive and drug-resistant population of tumor cells elicits similar immune responses. The resistant population of cells represents a fraction of the tumor cells that are unresponsive to the conventional treatment strategies. Thus, the difference in their behavior arises when the

treatment/control is applied. Our novel modeling approach and strategy for the design of treatment protocol throws light on the ways to optimize drug schedules, dosage and treatment cycles required for the elimination of the tumor cells. This model may be used as a potential tool for the prediction of Cancer prognosis and calculation of fold changes in the tumor sub-populations in response to a new treatment regimen.

2. Model

The tumor-immune interaction model, depicted in Fig 1A, can be perceived as three regulatory modules – (i) the core tumor along with the tumor infiltrated Tc cells (red box), (ii) the immune-stimulators consisting of M1 cells, T_{H1} cells, IL2 and IFN- γ cytokines (green box) and (c) the immune-suppressors consisting of M2 cells, T_{H2} cell, Treg cells and IL10 cytokines (orange box). The interactions between these components of the model are based on known experimental evidences and immunological relevance. A detailed description of the model along with the mathematical assumptions, based on the biological phenomenon, used in its mathematical formulation has been described in the *Methods* section.

Based on these biological relevances and mathematical assumptions, the tumor-immune interaction network has been modelled using 13 Ordinary Differential Equations (Eqs 1–13) and 71 parameters (as enlisted in the *Methods* section). The state variables and parameters used in the formulation of the model have been listed in the *S1 Text*. The initial values of the

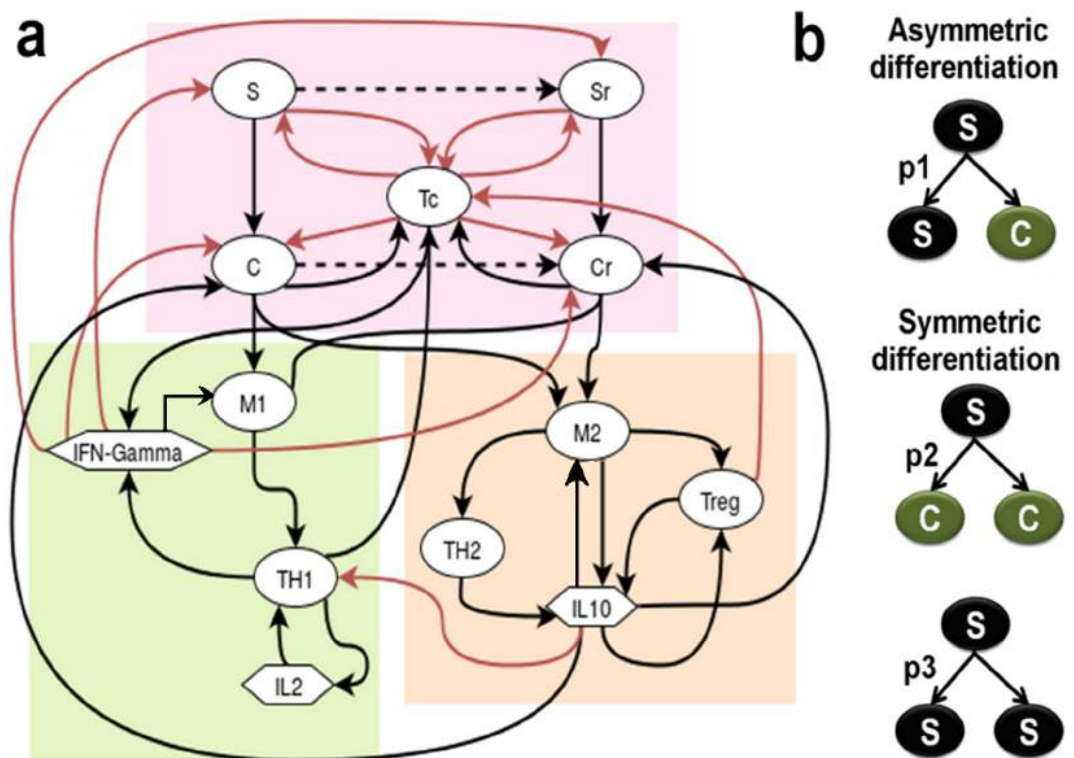


Fig 1. Diagrammatic representation of the tumor-immune interaction model. (a) Cellular interaction network representing the key players of the tumor microenvironment, viz. Cancer Stem Cells (S), Cancer cells (C), their drug resistant counterparts (S_R and C_R), M1-TAM, M2-TAM, T_{H1}, T_{H2}, Tc, Treg immune cells, and cytokines IL10, IFN- γ and IL-2; The tumor microenvironment has been grouped into three parts, viz.- core tumor and infiltrated Tc cells (red box), the immune-stimulators (green box) and the immune-suppressors (orange box); the Black arrows represent Activation, while the Red arrow represent Inhibition; (b) Stem cell differentiation pattern.

<https://doi.org/10.1371/journal.pone.0203030.g001>

model variables have been listed in the [S1 Text](#). Here the initial value of the stem cell $S_0 = 1$, while S_R , C , C_R have been initialized as zero such that all the tumor sub-populations develop from the symmetric and asymmetric differentiation of a single stem cell that ensures the conservation of the stem cell hypothesis.

3. Therapeutic intervention

The protocols are designed using various combinations of *Radiotherapy*, *Chemotherapy* and *Immunotherapy*. The dosage, time duration and number of cycles for each therapy are varied to determine the optimal combination that gives us maximum fold changes in the tumor reduction as well as enhance the T_{H1}/T_{H2} ratio to ensure better treatment efficacy. Two treatment protocols have been tested in our model. Protocol 1 is an adaptation from a previously reported protocol involving Chemotherapy and Radiotherapy, while Protocol 2 is novel combinatorial protocol proposed where we have introduced Immunotherapy by triggering the immune cells of our model (detailed discussion in the *Methods* section).

4. Results

4.1. Model validation with experimental data

4.1.1. Tumor growth (without therapy). The growth kinetics of the tumor is estimated by four variables of our model, S , S_R , C and C_R , signifying the four sub-populations of cells that are found in the tumor. In order to validate the growth kinetics of these tumor cell sub-populations of our model, we have used data from different experimental and theoretical studies of tumor growth estimation. The early temporal growth kinetics of the Stem (S) and Resistant Stem cells (S_R) were validated over a period of 5 days, with the reports of Tomasetti and Levy [3], by choosing the parameter values $\gamma_S = 2 \text{ day}^{-1}$ and $\delta_S = 0.2 \text{ day}^{-1}$ (Fig 2A). Here, it was observed that the Stem cells (S) start proliferating exponentially during this initial growth phase of tumor formation. During this time frame, the stem cells also start acquiring mutations and start producing the Resistant Stem Cells (S_R) that gradually starts proliferating slowly and is maintained in very low numbers inside the tumor [3]. It is to be noted that for all our subsequent simulations we have used $\gamma_S = 0.15 \text{ day}^{-1}$ and $\delta_S = 2 \times 10^{-7} \text{ day}^{-1}$, as reported in the [S1 Text](#).

Temporal behaviors of the Cancer (C) and Resistant Cancer (C_R) sub-populations have been simulated to validate our model with experimental data (Fig 2B; See [Methods Section 7.7](#)). Fig 2B depicts the temporal growth kinetics of the Breast cancer cell line MCF-7/TAX-resistant to Paclitaxel [31], Hepatocellular Carcinoma cell line SK-Hep1/CDDP3-resistant to Cisplatin [32], and Colon Cancer cell lines SW-620-L-OHP and LoVo-L-OHP-resistant to Oxaliplatin [33]. Our simulation result mimics the average behavior of the resistant cancer cell lines over the time period of 5 days (Fig 2B), using the parameter set estimated through the MCMC method.

The model was simulated for a sufficiently long time to study the temporal evolution of the drug-sensitive and drug-resistant cancer cells without any therapeutic interventions (Fig 2C). Here, it was observed that during the early stages of tumor development, the stem cells (S) show a very slow rate of proliferation. According to our simulation results, it is observed that although a single stem cell initiates the formation of the entire tumor, the stem cells maintain a very low number during the first few months of tumor development. The rapid proliferation of the Cancer cells (C) during the early growth phase lead to their transformation to the resistant C_R species that soon start proliferating rapidly, thereby giving rise to a tumor. At the end of the exponential growth phase, the cancer progression is impeded by the activated $M1$, T_{H1} and T_c immune cells and the systems stay relatively stable for some time until the stem cells

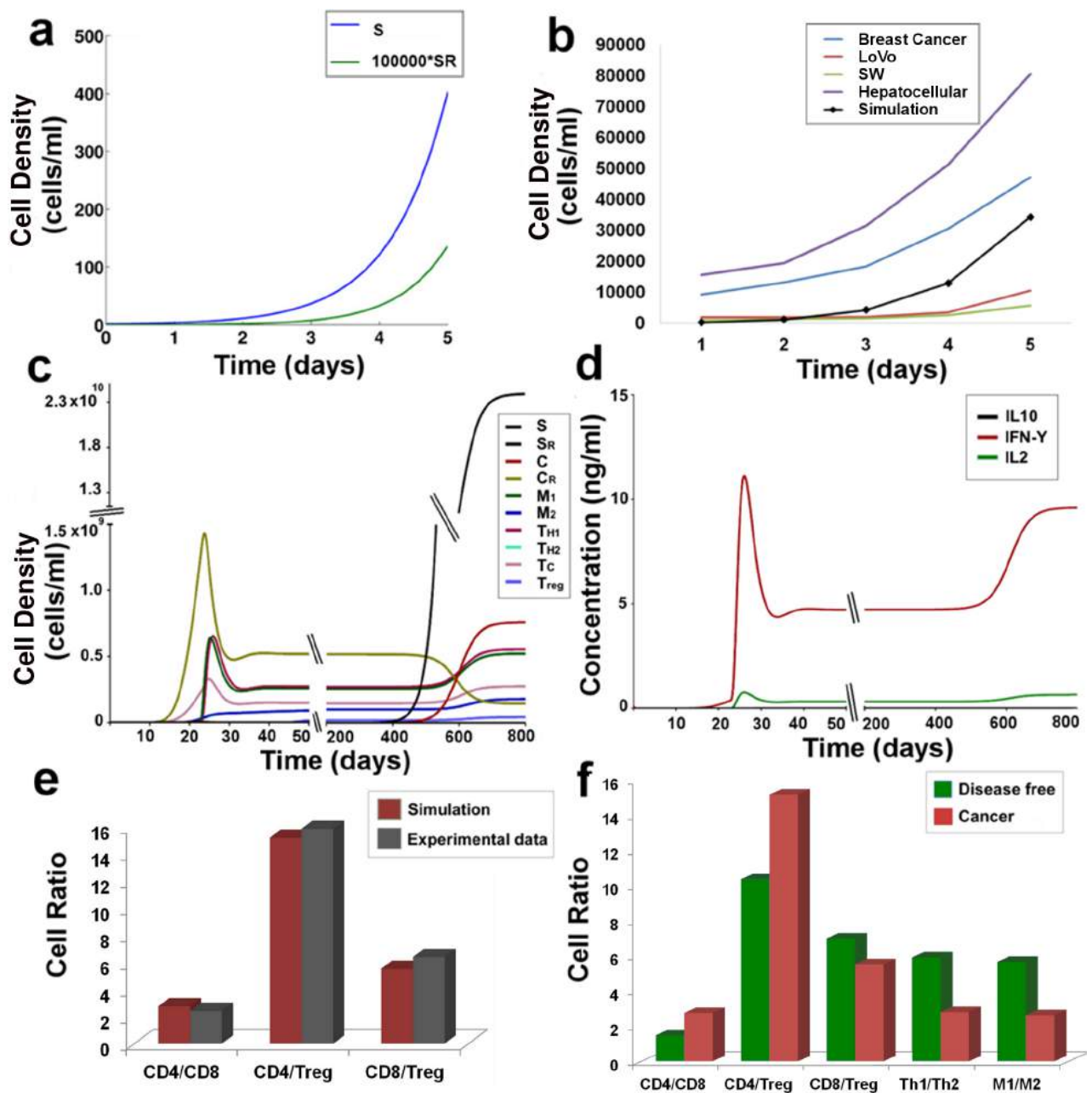


Fig 2. Model validation with experimental data: (a) Stem and Stem resistant cell proliferation at $\gamma_S = 2 \text{ day}^{-1}$ and $\delta_S = 0.2 \text{ day}^{-1}$; (b) Proliferation of the Cancer Resistant cells as observed in experiments along with the observations from our simulation; figure depicts growth kinetics of the Breast cancer cell line MCF-7/TAX-resistant to Paclitaxel, Hepatocellular Carcinoma cell line SK-Hep1/CDDP3-resistant to Cisplatin, and Colon Cancer cell lines SW-620-L-OHP and LoVo-L-OHP-resistant to Oxaliplatin; (c) Temporal cellular behavior of the components of the model during tumor formation; (d) Temporal cytokine expression pattern during tumor formation; (e) Immune Cell Ratio at steady state- experiment versus simulation results (f) Immune cell ratio in the disease free condition versus cancer scenario. Note: $CD4 = T_{H1} + T_{H2}$; $CD8 = T_c$.

<https://doi.org/10.1371/journal.pone.0203030.g002>

start proliferating exponentially and form the main bulk of the tumor. Our simulation results indicate that the first resistant stem cell of the tumor is detected at 400 days. Around 800 days the model reaches its steady state. The total tumor density at steady state can be estimated to be around 2.5×10^{10} cells/ml, i.e. 25 times higher than the reported minimum threshold of a

clinically detectable tumor [3]. From here we calculate the relative abundance of the sub-populations of the tumor cells and derive that at steady state, the tumor is composed of 94.59% Stem cells (S), 4.49% Cancer cells (C), 1% Cancer Resistant cells (C_R) and small fraction of Stem Resistant cells (S_R) that comprises 0.001% of the tumor mass.

4.1.2. Immune cell-ratio comparison with cytometric data. Our simulation results revealed the dynamics of the adaptive immune responses generated during the tumor development (Fig 2C). Here we observe that as the tumor sub-populations begins to proliferate, the Tc cells show enhanced activation that is required for the natural regression of the tumor (Fig 2C). However, as the tumor continues to proliferate and the resistant cancer cells (C_R) peaks to 1.5×10^9 cells/ml, there is a sharp rise in the M1 and T_{H1} cells proliferation. The combined effect of the Tc, M1 and T_{H1} cells helps to impede the tumor development and decrease it by 3 folds which then falls below the limit of tumor detection (i.e. 10^9 cells/ml, [3]) and apparently stays dormant till 400 days. Thereafter, as the stem (S) and resistant stem (S_R) cells start proliferating, the adaptive immunity becomes active again. However, this is also accompanied with the increase in abundance of M2 and Treg cells (Fig 2C), that helps in the sustenance and continued survival of the tumor cells.

In order to analyse the changes in the immune activation state before and after tumor formation, the immune cell ratio values obtained at the steady state are estimated and compared to the cell ratios in the normal disease-free condition (Fig 2F). It may be mentioned here, in Fig 2E and 2F, CD4 depicts the summation of both the T_{H1} and T_{H2} cells of our model, while CD8 implies Tc cells. From our model analysis, we observe that, during Cancer, the ratio of CD4 and CD8 cells reaches a mean value of 2.75, that is in sharp contrast to the normal healthy individuals which show a value of 1.48 (Fig 2F) [34]. On the other hand, the value of CD4:Treg ratio in Cancer shows a value of 15.2 that is higher than the ratio observed in the normal scenario. This happens due to the enhanced T_{H2} proliferation during tumor development. This also explains the reason for the elevated CD4/Treg ratio. However, the CD8:Treg ratio shows a decrease in Cancer patients and reaches to about 5.5, which is a characteristic of resistant tumors in mammals [35]. In Fig 2E we have compared these results of our numerical simulation with experimental data obtained from various literatures. Here, we clearly observe that our simulation corroborates very well with the experimental observations made from blood samples of Cancer patients (Fig 2E) [36, 37]. Additionally, we have observed the changes in the $T_{H1}:T_{H2}$ and M1:M2 ratios that have important implications in Cancer prognosis. We find that both $T_{H1}:T_{H2}$ ratio and M1:M2 ratio get decreased during Cancer as compared to the normal disease-free conditions (Fig 2F) [38, 39]. These results are in excellent agreement to the literature that suggests Cancer patients showing $T_{H1}:T_{H2}$ ratio below 8 show poor disease prognosis [39].

4.1.3. Cytokine production. IL10 production is a characteristic feature for Cancer detection. During Cancer, the marked increase in IL10 production has been noted in blood samples of various cancer patients, where an average concentration of 0.01 ng/ml has been recorded in various protein expression studies [40–42]. The temporal protein expression profile, from our simulations, suggests the IL10 expression starts increasing around the 15th day until it reaches to a concentration of 0.005 ng/ml (Fig 2D). The IFN- γ production begins along with the proliferation of the Tc cells and increases sharply with the activation of the T_{H1} cells (Fig 2D). This is accompanied by IL2 production that helps in the continued proliferation of the T_{H1} cells. After the proliferation of the stem cells, the cytokine production increases further. The IL10 concentration starts increasing rapidly and attains a concentration of 0.009 ng/ml at steady state. The steady state concentrations of IFN- γ and IL2 reach 9.6 ng/ml and 0.6 ng/ml respectively. The cytokine expression levels from our simulation lie close to the experimentally observed ranges of protein expression of cancer treatment prior to their treatment [40].

4.2. Model analysis

4.2.1. Development of drug resistance is governed by the pattern of stem cell differentiation. With the assumption that the stem cells predominantly tend to renew their pool of stem cells, i.e. with a probability p_3 , we have varied the values of p_1 and p_2 to observe the effect of the asymmetric and symmetric differentiation of the stem cell on the development of drug resistance (Fig 3A–3D). Here it may be observed that as we increase the values of p_1 and p_2 , the rate of the stem cell renewal decreases gradually, thereby leading to decrease in the steady state values of S and S_R (Fig 3A and 3B). However, in the case of C cells (Fig 3C), we observe that as we increase the value of p_1 , the steady state values of C decreases, whereas the variation of p_2 has little effect on the steady states of C (Fig 3C). The steady state level of C_R on the other hand, is greatly influenced by p_1 and p_2 (Fig 3D). With the increase in the value of p_1 and p_2 , the steady states value of C_R increases, signifying as the mode of stem cell differentiation changes, the tumor cell sub-populations tend to transform into the resistant Cancer cells. Hence, from our results, we may infer that higher asymmetric stem cell division may be associated with a high rate of drug resistance.

4.2.2. Dual role of tumor associated macrophages. The differential regulatory behavior of the type I and type II TAMs on the tumor cells was studied by varying the γ_{M1} and γ_{M2} parameters, governing the growth rate of the M1 and M2 macrophages (Fig 3E–3H). Here it was observed, as we increase the birth rate of M1, the steady state values of all the sub-populations of the tumor decreases. However, on varying γ_{M2} , we observe that although the S , S_R and C sub-populations show a decrease in the steady state values, the C_R population increases (Fig 3E–3H). This result corroborates with the experimental observations that indicate that while M1 macrophages may have an important role in suppression of the tumor growth, a higher abundance of M2 macrophages may lead to poor disease prognosis [43]. From our model analysis, we infer that a higher proliferation of M2 TAMs leads to an increased accumulation of resistant cancer cells in the tumor. This is primarily because of the feedback regulations that govern the dynamics of the tumor-immune interaction network.

4.2.3. IFN-gamma and IL10 feedbacks regulate Cancer progression. The cytokines are the key regulators of the Tumor-Immune interaction network. The IFN- γ produced by the T_{H1} cells helps in maintaining the steady state dynamics of the entire system. Parameter variation studies reveal that as we increase IFN- γ production from the T_{H1} cells by changing the value of β_{Th1Ck2} between 10^{-7} and 10^{-2} ng/cell/day, the S and S_R cells show a dampening oscillation in their temporal behavior and these stem cell populations gradually decrease to a very low value. On the other hand, with the increasing β_{Th1Ck2} values, the temporal behavior of C and C_R cell population changes from dampening to stable oscillations at $\beta_{Th1Ck2} = 0.1$ (Fig 3I). The increased production of IFN- γ leads to the rapid killing of the S and S_R populations, whose oscillations dampen with time resulting in complete elimination of the stem cells from the system (Fig 3J). However, the high rate of C proliferation balances out the negative feedback effect of the high IFN- γ production, which keeps oscillating the system (Fig 3K). The phase-plot depicts the feedback regulation that operates between the Cancer (C) cells and IFN- γ that regulates the Cancer relapse. As the Cancer proliferation reaches 4×10^6 cells, the IFN- γ production starts increasing which reduces the Cancer proliferation. When the Cancer cells fall below 1×10^6 cells, the IFN- γ production also starts decreasing. However, at low levels IFN- γ , the Cancer cells start proliferating again (Fig 3K). This leads the system into stable steady state oscillations.

Another important feedback regulation that is crucial for the determination of tumor progression is the negative feedback effect of the IL10 cytokine on the T_{H1} proliferation. This is governed by the parameter μ_{Th1Ck1} . As the value of μ_{Th1Ck1} is increased, the T_{H1}/T_{H2} ratio

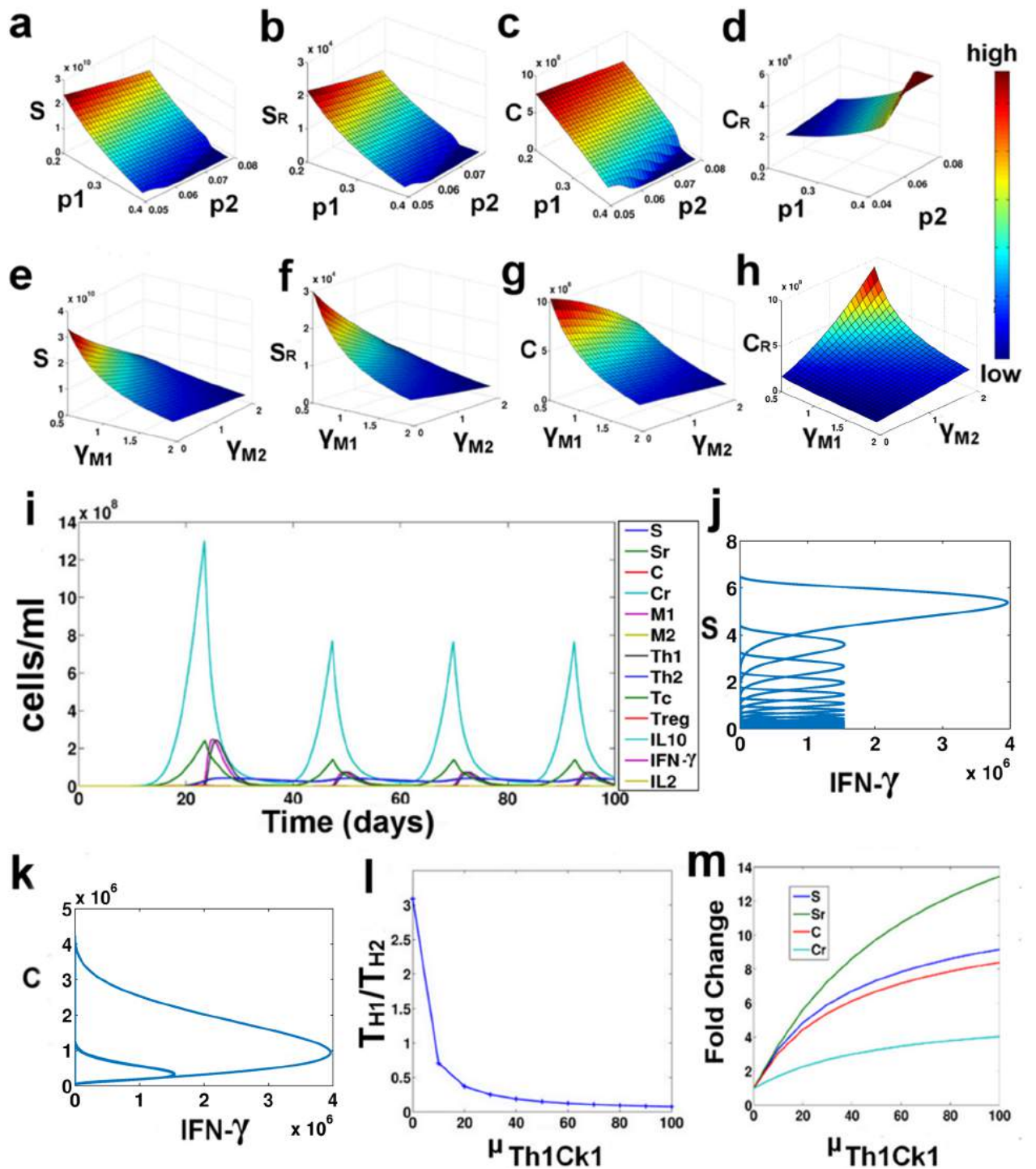


Fig 3. Parameter variation study. (a-d) Surface plot of the steady state values of S, S_R , C and C_R under varying p_1 and p_2 ; (e-h) Surface plot of the steady state values of S, S_R , C and C_R under varying γ_{M1} and γ_{M2} ; (i) Temporal Plot at $\beta_{Th1Ck2} = 0.1$; (j-k) Phase plane of S vs. IFN- γ and C vs. IFN- γ at $\beta_{Th1Ck2} = 0.1$; (l) T_{H1}/T_{H2} ratio at varying μ_{Th1Ck1} ; (m) Fold change in steady states at varying μ_{Th1Ck1} .

<https://doi.org/10.1371/journal.pone.0203030.g003>

decreased rapidly (Fig 3L). This results in the further proliferation of all the tumor sub-populations, i.e., S, S_R , C and C_R , and the fold changes in the steady state values of all four increases with increasing μ_{Th1Ck1} values (Fig 3M). Here it may be observed that inhibition of T_{H1} cells by IL10, results in higher fold changes of the steady state of S_R cells.

4.3. Development of treatment strategies

4.3.1. Failure of chemo and radiotherapies due to the presence of resistant cells. Chemotherapy and Radiotherapy are effective for controlling tumor proliferation in the absence of the resistant cells, i.e. when the rate of transformation of the stem and cancer cells to their resistant counterparts reduces. Here we have tried to simulate the cancer scenario without any mutational pressure, i.e. $m_C = 0$ and $m_S = 0$. Under such conditions, when we apply the Treatment Protocol 1, we observe the Stem and the Cancer cells population decreases rapidly and an overall reduction in the tumor population is observed (Fig 4). However, during the formation of a tumor, a certain fraction of the tumor cells acquire resistance to drugs. Under such conditions, i.e. $m_C > 0$ and $m_S > 0$, when the Treatment Protocol 1 is applied at the end of the detection time ($DT = 200$ days), we observe that even though the drug-sensitive populations viz. S and C decreases, the resistant populations S_R and C_R remain unaffected during the chemotherapeutic cycles. Thereafter, during the Radiotherapy cycles, the S_R cell population being completely unaffected by radiation proliferates rapidly, while the C and C_R population sharply decreases for some time and then becomes stable. In the next treatment-free stage, S_R , C and C_R start proliferating again. This activates the IFN- γ from the T_{H1} and T_C cells that help to bring down the S_R and C_R populations a little, that are then sustained at by the M2 and the Treg cells of the tumor microenvironment. The last phase of Chemotherapy does not have any effect on S_R and C_R populations. Hence the reduction in the overall tumor mass is not substantial. Also, it may be noticed here that at the end of this treatment regimen the T_{H1}/T_{H2} ratio is reduced to 2.5 that is indicative of poor disease prognosis.

4.3.2. Immune interventions for effective tumor remission. Combinatorial treatment protocol was designed to reduce the tumor burden and restore healthy T_{H1}/T_{H2} ratio. Parameter variation studies revealed the importance of the T_C and the T_{H1} cells in the regulation of the steady state levels of the tumor cells. Here, Immunotherapy was introduced as two control variables, i.e., $u_3_{T_C}$ and $u_3_{T_{H1}}$, which boost the production of the T_C and T_{H1} respectively. The stimulus to the T_{H1} and T_C cells was started at the end of the last chemotherapeutic cycle and was administered for 20 days followed by 1 day rest. This was repeated for 10 cycles. The dosage of each therapy was varied in wide ranges, and it was observed that when Immunotherapy is low, the change in Radio and Chemotherapies does not affect the tumor population significantly which is reflected in the very small tumor fold change and low T_{H1}/T_{H2} ratio (S1 Fig). As the Immunotherapy is increased, the fold change of tumor population increases along with the T_{H1}/T_{H2} . However at very high doses of immunostimulation, the fold changes decreases and the T_{H1}/T_{H2} ratio increases abruptly that leads to extreme suppression of the T_{H2} cells in the system. Hence the region $1.5 < d_I < 2.5$ can be considered as the ideal dosage of immunostimulation required for triggering the remission of Tumor. Using the leads from this analysis, the Protocol 2 was designed. At the end of this treatment regimen, it was observed that all the four tumor sub-populations showed a huge reduction in their proliferation, i.e. 136 fold reduction in tumor mass (Protocol 2). The T_{H1}/T_{H2} ratio was boosted to 8.8.

5. Discussion

The model developed here throws light into the development of a full grown tumor from a single cancer stem cell (S), and the influence of the tumor microenvironment during its

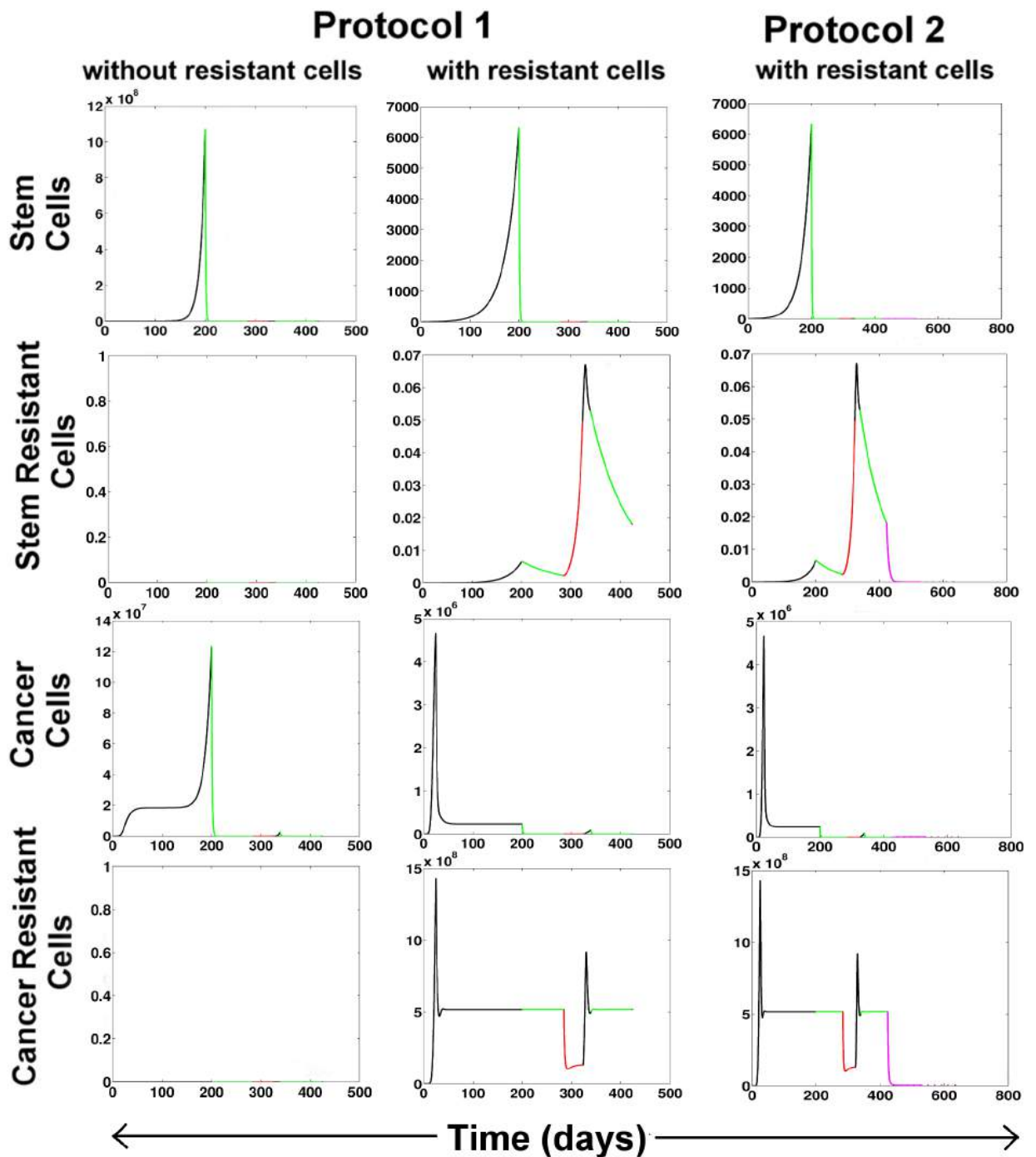


Fig 4. Changes in the tumor growth after therapeutic interventions. Protocol 1 has been applied without and with the presence of resistant cells. Protocol 2 efficiently suppresses tumor in spite of the presence of resistant cells. Color code: Black-without treatment, Green-Chemotherapy, Red-Radiotherapy, Pink-Immunotherapy.

<https://doi.org/10.1371/journal.pone.0203030.g004>

maturation. The study of the temporal evolution of tumor development shows that although the cancer stem cell forms the 'seed' from which the tumor emanate, the stem cell population remains low in the beginning. These cancer stem cells, owing to their slow replication, are

intrinsically resistant to radiotherapy and are only partially sensitive to chemotherapy [44, 45]. Additionally, the stem cell sub-populations have a strong immune-suppressive effect on the tumor microenvironment [46]. This phenomenon has been captured in our model in the study of the temporal evolution of the tumor-immune interaction dynamics, where we observe that coincident with the proliferation of the stem and resistant stem cell there is also an increased proliferation of the M2 and Treg cells (Fig 2C). This consequently leads to the lowering of the M1/M2 and T_{H1}/T_{H2} ratio that is associated with the formation of resistant tumors (Fig 2F). Moreover, it has been observed in our study that the proliferation of stem cell sub-populations leads to suppression of the Tc cells and the activation of the Treg cells, that results in the lowering the CD8/Treg ratio during Cancer (Fig 2F). This happens primarily because of the direct negative regulatory effects of the stem and resistant stem cells on the growth of the Tc cells. Hence, an early detection of the tumor is crucial for an effective treatment, when the stem cell population in the tumor remains low and the resistant stem cell population is not yet formed.

The model also captures the different patterns of CSC differentiation and its role in determining the fate of the tumor. Here, it has been observed that as the differentiation pattern of CSC shifts towards the asymmetric pattern, the CSC pool begins to deplete and the CSC starts producing the terminally differentiated cancer cells that have a finite lifespan. The reduction in the stem cell population helps in the reduction of its immune-suppressive effects on the Tc cells. At the same time, the differentiation of the stem into the cancer cells stimulates the Tc cells to get activated that now inhibit the tumor via the negative feedback regulation. However, the steady state value of the resistant cancer cells increases and overrides the negative feedback effect of the immune cells, reinforcing the observations that a higher asymmetric stem cell differentiation may be associated with the formation of more resistant tumors. Our model analysis also indicates that at low p_1 value, as the probability of symmetric differentiation (p_2) of stem cells is increased, the steady state levels of stem cells rapidly decreases, however it has little effect on the steady state value of Cancer cells. On the contrary, at high p_1 value, the increase in p_2 leads to the transformation of the cancer to resistant cancer cells. These results signify that reduction in stem cell symmetric renewal (p_3) of the cell leads to its differentiation into more resistant tumors.

The model further elucidates a dual role of the M2-TAMs in regulating the tumor formation (Fig 3E–3H). Here we observe that on one hand, the M2-TAMs aid in the suppression of the S, S_R and C cells of the tumor. This is because M2 is a prime source for the production of IL10 cytokine that has an important role in positively regulating the proliferation of the Cancer (C) cells. Hence, as the M2-TAMs increase in abundance, the cancer cells begin to proliferate via a positive feedback loop (Fig 5A). This leads to the activation of both the Tc and T_{H1} cells that inhibits the tumor cells *via* their negative feedback by producing a higher amount of IFN- γ and higher cytotoxic activity of the Tc cells (Fig 5A). However, on the other hand, it may be observed that M2-TAMs help in the growth of the C_R cells via the positive feedback loop, while the negative feedback has little effect on the C_R sub-population. This observation explains the reason for the refractory behavior of the tumor to treatment strategies under the presence of the M2-TAMs [47].

Our study reveals the functional behavior of the feedback mechanisms that regulate the behavior of the entire tumor-immune interaction network. From our parameter variation studies, the importance of the IFN- γ production in regulating the temporal behavior of the tumor development is observed. Here, we found that as the rate of IFN- γ production from the T_{H1} cells increases, the negative feedback effect of IFN- γ on the tumor helps in the suppression of the tumor cells (Figs 3I and 5B). However, the replicative potential of the Cancer and resistant Cancer balances out the negative effect of the IFN- γ leading to an oscillatory tumor-

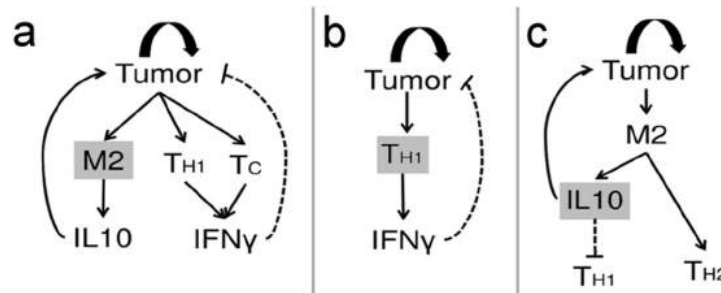


Fig 5. Regulatory feedback loops. (a) The M2 macrophage triggers two feedback loops. The first loop through IL10 is a positive feedback that triggers tumor proliferation. This, in turn, activates the second loop through IFN- γ that inhibits the tumor; (b) The T_{H1} derived IFN- γ inhibits the tumor via a negative feedback that leads to an oscillation in the population of tumor cells; (c) The positive feedback loop through IL10 is responsible for the maintenance of tumor and suppression of T_{H1}/ T_{H2} ratio.

<https://doi.org/10.1371/journal.pone.0203030.g005>

relapsing behavior, whereas the slowly replicating stem and resistant cells sub-populations gradually get eliminated from the tumor due to the high production of the IFN- γ cytokine (Fig 3J and 3K). This finding has important implications in the design of Immunotherapeutic protocols, where we observe the differential behavior of the tumor cells in response to high IFN- γ production. Using our model, we further explore the effects of the negative feedback of the IL10 cytokine on the T_{H1} cells (Figs 3L, 3M and 5C). We also make an important observation, where we find that as the sensitivity of T_{H1} cells to IL10 increases, the T_{H1}/T_{H2} ratio decreases sharply. This leads to the increased proliferation of the tumor cells. The fold change in the steady values of the resistant stem cells is the greatest signifying the prognostic role of the T_{H1}/T_{H2} ratio in predicting tumor progression and the formation of a resistant tumor with higher proportion of resistant stem cells.

With the knowledge of the regulatory mechanisms governing the differential response of the tumor sub-populations to the microenvironment, we have tried to explore the effect of treatment strategies conventionally adopted for the treatment of Cancer (Fig 4). Using our model we have been able to show that the reason for the failure of conventional Chemotherapy and Radiotherapy is primarily due to the formation of the resistant cancer stem cells S_R and resistant cancer cells C_R within the tumor. Under the conditions where there are no mutations conferring drug resistivity to the tumor, a significant reduction in tumor mass may be achieved using Chemo and Radio therapy alone. However, in reality, a small population of resistant tumor cells exists in the tumor that remains refractory to these treatment protocols. In order to successfully remove the tumor, a combination of the conventional treatment protocol along with Immuno-therapy can help alleviate the disease scenario. There can be several ways of boosting the immune system. However, in this work, we propose that a synergistic stimulus to both T_{H1} and T_C cells is required for the generation of an adaptive immune response that is capable of reducing both the drug-sensitive as well as the drug-resistant sub-populations of the tumor. In order to achieve this, dosage of Radio, Chemo and Immunotherapies were varied to create 1000 different treatment combinations and thereafter a treatment protocol (Protocol 2) has been designed to ensure maximal reduction in the tumor mass, as well as the restoration of a healthy T_{H1}/T_{H2} balance.

In this model, we try to capture the high complexity of the tumor microenvironment with a simple ODE model that represents the interaction of the tumor cell sub-populations and the immune cells at the phenotypic level. Here we assume that the parameters governing these cellular interactions are a cumulative outcome of the various molecular and the intracellular signalling events occurring in the microenvironment that influence the immune evasion but have

not been explicitly considered in this model for its simplification. However, it is worth mentioning that depending on the availability of data and hybrid modeling techniques involving a combination of different mathematical tools and strategies, this model may further be improved by considering the effect of the various molecular events such as angiogenesis, the role of the miRNA, exosomes and chemokines in mediating the cellular interactions, the metabolic pathways as well as the hypoxic conditions [48], that may further help us unravel unknown regulations underlying the tumor immune interaction and the development of drug-resistance.

6. Conclusion

With respect to the long standing ‘seed and soil’ hypothesis, we propose a model that throws light into the previously unexplored regulations governing tumor-immune interaction. This novel approach of developing of a tumor-immune interaction model considering both the stem cell differentiation pattern as well as the effect of the microenvironment has helped us in unveiling the effect of stem cell differentiation on the development of drug resistance and the different mechanistic regulations governing the tumor-immune interaction dynamics. However, this model does not capture the diffusion kinetics of the cytokines or the time delay associated with the cytokine regulations. Nonetheless, the observations derived from the model have been corroborated extensively with the experimental observations in cytometric and protein expression studies that strengthen the reliability of our model for the prediction of mechanistic regulations of tumor-immune interaction and design of the treatment protocols. This study can further be used to optimize treatment strategies, drug dosage and time schedules for designing advanced treatment protocols for Cancer.

7. Methods

7.1. Model development

7.1.1. Tumor formation. The core tumor consists of the Cancer Stem Cells (S), the Cancer Cells (C) and their drug resistant counterparts Resistant Stem Cells (S_R) and Resistant Cancer Cells (C_R) (Fig 1A, red box). The model takes into consideration the different patterns of stem cell differentiation, viz. the symmetric and asymmetric stem cell differentiation (Fig 1B). In the asymmetric differentiation, one stem cell (S) produces one daughter stem cell (S) and a differentiated progenitor Cancer cell (C) with probability p_1 , while in the symmetric differentiation one stem cell (S) produce either two Cancer cells (C) with probability p_2 or two stem cells (S) with probability p_3 (where, $p_1+p_2+p_3 = 1$). The stem cells undergoing asymmetric differentiation acquire mutation (represented with black dotted line in Fig 1A) with a probability m_S that leads to the transformation of a stem cell (S) to a resistant stem cell (S_R). Since the probability that this mutation hits the daughter stem cell and not the differentiated cancer cell is 0.5, the probability of formation of S_R from S is further multiplied by $p_1/2$. The symmetric differentiation leads to the renewal of the non-mutant stem cell (S) pool with a probability $(1-m_S)(1-p_1-p_2)$ [3]. Considering these factors (as described by Tomasetti and Levy [3]), we assume that the growth rate of S can be mathematically represented as $(\gamma_S(1 - m_S)(1 - p_1 - p_2))S$, while the rate of depletion of the stem cell pool, that includes the differentiation of S to C and the transformation S to S_R can be represented as $(\delta_S + (p_2 * \gamma_S) + \gamma_S * \frac{m_S * p_1}{2})S$. It may be mentioned here that γ_S and δ_S represents that natural birth and death rates of S cells. A similar nomenclature has been followed for all the other cell types.

The resistant stem cells are formed from the transformation of an S to S_R . The S_R follows a similar pattern of self-renewal and differentiation that leads to the replenishment of the S_R

pool and the formation of differentiated C_R cells [3]. Here, it may be assumed that the S_R represents the compartment of stem cells that accumulate all the mutations in its pool, such that no separate compartment for any secondary mutations has been considered here in this model.

The Cancer cells (C) are formed from the stem cells (S) with the probability p_1+p_2 . These C cells follow a Gompertzian growth kinetics that can be mathematically represented by $\gamma_C * \log\left(\frac{C_{max}}{C+r_1}\right)$, where C_{max} is the carrying capacity of the tumor [49]. Here, it has been assumed that during proliferation these C cells acquire mutations with a probability m_C and get transformed into C_R cells. Hence the probability of proliferation of the non-mutant C cell is further multiplied by a factor $(1-m_C)$. The C_R cells are formed from the differentiation of the S_R cells with probability p_1+p_2 and the transformation of the C to C_R cells with probability m_C . The C_R cells also follow similar Gompertzian growth kinetics. The total carrying capacity of these non-stem tumor cells has been considered as K_{tumor} , while each of C and C_R has a carrying capacity of $K_{tumor}/2$, so that both the cell populations can use the nutrients equally and have an equal advantage in proliferation.

7.1.2. Immune cells in the tumor microenvironment. As the tumor develops the resident TAMs, both M1 and M2, encounters the C and C_R cells of the tumor and gets activated (Fig 1A) [38]. It may be assumed that this cell to cell interaction will follow a saturating kinetics where even in the presence of a high number of tumor cells, the availability of TAMs acts as the limiting condition. Hence a Michaelis-Menten type functional form may be used to represent the TAM activation, e.g. $\gamma_{M1} * \left(\frac{M_1 * (C+C_R)}{M_1 + \lambda_{M1}}\right)$. These M1 and M2 TAMs now activate the T_{H1} and T_{H2} cells respectively [50]. Here the abundance of the T_H cells acts as the limiting condition. In a similar way, the M2-TAMs also activate the Treg cells present in the tumor microenvironment [51]. The Tc cells, on the other hand, infiltrate the tumor, gets directly activated by C and C_R cells (Fig 1A). However, the S and S_R cells of the tumor inhibit the Tc cell proliferation [9]. This is a bidirectional reaction, as the activated Tc also tries to kill the tumor cell sub-populations via its cytotoxic activity [52, 53]. The Treg cells act as immune-suppressor of the system and try to inhibit Tc proliferation, whereas the T_{H1} cells act as immune-stimulator of the system that helps in Tc proliferation and tumor infiltration [54, 55]. All these cell to cell interactions tend to follow saturation growth kinetics and hence have been modelled using the Michaelis Menten form discussed earlier [23].

7.1.3. Cytokines and feedbacks. Tumor formation triggers the immune system to produce cytokines. In this model, three important cytokines have been considered, viz. IFN- γ , IL-2 and IL-10 (Fig 1A). The activation of the T_{H1} cells stimulates the production of IL-2 cytokine from them. The amount of cytokine produced is directly proportional to the abundance of effector cells activated. Hence, this has been modelled using the Law of Mass Action, e.g. $(\beta_{Th1CK3} * T_{H1})$, where β_{Th1CK3} (units: ng cell⁻¹day⁻¹) is the rate of production of IL2 from T_{H1} cells [56]. This IL2 is responsible for the auto-regulation and sustained proliferation of the T_{H1} cells. Hence, we have considered a positive feedback loop from IL-2 to T_{H1} cell that has been modelled using a saturating function $\frac{\beta_{Th1CK3} * IL2 * T_{H1}}{IL2 + k_9}$, where the cytokine acts as the limiting factor [23, 56]. Similarly, the IFN- γ is produced by T_{H1} and Tc cells which have a negative feedback effect on all the tumor cell sub-populations. The production of IL-10 is regulated by M2, Treg and T_{H2} cells. An auto-regulatory positive feedback loop exists between IL10 and the Treg cells. IL10 also plays an important role in the proliferation of the C and C_R cells and inhibition of the T_{H1} cells. This IL10 mediated regulation captures the inhibitory actions of T_{H2} on T_{H1} cells that are often observed in Cancer scenario.

7.2. Model equations

Based on the biological relevance and mathematical assumptions discussed above, the equations representing the tumor-immune interaction network comprising of 13 Ordinary Differential Equations (Eqs 1-13) and 71 parameters have been enlisted below:

$$\bullet \frac{dS}{dt} = (\gamma_s(1 - m_s)(1 - p_1 - p_2))S - (\delta_s + (p_2 * \gamma_s) + \gamma_s * \frac{m_s * p_1}{2}) S - \left(\frac{\mu_s * S * IFN\gamma}{k_1 + IFN\gamma} \right) - \left(\frac{tck * S * Tc}{k_{tc1} + Tc} \right) \tag{Eq 1}$$

$$\bullet \frac{dS_R}{dt} = (\gamma_s(1 - p_1 - p_2) - (\delta_s + (p_2 * \gamma_s))) S_R + m_s * \gamma_s * \left(1 - \frac{p_1}{2} - p_2 \right) S - \left(\frac{\mu_{SR} * S_R * IFN\gamma}{k_2 + IFN\gamma} \right) - \left(\frac{tck * S_R * Tc}{k_{tc2} + Tc} \right) \tag{Eq 2}$$

$$\bullet \frac{dC}{dt} = \gamma_c * (1 - m_c) * \log \left(\frac{0.5 * K_{tumor}}{C + r_1} \right) * C + \gamma_s * (p_1 + p_2) * S - \delta_c * C - m_c * \gamma_c * C + \left(\frac{\mu_{C1} * C * IL10}{IL10 + k_3} \right) - \left(\frac{\mu_{C2} * C * IFN\gamma}{IFN\gamma + k_4} \right) - \left(\frac{tck * C * Tc}{k_{tc3} + Tc} \right) \tag{Eq 3}$$

$$\bullet \frac{dC_R}{dt} = \gamma_c * C_R * \log \left(\frac{0.5 * K_{tumor}}{C_R + r_2} \right) + \gamma_s * S_R * (p_1 + p_2) + m_c * \gamma_c * C - \delta_{CR} * C_R + \left(\frac{\mu_{C1} * C_R * IL10}{IL10 + k_5} \right) - \left(\frac{\mu_{C2} * C_R * IFN\gamma}{IFN\gamma + k_6} \right) - \left(\frac{tck * C_R * Tc}{k_{tc4} + Tc} \right) \tag{Eq 4}$$

$$\bullet \frac{dM_1}{dt} = \gamma_{M1} * M_1 * \left(\frac{C + C_R}{M_1 + \lambda_{M1}} \right) - \delta_{M1} * M_1 + \left(\frac{\mu_{M1Ck2} * M_1 * IFN\gamma}{IFN\gamma + k_7} \right) \tag{Eq 5}$$

$$\bullet \frac{dM_2}{dt} = \gamma_{M2} * M_2 * \left(\frac{C + C_R}{M_2 + \lambda_{M2}} \right) - \delta_{M2} * M_2 + \left(\frac{\mu_{M2Ck1} * M_2 * IL10}{IL10 + k_{10}} \right) \tag{Eq 6}$$

$$\bullet \frac{dT_{H1}}{dt} = \gamma_{TH1} * \left(\frac{T_{H1} * M_1}{\lambda_{TH1} + T_{H1}} \right) - (\delta_{TH1} * T_{H1}) - \frac{\mu_{TH1Ck1} * IL10 * T_{H1}}{IL10 + k_8} + \frac{\mu_{Th1Ck3} * IL2 * T_{H1}}{IL2 + k_9} \tag{Eq 7}$$

$$\bullet \frac{dT_{H2}}{dt} = \gamma_{TH2} * \left(\frac{T_{H2} * M_2}{\lambda_{TH2} + T_{H2}} \right) - (\delta_{TH2} * T_{H2}) \tag{Eq 8}$$

$$\bullet \frac{dTc}{dt} = \gamma_{Tc} * Tc * \left(\frac{C + C_R}{Tc + \lambda_{Tc1}} \right) + \gamma_{Tc} * \frac{Tc * T_{H1}}{Tc + \lambda_{Tc4}} - \mu_{TcS} * Tc * \left(\frac{S + S_R}{Tc + \lambda_{Tc2}} \right) - \delta_{Tc} * Tc - \mu_{TcTreg} * Tc * \left(\frac{T_{reg}}{\lambda_{Tc3} + T_{reg}} \right) \tag{Eq 9}$$

$$\bullet \frac{dT_{reg}}{dt} = \gamma_{Treg} * \left(\frac{T_{reg} * M_2}{T_{reg} + \lambda_{Treg2}} \right) - \delta_{Treg} * T_{reg} + \left(\mu_{TregCk1} * \frac{IL10 * T_{reg}}{T_{reg} + k_{11}} \right) \quad (\text{Eq 10})$$

$$\bullet \frac{dIL10}{dt} = \beta_{M2} * M_2 - \delta_{Ck1} * IL10 + \beta_{Treg} * T_{reg} + \beta_{Th2} * T_{H2} \quad (\text{Eq 11})$$

$$\bullet \frac{dIFN\gamma}{dt} = \beta_{Th1CK2} * T_{H1} + \beta_{Tc} * Tc - \delta_{Ck2} * IFN\gamma \quad (\text{Eq 12})$$

$$\bullet \frac{dIL2}{dt} = \beta_{Th1CK3} * T_{H1} - \delta_{Ck3} * IL2 \quad (\text{Eq 13})$$

7.3. Control and therapeutic strategies

- a. **Radiotherapy (R)** - With the aim to reduce the tumor cell proliferation, control variables were introduced in our model. Here, the control variable u_1 signifies the probability of cell death due to Radiotherapy (Eq 14),

$$u_1 = 1 - \exp(-\alpha d_r - \beta d_r^2) \quad (\text{Eq 14})$$

where α and β are the parameters governing the radio-sensitivity of the cells, and d_r is the dose of radiotherapy applied, measured in Grey (Gy) units [57]. The value of α and β depends on the oxygenation state of the cell [58]. In our model it has been considered that Radiotherapy affects only the Cancer (C) and the Cancer Resistant (Cr) populations of the tumor. It has no effect on the stem cells owing to their slow growth rate.

- b. **Chemotherapy (C)** - The control variable u_2 , signifying chemotherapy has an effect on the drug-sensitive stem (S) and cancer (C) cells of the tumor (Eq 15). u_{2_S} and u_{2_C} are defined as the probabilities of cell death, due to chemotherapy, of Stem cells and Cancer cells respectively (Eq 15 and Eq 16).

$$u_{2_S} = f_c * (1 - \exp(-M_c * d_c)) - k_s \quad (\text{Eq 15})$$

$$u_{2_C} = f_c * (1 - \exp(-M_c * d_c)) \quad (\text{Eq 16})$$

Here, f_c denotes the frequency of chemotherapy per day, M is defined as the efficiency of the chemotherapeutic drug in $m^2 mg^{-1}$ denoting the area of the tumor affected per mg of the drug and d_c is the concentration of the drug in $mg m^{-2}$. The efficacy of the chemotherapy of the stem cells depends on the factor k_s that represent the inhibitory effect of IL-4 on the stem cells that reduces the efficacy of the drugs. Sequestration of IL-4 makes the stem cells sensitive to chemotherapy [44, 59].

- c. **Immunotherapy (I)** - The parameter set was systematically screened to identify key parameters governing the negative feedback of the immune cells on the Tumor population. Then, the immunotherapy was introduced in our model as perturbations to the system in order to overcome the immunosuppressive effect of the tumor cells and to restore a healthy

T_{H1} / T_{H2} balance.

$$u3_Tc = d_I * M_{TC} \tag{Eq 17}$$

$$u3_TH1 = d_I * M_{TH1} \tag{Eq 18}$$

Eq 17 and Eq 18 depicts the control variables for providing immune-boost to the T_C and T_{H1} cells, respectively. d_I signifies the dose of immunostimulant, measured in $mg\ day^{-1}$ that must be given to the system, while M_{TC} and M_{TH1} are the measures of the sensitivity of the T_C and T_{H1} cells, respectively.

7.4. Designing treatment protocols

The protocols are designed using various combination of the above mentioned treatment strategies, viz. *Radiotherapy*, *Chemotherapy* and *Immunotherapy*. The dosage, time duration and number of cycles for each therapy are varied to determine the optimal combination that gives us maximum fold changes in the tumor reduction. The general form of the protocols can be described as follows:

$$DT_{200} \rightarrow (R_{iR}^{dR/n})_{nR} \rightarrow FT_{tFT} \rightarrow (Ch_{iC}^{dC})_{nC} \rightarrow (I_{tI}^{dI})_{nI}$$

Here, Ch denotes Chemotherapy, R denotes Radiotherapy and FT signifies a treatment-free period or relaxation time. The model was run till 200 days before the start of any therapeutic interventions. This has been considered as the standard detection time (DT) for a full grown tumor. Here the subscripts (t_R , t_C and t_I) denotes the time duration for which the treatment was given, and the superscripts (d_R , d_C and d_I) represent the dosage. The subscript outside the bracket (n_R , n_C and n_I) denotes the number of cycles for which that treatment was repeated.

7.4.1. Protocol 1. This Protocol is an adaptation of the standard treatment protocol used for applying chemo and radiotherapy (adapted from British Columbia Cancer Agency Protocol GIGAJCPRT - <http://www.bccancer.bc.ca/>). It was applied to our model to observe the fold changes in the tumor cell population. The protocol can be summarized as follows:

$$DT_{200} \rightarrow (Ch_{14}^{800})_6 \rightarrow (R_{40}^{60/28}) \rightarrow FT_{15} \rightarrow (Ch_{14}^{800})_6$$

7.4.2. Protocol 2. This Protocol was designed as a combinatorial treatment protocol of Chemotherapy, Radiotherapy and Immunotherapy to enhance the treatment efficacy. Based on Protocol 1, this Protocol is an improvisation where Immunotherapy has been included that boosts both the T_{H1} and T_C simultaneously. In order to design this combinatorial treatment protocol, the dose of Radio, Chemo and Immunotherapy were varied over wide ranges in order to create 1000 treatment combinations. The treatment efficacy of each combination was plotted in a 4-dimensional scatter plot, measured in terms of fold change and T_{H1}/T_{H2} ratio (S1 Fig). The Protocol 2 can be summarized as follows:

$$DT_{200} \rightarrow (Ch_{14}^{800})_6 \rightarrow (R_{40}^{60/28}) \rightarrow FT_{15} \rightarrow (Ch_{14}^{800})_6 \rightarrow (I_{20}^2)_{10}$$

7.4.3. Measuring treatment efficacy. The efficacy of a treatment protocol is measured by the reduction in the size of the tumor and the overall recovery from the immune-suppression induced by the tumor, to ensure minimal chances of tumor relapse. Hence we have defined two parameters that can be used as an indicator of Cancer prognosis:

- a. **Fold Change** – The treatment efficacy was estimated by measuring the fold change of the tumor mass at the end of the treatment period as compared to the tumor mass measured at the time of detection.
- b. **T_{H1}/T_{H2} ratio** - In order to ensure maximum treatment efficacy and minimize chances of Cancer relapse, the T_{H1}/T_{H2} ratio was used as an indicator for disease prognosis. A minimum threshold of T_{H1}/T_{H2} ≥ 5 was chosen to optimize treatment protocol.

7.5. Positivity and boundedness

This system of equations (Section 1.2, Eqs 1–13) can be analyzed with the initial conditions (S1 Text) defined in the thirteen dimensional variable space

$$R_+^{13} = [(S, S_R, C, C_R, M1, M2, T_{H1}, T_{H2}, Tc, Treg, IL10, IFN\gamma, IL2) \in \mathfrak{R}^{13} | (S, S_R, C, C_R, M1, M2, T_{H1}, T_{H2}, Tc, Treg, IL10, IFN\gamma, IL2) \geq 0]$$

It can be proven, that all solutions of the system in R_{0+}^{13} remain in R_{0+}^{13} . Hence, R_{0+}^{13} is positively invariant, and it is sufficient to consider solutions only in R_{0+}^{13} . In this region, the usual existence, uniqueness and continuation results hold for the system. From our numerical simulations also, we have observed the existence of positive solutions. The solution set we get for the set of ODEs represents the effective cell population and protein concentrations of the species considered in the model at different time points during the tumor development. The fixed point attained by all the variables of the model is a part of this positive solution space.

Also, we observe that the right-hand side of Eqs 1–13 (Section 1.2) are smooth functions of the variables (S, S_R, C, C_R, M1, M2, T_{H1}, T_{H2}, Tc, Treg, IL10, IFN γ , IL2). Also, since all the parameters are non-negative, local existence and uniqueness properties hold in R_+^{13} , and if the following necessary conditions are satisfied,

1. $S_0 > 0$
2. $p_1 + p_2 < 1$
3. $m_S < 1$
4. $m_C < 1$
5. $\gamma_S(1 - p_2) > \delta_S$

then, we can state the following proposition.

Proposition 1: All the solutions of Eqs 1–13 (Section 1.2) which initiate in R_+^{13} are uniformly bounded.

Proof: The proof of Proposition 1 is obvious as all the variables satisfy the condition of positive invariance for all the solutions of Eqs 1–13 (Section 1.2) which initiate in R_+^{13} , the assumptions and necessary conditions (stated in Section 1.3) [60].

7.6. Sensitivity analysis

The sensitivity analysis of the model was performed by the extended Fourier Amplitude Sensitivity Test eFAST technique using a MATLAB based toolbox [61]. The sensitivity analysis was carried out using the whole set of parameters [k = 71]. 100 samples were chosen per search curve and resampling of the search curves was carried out 5 times [N_S = 100, N_R = 5]. Hence, the total number of model simulations N = (k+1)*N_S*N_R = 36000. The Sensitivity Indices (Si) of the parameters (p < 0.05) for the variables governing the growth of the tumor sub-

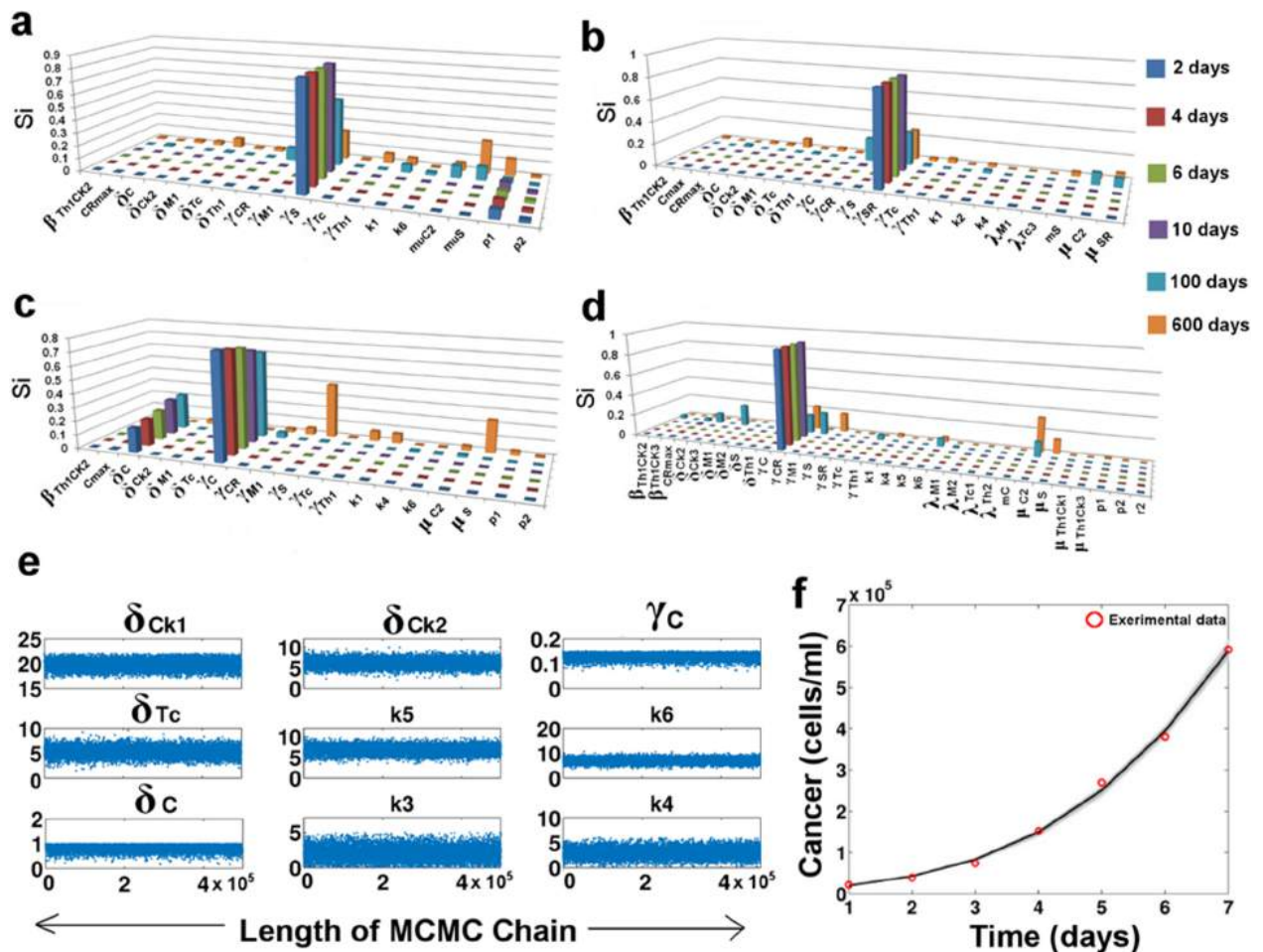


Fig 6. Sensitivity analysis and parameter estimation: (a-d) Sensitivity Analysis plots for S, S_R , C and C_R respectively. The x-axis represents the parameters with $p < 0.05$; (e) Trace Plot showing the best fitting parameter values as estimated by the MCMC algorithm; (f) Predictive plot of cancer proliferation using the estimated parameter values. The red circles represent the cancer cell proliferation values as obtained from Cell Counting experiments using Gastric Cancer cell line [29].

<https://doi.org/10.1371/journal.pone.0203030.g006>

populations, *viz.* S, S_R , C and C_R were estimated at different stages of the tumor development (Fig 6A–6D). Here it may be observed that at different time points that Si values of the parameters change, signifying the importance of the parameters in the different stages of the tumor development. The knowledge from this sensitivity analysis was used to determine the parameters that have a maximum effect on the tumor development.

7.7. Parameter estimation from Cancer cell line data

The model comprises of a total of 71 parameters. The values of 21 parameters of the model were curated from the existing literature. The unknown parameters were estimated (few were assumed within the biological feasible ranges) using the MATLAB based toolbox that employs the MCMC-DRAM algorithm for parameter estimation [62]. The time course experiment cytometric data for cancer cell proliferation obtained for 7 days in for Gastric cancer cell line (SGC7901) that was fitted for approximating the cancer cell behavior during the growth phase (Fig 6F) [29]. Parameters that were sensitive for the growth of the Cancer (C sub-population)

cells were varied in biologically feasible ranges. The prior distribution was assumed to be normal and the MCMC simulation was carried out for 5 lakh iterations to ensure the convergence of the chain (Fig 6E). The estimated parameter values for the model have been listed in S1 Text.

7.8. Experimental data for model calibration

Apart from the parameters estimated using the MCMC method, the remaining unknown parameters governing the steady state behavior of the system were manually adjusted within the biologically feasible ranges for the calibration of the model so as to ensure that the simulation results corroborated with the various experimental observations. These parameter values (labelled as 'Expected') used for the numerical simulation of the model have been enlisted in S1 Text. The experimental data used for this purpose were extracted from the available literature. For the validation of the growth kinetics of the resistant Cancer cells, time-course data of resistant cell lines were obtained from Breast cancer cell line MCF-7/TAX-resistant to Paclitaxel [31], Hepatocellular Carcinoma cell line SK-Hep1/CDDP3-resistant to Cisplatin [32], Colon Cancer cell lines SW-620-L-OHP and LoVo-L-OHP-resistant to Oxaliplatin [33]. The cytometric data obtained for the validation of the immune cell ratios were mostly obtained from Gastric Cancer, Ovarian Cancer and Osteosarcoma studies [34–39]. The data for the validation of cytokine expression were obtained from cases of Gastric and Breast Cancer studies [40–42]. These data used came from heterogeneous sources as none of the previously performed experiments were found to report the values of all cytometric data in a single experiment. Moreover, the use of data from the different Cancer studies ensures that the model is generic and mimics the average behavior observed in most Cancer studies. The use of data from both *in vitro* studies as well as data obtained from Cancer patients ensures the reliability of the model for its use in designing therapeutic control. In order to make the model specific for a single type of Cancer, one needs to simply obtain the cytometric data from a single experimental source and adjust the parameters accordingly.

7.9. Interior equilibria

To ensure positivity and existence of the interior equilibrium solutions, 36000 random parameter sets were generated (as mentioned in Section 7.6) within the biologically feasible ranges. Thereafter the model is simulated up to 800 days for each set of parameter. It was observed that each model simulation led to the positive interior equilibrium solution. Hence, we can state and prove the following Proposition.

Proposition 2: Positive interior equilibria exists for the set of equations Eqs 1–13 (Section 1.2).

Proof: The interior equilibrium points are the steady-state solutions of the Eqs 1–13 (Section 1.2) under the necessary conditions (Section 1.3) in the biologically feasible ranges of parameter values and initial conditions S1 Text.

7.10. Model initialization and numerical simulation

The tumor mass is formed by the sub-populations S , S_R , C , C_R . In our model, the S cell sub-population has been initialized to 1, while all the other tumor cell sub-populations have been considered as 0. The initial values of the remaining variables have been initialized based on cytometric data and cytokine expression values of healthy individuals, curated from the literature. The details have been provided in the S1 Text. The model was simulated numerically using the variable-step, variable order solver, ode15s, in MATLAB® 2017a platform.

Supporting information

S1 Text. Model parameters. The Supplementary Text contains the description of the parameters and state variables used for the model simulations.
(DOCX)

S1 Fig. Treatment conditions under varying dose of Radiotherapy, Chemotherapy and Immunotherapy. The scatter plot depicts (a) the fold change of tumor population and (b) T_{H1}/T_{H2} ratio under 1000 treatment combinations.
(TIF)

Acknowledgments

Piyali Ganguli acknowledges the Council of Scientific & Industrial Research (CSIR) for the Junior Research Fellowship.

Author Contributions

Conceptualization: Ram Rup Sarkar.

Data curation: Piyali Ganguli.

Formal analysis: Piyali Ganguli, Ram Rup Sarkar.

Methodology: Piyali Ganguli.

Supervision: Ram Rup Sarkar.

Validation: Piyali Ganguli.

Writing – original draft: Piyali Ganguli.

Writing – review & editing: Ram Rup Sarkar.

References

1. Tan BT, Park CY, Ailles LE, Weissman IL. The cancer stem cell hypothesis: a work in progress. *Laboratory Investigation*. 2006; 86(12):1203–7. <https://doi.org/10.1038/labinvest.3700488> PMID: 17075578
2. Fidler IJ. The pathogenesis of cancer metastasis: the 'seed and soil' hypothesis revisited. *Nature reviews Cancer*. 2003; 3(6):453–8. <https://doi.org/10.1038/nrc1098> PMID: 12778135.
3. Tomasetti C, Levy D. Role of symmetric and asymmetric division of stem cells in developing drug resistance. *Proceedings of the National Academy of Sciences of the United States of America*. 2010; 107(39):16766–71. <https://doi.org/10.1073/pnas.1007726107> PMID: 20826440; PubMed Central PMCID: PMC2947914.
4. Zahreddine H, Borden KLB. Mechanisms and insights into drug resistance in cancer. *Frontiers in Pharmacology*. 2013; 4:28. <https://doi.org/10.3389/fphar.2013.00028> PMC3596793. PMID: 23504227
5. Chew V, Toh HC, Abastado JP. Immune microenvironment in tumor progression: characteristics and challenges for therapy. *Journal of oncology*. 2012; 2012:608406. <https://doi.org/10.1155/2012/608406> PMID: 22927846; PubMed Central PMCID: PMC3423944.
6. Papaccio F, Paino F, Regad T, Papaccio G, Desiderio V, Tirino V. Concise review: cancer cells, cancer stem cells, and mesenchymal stem cells: influence in cancer development. *Stem cells translational medicine*. 2017; 6(12):2115–25. <https://doi.org/10.1002/sctm.17-0138> PMID: 29072369
7. Bellone G, Turletti A, Artusio E, Mareschi K, Carbone A, Tibaudi D, et al. Tumor-associated transforming growth factor- β and interleukin-10 contribute to a systemic Th2 immune phenotype in pancreatic carcinoma patients. *The American journal of pathology*. 1999; 155(2):537–47. PMID: 10433946
8. Ostuni R, Kratochvill F, Murray PJ, Natoli G. Macrophages and cancer: from mechanisms to therapeutic implications. *Trends in immunology*. 2015; 36(4):229–39. <https://doi.org/10.1016/j.it.2015.02.004> PMID: 25770924

9. Hirohashi Y, Torigoe T, Tsukahara T, Kanaseki T, Kochin V, Sato N. Immune responses to human cancer stem-like cells/cancer-initiating cells. *Cancer Science*. 2016; 107(1):12–7. <https://doi.org/10.1111/cas.12830> PMID: 26440127
10. Bell E, Taylor MA. Functional roles for exosomal microRNAs in the tumour microenvironment. *Computational and structural biotechnology journal*. 2017; 15:8–13. <https://doi.org/10.1016/j.csbj.2016.10.005> PMID: 27872688
11. Neviani P, Fabbri M. Exosomal microRNAs in the tumor microenvironment. *Frontiers in medicine*. 2015; 2:47. <https://doi.org/10.3389/fmed.2015.00047> PMID: 26258125
12. Ohm JE, Gabrilovich DI, Sempowski GD, Kisseleva E, Parman KS, Nadaf S, et al. VEGF inhibits T-cell development and may contribute to tumor-induced immune suppression. *Blood*. 2003; 101(12):4878–86. <https://doi.org/10.1182/blood-2002-07-1956> PMID: 12586633
13. Ziogas AC, Gavalas NG, Tsiatas M, Tsitsilonis O, Politi E, Terpos E, et al. VEGF directly suppresses activation of T cells from ovarian cancer patients and healthy individuals via VEGF receptor Type 2. *International journal of cancer*. 2012; 130(4):857–64. <https://doi.org/10.1002/ijc.26094> PMID: 21445972
14. Paino F, La Noce M, Di Nucci D, Nicoletti GF, Salzillo R, De Rosa A, et al. Human adipose stem cell differentiation is highly affected by cancer cells both in vitro and in vivo: implication for autologous fat grafting. *Cell death & disease*. 2017; 8(1):e2568.
15. Stellavato A, La Noce M, Corsuto L, Pirozzi AVA, De Rosa M, Papaccio G, et al. Hybrid complexes of high and low molecular weight hyaluronans highly enhance HASCs differentiation: implication for facial bioremodelling. *Cellular Physiology and Biochemistry*. 2017; 44(3):1078–92. <https://doi.org/10.1159/000485414> PMID: 29179206
16. Whiteside TL. The tumor microenvironment and its role in promoting tumor growth. *Oncogene*. 2008; 27(45):5904–12. <https://doi.org/10.1038/onc.2008.271> PMID: 18836471; PubMed Central PMCID: PMC3689267.
17. Gammaitoni L, Leuci V, Mesiano G, Giraudo L, Todorovic M, Carnevale-Schianca F, et al. Immunotherapy of cancer stem cells in solid tumors: initial findings and future prospective. *Expert opinion on biological therapy*. 2014; 14(9):1259–70. <https://doi.org/10.1517/14712598.2014.918099> PMID: 24835841
18. Liao T, Kaufmann AM, Qian X, Sangvatanakul V, Chen C, Kube T, et al. Susceptibility to cytotoxic T cell lysis of cancer stem cells derived from cervical and head and neck tumor cell lines. *Journal of cancer research and clinical oncology*. 2013; 139(1):159–70. <https://doi.org/10.1007/s00432-012-1311-2> PMID: 23001491
19. Chen H-C, Joalland N, Bridgeman JS, Alchami FS, Jarry U, Khan MWA, et al. Synergistic targeting of breast cancer stem-like cells by human $\gamma\delta$ T cells and CD8(+) T cells. *Immunology and Cell Biology*. 2017; 95(7):620–9. <https://doi.org/10.1038/icb.2017.21> PMC5550559. PMID: 28356569
20. Guo Y, Feng K, Wang Y, Han W. Targeting cancer stem cells by using chimeric antigen receptor-modified T cells: a potential and curable approach for cancer treatment. *Protein & cell*. 2017:1–11.
21. Agliano A, Calvo A, Box C. The challenge of targeting cancer stem cells to halt metastasis. *Seminars in Cancer Biology*. 2017; 44:25–42. <https://doi.org/10.1016/j.semcancer.2017.03.003> PMID: 28323021
22. McHale PT, Lander AD. The Protective Role of Symmetric Stem Cell Division on the Accumulation of Heritable Damage. *PLOS Computational Biology*. 2014; 10(8):e1003802. <https://doi.org/10.1371/journal.pcbi.1003802> PMID: 25121484
23. Kirschner D, Panetta JC. Modeling immunotherapy of the tumor-immune interaction. *Journal of mathematical biology*. 1998; 37(3):235–52. PMID: 9785481
24. de Pillis LG, Radunskaya AE, Wiseman CL. A Validated Mathematical Model of Cell-Mediated Immune Response to Tumor Growth. *Cancer Research*. 2005; 65(17):7950. <https://doi.org/10.1158/0008-5472.CAN-05-0564> PMID: 16140967
25. De Boer RJ, Hogeweg P, Dullens HF, De Weger RA, Den Otter W. Macrophage T lymphocyte interactions in the anti-tumor immune response: a mathematical model. *The Journal of Immunology*. 1985; 134(4):2748. PMID: 3156189
26. Robertson-Tessi M, El-Kareh A, Goriely A. A mathematical model of tumor-immune interactions. *Journal of Theoretical Biology*. 2012; 294:56–73. <https://doi.org/10.1016/j.jtbi.2011.10.027> PMID: 22051568
27. De Pillis LG, Radunskaya A. A mathematical tumor model with immune resistance and drug therapy: an optimal control approach. *Journal of Theoretical Medicine*. 2001; 3(2):79–100. <https://doi.org/10.1080/10273660108833067>
28. Krishnapriya P, Pitchaimani M. Optimal control of mixed immunotherapy and chemotherapy of tumours with discrete delay. *International Journal of Dynamics and Control*. 2015. <https://doi.org/10.1007/s40435-015-0221-y>

29. Ning X, Sun S, Hong L, Liang J, Liu L, Han S, et al. Calcyclin-binding protein inhibits proliferation, tumorigenicity, and invasion of gastric cancer. *Molecular cancer research: MCR*. 2007; 5(12):1254–62. <https://doi.org/10.1158/1541-7786.MCR-06-0426> PMID: 18171983.
30. Pan Q, Li Q, Liu S, Ning N, Zhang X, Xu Y, et al. Concise Review: Targeting Cancer Stem Cells Using Immunologic Approaches. *Stem Cells*. 2015; 33(7):2085–92. <https://doi.org/10.1002/stem.2039> PMID: 25873269
31. Chen S-Y, Hu S-S, Dong Q, Cai J-X, Zhang W-P, Sun J-Y, et al. Establishment of Paclitaxel-resistant Breast Cancer Cell Line and Nude Mice Models, and Underlying Multidrug Resistance Mechanisms in Vitro and in Vivo. *Asian Pacific Journal of Cancer Prevention*. 2013; 14(10):6135–40. <https://doi.org/10.7314/apjcp.2013.14.10.6135> PMID: 24289639
32. Ling X, Wen L, Zhou Y. Role of mitochondrial translocation of telomerase in hepatocellular carcinoma cells with multidrug resistance. *International journal of medical sciences*. 2012; 9(7):545–54. <https://doi.org/10.7150/ijms.4648> PMID: 22991493; PubMed Central PMCID: PMC3444975.
33. Liu Z, Qiu M, Tang QL, Liu M, Lang N, Bi F. Establishment and biological characteristics of oxaliplatin-resistant human colon cancer cell lines. *Chinese journal of cancer*. 2010; 29(7):661–7. PMID: 20591218.
34. Markowska J, Lacki J, Jaroszewski J, Wiktorowicz K. The usefulness of CD4/CD8 ratio evaluation in monitoring of ovarian cancer patients. *European journal of gynaecological oncology*. 1995; 16(1):54–8. PMID: 7744118
35. Biller BJ, Guth A, Burton JH, Dow SW. Decreased Ratio of CD8+ T Cells to Regulatory T Cells Associated with Decreased Survival in Dogs with Osteosarcoma. *Journal of veterinary internal medicine / American College of Veterinary Internal Medicine*. 2010; 24(5):1118–23. <https://doi.org/10.1111/j.1939-1676.2010.0557.x> PMC3557512. PMID: 20666983
36. Liu K, Yang K, Wu B, Chen H, Chen X, Chen X, et al. Tumor-Infiltrating Immune Cells Are Associated With Prognosis of Gastric Cancer. *Medicine*. 2015; 94(39):e1631. <https://doi.org/10.1097/MD.0000000000001631> PMC4616881. PMID: 26426650
37. Balachandran VP, Cavnar MJ, Zeng S, Bamboat ZM, Ocuin LM, Obaid H, et al. Imatinib potentiates antitumor T cell responses in gastrointestinal stromal tumor through the inhibition of Ido. *Nature medicine*. 2011; 17(9):1094–100. <https://doi.org/10.1038/nm.2438> PMID: 21873989; PubMed Central PMCID: PMC3278279.
38. Zhang M, He Y, Sun X, Li Q, Wang W, Zhao A, et al. A high M1/M2 ratio of tumor-associated macrophages is associated with extended survival in ovarian cancer patients. *Journal of Ovarian Research*. 2014; 7:19–. <https://doi.org/10.1186/1757-2215-7-19> PMC3939626. PMID: 24507759
39. Ubukata H, Motohashi G, Tabuchi T, Nagata H, Konishi S, Tabuchi T. Evaluations of interferon-gamma/interleukin-4 ratio and neutrophil/lymphocyte ratio as prognostic indicators in gastric cancer patients. *Journal of surgical oncology*. 2010; 102(7):742–7. <https://doi.org/10.1002/jso.21725> PMID: 20872813.
40. Hong CC, Yao S, McCann SE, Dolnick RY, Wallace PK, Gong Z, et al. Pretreatment levels of circulating Th1 and Th2 cytokines, and their ratios, are associated with ER-negative and triple negative breast cancers. *Breast cancer research and treatment*. 2013; 139(2):477–88. <https://doi.org/10.1007/s10549-013-2549-3> PMID: 23624818; PubMed Central PMCID: PMC3912696.
41. Szaflarska A, Szczepanik A, Siedlar M, Czupryna A, SIERŻĘGA M, Popiela T, et al. Preoperative plasma level of IL-10 but not of proinflammatory cytokines is an independent prognostic factor in patients with gastric cancer. *Anticancer research*. 2009; 29(12):5005–12. PMID: 20044609
42. Gupta M, Han JJ, Stenson M, Maurer M, Wellik L, Hu G, et al. Elevated serum IL-10 levels in diffuse large B-cell lymphoma: a mechanism of aberrant JAK2 activation. *Blood*. 2012; 119(12):2844–53. <https://doi.org/10.1182/blood-2011-10-388538> PMC3327462. PMID: 22323454
43. Yuan A, Hsiao Y-J, Chen H-Y, Chen H-W, Ho C-C, Chen Y-Y, et al. Opposite Effects of M1 and M2 Macrophage Subtypes on Lung Cancer Progression. *Scientific Reports*. 2015; 5:14273. <https://doi.org/10.1038/srep14273> <https://www.nature.com/articles/srep14273#supplementary-information>. PMID: 26399191
44. Rich JN, Bao S. Chemotherapy and cancer stem cells. *Cell stem cell*. 2007; 1(4):353–5. <https://doi.org/10.1016/j.stem.2007.09.011> PMID: 18371369.
45. Kim Y, Joo KM, Jin J, Nam D-H. Cancer Stem Cells and Their Mechanism of Chemo-Radiation Resistance. *International Journal of Stem Cells*. 2009; 2(2):109–14. PMC4021765. PMID: 24855529
46. Hazem G, Monther A-A. Do Cancer Stem Cells have an Immunomodulatory Role Different from the Bulk of Tumor Cells? *Journal of Carcinogenesis & Mutagenesis*. 2013;0(0):- . <https://doi.org/10.4172/2157-2518.S14-003>
47. Jiang X. Macrophage-produced IL-10 limits the chemotherapy efficacy in breast cancer. *Journal of Zhejiang University Science B*. 2015; 16(1):44–5. <https://doi.org/10.1631/jzus.B1400352> PMC4288943. PMID: 25559954

48. Mele L, Paino F, Papaccio F, Regad T, Boocock D, Stiuso P, et al. A new inhibitor of glucose-6-phosphate dehydrogenase blocks pentose phosphate pathway and suppresses malignant proliferation and metastasis in vivo. *Cell death & disease*. 2018; 9(5):572.
49. Demicheli R, Pratesi G, Foroni R. The exponential-Gompertzian tumor growth model: data from six tumor cell lines in vitro and in vivo. Estimate of the transition point from exponential to Gompertzian growth and potential clinical implications. *Tumori*. 1991; 77(3):189–95. PMID: [1862544](https://pubmed.ncbi.nlm.nih.gov/1862544/)
50. Mills CD, Ley K. M1 and M2 Macrophages: The Chicken and the Egg of Immunity. *Journal of Innate Immunity*. 2014; 6(6):716–26. <https://doi.org/10.1159/000364945> PMID: [25138714](https://pubmed.ncbi.nlm.nih.gov/25138714/)
51. Sun W, Wei F-Q, Li W-J, Wei J-W, Zhong H, Wen Y-H, et al. A positive-feedback loop between tumour infiltrating activated Treg cells and type 2-skewed macrophages is essential for progression of laryngeal squamous cell carcinoma. *British Journal Of Cancer*. 2017; 117:1631. <https://doi.org/10.1038/bjc.2017.329> <https://www.nature.com/articles/bjc2017329#supplementary-information>. PMID: [28949956](https://pubmed.ncbi.nlm.nih.gov/28949956/)
52. Kwiatkowska-Borowczyk EP, Gałbka-Buszek A, Jankowski J, Mackiewicz A. Immunotargeting of cancer stem cells. *Contemporary Oncology*. 2015; 19(1A):A52–A9. <https://doi.org/10.5114/wo.2014.47129> PMC4322523. PMID: [25691822](https://pubmed.ncbi.nlm.nih.gov/25691822/)
53. Beavis PA, Petley EV, Darcy PK. A novel combination strategy for effectively targeting cancer stem-like cells. *Immunology And Cell Biology*. 2017; 95:573. <https://doi.org/10.1038/icb.2017.39> PMID: [28529324](https://pubmed.ncbi.nlm.nih.gov/28529324/)
54. Chen M-L, Pittet MJ, Gorelik L, Flavell RA, Weissleder R, von Boehmer H, et al. Regulatory T cells suppress tumor-specific CD8 T cell cytotoxicity through TGF- β signals &in vivo>. *Proceedings of the National Academy of Sciences of the United States of America*. 2005; 102(2):419. <https://doi.org/10.1073/pnas.0408197102> PMID: [15623559](https://pubmed.ncbi.nlm.nih.gov/15623559/)
55. Huang H, Hao S, Li F, Ye Z, Yang J, Xiang J. CD4(+) Th1 cells promote CD8(+) Tc1 cell survival, memory response, tumor localization and therapy by targeted delivery of interleukin 2 via acquired pMHC I complexes. *Immunology*. 2007; 120(2):148–59. <https://doi.org/10.1111/j.1365-2567.2006.02452.x> PMC2265849. PMID: [17274112](https://pubmed.ncbi.nlm.nih.gov/17274112/)
56. de Pillis LG. *Mathematical Modeling of the Regulatory T Cell Effects on Renal Cell Carcinoma Treatment*. 2013.
57. Powathil GG, Adamson DJ, Chaplain MA. Towards predicting the response of a solid tumour to chemotherapy and radiotherapy treatments: clinical insights from a computational model. *PLoS Comput Biol*. 2013; 9(7):e1003120. <https://doi.org/10.1371/journal.pcbi.1003120> PMID: [23874170](https://pubmed.ncbi.nlm.nih.gov/23874170/); PubMed Central PMCID: PMC3708873.
58. Powathil G, Kohandel M, Milosevic M, Sivaloganathan S. Modeling the spatial distribution of chronic tumor hypoxia: implications for experimental and clinical studies. *Computational and mathematical methods in medicine*. 2012; 2012:410602. <https://doi.org/10.1155/2012/410602> PMID: [22400049](https://pubmed.ncbi.nlm.nih.gov/22400049/); PubMed Central PMCID: PMC3287099.
59. Abdullah LN, Chow EK. Mechanisms of chemoresistance in cancer stem cells. *Clinical and translational medicine*. 2013; 2(1):3. <https://doi.org/10.1186/2001-1326-2-3> PMID: [23369605](https://pubmed.ncbi.nlm.nih.gov/23369605/); PubMed Central PMCID: PMC3565873.
60. Birkhoff G, Rota G. *Ordinary differential equations*, John Wiley& Sons. Inc; 1978.
61. Marino S, Hogue IB, Ray CJ, Kirschner DE. A methodology for performing global uncertainty and sensitivity analysis in systems biology. *J Theor Biol*. 2008; 254(1):178–96. <https://doi.org/10.1016/j.jtbi.2008.04.011> PMID: [18572196](https://pubmed.ncbi.nlm.nih.gov/18572196/); PubMed Central PMCID: PMC2570191.
62. Haario H, Laine M, Mira A, Saksman E. DRAM: efficient adaptive MCMC. *Statistics and Computing*. 2006; 16(4):339–54.



T-Cell Activation and Differentiation: Role of Signaling and Metabolic Cross-Talk

6

Rupa Bhowmick, Piyali Ganguli, and Ram Rup Sarkar

Abstract

Different types of T effector cells function centrally in the immune-regulatory network, which acts as a line of defense for the body and elicits immune response during any diseased condition. At the molecular level, this functioning is maintained by an intricately designed network of signaling and metabolic pathways that function via multiple cross-talks to regulate complex immune responses during different antigenic challenges. These pathways regulate phenomena such as quiescence exit of naïve T cells, their activation, and differentiation into different effector T cells. Signaling properties of these T cells and their response to different cytokine signals have been well studied. Immune-metabolism is comparatively a new area of research that has been identified as driver for immune response. However, to gain a holistic understanding of the activation and differentiation of naïve T cells into the subtypes, the integration of signaling and metabolic pathway information is a prerequisite. The bidirectional mode of regulation between these cross-talking signaling and metabolic pathways governs the differentiation patterns. In this chapter, we review the activation and differentiation pattern of naïve T cells from both signaling and metabolic perspectives and also look into their cross-talk to understand their mutual regulation during differentiation into effector T cells.

R. Bhowmick · P. Ganguli · R. R. Sarkar (✉)
CSIR-National Chemical Laboratory, Pune, India

Academy of Scientific and Innovative Research (AcSIR), Ghaziabad, India
e-mail: rr.sarkar@ncl.res.in

© Springer Nature Singapore Pte Ltd. 2020
S. Singh (ed.), *Systems and Synthetic Immunology*,
https://doi.org/10.1007/978-981-15-3350-1_6

153

6.1 Introduction

The immune system forms the sentinel of the body that protects it from infectious disease and cancer. The adaptive immune system, composed mainly of the T and B lymphocytes, is responsible for maintaining this defense mechanism of the body as it helps to generate immune responses specific to the type of antigenic challenge that the body encounters [1]. The helper T cells (T_H) form the central orchestrators of the entire immune-regulatory network. They have been known to have an essential role in the recognition of the antigen when presented on the surface of the antigen-presenting cells and secrete cytokines that aid in the proliferation of the cytotoxic T cells and B cells, thereby playing an active role in stimulating both the humoral and the cell-mediated immunity [2]. The effector functions of these immune systems are mediated mainly by the cytokines and other microbicidal molecules secreted by them as a result of the activation of complex biochemical signaling pathways inside the immune cells. The T_H cells themselves produce a high amount of interferon and tumor necrosis factor via TCR and co-receptor mediated pathways that mediates apoptosis of infected and cancerous cells [3, 4].

The differentiation of the helper T cells is primarily influenced by the changes in the micro-environmental conditions that favor the proliferation of a certain subset of T cells that leads to disruption of the balance and ratio of the normal proportions of T-cell subsets present in a healthy individual [5, 6].

Naive T cells circulate in the body surveying for antigens. The metabolic activity of these cells is maintained low by allowing low uptake of glucose enough to fuel the TCA cycle and OXPHOS to produce ATP [7]. These cells are kept in a quiescent state that promotes their survival and persistence. On antigen stimulation, the metabolism of T cells is triggered via increased uptake of glucose, which allows quiescence exit and initiates clonal expansion and effector differentiation primarily by mTOR-mediated signaling responses [8]. Initially, the focus of studies remained on the immune receptors and transcriptional regulators involved in T-cell quiescence and activation, but recent findings highlight cell metabolism as a crucial regulator of these processes [9–12]. Receptor-induced signaling and metabolic networks in naïve T cells are mutually regulated by each other depending on the micro-environmental cues obtained by the cell that also influence quiescence exit. Here we will discuss the bidirectional communication of signaling and metabolic pathways that promotes proliferation, quiescence exit, and activation of naïve T cells and functioning of T cells upon activation. We will take into account the different signaling and metabolic events and their cross-talks that lead to differentiation of naïve T cells into T_{H1} , T_{H2} , T_{H17} , Treg, or Tfh effector cells. Understanding the cross-talks between T-cell signaling and metabolism under different environmental cues will be vital for understanding the differentiation patterns of naïve T cells during different pathogenic conditions. This will provide better prospects of developing novel approaches to modulate protective and pathological T-cell responses in human diseases.

6.2 Signaling and Metabolic Pathways Involved in Activation of Naïve T Cell

The activation of T_H cell is mediated by a complex chain of signaling events that involve the activation of distinct co-stimulators and co-inhibitors present on the surface of the lymphocyte. The interaction between the antigen-bound major histocompatibility complex (MHC) on the antigen-presenting cells (APCs) and the T-cell receptor (TCR) on T_H cells triggers the TCR-mediated signaling pathway. The phosphorylation of the LAT signalosome by LCK sends signal to three major cell-signaling pathways, viz. NF κ B, MAPK, and the calcium-mediated NFAT pathways [13]. Along with the TCR, the T cell also expresses several other co-receptor molecules that can be classified into two major functional groups. The first group consists of co-signaling receptors that have an immunoglobulin (Ig)-like fold in their ectodomains, such as CTLA-4, CD28, PD1, and BTLA [14]. The other co-signaling group belongs to the tumor necrosis factor receptor (TNFR) superfamily and includes DR3, OX40, 41BB, CD27, CD30, and HVEM [14]. Together with the TCR activation, a second signal from the co-stimulatory signal emanating from B7-CD28 interaction is also necessary for the T-cell activation. This is called the “two signal hypothesis” [13]. The B7 molecule present on the APC also binds with the CTLA-4 receptor of the T cell after the clearance of the antigen. This induces T-cell anergy after the antigen is cleared from the system and the T-cell activation is no longer required. The other co-receptor signaling pathway influences the type of cytokine expressed and regulates the T-cell differentiation pattern. Experimental studies have shown CD40-L, expressed on the surface of activated T cells, induces the APC to produce IL-12, thereby stimulating the T_H cells to differentiate into the T_{H1} cells [15, 16]. On the other hand, the TRAF2-mediated OX40 signaling pathway contributes to long-term survival of T_H cells [17]. OX40 has been implicated in the development of memory T cells, clonal expansion, and differentiation. It also mediates suppression of the Treg cells [17, 18]. The negative regulators of T-cell activation are required to maintain homeostasis and deactivate the T cells after the antigen is cleared out. This is mediated by the PD1-PDL axis that provides co-inhibitory signal to the T-cell activation. The T cell also expresses CD45, a phosphatase, that de-phosphorylates the carboxyl-terminal tyrosine of p56lck and p59fyn that aids T-cell activation [19]. Apart from these, the T cells express several other co-receptors that serve to regulate the cytokine expression and differentiation of the cell [20].

The calcium pathway also plays a major role in the proliferation of the T_H cell activation [21]. The influx of Ca^{2+} ions from the CRAC channels leads to the activation of the NFAT (Nuclear Factor of Activated T cell) transcription factor that acts as the master regulator of T-cell activation and T-cell anergy [22]. The activation of the calcium pathway in the T cell is initiated by the binding of the TCR with an antigenic peptide presented on MHC complexes of the APC that induces activation of PLC- γ that cleaves PIP2 into IP3 and DAG. This IP3 now activates the IP3-receptors located on the endoplasmic reticulum membranes inside the T cell, which causes the release

of intracellular stores of calcium, leading to a transient elevation in cytoplasmic calcium level. This activates the CRAC channels on the T-cell membrane that allows an inward flux of calcium from the extracellular environment. This triggers the calcium-mediated calmodulin-calcineurin pathway, which leads to the de-phosphorylation and nuclear translocation of NFAT proteins where it can cooperate with AP-1 complexes induced by co-stimulatory pathways. The NFAT/AP-1 complexes bind to the sites in the promoters of many cytokine genes to activate their transcription to mediate sustained T-cell activation and survival. In the absence of co-stimulation or in the presence of anergizing stimuli, sustained increases in intracellular calcium concentration activate NFAT proteins. However, in the absence of concomitant AP-1 activation, due to lack of co-stimulatory signals, NFAT proteins dimerize and translocate into the nucleus, inducing the expression of anergy-inducing genes that include E3-ubiquitin ligases, such as Itch, Grail, and Cbl-b that is known to ubiquitinate and inactivate the TCR signalosome and the co-stimulatory CD40-ligand, thereby destabilizing the immunological synapse in the anergic T cell. On the other hand, the calcium/NFAT-dependent activation of the Ikaros transcription factor in anergic T cells leads to the epigenetic changes in the IL-2 promoter by the recruitment of HDACs and other chromatin-modifying complexes, which results in stable silencing of the IL-2 gene expression [22].

Metabolic regulation of T cell is another aspect that determines activation and differentiation of naïve T cells and their functioning upon activation. Naïve T cells utilize glucose and glutamine metabolism for activation, and activation signals increase glucose and glutamine uptake by T cells through GLUT1 and ASCT2, respectively [23, 24]. Thus, both signaling and metabolism cooperate in a bidirectional manner to influence T-cell activation and differentiation. On encountering pathogenic antigens, a cascade of TCR signals and co-stimulatory signals are initiated, which leads to quiescence exit in naïve T cells. The first signal that initiates quiescence exit is the transduction of TCR signaling via PI3K/AKT/mTOR pathway, which induces glycolysis in the naïve T cells [25]. This initiation is marked by a trigger in the metabolism of T cells that suffices the increasing lipid, nucleotide, and amino acid requirement of differentiating cells. During quiescence exit, T cells produce lactate to sustain glycolysis. Lactate is also imported into cells through the monocarboxylate transporters and converted into pyruvate by lactate dehydrogenase A (LDHA). This reaction limits glycolytic programming and proliferation in T cells, potentially owing to the attenuated generation of glycolytic intermediates such as PEP that sustain glycolysis and biosynthesis reactions [26].

Glutamine metabolism regulates T-cell activation in different ways. It has an important role in determining differentiation to T_{H1} and T_{H17} cells. T_{H17} cells utilize both glucose and glutamine to fuel the TCA cycle and OXPHOS, which otherwise is optional for other T effector cells [27]. It regulates leucine uptake via regulation of LAT1-CD98 and together with leucine activates mTORC1 signaling [28]. Other amino acid metabolisms like tryptophan and arginine metabolism and their intermediate metabolites such as kynurenine and ornithine differentially regulate T-cell survival, apoptosis, and proliferation [29–31].

Glucose and glutamine metabolism also induce lipid metabolism via mTORC1-dependent regulation of AMPK [32]. These pathways are metabolically connected to the TCA cycle and OXPHOS, which also affect the redox and oxygen-sensing signals in T cells. The conversion of pyruvate to lactate via NAD⁺-NADH-dependent LDH reaction regulates redox signals, and impaired oxygen-sensing machinery of OXPHOS results in the formation of ROS, which induces ROS-dependent signaling that promotes IL-2 productions and induces T-cell proliferation by activating NFAT transcription factor [33].

6.3 T_H-Cell Differentiation and Diversity

The T_H cells display high plasticity that helps them to differentiate into specialized T_H cells according to the type of the antigenic challenge and the micro-environmental conditions (Fig. 6.1). The early events of the T-cell activation play a major role in the determination of the pattern of differentiation of the naïve T cell. The micro-environmental cues, in the form of cytokines, activate the signaling pathways of the T_H cells that eventually lead to the changes at the gene-regulatory levels [34]. The selective activation of specific transcription factors mediates the differentiation of the naïve cells into specialized CD4⁺ T_H effector cells, viz. T_{H1}, T_{H2}, T_{H17}, etc. (Table 6.1) [35]. Additionally, another type of CD4⁺ T_H cell called the regulatory T cells (iTreg) has a role in maintaining the T_H cell homeostasis.

The mechanism of T-cell differentiation is governed initially by the strength of the stimulus that the TCR receives from the APC. The strength of stimulus results in differential regulation of phosphatidylinositols that triggers different signaling

Fig. 6.1 Schematic diagram of signature signaling factors, cytokines, metabolites, and metabolic paths, which dictate T_H cell differentiation, proliferation, and effector function

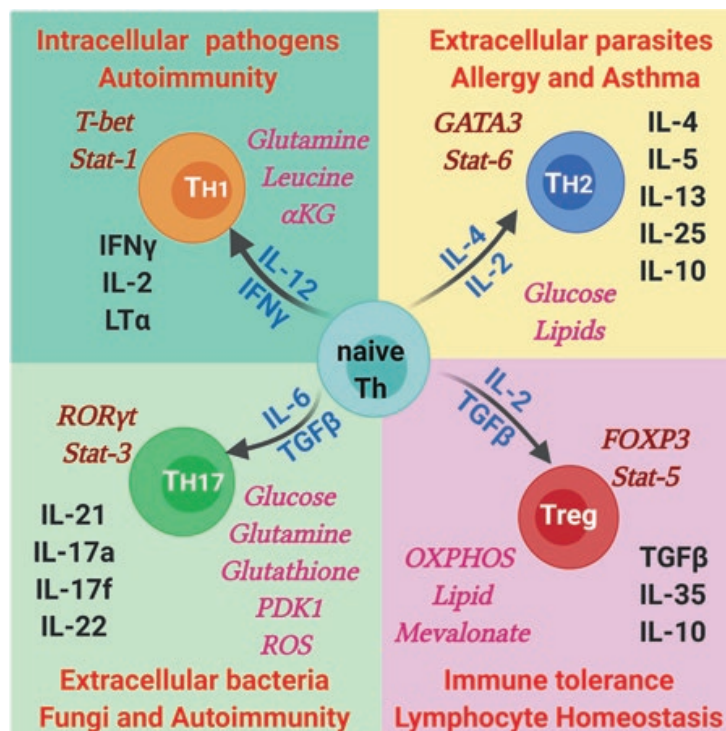


Table 6.1 Summary of T_H cell diversity, factors regulating T-cell plasticity and effector functions of each subtype

CD4 ⁺ subset	Polarizing cytokines	Transcription factors	Inhibitory transcription factors	Metabolic signature	Effector functions
T _{H1}	IL12, IFN γ	T bet, STAT1, STAT4, Runx 3, Eomes, Hlx	GATA3	Upregulated glycolysis, glutamine metabolism, leucine uptake, α KG production	Cell-mediated immunity against intracellular pathogens and phagocyte-dependent protective responses
T _{H2}	IL4, IL2	GATA3, STAT6, STAT5, STAT3, Gfi-1, c-Maf, IRF4	T-bet, Runx3	Downregulated glycolysis, upregulated lipid metabolism	Immune response against extracellular parasites, bacteria, allergens, and toxins. Help in activation and maintenance of humoral immune response and tissue repair
T _{H17}	IL6, IL 21, IL 23, TGF- β	ROR γ t, STAT3, ROR α , Runx1, Batf, IRF4, AHR	T-bet ⁺ Runx1, Smad3Runx1 ⁺ FOXP3	Uptake of both glucose and glutamine, glutathione production, upregulated PDK1 and ROS	Immune response against bacterial and fungal infection
T _H	IL6, IL21	Bcl6, STAT3	Not known	Not known	Help B cells produce antibody
iT _{Reg}	TGF- β , IL2	FOXP3, Smad2, Smad3, STAT5, NFAT	Not known	Inhibited glycolysis, upregulated OXPPOS, lipid and mevalonate metabolism	Suppression of immune response
T _{H9}	TGF- β , IL4	IRF4	Not known	Not known	Promotes mast cell and T-cell growth, stimulates mucous secretion to enhance innate immunity. Plays a role in allergic responses
Tr1	IL27, IL10	c-Maf, AhR	Not known	Not known	Suppression of T effector cells

pathways downstream. It has been observed that while a weak TCR signal generates a high level of PIP2 and lower levels of PIP3, which is required for the activation of the focal adhesion kinase and phosphorylation of AKT_{Thr308}, stronger signal favors the activation of mTORC2, and as a result, elevated level of PIP3 and reduced PIP2 are generated [36]. In vitro experiments have revealed that a stimulus of a lower strength induces the expression of the GATA-3 transcription factor, the master regulator of T_{H2} cells. Simultaneously, the expression of the IL-2 cytokine activates STAT5 that synergizes with GATA-3 to transcribe the IL-4 gene that eventually leads to the differentiation of the naïve cell into the T_{H2} subtype [37]. Recent advances in the field also divulged that during viral infection low TCR signals may also favor the formation of Tfh and memory T cells. On the other hand, a stronger stimulus favors the activation of the T-bet transcription factor that helps in the differentiation into the T_{H1} subtype and triggers the production of IFN- γ and IL12 cytokines. The differentiation of naïve CD4⁺ T cells into T_{H17} cells is induced by TGF- β /IL-6 in combination with TCR stimulation. This triggers the production of IL-23R, which induces the transcription factor ROR γ t, IL-17, and IL-21. The STAT-3 protein plays an important role in the production of the T_{H17} effector molecules and requires the activation of the ICOS co-stimulatory pathway. However, under the T_{H17}-inducing conditions, the presence of IL2/STAT5 induces the expression of the Foxp3 transcription factor that leads to the differentiation of the naïve cells into iTreg cells. The strength of TCR stimulus also plays a role in the T_{H17}/iTreg determination process, where it has been observed that a weak stimulus favors the differentiation into iTreg cells that is known to have a role in immune-suppression [37].

The effect of signaling in T_H cell differentiation is further augmented by the action of metabolism within these cells. On activation by the upstream TCR and co-stimulatory signals, metabolic pathways trigger the process of T-cell activation with the initiation of glycolysis in most of the cases [38]. The utilization of glucose is maintained nominal in naïve T cells, just to suffice ATP requirement enough to maintain survival during quiescence [39]. However, with the transduction of TCR signals via mTORC1/2 signaling, the rate of glucose utilization increases, leading to quiescence exit and activation of T_H cells [8, 38]. Upon activation, differentiation patterns are regulated by differential expression of metabolic pathways. For example, glutamine metabolism along with leucine induces proliferation and differentiation of T_{H1} and T_{H17} cells [27, 28]. In addition, α KG promotes initial programming in T_{H1} cells [40]. Further, glutaminolysis results in the formation of glutathione, which is required for T_{H17} differentiation [41]. An increase in glucose metabolism induces lipid metabolism to promote T_{H2} differentiation [42]. Inhibition of glycolysis and promotion of OXPHOS along with upregulated lipid and mevalonate metabolism induce Treg proliferation and differentiation [43, 44]. Intermediate metabolites of metabolic pathways, in return, regulate signaling processes as well. For example, tryptophan intermediate, kynurenine, and arginine intermediate ornithine regulate signaling processes in T cells, which have been discussed in the next section.

Each of the T_H sub-type has a specific effector function to perform [34, 35, 37, 45]. A balance between all the T_H cell subtypes is necessary for the proper functioning of the immune system. The effector molecules, in the form of interleukins,

interferons, tumor necrosis factor, etc., produced by these diverse groups of immune cells, maintain the integrity of the immune-regulatory network (Table 6.1). However, during any disease condition, this defense mechanism gets subdued. Changes in the micro-environmental conditions lead to alterations in the biochemical reaction network that disrupts the balance between the effector cell populations that favors the progression of the disease. This immune-suppression is observed very frequently in the cases of chronic infections (e.g., chronic *Leishmania* infection) and cancer.

6.4 Signaling and Metabolic Cross-Talk Mediated by mTOR Regulate Differentiation

Activation of naïve T cells is initiated with the tonic signals generated by T-cell receptor (TCR) on their interactions with self-peptides on MHC molecules. There is an intricate design of the signaling and metabolic interactions of these cells, which allow them to proliferate and produce effector molecules (Fig. 6.2). Sensitivity toward TCR signaling in the naïve T cells is partially mediated by the mechanistic target of Rapamycin complex (mTORC1 and mTORC2) [46]. Peripheral naïve T cells circulate in the blood and survey antigens. They maintain a low metabolic rate and import a small amount of glucose to fuel the TCA cycle and OXPHOS for ATP production [39]. Naive T-cell homeostasis is disrupted by the activation of mTOR signaling [47]. The activation of mTORC1 signaling enhances glycolytic metabolism in these cells, inducing entry to cell cycle and cell growth. The naïve T cells, which otherwise remain in a quiescence state, are activated by the enhanced glycolytic pathway. Different regulators of mTORC affect the process of naïve T-cell activation [46].

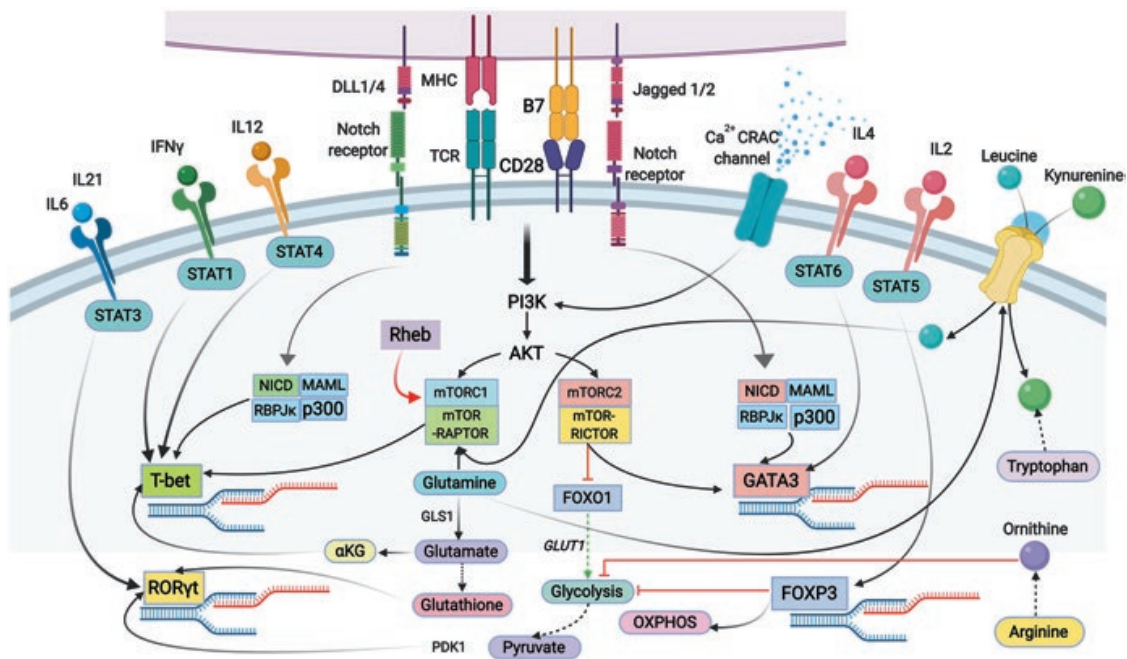


Fig. 6.2 Cross-talks of signaling and metabolic pathways regulating the activation of the T-bet, GATA3, ROR γ t, and FOXP3 transcription factors that mediate T-cell differentiation

mTOR signaling is regulated by a set of upstream signaling, which determines the formation of mTORC1 and mTORC2 and subsequent signaling. The signal induces upon activation of TCR and subsequently the PI3K/Akt pathway [48]. Raptor and rictor are the main components of mTORC1 and mTORC2 complexes, respectively. mTORC1 signaling is required for differentiation into T_{H1} and T_{H17} effector cells, and an inhibition of mTORC1 has been observed to induce T_{H2} differentiation and prevent T_{H1} and T_{H17} differentiation [25]. However, these observations differ according to the upstream signal received by the complex. Loss of tuberous sclerosis complex 1 (TSC1) results in mTORC1 activation [47]. The metabolic activity of naive T cells can also be enhanced by the exposure to IL-2 released by activated CD4⁺ effector cells [49]. Inhibition of mTORC1 by the TSC (Tuberous Sclerosis Complex) via Rheb inhibition leads to failure in differentiation into T_{H1} and T_{H17} effector cells [47].

mTORC1 is a master kinase that helps naive T cells to exit quiescence. TCR signaling along with costimulatory and IL-2 signals promote the activation of mTORC1 during quiescence exit. The magnitude and duration of mTORC1 activity likely determine quiescence exit. TCR signals must meet a certain threshold of activation to induce T-cell proliferation. This threshold is determined by the level of mTORC1 activation and expression of IRF4 and c-Myc [50, 51] that regulate anabolic and mitochondrial metabolism. mTORC1 also regulates sterol regulatory element-binding proteins (SREBPs) that has a role in metabolic reprogramming in naive T cells. Metabolism in turn regulates the activity of mTORC1. Leucine and glutamine coordinate with TCR and CD28 signaling to activate mTORC1 and sustain metabolic flux during quiescence exit [27, 28]. T-cell activation demands for the biosynthesis of lipids, cholesterol, nucleotides and amino acids in order to maintain the increase in metabolic rates of the activated cells. These increased demands are facilitated by the upregulation of hexokinase 2 (HK2), which is the rate-limiting enzyme for glycolysis [52, 53]. This induces increased utilization of glucose, which can also activate mTORC1 and inhibit the activation of AMP-activated protein kinase (AMPK) [32, 54]. AMPK induces lipid and cholesterol biosynthesis through the mTORC1-dependent upregulation of SREBP1 and SREBP2 [55]. mTORC1 forms a bridge between signaling and metabolic responses in T cells that senses metabolic cues and mediates signaling regulation over metabolic pathways and vice-versa. Thus, mTORC1-dependent responses are crucial in determining proliferation, activation, and functioning of T cells.

TCR signaling targets the transcription factor, c-Myc, in an mTORC1-dependent manner. It regulates the transcription of metabolic genes critical for T-cell activation. c-Myc induces the transcription factor AP4, which maintains the glycolytic transcriptional program initiated by c-Myc to support T-cell population expansion [50]. However, c-Myc expression is not continually sustained after T-cell activation [56].

Metabolites also influence T cells in an mTORC1-independent manner. For example, post-translational protein modifications by glycolytic, lipid, or mevalonate by-products allow receptors, enzymes, and scaffolding proteins to properly posit at their sites of activity [57, 58]. In T cells, extracellular ATP, glucose, and glutamine modulate AMPK activity to promote T-cell responses against bacteria and viruses

[54]. The glucose metabolite PEP regulates the activation of Ca^{2+} -calcineurin–NFAT signaling [59]. TCR signaling can be altered by cholesterol esters and cholesterol sulfate, which alter TCR clustering or affinity for antigens [60]. Also, N-glycans derived from the hexosamine pathway suppress TCR signaling [61].

mTORC2 also contributes to quiescence exit by enhancing glycolytic pathway. AKT/mTORC2 represses forkhead box protein O1 (FOXO1) function [62], which induces glucose transporter 1 (GLUT1) expression and enhances glycolytic flux [63]. Expression of glucose transporters contribute in determining naïve T-cell survival. IL-7–IL-7R signaling prevents degeneration of quiescent T cells by increasing glucose and amino acid catabolism [64]. Rate or quantity of glucose uptake via the GLUT1 receptor may have a role in determining quiescence versus quiescence exit as its expression is lower on naive T cells than on activated T cells. During quiescence exit, cell growth and clonal proliferation are favored by glucose metabolism upon survival [51].

Duration and strength of TCR signaling mediate both quiescence and activation of T cells. However, based on the type of initiation of these signaling cascades, i.e., tonic or antigen-driven, TCR signals differ in both duration and strength. In antigen-activated T cells, CD28-mediated co-stimulation of TCR signaling induces GLUT1 expression to increase glucose uptake [65]. Expression of the glutamine transporter ASCT2 and of sodium-coupled neutral amino acid transporters (SNATs) increases on TCR and CD28 co-stimulation [23]. Upregulation of SNATs on T-cell activation suggests that they also modulate the rate or quantity of glutamine uptake.

Glutamine metabolism plays a crucial role in determining differentiation to $T_{\text{H}1}$ and $T_{\text{H}17}$ cells. Glutamine affects LAT1–CD98 activity, which promotes leucine uptake to induce the proliferation and differentiation of $T_{\text{H}1}$ cells, $T_{\text{H}17}$ cells, and effector $\text{CD}8^+$ T cells [23, 66]. Glutamine along with leucine activates mTORC1 and sustains metabolic flux during quiescence exit [28]. Further, utilization of glutamine to generate glutathione via glutaminolysis is essential for T-cell proliferation and differentiation into $T_{\text{H}17}$ cells [27]. Glutaminolysis also generates α -ketoglutarate (α -KG), which promotes initial programming of $T_{\text{H}1}$ cells. Glutaminolysis also affects IL-2 signaling, as it has been observed to suppress IL-2-induced mTORC1 activation during type 1 inflammation [27]. However, impaired glutaminolysis may promote abnormal leucine uptake to increase mTORC1 activation under such inflammatory conditions [23, 66]. Thus, glutamine and glutaminolysis have different roles during quiescence exit and upon T-cell activation.

During impaired glutaminolysis, the oxidation of pyruvate acts as a crucial checkpoint. The mitochondrial pyruvate carrier (MPC) transports pyruvate into the mitochondria to fuel the TCA cycle and OXPHOS and depletes it from the cytoplasm. The inhibition of MPC favors glycolysis over OXPHOS, particularly when glutaminolysis is also impaired. Downregulation of OXPHOS in T cells require inhibition of both MPC and glutaminase 1 (GLS 1) [67]. $T_{\text{H}17}$ cells suffice their nutrient requirement using both glucose and glutamine, which otherwise is optional for other activated T cells. The plausible explanation for this phenomenon is the high-level expression of pyruvate dehydrogenase kinase 1 (PDK1) in $T_{\text{H}17}$ cells, which prevents conversion of pyruvate to acetyl-CoA in mitochondria [53].

High expression of PDK1 diverts the pyruvate flux away from TCA in T_{H17} cells, and hence, the cell depends on glutamine to fuel the TCA cycle. The regulation of PDK1 is not well understood in T_{H17} cells; however, studies suggest that hypoxia-inducible factor 1 α (HIF1 α) might induce PDK1, promoting T_{H17} cell responses [53]. Also, lactate dehydrogenase A (LDHA), which catalyzes lactate formation from pyruvate, sustains glycolytic metabolism and promotes interferon- γ (IFN γ) expression in activated T cells [68].

Upon activation, amino acids play an important role in the functioning of activated T cells. Certain amino acids promote quiescence exit and proliferation of naïve T cells, whereas others might suppress proliferation and promote quiescence-like programs in naïve T cells. Majority of the biomass of activated T cells is made by amino acids. Uptake of essential amino acids such as leucine or conditionally essential amino acids such as glutamine are taken up by amino acid transporters, such as LAT1-CD98 or ASCT2 [23], but non-essential amino acids accumulate in T cells due to influx or de novo biosynthesis from glucose or glutamine. Accumulation of amino acid intermediates impact the functioning of activated T cells. Accumulation of kynurenine, an intermediate of tryptophan metabolism, suppresses T-cell proliferation [30]. Kynurenine accumulation might also result from its uptake through the LAT1-CD98 transporters [69]. Ornithine, an arginine intermediate, reduced glucose consumption via glycolysis. However, arginine supplementation increases serine biosynthesis and OXPHOS [31], which increases T-cell survival and promotes secondary effector responses.

Balanced redox reactions are one of the prerequisites for T-cell activation [70]. The NAD⁺-NADH-dependent conversion of pyruvate to lactate is a major redox balancer of T cells. An accumulation of NAD⁺ increases lysosome biogenesis, which can suppress T-cell activation. Mitochondrial reduction of NAD⁺ levels is utilized to promote aspartate synthesis, which is necessary for T-cell proliferation [70]. Both NAD⁺ and ATP cooperatively influence T-cell responses. Extracellular ATP augments quiescence exit and T-cell proliferation via the expression of purinergic receptor P2XY, which induces IL-2 production [71]. Conversely extracellular NAD⁺ promotes T-cell death by increasing the ART2-dependent activation of P2XY [72].

Oxygen sensing by T cells also regulates their effector functioning [73]. OXPHOS, which requires oxygen, is essential for both T-cell quiescence and activation [70, 74]. OXPHOS generates ROS, which stimulates IL-2 production and promotes T-cell proliferation by activating nuclear factor of activated T-cell (NFAT) transcription factors [75]. Under pathological conditions, increased levels of mitochondria-derived ROS can have antagonizing T-cell responses, including T_{H17} cell differentiation [27, 53].

FOXP3 is an important determinant of Treg differentiation and the Treg cell responses and regulated via the metabolic regulation exerted by FOXP3 [76]. It promotes OXPHOS and inhibits glycolysis in Treg cells. Survival and function of these cells are reduced by excessive PI3K or mTOR activity as it decreases FOXP3 expression and increases glycolytic metabolism [77]. Treg cells, upon activation, upregulate mTOR signaling, which induces lipid synthesis, mevalonate metabolism, and mitochondrial function [78, 79]. These pathways influence activation programs to regulate Treg cell function.

Mitochondria-derived metabolites like acetyl-Coa, succinate, α KG, and 2-hydroxyglutarate (2-HG) alter epigenetic programs. Acetyl-CoA induces histone acetylation, which is permissive for transcription. α -KG promotes the activity of demethylases that target DNA or histones, whereas 2-HG antagonizes demethylases [80]. Demethylation in turn allows changes in gene transcription associated with specific T-cell effector programs. 2-HG accumulation downstream of the von Hippel–Lindau disease tumor suppressor (VHL)–HIF1 α axis in T cells induces changes in DNA and histone methylation that increase CD8⁺ T-cell proliferation [80].

Thus, we observe metabolic regulation of T-cell activation and functioning at different levels. Mitochondria-derived metabolites affect the functioning and/or expression of various transcription factors through methylation-demythylation, acetylation processes or by mitochondria-derived ROS regulations. The effects of glucose metabolism in mTOR and c-Myc regulation have been implicated. Metabolites also regulate transcription factor activity. For example, transcriptional regulators BAZ1B, PSIP1 are activated by arginine and lipids or sterols regulate the activities of LXRs, PPARs, and SREBPs [81–83]. Further, metabolic processes also regulate processes at post-transcriptional and translational levels. For example, amino acid deprivation is sensed by GCN2 (or EIF2AK4) and leads to inhibition of protein translation by the EIF2 α pathway, which supposedly leads to suppression of T-cell proliferation [84]. Also, GAPDH produced by the glycolytic pathway has been observed to suppress protein translational processes [85]. Metabolites also affect the activity of activated T cells by the regulation of transporter proteins and complexes. Amino acids like leucine, glutamine, tryptophan, and arginine and the intermediate metabolites generated during the biogenesis or catabolism of these amino acids like kynurenine, ornithine, etc., affect the functioning of T cells upon activation via the regulation of transporter proteins like LAT1-CD98 or ASCT2. To summarize, metabolism can influence the processes of T-cell differentiation, activation, and functioning by regulating molecular processes at different levels starting from gene and transcription regulation.

6.5 Methodologies to Unwind the Regulations of the Immune Response

A comprehensive understanding of the complex regulations underlying the immune responses under different environmental conditions, antigenic challenges, strength of stimulus, and metabolic demands have challenged the implementation of successful immunotherapy. A need to unveil these regulatory mechanisms has driven experimental researchers as well as computational biologists to implement different omic studies and model the immunome under different antigenic stimulus. In the following section, we have taken up examples of the studies of T-cell responses and differentiation during infectious diseases (e.g., Leishmaniasis) and cancer that will give a clear insight of how the immune responses are altered under specific antigenic challenges.

6.5.1 Immunomics and Enrichment Analysis

Transcriptomic analysis, e.g., microarray, RNAseq, have opened up new avenues of research that allows the analysis of gene expression profile of several patient cohorts under various disease conditions. While microarray involves detection and quantification of gene expression based on the pairing of an mRNA transcript with its probe on a chip, RNA-Seq involves direct sequencing of gene transcripts by high-throughput sequencing technologies. This enables the RNAseq technique to detect novel transcripts as it does not require transcript specific probes as well as confers higher specificity and sensitivity for the detection of a wider range of differentially expressed genes, allowing detection of genes even with low expression. Following the identification of differentially expressed genes, gene ontology (GO) and pathway enrichment tools enable the identification of the biological processes (BP), molecular functions (MF), cellular component (CC), and biochemical pathways that are significantly enriched or over-represented in a given scenario. Various online tools and web-servers such as DAVID, GeneCodis, Gene Set Enrichment Analysis, and Reactome are available freely for performing enrichment analysis [86–90].

Researchers have exploited these techniques to unearth the immunome landscape in the microenvironment where the spatio-temporal dynamics of 28 different immune cell-types (immunome) have been studied using 105 human colorectal cancer patient data. Here the immunome was made up of mRNA transcripts specific for most innate and adaptive immune cell subpopulations. Using an integrative analysis, it has been elucidated that the densities of T follicular helper (Tfh) cells and innate cells increased, whereas most other T-cell densities decreased along with tumor progression. However, the Tfh and B cell numbers are inversely correlated with the disease progression and recurrence, and CXCL13 and IL21 genes are essential for the Tfh/B cell axis that is correlated with higher chances of survival of the patient [91, 92].

RNAseq analyses in the case of Leishmaniasis have been performed, that has revealed *Leishmania* species-specific differences in the expression of mammalian macrophage genes due to infection [93]. Such analyses have helped in the understanding of the changes in immune response generated during infection by unveiling the notable changes induced in the cytokine expression profiles during the *Leishmania* invasion. Experiments using microarray techniques have been used to assess the host cell genes and pathways in human dendritic cells associated with early *Leishmania major* infection. The study revealed 728 genes were significantly differentially expressed in the infected cells, and molecular signaling pathway revealed that the type I IFN pathway was significantly enriched. Here it was elucidated that *L. major* induces expression of IRF2, IRF7, and IFIT5, which indicates that the regulation of type I IFN-associated signaling pathways is responsible for the production of IL-12. However, this is not observed in the case of *L. donovani* [94].

6.5.2 Computational Methods for the Study of Immune Responses

The understanding of intra-cellular and inter-cellular signaling pathways involved in the generation of immune responses requires the study of a complex network of biochemical pathways under different disease-affected micro-environmental conditions. This is an extremely challenging task that can rarely be achieved using in vitro or in vivo experimental techniques. In order to gain insight into the immune-regulatory modules involved in T-cell functioning as well as study the immune-modulatory mechanisms employed by pathogen and the tumor cells, computational tools and mathematical modeling approaches have been extremely useful in obtaining a systems-level understanding. These have also helped the researchers and medical practitioners in the prediction of immunotherapeutic strategies and design of treatment protocols. Here we will throw light onto some of the most popular tools and techniques used for such studies and also explore a few of the mathematical models that have helped us unravel some of the intriguing problems in immunology.

6.5.2.1 Signaling and Metabolic Pathway Databases

The signaling pathway databases are important sources of information that collate pathway data from experimental studies regarding the intracellular signaling pathways in different immune cells [95, 96]. The KEGG provides information regarding the core TCR-mediated pathway along with a few co-receptor signaling pathways. The database also contains the pathways responsible for the T_{H1} , T_{H2} , and T_{H17} differentiation. Another popular database called Reactome provides detailed biochemical reactions involved in each step of the protein–protein interactions involved in the T-cell signaling pathway. It also enlists the pathway information related to CD28 and PD-1 co-signaling pathways. Simultaneously, Reactome forms a very important source for cytokine signaling pathways that includes different interleukin families, interferons, tumor necrosis factor, and a few growth hormones. A list of few of the available databases and the available information in each has been listed down in Table 6.2. However, the information regarding the intercellular cross-talks in the immune system is lacking in most of these databases that can be extracted through a thorough literature survey.

Few databases also provide data regarding the changes in the pathway during disease condition. The KEGG database has a sufficient amount of pathway information regarding the endocytosis of the *Leishmania* pathogen as well as the signaling events that occurs inside the infected macrophage. BioLegend database contains the cancer immune-editing network that consists of the intercellular signaling cross-talks governing the immune responses generated during cancer.

For the analysis of these biochemical pathways, the BIOPYDB database also provides an integrated platform for performing network analysis, logical steady-state analysis, knock-out analysis, etc. It contains detailed information regarding each protein involved in the immunological pathways as well as links them to the specific diseases associated with them. Apart from the TCR co-receptor-mediated

Table 6.2 List of a few signaling and metabolic pathway databases containing T-cell-specific pathway data and related cytokine pathways

Database	T-cell activation/ differentiation pathways/network	Cytokine pathways	URL of database
Kyoto Encyclopedia of Genes and Genomes (KEGG)	T-cell receptor signaling pathway, T _{H1} and T _{H2} cell differentiation, T _{H17} cell differentiation	IL-17, TNF, calcium signaling pathway	http://www.genome.jp/kegg/
Reactome	TCR-mediated pathway, CD28 co-signaling pathway	IFN- α/β , IFN- γ , TNF- α , IL-1, IL-2, IL-3, IL-5, GM-CSF, IL-4, IL-13, IL-6, IL-7, IL-10, IL-12, IL-17, IL-20 family cytokines	https://reactome.org/
Wikipathways	TCR-mediated pathway, B7-CD28, B7-CTLA4, PDL- PD1 pathways	IL-2, IL4, IL-5, IL-7, IL-9, IL-11, Type-1 IFN, TNF- α pathways	http://www.wikipathways.org
NCI – Pathway Interaction Database (PID)	TCR signaling network in naïve CD4 cells, B7-CD28 signaling networks	IL-1, IL-2, IL-3, IL-4, IL-5, IL-6, IL-8, IL-12, IL-23, IL-27, TNF signaling networks	http://www.ndexbio.org
BioLegend	T-fh, T _{H1} , T _{H2} , T _{H17} , Treg, $\gamma\delta$ -T-cell signaling pathways	IL-1, IL-2, IL-4, IL-6, IL-10, IFN, TNF pathways and inter-cellular cytokine signaling network of immune cells	https://www.biolegend.com/pathways/
BIOPYDB	TCR-mediated pathway, co-receptor-mediated T-cell activation pathway	IL-1 α , IL- β , IL2, IL-4, IL-6, IL-12, IL-18, IL-36 α , IL-36 β , IL-36 γ , TNF α , TNF β , IFN α , IFN β , IFN γ , TGF β	http://biopydb.ncl.res.in/biopydb/index.php
HumanCyc	T _{H1} , T _{H2} , T _{H17} , Treg-associated processes and pathways	Cytokine pathways are not available separately, but integrated with the other immune processes	https://biocyc.org/HUMAN/
Brenda	T _{H1} , T _{H2} -related processes	IL-1, IL-3, IL-5, IL-6, IL-8, IL-12, IL-17, IL-18, IL-21, IL-33, IFN- α , IFN- β , IFN- γ , TNF- α , TNF- β ligands	https://www.brenda-enzymes.org/

and cytokine pathways, BIOPYDB also contains detailed information about the toll-like receptor (TLR) pathways that has an important role in the regulation of immune response [97].

With the realization of the importance of immune-metabolism as a decisive factor in eliciting immune responses, metabolic databases have started to incorporate such details into the database structure. Although the advent is very recent and

only a limited number of databases have included this information. Two of the popularly used metabolic databases, HumanCyc [98] and Brenda [99], include information about immune-metabolites that are linked to immune responses. HumanCyc is the *Homo sapiens*-specific repertoire of the metabolic database BioCyc, which enlists metabolism specific to human. The database enlists a range of “Biological Process” and “Proteins” related to immune system. The biological processes are linked to their “Gene Ontology” term. A few of the important immune processes listed are “leukocyte-mediated cytotoxicity,” “adaptive immune response,” “immune effector process,” “regulation of immune response,” and “immune system development.” The GO IDs of these processes link them to pathways and processes to which are linked/cross-linked, which are enlisted as “Parent Classes” and metabolites/proteins which are involved in these processes are enlisted under “Instances”. These metabolites/proteins are linked to their detailed descriptions along with reactions in which they are involved and the reaction mechanism [98]. Brenda also provides details of immune-metabolites. The database has a wide range of entries as search option. Upon search of immune processes, it provides a variety of immune-metabolites and proteins whose “Enzyme Nomenclature,” “Enzyme-Ligand Interactions,” “Diseases,” “Functional Parameters,” “Organism-related Information,” “General Information,” “Enzyme Structure,” “Molecular Properties,” “Applications,” and “References” are provided.

6.5.2.2 Graph Theoretical Analysis

The Graph Theory was initiated with Euler’s famous publication from 1736 on the Seven Bridges of Königsberg problem [100]. However, it was applied to biochemical networks much later with the advent of the concepts of small-world and scale-free networks in 1999 that describes the global architecture of any complex real-world network such as the network of biochemical reactions in a cell [101, 102]. Computational biologists have modeled biochemical pathways as network where each protein or metabolite has been considered a node and the reaction between any two such species have been denoted as an edge, thereby translating the entire reaction network as an interconnected mesh of nodes and edges. Various network parameters such as Degree (k), Betweenness Centrality, Closeness Centrality, Eccentricity, Edge Betweenness, and Clustering Coefficient are used to describe the topological properties of the network. These parameters help in the identification of important hubs, i.e., a highly connected node, and shortest paths in the biochemical reaction network that may have significant contribution in the functioning of the signaling or metabolic pathways. Tools such as Cytoscape, Gephi, Pajek are freely available for performing network analysis of large reaction network [103–105]. Cytoscape further offers downloadable plugins for identifying important motifs, extracting sub-networks, and performing enrichment analysis and a host of other functions required for visualizing and analyzing large biochemical reaction networks. These biochemical networks mostly follow the small-world property of a network that indicates a relatively short distance from any one node to another and a relatively high level of clustering. This network property, termed as scale-free property of a network, denotes a connectivity distribution that fits a power law

depicted in Eq. 6.1 where the value of γ lies in the range $2 < \gamma < 3$ [106]. It has been observed that networks following the scale-free property are generally resistant to perturbations and thus are highly robust:

$$P(k) = \alpha k^{-\gamma} \quad (6.1)$$

Graph Theory has successfully been applied to signaling pathway networks where the concept of shortest path has been used to hypothesize potential signaling mechanisms in Neuro2A cells downstream of CB1R receptors. Here the cells were stimulated with a CB1R agonist for the assessment of activity of transcription factors. This experiment revealed CB1R activation modulates the activity of 23 transcription factors [107]. Such methods are useful in the identification of important novel signaling routes between a cell-surface receptor and downstream transcription. In a recent study, Graph theoretic network analysis has been used to identify protein pathways responsible for cell death after neurotropic viral infection by Chandipura Virus (CHPV) [108]. Another important application of network analysis is that it can be used to identify important hub proteins that can be used as potential drug or immunotherapeutic target [109, 110].

6.5.2.3 Logic-Based Models

Logical modeling is gradually being recognized as a simple yet powerful tool in systems biology for the study of large and complex reaction networks. Here the information flow from one node to another in a network is determined by a combination of input nodes and their relation is specified using logic gates – AND, OR, NOT. It was first explained by Kauffmann where he modeled the gene as a binary device that can be either in the ‘ON’ or ‘OFF’ states signifying whether a gene expression is upregulated or downregulated, respectively [111]. Here he elucidated that a distinct advantage in this choice of a binary model for gene activity lies in the fact that the number of different possible rules by which a finite number (K) of inputs may affect the output behavior of a binary element is finite, i.e., 2^{2K} . Figure 6.3a shows a simple toy model of three nodes interacting with one another. The reaction network can be represented using Boolean rules or equations (Eqs. 6.2, 6.3 and 6.4). The truth tables and the state transitions graphs of the reaction network show the temporal evolution of the states (0 or 1) of the nodes starting from different input combinations (Fig. 6.3a). Here, in this example we observe under the different input conditions the system tends to reach certain point steady-state attractors, i.e. 1–0–0 and 1–1–1 or cyclic attractor, i.e. 1–0–1 \leftrightarrow 1–1–0:

$$v1 = v1 \text{ OR } (\text{NOT } v3) \quad (6.2)$$

$$v2 = v1 \text{ AND } v3 \quad (6.3)$$

$$v3 = v2 \quad (6.4)$$

Several software packages such as BoolNet (R-based), BooleanNet (Python based), and CellNetAnalyzer (software with GUI) are available for performing logical steady-state analysis of large biochemical networks [112–114]. This concept

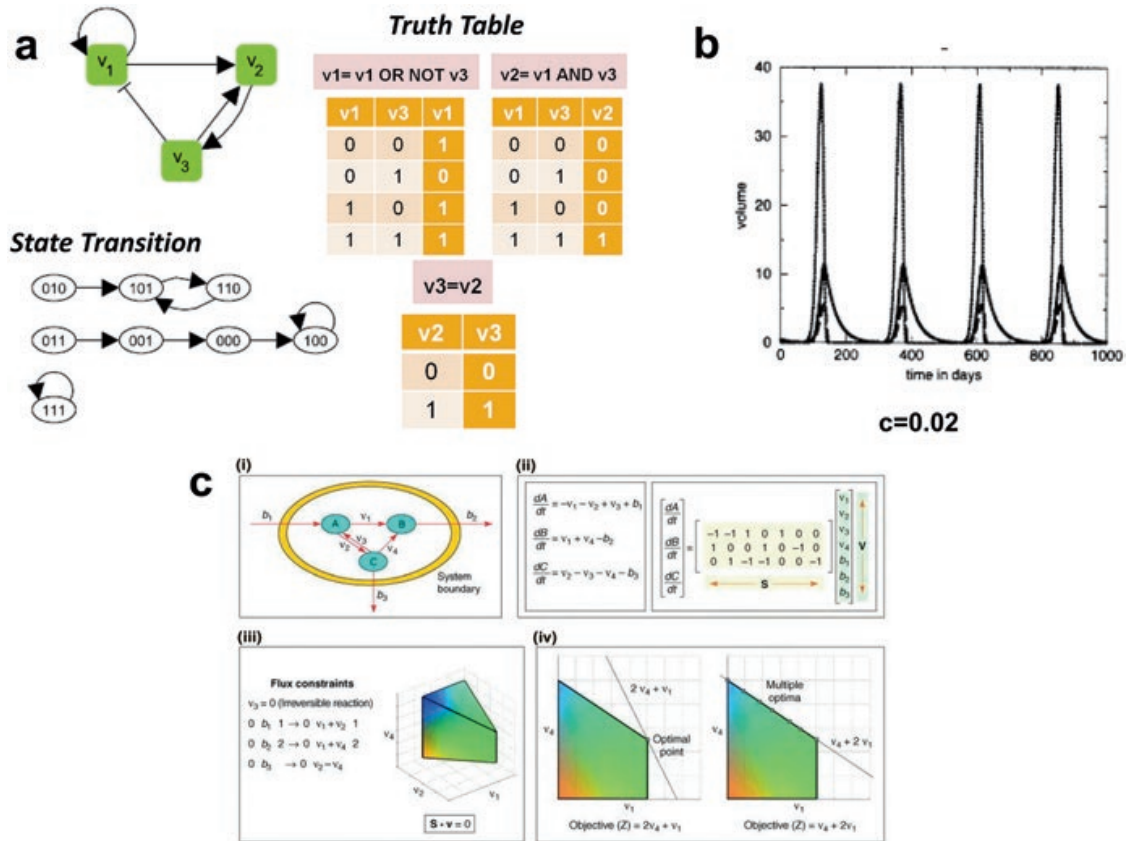


Fig. 6.3 Computational techniques used for study of large biochemical pathways. (a) Interaction Graph, Truth Table, and State Transition Graph for a Logic-Based Toy Model; (b) Temporal dynamics of Tumor, Effector cells, and IL-2 from an ODE-based model (adapted from Kirshner, et al. 1998 [150]); (c) A toy model describing (i) the flux distribution of metabolites A, B, and C through different reactions, (ii) the formation of stoichiometric matrix "S" and flux vector "v," (iii) defining constraints and (iv) defining objective and finding optimal solution within the solution space of linear optimization problem (Adapted from Kauffman et al. 2003 [157])

was later used by Huang and Ingber to model cell signaling networks for demonstrating that cellular phenotypes correspond to the dynamic steady states of the intracellular signaling molecules in a logic-based model. A key advantage of this strategy is that it does not require the knowledge of parameter values that is often not available for large biochemical networks. Later it has been extensively used for the study of cell signaling pathways and identification of drug targets for the treatment of cancer [109, 110]. Logical models have also been developed for the study of T-cell signaling pathways where the observations made from the *in silico* analysis were experimentally validated to establish the authenticity of their logic-based model. Using this model, the authors have predicted an alternative pathway of activation from CD28 to JNK that does not involve the canonical pathway involving LAT signalosome, nor does it involve the activation of PLC γ 1 or calcium flux, but depends on the activation of the nucleotide exchange factor Vav1, which activates MEKK1 via the small G-protein Rac1 [115]. A logical steady-state model that captures the effect of the co-receptor signaling pathway cross-talks has been developed that shows that simultaneous activation of the TCR:CD3, CRAC, and OX40

pathways are important for sustained T-cell proliferation. At the same time, it has been shown that the co-receptor CD27 and LTBR pathways are important for regulating the cytokine production [116]. A further extension of this work for the study of immune responses during Leishmaniasis explains how the differentiation of T cell is altered during infection [117]. Another model employing Boolean formalism has been used in the study of differentiation of naive cells into T_{H1} , T_{H2} , T_{H17} , and Treg subtypes under different environmental conditions [118]. This model provides evidences that $Foxp3^+$ Treg cells and T_{H17} cells are highly plastic and labile, whereas the T_{H1} and T_{H2} subtypes remain steady under different environmental conditions. However, this model also predicts the existence of hybrid states and cyclic attractors expressing markers characteristic of two or more canonical cell types under certain environmental conditions that lays the foundation for the oscillatory behavior of T-cell differentiation. This study further elucidates that under proper polarizing environments, the Treg cells may differentiate into T_{H1} or T_{H2} subtypes [118]. Later another model based on the Boolean formalism was developed to study the molecular mechanisms controlling the cytokine-driven T_H cell differentiation and plasticity. This model explained the role for peroxisome proliferator-activated receptor gamma ($PPAR\gamma$) in the regulation of T_{H17} to iTreg cell switching that gives promising cues for the prediction of therapeutic target for dysregulated immune responses and inflammation [119]. More recently, Probabilistic Boolean Control Network has also been employed for the study of T_H cell differentiation under varied environmental conditions. Here each input node is activated with a certain user-defined probability, which makes the system stochastic. Using this study, the authors have identified that the T-cell differentiation process is regulated by composition and dosage of signals that the cell receives from the environment. They have also predicted novel T-cell phenotypes using their model and have identified the specific environmental conditions that give rise to them [120].

6.5.2.4 Steady-State Metabolic Models

Immunometabolism has gained momentum in recent years as an emerging field of investigation at the interface between two highly discussed disciplines of immunology and metabolism [9, 10]. The idea of metabolism as a driver of the immune response [121] has been appreciated in recent years. However, capturing the bidirectional regulation of signaling and metabolism using a single computational platform is challenging. The mechanism of action of the two cascades is different, and the time scales in which the two processes occur also differ enormously. Mostly signaling cascades are faster than the metabolic reactions. This, along with the limitation of availability of information about how metabolism regulates immune cell responses and functioning, has limited the designing of immune-metabolic models to a small scale, mostly considering few parameters to design smaller dynamic models. An integrated systems-level computational model of immunometabolism is yet to be undertaken. Nevertheless, the currently employed computational approaches can be used to address immune-metabolism at a systems-level.

Genome-scale metabolic modeling (GSMM) is currently the most widely used systems-level modeling approach that accounts for whole-genome metabolism of

biological systems. It is a constraint-based mathematical modeling approach that assimilates biochemical, genetic, and genomic information within a single computational platform [122–126]. It allows the study of the metabolic genotype-phenotype relationship of an organism. Genome-scale metabolic models have been used in *in silico* metabolic engineering for the design of studies like defining essentiality of the reaction/gene [127, 128], the relevance of distant pathways [129] and overexpression or knockout analyses of metabolites, reactions, and metabolic pathways [130]. These are efficient tools for the prediction of growth in living cells/tissues exposed to different external conditions [131]. They have been used to predict conditional and absolute essentiality of metabolites and reactions in metabolic networks.

Flux balance analysis (FBA) is the most popularly used constraint-based approach in systems-level metabolic modeling, which works on the basic principles of linear optimization [132]. The technique assumes a steady-state approach, where all the metabolites of the network are considered to be in steady state; i.e., the rate of change of metabolites over time remains zero (Fig. 6.3c). This ensures that the rate of formation of a metabolite in the network is always equal to the rate of its consumption and hence a net difference in the metabolite concentration over time always remains zero. All reactions of the network work as constraints to the optimization problem. The reactions are bounded between a lower and an upper bound, which creates the constraint. The metabolites are connected to respective reactions in the form of a stoichiometric matrix, “ S ,” where the rows represent the metabolites (m) and the columns represent reactions (n). Thus, a “ $m \times n$ ” matrix is generated in which the involvement of a metabolite in a reaction is represented by its respective stoichiometry in that reaction. A positive stoichiometric value represents the formation of the metabolite and a negative stoichiometric value represents consumption. The flux through the reactions is represented in a separate flux matrix “ v ,” which is a “ $n \times 1$ ” matrix. The outcome of the optimization is obtained by matrix multiplication of “ $S \cdot v = 0$.” The matrix multiplication results in an optimized “ v ” matrix, which assigns an optimized flux to each of the reactions in the network. Generally, whole-genome models are large with a few hundreds of reactions and metabolites, which make it a multidimensional optimization problem. An objective is assigned to the model that depends on the biological question one wants to address. For example, if one wants to observe the behavior of the network when it tries to maximize ATP production, then one can assign ATP synthase (ATPS) reaction as the objective and try optimizing the model by maximizing the objective function. Thus, the model gets optimized a per the requirement of maximizing or minimizing the objective function.

A further extension of the modeling technique has been done to incorporate dynamic regulation of metabolic regulations by signaling pathways. This is popularly known as dynamic FBA (dFBA), where the initial activation of the metabolic FBA model depends on the output of signaling response generated by dynamic analysis. In yet another extension of FBA, the initial signaling response is analyzed using Boolean analysis. This is known as rFBA. The method that takes into account a combined FBA, Boolean regulatory, and ODE approach is known as integrative FBA (iFBA).

There are various tools available for performing these analyses. COBRA Toolbox is the most widely used platform for flux balance analysis [133]. This is a Matlab extension, which allows user-interface for ease in analysis. Other platforms are COBRAPy [134], PSAMM [135], OptFlux [136], FBASimVis [137], FluxViz [138], FlexFlux [139], FAME [140], and Escher-FBA [141].

6.5.2.5 Dynamic ODE-Based Immune Models

Several dynamic models have been developed for the study of immune responses for several diseases [142–146]. The study of immune responses during tumor formation using mathematical ODE-based models has helped clinicians in the prediction of tumor evolution and the determination of dosage schedules and treatment protocols [147–149]. A seminal work by Kirschner and Panetta has led to the development of many such similar models with further improvisations [150]. The model developed by them represents an ODE-based model of the tumor-immune interaction and the production of IL-2 that has important roles in the regulation of immune response generated during tumor progression (Eqs. 6.5, 6.6, and 6.7). The model considers that the proliferation of the effector immune cells increases proportional to the antigenicity of the tumor. The model equations comprise three variables, viz. tumor (T), effector cells (E), and IL2 (I_L), that interact among themselves, and 12 parameters that describe the rate at which these interactions occur. In this model the antigenicity, denoted with c , of the tumor has been considered as an essential parameter that regulates the dynamics of the effector cell population:

$$\frac{dE}{dt} = cT - \mu_2 E + \frac{p_1 E I_L}{g_1 + I_L} + s_1 \quad (6.5)$$

$$\frac{dT}{dt} = r_2 (1 - bT)T - \frac{aET}{g_2 + T} \quad (6.6)$$

$$\frac{dI_L}{dt} = \frac{p_2 ET}{g_3 + T} - \mu_3 I_L + s_2 \quad (6.7)$$

Figure 6.3b (adapted from Kirshner et al. 1998 [150]) shows the temporal evolution of the system and the oscillating steady state behavior of the variables when antigenicity parameter $c = 0.02$. This model explains short-term oscillations in tumor sizes as well as long-term tumor relapse. This model has been further used to explore the effects of adoptive cellular immunotherapy for the tumor elimination [150].

A more recent tumor-immune interaction model developed for understanding the dynamics of immune-mediated tumor rejection focuses mainly on the role of natural killer (NK) and CD8⁺ T cells in tumor surveillance. Here the techniques of parameter estimation and sensitivity analysis have been exploited for the model calibration and validation with experimental results. This study has revealed the variable to which the model is most sensitive is patient specific and that there exists a direct positive correlation between the patient-specific efficacy of the CD8⁺ T-cell response and the likelihood of a patient favorably responding to immunotherapy

treatments [151]. A more detailed model of immune responses during tumor progression has been developed using 13 variables and 71 parameters. The model considers cytokine feedbacks and five different immune cells present in the tumor microenvironment. This model is useful for optimizing combinatorial treatment dose and schedules for maximal tumor reduction using immunotherapy [152].

There is a range of ODE models that investigate various pathways involved in metabolism under different pathological conditions. Immune metabolic models are available for glucose metabolism [153], glutathione metabolism [154], folate-mediated one-carbon metabolism [154], and arsenic metabolism [155]. A composite review of these metabolic models is available in Nijhout et al.'s work [156]. The recent understanding from experimental research on the metabolic regulation of the immune response [9] will help to adapt these mathematical models to the reality of metabolic pathways inside immune cells.

6.6 Challenges and Future Directions

The immune-regulatory network forms a complex mesh of interacting cells and biochemical reactions that work in a coordinated fashion to eliminate the pathogen-infected cells and trigger the remission of any neoplastic growth inside the body. However, the intricacies of the immune signaling network are far from being completely understood, and the regulations governing the differential immune response of the T cells under varied antigenic challenges still remain elusive to immunologists. In this context, the knowledge regarding the signaling routes is essential to understand the mechanistic regulations such as the feedback and feed-forward loops and the alternative signaling pathways that govern the production of effector molecules from the lymphocytes. Hence, an in-depth study of the co-receptor signaling pathways and their cross-talks is essential that will provide valuable information regarding the pathways involved in the cytokine regulation and effector functions of the immune cells.

T-cell plasticity that determines their differentiation, de-differentiation, subtype specification, and T helper memory cell formation under different environmental conditions is yet another area that has remained very less explored. Although the recent developments in the field elucidate the process of T-cell differentiation with respect to changes in the cytokine milieu under *in vitro* conditions, the complex interactions in the human immunome needs to be studied using a holistic integrative approach in order to gain clear insights into the changes of immune responses due to changes in quality and quantity of the antigenic challenge, the strength of the stimulus, and the role of the other interacting immune cells. Such studies will throw light into the modulations of T-cell subtype ratios that has a substantial impact on the disease prognosis and response of a patient to an immunotherapeutic intervention.

Metabolic regulation of immune cell in determining T-cell activation, proliferation, and differentiation is a newer area of research; and studies are in progress to understand these processes. Many questions related to immune-metabolism still

remain unanswered. How metabolism alters during transition from quiescent T cells to activated effector T cells remains poorly understood. Although mTORC1 activity has been observed to be central to signaling and metabolic cross-talk and the master kinase in guiding quiescence exit of T cells, how nutrients tune mTORC1 activity remains to be explored further. Redox metabolism and oxygen sensing have been implicated in T-cell proliferation and activation; however, the exact mechanism of how they regulate T-cell quiescence and activation in different tissues remains unaddressed. Also, the cross-talks between signaling and metabolic pathways are only partially explored. A clear understanding of these mechanisms will help augment immune responses and pave way for immunotherapy under different pathogenic conditions.

References

1. Cruse JM, Lewis RE, Wang H (eds) (2004) Chapter 1 – Molecules, cells, and tissues of immunity. Immunology guidebook. Academic, San Diego, pp 1–15
2. Rabb H (2002) The T cell as a bridge between innate and adaptive immune systems: implications for the kidney. *Kidney Int* 61(6):1935–1946
3. Moticka EJ (2016) Chapter 20 – Activation of T lymphocytes and MHC restriction. A historical perspective on evidence-based immunology. Elsevier, Amsterdam, pp 169–179
4. Moticka EJ (2016) Chapter 37 – Tumor immunology. A historical perspective on evidence-based immunology. Elsevier, Amsterdam, pp 329–339
5. Kara EE, Comerford I, Fenix KA, Bastow CR, Gregor CE, McKenzie DR et al (2014) Tailored immune responses: novel effector helper T cell subsets in protective immunity. *PLoS Pathog* 10(2):e1003905
6. Moticka EJ (2016) Chapter 23 – T lymphocyte subpopulations. A historical perspective on evidence-based immunology. Elsevier, Amsterdam, pp 197–205
7. Pearce EL, Pearce EJ (2013) Metabolic pathways in immune cell activation and quiescence. *Immunity* 38(4):633–643
8. Zeng H, Chi H (2017) mTOR signaling in the differentiation and function of regulatory and effector T cells. *Curr Opin Immunol* 46:103–111
9. Ganeshan K, Chawla A (2014) Metabolic regulation of immune responses. *Annu Rev Immunol* 32:609–634
10. Assmann N, Finlay DK (2016) Metabolic regulation of immune responses: therapeutic opportunities. *J Clin Invest* 126(6):2031–2039
11. Patel CH, Leone RD, Horton MR, Powell JD (2019) Targeting metabolism to regulate immune responses in autoimmunity and cancer. *Nat Rev Drug Discov* 18(9):669–688
12. Jung J, Zeng H, Horng T (2019) Metabolism as a guiding force for immunity. *Nat Cell Biol* 21(1):85–93
13. Brownlie RJ, Zamoyska R (2013) T cell receptor signalling networks: branched, diversified and bounded. *Nat Rev Immunol* 13:257
14. Ware CF (2008) Targeting lymphocyte activation through the lymphotoxin and LIGHT pathways. *Immunol Rev* 223:186–201
15. Elgueta R, Benson MJ, de Vries VC, Wasiuk A, Guo Y, Noelle RJ (2009) Molecular mechanism and function of CD40/CD40L engagement in the immune system. *Immunol Rev* 229(1):152–172
16. Munroe ME, Bishop GA (2007) A Costimulatory function for T cell CD40. *J Immunol* 178(2):671–682
17. Redmond WL, Ruby CE, Weinberg AD (2009) The role of OX40-mediated co-stimulation in T cell activation and survival. *Crit Rev Immunol* 29(3):187–201

18. Croft M, So T, Duan W, Soroosh P (2009) The significance of OX40 and OX40L to T-cell biology and immune disease. *Immunol Rev* 229(1):173–191
19. Ledbetter JA, Deans JP, Aruffo A, Grosmaire LS, Kanner SB, Bolen JB et al (1993) CD4, CD8 and the role of CD45 in T-cell activation. *Curr Opin Immunol* 5(3):334–340
20. Chen L, Flies DB (2013) Molecular mechanisms of T cell co-stimulation and co-inhibition. *Nat Rev Immunol* 13(4):227–242
21. Feske S (2007) Calcium signalling in lymphocyte activation and disease. *Nat Rev Immunol* 7:690
22. Baine I, Abe Brian T, Macian F (2009) Regulation of T-cell tolerance by calcium/NFAT signaling. *Immunol Rev* 231(1):225–240
23. Nakaya M, Xiao Y, Zhou X, Chang J-H, Chang M, Cheng X et al (2014) Inflammatory T cell responses rely on amino acid transporter ASCT2 facilitation of glutamine uptake and mTORC1 kinase activation. *Immunity* 40(5):692–705
24. Palmer CS, Ostrowski M, Balderson B, Christian N, Crowe SM (2015) Glucose metabolism regulates T cell activation, differentiation, and functions. *Front Immunol* 6:1
25. Chi H (2012) Regulation and function of mTOR signalling in T cell fate decisions. *Nat Rev Immunol* 12(5):325
26. Chapman NM, Boothby MR, Chi H (2020) Metabolic coordination of T cell quiescence and activation. *Nat Rev Immunol* 20:55–70
27. Johnson MO, Wolf MM, Madden MZ, Andrejeva G, Sugiura A, Contreras DC et al (2018) Distinct regulation of Th17 and Th1 cell differentiation by glutaminase-dependent metabolism. *Cell* 175(7):1780–95.e19
28. Dodd KM, Tee AR (2012) Leucine and mTORC1: a complex relationship. *Am J Physiol Endocrinol Metab* 302(11):E1329–42
29. Fallarino F, Grohmann U, Vacca C, Bianchi R, Orabona C, Spreca A et al (2002) T cell apoptosis by tryptophan catabolism. *Cell Death Differ* 9(10):1069
30. Fallarino F, Grohmann U, Hwang KW, Orabona C, Vacca C, Bianchi R et al (2003) Modulation of tryptophan catabolism by regulatory T cells. *Nat Immunol* 4(12):1206
31. Geiger R, Rieckmann JC, Wolf T, Basso C, Feng Y, Fuhrer T et al (2016) L-arginine modulates T cell metabolism and enhances survival and anti-tumor activity. *Cell* 167(3):829–42.e13
32. Zhao Y, Hu X, Liu Y, Dong S, Wen Z, He W et al (2017) ROS signaling under metabolic stress: cross-talk between AMPK and AKT pathway. *Mol Cancer* 16(1):79
33. Franchina DG, Dostert C, Brenner D (2018) Reactive oxygen species: involvement in T cell signaling and metabolism. *Trends Immunol* 39(6):489–502
34. Zhu J, Yamane H, Paul WE (2010) Differentiation of effector CD4 T cell populations. *Annu Rev Immunol* 28:445–489
35. Luckheeram RV, Zhou R, Verma AD, Xia B (2012) CD4+T cells: differentiation and functions. *Clin Dev Immunol* 2012:925135
36. Hawse WF, Cattley RT (2019) T cells transduce T-cell receptor signal strength by generating different phosphatidylinositols. *J Biol Chem* 294(13):4793–4805
37. Yamane H, Paul WE (2013) Early signaling events that underlie fate decisions of naive CD4(+) T cells towards distinct T-helper cell subsets. *Immunol Rev* 252(1):12–23
38. Peter C, Waldmann H, Cobbold SP (2010) mTOR signalling and metabolic regulation of T cell differentiation. *Curr Opin Immunol* 22(5):655–661
39. MacIver NJ, Michalek RD, Rathmell JC (2013) Metabolic regulation of T lymphocytes. *Annu Rev Immunol* 31:259–283
40. Klysz D, Tai X, Robert PA, Craveiro M, Cretenet G, Oburoglu L et al (2015) Glutamine-dependent α -ketoglutarate production regulates the balance between T helper 1 cell and regulatory T cell generation. *Sci Signal* 8(396):ra97
41. Mak TW, Grusdat M, Duncan GS, Dostert C, Nonnenmacher Y, Cox M et al (2017) Glutathione primes T cell metabolism for inflammation. *Immunity* 46(4):675–689
42. Stark JM, Tibbitt CA, Coquet JM (2019) The metabolic requirements of Th2 cell differentiation. *Front Immunol* 10:2318

43. Gerriets VA, Kishton RJ, Johnson MO, Cohen S, Siska PJ, Nichols AG et al (2016) Foxp3 and Toll-like receptor signaling balance T reg cell anabolic metabolism for suppression. *Nat Immunol* 17(12):1459
44. Angelin A, Gil-de-Gómez L, Dahiya S, Jiao J, Guo L, Levine MH et al (2017) Foxp3 reprograms T cell metabolism to function in low-glucose, high-lactate environments. *Nat Immunol* 25(6):1282–93.e7
45. Geginat J, Paroni M, Maglie S, Alfen JS, Kastirr I, Gruarin P et al (2014) Plasticity of human CD4 T cell subsets. *Front Immunol* 5:630
46. Pollizzi KN, Powell JD (2015) Regulation of T cells by mTOR: the known knowns and the known unknowns. *Trends Immunol* 36(1):13–20
47. Yang K, Neale G, Green DR, He W, Chi H (2011) The tumor suppressor Tsc1 enforces quiescence of naive T cells to promote immune homeostasis and function. *Nat Immunol* 12(9):888
48. Sauer S, Bruno L, Hertweck A, Finlay D, Leleu M, Spivakov M et al (2008) T cell receptor signaling controls Foxp3 expression via PI3K, Akt, and mTOR. *Proc Natl Acad Sci U S A* 105(22):7797–7802
49. Macintyre AN, Gerriets VA, Nichols AG, Michalek RD, Rudolph MC, Deoliveira D et al (2014) The glucose transporter Glut1 is selectively essential for CD4 T cell activation and effector function. *Cell Metab* 20(1):61–72
50. Wang R, Dillon CP, Shi LZ, Milasta S, Carter R, Finkelstein D et al (2011) The transcription factor Myc controls metabolic reprogramming upon T lymphocyte activation. *Immunity* 35(6):871–882
51. Yang K, Shrestha S, Zeng H, Karmaus PW, Neale G, Vogel P et al (2013) T cell exit from quiescence and differentiation into Th2 cells depend on Raptor-mTORC1-mediated metabolic reprogramming. *Immunity* 39(6):1043–1056
52. Tan H, Yang K, Li Y, Shaw TI, Wang Y, Blanco DB et al (2017) Integrative proteomics and phosphoproteomics profiling reveals dynamic signaling networks and bioenergetics pathways underlying T cell activation. *Immunity* 46(3):488–503
53. Gerriets VA, Kishton RJ, Nichols AG, Macintyre AN, Inoue M, Ilkayeva O et al (2015) Metabolic programming and PDHK1 control CD4+ T cell subsets and inflammation. *J Clin Invest* 125(1):194–207
54. Blagih J, Coulombe F, Vincent EE, Dupuy F, Galicia-Vázquez G, Yurchenko E et al (2015) The energy sensor AMPK regulates T cell metabolic adaptation and effector responses in vivo. *Immunity* 42(1):41–54
55. Mossmann D, Park S, Hall MN (2018) mTOR signalling and cellular metabolism are mutual determinants in cancer. *Nat Rev Cancer* 18(12):744–757
56. Buck MD, O'sullivan D, Pearce EL (2015) T cell metabolism drives immunity. *J Exp Med* 212(9):1345–1360
57. Mullen PJ, Yu R, Longo J, Archer MC, Penn LZ (2016) The interplay between cell signalling and the mevalonate pathway in cancer. *Nat Rev Cancer* 16(11):718
58. Doerig C, Rayner JC, Scherf A, Tobin AB (2015) Post-translational protein modifications in malaria parasites. *Nat Rev Microbiol* 13(3):160–172
59. Ho P-C, Bihuniak JD, Macintyre AN, Staron M, Liu X, Amezquita R et al (2015) Phosphoenolpyruvate is a metabolic checkpoint of anti-tumor T cell responses. *Cell* 162(6):1217–1228
60. Wang F, Beck-García K, Zorzín C, Schamel WW, Davis MM (2016) Inhibition of T cell receptor signaling by cholesterol sulfate, a naturally occurring derivative of membrane cholesterol. *Nat Immunol* 17(7):844–50
61. Demetriou M, Granovsky M, Quaggin S, Dennis JW (2001) Negative regulation of T-cell activation and autoimmunity by Mgat5N-glycosylation. *Nature* 409(6821):733–9
62. Lee K, Gudapati P, Dragovic S, Spencer C, Joyce S, Killeen N et al (2010) Mammalian target of rapamycin protein complex 2 regulates differentiation of Th1 and Th2 cell subsets via distinct signaling pathways. *Immunity* 32(6):743–753
63. Frauwirth KA, Riley JL, Harris MH, Parry RV, Rathmell JC, Plas DR et al (2002) The CD28 signaling pathway regulates glucose metabolism. *Immunity* 16(6):769–777

64. Kimura MY, Pobezinsky LA, Guinter TI, Thomas J, Adams A, Park J-H et al (2013) IL-7 signaling must be intermittent, not continuous, during CD8+ T cell homeostasis to promote cell survival instead of cell death. *Nat Immunol* 14(2):143–51
65. Jacobs SR, Herman CE, MacIver NJ, Wofford JA, Wieman HL, Hammen JJ et al (2008) Glucose uptake is limiting in T cell activation and requires CD28-mediated Akt-dependent and independent pathways. *J Immunol* 180(7):4476–4486
66. Sinclair LV, Rolf J, Emslie E, Shi Y-B, Taylor PM, Cantrell DA (2013) Control of amino-acid transport by antigen receptors coordinates the metabolic reprogramming essential for T cell differentiation. *Nat Immunol* 14(5):500
67. Bricker DK, Taylor EB, Schell JC, Orsak T, Boutron A, Chen Y-C et al (2012) A mitochondrial pyruvate carrier required for pyruvate uptake in yeast, *Drosophila*, and humans. *Science* 337(6090):96–100
68. Shi LZ, Wang R, Huang G, Vogel P, Neale G, Green DR et al (2011) HIF1 α -dependent glycolytic pathway orchestrates a metabolic checkpoint for the differentiation of TH17 and Treg cells. *J Exp Med* 208(7):1367–1376
69. Sinclair LV, Neyens D, Ramsay G, Taylor PM, Cantrell DA (2018) Single cell analysis of kynurenine and System L amino acid transport in T cells. *Nat Commun* 9(1):1981
70. Baixauli F, Acín-Pérez R, Villarroya-Beltrí C, Mazzeo C, Nuñez-Andrade N, Gabandé-Rodríguez E et al (2015) Mitochondrial respiration controls lysosomal function during inflammatory T cell responses. *Cell Metab* 22(3):485–498
71. Seman M, Adriouch S, Scheuplein F, Krebs C, Freese D, Glowacki G et al (2003) NAD-induced T cell death: ADP-ribosylation of cell surface proteins by ART2 activates the cytolytic P2X7 purinoceptor. *Immunity* 19(4):571–582
72. Adriouch S, Hubert S, Pechberty S, Koch-Nolte F, Haag F, Seman M (2007) NAD⁺ released during inflammation participates in T cell homeostasis by inducing ART2-mediated death of naive T cells in vivo. *J Immunol* 179(1):186–194
73. Clever D, Roychoudhuri R, Constantinides MG, Askenase MH, Sukumar M, Klebanoff CA et al (2016) Oxygen sensing by T cells establishes an immunologically tolerant metastatic niche. *Cell* 166(5):1117–31.e14
74. Tarasenko TN, Pacheco SE, Koenig MK, Gomez-Rodriguez J, Kapnick SM, Diaz F et al (2017) Cytochrome c oxidase activity is a metabolic checkpoint that regulates cell fate decisions during T cell activation and differentiation. *Cell Metab* 25(6):1254–68.e7
75. Sena LA, Li S, Jairaman A, Prakriya M, Ezponda T, Hildeman DA et al (2013) Mitochondria are required for antigen-specific T cell activation through reactive oxygen species signaling. *Immunity* 38(2):225–236
76. Chinen T, Kannan AK, Levine AG, Fan X, Klein U, Zheng Y et al (2016) An essential role for the IL-2 receptor in T reg cell function. *Nat Immunol* 17(11):1322
77. Yang K, Blanco DB, Neale G, Vogel P, Avila J, Clish CB et al (2017) Homeostatic control of metabolic and functional fitness of T reg cells by LKB1 signalling. *Nature* 548(7669):602
78. Zeiser R, Maas K, Youssef S, Dürr C, Steinman L, Negrin RSJI (2009) Regulation of different inflammatory diseases by impacting the mevalonate pathway. *Immunology* 127(1):18–25
79. Huynh A, DuPage M, Priyadharshini B, Sage PT, Quiros J, Borges CM et al (2015) Control of PI (3) kinase in T reg cells maintains homeostasis and lineage stability. *Nat Immunol* 16(2):188
80. Tyrakis PA, Palazon A, Macias D, Lee KL, Phan AT, Veliça P et al (2016) S-2-hydroxyglutarate regulates CD8+ T-lymphocyte fate. *Nature* 540(7632):236
81. Kidani Y, Elsaesser H, Hock MB, Vergnes L, Williams KJ, Argus JP et al (2013) Sterol regulatory element-binding proteins are essential for the metabolic programming of effector T cells and adaptive immunity. *Nat Immunol* 14(5):489
82. Bensinger SJ, Bradley MN, Joseph SB, Zelcer N, Janssen EM, Hausner MA et al (2008) LXR signaling couples sterol metabolism to proliferation in the acquired immune response. *Cell* 134(1):97–111
83. Angela M, Endo Y, Asou HK, Yamamoto T, Tumes DJ, Tokuyama H et al (2016) Fatty acid metabolic reprogramming via mTOR-mediated inductions of PPAR γ directs early activation of T cells. *Nat Commun* 7:13683

84. Munn DH, Sharma MD, Baban B, Harding HP, Zhang Y, Ron D et al (2005) GCN2 kinase in T cells mediates proliferative arrest and anergy induction in response to indoleamine 2, 3-dioxygenase. *Immunity* 22(5):633–642
85. Chang C-H, Curtis JD, Maggi LB Jr, Faubert B, Villarino AV, O’Sullivan D et al (2013) Posttranscriptional control of T cell effector function by aerobic glycolysis. *Cell* 153(6):1239–1251
86. Sherman BT, Lempicki RA (2009) Systematic and integrative analysis of large gene lists using DAVID bioinformatics resources. *Nat Protoc* 4(1):44–57
87. Huang DW, Sherman BT, Lempicki RA (2008) Bioinformatics enrichment tools: paths toward the comprehensive functional analysis of large gene lists. *Nucleic Acids Res* 37(1):1–13
88. Carmona-Saez P, Chagoyen M, Tirado F, Carazo JM, Pascual-Montano A (2007) GENECODIS: a web-based tool for finding significant concurrent annotations in gene lists. *Genome Biol* 8(1):R3
89. Subramanian A, Tamayo P, Mootha VK, Mukherjee S, Ebert BL, Gillette MA et al (2005) Gene set enrichment analysis: a knowledge-based approach for interpreting genome-wide expression profiles. *Proc Natl Acad Sci U S A* 102(43):15545–15550
90. Croft D, Mundo AF, Haw R, Milacic M, Weiser J, Wu G et al (2013) The Reactome pathway knowledgebase. *Nucleic Acids Res.* 42(D1):D472–D477
91. Bindea G, Mlecnik B, Tosolini M, Kirilovsky A, Waldner M, Obenauf Anna C et al (2013) Spatiotemporal dynamics of Intratumoral immune cells reveal the immune landscape in human cancer. *Immunity* 39(4):782–795
92. Fridman WH, Pagès F, Sautès-Fridman C, Galon J (2012) The immune contexture in human tumours: impact on clinical outcome. *Nat Rev Cancer* 12:298
93. Dillon LAL, Suresh R, Okrah K, Corrada Bravo H, Mosser DM, El-Sayed NM (2015) Simultaneous transcriptional profiling of *Leishmania major* and its murine macrophage host cell reveals insights into host-pathogen interactions. *BMC Genomics* 16:1108
94. Favila MA, Geraci NS, Zeng E, Harker B, Condon D, Cotton RN et al (2014) Human dendritic cells exhibit a pronounced type I IFN signature following *Leishmania major* infection that is required for IL-12 induction. *J Immunol* 192(12):5863–5872
95. Chowdhury S, Sarkar RR (2015) Comparison of human cell signaling pathway databases—evolution, drawbacks and challenges. *Database* 2015:bau126
96. Sherriff MR, Sarkar RR (2008) Computational approaches and modelling of signaling processes in immune system. *Proc Indian Natl Sci Acad* 74:187–200
97. Chowdhury S, Sinha N, Ganguli P, Bhowmick R, Singh V, Nandi S et al BIOPYDB: a dynamic human cell specific biochemical pathway database with advanced computational analyses platform. *J Integr Bioinform* 15(3):20170072
98. Trupp M, Altman T, Fulcher CA, Caspi R, Krummenacker M, Paley S et al (2010) Beyond the genome (BTG) is a (PGDB) pathway genome database: HumanCyc. *Genome Biol* 11(1):O12
99. Schomburg I, Chang A, Schomburg D (2002) BRENDA, enzyme data and metabolic information. *Nucleic Acids Res* 30(1):47–49
100. Euler L (1736) *Commentarii Academiae Scientiarum Imperialis Petropolitanae* 8:128
101. Watts DJ, Strogatz SH (1998) Collective dynamics of ‘small-world’ networks. *Nature* 393(6684):440
102. Barabási A-L, Albert R (1999) Emergence of scaling in random networks. *Science* 286(5439):509–512
103. Smoot ME, Ono K, Ruscheinski J, Wang P-L, Ideker T (2010) Cytoscape 2.8: new features for data integration and network visualization. *Bioinformatics* 27(3):431–432
104. Bastian M, Heymann S, Jacomy M (2009) Gephi: an open source software for exploring and manipulating networks. Third international AAAI conference on weblogs and social media.
105. Batagelj V, Mrvar A (1998) Pajek-program for large network analysis. *Connect* 21(2):47–57
106. Pavlopoulos GA, Secrier M, Moschopoulos CN, Soldatos TG, Kossida S, Aerts J et al (2011) Using graph theory to analyze biological networks. *BioData Min* 4(1):10
107. Bromberg KD, Ma’ayan A, Neves SR, Iyengar R (2008) Design logic of a cannabinoid receptor signaling network that triggers neurite outgrowth. *Science* 320(5878):903–909

108. Ghosh S, Kumar GV, Basu A, Banerjee A (2015) Graph theoretic network analysis reveals protein pathways underlying cell death following neurotropic viral infection. *Sci Rep* 5:14438
109. Chowdhury S, Pradhan RN, Sarkar RR (2013) Structural and logical analysis of a comprehensive hedgehog signaling pathway to identify alternative drug targets for glioma, colon and pancreatic cancer. *PLoS One* 8(7):e69132
110. Chowdhury S, Sarkar R (2013) Drug targets and biomarker identification from computational study of human notch signaling pathway. *Clin Exp Pharmacol* 3(137):2161–1459
111. Kauffman SA (1969) Metabolic stability and epigenesis in randomly constructed genetic nets. *J Theor Biol* 22(3):437–467
112. Müssel C, Hopfensitz M, Kestler HA (2010) BoolNet—an R package for generation, reconstruction and analysis of Boolean networks. *Bioinformatics* 26(10):1378–1380
113. Albert I, Thakar J, Li S, Zhang R, Albert R (2008) Boolean network simulations for life scientists. Source code for biology and medicine. *Source Code Biol Med* 3(1):16
114. Klamt S, Saez-Rodriguez J, Gilles ED (2007) Structural and functional analysis of cellular networks with CellNetAnalyzer. *BMC Syst Biol* 1(1):2
115. Saez-Rodriguez J, Simeoni L, Lindquist JA, Hemenway R, Bommhardt U, Arndt B et al (2007) A logical model provides insights into T cell receptor signaling. *PLoS Comp Biol* 3(8):e163
116. Ganguli P, Chowdhury S, Bhowmick R, Sarkar RR (2015) Temporal protein expression pattern in intracellular signalling cascade during T-cell activation: a computational study. *J Biosci* 40(4):769–789
117. Ganguli P, Chowdhury S, Chowdhury S, Sarkar RR (2015) Identification of Th1/Th2 regulatory switch to promote healing response during leishmaniasis: a computational approach. *EURASIP J Bioinform Syst Biol* 2015(1):13
118. Naldi A, Carneiro J, Chaouiya C, Thieffry D (2010) Diversity and plasticity of Th cell types predicted from regulatory network modelling. *PLoS Comp Biol* 6(9):e1000912
119. Carbo A, Hontecillas R, Kronsteiner B, Viladomiu M, Pedragosa M, Lu P et al (2013) Systems modeling of molecular mechanisms controlling cytokine-driven CD4+ T cell differentiation and phenotype plasticity. *PLoS Comp Biol* 9(4):e1003027
120. Puniya BL, Todd RG, Mohammed A, Brown DM, Barberis M, Helikar T (2018) A mechanistic computational model reveals that plasticity of CD4+ T cell differentiation is a function of cytokine composition and dosage. *Front Physiol* 9:878
121. Kelly PN (2019) Metabolism as a driver of immune response. *Science* 363(6423):137–139
122. Price ND, Reed JL, Palsson BØ (2004) Genome-scale models of microbial cells: evaluating the consequences of constraints. *Nat Rev Microbiol* 2(11):886
123. Blazier AS, Papin JA (2012) Integration of expression data in genome-scale metabolic network reconstructions. *Front Physiol* 3:299
124. Orth JD, Palsson BØ (2010) Systematizing the generation of missing metabolic knowledge. *Biotechnol Bioeng* 107(3):403–412
125. O'Brien EJ, Monk JM, Palsson BO (2015) Using genome-scale models to predict biological capabilities. *Cell* 161(5):971–987
126. Bordbar A, Monk JM, King ZA, Palsson BO (2014) Constraint-based models predict metabolic and associated cellular functions. *Nat Rev Genet* 15(2):107–120
127. Patil KR, Nielsen J (2005) Uncovering transcriptional regulation of metabolism by using metabolic network topology. *Proc Natl Acad Sci U S A* 102(8):2685–2689
128. AbuOun M, Suthers PF, Jones GI, Carter BR, Saunders MP, Maranas CD et al (2009) Genome scale reconstruction of a salmonella metabolic model comparison of similarity and differences with a commensal *Escherichia coli* strain. *J Biol Chem* 284(43):29480–29488
129. Pharkya P, Burgard AP, Maranas CD (2004) OptStrain: a computational framework for redesign of microbial production systems. *Genome Res* 14(11):2367–2376
130. Pharkya P, Maranas CD (2006) An optimization framework for identifying reaction activation/inhibition or elimination candidates for overproduction in microbial systems. *Metab Eng* 8(1):1–13

131. Förster J, Famili I, Fu P, Palsson BØ, Nielsen J (2003) Genome-scale reconstruction of the *Saccharomyces cerevisiae* metabolic network. *Genome Res* 13(2):244–253
132. Orth JD, Thiele I, Palsson BØ (2010) What is flux balance analysis? *Nat Biotechnol* 28(3):245
133. Becker SA, Feist AM, Mo ML, Hannum G, Palsson BØ, Herrgard MJ (2007) Quantitative prediction of cellular metabolism with constraint-based models: the COBRA Toolbox. *Nat Protoc* 2(3):727
134. Ebrahim A, Lerman JA, Palsson BO, Hyduke DR (2013) COBRApy: constraints-based reconstruction and analysis for python. *BMC Syst Biol* 7(1):74
135. Steffensen JL, Dufault-Thompson K, Zhang Y (2016) PSAMM: a portable system for the analysis of metabolic models. *PLoS Comput Biol* 12(2):e1004732
136. Rocha I, Maia P, Evangelista P, Vilaça P, Soares S, Pinto JP et al (2010) OptFlux: an open-source software platform for in silico metabolic engineering. *BMC Syst Biol* 4(1):45
137. Grafahrend-Belau E, Klukas C, Junker BH, Schreiber F (2009) FBA-SimVis: interactive visualization of constraint-based metabolic models. *Bioinformatics* 25(20):2755–2757
138. König M, Holzhütter H-G (2010) Fluxviz—Cytoscape plug-in for visualization of flux distributions in networks. *Genome Inform* 24:96–103
139. Marmiesse L, Peyraud R, Cottret L (2015) FlexFlux: combining metabolic flux and regulatory network analyses. *BMC Syst Biol* 9(1):93
140. Kirchmair J, Williamson MJ, Afzal AM, Tyzack JD, Choy AP, Howlett A et al (2013) FAsT MEtabolizer (FAME): a rapid and accurate predictor of sites of metabolism in multiple species by endogenous enzymes. *J Chem Inf Model* 53(11):2896–2907
141. Rowe E, Palsson BO, King ZA (2018) Escher-FBA: a web application for interactive flux balance analysis. *BMC Syst Biol* 12(1):84
142. Beerenwinkel N, Schwarz RF, Gerstung M, Markowitz F (2015) Cancer evolution: mathematical models and computational inference. *Syst Biol* 64(1):e1-25
143. Banerjee S, Sarkar RR (2008) Delay-induced model for tumor-immune interaction and control of malignant tumor growth. *Biosystems* 91(1):268–288
144. d’Onofrio A, Gatti F, Cerrai P, Freschi L (2010) Delay-induced oscillatory dynamics of tumour–immune system interaction. *Math Comput Model* 51(5–6):572–591
145. dePillis L, Caldwell T, Sarapata E, Williams H (2013) Mathematical modeling of regulatory T cell effects on renal cell carcinoma treatment. *Discrete Cont Dyn-B* 18(4):915–943
146. d’Onofrio A (2008) Metamodeling tumor–immune system interaction, tumor evasion and immunotherapy. *Math Comput Model* 47(5–6):614–637
147. Leder K, Pitter K, Laplant Q, Hambardzumyan D, Ross BD, Chan TA et al (2014) Mathematical modeling of PDGF-driven glioblastoma reveals optimized radiation dosing schedules. *Cell* 156(3):603–616
148. Robertson-Tessi M, El-Kareh A, Goriely A (2012) A mathematical model of tumor-immune interactions. *J Theor Biol* 294:56–73
149. Powathil GG, Adamson DJ, Chaplain MA (2013) Towards predicting the response of a solid tumour to chemotherapy and radiotherapy treatments: clinical insights from a computational model. *PLoS Comput Biol* 9(7):e1003120
150. Kirschner D, Panetta JC (1998) Modeling immunotherapy of the tumor–immune interaction. *JMB* 37(3):235–252
151. de Pillis LG, Radunskaya AE, Wiseman CL (2005) A validated mathematical model of cell-mediated immune response to tumor growth. *Cancer Res* 65(17):7950
152. Ganguli P, Sarkar RR (2018) Exploring immuno-regulatory mechanisms in the tumor microenvironment: model and design of protocols for cancer remission. *PLoS One* 13(9):e0203030
153. Chew YH, Shia YL, Lee CT, Majid FAA, Chua LS, Sarmidi MR et al (2009) Modeling of glucose regulation and insulin-signaling pathways. *Mol Cell Endocrinol* 303(1–2):13–24
154. Reed MC, Thomas RL, Pavisic J, James SJ, Ulrich CM, Nijhout HF et al (2008) A mathematical model of glutathione metabolism. *J Theor Biol* 5(1):8
155. Lawley SD, Yun J, Gamble MV, Hall MN, Reed MC, Nijhout HF et al (2014) Mathematical modeling of the effects of glutathione on arsenic methylation. *J Theor Biol* 11(1):20

-
156. Nijhout HF, Best JA, Reed MC (2015) Using mathematical models to understand metabolism, genes, and disease. *BMC Biol* 13(1):79
 157. Kauffman KJ, Prakash P, Edwards JS (2003) Advances in flux balance analysis. *J Coib* 14(5):491–496



Study of Combinatorial Drug Synergy of Novel Acridone Derivatives With Temozolomide Using *in-silico* and *in-vitro* Methods in the Treatment of Drug-Resistant Glioma

Malobika Chakravarty^{1†}, Piyali Ganguli^{2,3†}, Manikanta Murahari⁴, Ram Rup Sarkar^{2,3*}, Godefridus Johannes Peters^{5,6} and Y. C. Mayur^{1*}

OPEN ACCESS

Edited by:

Fanfan Zhou,
The University of Sydney, Australia

Reviewed by:

Gunjan Arora,
National Institutes of Health (NIH),
United States
Tsung-I Hsu,
Taipei Medical University, Taiwan

*Correspondence:

Y. C. Mayur
mayuryc@rediff.com;
mayuryc@hotmail.com
Ram Rup Sarkar
rr.sarkar@ncl.res.in

[†]These authors have contributed
equally to this work and share first
authorship

Specialty section:

This article was submitted to
Pharmacology of Anti-Cancer Drugs,
a section of the journal
Frontiers in Oncology

Received: 04 November 2020

Accepted: 16 February 2021

Published: 15 March 2021

Citation:

Chakravarty M, Ganguli P, Murahari M,
Sarkar RR, Peters GJ and Mayur YC
(2021) Study of Combinatorial Drug
Synergy of Novel Acridone Derivatives
With Temozolomide Using *in-silico* and
in-vitro Methods in the Treatment of
Drug-Resistant Glioma.
Front. Oncol. 11:625899.
doi: 10.3389/fonc.2021.625899

¹ Department of Pharmaceutical Chemistry, Shobhaben Pratapbhai Patel School of Pharmacy and Technology Management, SVKM's NMIMS, Mumbai, India, ² Chemical Engineering and Process Development Division, CSIR-National Chemical Laboratory, Pune, India, ³ Academy of Scientific and Innovative Research (AcSIR), Ghaziabad, India, ⁴ Department of Pharmaceutical Chemistry, Faculty of Pharmacy, M.S. Ramaiah University of Applied Sciences, Bengaluru, India, ⁵ Department of Biochemistry, Medical University of Gdansk, Gdansk, Poland, ⁶ Laboratory Medical Oncology, Amsterdam University Medical Centers, Location VUMC, Amsterdam, Netherlands

Drug resistance is one of the critical challenges faced in the treatment of Glioma. There are only limited drugs available in the treatment of Glioma and among them Temozolomide (TMZ) has shown some effectiveness in treating Glioma patients, however, the rate of recovery remains poor due to the inability of this drug to act on the drug resistant tumor sub-populations. Hence, in this study three novel Acridone derivative drugs AC2, AC7, and AC26 have been proposed. These molecules when combined with TMZ show major tumor cytotoxicity that is effective in suppressing growth of cancer cells in both drug sensitive and resistant sub-populations of a tumor. In this study a novel mathematical model has been developed to explore the various drug combinations that may be useful for the treatment of resistant Glioma and show that the combinations of TMZ and Acridone derivatives have a synergistic effect. Also, acute toxicity studies of all three acridone derivatives were carried out for 14 days and were found safe for oral administration of 400 mg/kg body weight on albino Wistar rats. Molecular Docking studies of acridone derivatives with P-glycoprotein (P-gp), multiple resistant protein (MRP), and O6-methylguanine-DNA methyltransferase (MGMT) revealed different binding affinities to the transporters contributing to drug resistance. It is observed that while the Acridone derivatives bind with these drug resistance causing proteins, the TMZ can produce its cytotoxicity at a much lower concentration leading to the synergistic effect. The *in silico* analysis corroborate well with our experimental findings using TMZ resistant (T-98) and drug sensitive (U-87) Glioma cell lines and we propose three novel drug combinations (TMZ with AC2, AC7, and AC26) and dosages that show high synergy, high selectivity and low collateral toxicity for the use in the treatment of drug resistant Glioma, which could be future drugs in the treatment of Glioblastoma.

Keywords: acridone derivatives, drug combinations, synergy index, mathematical model, Glioma, drug resistance

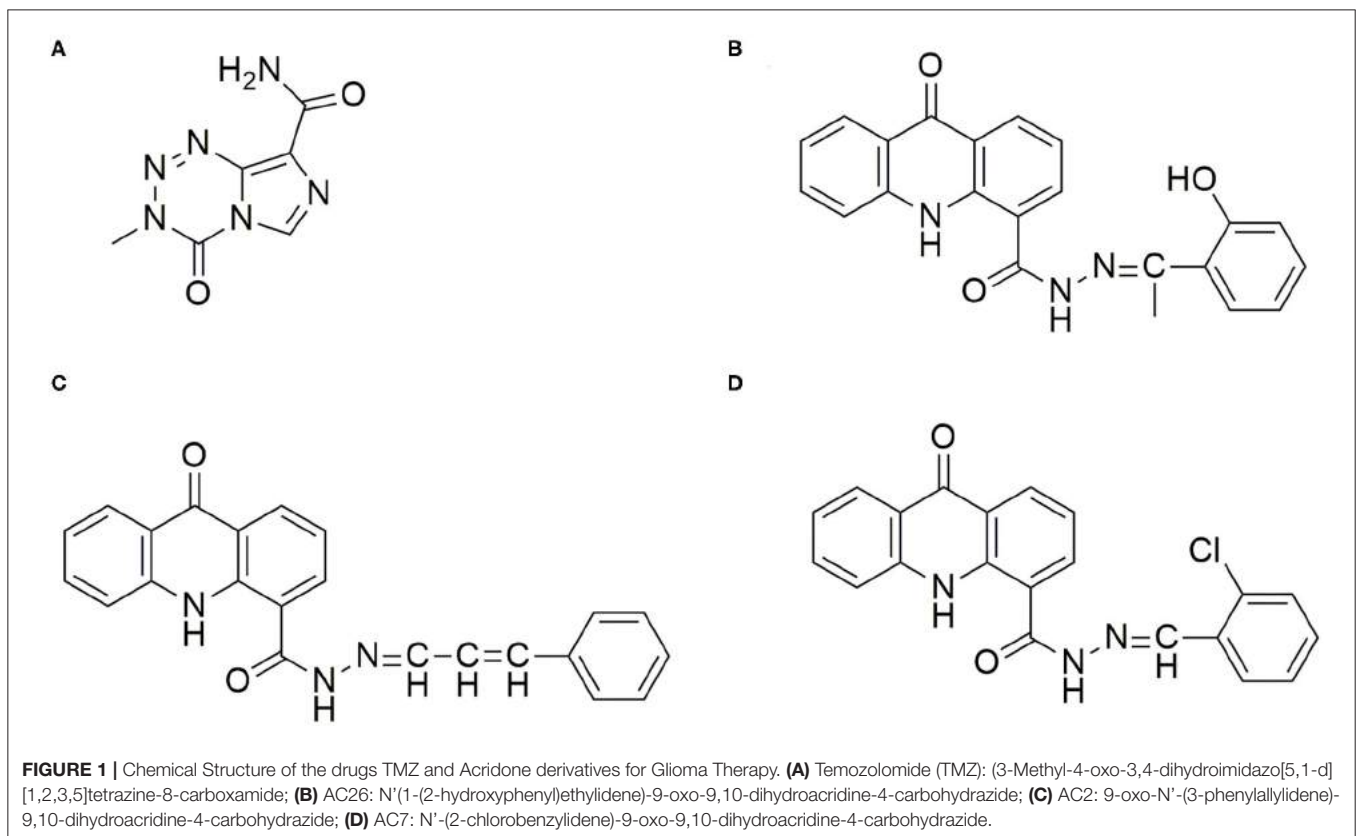
INTRODUCTION

Glioblastoma multiforme or Gliomas are the most commonly occurring primary tumors in the brain and spinal cord. Repeated failures and multiple challenges are seen in treating Glioma due to the development of drug resistance, recurrence, collateral toxicity to healthy cells, and detrimental adverse effects. Amongst these, one of the greatest challenges faced is the development of drug resistance, which can occur as a result of several complex mechanisms. These include poor absorption of the drug, efflux transport pumps, metabolic reprogramming, de-regulation in gene, and protein expression responsible for apoptosis as well as tumor heterogeneity (1–3).

Over the past few decades, several chemotherapeutic drugs like Carmustine, Lomustine, Vincristine, Cisplatin, Bevacizumab etc., have been studied for the treatment of Glioma (4, 5). However, at present, Temozolomide (TMZ) is the one of the well-known and the most effective drug used for the treatment and management of Glioma. It is an alkylating agent belonging to the tetrazine class (**Figure 1A**) having a molecular weight of 194 g/mol and has shown the ability to penetrate the Blood Brain Barrier (BBB) (6). Reports suggest TMZ increases survival advantage by 2.5 times when the drug is administered along with surgery and radiotherapy (7). It is an alkylating agent that transfers a methyl group (CH₃) to a purine base of DNA (N7-guanine, O6-guanine, and N3-adenine) causing both single and double stranded breaks leading to apoptotic

cell death (8). However, it has been observed that although the malignant cells respond to this TMZ induced apoptosis during the initial phases, they gradually develop resistance to it during the later phase of cancer progression. This is because the cytotoxic action of TMZ is reversed by removal of methyl group from O6-methylguanine (O6-MeG) by the methylguanine methyltransferase enzyme (MGMT) (9). The MGMT is an enzyme that is overexpressed in the tumor and the most common reason for the development of drug resistance. Additionally, administration of TMZ results in certain side effects like alopecia, fatigue, nausea, vomiting, headache, constipation, anorexia, convulsions, rash, fever, dizziness, amnesia, insomnia, lymphopenia, thrombocytopenia, neutropenia, and leucopenia, and also leads to severe toxicity at high doses (more than 250 μM) (10). Furthermore, as per equation proposed by Levin-log permeability it was observed that TMZ has a very low brain capillary permeability with a value close to 2.7×10^{-6} cm/s (11). Hence, it may be assumed that permeability of TMZ can be improved by combining it with another lipophilic drug and these acridone molecules fulfill this gap.

However, regardless of these obstacles, TMZ is used as a standard drug in treating Glioma and is the most promising drug known to treat Glioma till today. Hence, in this present study we aim to thwart resistance by combining TMZ with acridone molecules which may have a synergistic effect and help in effectively treating the drug resistant tumor cells. Nevertheless, the question arises which other drugs should be selected that



would give synergistic effect with TMZ? In order to circumvent the shortcomings faced due to the use of the known drugs, it has become crucial to consider novel drugs for fighting Glioma and the drug resistance. In one of our recent work, we have shown that certain novel acridone derivatives have shown high cytotoxic effect against Cervical, Lung, and Breast Cancers (12, 13). In Breast Cancer studies, using MCF-7 cell lines, it has been observed that certain acridone derivatives have the ability to bind to multiple targets and prevent multiple mechanisms responsible for drug resistance in cancer. These molecules can intercalate with DNA and inhibit the process of cell division, initiate reactive oxygen species (ROS) mediated oxidative stress, and bind to the proteins expressed in the plasma membrane responsible for efflux of the drugs like P-glycoprotein(P-gp) (14). The studies have revealed that overexpression of proteins and actions of efflux pumps are the main reason for the drug resistance as this leads to drugs failing to accumulate and exert their activity at the site of action. Apart from this, acridone moieties also showed unique properties of high lipophilicity enabling penetration of the drug into the BBB. It has also been observed that certain structural modifications in these acridone derivatives could result into more potent drugs AC2, AC7, and AC26 which have shown 100 times more cytotoxicity in comparison to the other acridone derivatives (15) (Figures 1B–D). These Acridone compounds (AC2, AC7, and AC26) on evaluation of histopathology demonstrated liver with minimal hyperchromatic, anaplasia, and cellular infiltration. Studies conducted using these compounds showed no cardiotoxicity, nephrotoxicity and necrosis. In recent past, these acridone molecules were able to successfully act on breast cancer MCF-7 cell line (Michigan Cancer Foundation-7) at lower concentration and have shown ability to modulate cytotoxicity in drug resistant MCF-7/ADR (Adriamycin) cell lines when administered in combination with Vinblastine (14). Thus, due to high cytotoxicity of acridone compounds at low dose in MCF-7/ADR cell lines and because of their ability to overcome drug resistance, we aim to test its effectiveness in the treatment of Glioma. In order to have an effective Glioma therapy with minimal toxicity and to overcome drug resistance, in this study, we have tested different combinations of acridone derivatives with TMZ. Here, for the first time *in-vitro* and *in-silico* strategies have been employed together to evaluate efficacy of combinatorial drugs-TMZ + AC26, TMZ + AC2, and TMZ + AC7 in the treatment of Glioma and to evaluate their synergistic action to overcome the drug resistance in Glioma.

Sulforhodamine B (SRB) Assay of the novel acridone derivatives, *viz.*, AC2, AC7, and AC26 have been performed on U-87 (Uppsala 87-WT) and T-98 (Temozolomide resistant) malignant Glioma cell lines to determine the effectiveness of the individual drugs on the drug sensitive and drug resistant cancer cells. In order to gain insights into the molecular mechanism underlying the effectiveness of the Acridone derivatives in overcoming the drug resistance in Glioma, Molecular Docking studies have been performed to compare the binding affinities of the three Acridone derivatives with MGMT, P-gp, and MRP proteins which are responsible for conferring resistance to the Glioma cells. Thereafter, to determine the effectiveness of these drugs in combination with TMZ and to observe the

dose responses under different dosage combinations, we have developed a mathematical model to mimic the effect of these drugs on heterogeneous subpopulation of cancer cells (drug sensitive cancer cells and drug resistant cancer cells) in a tumor. The model has been parameterized using the experimental data and its outcome have been validated with our *in vitro* experiments on the Glioma cell lines in order to ensure correct predictions and to provide the optimum concentration of both the drugs within the toxicity limits for maximum efficacy. The dose response matrices generated from the simulation of the mathematical model have been used for screening 10,000 combinations of doses for each pair of drugs for evaluating the synergistic intensity of each dose combinations of the TMZ and Acridone derivative using *in-silico* method. Experimental studies have also been performed to validate the synergistic dosage combinations of each pair of drugs. This study throws light on new treatment strategies for Glioma by the selection of most beneficial doses of the combinatorial drugs with minimum side effects and determination of the optimum doses for synergy and highest efficacy.

MATERIALS AND METHODS

Drugs Characterization

Characterization of acridone derivatives AC2, AC7, and AC26 were carried out by using all the chemicals of analytical grade. Hydrochloric acid and sodium hydroxide were procured from Sisco Research Lab Pvt. Ltd (Mumbai, India). Potassium dihydrogen orthophosphate, methanol and ortho-phosphoric acid (85% pure) was received from Loba Chemie Pvt. Ltd. (Mumbai, India). Sodium chloride was received from SD Fine-Chem Limited (Mumbai, India). Milli-pore water was used throughout the study. Chemical information like the molecular weight of compounds was determined by obtaining ESI-MS spectroscopy using methanol as solvent. pH calculated by using pH analyzer (Lab India) and PKa determined by using UV-Vis spectrophotometer (Shimadzu, Japan). Melting point was calculated by Digital Melting point apparatus (Veego India). Lipophilicity was determined by using software like Chem Draw 15 and ALGOPS 2.1 (16). In order to determine the Blood Brain Barrier (BBB) permeability of the compounds, we have used Online BBB Predictor (<https://www.cbligand.org/BBB/predictor.php>) using SVM Machine Learning algorithm and PubChem as the fingerprint (17).

Molecular Docking

Molecular docking of the Acridone derivatives AC2, AC7, and AC26 were performed to investigate the binding interactions and patterns at the active pockets of the drug resistance causing target proteins. X-ray crystallographic structures of the target proteins [i.e., P-gp (PDB ID- 6QEX), MRP (PDB ID- 2CBZ), and MGMT (PDB ID- 1QNT) were retrieved from Protein Data Bank (PDB) (18)]. All the crystallographic structures were processed individually in Discovery Studio Visualizer. All the water molecules, unwanted chains, heteroatoms of respective protein structure were removed and hydrogen atoms were added in Discovery Studio Visualizer (19). Receptor cavities of individual

proteins were identified by selecting the co-crystallized ligand in the Discovery Studio Visualizer and attributes were documented for docking calculations (19). Thereafter the processed proteins were loaded to AutoDock Tools, both Kollman and Gasteiger charges were added and saved in pdbqt format (20). All the ligands were sketched in Avogadro software and optimized with Universal Force Field (UFF) and Steepest Descent algorithm (21). Prepared ligands were loaded to AutoDock and saved in pdbqt format. Attributes of individual target protein obtained from Discovery Studio (**Supplementary Table 1**), name of protein and ligands were written in configuration file and submitted to molecular docking. Docking parameters were optimized using Genetic Algorithm (GA) approach with 1,000 runs. Docked pose with highest binding affinity was visualized and interaction analysis was performed in Biovia Discovery Studio Visualizer. All the docking calculations were carried out in a laptop running with Windows 10 64 bit operating system, 8GB RAM and i3 processor.

Sulforhodamine B Assay for Individual Drugs

In order to test the growth inhibition potential of the TMZ and Acridone derivatives on Glioma, the U-87 (Uppsala 87) Glioma cell lines and T-98 (Temozolomide resistant) Glioma cell lines were treated with Temozolomide (TMZ) and Acridone derivatives AC2, AC7, and AC26. The African Green Monkey Kidney Vero cell lines were used as control for the study. The Vero cell lines were obtained from the National Center for Cell Sciences (NCCS), Pune, while the U-87 and T-98 cell lines were carried in the lab of Dr. GJ Peters, Cancer Center Amsterdam (CCA), VU University Medical Center, Amsterdam, Netherlands. The Mycoplasma testing was done by using the Universal Mycoplasma Detection Kit (ATCC® 30-1012K™) every 6 months. The Vero cell lines have been used as control as they are normal kidney epithelial cells and are non-cancerous in nature. The Vero cell lines have been routinely used for testing cytotoxicity of small molecules by various researchers (22, 23). Also, in our previous study, Vero cell lines have been used for testing safety and efficacy of Acridone derivatives for Lung, Cervical, and Breast Cancer studies (13).

Cell viability was found using the Sulforhodamine B (SRB) assay to measure the cellular protein content which provides better sensitivity in comparison to MTT assay (24). Moreover, as this method is dependent on the property of the SRB dye, it acts by binding to proteins under slightly acidic conditions and can be exposed to basic conditions for its extraction. The resulting amount of bound dye is then utilized as a proxy for cell mass (25). This cell mass can then be extrapolated to measure cell growth.

Glioma cells were cultured in Gibco (RPMI 1640) complemented with 10% fetal calf serum (Gibco). The cultures were then treated with trypsin-EDTA in order to detach/separate the cells from their culture flasks. The quickly proliferating cells were harvested, counted and plated at suitable concentrations in 96-well microplates. These microplates were subsequently incubated for 24 h. After incubation, drug compounds were dissolved in the culture media and placed in 96 well plates in

triplicates, which were again incubated at 37°C under 5% CO₂ for 72 h. 72 h later, the plates were removed and the cells were treated with cold Trichloroacetic acid (TCA) to fix the cultures and 0.4% of SRB dissolved in 1% acetic acid was then added to the culture in order to stain the cells. Next, the bound stain was dissolved in 150 µl of 10 mM unbuffered Tris base left on a gyrator shaker. Thereafter, absorbance of the solution was measured at 540 nm utilizing a microplate reader. Absorbance readings (triplicate values) recorded were used to calculate percentage growth inhibition due to the effect of drugs using the following equations.

$$\% \text{ Cell growth} = \text{Absorbance sample} / \text{Absorbance of control or untreated} \times 100$$

$$\% \text{ Growth inhibition} = 100 - \% \text{ cell growth}$$

The Inhibitory concentration (IC₅₀) of the drugs were determined on the basis of concentration that induced 50% growth inhibition of the treated cells in comparison to untreated cells after 72-h treatment (as given in **Table 4**). The IC₅₀ was calculated based on the log graph sheet which was developed in-house at the CCA, VU University Medical Center.

Selectivity Index

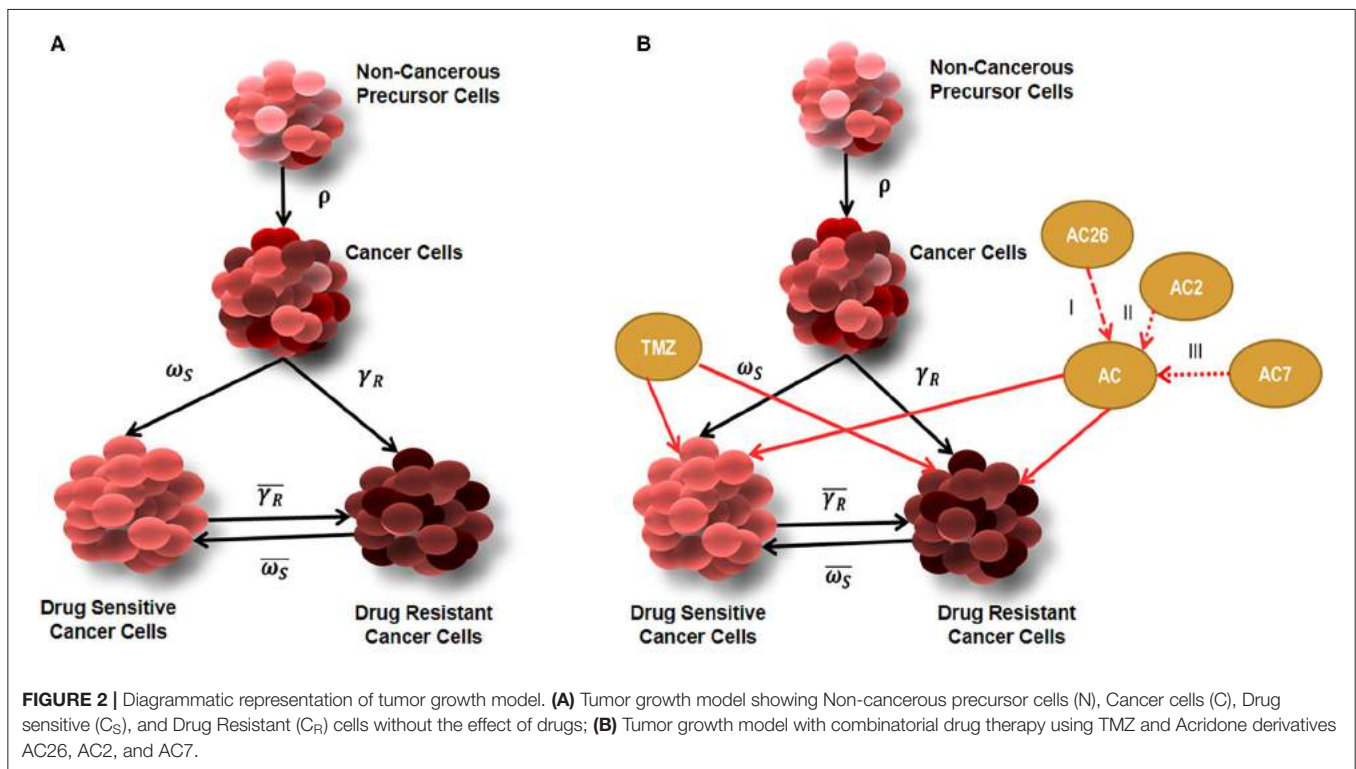
Selectivity Index (SI) is a ratio that measures the window between cytotoxicity and anticancer activity of the drugs (26). Thus, to evaluate effectiveness of all the 4 drugs, SI has been calculated using the formula $SI = CC_{50} \text{ of Vero cell line} / IC_{50} \text{ of Cancer cell line}$, after 72 h of TMZ/AC treatment (27). Here, IC₅₀ is the inhibition concentration for inhibiting 50% of cancer cells and CC₅₀ is cytotoxic concentration causing death of 50% viable cells in the host. Ideally, IC₅₀ concentration should be below CC₅₀ concentration suggesting that cancer cells are killed before host cells.

Model Development

The data obtained from the *in-vitro* experiments were used to develop an Ordinary Differential Equations (ODEs) based model that can mimic the tumor development *in-silico*. The model consists of 4 variables representing the heterogeneous sub-populations of cells in a tumor and 29 parameters that govern the differentiation pattern and growth dynamics of each sub-population. The model has been calibrated and parameters set to capture the growth dynamics of U-87 and T-98 cells that represent the drug resistant and drug sensitive cell sub-populations in a developing tumor. The primary objective of this model development is to screen the effect of varying dosage combinations of TMZ and the Acridone derivatives on the tumor growth to determine the dosage combinations showing high synergistic effects within the toxicity limits.

Tumor Growth Model

The tumor growth model developed (**Figure 2**), assumes existence of few non-cancerous precursor cells (N) which tend to acquire mutation (ρ) over a period of time to form cancerous cells (C) (**Equations 1–4**). The process of acquisition of mutation in non-cancerous precursor cell population can be the result of their exposure to several factors like radiations, air pollution, chemicals, other factors (such as Viruses,) etc.,



(28). Since non-cancerous cells are acquiring mutation with a probability ρ to form cancer cells, the non-cancerous precursor cell population tend to renew their pool of cells with $(1 - \rho)$ probability (**Equation 1**). The model further considers that cancer cell population undergoes differentiation to give rise to heterogeneous subpopulations consisting of the resistant cancer cells (C_R) and sensitive cancer cells (C_S) (29). The sensitive cells are susceptible to therapy, while therapy is hardly effective against resistant cells. The probability that cancer population would differentiate into Drug resistant cancer population (C_R) is γ_R and into Drug sensitive cancer (C_S) population is ω_S where $\gamma_R + \omega_S = 1$. Tracing the past footprints in the literature, it can be understood that transitions are allowed between drug sensitive cancer cells and drug resistant cancer cells with more probability ($\tilde{\gamma}_R$) of transformation occurring in forward direction and less probability ($\tilde{\omega}_S$), that resistant cell population will switch back into sensitive cancer cell population (29, 30). This rare transformation process is well-documented in literature where experiments show that drug resistant cell population reduces in drug free medium (31) or refractoriness to drug therapy can be sometimes reversed by epigenetic programming (32). In mathematical terms, it may be noted here that α_C and δ_C denote the natural birth and death rates of C cells. An identical nomenclature has been followed for other types of cells. The resistant cancer cells are developed from the conversion of a C to C_R. The C_R trail an identical pattern of self-renewal and differentiation resulting in the replenishment of the C_R pool and development of C_S.

Though a plethora of models exist on the basis of the assumption that proliferation of a constant fraction of tumor

volume follows exponential growth but in this model we have considered the widely accepted and well-known model of Gompertz to describe growth dynamics of cancer cells and their heterogeneous subpopulations (33, 34). Mathematical representation of growth kinetics followed by cancer cells can be given as $\alpha_C * C * \log \frac{K}{C + \mu}$, where K denotes carrying capacity of the cancerous cells (35). In this model, it has been considered that C_R and C_S follow identical Gompertzian growth kinetics and all types of cancerous cells have a common carrying capacity. On the contrary, the model assumes that non-cancerous precursor cells are growing logistically, which can be mathematically represented as $\alpha_N * N * (1 - \rho) * (1 - \frac{N}{K})$ (36, 37).

Model Equations

Based on the biological significance and mathematical assumptions, four ODEs were developed for four different types of tumor cells using 29 parameters (**Supplementary Table 2**) in order to describe evolutionary dynamics of tumor growth. The model equations have been listed below:

$$\frac{dN}{dt} = \alpha_N * N * (1 - \rho) * \left(1 - \frac{N}{K}\right) - \delta_N N - \alpha_N * N * \rho \quad (1)$$

$$\frac{dC}{dt} = \alpha_N * \rho * N + \alpha_C * C * \log \frac{K}{C + \mu} - \gamma_R \alpha_C C - \omega_S \alpha_C C - \delta_C C \quad (2)$$

$$\frac{dC_R}{dt} = \gamma_R \alpha_C C + \tilde{\gamma}_R \alpha_{CS} C_S + \alpha_{CR} * C_R * \log \frac{K}{C_R + \mu} - \delta_R C_R - \tilde{\omega}_S \alpha_{CR} C_R \quad (3)$$

$$\frac{dC_S}{dt} = \overline{\omega_S}\alpha_{CR}C_R + \omega_S\alpha_C C + \alpha_{CS}*C_S*\log \frac{K}{C_S + \mu} - \delta_S C_S - \overline{\gamma_R}\alpha_{CS}C_S \quad (4)$$

Parameter Estimation and Validation of Tumor Growth Model

For the simulation and validation of the tumor growth dynamics, the calibration of the model has been carried out and the unknown parameters present in the model have been estimated by appropriately fitting the initial growth kinetics of the model with experimental data of drug sensitive and resistant cell lines of Glioma origin (without the effect of any drugs) for 96 h (38–40). The parameter estimation was performed using the MATLAB based toolbox that uses Markov Chain Monte Carlo (MCMC)-DRAM algorithm (41). Trace plots and Histograms are given in **Supplementary Figure 1**. For this purpose, the U-87 cell growth data has been considered as drug sensitive Glioma cells as U87 cells express low level of MGMT (42). On the other hand, T-98 has been considered as drug resistant cell line due to high expression of cystine-glutamate exchanger (xCT), MGMT, NAMPT (nicotinamide phosphoribosyl transferase), BER (base excision repair), ubiquitin-specific peptidase (Usp18) etc. (42). These protein expressions have been correlated in literature with activity of the transporters (influx, efflux), metabolism, increased DNA repair activity and other processes leading to drug resistance (43).

In this study, the tumor growth model (without drug) consists of four variables and 15 parameters. Out of these values, three parameter values are known from experiments and literature, 10 parameters were estimated using the MCMC technique, and other two parameters were assumed and labeled as expected values as these have been estimated to obtain a close fit of all the four variables during the model simulation. The MATLAB codes for performing the parameter estimation have been made available in **Supplementary Text 2 (Scripts 1–4)**. The model contains additional 14 parameters related to TMZ and the Acridone derivative that regulates drug response behavior of the model (Section model initialization and numerical simulations). The parameter values used for the simulation have been enlisted in **Supplementary Table 2**.

Model Initialization and Numerical Simulations

Using the parameter values and initial values, the system of ODEs were solved numerically utilizing Runge-Kutta methods (RK). In this model, two types of cells non-cancerous cells (N) and Cancer cells (C) have been considered. The C is thought to be consisting of subpopulations-Drug resistant cancer cells (C_R) and Drug sensitive cancer cells (C_S). Numerical simulation of this model was carried out using ODE45, variable order solver present in MATLAB® 2017a platform. The model was initialized and simulated by considering initial values of N, C, C_R , and C_S similar to that of the initial values considered in experiments (**Supplementary Table 3**).

Incorporation of Effects of TMZ and Acridone Derivative

After validating the natural growth dynamics of the tumor, without incorporating the effect of any drug, the model equations

have been modified with additional terms to capture the cell kill dynamics under the influence of individual drugs (TMZ and Acridone derivative) and when administered in combination. For this, the Maximum response (E_{max}) model for drug induced cell death has been considered in our model for comparing efficacy of the drugs. Functional form of E_{max} model along with an additional parameter (Hill exponent to show steeper relationship of concentration) to the concentration can be depicted as $\left[\frac{\epsilon_{max}(Conc)^{Hill}}{C_{50}^{Hill} + Conc^{Hill}} \right]$, where C_{50} is the concentration at 50% of E_{max} (44, 45). Similarly, effects of drugs on two different cancerous cells have been introduced in this mathematical model. In order to capture this, **Equations 3, 4** have been modified as follows:

$$\begin{aligned} \frac{dC_R}{dt} = & \gamma_R\alpha_C C + \overline{\gamma_R}\alpha_{CS}C_S + \alpha_{CR}*C_R*\log \frac{K}{C_R + \mu} \\ & - \delta_R C_R - \overline{\omega_S}\alpha_{CR}C_R - \left[\epsilon_{max}^{D1r} \frac{D_1^{\eta_{D1r}}}{IC_{50D1r}^{\eta_{D1r}} + D_1^{\eta_{D1r}}} \right] C_R \\ & - \left[\epsilon_{max}^{D2r} \frac{D_2^{\eta_{D2r}}}{IC_{50D2r}^{\eta_{D2r}} + D_2^{\eta_{D2r}}} \right] C_R \end{aligned} \quad (5)$$

$$\begin{aligned} \frac{dC_S}{dt} = & \overline{\omega_S}\alpha_{CR}C_R + \omega_S\alpha_C C + \alpha_{CS}*C_S*\log \frac{K}{C_S + \mu} \\ & - \delta_S C_S - \overline{\gamma_R}\alpha_{CS}C_S - \left[\epsilon_{max}^{D1s} \frac{D_1^{\eta_{D1s}}}{IC_{50D1s}^{\eta_{D1s}} + D_1^{\eta_{D1s}}} \right] C_S \\ & - \left[\epsilon_{max}^{D2s} \frac{D_2^{\eta_{D2s}}}{IC_{50D2s}^{\eta_{D2s}} + D_2^{\eta_{D2s}}} \right] C_S \end{aligned} \quad (6)$$

Here D_1 is the dose of the TMZ in μM , while D_2 is the dose updated every time with the parameter values of the Acridone derivatives for AC2, AC7, and AC26 in μM , ϵ_{max} is given for Drug 1 and Drug 2 in different cancer cells (Drug resistant cancer cells and drug sensitive cancer cells), η_{D1r} and η_{D2r} (Hill exponents) represents efficacy of the Drug 1 and Drug 2 in for resistant cancer cells (similarly η_{D1s} and η_{D2s} are for sensitive cells), while IC_{50} stands for inhibitory concentration of Drug 1 and Drug 2 at which 50% of tumor response is inhibited. After incorporation of the effect of drugs (TMZ and Acridone derivative) the model now consists of 29 parameters. However, it is to be noted that each of the parameters related to the Acridone derivative (Drug 2 or D_2) can have three possible values related to AC2, AC7, and AC26, thereby making the total number of possible values of the parameters 43 (**Supplementary Table 2, Supplementary Text 2: Scripts 5 and 6**). Here, the doses for the four drugs (TMZ, AC2, AC7, and AC26) were varied to study the change in cellular dynamics under different dosages. The parameter values related to these drugs considered in our model equations have been determined by varying the parameters to obtain a close fit with the experimental observations from the SRB Assay.

Numerical Simulation With Drug Therapy

Numerical simulations were carried out by varying the dose of the drug (D_1) [i.e., TMZ while keeping the dose of the Acridone derivative drug (D_2) as zero]. Simulations were run using an ODE variable solver in MATLAB until a steady state solution was reached. For the study of the effect of the individual drugs on the inhibition of cellular growth, simulations for AC2, AC7, and

AC26 were also performed in a similar way by varying the dose of the Acridone derivatives. These simulation results in capturing the effect of the individual drugs on the drug sensitive and resistant cell lines were fitted and validated with our experimental findings obtained from the Sulforhodamine B Assay mentioned in Section Sulforhodamine B assay for individual drugs.

Administration of Combinatorial Drugs

After studying the effect of drugs individually on the growth of different Glioma cells, combinational studies were carried out to observe how the growth inhibition of TMZ resistant Glioma cells could be achieved when TMZ and Acridone derivatives were administered in combination. For this, combinational drugs (AC26 + TMZ, AC2 + TMZ, and AC7 + TMZ) were administered and their effect on growth of drug resistant cancer cells and drug sensitive cancer cells were observed. Simulations were performed by varying doses of both the drugs for each combinational drug within the range that would not lead to drug toxicity. Toxicity range was considered as more than 100 μM for Acridone compounds and more than 250 μM for TMZ (42). Also, because it was observed from the experiment and the previous simulations that Acridone compounds were highly cytotoxic and potent at lower concentrations so the range of Acridone moieties in simulations were varied from 0 to 6 μM only. For each of the drugs, both TMZ and the Acridone derivatives, 100 dosages were considered and simulated using our mathematical model to generate $100 \times 100 = 10,000$ dosage combinations *in silico* (Supplementary Text 2: Scripts 7 and 8). The dose response matrix of C_R and C_S generated from the simulation was used to calculate the Synergy Scores (SC) of each combination.

Sensitivity Analysis

In order to determine the effect of the different model parameters and the dosages of TMZ and Acridone derivatives on the model variables and the dose response matrices, the Sensitivity Analysis was performed using LHS-PRCC (Latin Hypercube Sampling - Partial Rank Correlation Coefficient) method in MATLAB (46). This method is useful for global uncertainty analysis for monotonic systems. The sensitivity analysis was performed on 29 parameters including the parameters related to TMZ (D1) and Acridone derivatives (D2). The parameters range related to the Acridone derivatives (D2) were considered such that it covers the values of all the three derivatives, viz., AC2, AC7, and AC26. The sensitive parameters were identified for all the four variables based on their PRCC values with a $p < 0.05$ (Supplementary Text 2: Scripts 10–12).

In-silico Drug Synergy Estimation

The synergy scores (SC) for each pair of drug combinations in the resistant cells were calculated using the R-based package Synergy Finder using the Bliss reference model (47). The dose-response matrix obtained from the numerical simulation of the model for the C_R cells was used as an input matrix (100×100) for Synergy Finder to calculate the synergy scores (SC). For the calculation of synergy scores, the assumption is that if an experiment drug A at dose x_1 is combined with drug B at dose x_2 , then the effect of

such a combination is y_c as compared to the monotherapy effect of A at x_1 and B at x_2 . In order to quantify the degree of synergy, the value of y_c needs to be compared with the expected effect y_e of non-interaction. In the Bliss model y_c is calculated as

$$y_c = y_A + y_B - y_A y_B \quad (7)$$

The synergy score is calculated as the difference between the observed effect (y_c) and the expected effect (y_e). This method has been used when the two drugs are acting independently on the phenotype.

Sulforhodamine B Assay for Combinatorial Drugs

Sulforhodamine B Assay procedure used for evaluation of combinational drugs is the same as that of the individual drugs. Cell lines were treated with various concentrations of drug combinations TMZ+AC2, TMZ+AC7, and TMZ+AC26 instead of individual drugs. Combination index (CI) of these combinational drugs were evaluated in drug-sensitive (U-87) and drug-resistant (T-98) cancer cell lines. The 100 μM concentration of TMZ with IC_{10} concentration of the AC2, AC7, and AC26 were used for the combination assay. Based on CI values obtained for these drug combinations, it is possible to determine the type of interaction. If CI value is <0.8 , then combinational drugs show synergism (i.e., its effect is better than the expected theoretical effect); when CI value lies between 0.8 and 1.2, combinational drugs show additive behavior i.e., it means the effect of combination will be equal to sum or product of each separate effect; and when CI value is more than 1.2, combinational drugs show antagonism i.e., its effect is worse than expected theoretical effect (48, 49).

Acute Toxicity Study of Acridone Derivatives

Animal study was conducted for acridone derivatives AC2, AC7, and AC26 alone and in combination with Temozolomide for Acute Oral Toxicity - Fixed Dose procedure. The Institutional Animal Ethics Committee bearing CPCSEA/IAEC/P-52/2016 was approved for undertaking the study. Acute oral toxicity was conducted on female albino Wistar rats for 8–12 weeks and were maintained at $25 \pm 2^\circ\text{C}$ in a conditioned room with 50–60% of humidity and free access to food and water was given. Rats were kept for fasting overnight (12 h) before dosing and weights were recorded periodically. Rats in two groups were given acridone derivatives alone at a dose of 300 and 2,000 mg, rats in two groups were given a combination of Temozolomide : acridone derivatives at dose of 10:1 mg/kg and 15:1.5 mg/kg body weight and one group was kept as control. Dose of Temozolomide was taken as per previously published article (50). Compounds alone and combination were suspended in 2.0% of Tween 80 in normal saline and control group was taken for vehicle only. After administering the compound, food was not provided for 3 h. All the rats were monitored periodically for 1 h upto 12 h on the 1st day and thereafter twice in a day for mortality, behavioral changes, signs and symptoms of toxicity for 14 days. Individual

TABLE 1 | Physical data for acridone derivatives.

Compound name	Molecular formula	Molecular weight (g/mol)	Melting point (°C)	Log P	pKa
AC-26	C ₂₂ H ₁₇ N ₃ O ₃	371.39	246–250	3.17	6.517
AC-2	C ₂₃ H ₁₇ N ₃ O ₂	367.40	238–242	3.92	8.028
AC-7	C ₂₁ H ₁₄ ClN ₃ O ₂	375.81	129–134	4.54	9.234

TABLE 2 | Docking of acridones with P-gp and MRP.

S. No.	Target	Compound code	Binding affinity (kcal/mol)	Interactions at the active pocket	
				Type of interactions	Residue information
1	P-glycoprotein (P-gp)	AC26	−10.2	Hydrogen bonding Pi-Pi Stacking Pi-Alkyl	TYR A:310 TRP A:232; PHE A:343 ALA A:229
2		AC2	−10.1	Hydrogen bonding Pi-Pi Stacking Pi-Sulfur Pi-Alkyl	GLN A:725 TRP A:232; PHE A:343; PHE A:983 MET A:986 ALA A:229; ALA A:987
3		AC7	−9.5	Pi-Sigma Pi-Pi Stacking Pi-Alkyl	ILE A:306; PHE A:343 TRP A:232 ALA A:229; MET A:986
1	Multidrug Resistance Protein (MRP)	AC26	−7.5	Hydrogen bonding Pi-Anion Pi-Alkyl	SER A:796; SER A:828; SER A:830; TYR A:831 HIS A:872 LEU A:795; ALA A:800
2		AC2	−7.1	Van Der Waals Hydrogen bonding Pi-Pi Stacking Pi-Anion Pi-Sigma Pi-Alkyl	HIS A:801 SER A:830 ALA A:800 HIS A:872 ALA A:800 LEU A:795
3		AC7	−7.2	Hydrogen bonding Pi-Anion Pi-Alkyl	SER A:796; ALA A:800; SER A:828; TYR A:831 HIS A:872 LEU A:795

weights of rats were taken for all the 14 days and study was conducted twice for each dose.

RESULTS

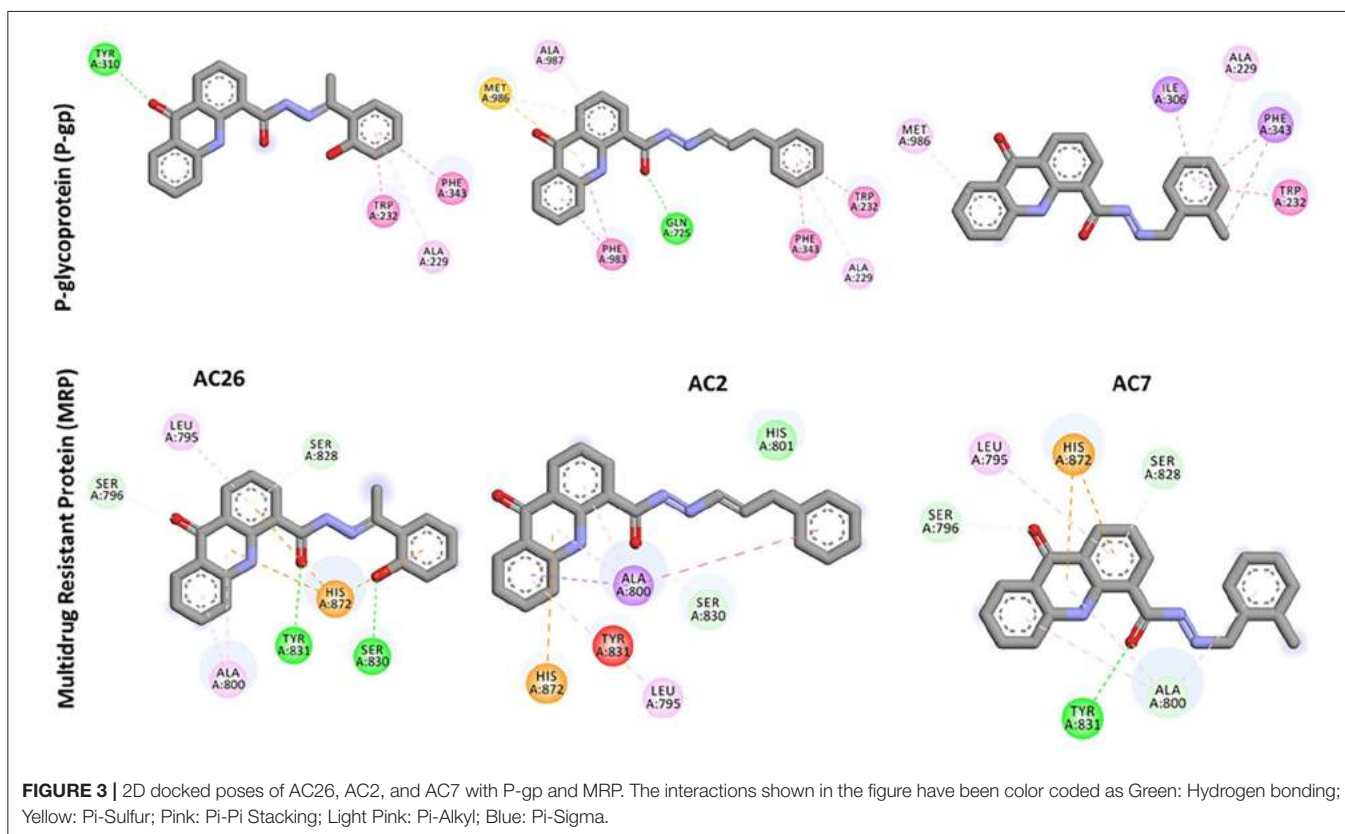
Characterization of the Drugs

Successful delivery of any anti-cancer drug across the blood brain barrier depends mainly on the lipophilicity of the drug (51). The Acridone derivatives (AC2, AC7, and AC26) are weak bases existing in both the uncharged (unprotonated) and charged (protonated) forms (52). Characteristics of novel Acridone derivatives like molecular weight, melting point, Log P (or partition co-efficient) and pKa have been evaluated and results of the same are shown in **Table 1**. It seems that the lipophilicity of the compounds contributes to the anti-neoplastic activity to some extent. The results from the Online BBB Predictor show that all the three Acridone derivatives AC2, AC7, and AC26 have blood brain barrier permeability with BBB scores 0.238, 0.236, and 0.144, respectively. On the other hand, the tool predicts TMZ to have a BBB score of 0.034 (**Supplementary Figure 3**) (17).

Molecular Docking of Acridones With P-gp, MRP, and MGMT

In order to determine the binding affinities of these Acridone derivatives with drug resistant causing proteins P-gp, MRP, and MGMT, Molecular docking studies have been performed. Acridone derivatives are very much recognized as substrates of efflux pumps P-gp and MRP proteins with potential DNA intercalating property for multidrug resistant (MDR) cancers (52). Acridones being substrates or inhibitors of these efflux pumps enhances the concentration of drugs like Temozolomide inside the cell, which can lead to cell death. Also the combination of anticancer drugs with acridone derivatives can modulate or prevent the cause of drug resistance (53). Same hypothesis might have improved the cytotoxicity against drug resistant cancer cells in SRB assay. To further verify the experimental results and predict the binding affinity of acridone derivatives, molecular docking was performed against P-gp, MRP, and MGMT target proteins.

Docking of Acridones with P-gp has identified AC26 with highest binding affinity of −10.2 kcal/mol (**Table 2**). Complex was found stabilized by hydrogen bonding with TYR A:310;



Pi-Pi Stacking with TYR A:232, PHE A:343, and Pi-Alkyl interactions with ALA A:229 residues (**Figure 3**). The AC2 has demonstrated binding affinity of -10.1 kcal/mol by hydrogen bonding with GLN A:725, Pi-Pi Stacking with TRP A:232; PHE A:343; PHE A:983, Pi-Sulfur with MET A:986, and Pi-Alkyl interactions with ALA A:229, ALA A:987 residues. Most of the interactions were found common with AC26 unlike hydrogen bonding and Pi-Sulfur interacting residues. Surprisingly, AC7 was found stabilized with -9.5 kcal/mol without hydrogen bonding interactions. All the three compounds have interacted with different binding patterns and interactions with P-gp. Complex structure and size of active pocket might have led to different interactions.

Similarly, docking of Acridones with MRP has identified AC26 with binding affinity of -7.5 kcal/mol (**Table 2**). Interestingly, complex was found stabilized by hydrogen bonding with four residues [i.e., SER A:796; SER A:828; SER A:830; TYR A:831, Pi-anion with HIS A:872, and Pi-alkyl interactions with LEU A:795; ALA A:800 (**Figure 3**)]. AC2 and AC7 have exhibited -7.1 and -7.2 kcal/mol. Only AC2 has formed Van der Waals interaction with HIS A:801. Pi-alkyl interaction with LEU A:795 and Pi-anion with HIS A:872 was found common with all the three compounds. AC7 also demonstrated four hydrogen bonding interactions. Unlike AC26 and AC2 hydrogen bonding with SER A:830 was found missing with AC7. This particular interaction might have reduced the binding affinity to -7.2 kcal/mol. All the

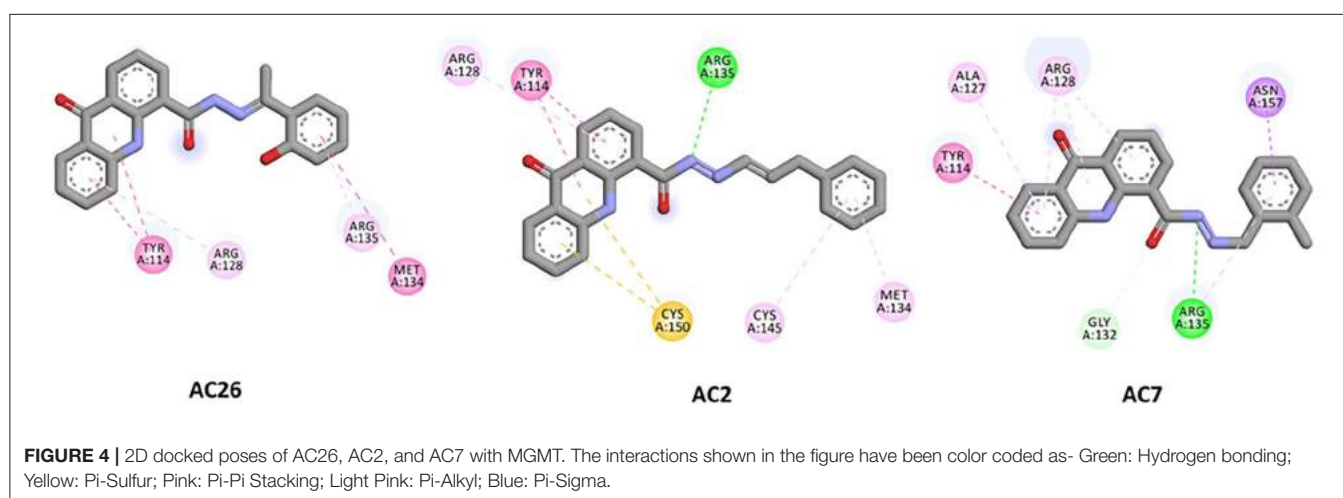
three compounds have exhibited a good number of interactions at the active pocket of MRP.

Finally, docking of Acridones with MGMT has revealed interesting insights. The AC2 and AC26 were found stabilized with good binding affinity of -7.8 and -7.7 kcal/mol (**Table 3**). Also AC2 has demonstrated hydrogen bonding with ARG A:135, Pi-Pi stacking with TYR A:114, Pi-alkyl with ARG A:128; MET A:134; CYS A:145, and Pi-sulfur with CYS A:150. Only AC2 has formed Pi-sulfur interaction among the three compounds (**Figure 4**). AC7 has also exhibited hydrogen bonding interactions with ARG A:135; GLY A:132, and other Pi-Pi stacking, Pi-alkyl, Pi-sigma interactions at the active pocket of MGMT. Also, only compounds formed Pi-sigma interactions. Surprisingly, AC26 was found stabilized by Pi-Pi Stacking with TYR A:114; MET A:134 and Pi-alkyl with ARG A:128; ARG A:135 interactions. Compound has shown -7.7 kcal/mol binding affinity with no hydrogen bonding interactions. Pi-Pi stacking with TYR A:114 and Pi-alkyl with ARG A:128 were found common with all the three compounds.

Overall, docking calculations revealed that acridones have good binding affinity to P-gp and MGMT. Compounds have exhibited lesser binding affinity with MRP compared to other targets. Particularly, AC26 has demonstrated highest binding affinity with all the three target proteins. Molecular docking studies of acridones against P-gp target has revealed that compounds have the ability to modulate or reverse

TABLE 3 | Docking of acridones with MGMT.

S. No.	Compound code	Binding affinity (kcal/mol)	Interactions at the active pocket	
			Type of interactions	Residue information
1	AC26	-7.7	Pi-Pi Stacking Pi-Alkyl	TYR A:114; MET A:134 ARG A:128; ARG A:135
2	AC2	-7.8	Hydrogen bonding Pi-Pi Stacking Pi-Alkyl Pi-Sulfur	ARG A:135 TYR A:114 ARG A:128; MET A:134; CYS A:145 CYS A:150
3	AC7	-7.1	Hydrogen bonding Pi-Pi Stacking Pi-Alkyl Pi-Sigma	ARG A:135; GLY A:132 TYR A:114 ALA A:127; ARG A:128 ASN A:157

**TABLE 4** | Dose-effect relationships of TMZ and AC in Glioma cell lines[#].

Name of cell lines	Vero cell Line	U-87/WT			T-98/TMZRES	
		CC ₅₀ (μM)	IC ₅₀ (μM)	SI	IC ₅₀ (μM)	SI
TMZ	482	23.33 ± 7.57	20.66	190 ± 0.16	2.53	
AC26	66.08	0.9 ± 0.1	73.42	0.76 ± 0.053	86.94	
AC2	56.21	1.53 ± 0.85	36.73	1.53 ± 0.25	36.73	
AC7	48.17	5.67 ± 0.58	8.49	1.05 ± 0.18	45.87	

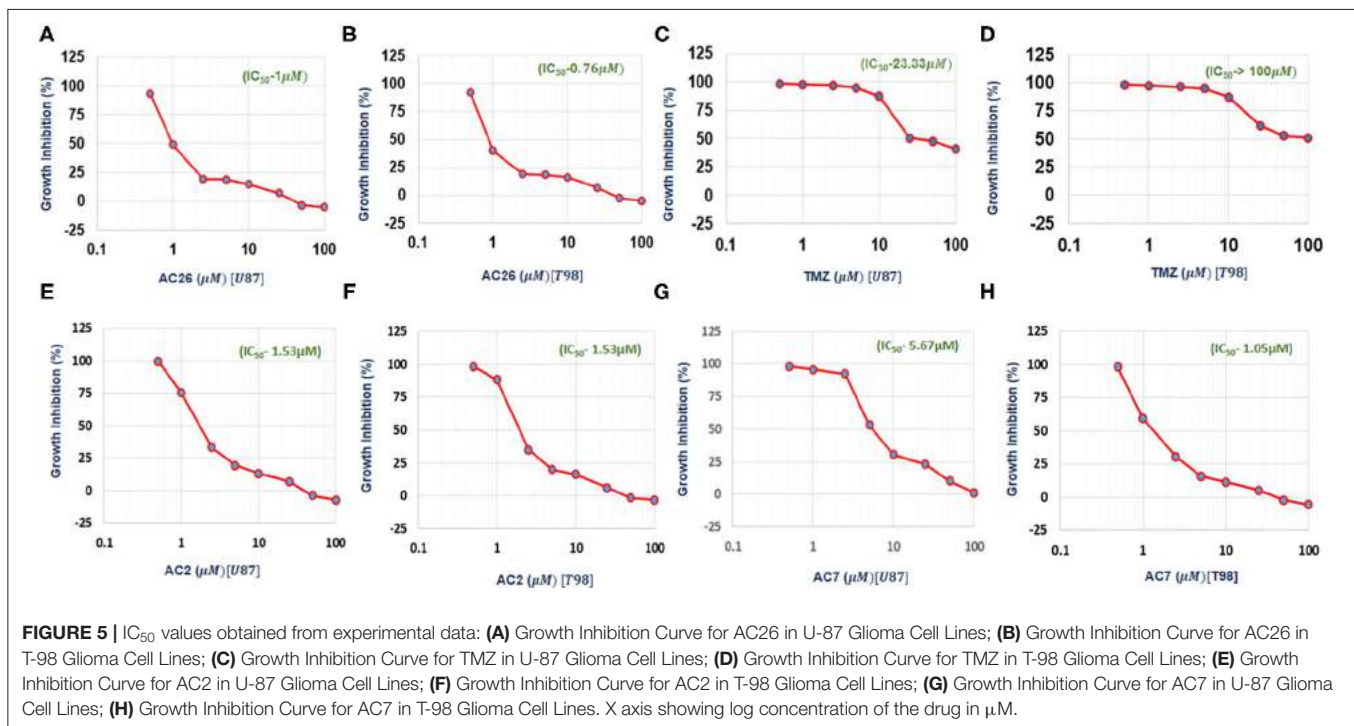
[#]Selectivity Index (SI) = CC₅₀ of Vero cell line / IC₅₀ of Cancer cell line after 72 h of TMZ or AC.

[#]IC₅₀ values are represented in the form of Mean ± Standard Deviations for both the cell lines.

drug resistance mediated by efflux pumps like P-gp with good binding affinity. Docking studies have once again supported that Acridones are known to modulate MDR as P-gp substrate/inhibitor. Study suggests that Acridone derivatives can be further optimized for the design of safe and potent MGMT inhibitors.

Sulforhodamine B Assay for Individual Drugs

The cell growth inhibition potential of the Acridone derivatives on the drug sensitive and drug resistant Glioma is studied using the Sulforhodamine B (SRB) assay. Here the IC₅₀ (μM) values for the drugs AC2, AC7, AC26, and TMZ were determined and tabulated in **Table 4**. We have found out IC₅₀ values of acridone derivatives using SRB Assay and have confirmed safety dose by conducting acute toxicity studies on albino Wistar rats. However, the reported IC₅₀ values of acridone derivatives are based on *in vitro* study only and is yet to be tested for clinical application. Also, this experimental data was used to plot growth inhibition curves for AC2, AC7, AC26, and TMZ in U-87 drug sensitive Glioma cell lines and T-98 TMZ resistant Glioma cell lines (**Figure 5**). All the four compounds AC26, AC2, AC7, and TMZ were found active. Here we observe that the compound AC26 containing substituent like 1-(2-hydroxyphenyl) ethylidene have shown better results in both drug resistant and sensitive types of Glioma cell lines (U-87 and T-98). Results show that this substitution is responsible for high anti-proliferative activity. Also, substitution of -Cl in phenyl group in AC7 was found to overcome drug resistance to a larger extent in comparison to



having no substitution in phenyl group in AC2. One important aspect related to AC7 is that the presence of $-\text{Cl}$ group in the phenyl group is also one of the main reasons for the drug not being effective on U-87. From this we observe that in comparison to other Acridone derivatives, AC26 showed highest cytotoxicity when compared with AC7 and AC2, respectively.

Selectivity Index

Selectivity indices (SI) of all the four drugs, were obtained from the experiments, have been tabulated (Table 4). A drug with high SI is able to act against cancer cells effectively at concentrations below its cytotoxic concentration. The SI data shows that AC26 is more selective toward T-98 (drug resistant cancer cell line) and U-87 (drug sensitive cancer cell lines) than its selectivity toward Vero cell lines. These results indicate the supremacy of AC26 as a better choice of drug for treatment of cancer that would be effective both on T-98 and U-87 drug lines.

Numerical Simulations and Parameter Estimation (Without Drug)

In order to mimic the experimental observations *in silico*, first the Glioma cell growth model was developed without the administration of any drug (Equations 1–4). The unknown values of 10 parameters were estimated by MCMC method. Sensitive parameters regulating the growth of the variables C , C_R , and C_S were varied within biologically feasible ranges. Time course cell growth experimental data of 96 h for Glioma, U-87 and T-98 cells lines were used to fit the model parameters (red circles, Figure 6) (29–31). It was assumed that the prior distribution is normal. The MCMC simulation was run for

500,000 iterations to assure convergence of the chain. The final parameter values estimated by MCMC algorithm for the mathematical model have been listed in Supplementary Table 2. The simulated predictive plots, with the estimated parameters, obtained for cancer cells C (Figure 6A), Cancer Resistant C_R (Figure 6B), and Cancer Sensitive cells C_S (Figure 6C) show a good fit with the experimental data points (indicated with red circles) and mostly lie within the 95% confidence interval. This ensures the validity of the parameter chosen and the mathematical model for closely mimicking the *in vitro* experiments.

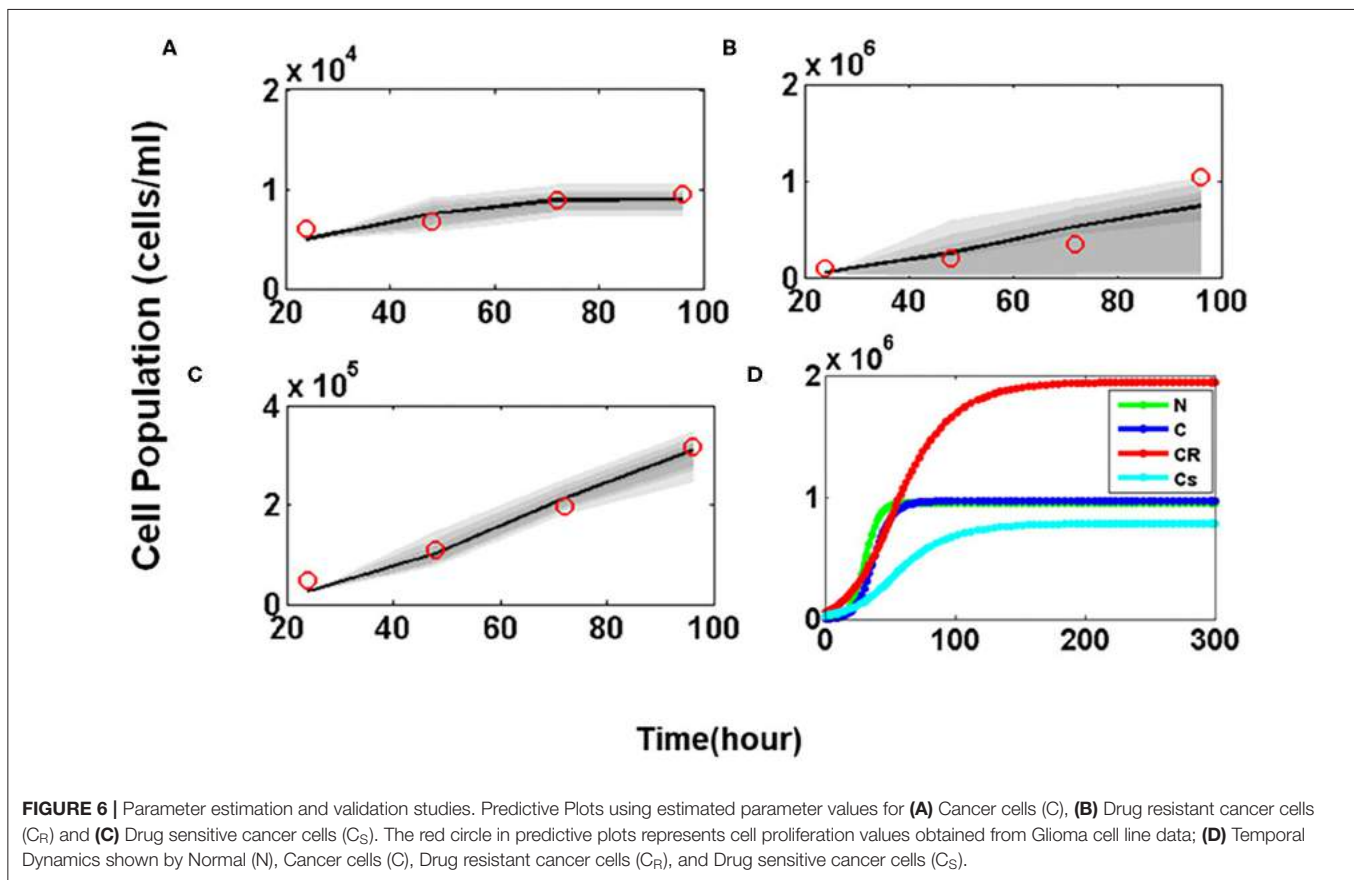
The model was then simulated for 300 h to ensure that all four variables representing the tumor sub-populations reach steady state. Figure 6D shows the temporal dynamics of all four of cellular sub-populations. Here it is observed that at steady state the C_R population reaches a much higher concentration as compared to the C_S cells which makes the tumor resistant to therapeutic interventions.

Numerical Simulations With TMZ and the Combinations

After successful validation of the tumor cell growth model, it is now used to test the cellular inhibition effect of the drugs individually and then in combinations. Experimental data from the SRB assay was used to calibrate and validate the model outcome.

Administration of Individual Drugs

Numerical simulations were performed to study the growth inhibition of the drug sensitive C_S and drug resistant C_R cancer



cells by varying the doses of TMZ, AC26, AC2, and AC7 individually. The **Figures 7A,B** obtained shows relative tumor growth (%) with the changing concentration of TMZ. Here, it can be observed that both the simulated data (cyan) and experimental data (royal blue) closely fit. The spearman's rank-order correlation R^2 values for both drug resistant cancer cells (T-98) and drug sensitive cancer cells (U-87) indicating very strong correlation between both the experimental data and simulated results. The IC_{50} values obtained from the simulations also match with the experimental data pretty well.

Similarly, the growth inhibition effect of the Acridone derivatives AC26 (**Figures 7C,D**), AC2 (**Figures 7E,F**), and AC7 (**Figures 7G,H**) were also studied on the drug resistant C_R and drug sensitive C_S cancer cells. The simulation results show a good fit of experimental data for all the three drugs ($R^2 > 0.98$).

Administration of Combinatorial Drugs—TMZ With Acridone Derivative

Various doses of combinatorial drugs D_1 -TMZ and D_2 -Acridone derivatives (AC26/AC2/AC7) were administered to the model and the simulations were run until steady state was reached. The dose response matrix showing the relative growth percentage (along Z-axis) of drug resistant cancer cells and drug sensitive cancer cells have been depicted through surface plots (**Figure 8**) for 10,000 dosage combinations of each pair of TMZ and Acridone derivative (AC26/AC2/AC7). The **Figure 8A** shows

that when dose of D_1 (TMZ) is 0, tumor growth is maximum (represented by red color), but as dose is increased slowly from 0 to 200, the TMZ inhibits tumor growth reduction by 50%. Here we also observe that, alongside TMZ, as dose of D_2 (i.e., AC26) is increased, drastic fall in the number of drug resistant cancer cells is observed (more than 20% tumor growth reduction). While comparing the efficacy of both the drugs, it was observed that AC26 was more successful in inhibiting drug resistant cancer cell growth at lower concentration than TMZ. Conversely, **Figure 8B** shows that increase in the dose of TMZ results in sudden fall in concentration of drug sensitive cancer cells (40% tumor growth reduction) whereas increase in the dose of AC26 leads to moderate reduction in drug sensitive cancer population (10–20% of tumor growth reduction).

Similarly, the dosage of the drugs TMZ and AC2 were varied from 0 to 200 and 0 to 2, respectively (**Figures 8C,D**), while in the third drug combination study, TMZ and AC7 were varied from 0 to 200 and 0 to 6, respectively (**Figures 8E,F**). In both the cases we observed a better growth inhibition of the resistant tumor cells on administration of the Acridone derivative AC2 and AC7 when combined with TMZ as opposed to when they were administered individually. From the dose response matrices, the fold change in the IC_{50} values of TMZ and the Acridone derivatives when used in combinations as opposed to when they are administered individually were also calculated (**Table 6**). Here we observe that when the drugs are used in combination, the IC_{50} value of TMZ

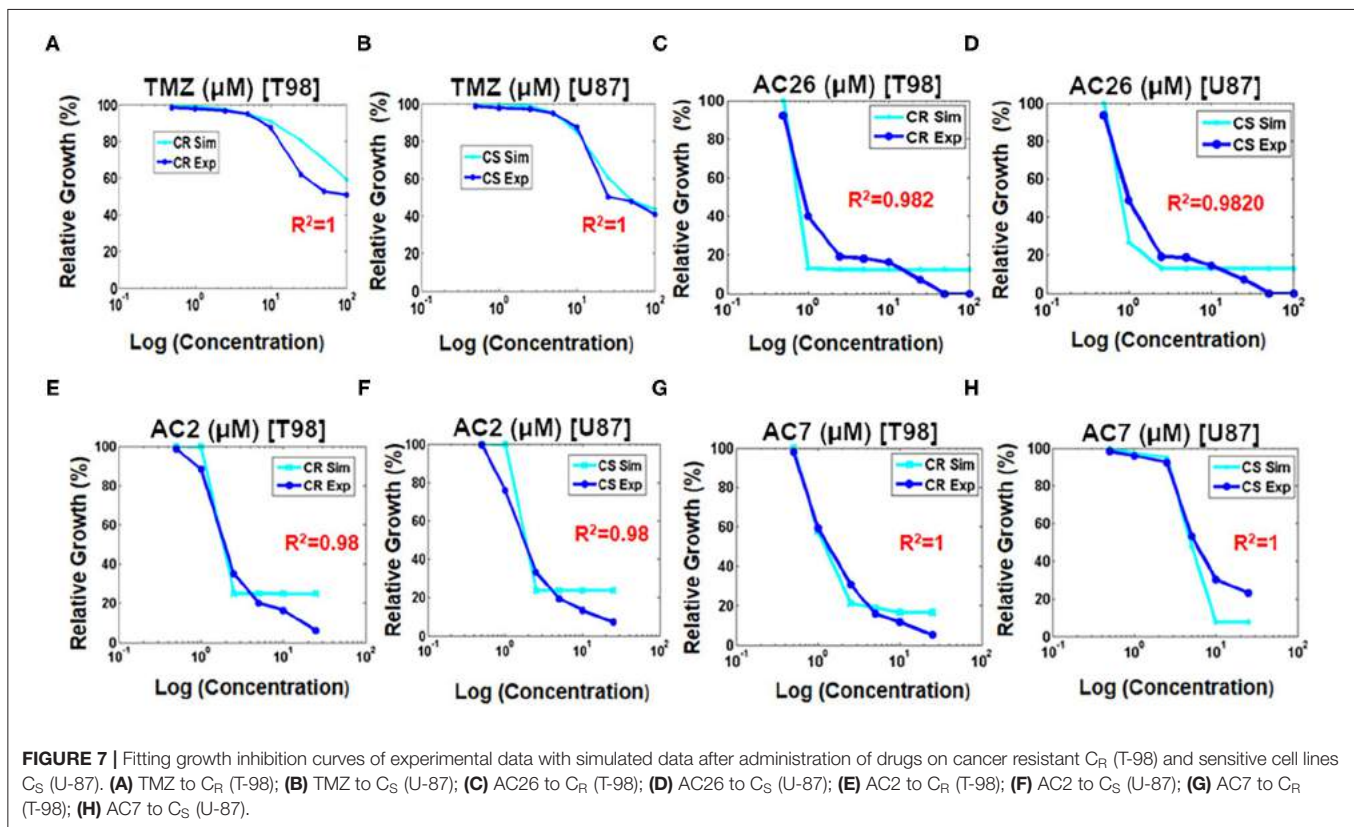


FIGURE 7 | Fitting growth inhibition curves of experimental data with simulated data after administration of drugs on cancer resistant C_R (T-98) and sensitive cell lines C_S (U-87). (A) TMZ to C_R (T-98); (B) TMZ to C_S (U-87); (C) AC26 to C_R (T-98); (D) AC26 to C_S (U-87); (E) AC2 to C_R (T-98); (F) AC2 to C_S (U-87); (G) AC7 to C_R (T-98); (H) AC7 to C_S (U-87).

and Acridone derivatives reduces substantially. This observation throws light on the possibility of existence of synergistic effects of the drugs when used in combination with TMZ in the drug resistant cancer cells.

In order to determine the parameters that govern this dose response dynamics of the C_R and C_S cells, to the administration of the TMZ and Acridone derivatives, sensitivity analysis was performed. Here it was observed that the C_R cells were sensitive to 13 out of 29 parameter values ($p < 0.05$), while the C_S cells were sensitive to 12 parameters ($p < 0.05$) (Supplementary Figure 2). However, the Partial Rank Correlation Coefficient calculated for the parameters show that while the C_S cells are more sensitive ($|\text{PRCC}| > 0.5$) to the parameters governing cellular growth such as $\alpha_N, \alpha_{CS}, \alpha_{CR}, K$ (carrying capacity of the tumor), and the efficacy of TMZ ε_{\max}^{D1s} the parameters of C_R cells with $|\text{PRCC}| > 0.5$ comprises the dosage of Acridone derivative (D_2), IC_{50}^{D2r} and the efficacy of TMZ on the resistant cells ε_{\max}^{D1r} . The outcome of the analysis show that there is a strong correlation of the dosage of the Acridone derivative (D_2) with response of the C_R cells which further motivates to determine the dosage combinations where synergy of the two drugs can be obtained for maximal inhibition of the drug resistant Glioma cells.

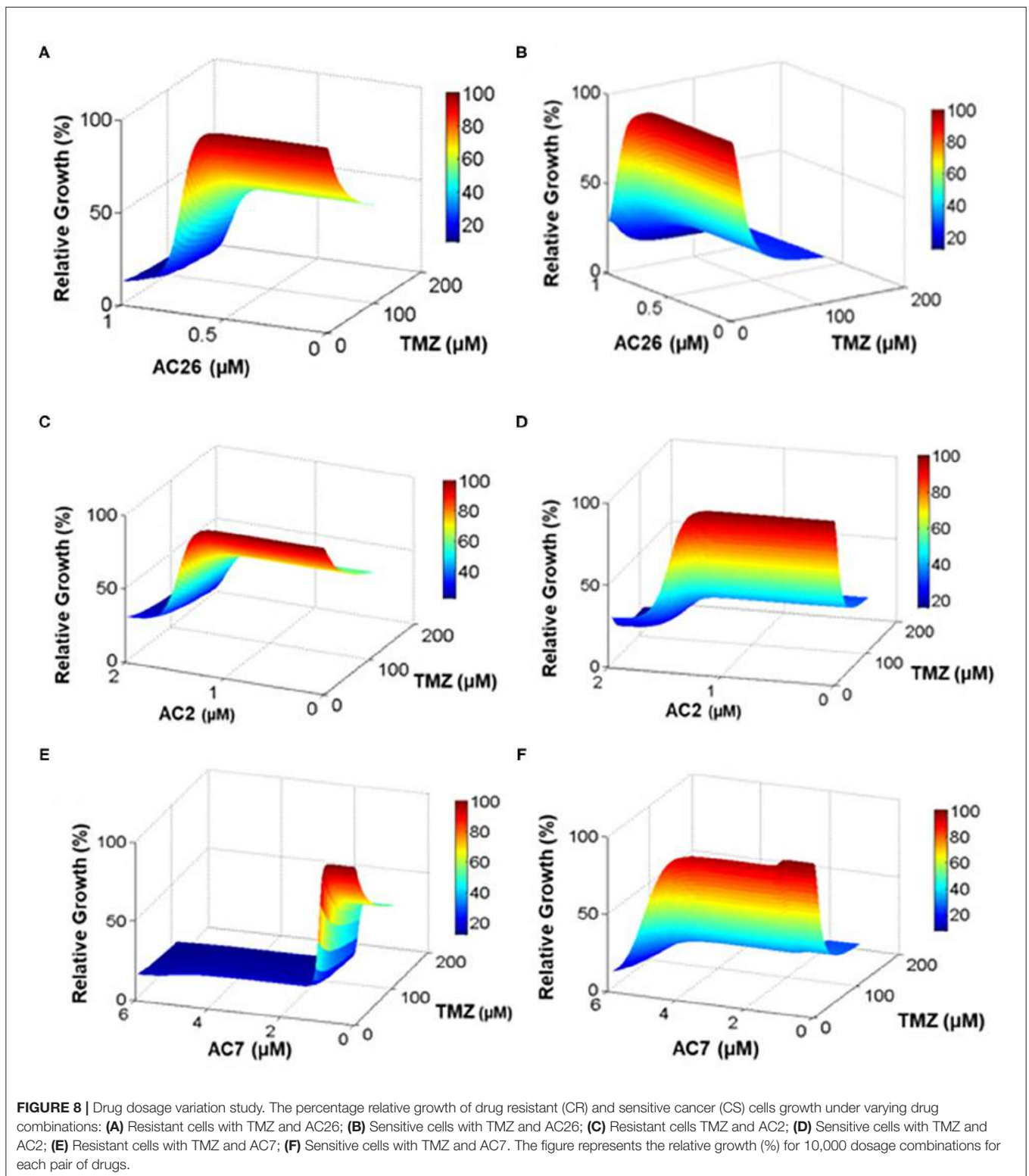
Drug Synergy Estimation

In order to determine the dosage combinations of the drug pairs (TMZ and Acridone derivatives) that show synergism for the drug resistant cells, the dose response matrix (Figures 8A,C,E) for the resistant cells (C_R) for all the 10,000 dosage combinations

of each of the three drug pairs (as obtained from the mathematical model) was tested for synergy. The synergy scores (SC) have been calculated based on the observed growth inhibition data obtained from the simulation (Figures 8A,C,E) with each drug pair for the resistant cell line using the Bliss Independence method. The corresponding synergy scores (SC) calculated for each combination have been shown in Figures 9A–C. Here a positive SI score shows antagonism while a negative SC score shows synergy. The 10,000 combinations were simulated for each drug pair and we observed good synergy of all the three Acridone derivatives, AC2, AC7, and AC26 when combined with TMZ for a large number of dosage combinations. The Figure 9 also shows three points on the surface plots that denote the combination that have been tested using experiment for the validation of our simulation results.

Sulforhodamine B Assay for Combinatorial Drugs

With the leads obtained from the synergy estimations *in-silico*, CI was calculated for all the three combinatorial drug pairs using SRB assay (Table 5). The observations from the experiments showed that combinatorial drugs (TMZ+AC2, TMZ+AC7, and TMZ+AC26) showed synergistic inhibitory effect on growth of T-98 cell lines at low concentration (IC_{50}) with respective CIs of 0.4, 0.41, and 0.32 (marked with red on Figures 9A–C). It has to be noted here that the Synergy Score (SC) estimated using the Bliss Independence method



in silico (Figure 9) has been performed independently from the CI calculated from the SRB assay (Table 5). However, the result obtained from the SRB assay corroborates well within the *in-silico* findings and we observe synergy for the

same drug dosage combinations from both the *in silico* and experimental studies. Our results indicate that, TMZ+AC26 shows the highest synergistic inhibitory effect amongst all the combinations.

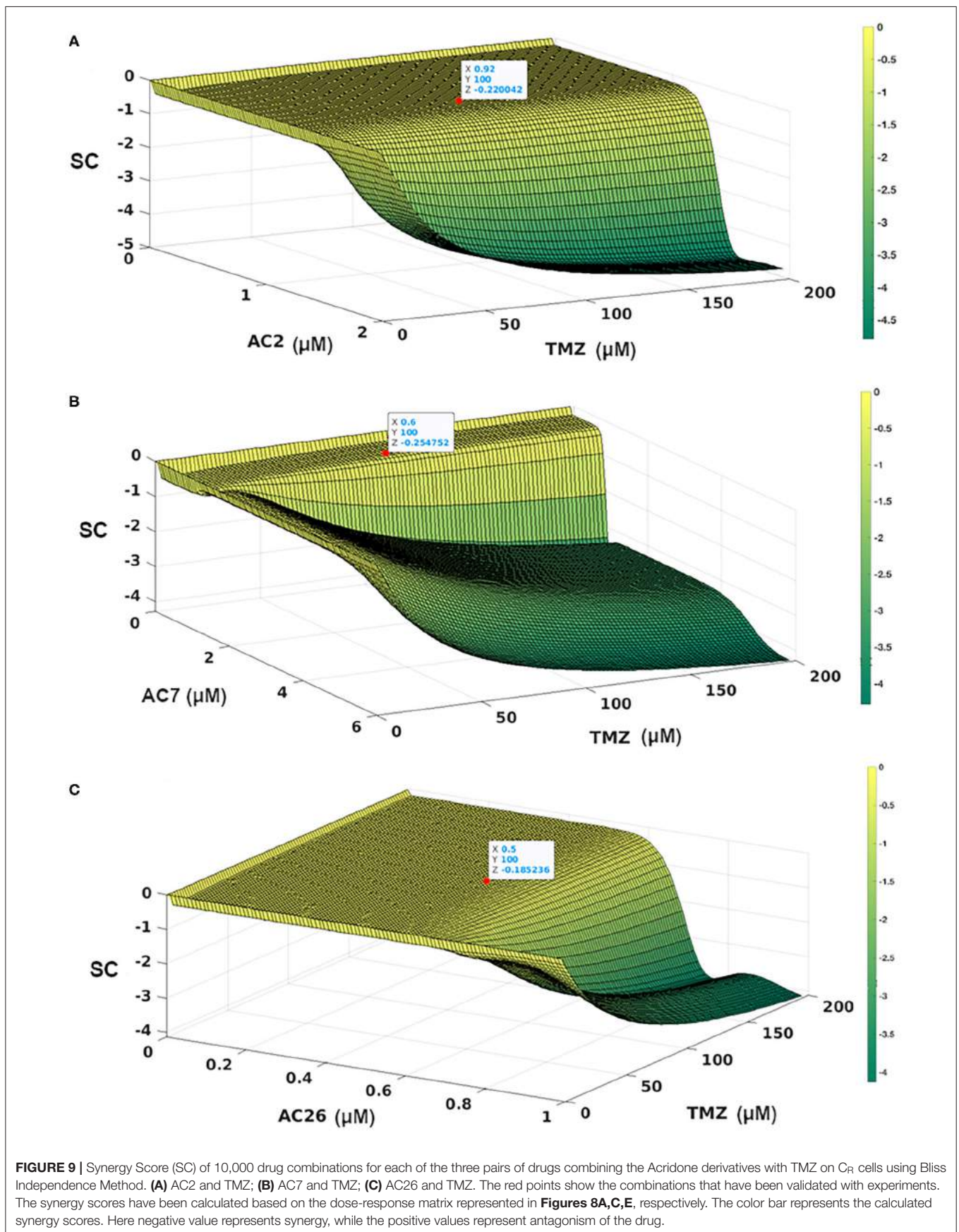


TABLE 5 | Dose-effect relationships of TMZ and AC in Glioma cell lines.

Drugs	CI (T-98/TMZRES) at IC ₅₀ (μM)
AC26 (IC ₁₀) + TMZ (100 μM)	0.32 ± 0.1
AC2 (IC ₁₀) + TMZ (100 μM)	0.4 ± 0.32
AC7 (IC ₁₀) + TMZ (100 μM)	0.41 ± 0.5

TABLE 6 | Fold change of the combinatorial drugs.

	Initial IC ₅₀	Final IC ₅₀	Fold change = final IC ₅₀ /initial IC ₅₀	% fold change [[final- initial]/initial]*100
TMZ + AC26				
TMZ	190	102.3	0.54	46.17
AC26	0.76	0.67	0.88	11.84
TMZ + AC7				
TMZ	190	46.2	0.24	75.68
AC7	1.05	0.96	0.91	8.5
TMZ + AC2				
TMZ	190	36.3	0.19	80.8
AC2	1.53	1.48	0.96	3.26

Acute Toxicity

Acridone derivatives AC2, AC7, and AC26 alone and in combination with Temozolomide were evaluated for oral toxicity by administering compounds suspended in normal saline with Tween 80 through oral route. Rats were kept for overnight night fasting before the day of dosing and for 3 h after dosing. On the 1st day of dosing, they were monitored periodically for every hour upto 12 h for mortality, clinical signs, and behavioral changes. And thereafter observed twice in a day for 14 days and body weight was recorded daily. No clinical sign of toxicity was observed during the period of 14 days under observation among the control and treated groups. The gain in body weight of rats was found to be normal in the control and treated groups (Supplementary Tables 4–6). Present study suggests that acridone derivatives alone (of 2,000 mg/kg) and in combination with Temozolomide (15:1.5 mg/kg) are safe for oral administration in single dose to albino Wistar rats of female.

DISCUSSION

Drug resistance and recurrence are one of the major issues associated in the treatment of Glioma. Better strategies are required to be adapted for enhancing the efficacy of the treatment of Glioma patients. Development of experimentally validated mathematical models is a promising approach to estimate the efficacy of a particular therapy and predicting what percentage of tumor growth inhibition can be achieved under a particular therapy. Given the current scenario, various trial and error experiments for drug screening and drug combination study with high synergy can be carried out at economical costs and rapid rate by employing mathematical models for designing effective cancer therapy.

In this study, we propose three novel drug combinations using TMZ and Acridone derivatives as well as show their efficacy of tumor inhibition over a wide range of dosage combinations using both *in-silico* and *in-vitro* studies. The simple four variable mathematical model developed in this study captures the formation and development of a malignant Glioma and its differentiation into drug resistant and sensitive cells. This model effectively captures the cellular dynamics of a growing tumor using simple mathematical assumptions and minimal unknown parameters. The model here has been parameterized to closely mimic the behavior of U-87 drug sensitive and T-98 drug resistant Glioma cells using experimental data (Figure 6). This has been useful in screening the effectiveness and growth inhibition potential of TMZ and Acridone derivatives individually and also in combination for a wide range of doses (Figures 7, 8). Sensitivity Analysis performed on the model parameters revealed that the inhibition of the drug resistant cells correlated highly with the dosage of the Acridone derivative (D₂) and the efficacy of TMZ on the drug resistant cells (ϵ_{max}^{D1r}) (Supplementary Figure 2). This analysis indicates a need to determine the optimum dosage of Acridone derivatives as well as the throws light on the necessity to enhance the effectiveness of the TMZ on the drug resistant cells which may be achieved through the inhibition of the resistance causing target proteins. Our analysis also reveals a significant fold change in the IC₅₀ value of the drugs when used individually as opposed to when they are used in combination (Table 6). This indicates the plausibility of synergy between the drugs TMZ and Acridone derivatives. Hence, the dose response matrix obtained from the model simulations of the drug resistant cells was used to analyse the existence of synergy between TMZ and Acridone derivatives for the treatment of resistant Glioma (Figure 9). Although a key limitation of this model may be that being a deterministic model, it is governed by fixed parameters values and thus fails to capture the immense heterogeneity of Cancer cells, the effect of angiogenesis, the influence surrounding immune cells and other micro-environmental factors explicitly, it may be noted that the parameters are estimated using experimental data that has helped in calibrating the model to closely mimic a real life scenario. Nevertheless, the outcomes from our *in-silico* mathematical model corroborate well with our experimental findings and provide insights into the entire synergy landscape of these drugs when used in combination for the treatment of resistant tumors.

The study of drug synergy revealed that the combination of TMZ and AC26 was found to show synergistic effect on the drug resistant Glioma cell lines (T-98) as well as drug sensitive Glioma cell lines (U-87) with CI 0.6. Here we also observe that 100 μM of TMZ and IC₁₀ of AC26 could effectively destroy drug sensitive cancer cells and IC₁₀ of TMZ and IC₅₀ of AC26 could exterminate drug resistant cancer cells. Thus, we put forward a treatment strategy i.e., use of combinatorial drugs 100 μM of TMZ and IC₁₀ of AC26, which is the lowest dose possible, in order to combat drug resistance in cancers. Furthermore, we also show that these doses showing synergistic effect are below the toxicity levels shown by the individual drugs. All these results have been experimentally validated to confirm effectiveness of these combinatorial drugs.

A close observation from the results obtained, reveal a comparison between the individual activity of acridone derivatives where we note that the relative efficacy of the drugs may vary as $AC26 > AC7 > AC2$. These results are also confirmed from the experimental observations of drug combinations, synergy and selectivity index calculations of the drugs (**Table 4**) which reinforce the efficacy of the drug combinations on drug resistant cancer cells in the order $TMZ + AC26 > TMZ + AC7 > TMZ + AC2$. Acute toxicity studies for 14 days as per OECD guidelines have indicated that all the acridone derivatives alone and in combination with Temozolomide were found safe in single dose to female albino Wistar rats. Additionally, using *in silico* prediction tool, it has been observed that all the Acridone derivatives show BBB permeability higher than TMZ which gives hope for its clinical efficacy (**Supplementary Figure 3**). However, to establish the clinical usefulness of the proposed combination, further *in vitro* and *in vivo* assays are currently being undertaken for the determination of other pharmacokinetic parameters.

The molecular docking study shows that the synergistic effect of combining TMZ and Acridone derivatives might be due to inhibitory action exerted by the acridone derivatives on the resistant cells due to interactions with P-gp, MRP, and MGMT proteins that contributes to the development of drug resistance. Through the *in silico* studies it has been observed that the acridone derivatives show particularly good binding affinity to P-gp and MGMT compared to MRP. Particularly, AC26 have demonstrated highest binding affinity to all three targets P-gp, MRP, and MGMT and observed same with experimental findings. Study suggests that acridone derivatives can be further optimized for the design of safe and potent MGMT inhibitors. Good interactions at the active pocket and binding affinity of AC26 with efflux pumps and MGMT might be responsible for synergistic effect against resistant Glioma cells in combination with TMZ. Through our previous studies we have demonstrated that Acridone derivatives have DNA intercalating property which implicates that these derivatives might also be effective in killing resistant glioblastoma through MGMT-independent mechanisms as well (15, 54, 55). Whether these acridone derivatives also have an effect on the expression levels of P-gp, MRP, and MGMT proteins is currently under investigation and will be reported in another study. It is to be mentioned here that, although, in this study we have only reported the experimental verification of one dosage per drug combinations (**Table 5**), using our *in silico* analysis, we have been able to show the entire synergy landscape for each drug combination pair that can be tested *in vivo* using orthotopic xenografts for establishing its clinical efficacy. Along with the novel drug combinations reported in this study, we also propose a validated mathematical model, albeit simple, and *in-silico* approach to test the efficacy and synergy of novel drugs combinations in future.

CONCLUSION

The novel drug combinations, involving TMZ and Acridone derivatives, proposed in this study provides new insights for

the treatment of drug resistant Gliomas. The effective dosages of each of these combinations suggested in our study have been supported using both our simulation outcomes as well as experimental data. For this, the mathematical model developed here throws light on the effectiveness of each of these dosage combinations in terms of tumor reduction for wide range dosages that is not possible to screen experimentally. This is an extremely important step for the estimation of the synergistic effect of the drug pairs. Hence, it may be mentioned here that, albeit the simplicity of the model, which can be further modified in future with the inclusion of new variables, parameters and stochasticity to capture the tumor heterogeneity, the model provides useful insights in the tumor development and drug effectiveness that have been corroborated experimentally in its present form. Thus, not only does the experimental finding and docking studies of this work provide new hopes for the treatment of drug resistant Glioma, but the mathematical model developed in this study will be an invaluable tool to estimate dosage and effectiveness of other drugs for Glioma therapy in future.

DATA AVAILABILITY STATEMENT

The original contributions presented in the study are included in the article/**Supplementary Material**, further inquiries can be directed to the corresponding author/s.

ETHICS STATEMENT

The animal study was reviewed and approved by The Institutional Animal Ethics Committee bearing CPCSEA/IAEC/P-52/2016 approved for undertaking the study.

AUTHOR CONTRIBUTIONS

MC, PG, and RS developed the mathematical model and performed the *in-silico* analysis of drug synergy. MM performed the molecular docking studies. YM and GP contributed toward experimental validation. MC, PG, and MM wrote the manuscript. RS, YM, and GP reviewed the manuscript and supervised the work. All authors contributed to the article and approved the submitted version.

FUNDING

Funding was received by Dr. YM from Department of Health Research, Govt. of India (grant no. F. No. V. 25011/547-HRD/2016-HR). We thank SERB, Department of Science and technology, Govt. of India (file no. EMR/2016/000516), for providing financial support to RS. PG acknowledges Council of Scientific & Industrial Research (CSIR) for the Senior Research Fellowship. The present study was funded by the Science Engineering and Research Board, Department of Science and Technology, Government of India (CRG/2019/001452).

ACKNOWLEDGMENTS

The authors thank Dr. Noopur Sinha and Ms. Rupa Bhowmick for their useful suggestions, discussions, and timely help.

SUPPLEMENTARY MATERIAL

The Supplementary Material for this article can be found online at: <https://www.frontiersin.org/articles/10.3389/fonc.2021.625899/full#supplementary-material>

Supplementary Text 1 | This supplementary material contains Target Proteins and Attributes of grid (**Supplementary Table 1**); List of parameter values (**Supplementary Table 2**); List of Initial Values of Model Variables (**Supplementary Table 3**); Toxicity Study Data of the Compound AC2 (**Supplementary Table 4**); Toxicity Study Data of the Compound AC7 (**Supplementary Table 5**); Toxicity Study Data of the Compound AC26

(**Supplementary Table 6**); Toxicity Study Data of Temozolomide with Compound AC2 (**Supplementary Table 7**); Toxicity Study Data of Temozolomide with Compound AC7 (**Supplementary Table 8**); Toxicity Study Data of Temozolomide with Compound AC26 (**Supplementary Table 9**); Histogram plots and Trace plots for Parameter Estimation using MCMC-DRAM algorithm (**Supplementary Figure 1**); Sensitivity Analysis of model parameters using LHS-PRCC (**Supplementary Figure 2**); Blood Brain Barrier Permeability results for the Acridone derivatives and TMZ (**Supplementary Figure 3**).

Supplementary Text 2 | The codes developed for the simulation of the mathematical model have been provided. It includes the codes for (a) Parameter Estimation using the MCMC DRAM toolbox in Matlab (Scripts 1–4); (b) Determination of IC50 of TMZ and Acridone derivations from dose response curves of each drug individually in Matlab (Scripts 5 and 6); (c) Dose response matrix for each drug combinations from parameter variation studies in Matlab (Scripts 7 and 8); (d) Synergy Index calculation using Bliss Independence using SynergyFinder package in R (Script 9); (e) Sensitivity Analysis using LHS PRCC method in Matlab (Scripts 10–12).

REFERENCES

- Alfarouk KO, Stock C-M, Taylor S, Walsh M, Muddathir AK, Verduzco D, et al. Resistance to cancer chemotherapy: failure in drug response from ADME to P-gp. *Cancer Cell Int.* (2015) 15:71. doi: 10.1186/s12935-015-0221-1
- Zaal EA, Berkers CR. The influence of metabolism on drug response in cancer. *Front Oncol.* (2018) 8:500. doi: 10.3389/fonc.2018.00500
- Mansoori B, Mohammadi A, Davudian S, Shirjang S, Baradaran B. The different mechanisms of cancer drug resistance: a brief review. *Tabriz Univ Med Sci.* (2017) 7:339–48. doi: 10.15171/apb.2017.041
- National Cancer Institute. *Drugs Approved for Brain Tumors*. National Cancer Institute. Available online at: <https://www.cancer.gov/about-cancer/treatment/drugs/brain> (accessed December 17, 2020).
- Hanif E, Muzaffar K, Perveen K, Malhi SM, Simjee SU. Glioblastoma multiforme: a review of its epidemiology and pathogenesis through clinical presentation and treatment. *Asian Pacific J Cancer Prev.* (2017) 18:3–9. doi: 10.22034/APJCP.2017.18.1.3
- Strobel H, Baisch T, Fitzel R, Schilberg K, Siegelin MD, Karpel-Massler G, et al. Temozolomide and other alkylating agents in glioblastoma therapy. *Biomedicines.* (2019) 7:69. doi: 10.3390/biomedicines7030069
- McGirt MJ, Than KD, Weingart JD, Chaichana KL, Attenello FJ, Olivi A, et al. Gliadel (BCNU) wafer plus concomitant temozolomide therapy after primary resection of glioblastoma multiforme. *J Neurosurg.* (2009) 110:583–8. doi: 10.3171/2008.5.17557
- Fan C-H, Liu W-L, Cao H, Wen C, Chen L, Jiang G. O6-methylguanine DNA methyltransferase as a promising target for the treatment of temozolomide-resistant gliomas. *Cell Death Dis.* (2013) 4:e876. doi: 10.1038/cddis.2013.388
- Jiapaer S, Furuta T, Tanaka S, Kitabayashi T, Nakada M. Potential strategies overcoming the temozolomide resistance for glioblastoma. *Neurol Med Chir.* (2018) 58:405–21. doi: 10.2176/nmc.ra.2018-0141
- Chamberlain MC. Temozolomide: therapeutic limitations in the treatment of adult high-grade gliomas. *Expert Rev Neurother.* (2010) 10:1537–44. doi: 10.1586/ern.10.32
- Zhou Q, Gallo JM. Differential effect of sunitinib on the distribution of temozolomide in an orthotopic glioma model. *Neuro Oncol.* (2009) 11:301–10. doi: 10.1215/15228517-2008-088
- Yergeri M, Murahari M, Peters. GJ. *Design and synthesis of novel acridone based derivatives as multidrug resistant modifiers and their membrane perturbing potency in cancer cells*. Indian Patent No: 201822004910. Mumbai: Indian Patent Office.
- Murahari M, Prakash KV, Peters GJ, Mayur YC. Acridone-pyrimidine hybrids-design, synthesis, cytotoxicity studies in resistant and sensitive cancer cells and molecular docking studies. *Eur J Med Chem.* (2017) 139:961–81. doi: 10.1016/j.ejmech.2017.08.023
- Murahari M, Kharkar PS, Lonikar N, Mayur YC. Design, synthesis, biological evaluation, molecular docking and QSAR studies of 2,4-dimethylacridones as anticancer agents. *Eur J Med Chem.* (2017) 130:154–70. doi: 10.1016/j.ejmech.2017.02.022
- (**Supplementary Table 6**); Toxicity Study Data of Temozolomide with Compound AC2 (**Supplementary Table 7**); Toxicity Study Data of Temozolomide with Compound AC7 (**Supplementary Table 8**); Toxicity Study Data of Temozolomide with Compound AC26 (**Supplementary Table 9**); Histogram plots and Trace plots for Parameter Estimation using MCMC-DRAM algorithm (**Supplementary Figure 1**); Sensitivity Analysis of model parameters using LHS-PRCC (**Supplementary Figure 2**); Blood Brain Barrier Permeability results for the Acridone derivatives and TMZ (**Supplementary Figure 3**).
- Rajendra Prasad VVS, Peters GJ, Lemos C, Kathmann I, Mayur YC. Cytotoxicity studies of some novel fluoro acridone derivatives against sensitive and resistant cancer cell lines and their mechanistic studies. *Eur J Pharm Sci.* (2011) 43:217–24. doi: 10.1016/j.ejps.2011.04.010
- Tetko IV, Gasteiger J, Todeschini R, Mauri A, Livingstone D, Ertl P, et al. Virtual computational chemistry laboratory – design and description. *J Comput Aided Mol Des.* (2005) 19:453–63. doi: 10.1007/s10822-005-8694-y
- Liu H, Wang L, Lv M, Pei R, Li P, Pei Z, et al. AlzPlatform: an Alzheimer's disease domain-specific chemogenomics knowledgebase for polypharmacology and target identification research. *J Chem Inf Model.* (2014) 54:1050–60. doi: 10.1021/ci500004h
- Berman HM. The protein data bank. *Nucl Acids Res.* (2000) 28:235–42. doi: 10.1093/nar/28.1.235
- Discovery Studio Visualizer. *Dassault Systèmes BIOVIA*. San Diego, CA: Discovery Studio Visualizer (2020).
- Trott O, Olson AJ. AutoDock Vina: improving the speed and accuracy of docking with a new scoring function, efficient optimization, and multithreading. *J Comput Chem.* (2009) 31:21334. doi: 10.1002/jcc.21334
- Hanwell MD, Curtis DE, Lonie DC, Vandermeersch T, Zurek E, Hutchison GR. Avogadro: an advanced semantic chemical editor, visualization, and analysis platform. *J Cheminform.* (2012) 4:17. doi: 10.1186/1758-2946-4-17
- Wiji Prasetyaningrum P, Bahtiar A, Hayun H. Synthesis and cytotoxicity evaluation of novel Asymmetrical Mono-Carbonyl Analogs of Curcumin (AMACs) against Vero, HeLa, and MCF7 cell lines. *Sci Pharm.* (2018) 86:25. doi: 10.3390/scipharm86020025
- Khan MA, Ahmad R, Srivastava AN. Effect of ethyl acetate aroma on viability of human breast cancer and normal kidney epithelial cells *in vitro*. *Integr Med Res.* (2017) 6:47–59. doi: 10.1016/j.imr.2016.11.004
- Keepers YP, Pizao PE, Peters GJ, van Ark-Otte J, Winograd B, Pinedo HM. Comparison of the sulforhodamine B protein and tetrazolium (MTT) assays for *in vitro* chemosensitivity testing. *Eur J Cancer Clin Oncol.* (1991) 27:897–900. doi: 10.1016/0277-5379(91)90142-Z
- Voigt W. Sulforhodamine B assay and chemosensitivity. *Humana Press.* (2005) 110:39–48. doi: 10.1385/1-59259-869-2:039
- Peña-Morán O, Villarreal M, Álvarez-Berber L, Meneses-Acosta A, Rodríguez-López V. Cytotoxicity, post-treatment recovery, and selectivity analysis of naturally occurring podophyllotoxins from *Bursera fagaroides* var. *fagaroides* on breast cancer cell lines. *Molecules.* (2016) 21:1013. doi: 10.3390/molecules21081013
- Majoumou MS, Tincho MB, Morris T, Hiss DC, Boyom FF, Mandal C. Antiproliferative potential of methanolic and aqueous extracts and their methanolic fractions derived from fruits of *Bersama engleriana* against a panel of four cancer cell lines. *Cogent Biol.* (2020) 6:1727636. doi: 10.1080/23312025.2020.1727636
- Parsa N. Environmental factors inducing human cancers. *Iran J Public Health.* (2012) 41:1–9.

29. Yin A, Moes DJAR, Hasselt JGC, Swen JJ, Guchelaar H. A review of mathematical models for tumor dynamics and treatment resistance evolution of solid tumors. *CPT Pharmacometrics Syst Pharmacol.* (2019) 8:720–37. doi: 10.1002/psp4.12450
30. Housman G, Byler S, Heerboth S, Lapinska K, Longacre M, Snyder N, et al. Drug resistance in cancer: an overview. *Cancers.* (2014) 6:1769–92. doi: 10.3390/cancers6031769
31. Ledzewicz U, Schättler H. Analysis of models for evolving drug resistance in cancer chemotherapy. In: *Dynamics of Continuous, Discrete and Impulsive Systems - DCDIS, Proceedings 2.* (2006). p. 291–304.
32. Salgia R, Kulkarni P. The genetic/non-genetic duality of drug “resistance” in cancer. *Trends Cancer.* (2018) 4:110–8. doi: 10.1016/j.trecan.2018.01.001
33. Ganguli P, Sarkar RR. Exploring immuno-regulatory mechanisms in the tumor microenvironment: model and design of protocols for cancer remission. *PLoS ONE.* (2018) 13:1–25. doi: 10.1371/journal.pone.0203030
34. Vaghi C, Rodallec A, Fanciullino R, Ciccolini J, Mochel JP, Matri M, et al. Population modeling of tumor growth curves and the reduced Gompertz model improve prediction of the age of experimental tumors. *PLoS Comput Biol.* (2020) 16:e1007178. doi: 10.1371/journal.pcbi.1007178
35. Demicheli R, Pratesi GFR. The exponential-Gompertzian tumor growth model: data from six tumor cell lines *in vitro* and *in vivo*. Estimate of the transition point from exponential to Gompertzian growth and potential clinical implications. *Tumori.* (1991) 77:189–95. doi: 10.1177/030089169107700302
36. Murphy H, Jaafari H, Dobrovolsky HM. Differences in predictions of ODE models of tumor growth: a cautionary example. *BMC Cancer.* (2016) 16:163. doi: 10.1186/s12885-016-2164-x
37. Charlebois DA, Balázsi G. Modeling cell population dynamics. *In silico Biol.* (2019) 13:21–39. doi: 10.3233/ISB-180470
38. Li B, Fei C, Zhang J, Guo F, Sun A, Huan L, et al. Histamine induced apoptosis in primary-cultured glioma. *Biomed Res.* (2017) 28:6725–9. Available online at: <https://www.alliedacademies.org/articles/histamineinduced-apoptosis-in-primarycultured-glioma-8100.html>
39. Bigner DD, Winters A, Choudhury GR, Yuan F, Liu R, Keir ST, et al. Reversing the warburg effect as a treatment for glioblastoma. *J Biol Chem.* (2013) 288:9153–64. doi: 10.1074/jbc.M112.440354
40. Castaño E, Giménez-Bonafé P, Tortosa A, Martínez-Soler F, Acebes J-J, Coll-Mulet L, et al. Activation of p53 by nutlin-3a induces apoptosis and cellular senescence in human glioblastoma multiforme. *PLoS ONE.* (2011) 6:e18588. doi: 10.1371/journal.pone.0018588
41. Saksman E, Mira A, Haario H, Laine M. DRAM: efficient adaptive MCMC. *Stat Comput.* (2006) 16:339–54. doi: 10.1007/s11222-006-9438-0
42. Lee SY. Temozolomide resistance in glioblastoma multiforme. *Genes Dis.* (2016) 3:198–210. doi: 10.1016/j.gendis.2016.04.007
43. Goellner EM, Grimme B, Brown AR, Lin Y-C, Wang X-H, Sugrue KF, et al. Overcoming temozolomide resistance in glioblastoma *via* dual inhibition of NAD⁺ biosynthesis and base excision repair. *Cancer Res.* (2011) 71:2308–17. doi: 10.1158/0008-5472.CAN-10-3213
44. Mould D, Walz A-C, Lave T, Gibbs J, Frame B. Developing exposure/response models for anticancer drug treatment: special considerations. *CPT Pharmacometrics Syst Pharmacol.* (2015) 4:12–27. doi: 10.1002/psp4.16
45. Holford N. Pharmacodynamic principles and the time course of immediate drug effects. *Transl Clin Pharmacol.* (2017) 25:157. doi: 10.12793/tcp.2017.25.4.157
46. Marino S, Hogue IB, Ray CJ, Kirschner DE. A methodology for performing global uncertainty and sensitivity analysis in systems biology. *J Theor Biol.* (2008) 254:178–96. doi: 10.1016/j.jtbi.2008.04.011
47. He L, Kuleskiy E, Saarela J, Turunen L, Wennerberg K, Aittokallio T, et al. Methods for high-throughput drug combination screening and synergy scoring. *Cancer Syst Biol.* (2018) 17:351–98. doi: 10.1007/978-1-4939-7493-1_17
48. Bijnsdorp IV, Giovannetti E, Peters GJ. Analysis of drug interactions. *Methods Mol Biol.* (2011) 731:421–34. doi: 10.1007/978-1-61779-080-5_34
49. El Hassouni B, Mantini G, Li Petri G, Capula M, Boyd L, Weinstein HNW, et al. To combine or not combine: drug interactions and tools for their analysis. Reflections from the EORTC-PAMM course on preclinical and early-phase clinical pharmacology. *Anticancer Res.* (2019) 39:3303–9. doi: 10.21873/anticancer.13472
50. Dertinger SD, Avlasevich SL, Torous DK, Singh P, Khanal S, Kirby C, et al. 3Rs friendly study designs facilitate rat liver and blood micronucleus assays and Pig-a gene mutation assessments: proof-of-concept with 13 reference chemicals. *Environ Mol Mutagen.* (2019) 60:704–39. doi: 10.1002/em.22312
51. Upadhyay RK. Drug delivery systems, CNS protection, and the blood brain barrier. *Biomed Res Int.* (2014) 2014:1–37. doi: 10.1155/2014/869269
52. Mayur YC. Design of new drug molecules to be used in reversing multidrug resistance in cancer cells. *Curr Cancer Drug Targets.* (2009) 9:298–306. doi: 10.2174/156800909788166619
53. Mayur YC, Padma T, Parimala B, Chandramouli K, Jagadeesh S, Gowda NM, et al. Sensitization of Multidrug Resistant (MDR) cancer cells to vinblastine by novel acridones: correlation between anti-calmodulin activity and anti-MDR activity. *Med Chem.* (2006) 2:63–77. doi: 10.2174/157340606775197732
54. Mayur YC, Zaheeruddin, Peters GJ, Lemos C, Kathmann I, Prasad VVSR. Synthesis of 2-fluoro N 10 -substituted acridones and their cytotoxicity studies in sensitive and resistant cancer cell lines and their DNA intercalation studies. *Arch Pharm.* (2009) 342:640–50. doi: 10.1002/ardp.200900046
55. Rajendra Prasad VVS, Venkat Rao J, Giri RS, Sathish NK, Shanta Kumar SM, Mayur YC. Chloro acridone derivatives as cytotoxic agents active on multidrug-resistant cell lines and their duplex DNA complex studies by electrospray ionization mass spectrometry. *Chem Biol Interact.* (2008) 176:212–9. doi: 10.1016/j.cbi.2008.06.007

Conflict of Interest: The authors declare that the research was conducted in the absence of any commercial or financial relationships that could be construed as a potential conflict of interest.

Copyright © 2021 Chakravarty, Ganguli, Murahari, Sarkar, Peters and Mayur. This is an open-access article distributed under the terms of the Creative Commons Attribution License (CC BY). The use, distribution or reproduction in other forums is permitted, provided the original author(s) and the copyright owner(s) are credited and that the original publication in this journal is cited, in accordance with accepted academic practice. No use, distribution or reproduction is permitted which does not comply with these terms.